MEDICINAL PLANTS IN THE TREATMENT OF MYOCARDIAL INJURY AND VASCULAR DISEASES

EDITED BY: Yusof Kamisah, Zakiah Jubri, Mas Rizky A. A. Syamsunarno and Yue Liu

PUBLISHED IN: Frontiers in Pharmacology

frontiers Research Topics

frontiers

ISSN 1664-8714
ISBN 978-2-88974-999-7
DOI 10.3389/978-2-88974-999-7

About Frontiers

Frontiers is more than just an open-access publisher of scholarly articles: it is a pioneering approach to the world of academia, radically improving the way scholarly research is managed. The grand vision of Frontiers is a world where all people have an equal opportunity to seek, share and generate knowledge. Frontiers provides immediate and permanent online open access to all its publications, but this alone is not enough to realize our grand goals.

Frontiers Journal Series

The Frontiers Journal Series is a multi-tier and interdisciplinary set of open-access, online journals, promising a paradigm shift from the current review, selection and dissemination processes in academic publishing. All Frontiers journals are driven by researchers for researchers; therefore, they constitute a service to the scholarly community. At the same time, the Frontiers Journal Series operates on a revolutionary invention, the tiered publishing system, initially addressing specific communities of scholars, and gradually climbing up to broader public understanding, thus serving the interests of the lay society, too.

Dedication to Quality

Each Frontiers article is a landmark of the highest quality, thanks to genuinely collaborative interactions between authors and review editors, who include some of the world's best academicians. Research must be certified by peers before entering a stream of knowledge that may eventually reach the public - and shape society; therefore, Frontiers only applies the most rigorous and unbiased reviews.
Frontiers revolutionizes research publishing by freely delivering the most outstanding research, evaluated with no bias from both the academic and social point of view. By applying the most advanced information technologies, Frontiers is catapulting scholarly publishing into a new generation.

What are Frontiers Research Topics?

Frontiers Research Topics are very popular trademarks of the Frontiers Journals Series: they are collections of at least ten articles, all centered on a particular subject. With their unique mix of varied contributions from Original Research to Review Articles, Frontiers Research Topics unify the most influential researchers, the latest key findings and historical advances in a hot research area! Find out more on how to host your own Frontiers Research Topic or contribute to one as an author by contacting the Frontiers Editorial Office: frontiersin.org/about/contact

MEDICINAL PLANTS IN THE TREATMENT OF MYOCARDIAL INJURY AND VASCULAR DISEASES

Topic Editors:
Yusof Kamisah, Faculty of Medicine Universiti Kebangaan Malaysia, Malaysia
Zakiah Jubri, National University of Malaysia, Malaysia
Mas Rizky A. A. Syamsunarno, Padjadjaran University, Indonesia
Yue Liu, Cardiovascular Diseases Center, Xiyuan Hospital, China

Citation: Kamisah, Y., Jubri, Z., Syamsunarno, M. R. A. A., Liu, Y., eds. (2022). Medicinal Plants in the Treatment of Myocardial Injury and Vascular Diseases. Lausanne: Frontiers Media SA. doi: 10.3389/978-2-88974-999-7

Table of Contents

frontiers | Frontiers in Pharmacology

EDITORIAL
published: 01 April 2022
doi: 10.3389/fphar.2022.879557

Editorial: Medicinal Plants in the Treatment of Myocardial Injury and Vascular Diseases

*Mas Rizky AA Syamsunarno[1], Zakiah Jubri[2,3], Yue Liu[4] and Yusof Kamisah[3,5]**

[1]Department of Biomedical Sciences, Faculty of Medicine, Universitas Padjadjaran, Bandung, Indonesia, [2]Department of Biochemistry, Faculty of Medicine, Universiti Kebangsaan Malaysia, Kuala Lumpur, Malaysia, [3]Cardiovascular Health Research Group, Faculty of Medicine, Universiti Kebangsaan Malaysia, Kuala Lumpur, Malaysia, [4]Cardiovascular Diseases Center, Xiyuan Hospital, Beijing, China, [5]Department of Pharmacology, Faculty of Medicine Universiti Kebangaan Malaysia, Kuala Lumpur, Malaysia*

Keywords: traditional medicine, ethnopharmacology, heart, vascular, traditional Chinese medicine

Editorial on the Research Topic

Medicinal Plants in the Treatment of Myocardial Injury and Vascular Diseases

Cardiovascular diseases are the number one killer worldwide; approximately 17.9 million deaths were attributed to cardiovascular diseases in 2019, accounting for 32% of all global mortalities. The most common cardiovascular diseases are hypertension, atherosclerosis, heart failure, and ischemic heart disease (World Health Organization, 2021). These diseases are managed pharmacologically using modern medicines, such as statins (Bruikman et al., 2017), angiotensin-converting enzyme inhibitors, diuretics (Hui, 2020; Lin and Fang, 2020), and aspirin (Wan et al., 2020). However, the use of these drugs is not without several adverse effects. Because of this awareness, several studies have been conducted in search of alternative medicines, especially those from plants.

Approximately 24% of drugs approved by the United States Food and Drug Administration and other drug regulatory bodies from 1981 to September 2019 originated from natural sources, and approximately 12% of these newly approved drugs derived from natural products were cardiovascular drugs (Newman and Cragg, 2020). This development indicates that natural products, such as plants and microbes, are one of the key sources of new drugs. Many plants have potential medicinal values, and most of them have been used traditionally for various ailments since ancient times. Traditional medicines play a crucial role in the development of new drugs, many of which have progressed into orderly-regulated systems of medicine, such as traditional Chinese medicine (Yuan et al., 2016).

The Research Topic Medicinal plants in the treatment of myocardial injury and vascular diseases collected studies carried out on crude extracts (typically used in a traditional context) and isolated bioactive compounds for the treatment of myocardial injury and vascular disease, focusing on the possible mechanisms of action. It is a collection of 15 articles that explore the effects of various medicinal plants against cardiovascular disease. More than two-thirds of the articles were original research articles and study protocol, and the remaining were reviews (**Figure 1A**), suggesting that research has actively explored medicinal plants in search of new drugs against cardiovascular diseases. The most common focus of articles submitted to the Research Topic was traditional medicinal plant extracts, followed by traditional Chinese medicines (**Figure 1B**). One-third of the articles studied bioactive compounds isolated from medicinal plants.

Danlou tablet is a commercially available traditional Chinese medicine composed of 10 herbs. Wang et al. and Liu et al. investigated its effects on atherosclerosis using apolipoprotein E-deficient ($ApoE^{-/-}$) mice (an atherosclerotic mouse model) fed a high-fat diet. The medication improved the blood lipid profile, reduced blood inflammatory biomarkers, and decreased lipid deposition and

OPEN ACCESS

Edited by:
Javier Echeverria,
University of Santiago, Chile

Reviewed by:
Min Wu,
China Academy of Chinese Medical Sciences, China

****Correspondence:***
Yusof Kamisah
kamisah_y@yahoo.com

Specialty section:
This article was submitted to Ethnopharmacology, a section of the journal Frontiers in Pharmacology

Received: *19 February 2022*
Accepted: *09 March 2022*
Published: *01 April 2022*

Citation:
Syamsunarno MRAA, Jubri Z, Liu Y and Kamisah Y (2022) Editorial: Medicinal Plants in the Treatment of Myocardial Injury and Vascular Diseases. Front. Pharmacol. 13:879557. doi: 10.3389/fphar.2022.879557

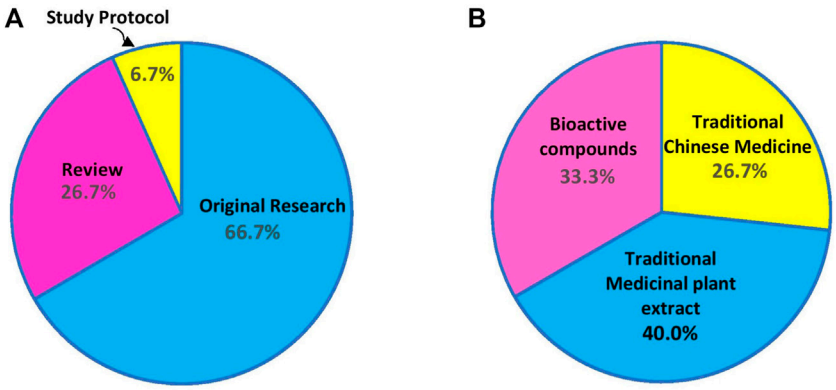

FIGURE 1 | (A) The proportion of article types and **(B)** the type of studied medicinal plants published in the Research Topic.

fibrous plaque formation in atherosclerotic plaque. Its protective mechanism was most likely the activation of autophagy mediated by the phosphatidylinositol 3-kinase/protein kinase B/mammalian target of rapamycin (PI3K/Akt/mTOR) signaling pathway in vascular adventitial fibroblasts (Wang et al.) and macrophages (Liu et al.). Additionally, Liu et al. reported reduced $CD68^+$ macrophage infiltration and inflammatory factor expression in the plaque.

Exposure to secondhand tobacco smoke that contains nicotine can lead to severe health consequences, such as an increased risk of vascular dysfunction (Whitehead et al., 2021). Md Salleh et al. reported that *Piper sarmentosum* Roxb. protected against nicotine-induced vascular endothelial dysfunction *in vitro*. They observed that the plant extract promoted vasorelaxation by enhancing vascular nitric oxide and antioxidant levels in nicotine-administered rats. Kim et al. investigated the effects of the seaweed *Codium fragile* (Suringer) Hariot on thrombosis and platelet aggregation by suppressing the activation of sarcoma tyrosine-protein kinase, spleen tyrosine kinase, phospholipase Cγ2, PI3K, Akt, and mitogen-activated protein kinases (MAPKs). The suppression inhibited the signaling of αIIbβ3 integrin, a primary mediator of platelet aggregation. Phytol detected in the seaweed may be the bioactive compound responsible for the observed effects.

In addition, oroxylin A purified from *Scutellaria baicalensis* Georgi conferred beneficial effects against ischemia after artery blockage due to peripheral artery disease (Zhang et al.). It attenuated tissue injury and promoted perfusion recovery, angiogenesis, and endothelial cell migration, most likely by stimulating the T-box20/prokineticin 2 and Ras homolog gene family member A (RhoA)/Rho-associated coiled-coil kinase 2 signaling pathways. On the basis of these findings, oroxylin A could be developed as a drug candidate for treating medical problems related to peripheral artery disease. Additionally, Vijakumaran et al. described the effects of hydroxytyrosol, a polyphenol from the olive plant (*Olea europaea* L.), on the progression of intimal hyperplasia in a scoping review. Hydroxytyrosol has an anti-inflammatory effect, which prevents intimal hyperplasia arising from endothelial inflammation. This effect is mediated by the upregulation of the PI3K/Akt/mTOR pathway; the inhibition of extracellular signal-regulated protein kinase pathway activation, which is involved in inflammation; and the inhibition of the stress-activated protein kinase pathway (also known as the c-Jun N-terminal kinase pathway), which is involved in apoptosis. Leong et al. described the anti-inflammatory effects of thymoquinone on atherosclerosis. Thymoquinone, a compound isolated from *Nigella sativa* L., modulates inflammatory events in atherosclerosis by suppressing the nuclear factor kappa-light-chain-enhancer of activated B cells and MAPK pathways.

Heart failure has become a serious global medical problem (Maraey et al., 2021). It is manifested as cardiac hypertrophy, the presence of fibrotic tissues, and impaired cardiac function (Siti et al., 2020). Various plants have demonstrated protective effects against heart failure in animal models. Huangqi Shengmai Yin, another traditional Chinese medicine, was studied in isoprenaline-induced heart failure in rats (Pan et al.). The medication reduced myocardial fibrosis and improved cardiac function in the rats, possibly by activating sirtuin 3 and inhibiting the transforming growth factor-β/Smad pathway. Moreover, *Parkia speciosa* Hassk., which is rich in flavonoids, protected against angiotensin II (Ang II)-induced cardiomyocyte hypertrophy *in vitro*, most likely by suppressing the activation of the MAPK signaling pathway, which is involved in inflammatory regulation and the Ang II/reactive oxygen species/nitric oxide axis (Siti et al.). Bunaim et al. also demonstrated that *Centella asiatica* (L.) Urb extract administered orally for 8 weeks prevented heart damage and the development of hypertension induced by N(G)-nitro-L-arginine methyl ester, a nitric oxide synthase inhibitor. The plant extract provided protection by inhibiting serum nitric oxide loss and myocardial angiotensin-converting enzyme activity, most likely through its antioxidant properties. Liu et al. described a study protocol for a basket trial involving BuqiTongluo granule for patients with ischemic stroke, stable angina pectoris, and diabetic peripheral neuropathy associated with qi deficiency and blood stasis syndrome. The treatment would be given for 6 weeks. This was the only clinical study included in the Research Topic.

The effects of two bioactive metabolites—ferruginol and aconitine—were studied in the hearts. Ferruginol, a terpenoid, is abundant in *Salvia spp.* plants, whereas aconitine, a diterpenoid, is found in *Aconitum spp.* Ferruginol afforded cardioprotection against doxorubin-induced cardiotoxicity by rescuing mitochondrial biogenesis and fatty acid oxidation via the sirtuin 1–peroxisome proliferator-activated receptor gamma coactivator-1α axis (Li et al.); this protection was observed as an improvement in cardiac function and a reduction in myocardial damage in rats. Qiu et al. also reported cardiotonic effects of repeated low-dose administration of aconitine in neonatal rat ventricular myocytes. These findings suggest that the metabolite promotes remodeling of mitochondrial function and thus increases energy metabolism, possibly via the AMP-activated protein kinase–optic atrophy 1–ATP synthase α-subunit pathway.

Syamsunarno et al. contributed an in-depth review of the effects of *Caesalpinia sappan* Linn. on the cardiovascular organs. They described the molecular mechanisms of the plant extract's protective effects and its bioactive compounds—brazilin, sappanone A, and brazilein—against myocardial and vascular injuries. The protective effects of *Moringa oleifera* Lam. were also comprehensively reviewed, especially against cardiovascular-related metabolic syndrome (Alia et al.).

In conclusion, this Research Topic stipulates updated research studies and reviews that provide insights into the molecular mechanisms of the protective effects of various medicinal plants and their bioactive compounds against cardiovascular diseases. The bioactive compounds that have been reported in plants could potentially be developed as candidate drugs. Unfortunately, the Research Topic lacks findings from clinical studies. Thus, more studies in the clinical setting should be pursued to confirm the protective effects observed in the laboratory.

AUTHOR CONTRIBUTIONS

YK drafted the manuscript. MS, ZJ, and YL critically revised the manuscript. All authors made a substantial intellectual contribution to the work and approved it for publication.

FUNDING

The study was funded by Ministry of Higher Education of Malaysia (FRGS-1-2019-SKK10-UKM-02-1).

ACKNOWLEDGMENTS

We wish to express our gratitude and appreciation to all contributing authors to the Frontiers Research Topic, reviewers who had given their professional input, invited editors who had helped out with editing process, and Editorial and Production team of Frontiers for their support throughout the publication process.

REFERENCES

Bruikman, C. S., Stoekenbroek, R. M., Hovingh, G. K., and Kastelein, J. P. (2017). New Drugs for Atherosclerosis. *Can. J. Cardiol.* 33 (3), 350–357. doi:10.1016/j.cjca.2016.09.010

Hui, R. (2020). Hypertension Drug Therapy. *Adv. Exp. Med. Biol.* 1177, 149–268. doi:10.1007/978-981–15-2517-9_6

Lin, X., and Fang, L. (2020). Pharmaceutical Treatment for Heart Failure. *Adv. Exp. Med. Biol.* 1177, 269–295. doi:10.1007/978-981-15-2517-9_7

Maraey, A., Salem, M., Dawoud, N., Khalil, M., Elzanaty, A., Elsharnoby, H., et al. (2021). Predictors of Thirty-Day Readmission in Nonagenarians Presenting with Acute Heart Failure with Preserved Ejection Fraction: A Nationwide Analysis. *J. Geriatr. Cardiol.* 18 (12), 1008–1018. doi:10.11909/j.issn.1671–5411.2021.12.005

Newman, D. J., and Cragg, G. M. (2020). Natural Products as Sources of New Drugs over the Nearly Four Decades from 01/1981 to 09/2019. *J. Nat. Prod.* 83 (3), 770–803. doi:10.1021/acs.jnatprod.9b01285

Siti, H. N., Jalil, J., Asmadi, A. Y., and Kamisah, Y. (2020). Roles of Rutin in Cardiac Remodeling. *J. Funct. Foods* 64, 103606. doi:10.1016/j.jff.2019.103606

Wan, Q., Qian, S., Huang, Y., Zhang, Y., Peng, Z., Li, Q., et al. (2020). Drug Discovery for Coronary Artery Disease. *Adv. Exp. Med. Biol.* 1177, 297–339. doi:10.1007/978-981-15-2517-9_8

Whitehead, A. K., Erwin, A. P., and Yue, X. (2021). Nicotine and Vascular Dysfunction. *Acta Physiol.* 231, 1–13. doi:10.1111/apha.13631

World Health Organization (2021). Cardiovascular Diseases (CVDs). Available at: https://www.who.int/news-room/fact-sheets/detail/cardiovascular-diseases-(cvds) (Accessed on February 6, 2022).

Yuan, H., Ma, Q., Ye, L., and Piao, G. (2016). The Traditional Medicine and Modern Medicine from Natural Products. *Molecules* 21 (5), 559. doi:10.3390/molecules21050559

Conflict of Interest: The authors declare that the research was conducted in the absence of any commercial or financial relationships that could be construed as a potential conflict of interest.

The reviewer (MW) declared a past co-authorship with the author (YL) to the handling editor.

frontiers in Pharmacology

SYSTEMATIC REVIEW
published: 21 May 2021
doi: 10.3389/fphar.2021.663266

Molecular Action of Hydroxytyrosol in Attenuation of Intimal Hyperplasia: A Scoping Review

*Ubashini Vijakumaran[1], Muhammad Dain Yazid[1], Ruszymah Bt Hj Idrus[1,2], Mohd Ramzisham Abdul Rahman[3] and Nadiah Sulaiman[1]**

[1]Centre for Tissue Engineering and Regenerative Medicine, Universiti Kebangsaan Malaysia Medical Centre, Kuala Lumpur, Malaysia, [2]Department of Physiology, Faculty of Medicine, Universiti Kebangsaan Malaysia Medical Centre, Kuala Lumpur, Malaysia, [3]Department of Surgery, Faculty of Medicine, Universiti Kebangsaan Malaysia Medical Centre, Kuala Lumpur, Malaysia

OPEN ACCESS

Edited by:
Masliza Mahmod, University of Oxford, United Kingdom

Reviewed by:
Jian Yang, The First People's Hospital of Yichang, China
Juan Carlos Sepúlveda-Arias, Technological University of Pereira, Colombia

***Correspondence:**
Nadiah Sulaiman
nadiahsulaiman@ukm.edu.my

Specialty section:
This article was submitted to Ethnopharmacology, a section of the journal Frontiers in Pharmacology

Received: *02 February 2021*
Accepted: *29 April 2021*
Published: *21 May 2021*

Citation:
Vijakumaran U, Yazid MD, Hj Idrus RB, Abdul Rahman MR and Sulaiman N (2021) Molecular Action of Hydroxytyrosol in Attenuation of Intimal Hyperplasia: A Scoping Review. Front. Pharmacol. 12:663266. doi: 10.3389/fphar.2021.663266

Objective: Hydroxytyrosol (HT), a polyphenol of olive plant is well known for its antioxidant, anti-inflammatory and anti-atherogenic properties. The aim of this systematic search is to highlight the scientific evidence evaluating molecular efficiency of HT in halting the progression of intimal hyperplasia (IH), which is a clinical condition arises from endothelial inflammation.

Methods: A systematic search was performed through PubMed, Web of Science and Scopus, based on pre-set keywords which are Hydroxytyrosol OR 3,4-dihydroxyphenylethanol, AND Intimal hyperplasia OR Neointimal hyperplasia OR Endothelial OR Smooth muscles. Eighteen *in vitro* and three *in vitro* and *in vivo* studies were selected based on a pre-set inclusion and exclusion criteria.

Results: Based on evidence gathered, HT was found to upregulate PI3K/AKT/mTOR pathways and supresses inflammatory factors and mediators such as IL-1β, IL-6, E-selectin, P-selectin, VCAM-1, and ICAM-1 in endothelial vascularization and functioning. Two studies revealed HT disrupted vascular smooth muscle cells (SMC) cell cycle by dephosphorylating ERK1/2 and AKT pathways. Therefore, HT was proven to promote endothelization and inhibit vascular SMCs migration thus hampering IH development. However, none of these studies described the effect of HT collectively in both vascular endothelial cells (EC) and SMCs in IH *ex vivo* model.

Conclusions: Evidence from this concise review provides an insight on HT regulation of molecular pathways in reendothelization and inhibition of VSMCs migration. Henceforth, we propose effect of HT on IH prevention could be further elucidated through *in vivo* and *ex vivo* model.

Keywords: hydroxytyrosol, intimal hyperplasia, neointimal hyperplasia, smooth muscle cell, endothelial cell

INTRODUCTION

Intimal Hyperplasia and Current Treatments

Annually, millions of coronary artery bypass surgery (CABG) and percutaneous coronary interventions (PCI) are performed to treat ischemic heart disease. However, the development of intimal hyperplasia (IH) limits the long-term efficacy of these cardiovascular interventions (Mylonaki et al., 2018). Intimal hyperplasia is defined by thickening of the intimal layer of a blood vessel as a response to endothelial injury, which occurs during or post-surgical procedures such as PCI or CABG (Gellman et al., 1991). Endothelial injury triggers inflammation and platelet activation which subsequently stimulates the proliferation and migration of smooth muscle cells (SMCs) from media toward the intimal layer. SMCs migration is highly assisted by the secretion of inflammatory factors and mediators and degradation of multiple extracellular matrix (ECM) components in the media and adventitia (Jennette and Stone, 2014). This cascade reaction eventually leads to atherosclerosis where the blood vessel narrowed, and surrounding tissues falls into ischemic condition. Unfortunately, the formation of IH decreases the patency of bypass grafted veins to 40% after 10–20 years following surgery (de Vries and Quax, 2018).

Despite cutting edge therapies, IH remains as the main risk after CABG with no known remedy to reduce or relinquish the ever-progressing condition. Antithrombotic drugs are the classic approach to prevent IH (Hillis et al., 2012; Anderson et al., 2013). However, prolonged dual-antiplatelet therapy post angioplasty and stent implantation increases the risk of internal bleeding (Costa et al., 2015; Urban et al., 2019). First-generation drug-eluting stent (DES) incorporated with antiproliferative drugs like Sirolimus and Paclitaxel, were used to replace bare-metal stent (BMS) (Stone et al., 2007) has significantly reduced the recurrence of occlusion (Stettler et al., 2007; Jennette and Stone, 2014). Unfortunately, increased late stent thrombosis were also reported (Stone et al., 2007). DES efficiently prevent the migration of SMCs by disrupting SMCs cell cycle but with the price of delayed re-endothelization due to the antiproliferative effect of the drug on endothelial cells (ECs) (Camenzind et al., 2007; Joner et al., 2008).

Moving forward, bioresorbable stent (BRS) technology were introduced where the stents could be completely resolved after six months of implantation (Luo et al., 2014) leaving zero traces of stents material. This ultimately reduces future complications like stent migration, endothelial dysfunction, and restenosis (Gonzalo and Macaya, 2012). Unfortunately, BRS mechanical properties i.e. strut thickness, causes vessel injury and subsequently leads to platelet recruitment and thrombosis (Lee and Hernandez, 2018). In addition to that, concern about the degradation and disintegration of BRS into its by-products and its elimination in the coronary artery adds more challenges to the use of BRS. Large and small randomized trials of BRS implantation, unveiled thrombosis and intimal proliferation at one year follow up (Jinnouchi et al., 2019). Moreover, Optical Coherence Tomography (OCT) of an implanted Bioresorbable Novolimus-Eluting Coronary in patient revealed that the implanted scaffold collapsed and increased of neointimal proliferation in the artery (Alfonso and García-Guimaraes, 2017); Braun et al., 2016). Absorb Bioresorbable Vascular Scaffold (BVS; Abbott Vascular) is the first FDA-approved BRS, but it failed to ensure sustained success with increased late thrombosis events reported that leads to its withdrawal from the market due to low demand (Jinnouchi et al., 2019). BRSs are being redeveloped by taking into consideration several issues that include the strut thickness, degradation efficiency, scaffold thrombosis, and currently waiting to be evaluated in large-scale clinical trials (Regazzoli et al., 2017).

Plant-Based Approach for IH

Various herbal plant-based components were studied for their cardiovascular protection effect (Barnard et al., 2019; Kim et al., 2019; Tuso et al., 2015). Xu et al. compiled a list of natural plant derived compounds such as flavonoids, polyphenols, alkaloids, and terpenes that were found to efficiently suppress VSMCs migration and proliferation (Xu et al., 2018). They further elucidated the involvement of typical cell regulatory and inflammatory pathways including MAPKs, PI3K/Akt, JAK-STAT, FAK, and NF-κB in VSMCs migration. However, they focused solely on activity of plant base compounds on VSMCs and not collectively with endothelial cells which is also an essential cell in pathophysiology of IH.

Polyphenol such as resveratrol is the most studied compound in IH prevention. Balloon catheters coated with resveratrol effectively deliver resveratrol to the targeted site and successfully reduce IH development in rabbit models (Tolva et al., 2016). In addition to that, a series of *in vivo* animal studies showed that resveratrol promoted re-endothelization and vascular healing post-surgical anastomosis (Yurdagul et al., 2014; Karaarslan et al., 2015; Kamann et al., 2019). Kamann et al. reported that resveratrol increases ECs proliferation via activating extracellular signal-regulated kinase (ERK) and estrogen receptor-dependent pathway under laminar shear stress (Yurdagul et al., 2014). Interestingly, curcumin also ameliorated IH by increasing endothelial angiogenesis and proliferation in an artery injured rat (Chen et al., 2015).

Alternatively, quercetin (Khandelwal et al., 2012) and salvianolic acid A (SAA) (Sun et al., 2012) were also found to inhibit proliferation of VSMCs too. Intriguingly, a green tea polyphenol, epigallocatechin-3-gallate (EGCg), suppressed neointimal hyperplasia (NIH) in rabbit model by inhibiting the proliferation of VSMCs via inactivation of MAPKs pathway In a recent study, Wei delivered mesoporous silica nanoparticles encapsulated honokiol (HNK), a small molecule polyphenol after balloon injury and HNK greatly suppressed intimal thickening by reducing phosphorylation of Smad3 (Wei et al., 2020).

Hydroxytyrosol as an Innovative Approach

Olive oil is the primary source of fat and polyphenols in Mediterranean Diet (MD) (Widmer et al., 2015). In 2013, the United Nations Educational, Scientific and Cultural Organization

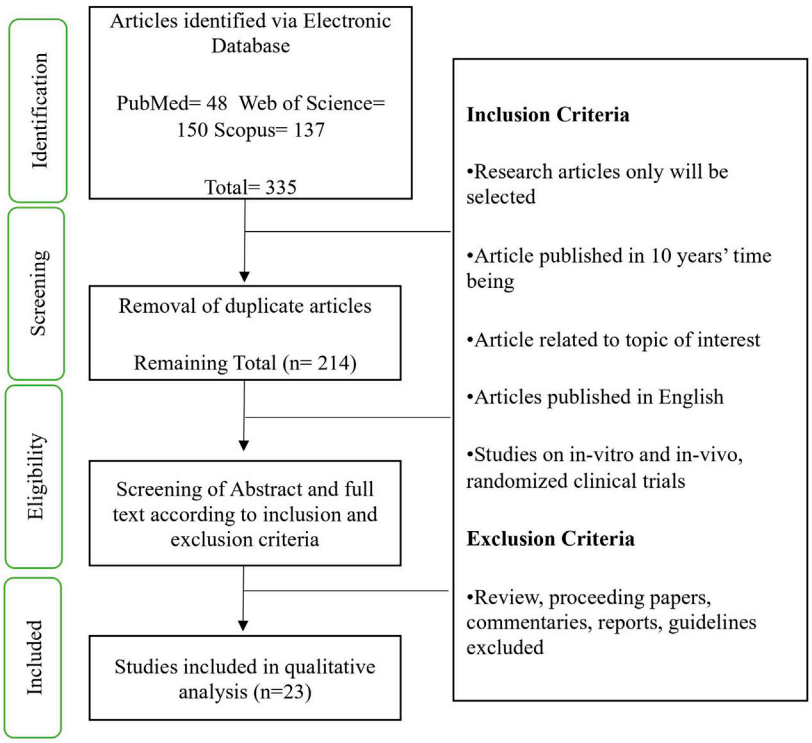

FIGURE 1 | Flow chart represent selection and screening process based on PRISMA.

(UNESCO) include MD in the "Representative List of the Intangible Cultural Heritage of Humanity". MD was also classified in the 2015–2020 Dietary Guidelines for Americans as a healthy diet (Romagnolo and Selmin, 2017). Phytochemicals from olive plant showed positive correlation with the reduction of cardiovascular diseases symptoms and risk factors (Tejada et al., 2016; Guasch-ferré et al., 2019).

Hydroxytyrosol (HT) is a most potent antioxidant, with 154.16 g/mol M mass found in the olive plant (Granados-Principal et al., 2010). HT is naturally derived from the hydrolysis of oleuropein (Tagliafierro et al., 2015) and alternatively, from dopamine metabolism in humans (Rodríguez-Morató et al., 2016). In nature, HT is hydrophilic hence readily absorb in a dose-dependent manner in animals and humans and are excreted in the urine as glucuronide conjugates (Kamil et al., 2020). HT is a well-studied phytochemical for its vascular protection (Hernáez et al., 2017; Nemzer et al., 2019), antioxidant (Adawiyah Razali et al., 2019; Soler-Cantero et al., 2012; Tejada et al., 2016), anti-inflammatory (Chin and Pang, 2017; Ng et al., 2017; Vilaplana-Pérez et al., 2014; Li et al., 2017), anti-atherogenic properties including the inhibition of LDL oxidation (Storniolo et al., 2019); and anti-platelet aggregation (De Roos et al., 2011). A couple of independent research elucidated HT potential in the attenuation of IH development (Xu et al., 2018; Man et al., 2020) However, HT has not been employed in any *in vivo* model to treat IH. Therefore, we aim to collect the scientific evidence of HT in the suppression of IH. This systematic review collate *in vitro* and *in vivo* studies that elucidate the underlying molecular action of HT in the attenuation of IH.

METHODOLOGY

Search Strategy

The selection and screening process were carried out based on PRISMA guideline as presented in **Figure 1**. A systematic screening through three databases (PubMed, Scopus and Web of Science) were performed. Original articles related to the molecular action of Hydroxytyrosol in intimal hyperplasia were searched using the following keywords: Hydroxytyrosol OR 3,4-dihydroxyphenylethanol AND Intimal hyperplasia OR Neointimal hyperplasia OR Endothelial OR Smooth muscle cells.

Selection Criteria

Full-text articles published between 2011–2020 in English were included. Only research/original articles were selected while review articles, proceeding abstract, and case studies were excluded. The search included all *in vitro* and *in vivo* studies. Titles and abstracts were meticulously screened and only articles that correlate to the molecular and cellular mechanism of action of Hydroxytyrosol in intimal hyperplasia were selected.

Data Extraction and Management

Two independent reviewers thoroughly screen the selected research articles. All related articles from the database searches were

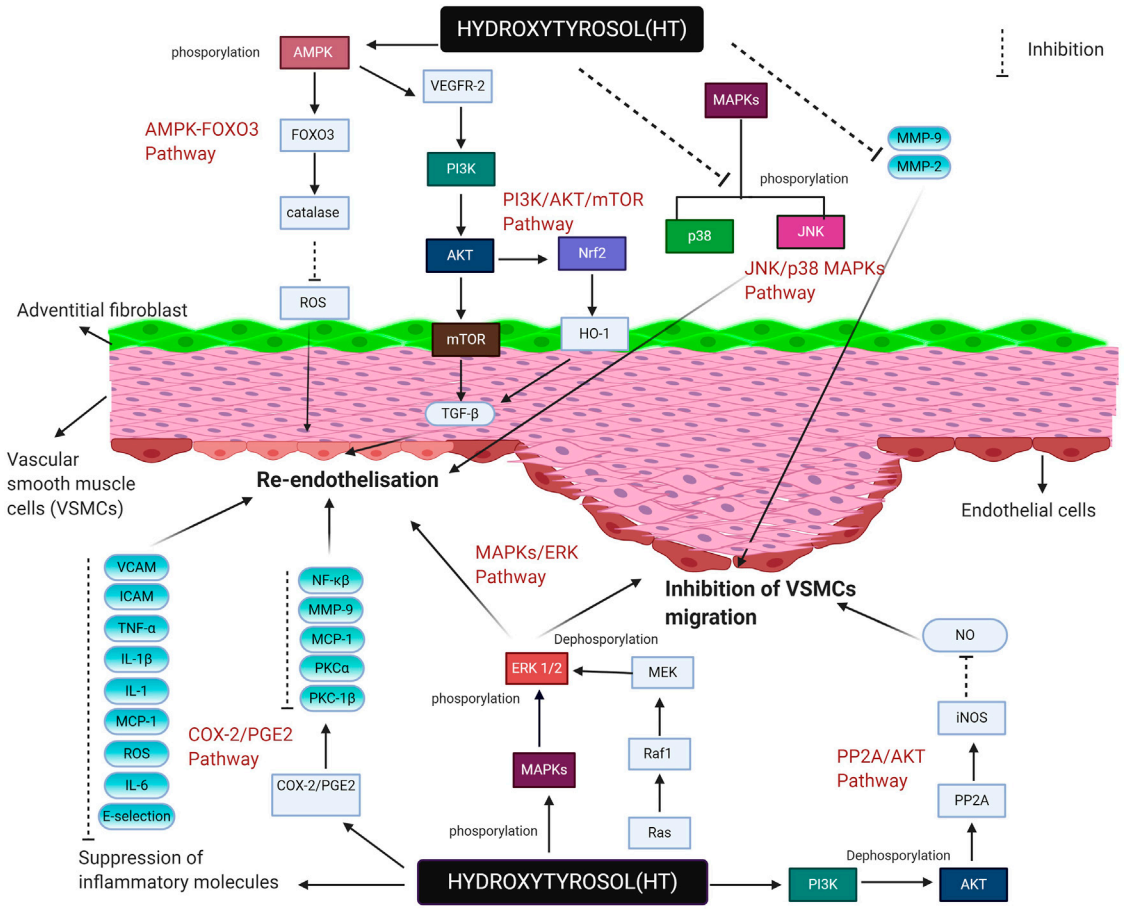

FIGURE 2 | Hydroxytyrosol regulating key genes, inflammatory molecules and pathways in reendotelisation and inhibition of VSMCs

combined and duplicates were removed. The rest of the articles were screened further to meet the selection criteria. The title was first screened, follow by the abstracts for relevance to the selected topic. Unrelated articles that do not fall into the inclusion criteria were removed. The extracted data are tabulated concisely as follows: 1) Reference 2) Aim 3) Cells and Treatment 4) Test(s) 5) Finding(s) 6) Signaling molecules/Pathways 7) Conclusion/correlation with IH.

Quality Evaluation

The quality of the selected studies was validated using a modified version of Office of Health Assessment and Translation (OHAT). The checklist is designed as presented in **Table 3** to evaluate the potential risk of bias of both *in vivo* and *in vitro* studies by assessing 1) reporting bias, 2) performance bias, 3) detection bias, and 4) selection bias.

RESULT

Search Results

Initially, a total of 335 articles were identified from all database search and 216 articles remained after the removal of duplicates. The reviewers validate selected articles independently according to designed inclusion and exclusion criteria to minimize bias. Screening of title and abstract were done twice and a total of 35 papers were identified. During the final screening of the full text, 11 non-related articles, and 3 articles that used nonvascular cells were excluded. In the end, a total of 19 *in vitro* and 4 both *in vitro* and *in vivo* studies were selected for the review. **Figure 1** shows the selection and screening process based on PRISMA guidelines.

Study Characteristics

Three electronic database searches identified 19 *in vitro* (**Table 1**) and 4 studies that include both *in vivo* and *in vitro* (**Table 2**) analysis related to the action of HT in enhancing endothelial function and inhibiting proliferation of VMSCs which are involved in the suppression of intimal hyperplasia development. Data extracted from the selected articles is presented in **Table 1**. Most experiments were conducted utilizing human umbilical vein endothelial cells (HUVECs), human vascular endothelial cells (HVEC) and porcine pulmonary artery endothelial cells (PAECs). However, monocyte cell lines such as U937 and Jurkat were also used in 3 studies. Bovine vascular smooth muscle cells (BVSMVs) and

TABLE 1 | *In vitro* studies outcomes.

No	References	Aim	Cells and treatment	Tests	Findings	Signaling molecules/ Pathways	Conclusion/correlation with IH
1	Nakbi et al. (2011)	To investigate the potential of HT and T on oxidative damage caused by ROS production and MMP-9 expression in PMA induced THP-1	Cells THP-1 Treatment HT (1, 5, 10 and 50 μM) and T (0.05, 0.15, 0.5 and 2 mM) for 4, 15 and 24 h followed by addition of PMA (0.1 μM)	1. Superoxide anion production 2. MMP-9 expression	1. HT and T reduced superoxide release	ROS	HT reduced MMP-9 production that could prevent the migration of smooth muscle cell
2	Scoditti et al. (2012)	To study polyphenols effect on COX-2 and MMP-9 expression induced by pro-angiogenic factor PMA	Cells 1. HUVEC 2. HMEC-1 Treatment HT (0.1–50 μMmol/L)	1. Cell cytotoxicity 2. MMP-9 release 3. MMP-9 gelatinolytic activity 4. PGE2 production 5. COX-2, COX-1, b-actin, and p65 NF-kB expression 6. ROS production	1. HT prevented inflammatory tube formation and cell migration 2. HT inhibited MMP-9 expression 3. HT inhibited COX-2 activity 4. HT decreased ROS level 5. HT suppressed translocation and transactivation of p65 NF-κB	NF-κB	HT suppressed the ROS level and NF-κB activation that regulates the proliferation of endothelial and smooth muscle cells
3	Lamy et al. (2014)	To investigate effect of phenolic compounds toward endothelial cell angiogenesis	Cells 1. HUVECs (HMVECs-d-Ad) Treatment 50 μM olive oil compounds for 18 followed by addition of 1 μg/ml VEGF	1. Tube formation 2. Cell proliferation 3. Cell migration 4. VEGFR-2 phosphorylation study	1. HT suppressed VEGF-induced tube formation 2. HT inhibited cell proliferation 3. HT inhibited phosphorylation of VEGFR-2 4. HT suppressed phosphorylation of ERK-1/2 and SAPK/JNK	1. VEGF 2 2. ERK-1/2 3. SAPK/JNK	HT potently suppressed ERK-1/2, SAPK and JNK pathways involved in endothelial apoptosis
4	Scoditti et al. (2014)	To study the HT effect on MMP-9 expression involved in COX-2/ PGE2 pathway in PMA stimulated human monocytes stimulated	Cells 1. PBMC 2. U937 Treatment HT (1–10 μmol/L) for 1 h followed by stimulation with 30 nmol/L PMA for 0–24 h	1. MMP-9 and TIMP-1 secretion 2. PGE2 production 3. COX-2, COX-1, PKCa, PKCb1, NF-kB expression 4. MMP-9, COX-2, MCP-1, ICAM-1, IL-1b, TNF-a gene expression 5. NF-kB activation 6. PKC translocation	1. HT suppressed MMP-9 secretion 2. HT reduced MMP-9 mRNA levels 3. HT suppressed PGE2 production 4. HT inactivated NF-kB 5. HT decreased MCP-1, ICAM-1, IL-1b, and TNF-α mRNA level 6. HT inactivated PKCα and PKCβ1	1. PGE2 2. NF-kB	HT exhibits protection against vascular endothelial inflammation by suppressing inflammatory cytokines and activating COX-2 and PGE2 pathway
5	Zrelli et al. (2011b)	To study the potential of HT on ROS reduction by enhancing catalase activity through AMPK-FOXO3a pathway	Cells PPAECs Treatment HT (10, 30 and 50 μM)	1. ROS production 2. Catalase mRNA level 3. Phosphorylation of AMPKα and AMPKβ1 4. Protein level of catalase, FOXO3a and AMPK	1. HT reduced ROS 2. HT increased catalase expression 3. HT upregulated FOXO3a expression and mediated nuclear translocation 4. HT activated AMPK phosphorylation	AMPK–FOXO3	HT positively regulated endothelial oxidative defense while prevents endothelial dysfunction and apoptosis by activating AMPK-FOXO3 pathways

(Continued on following page)

TABLE 1 | (*Continued*) *In vitro* studies outcomes.

No	References	Aim	Cells and treatment	Tests	Findings	Signaling molecules/ Pathways	Conclusion/correlation with IH
6	Zrelli et al. (2013)	To study the effect of hydroxytyrosol with carbon monoxide-releasing Molecule-2 in prevention of endothelial dysfunction through NO production and NFκB inactivation	Cells PAECs Treatment HT (1, 10, or 100) μmol/L	1. eNOS,NFκBp65, IκBα, cleaved 2. caspase-3 expression 3. NO production 4. Cell cytotoxicity 5. Cell morphology 6. NFκB activation	1. HT inhibited cytotoxicity 2. HT suppressed cellular damage 3. HT inhibited apoptotic morphology changes and apoptotic cell death 4. HT alone and HT + CORM-2 reduced NFκBp65 protein level 5. HT + CORM-2 increased Enos phosphorylation 6. HT + CORM-2 increased NO release 7. HT + CORM-2 blocked activation of caspase-3 8. HT alone inhibited NFκBp65 phosphorylation while CORM-2 enhanced it 9. HT + CORM-2 inactivates NFκB	NFκB	HT + CORM-2 potentially inhibited endothelial apoptosis by inhibiting caspase 3 and NFκB pathway while supported vascular healing through NO production
7	Abe et al. (2012)	To examine the potential of olive oil phenols in inhibition of smooth muscle cell proliferation through a G1/S cell cycle block regulated by ERK1/2	Cells BVSMCs Treatment HT (1, 10, or 100 μmol/L)	1. Cell proliferation 2. Cell cycle 3. (ERK)1/2 phosphorylation	1. HT inhibited cell proliferation 2. HT disrupted cell cycle and controlled over proliferation 3. HT inhibited ERK1/2 phosphorylation	ERK1/2	HT has potential to inhibit intimal hyperplasia by reducing migration and proliferation of SMC via blocking cell cycle regulated by ERK1/2 phosphorylation
8	Torul et al. (2020)	To evaluate phenolic compounds of olive extract on endothelial toxicity induced by hydrogen peroxide	Cells HUVECs Treatment HT (1.0–10.0 μmol/L	1. Determination of phenolic compounds 2. Induction of ROS 3. Cell cytotoxicity	1. HT suppressed cell toxicity 2. HT decreased ROS production	ROS	HT shown to decrease ROS generation in endothelial which could promote vascular healing
9	Fortes et al. (2012)	To investigate effect of hydroxytyrosol and tyrosol in preventing inflammatory angiogenesis	Cells 1. HUVECs 2. HMECs 3. BAECs Treatment HT 10 mg/ml	1. Cell cytotoxicity 2. Cell migration 3. Tube formation 4. Cell cycle analysis 5. MMP-2 production	1. HT inhibited cell proliferation 2. HT inhibited cell migration 3. HT suppressed tube formation 4. HT enhances apoptosis 5. HT regulated cell cycle 6. HT inhibited MMP-2 activity		HT regulated endothelial cell cycle while decreased production of MMP-2 that possibly could prevent smooth muscle cells migration
10	Abate et al. (2020)	To investigate the effect of HT in endothelial vascularization	Cells 1. HUVECs 2. HVECs Treatment (0–160 μM) for 24 and 48 h	1. Cell viability 2. Cell proliferation 3. Wound healing 4. Cell migration 5. Tube formation 6. Angiogenesis protein expression	1. HT safe for cells up to 160 μM 2. HT enhanced wound healing process 3. HT stimulated HUVEC migration 4. HT upregulated migration and adhesion related protein expression such as ROCK, MMP-2, Phospho-Src, Src, Phospho Erk1/2, Erk1/2, RhoA, Rac1 and Ras 5. HT enhanced tube formation 6. HT upregulated VEGF) receptor 2 7. eNOS, PI3-Kinase, m-TOR, AMPK and Akt	1. PI3K/AKT/ mTor 2. Erk1/2	HT positively regulated vascular remodeling by promoting reendothelization and wound healing by activating PI3K/AKT/ mTor pathways

(Continued on following page)

TABLE 1 | (*Continued*) *In vitro* studies outcomes.

No	References	Aim	Cells and treatment	Tests	Findings	Signaling molecules/ Pathways	Conclusion/correlation with IH
11	Wang et al. (2018)	To assess the effect of HT on autophagosis of VAFs and its related signaling pathways	Cells VAFs Treatment HT (12.5, 25, 50, 100, 200 and 400 μM) for 1 h followed by induction of TNF-α (5 ng/ml) for 24 h	1. Cell viability 2. SIRT1 siRNA level 3. Autophagy related protein level 4. Inflammatory cytokines level	1. HT was shown no cytotoxicity up to 100 μM 2. HT upregulated conversion of LC3 I to LC3 II and the expression of LC3 mRNA in VAFs stimulated with TNF-α 3. HT increased protein level and mRNA expression of Beclin1 4. HT regulated the expression of SIRT1 5. HT and SIRT1 shown compatibility in molecular docking 6. HT activated Akt/mTOR signaling pathway 7. HT decreased TNF-α induced inflammatory cytokine IL-1β	1. SIRT1 2. Akt/mTOR	Hydroxytyrosol promoted autophagy of VAFs via SIRT1-signaling pathway and inhibited inflammatory cytokines in vascular inflammation pathophysiology
12	Cheng et al. (2017)	To study the potential of HT together with PEMFs on HUVECs proliferation	Cells HUVECs Treatment PEMFs at days 0, 1, 2, 3 or 4, or treated with HTY (0, 10, 30, 50, 100, 150 μM) at day 2, or treated with a combination on days 0, 1, 2 or 4	1. Cell viability 2. Cell migration 3. Cell apoptosis	1. HTY + PEMF increases cell proliferation 2. HTY + PEMF enhanced cell migration 3. HTY + PEMFs prevented apoptosis 4. HTY increases mRNA and protein level of Akt, mTOR and TGF-β, but not p53	1. Akt 2. mTOR 3. TGF-β	PEMFs and HTY enhanced endothelial migration and proliferation that could promote reendothelization in vascular remodeling
13	Kouka et al. (2017)	To examine antioxidant property of pure HT from EVOO phenolic fraction	Cells 1. EA. hy926 2. C2C12 Treatment HT (0–40 μg/ml)	1. Extraction of TPF from EVOO 2. Purification of HT from TPF 3. radical scavenging assay 4. Cell viability 5. Assessment of GSH and ROS levels	1. HT exhibited highest antioxidant DPPH 2. HT reduced ROS 3. HT increased GSH		HT found to have decreased ROS and increased GSH which possibly enhance endothelial proliferation and functioning
14	Kitsati et al. (2016)	To assess the potential of HT in rescuing cells from oxidative stress induced by H_2O_2	Cells Jurkat cells Treatment HT (0.05 and 0.1 mM) for 30 min	1. Comet assay 2. Labile iron level 3. H_2O_2 generation	1. HT inhibited H_2O_2 induced labile iron level 2. Hydroxytyrosol inhibits H_2O_2-induced and mitochondrial-mediated apoptosis 3. Hydroxytyrosol inhibits H_2O_2-induced apoptosis 4. inhibits H2O 5. HT inhibited phosphorylation and activation of the JNK and p38 MAPKs	1. JNK 2. p38 MAPKs	HT prevented cellular apoptosis by inactivating JNK and p38 MAPKs pathway

(Continued on following page)

TABLE 1 | (*Continued*) *In vitro* studies outcomes.

No	References	Aim	Cells and treatment	Tests	Findings	Signaling molecules/ Pathways	Conclusion/correlation with IH
15	Zrelli et al. (2015)	To examine the action of hydroxytyrosol in the vascular wound healing mechanism	Cells PPAECs Treatment HT (10–100 μM) 0–24 h	1. Expression of HO-1 and Nrf2 2. Wound healing	1. HT inclined HO-1 mRNA and protein level 2. HT induced HO-1 expression supported by PI3K/Akt and ERK1/2 3. HT mediated Nrf2 expression and nuclear localization	1. PI3K/Akt 2. ERK1/2 3. Nrf2	HT enhanced wound healing process in endothelial through activating expression of HO-1 and Nrf2
16	Zrelli et al. (2011a)	To study the effect of HT in vascular smooth muscle cell VSMCs proliferation	Cells RVSMCs Treatment HT (10, 30, and 100 μM) with and without 20 ng/mL of PDGF	1. Cell migration 2. Cell viability 3. NO production 4. Akt phosphorylation	1. HT decreased the number of viable VSMCs either in the presence or not of PDGF 2. HT promotes VSMCs apoptosis 3. HT increased NO production 4. HT increased iNOS protein expression 5. HT dephosphorylate Akt 6. PP2A mediated HT induced Akt phosphorylation	1. Akt 2. PPA	HT prevents VSMCs apoptosis through NO production and Akt dephosphorylation via activation of PP2A
17	Zrelli et al. (2011b)	To assess the proliferation and protective effect of HT on oxidative injury induced VECs injury	Cells PPAECs Treatment HT (10–100 μM) for 24 h followed by 0–700 3M) of H_2O_2 for 24 h	1. Cell viability 2. Wound healing 3. HO-1 mRNA expression 4. phosphorylation of Akt, p38 MAPK, and ERK1/2 5. ROS production	1. HT enhanced cell proliferation 2. HT repaired wound healing 3. HT prevented H2O2-Induced cytotoxicity 4. HT-induced phosphorylation of Akt, p38 MAPK, and ERK1/2 5. HT accumulates Nrf2 in nucleus 6. HT reduced ROS generation 7. HT increased mRNA and protein level of HO-1	1. Akt 2. MAPK 3. ERK1/2 4. Nrf2	HT protects VECs from oxidative damage through activation of the PI3K/Akt and ERK1/2 pathways
18	Catalan et al. (2015)	To evaluate the effect of hydroxytyrosol and its plasma metabolites toward endothelial protection	Cells HAEC Treatment HT (1, 2, 5, and 10 μM) co-incubated with TNF -α (10 ng/ml) for 18 and 24 h	1. HT metabolites production 2. Adhesion molecules production 3. Chemokine protein production 4. Cytotoxicity	1. HT and HT metabolites reduced E-selectin, P-selectin, VCAM-1, and ICAM-1 2. HT metabolites only reduced MCP-1		HT and HT metabolites exhibited vascular protection by reducing endothelial inflammation cytokines
19	Terzuoli et al. (2020)	To investigate the HT-3Os effects on endothelial-to-mesenchymal transition (EndMT) in the inflamed endothelium	Cells 1. EC 2. HUVEC 3. HREC Treatment 1. IL-1β (10 ng/ml) with or without HT-3Os (10 μM, every 24 h for 7 days	1. Morphology evaluation 2. Immunomarkers detection 3. Cytoplasmic and nuclear protein detection 4. miRNA expression analysis 5. Cytotoxicity	1. HT-3Os reverses EndMT-phenotypic changes induced by IL-1β 2. HT-3Os restores let-7 miRNA expression and inhibits TGF-β signaling 3. HT-3Os upregulated CD31 in IL-1β induced HUVEC and HREC 4. HT-3Os decreased fibroblast markers as FN1 and VIM or SMCin IL-1β induced HUVEC and HREC) 5. HT-3Os upregulated NOTCH3 and MMP2 and MMP9	1. let-7 miRNA 2. MMP 2 3. MMP 9	HT-3Os halts EndMT process in inflamed EC, by increasing let-7 miRNA expression and preventing activation of TGF-β signaling

human microvascular endothelial cells (HMVECs) were utilized in 2 studies. Human microvascular cell line, bovine aorta endothelial cells (BAECs), human peripheral blood cells, myoblast, rat vascular smooth muscle cells, and vascular adventitia fibroblast were also utilized. Two *in vivo* studies were conducted on mice while one was done in a rat model.

Quality Evaluation

Risk bias analysis was conducted using modified version of Office of Health Assessment and Translation (OHAT). Overall, twenty-one out of twenty-three studies showed low risk bias. Two *in vitro*, two *in vivo* and one *in vitro* and *ex vivo* studies showed low risk of bias when they fulfill the selection criteria and reported all outcomes. In contrast, two studies showed high substantial risk of bias due to insufficient sample number and unclear adverse event reporting. A summary of risk bias analysis presented in **Table 3**.

HT Role as an Antioxidant

Antioxidant potential of HT comes from its chemical presence of hydroxyl (OH) groups in the ortho position. These OH groups are responsible in forming stable hydrogen bonds by scavenging reactive oxygen species (ROS) such as hydrogen peroxide (H_2O_2), superoxide ion (O_2^-), hydroxyl radical (OH^-), and reactive nitrogen species (RNS) (Napolitano et al., 2010). HT regulates vascular homeostasis by balancing cellular oxidation stress and in addition to that, treatment with HT increase the production of nitric oxide (NO) which directly plays a crucial role in endothelial cells (ECs) functioning (Sandoo et al., 2010) such as inhibition of inflammation, cell adhesion (Reglero-Real et al., 2016), platelets interactions (Hamilos et al., 2018) as well as maintaining vessel tone (Norton and Popel, 2016).

Imbalance cellular redox reactions in ECs arise from vascular complications like thrombosis (Yang et al., 2017), intimal growth (Nedeljkovic et al., 2003), inflammation, and infarction (Pober and Sessa, 2007). These events are likely activate transcription factors which mediate the secretion of inflammatory factors and cells to the site of inflammation which eventually, delays the healing process (Martinon, 2010; Yang et al., 2017). Interestingly, Pi et al. showed that organic compound extracted from plant i.e. apocynin reduces endogenous ROS level in mice with carotid injury that subsequently suppressed the secretion of pro-inflammatory molecules and VSMC proliferation (Pi et al., 2013). Similarly, heart failure drug like simvastatin and Ivabradine reduces the generation of ROS in IH progression in hyperlipidaemic rabbits (Koniari et al., 2016).

These findings strongly support the correlation between oxidation machinery and the prevention of IH. From our database search, 9 studies reported that HT efficiently prevented ROS production (Nakbi et al., 2011; Zrelli et al., 2011a; Zrelli et al., 2011b; Scoditti et al., 2012; Zrelli et al., 2013; Kouka et al., 2017; Torul et al., 2020). HT was also reported to be able to phosphorylate endothelial nitric oxide synthase (eNOS) which increases nitric oxide (NO) synthesis that essentially needed for vascular integrity and protection (Tousoulis et al., 2011; Zhao et al., 2015; Loscalzo and Jin, 2010). This effect could potentially promote reendothelization in IH repair.

In addition to that, HT also protect cells from H_2O_2 induced cytotoxicity and apoptosis by decreasing superoxide release (Nakbi et al., 2011; Torul et al., 2020) while activating JNK and p38 MAPKs pathways (Kitsati et al., 2016). Interestingly, a particular study by Zrelli found that HT activate the AMPK-FOXO3 pathway by enhancing catalase activity to reduce oxidative stress (Zrelli et al., 2011b). Expression of FOXO3 appears to protect cells from oxidative injury by regulating the expression of the antioxidant enzyme such as catalase and peroxiredoxin (Hou et al., 2010; Olmos et al., 2009). Similarly, another set of studies stated AMPK directly activates FOXO3 transcriptional activity to provide cellular resistance toward oxidative stress (Greer et al., 2007; Li et al., 2009).

HT Reduces Vascular Inflammatory Markers

Endothelial injury is a precursor for intimal hyperplasia (Garg and Hassid, 1989; de Vries and Quax, 2018). Inflammatory cytokines, chemokines, immune cells, and platelets are recruited to the site of injury to initiate repair mechanism which starts off with vascular inflammation and followed with healing process that are regulated by the immune system to maintain vascular health (D'Angelo et al., 2020). However, prolonged exposure to inflammatory molecules has a detrimental effect on vascular cells. Especially, during vascular injury, the secretion of ICAM-1 and MCP-1 attract platelet and leukocyte to the injured site. Gradually, the activated platelets trigger Thromboxane A2 and PDGF release which causes the VSMC to proliferate and migrate (Davies and Hagen, 1989; Huang et al., 2002). Thus, downregulating inflammatory factors and mediators potentially could prevent further progression of IH. Olive oil extracts have been shown to decrease the inflammatory activation in endothelial cells (Burja et al., 2019).

In ECs inflammation, nuclear factor-kappa B (NFκB) transcription factor regulates inflammatory mediators such as MCP-1, VCAM-1, ICAM-1, and E-selectin which recruits leukocytes, IL-6, and IL-8. (Pamukcu et al., 2011). From our systematic search, Scoditti et al. found that HT treatment decrease the expression of MMP-9, ICAM-1, IL-1b, TNF-α, and COX-2 by inactivating NF-κβ, PKCβ1, and PKCα in PMA activated human monocytes (Scoditti et al., 2014). Upon consumption, HT metabolized into glucuronide, sulfate methyl and methyl–sulphate conjugates (Kotronoulas et al., 2013; Rubió et al., 2014). It is crucial to test biological activity of HT metabolites together with HT assessing in vascular protection ability of HT. Catalan and colleagues synthesized physiological HT metabolites using Caco-2 cells. They reported that HT with its metabolites decrease inflammatory mediatorssuch as E-selectin, P-selectin, ICAM-1, and VCAM-1 but HT metabolite alone could only decrease MCP-1 level (Catalán et al., 2015). They further elucidate HT and HT metabolites potential in rat and endothelial cell model where they reported that HT and HT derivate supplemented aorta, stained less for E-selectin, MCP-1, and

TABLE 2 | *In vitro* and *in vivo* studies outcome.

1	García et al. (2017)	To study effects of Hydroxytyrosol in endothelial cell expressing extracellular matrix remodeling enzymes in inhibition of angiogenesis	Animal and Cells 1. Rats 2. BAECs Treatment *In vitro*-HT 0–800 nmol) and 1 mM of HT for 24 h cells *In vivo*-HT 31.2,62.5, 125 and 250 μm) for 48 hours	1. *Ex vivo* rat aortic ring assay 2. *In vivo* chorioallantoic membrane (CAM) assay 3. mRNAs for some extracellular matrix remodeling enzymes	1. HT reduced MMP-1 and MMP-2, uPA mRNA expression 2. HT inhibit *ex vivo* angiogenesis, yet endothelial outgrowing observed 3. HT prevented *in vivo* angiogenesis		HT decreased expression of extracellular matrix remodeling enzyme that could supress migration of smooth muscle cells
2	Catalán et al. (2018)	To study the potential of hydroxytyrosol (HT) and its plasmatic metabolites (HTmet) in enhancement of endothelial function	Animal and cells 1. Apolipoprotein E knockout mice 2. HAEC 3. Jurkat Treatment Invivo-10 mg/kg/day of HT derivatives for 12 weeks Invitro-cells (1, 2 and 5 μM) and TNF-α (10 ng/ml) for 24 h	1. VCAM-1, E-selectin, MCP-1, ICAM-1 expression 2. Human Phospho-MAPK Array 3. NF-B (p65) expression	1. Mice aortas stained less for E-selectin, MCP-1, and ICAM-1 2. HTmet reduced Jurkat T adhesion 3. HTmet decreased E-selectin and VCAM-1 mRNA expression in HAECs 4. HT and HTmet decreased CREB, ERK, JNK pan, JNK, p38δ, p70 S6 kinase	1. ERK 2. JNK 3. MAPK	HT and its metabolites shown to have endothelial protection potential which regulated by the MAPK pathway
3	Yaoa et al. (2019)	To examine the potential of hydroxytyrosol acetate on vascular endothelial inflammation mechanism	Animal and Cells 1. Specific Sirt6 knockout mice hypercholesteraemic 2. HUVECs Treatment Invivo- P-407 (0.5 g/kg), P-407 + HT (5, 10, 20 mg/kg), and P-407+HT-AC (5, 10, 20 mg/kg) groups Invitro-HT or HT-AC (25, 50, or 100 μmol/L) for 1 h, and then stimulated with TNF (10 ng/ml) for 8 h	1. Cell viability 2. SOD, MDA and ROS level 3. SIRT6 siRNA transfection 4. SIRT6 and PKM2 expression 5. HT-AC molecular docking	1. HT and HT-AC decreased TNF and IL1B in mice serum 2. HT and HT-AC decreased mRNA expression of Il-b, Il6 and Ccl2 and TNF 3. HT and HT-AC decreased mRNA expressions of IL1B, IL6 and CCL2 in HUVECs 4. HT-AC increased SOD while decreased MDA and ROS level in TNF- induced HUVECs 5. HT-AC decreased TNFRSF1A protein and mRNA in HUVECs 6. HT-AC upregulated SIRT6 protein and mRNA expression in mice 7. Molecular docking shown good compatibility between HT-AC and SIRT6 8. HT-AC decreased expression of PKM2 in mice and TNF-stimulate HUVECs	1. PKM2	HT and HT-AC exhibited protection against endothelial inflammation in mice and HUVECs cells by mediating PKM2 signaling pathway
4	Fuccelli et al. (2018)	To study the effect of HT in inflammatory markers Cyclooxygenase-2 (COX2) And tumor necrosis factor alfa (TNF-α) and oxidative stress reduction in *vivo* systematic inflammation model	Animal Balb/c mice Treatment 1. HT (40 and 80 mg/kg) 2. LPS induction (50 μg/mouse)	1. COX2 mRNA detection 2. TNF-a cytokine determination 3. DNA damage assessment 4. Antioxidant plasma power quantification	1. HT inhibits the COX2 gene expression 2. HT reduces the TNF-α cytokine secretion 3. HT improves the antioxidant power of plasma 4. HT prevents the DNA damage induced	1. COX2 2. TNF-α	HT inhbited LPS induced COX2 expression, TNF-α production and the DNA damage while enhance antioxidant potential of plasma in *vivo* model

Abbreviations: THP-1, human monocyte cell line; U937, Monocytic cell line; HUVECs, Human umbilical vein endothelial cells; HMEC-1, Human microvascular endothelial cell line; PBMC, Human peripheral blood mononuclear cells; PPAECs, Porcine pulmonary artery endothelial cells; BVSMC, Bovine Vascular smooth muscle cells; HMECs, Human microvascular endothelial cells; VAFs, vascular adventitial fibroblasts; HVECs, Human vascular endothelium cells; BAECs, Bovine aorta endothelial cells; HAECs, human aortic endothelial cells; EA, hy926-endothelial cells; C2C12, myoblasts cells; HREC, Human retinal endothelial cells; RVSMCs, Rat Vascular smooth muscle cells; PMA, phorbol myristate acetate; MMP, matrix metalloproteinase; ROS, Reactive oxygen species; COX-2, cyclooxygenase 2; NF-κβ, nuclear factor kappa-light-chain-enhancer of activated B cells; MCP-1, monocyte chemoattractant protein-1; ICAM-1, intercellular adhesion molecule-1; VCAM-1, vascular cell adhesion molecule-1; IL-1β, interleukin-1β; TNF-α, tumour necrosis factor-α; HMVECs-d-Ad, Human dermal microvascular endothelial cells; VEGF, Vascular endothelial growth factor; prostaglandin (PG)E2; protein kinase C (PKC); FOXO3a, forkhead transcription factor 3a; AMPK-AMP, activated protein kinase; Akt, protein kinase B; CORM-2, Carbon Monoxide-Releasing Molecule-2; PEMF, Pulsed electromagnetic fields; mTOR-mechanistic target of rapamycin; TGF-β1, Transforming growth factor; MAPK, mitogen-activated protein kinase; EndMT, Endothelial-to-mesenchymal transition; HT-3Os, plasma metabolite HT-3O sulfate; FGFR1, fibroblast growth factor receptor 1

ICAM-1. Furthermore, they found that HT and HT metabolites provide endothelial protection through regulation of ERK, JNK, and MAPK interrelated pathways (Catalán et al., 2018). Moreover, Hydroxytyrosol acetate (HT-Ac), were also found to be able to suppress inflammatory response by upregulating SIRT-6 expression in hypercholesterolemic mice and TNF-α treated HUVECs. These studies shed light on the activation of TNFRSF1A and PKM2 pathways which are responsible for anti-inflammatory activity (Yao et al., 2019) thus proves HT inhibits inflammatory angiogenesis.

Inflammatory angiogenesis contribute immensely in the formation of tumor vasculature. Tumor angiogenesis produces new blood vessels from existing vessels to supply nutrients and oxygen to tumor cells (Aguilar-Cazares et al., 2019). HT successfully inhibited inflammatory angiogenesis in phorbol myristate acetate (PMA) stimulated endothelial cells through inhibition of proinflammatory enzyme cyclooxygenase (COX)-2 and matrix degrading enzymes matrix metalloproteinases (MMPs) which are proinflammatory mediators in cancer and atherosclerosis (Fortes et al., 2012; Scoditti et al., 2012).

HT Enhances Re-endothelization

Re-endothelization is a prime event in IH repair. Delay in re-endothelization results in non-successful vascular interventions. Abate et al. reported that HT promote angiogenesis and wound healing in HUVECs cells via activating PI3K/AKT/mTOR pathways while upregulating the migration and adhesion-related protein expression (Abate et al., 2020). In another study, HT combined with pulsed electromagnetic field treatment, enhanced HUVECs migration and proliferation via regulation of Akt, mTOR, and TGF-β pathways (Cheng et al., 2017). Besides, two independent research by Zrelli et al. (2011b, 2015) demonstrates HT action of vascular healing through heme oxygenase-1 (HO-1) activation. High HO-1 expression protects cells from endothelial injury (Marcantoni et al., 2012; Kim et al., 2013). Additionally, they also reported that HT promotes vascular healing by stimulating the Nrf2 pathway which upregulates expression of HO-1 that is supported by PI3K, Akt, Erk ½. Lamy and colleagues, revealed that HT prevent endothelial apoptosis by suppressing ERK-1/2, SAPK and JNK pathways (Lamy et al., 2014).

HT Inhibit VMSCs Proliferation and Migration

Proliferation and migration of VMSCs are huge contributors to intimal thickening. Naturally, VSMCs exist in both contractile and synthetic phenotypes which are responsible to maintain vascular homeostasis (Michel et al., 2012; Basatemur et al., 2019). Endothelial injury tends to trigger generation of inflammatory factors such as platelet-derived growth factor (PDGF), fibroblast growth factor (FGF), and transforming growth factor-beta (TGFβ), which accelerate the migration of VMSCs into the intima layer (Lindqvist et al., 2001). HT promote VMSCs apoptosis via the production of NO and subsequent inactivation of Akt mediated by PP2A pathway in PDGF induced rat VMSCs (Zrelli et al., 2011a).

Regulation of VSMCs proliferation determines by MAPKs family members such as c-Jun N terminal kinase (JNK), extracellular signal-regulated kinase ½ (ERK), and p38 (Xu et al., 2018). MAPK chains also promote PDGF-stimulated VSMCs migration in the vascular injury model (Zhan et al., 2003). In a study by Liu et al., sulphur dioxide prevented VSMCs proliferation by inactivating Erk/MAP kinase pathway (Liu et al., 2014). Therefore, HT successfully inhibit bovine VMSCs proliferation in the same manner by disrupting the cell cycle regulated by ERK ½ (Abe et al., 2012).

On another hand, Matrix Metalloproteinases (MMP) are crucial extracellular matrix (ECM) components in maintaining vessel integrity and angiogenesis (Raffetto and Khalil, 2008). Amongst the different type of MMPs, MMP-2 were shown to enhanced VMSCs migration by disrupting the ECM in an *in vitro* model (Belo et al., 2015). Therefore, HT's ability to inhibit MMP-2 expression (Fortes et al., 2012) could therefore suppress VSMCs migration. Just as important, expression of MMP-9 that breaks the barrier between VSMCs and ECs were found to be downregulated by HT treatment (Nakbi et al., 2011; Scoditti et al., 2012; Scoditti et al., 2014). Phenotype switching of VSMCs from contractile to synthetic, marks the beginning of VSMCs remodeling (Wadey et al., 2018). In a past study, Resveratrol stimulate differentiation of VSMCs and inhibit migration by activating SIRT1 and AMPK (Thompson et al., 2014). In the same way, HT regulate the expression of SIRT1 in TNF-α stimulated vascular adventitia fibroblast (VAFs). HT and SIRT1 were shown to have good compatibility (Wang et al., 2018). These findings thus support HT ability in prevention of excessive vascular remodeling.

DISCUSSION

Ethnopharmacology has been an ever-growing field especially in the discovery of new compound in treatments of various diseases. Linking our ancestor knowledge in medicinal plants and giving it

TABLE 3 | Presentation of risk bias analysis.

Bias domain	Nakbi et l., 2011	Scoditti et., 2012	Lamy et al., 2014	Scoditti et al., 2014	Zrelli et al., 2011	Zrelli et al., 2013	Abe et al., 2012	Torul et., 2020	Fortes., 2012	Abate et al., 2020	Wang et al., 2017	Cheng et al., 2017	Kouka et al., 2017	Kitsati., 2016	Zrelli et al., 2015	Zrelli et al., 2011a	Zrelli et al., 2011b	Catalan et al., 2015	Vilas et al., 2017	Catalán et al., 2018	Yaoa et al., 2019	Terzuoli et al., 2019	Fuccelli et al., 2018
Definitely low risk of bias (‡‡)	‡‡	‡‡	‡‡	‡‡	‡‡	‡‡	‡‡	‡‡	‡‡	‡‡	‡‡	‡‡	‡‡	‡‡	‡‡	‡‡	‡‡	‡‡	‡‡	‡‡	‡‡	‡‡	‡‡
Probably low risk of bias (+)	+	+	‡‡	‡‡	+	‡‡	‡‡	‡‡	‡‡	+	‡‡	‡‡	‡‡	‡‡	‡‡	NR	‡‡	‡‡	‡‡	‡‡	‡‡	‡‡	‡‡
Probably high risk of bias (-/NR)	‡‡	‡‡	‡‡	‡‡	‡‡	‡‡	-	‡‡	‡‡	‡‡	‡‡	‡‡	‡‡	‡‡	‡‡	‡‡	‡‡	‡‡	‡‡	‡‡	‡‡	‡‡	‡‡
Definitely high risk of bias (-)	‡‡	‡‡	‡‡	‡‡	‡‡	‡‡	‡‡	‡‡	‡‡	‡‡	‡‡	‡‡	‡‡	‡‡	‡‡	‡‡	‡‡	‡‡	‡‡	‡‡	‡‡	‡‡	‡‡
Not applicable (N/A)	‡‡	‡‡	‡‡	‡‡	‡‡	‡‡	‡‡	‡‡	‡‡	‡‡	‡‡	‡‡	‡‡	‡‡	‡‡	‡‡	‡‡	‡‡	‡‡	‡‡	‡‡	‡‡	‡‡
Clear hypothesis/objectives	‡‡	‡‡	‡‡	‡‡	‡‡	‡‡	‡‡	‡‡	‡‡	‡‡	‡‡	‡‡	‡‡	‡‡	‡‡	‡‡	‡‡	‡‡	‡‡	‡‡	‡‡	‡‡	‡‡
Interventions clearly described	‡‡	‡‡	‡‡	‡‡	‡‡	‡‡	‡‡	‡‡	‡‡	‡‡	‡‡	‡‡	‡‡	‡‡	‡‡	‡‡	‡‡	‡‡	‡‡	‡‡	‡‡	‡‡	‡‡
Was administered dose or exposure level adequately randomized	N/A	N/A	N/A	N/A	N/A	N/A	N/A	N/A	N/A	N/A	N/A	N/A	N/A	N/A	N/A	N/A	N/A	N/A	N/A	‡‡	‡‡	N/A	‡‡
Was allocation to study groups adequately concealed	N/A	N/A	N/A	N/A	N/A	N/A	N/A	N/A	N/A	N/A	N/A	N/A	N/A	N/A	N/A	N/A	N/A	N/A	N/A	‡‡	‡‡	N/A	‡‡
Were experimental conditions identical across study groups	‡‡	‡‡	‡‡	‡‡	‡‡	‡‡	‡‡	‡‡	‡‡	‡‡	‡‡	‡‡	‡‡	‡‡	‡‡	‡‡	‡‡	‡‡	‡‡	‡‡	‡‡	‡‡	‡‡
Can we be confident in the exposure characterization	‡‡	‡‡	‡‡	‡‡	‡‡	‡‡	‡‡	‡‡	‡‡	‡‡	‡‡	‡‡	‡‡	‡‡	‡‡	‡‡	‡‡	‡‡	‡‡	‡‡	‡‡	‡‡	‡‡
Were the research personnel and human subjects blinded to the study group during the study	N/A	N/A	N/A	N/A	N/A	N/A	N/A	N/A	N/A	N/A	N/A	N/A	N/A	N/A	N/A	N/A	N/A	N/A	N/A	‡‡	‡‡	N/A	‡‡
Were outcome data complete without attrition or exclusion from analysis	‡‡	‡‡	‡‡	‡‡	‡‡	‡‡	‡‡	‡‡	‡‡	‡‡	‡‡	‡‡	‡‡	‡‡	‡‡	‡‡	‡‡	‡‡	‡‡	‡‡	‡‡	‡‡	‡‡
Can we be confident in the outcome assessment	‡‡	‡‡	‡‡	‡‡	‡‡	‡‡	-	‡‡	‡‡	‡‡	‡‡	‡‡	‡‡	‡‡	‡‡	‡‡	‡‡	‡‡	‡‡	‡‡	‡‡	‡‡	‡‡
Were all measured outcomes reported	‡‡	‡‡	‡‡	‡‡	‡‡	‡‡	‡‡	‡‡	‡‡	‡‡	‡‡	‡‡	‡‡	‡‡	‡‡	‡‡	‡‡	‡‡	‡‡	‡‡	‡‡	‡‡	‡‡
Were n , N and statistical methods appropriate	‡‡	‡‡	‡‡	‡‡	‡‡	‡‡	-	‡‡	‡‡	‡‡	‡‡	‡‡	‡‡	‡‡	‡‡	‡‡	‡‡	‡‡	‡‡	‡‡	‡‡	‡‡	‡‡
Do adverse event reported	+	+	‡‡	‡‡	+	‡‡	‡‡	‡‡	‡‡	+	‡‡	‡‡	‡‡	‡‡	‡‡	NR	‡‡	‡‡	‡‡	‡‡	‡‡	‡‡	‡‡

a scientific prove are both exciting and beneficial in future medical treatment. The association of plant derived antioxidants, specifically Hydroxytyrosol (HT) with lower risk factor and mortality in cardiovascular disease patients that consume olives products are well recognized. HT were found to exerted cardioprotective and anti-atherosclerotic effects in a randomized, double-blinded, placebo-controlled, crossover trial that were performed for 20 weeks (Quirós-Fernández et al., 2019). However, until now HT has not been investigated in attenuating intimal hyperplasia (IH) which if found beneficial could change the treatment of CVD patients significantly.

Therefore, we compile studies that utilize HT in vascular remodeling and critically review the mechanism that were elucidated. Endothelial functioning and healing are a crucial point in preventing further progression of IH, as endothelial injury triggers migration of SMCs. HT antioxidant property provides an oxidative stress defense friendly environment that prevents endothelial dysfunction and apoptosis. This is facilitated by the activation of AMPK-FOXO3 (Zrelli et al., 2011b). The molecular action of HT downregulates NFκB pathway which improves NO production. HT also promote cellular survival from ROS induction (Torul et al., 2020). These series of evidence, allow us to proposed HT that could promote reendothelization in the site of endothelial injury.

Migration of smooth muscle cell (SMCs) is the direct causal effect following EC disruption in IH. Overall, direct effect of HT on SMCs were inhibition of proliferation and migration. HT inhibited SMCs migration and proliferation via blocking cell cycle regulated by ERK1/2 phosphorylation (Abate et al., 2012). Zrelli proved that NO production and Akt dephosphorylation could prevent VSMCs proliferation. He also reported these events triggered by activation of PP2A that leads to cell apoptosis (Zrelli et al., 2011a). Correspondingly, HT directly effect MMP 9 and MMP 2 reduction which indirectly inhibits migration of SMCs (Nakbi et al., 2011; Scoditti et al., 2012; Fortes et al., 2012; Scoditti et al., 2014).

With regards to dosage, up to 160 μM, HT promotes endothelial proliferation and functioning endothelium. HT efficiently reduced SMCs proliferation at a dosage of 100 μM. These findings strongly support our theory for the use HT as treatment for intimal hyperplasia where with further research, a perfect dosage that enables HT enhance reendothelization while inhibits SMCs migration. Therefore, we hope this evidence compilation will encourage researchers to investigate the use of HT in *ex vivo* intimal hyperplasia organ culture models in future.

CONCLUSION

This systematic review collect evidences on molecular action of HT in the attenuation of IH in both *in vitro* and *in vivo* models. Supporting study on HT activity at the molecular level is presented in **Tables 1 and 2** and further simplified in **Figure 2**. These consolidated findings uncovered the underlying pathways influenced by HT in IH suppression. HT promotes reendothelization by activating cell regulation pathways including AMPK/FOXO3, PI3K/AKT/mTOR and supressing VSMCs migration by disrupting cell cycle via inactivation of ERK1/2 and AKT. These findings can be further be applied in the treatment of IH by delivery of HT in future translational studies.

DATA AVAILABILITY STATEMENT

The original contributions presented in the study are included in the article/Supplementary Material, further inquiries can be directed to the corresponding author.

AUTHOR CONTRIBUTIONS

NS, MY, RI, and MR designed the research topic and questions of the systematic review. UV, NS, MY, and RI designed the study. UV, NS, and MY performed article selection and screening. UV, and NS carried out data collection, extraction, manuscript writing and data analysis. MY, RI, and MR performed final proofread of the manuscript.

FUNDING

This research is fully funded under the Fundamental Research Grant Scheme (FRGS) FRGS/1/2019/SKK08/UKM/03/3 by the Ministry of Education Malaysia. The funder does not have any contribution and decision on publishing or preparation of the manuscript.

ACKNOWLEDGMENTS

All the authors would like to thank the Faculty of Medicine, UKM, for the resources use to complete this review.

REFERENCES

Abate, M., Pisanti, S., Caputo, M., Citro, M., Vecchione, C., and Martinelli, R. (2020). 3-Hydroxytyrosol Promotes Angiogenesis In Vitro by Stimulating Endothelial Cell Migration. *Int. J. Mol. Sci.* 21 (10), 3657. doi:10.3390/ijms21103657

Abe, R., Beckett, J., Abe, R., Nixon, A., Rochier, A., Yamashita, N., et al. (2012). Olive Oil Polyphenols Differentially Inhibit Smooth Muscle Cell Proliferation through a G1/S Cell Cycle Block Regulated by ERK1/2. *Int. J. Angiol.* 21 (2), 069–076. doi:10.1055/s-0032-1315630

Adawiyah Razali, R., Lokanathan, Y., Yazid, M. D., Ansari, A. S., Bin Saim, A., and Bt Hj Idrus, R. (2019). Modulation of Epithelial to Mesenchymal Transition Signaling Pathways by Olea Europaea and its Active Compounds. *Int. J. Mol. Sci.* 20 (14), 3492. doi:10.3390/ijms20143492

Aguilar-Cazares, D., Chavez-Dominguez, R., Carlos-Reyes, A., Lopez-Camarillo, C., Hernadez de la Cruz, O. N., and Lopez-Gonzalez, J. S. (2019). Contribution of Angiogenesis to Inflammation and *Cancer*. *Front. Oncol.* 9, 1399. doi:10.3389/fonc.2019.01399

Alfonso, F., and García-Guimaraes, M. (2017). Restenosis of Coronary Bioresorbable Vascular Scaffolds. *Revista Española de Cardiología (English Edition)* 70 (7), 527–531. doi:10.1016/j.rec.2017.02.024

Anderson, J. L., Halperin, J. L., Albert, N. M., Bozkurt, B., Brindis, R. G., Curtis, L. H., et al. (2013). Management of Patients with Peripheral Artery Disease (Compilation of 2005 and 2011 ACCF/AHA Guideline Recommendations). *Circulation* 127 (13), 1425–1443. doi:10.1161/cir.0b013e31828b82aa

Barnard, N. D., Goldman, D. M., Loomis, J. F., Kahleova, H., Levin, S. M., Neabore, S., et al. (2019). Plant-based Diets for Cardiovascular Safety and Performance in Endurance Sports. *Nutrients* 11 (1), 1–10. doi:10.3390/nu11010130

Basatemur, G. L., Jørgensen, H. F., Clarke, M. C. H., Bennett, M. R., and Mallat, Z. (2019). Vascular Smooth Muscle Cells in Atherosclerosis. *Nat. Rev. Cardiol.* 16 (12), 727–744. doi:10.1038/s41569-019-0227-9

Belo, V. A., Guimarães, D. A., and Castro, M. M. (2015). Matrix Metalloproteinase 2 as a Potential Mediator of Vascular Smooth Muscle Cell Migration and Chronic Vascular Remodeling in Hypertension. *J. Vasc. Res.* 52 (4), 221–231. doi:10.1159/000441621

Braun, D., Baquet, M., Massberg, S., Mehilli, J., and Hausleiter, J. (2016). Collapse of a Bioresorbable Novolimus-Eluting Coronary Scaffold. *JACC: Cardiovasc. Interventions* 9 (1), e13–e14. doi:10.1016/j.jcin.2015.10.019

Burja, B., Kuret, T., Janko, T., Topalović, D., Živković, L., Mrak-Poljšak, K., et al. (2019). Olive Leaf Extract Attenuates Inflammatory Activation and DNA Damage in Human Arterial Endothelial Cells. *Front. Cardiovasc. Med.* 6, 56. doi:10.3389/fcvm.2019.00056

Camenzind, E., Steg, P. G., and Wijns, W. (2007). Response to Camenzind et al: Commentary. *Circulation* 115 (11), 1455. doi:10.1161/circulationaha.106.666800

Catalán, Ú., López de las Hazas, M.-C., Piñol, C., Rubió, L., Motilva, M.-J., Fernandez-Castillejo, S., et al. (2018). Hydroxytyrosol and its Main Plasma Circulating Metabolites Attenuate the Initial Steps of Atherosclerosis through Inhibition of the MAPK Pathway. *J. Funct. Foods* 40, 280–291. doi:10.1016/j.jff.2017.11.007

Catalán, Ú., López de las Hazas, M.-C., Rubió, L., Fernández-Castillejo, S., Pedret, A., de la Torre, R., et al. (2015). Protective Effect of Hydroxytyrosol and its Predominant Plasmatic Human Metabolites against Endothelial Dysfunction in Human Aortic Endothelial Cells. *Mol. Nutr. Food Res.* 59 (12), 2523–2536. doi:10.1002/mnfr.201500361

Chen, D., Tao, X., Wang, Y., Tian, F., Wei, Y., Chen, G., et al. (2015). Curcumin Accelerates Reendothelialization and Ameliorates Intimal Hyperplasia in Balloon-Injured Rat Carotid Artery via the Upregulation of Endothelial Cell Autophagy. *Int. J. Mol. Med.* 36 (6), 1563–1571. doi:10.3892/ijmm.2015.2365

Cheng, Y., Qu, Z., Fu, X., Jiang, Q., and Fei, J. (2017). Hydroxytyrosol Contributes to Cell Proliferation and Inhibits Apoptosis in Pulsed Electromagnetic Fields Treated Human Umbilical Vein Endothelial Cells In Vitro. *Mol. Med. Rep.* 16 (6), 8826–8832. doi:10.3892/mmr.2017.7701

Chin, K. Y., and Pang, K. L. (2017). Therapeutic Effects of Olive and its Derivatives on Osteoarthritis: From Bench to Bedside. *Nutrients* 9 (10), 1–18. doi:10.3390/nu9101060

Costa, F., Vranckx, P., Leonardi, S., Moscarella, E., Ando, G., Calabro, P., et al. (2015). Impact of Clinical Presentation on Ischaemic and Bleeding Outcomes in Patients Receiving 6- or 24-month Duration of Dual-Antiplatelet Therapy after Stent Implantation: a Pre-specified Analysis from the PRODIGY (Prolonging Dual-Antiplatelet Treatment after Grading Stent-Induced Intimal Hyperplasia) Trial. *Eur. Heart J.* 36 (20), 1242–1251. doi:10.1093/eurheartj/ehv038

D'Angelo, C., Goldeck, D., Pawelec, G., Gaspari, L., Di Iorio, A., and Paganelli, R. (2020). Exploratory Study on Immune Phenotypes in Alzheimer's Disease and Vascular Dementia. *Eur. J. Neurol.* 27 (10), 1887–1894. doi:10.1111/ene.14360

Davies, M. G., and Hagen, P.-0. (1989). Pathobiology of Intimal Hyperplasia. *Br. J. Surg.*, 81(9), 1254–1269. doi:10.1002/bjs.1800810904

De Roos, B., Zhang, X., Rodriguez Gutierrez, G., Wood, S., Rucklidge, G. J., Reid, M. D., et al. (2011). Anti-platelet Effects of Olive Oil Extract: *In vitro* Functional and Proteomic Studies. *Eur. J. Nutr.* 50 (7), 553–562. doi:10.1007/s00394-010-0162-3

de Vries, M. R., and Quax, P. H. A. (2018). Inflammation in Vein Graft Disease. *Front. Cardiovasc. Med.* 5, 1–13. doi:10.3389/fcvm.2018.00003

Fortes, C., García-Vilas, J. A., Quesada, A. R., and Medina, M. Á. (2012). Evaluation of the Anti-angiogenic Potential of Hydroxytyrosol and Tyrosol, Two Bio-Active Phenolic Compounds of Extra Virgin Olive Oil, in Endothelial Cell Cultures. *Food Chem.* 134 (1), 134–140. doi:10.1016/j.foodchem.2012.02.079

Fuccelli, R., Fabiani, R., and Rosignoli, P. (2018). Hydroxytyrosol exerts anti-inflammatory and anti-oxidant activities in a mouse model of systemic inflammation. *Molecules* 23 (12). doi:10.3390/molecules23123212

García-Vilas, J. A., Quesada, A. R., and Medina, M. Á. (2017). Hydroxytyrosol Targets Extracellular Matrix Remodeling by Endothelial Cells and Inhibits Both Ex Vivo and In Vivo Angiogenesis. *Food Chem.* 221, 1741–1746. doi:10.1016/j.foodchem.2016.10.111

Garg, U. C., and Hassid, A. (1989). Nitric Oxide-Generating Vasodilators and 8-Bromo-Cyclic Guanosine Monophosphate Inhibit Mitogenesis and Proliferation of Cultured Rat Vascular Smooth Muscle Cells. *J. Clin. Invest.* 83 (5), 1774–1777. doi:10.1172/jci114081

Gellman, J., Ezekowitz, M. D., Sarembock, I. J., Azrin, M. A., Nochomowitz, L. E., Lerner, E., et al. (1991). Effect of Lovastatin on Intimal Hyperplasia after Balloon Angioplasty: A Study in an Atherosclerotic Hypercholesterolemic Rabbit. *J. Am. Coll. Cardiol.* 17 (1), 251–259. doi:10.1016/0735-1097(91)90735-r

Gonzalo, N., Gonzalo, N., and Macaya, C. (2012). Absorbable Stent: Focus on Clinical Applications and Benefits. *Vhrm* 8 (1), 125–132. doi:10.2147/vhrm.s22551

Granados-Principal, S., Quiles, J. L., Ramirez-Tortosa, C. L., Sanchez-Rovira, P., and Ramirez-Tortosa, M. C. (2010). Hydroxytyrosol: From Laboratory Investigations to Future Clinical Trials. *Nutr. Rev.* 68 (4), 191–206. doi:10.1111/j.1753-4887.2010.00278.x

Greer, E. L., Oskoui, P. R., Banko, M. R., Maniar, J. M., Gygi, M. P., Gygi, S. P., et al. (2007). The Energy Sensor AMP-Activated Protein Kinase Directly Regulates the Mammalian FOXO3 Transcription Factor. *J. Biol. Chem.* 282 (41), 30107–30119. doi:10.1074/jbc.m705325200

Guasch-ferré, M., Merino, J., Sun, Q., Fitó, M., Salas-salvadó, J., Fern, D., et al. (2019). Supplementation in a Physically Active Population . *Sports Med. - Open* 20 (1), 1–17. doi:10.3390/ijms20184567

Hamilos, M., Petousis, S., and Parthenakis, F. (2018). Interaction between Platelets and Endothelium: From Pathophysiology to New Therapeutic Options. *Cardiovasc. Diagn. Ther.* 8 (5), 568–580. doi:10.21037/cdt.2018.07.01

Hernáez, Á., Castañer, O., Elosua, R., Pintó, X., Estruch, R., Salas-Salvadó, J., et al. (2017). Mediterranean Diet Improves High-Density Lipoprotein Function in High-Cardiovascular-Risk Individuals. *Circulation* 135 (7), 633–643. doi:10.1161/circulationaha.116.023712

Hillis, L. D., Smith, P. K., Anderson, J. L., Bittl, J. A., Bridges, C. R., Byrne, J. G., et al. (2012). 2011 ACCF/AHA guideline for coronary artery bypass graft surgery: executive summary: a report of the American College of Cardiology Foundation/American Heart Association Task Force on Practice Guidelines. *J. Thorac. Cardiovasc. Surg.* 143 (1), 4–34. doi:10.1016/j.jtcvs.2011.10.015

Hou, X., Song, J., Li, X.-N., Zhang, L., Wang, X., Chen, L., et al. (2010). Metformin Reduces Intracellular Reactive Oxygen Species Levels by Upregulating Expression of the Antioxidant Thioredoxin via the AMPK-FOXO3 Pathway. *Biochem. Biophysical Res. Commun.* 396 (2), 199–205. doi:10.1016/j.bbrc.2010.04.017

Huang, B., Dreyer, T., Heidt, M., Yu, J. C. M., Philipp, M., Hehrlein, F. W., et al. (2002). Insulin and Local Growth Factor PDGF Induce Intimal Hyperplasia in Bypass Graft Culture Models of Saphenous Vein and Internal Mammary Artery. *Eur. J. Cardio-Thoracic Surg.* 21 (6), 1002–1008. doi:10.1016/s1010-7940(02)00111-2

Jennette, J. C., and Stone, J. R. (2014). "Diseases of Medium-Sized and Small Vessels," in Cellular and Molecular Pathobiology of Cardiovascular Disease, 197–219. doi:10.1016/B978-0-12-405206-2.00011-9

Jinnouchi, H., Torii, S., Sakamoto, A., Kolodgie, F. D., Virmani, R., and Finn, A. V. (2019). Fully Bioresorbable Vascular Scaffolds: Lessons Learned and Future Directions. *Nat. Rev. Cardiol.* 16 (5), 286–304. doi:10.1038/s41569-018-0124-7

Joner, M., Nakazawa, G., Finn, A. V., Quee, S. C., Coleman, L., and Acampado, E. (2018). Endothelial cell recovery between comparator polymer-based drug-eluting stents. *J. Am. Coll. Cardiol.* 52 (5), 333–342. doi:10.1016/j.jacc.2008.04.030

Kamann, S., Haase, T., Stolzenburg, N., Löchel, M., Peters, D., and Schnorr, J. (2019). Resveratrol- Coated Balloon Catheters in Porcine Coronary and Peripheral Arteries. *Int. J. Mol. Sci.* 20 (9), 2285. doi:10.3390/ijms20092285

Kamil, K., Yazid, M. D., Idrus, R. B. H., and Kumar, J. (2020). Hydroxytyrosol Promotes Proliferation of Human Schwann Cells: An In Vitro Study. *Int. J. Environ. Res. Public Health* 17 (12), 1–11. doi:10.3390/ijerph17124404

Karaarslan, K., Abud, B., Albayrak, G., Aykut, K., Ergür, B. U., and Silistreli, E. (2015). The Effect of Resveratrol on Intimal Hyperplasia and Endothelial Proliferation of Rabbit Carotid Artery Anastomosis. *Interactive Cardiovasc. Thorac. Surg.* 20 (1), 15–20. doi:10.1093/icvts/ivu316

Khandelwal, A. R., Hebert, V. Y., Kleinedler, J. J., Rogers, L. K., Ullevig, S. L., Asmis, R., et al. (2012). Resveratrol and Quercetin Interact to Inhibit Neointimal Hyperplasia in Mice with a Carotid Injury. *J. Nutr.* 142 (8), 1487–1494. doi:10.3945/jn.112.162628

Kim, H., Caulfield, L. E., Garcia-Larsen, V., Steffen, L. M., Coresh, J., and Rebholz, C. M. (2019). Plant-Based Diets Are Associated with a Lower Risk of Incident Cardiovascular Disease, Cardiovascular Disease Mortality, and All-Cause Mortality in a General Population of Middle- Aged Adults. *J. Am. Heart Assoc.* 8 (16), e012865. doi:10.1161/jaha.119.012865

Kim, N., Hwangbo, C., Lee, S., and Lee, J.-H. (2013). Eupatolide Inhibits PDGF-Induced Proliferation and Migration of Aortic Smooth Muscle Cells through ROS-dependent Heme Oxygenase-1 Induction. *Phytother. Res.* 27 (11), 1700–1707. doi:10.1002/ptr.4924

Kitsati, N., Mantzaris, M. D., and Galaris, D. (2016). Hydroxytyrosol Inhibits Hydrogen Peroxide-Induced Apoptotic Signaling via Labile Iron Chelation. *Redox Biol.* 10 , 233–242. doi:10.1016/j.redox.2016.10.006

Koniari, I., Mavrilas, D., Apostolakis, E., Papadimitriou, E., Papadaki, H., Papalois, A., et al. (2016). Inhibition of Atherosclerosis Progression, Intimal Hyperplasia, and Oxidative Stress by Simvastatin and Ivabradine May Reduce Thoracic Aorta's Stiffness in Hypercholesterolemic Rabbits. *J. Cardiovasc. Pharmacol. Ther.* 21 (4), 412–422. doi:10.1177/1074248415617289

Kotronoulas, A., Pizarro, N., Serra, A., Robledo, P., Joglar, J., Rubió, L., et al. (2013). Dose-dependent Metabolic Disposition of Hydroxytyrosol and Formation of Mercapturates in Rats. *Pharmacol. Res.* 77, 47–56. doi:10.1016/j.phrs.2013.09.001

Kouka, P., Priftis, A., Stagos, D., Angelis, A., Stathopoulos, P., Xinos, N., et al. (2017). Assessment of the Antioxidant Activity of an Olive Oil Total Polyphenolic Fraction and Hydroxytyrosol from a Greek Olea Europea Variety in Endothelial Cells and Myoblasts. *Int. J. Mol. Med.* 40 (3), 703–712. doi:10.3892/ijmm.2017.3078

Lamy, S., Ouanouki, A., Béliveau, R., and Desrosiers, R. R. (2014). Olive Oil Compounds Inhibit Vascular Endothelial Growth Factor Receptor-2 Phosphorylation. *Exp. Cel Res.* 322 (1), 89–98. doi:10.1016/j.yexcr.2013.11.022

Lee, D. H., and Hernandez, J. M. d. la. T. (2018). The Newest Generation of Drug-Eluting Stents and beyond. *Eur. Cardiol. Rev.* 13 (1), 54–59. doi:10.15420/ecr.2018:8:2

Li, Q., Wu, X., Liu, Y., Zhang, M., Bai, X., and Chen, C. (2017). The Effect of Anagliptin on Intimal Hyperplasia of Rat Carotid Artery after Balloon Injury. *Mol. Med. Rep.* 16 (6), 8003–8010. doi:10.3892/mmr.2017.7667

Li, X. N., Song, J., Zhang, L., LeMaire, S. A., Hou, X., Zhang, C., et al. (2009). Activation of the AMPK-FOXO3 Pathway Reduces Fatty Acid-Induced Increase in Intracellular Reactive Oxygen Species by Upregulating Thioredoxin. *Diabetes* 58 (10), 2246–2257. doi:10.2337/db08-1512

Lindqvist, A., Nilsson, B. O., Ekblad, E., and Hellstrand, P. (2001). Platelet-derived Growth Factor Receptors Expressed in Response to Injury of Differentiated Vascular Smooth Muscle In Vitro: Effects on Ca2+ and Growth Signals. *Acta Physiol. Scand.* 173 (2), 175–184. doi:10.1046/j.1365-201x.2001.00873.x

Liu, D., Huang, Y., Bu, D., Liu, A. D., Holmberg, L., Jia, Y., et al. (2014). Sulfur Dioxide Inhibits Vascular Smooth Muscle Cell Proliferation via Suppressing the Erk/MAP Kinase Pathway Mediated by cAMP/PKA Signaling. *Cel Death Dis.* 5. doi:10.1038/cddis.2014.229

Loscalzo, J., and Jin, R. C. (2010). Vascular Nitric Oxide: Formation and Function. *J. Blood Med.* 2010 (1), 147–162. doi:10.2147/JBM.S7000

Luo, Q., Liu, X., Li, Z., Huang, C., Zhang, W., Meng, J., et al. (2014). Degradation Model of Bioabsorbable Cardiovascular Stents. *PLoS ONE* 9 (11), 1–9. doi:10.1371/journal.pone.0110278

Man, R. C., Sulaiman, N., Ishak, M. F., Idrus, R. B. H., Rahman, M. R. A., and Yazid, M. D. (2020). The Effects of Pro-inflammatory and Anti-inflammatory Agents for the Suppression of Intimal Hyperplasia: An Evidence-Based Review. *Int. J. Environ. Res. Public Health* 17 (21), 1–22. doi:10.3390/ijerph17217825

Marcantoni, E., Di Francesco, L., Dovizio, M., Bruno, A., and Patrignani, P. (2012). Novel Insights into the Vasoprotective Role of Heme Oxygenase-1. *Int. J. Hypertens.* 2012, 127910. doi:10.1155/2012/127910

Martinon, F. (2010). Signaling by ROS Drives Inflammasome Activation. *Eur. J. Immunol.* 40 (3), 616–619. doi:10.1002/eji.200940168

Michel, J. B., Li, Z., and Lacolley, P. (2012). Smooth Muscle Cells and Vascular Diseases. *Cardiovasc. Res.* 95 (2), 135–137. doi:10.1093/cvr/cvs172

Mylonaki, I., Allain, E., Strano, F., Allémann, E., Corpataux, J. M., Meda, P., et al. (2018). Evaluating Intimal Hyperplasia under Clinical Conditions. *Interactive Cardiovasc. Thorac. Surg.* 27 (3), 427–436. doi:10.1093/icvts/ivy101

Nakbi, A., Dabbou, S., Champion, S., Fouchier, F., Mehri, S., Attia, N., et al. (2011). Modulation of the Superoxide Anion Production and MMP-9 Expression in PMA Stimulated THP-1 Cells by Olive Oil Minor Components: Tyrosol and Hydroxytyrosol. *Food Res. Int.* 44 (2), 575–581. doi:10.1016/j.foodres.2010.12.010

Napolitano, A., De Lucia, M., Panzella, L., and d'Ischia, M. (2010). "The Chemistry of Tyrosol and Hydroxytyrosol: Implications for Oxidative Stress," in Olives and Olive Oil in Health and Disease Prevention, 1225–1232. doi:10.1016/B978-0-12-374420-3.00134-0

Nedeljkovic, Z. S., Gokce, N., and Loscalzo, J. (2003). Mechanisms of Oxidative Stress and Vascular Dysfunction. *Postgrad. Med. J.* 79 (930), 195–200. doi:10.1136/pmj.79.930.195

Nemzer, B. V., Yashin, A. Y., Vedenin, A. N., Yashin, Y. I., Yashunsky, D. V., Nifantiev, N. E., et al. (2019). Selected Powerful Natural Antioxidants: Structure, Food Sources, Antioxidant Activities, and Important Health Benefits. *J. Food Res.* 8 (1), 60. doi:10.5539/jfr.v8n1p60

Ng, S. F., Tan, L. S., and Buang, F. (2017). Transdermal Anti-inflammatory Activity of Bilayer Film Containing Olive Compound Hydroxytyrosol: Physical Assessment, In Vivo Dermal Safety and Efficacy Study in Freund's Adjuvant-Induced Arthritic Rat Model. *Drug Dev. Ind. Pharm.* 43 (1), 108–119. doi:10.1080/03639045.2016.1224893

Norton, K. A., and Popel, A. S. (2016). Effects of Endothelial Cell Proliferation and Migration Rates in a Computational Model of Sprouting Angiogenesis. *Scientific Rep.* 6, 1–10. doi:10.1038/srep36992

Olmos, Y., Valle, I., Borniquel, S., Tierrez, A., Soria, E., Lamas, S., et al. (2009). Mutual Dependence of Foxo3a and PGC-1α in the Induction of Oxidative Stress Genes. *J. Biol. Chem.* 284 (21), 14476–14484. doi:10.1074/jbc.m807397200

Pamukcu, B., Lip, G. Y. H., and Shantsila, E. (2011). The Nuclear Factor - Kappa B Pathway in Atherosclerosis: A Potential Therapeutic Target for Atherothrombotic Vascular Disease. *Thromb. Res.* 128 (2), 117–123. doi:10.1016/j.thromres.2011.03.025

Pi, Y., Zhang, L. L., Li, B. H., Guo, L., Cao, X. J., Gao, C. Y., et al. (2013). Inhibition of Reactive Oxygen Species Generation Attenuates TLR4-Mediated Proinflammatory and Proliferative Phenotype of Vascular Smooth Muscle Cells. *Lab. Invest.* 93 (8), 880–887. doi:10.1038/labinvest.2013.79

Pober, J. S., and Sessa, W. C. (2007). Evolving Functions of Endothelial Cells in Inflammation. *Nat. Rev. Immunol.* 7 (10), 803–815. doi:10.1038/nri2171

Quirós-Fernández, R., López-Plaza, B., Bermejo, L. M., Palma-Milla, S., and Gómez-Candela, C. (2019). Supplementation with Hydroxytyrosol and Punicalagin Improves Early Atherosclerosis Markers Involved in the Asymptomatic Phase of Atherosclerosis in the Adult Population: A Randomized, Placebo-Controlled, Crossover Trial. *Nutrients* 11 (3), 1–16. doi:10.3390/nu11030640

Raffetto, J. D., and Khalil, R. A. (2008). Matrix Metalloproteinases and Their Inhibitors in Vascular Remodeling and Vascular Disease. *Biochem. Pharmacol.* 75 (2), 347–359. doi:10.1016/j.bcp.2007.07.004

Regazzoli, D., Leone, P. P., Colombo, A., and Latib, A. (2017). New Generation Bioresorbable Scaffold Technologies: An Update on Novel Devices and Clinical Results. *J. Thorac. Dis.* 9 (Suppl. 9), S979–S985. doi:10.21037/jtd.2017.07.104

Reglero-Real, N., Colom, B., Bodkin, J. V., and Nourshargh, S. (2016). Endothelial Cell Junctional Adhesion Molecules. *Arteriosclerosis, Thromb. Vasc. Biol.* 36 (10), 2048–2057. doi:10.1161/atvbaha.116.307610

Rodríguez-Morató, J., Boronat, A., Kotronoulas, A., Pujadas, M., Pastor, A., Olesti, E., et al. (2016). Metabolic Disposition and Biological Significance of Simple Phenols of Dietary Origin: Hydroxytyrosol and Tyrosol. *Drug Metab. Rev.* 48 (2), 218–236. doi:10.1080/03602532.2016.1179754

Romagnolo, D. F., and Selmin, O. I. (2017). Mediterranean Diet and Prevention of Chronic Diseases. *Nutr. Today* 52 (5), 208–222. doi:10.1097/nt.0000000000000228

Rubió, L., Farràs, M., de La Torre, R., Macià, A., Romero, M. P., Valls, R. M., et al. (2014). Metabolite Profiling of Olive Oil and Thyme Phenols after a Sustained Intake of Two Phenol-Enriched Olive Oils by Humans: Identification of Compliance Markers. *Food Res. Int.* 65 59–68. doi:10.1016/j.foodres.2014.05.009

Sandoo, A., Veldhuijzen van Zanten, J. J. C. ., Metsios, G. S., Carroll, D., and Kitas, G. D. (2010). The Endothelium and its Role in Regulating Vascular Tone. *Open Cardiovasc. Med. J.* 4 (1), 302–312. doi:10.2174/1874192401004010302

Scoditti, E., Calabriso, N., Massaro, M., Pellegrino, M., Storelli, C., Martines, G., et al. (2012). Mediterranean Diet Polyphenols Reduce Inflammatory Angiogenesis through MMP-9 and COX-2 Inhibition in Human Vascular Endothelial Cells: A Potentially Protective Mechanism in Atherosclerotic Vascular Disease and Cancer. *Arch. Biochem. Biophys.* 527 (2), 81–89. doi:10.1016/j.abb.2012.05.003

Scoditti, E., Nestola, A., Massaro, M., Calabriso, N., Storelli, C., De Caterina, R., et al. (2014). Hydroxytyrosol Suppresses MMP-9 and COX-2 Activity and Expression in Activated Human Monocytes via PKCα and PKCβ1 Inhibition. *Atherosclerosis* 232 (1), 17–24. doi:10.1016/j.atherosclerosis.2013.10.017

Soler-Cantero, A., Jové, M., Cacabelos, D., Boada, J., Naudí, A., Romero, M. P., et al. (2012). Plant-Derived Phenolics Inhibit the Accrual of Structurally Characterised Protein and Lipid Oxidative Modifications. *PLoS ONE* 7 (8), e43308. doi:10.1371/journal.pone.0043308

Stettler, C., Wandel, S., Allemann, S., Kastrati, A., Morice, M. C., Schömig, A., et al. (2007). Outcomes Associated with Drug-Eluting and Bare-Metal Stents: a Collaborative Network Meta- Analysis. *Lancet* 370 (9591), 937–948. doi:10.1016/s0140-6736(07)61444-5

Stone, G. W., Moses, J. W., Ellis, S. G., Schofer, J., Dawkins, K. D., Morice, M.-C., et al. (2007). Safety and Efficacy of Sirolimus- and Paclitaxel-Eluting Coronary Stents. *New Engl. J. Med.* 356 (10), 998–1008. doi:10.1056/nejmoa067193

Storniolo, C. E., Sacanella, I., Mitjavila, M. T., Lamuela-Raventos, R. M., and Moreno, J. J. (2019). Bioactive Compounds of Cooked Tomato Sauce Modulate Oxidative Stress and Arachidonic Acid Cascade Induced by Oxidized LDL in Macrophage Cultures. *Nutrients* 11 (8), 1880. doi:10.3390/nu11081880

Sun, L., Zhao, R., Zhang, L., Zhang, T., Xin, W., Lan, X., et al. (2012). Salvianolic acid A inhibits PDGF-BB induced vascular smooth muscle cell migration and proliferation while does not constrain endothelial cell proliferation and nitric oxide biosynthesis. *Molecules.* 17 (3), 3333–3347.

Tagliafierro, L., Officioso, A., Sorbo, S., Basile, A., and Manna, C. (2015). The Protective Role of Olive Oil Hydroxytyrosol against Oxidative Alterations Induced by Mercury in Human Erythrocytes. *Food Chem. Toxicol.* 82, 59–63. doi:10.1016/j.fct.2015.04.029

Tejada, S., Pinya, S., Mar Bibiloni, M. del., Tur, J. A., Pons, A., and Sureda, A. (2016). Cardioprotective Effects of the Polyphenol Hydroxytyrosol from Olive Oil. *Curr. Drug Targets* 18 (13), 1477–1486. doi:10.2174/1389450117666161005150650

Terzuoli, E., Nannelli, G., Giachetti, A., Morbidelli, L., Ziche, M., and Donnini, S. (2020). Targeting endothelial-to-mesenchymal transition: the protective role of hydroxytyrosol sulfate metabolite. *Eur. J. Nutrit.* 59. doi:10.1007/s00394-019-01920-x

Thompson, A. M., Martin, K. A., and Rzucidlo, E. M. (2014). Resveratrol Induces Vascular Smooth Muscle Cell Differentiation through Stimulation of SirT1 and AMPK. *PLoS ONE* 9 (1), 1–10. doi:10.1371/journal.pone.0085495

Tolva, V., Mazzola, S., Zerbi, P., Casana, R., Albertini, M., Calvillo, L., et al. (2016). A Successful Experimental Model for Intimal Hyperplasia Prevention Using a Resveratrol- Delivering Balloon. *J. Vasc. Surg.* 63 (3), 788–794. doi:10.1016/j.jvs.2014.09.035

Torul, H., Küçükboyaci, N., Tamer, U., and Karasu, Ç. (2020). Evaluation of Phenolic Compounds and Protective Effects of Olive (Olea Europaea L.) Leaf Extracts on Endothelial Cells against Hydrogen Peroxide-Induced Toxicity. *J. Res. Pharm.* 24 (4), 497–507. doi:10.35333/jrp.2020.198

Tousoulis, D., Kampoli, A.-M., Tentolouris Nikolaos Papageorgiou, C., and Stefanadis, C. (2011). The Role of Nitric Oxide on Endothelial Function. *Curr. Vasc. Pharmacol.* 10 (1), 4–18. doi:10.2174/157016112798829760

Tuso, P., Stoll, S. R., and William, W. Li. (2015). "A Plant-Based Diet, Atherogenesis, and Coronary Artery Disease Prevention," in *Ethnicity*, 19, 62–67. doi:10.7812/TPP/14-0361

Urban, P., Mehran, R., Colleran, R., Angiolillo, D. J., Byrne, R. A., Capodanno, D., et al. (2019). Defining High Bleeding Risk in Patients Undergoing Percutaneous Coronary Intervention. *Circulation* 140 (3), 240–261. doi:10.1161/circulationaha.119.040167

Vilaplana-Pérez, C., Auñón, D., García-Flores, L. A., and Gil-Izquierdo, A. (2014). Hydroxytyrosol and Potential Uses in Cardiovascular Diseases, *Cancer*, and AIDS. *Front. Nutr.* 1, 1–11. doi:10.3389/fnut.2014.00018

Wadey, K., Lopes, J., Bendeck, M., and George, S. (2018). Role of Smooth Muscle Cells in Coronary Artery Bypass Grafting Failure. *Cardiovasc. Res.* 114 (4), 601–610. doi:10.1093/cvr/cvy021

Wang, W., Jing, T., Yang, X., He, Y., Wang, B., Xiao, Y., et al. (2018). Hydroxytyrosol Regulates the Autophagy of Vascular Adventitial Fibroblasts through the SIRT1-Mediated Signaling Pathway. *Can. J. Physiol. Pharmacol.* 96, 88–96. doi:10.1139/cjpp-2016-0676

Wei, X., Fang, Z., Sheng, J., Wang, Y., and Lu, P. (2020). Honokiol-mesoporous Silica Nanoparticles Inhibit Vascular Restenosis via the Suppression of TGF-β Signaling Pathway. *Int. J. Nanomedicine* 15, 5239–5252. doi:10.2147/ijn.s250911

Widmer, R. J., Flammer, A. J., Lerman, L. O., and Lerman, A. (2015). The Mediterranean diet, its components, and cardiovascular disease. *Am. J. Med.* 128 (3), 229–238. doi:10.1016/j.amjmed.2014.10.014

Xu, K., Al-Ani, M. K., Pan, X., Chi, Q., Dong, N., and Qiu, X. (2018). Plant-derived Products for Treatment of Vascular Intima Hyperplasia Selectively Inhibit Vascular Smooth Muscle Cell Functions. *Evidence-Based Complement. Altern. Med.* 2018, 3549312. doi:10.1155/2018/3549312

Yang, X., Li, Y., Li, Y., Ren, X., Zhang, X., Hu, D., et al. (2017). Oxidative Stress-Mediated Atherosclerosis: Mechanisms and Therapies. *Front. Physiol.* 8, 1–16. doi:10.3389/fphys.2017.00600

Yao, F., Yang, G., Xian, Y., Wang, G., Zheng, Z., Jin, Z., et al. (2019). The Protective Effect of Hydroxytyrosol Acetate against Inflammation of Vascular Endothelial Cells Partly through the SIRT6-Mediated PKM2 Signaling Pathway. *Food Funct.* 10 (9), 5789–5803. doi:10.1039/c9fo00586b

Yurdagul, A., Kleinedler, J. J., McInnis, M. C., Khandelwal, A. R., Spence, A. L., Orr, A. W., et al. (2014). Resveratrol Promotes Endothelial Cell Wound Healing under Laminar Shear Stress through an Estrogen Receptor-α-dependent Pathway. *Am. J. Physiol. - Heart Circulatory Physiol.* 306 (6), 797–806. doi:10.1152/ajpheart.00892.2013

Zhan, Y., Kim, S., Izumi, Y., Izumiya, Y., Nakao, T., Miyazaki, H., et al. (2003). Role of JNK, P38, and ERK in Platelet-Derived Growth Factor-Induced Vascular Proliferation, Migration, and Gene Expression. *Arteriosclerosis, Thromb. Vasc. Biol.* 23 (5), 795–801. doi:10.1161/01.ATV.0000066132.32063.F2

Zhao, Y., Vanhoutte, P. M., and Leung, S. W. S. (2015). Vascular Nitric Oxide: Beyond eNOS. *J. Pharmacol. Sci.* 129 (2), 83–94. doi:10.1016/j.jphs.2015.09.002

Zrelli, H., Kusunoki, M., and Miyazaki, H. (2015). Role of Hydroxytyrosol-dependent Regulation of HO-1 Expression in Promoting Wound Healing of Vascular Endothelial Cells via Nrf2 De Novo Synthesis and Stabilization. *Phytotherapy Res.* 29 (7), 1011–1018. doi:10.1002/ptr.5339

Zrelli, H., Matsuka, M., Araki, M., Zarrouk, M., and Miyazaki, H. (2011a). Hydroxytyrosol Induces Vascular Smooth Muscle Cells Apoptosis through No Production and PP2A Activation with Subsequent Inactivation of Akt. *Planta Med.* 77 (15), 1680–1686. doi:10.1055/s-0030-1271073

Zrelli, H., Matsuoka, M., Kitazaki, S., Zarrouk, M., and Miyazaki, H. (2011b). Hydroxytyrosol Reduces Intracellular Reactive Oxygen Species Levels in Vascular Endothelial Cells by Upregulating Catalase Expression through the AMPK-FOXO3a Pathway. *Eur. J. Pharmacol.* 660 (2–3), 275–282. doi:10.1016/j.ejphar.2011.03.045

Zrelli, H., Wei Wu, C., Zghonda, N., Shimizu, H., and Miyazaki, H. (2013). Combined Treatment of Hydroxytyrosol with Carbon Monoxide-Releasing Molecule-2 Prevents TNF α -induced Vascular Endothelial Cell Dysfunction through No Production with Subsequent NF B Inactivation. *Biomed. Res. Int.* 2013, 912431. doi:10.1155/2013/912431

Conflict of Interest: The authors declare that the research was conducted in the absence of any commercial or financial relationships that could be construed as a potential conflict of interest.

frontiers in Pharmacology

ORIGINAL RESEARCH
published: 10 June 2021
doi: 10.3389/fphar.2021.646121

Repeated Aconitine Treatment Induced the Remodeling of Mitochondrial Function *via* AMPK–OPA1–ATP5A1 Pathway

Li-Zhen Qiu[1,2†], *Wei Zhou*[2†], *Lan-Xin Yue*[2], *Yi-Hao Wang*[2], *Fei-Ran Hao*[2], *Peng-Yan Li*[3] *and Yue Gao*[1,2*]

[1]State Key Laboratory of Component-based Chinese Medicine, Tianjin University of Traditional Chinese Medicine, Tianjin, China, [2]Department of Pharmaceutical Sciences, Beijing Institute of Radiation Medicine, Beijing, China, [3]The Fifth Medical Center, General Hospital of PLA, Beijing, China

OPEN ACCESS

Edited by:
Yue Liu,
Xiyuan Hospital, China

Reviewed by:
Zhong-qiu Liu,
Guangzhou University of Chinese Medicine, China
Jinfan Tian,
Capital Medical University, China

***Correspondence:**
Yue Gao
gaoyue@bmi.ac.cn

[†]These authors have contributed equally to this work

Specialty section:
This article was submitted to Ethnopharmacology, a section of the journal Frontiers in Pharmacology

Received: 25 December 2020
Accepted: 08 March 2021
Published: 10 June 2021

Citation:
Qiu L-Z, Zhou W, Yue L-X, Wang Y-H, Hao F-R, Li P-Y and Gao Y (2021) Repeated Aconitine Treatment Induced the Remodeling of Mitochondrial Function via AMPK–OPA1–ATP5A1 Pathway. Front. Pharmacol. 12:646121. doi: 10.3389/fphar.2021.646121

Aconitine is attracting increasing attention for its unique positive inotropic effect on the cardiovascular system, but underlying molecular mechanisms are still not fully understood. The cardiotonic effect always requires abundant energy supplement, which is mainly related to mitochondrial function. And OPA1 has been documented to play a critical role in mitochondrial morphology and energy metabolism in cardiomyocytes. Hence, this study was designed to investigate the potential role of OPA1-mediated regulation of energy metabolism in the positive inotropic effect caused by repeated aconitine treatment and the possible mechanism involved. Our results showed that repeated treatment with low-doses (0–10 μM) of aconitine for 7 days did not induce detectable cytotoxicity and enhanced myocardial contraction in Neonatal Rat Ventricular Myocytes (NRVMs). Also, we first identified that no more than 5 μM of aconitine triggered an obvious perturbation of mitochondrial homeostasis in cardiomyocytes by accelerating mitochondrial fusion, biogenesis, and Parkin-mediated mitophagy, followed by the increase in mitochondrial function and the cellular ATP content, both of which were identified to be related to the upregulation of ATP synthase α-subunit (ATP5A1). Besides, with compound C (CC), an inhibitor of AMPK, could reverse aconitine-increased the content of phosphor-AMPK, OPA1, and ATP5A1, and the following mitochondrial function. In conclusion, this study first demonstrated that repeated aconitine treatment could cause the remodeling of mitochondrial function *via* the AMPK–OPA1–ATP5A1 pathway and provide a possible explanation for the energy metabolism associated with cardiotonic effect induced by medicinal plants containing aconitine.

Keywords: aconitine, mitochondrial homeostasis, mitochondrial fusion, OPA1, ATP5A1

Abbreviations: AMPK, AMP-activated protein kinase; ATP5A1, ATP synthase α-subunit; CC, compound C; DA, dopamine; NRVMs, neonatal rat ventricular myocytes; OPA1, optic atrophy 1.

INTRODUCTION

Aconitine is one of the main bioactive ingredients in *Aconitum L.* Apart from the toxicity, this aconite alkaloid is attracting ever-growing attention for its potential pharmacological effects on the cardiovascular system, such as anti-shock, anti-inflammatory, and myocardial protection effects induced at low doses (Xie and Peng, 2017). Notably, since the inotropic effects of aconitine were detected in the isolated muscles, some scholars had focused on the potential cardiotonic effect of low-dose aconitine. For instance, 0.01 mg/kg of acontine has been identified to significantly improve the cardiac function of rats by enhancing left ventricular systolic pressure and left ventricular end-diastolic pressure. Recent studies also found that low doses of aconitine could generate obvious cardiotonic effect in heart failure (Zhang and Wu 2001; Wen et al., 2012; Wang et al., 2019; Liu et al., 2020), especially combining with acupuncture treatment. Hence, Chan et al. and many Chinese experts on aconite shared a viewpoint that aconitine could generate a positive inotropic effect possibly by increasing the intracellular sodium content during the action potential (Chan, 2009), providing a novel pharmaceutical use of this compound.

The maintenance of the positive inotropic effect featuring enhanced cardiac contractility with high frequency always requires coordinated energy supply in cardiomyocytes. However, how to guarantee proper regulation of energy metabolism that fits for cardiotonic effects induced by aconitine in cardiac myocytes remains to be explored. As the major sites of energy synthesis in the heart, mitochondria are double-membraned subcellular organelles that consist of outer membranes, inner membranes, and soluble matrix surrounded by the inner membrane (Marin-Garcia and Akhmedov, 2016). The inner mitochondrial membrane folds inwardly to form highly organized invaginations known as cristae, which are studded with various protein complexes, such as respiratory chain supercomplexes, and participate in the generation of ATP (Upadhyay and Agarwal, 2020). Our latest work has shown that low dose of aconitine could improve the energy metabolism disorder by reducing CypD-mediated mPTP, resulting in the restoration of angiotensin II–induced myocardial mitochondrial dysfunction (Wang et al., 2021). Thus, a synchronized supply of ATP and/or energy metabolism in elevated contracted cardiomyocytes could be ascribed to aconitine-induced alterations in mitochondrial function.

Structurally, mitochondria are being dynamic homeostasis (mitochondrial turnover), that is, the principal regulator of mitochondrial morphology and function and is largely facilitated by mitochondrial fission, mitochondrial fusion, and mitophagy (Fuhrmann and Brune, 2017; Fu et al., 2019). Generally, mitochondrial biogenesis and fusion both optimize mitochondrial function and counteract the increasing demand of energy (Panchal and Tiwari, 2019). In recent, benzoylaconine, the main metabolite of aconitine, has been demonstrated to enhance the mitochondrial mass *via* promoting mitochondrial biogenesis, suggesting that aconitine might increase myocardial ATP content by exerting a crucial impact on mitochondrial turnover. However, the underlying mechanism is not fully elucidated, nor does the effect of aconitine on mitochondrial fusion.

OPA1, a dynamin-like 120 kDa protein that could promote the formation and modification of crista, mainly participates in the regulation of mitochondrial fusion and following ATP production (Baker et al., 2014). Besides, AMP-activated protein kinase (AMPK), acting as a key regulator of mitochondrial function and energy metabolism, has been found to improve mitochondrial quality control through increasing OPA1 expression in the myocardium (Zhang et al., 2019; Xin et al., 2020), implying that the potential role of AMPK/OPA1 signaling in mitochondrial fusion. But so far, there is no direct evidence of AMPK/OPA1 signaling-mediated mitochondrial fusion present in acontine-induced positive inotropic effect on the myocardium.

Hence, we hypothesized that repeated administration of low doses of aconitine could generate a positive inotropic effect on ventricular cardiomyocytes through AMPK/OPA1-mediated remodeling of mitochondrial function. Also, this study was designed to verify the hypothesis and explored the possible mechanism involved.

MATERIALS AND METHODS

Study Animals

Neonatal Wistar rats (1 day) were purchased from SPF Laboratories (Beijing, China, Beijing Vital River, certificate No. SCXK 2016–0011). All animal experiments were approved by the Ethics Committee of the Beijing Institute of Radiation Medicine (Approval No. IACUC-DWZX-2020–771).

Primary Neonatal Rat Ventricular Myocyte Culture

NRVMs were obtained from neonatal Wistar rat pups *via* serial enzymatic digestion. In brief, after cervical dislocation and disinfection, the heart tissues were immediately isolated and placed into the ice-cold phosphate buffer solution (PBS) (Gibco, Thermo Fisher Scientific, Waltham, MA, United States). After rinsing 4 times, the ventricular tissues were cut into less than 1 mm^3 tissue block and digested in trypsin (0.0625%, Sigma-Aldrich, St. Louis, MO, United States) for 5 min at room temperature (RT), followed by 5 min collagenase II (1 mg/ml, Solarbio, Beijing, China) enzymolysis at 37°C. Then the supernatant fluid was filtered using a sterile 70 μm cell strainer and transferred into a centrifuge tube containing Dulbecco's modified Eagle medium (DMEM) (Gibco) supplemented with 15% fetal bovine serum (FBS) (Gibco) and 1% penicillin/streptomycin (Hyclone, Logan, UT, United States). After further purification by eliminating fibroblasts, NRVMs were replanted into the 100 mm dishes (2×10^6 cells/ml), combining with 5-BrdU to inhibit cardiac fibroblast growth for 48 h. 0.1 mM 5-BrdU (Sigma-Aldrich), and cultured in a humidified atmosphere at 37°C and 5% CO_2.

Drug Treatment and CCK-8 Assay

NRVMs were repeatedly treated with aconitine (purity ≥98%, ManSiTe, Chengdu, China) at a series of diluted concentrations

(0, 2.5, 5, 10, 20, 40, and 80 μM, respectively) or dopamine (DA, 50 μM, Solarbio) for 7 days, and the drug was refreshed every 24 h. At the end of treatment, cell viability was detected by the Cell Counting Kit-8 assay (CCK-8, Dojindo, Tokyo, Japan) according to the manufacturer's instruction. In brief, NRVMs were washed twice and cultured with DMEM medium containing 10% CCK-8 reagent for another 2 h, and then the absorbance was detected using a microplate reader at 450 nm (Multiskan MK3, Thermo Fisher Scientific). The cell viabilities were presented as the percentages of that of the control group.

Quantification of Mitochondrial Superoxide

Mitochondrial superoxide was determined using the MitoSOX Red indicator (M36008, Thermo Fisher Scientific). NRVMs were seeded into a black 96-well plate (clear bottom with lid) and repeatedly exposed to aconitine (0, 2.5, 5, 10, 20, 40, and 80 μM, respectively) or DA (50 μM) for 7 days. After treatment, cells were washed with PBS buffer and then incubated with 5 μM MitoSOX Red for 10 min at 37°C. Next, fluorescence intensities of each group were detected with a multilabel microplate reader (Victor X5, PerkinElmer, Waltham, MA, United States), and results were presented as mean ± SD.

Western Blotting

Western blotting was performed according to the previous description, and treated NRVMs were harvested and immediately lysed using a Minute™ Total Protein Extraction Kit (SD-001, Invent, Beijing, China) supplemented with protease/phosphatase inhibitor cocktail (P1265/P1260, Applygen, Beijing, China), according to the manufacturer's instruction. The supernatants of total proteins were collected, and the concentrations were quantified *via* a BCA assay kit (P1510, Applygen). The denatured proteins were separated by SDS-PAGE gels and electrotransferred onto polyvinylidene fluoride (PVDF) membranes (Millipore, Billerica, MA, United States). After overnight blocking in 5% nonfat milk at 4°C, the membranes were incubated orderly with primary antibodies and corresponding secondary antibodies (detailed information for all indicated antibodies was listed in **Supplementary Table S1**). After rinsing three times with TBST, the protein blots were visualized with a chemiluminescence ECL Western blot system (Millipore) and an automatic exposure system (Image Quant LAS500, GE, Fairfield, CT, United States). The grayscale values of the bands were determined by ImageJ software; GAPDH or ß-actin were used as loading controls for total proteins.

Transmission Electron Microscopy

At the end of treatment, NRVMs were harvested and were fixed in 100 mM phosphate buffer (PB) (pH = 7.2) containing 2% formaldehyde and 2.5% glutaraldehyde overnight at 4°C. Then, the samples were washed three times with 0.1 M PBS and postfixed using 1% osmium tetroxide for 4 h at RT, followed by dehydration in a series of ascending concentrations of ethanol solutions (50, 70, 80, and 100%). Subsequently, cells were subject to propylene oxide and embedded in epoxy resin. Afterward, the blocks were sliced into ultrathin sections, which were then double-stained with 2% uranyl acetate and 5% lead citrate and finally observed using a transmission electron microscope (H-7650, HITACHI, Japan). The area and the number of mitochondria were analyzed by ImageJ software.

Confocal Microscopy and Quantification of Mitochondrial Fusion

NRVMs suspensions (1×10^5 cells/ml) were seeded in confocal dishes and exposed to aconitine (0 or 5 μM) with or without CC co-treatment for 7 days. At the end of treatment, cells were incubated with DMEM containing 200 nM MitoTracker Red CMXRos probe (M7512, Thermo Fisher Scientific) for 30 min at 37°C. After two rinses with PBS, cells were fixed with 4% formaldehyde for 10 min and blocked with blocking buffer (P0102, Beyotime, Beijing, China) for 1 h at RT. Next, the nuclei were counterstained with 4′,6-diamidino-2-phenylindole (5 μg/ml, DAPI, Sigma-Aldrich) for 7 min at RT. After 5 min wash (×3), the cells were visualized using a laser scanning confocal microscope (LSM 880, Carl Zeiss, Jena, Germany).

The obtained confocal images were subjected to the quantitative analysis of mitochondrial morphology using ImageJ software. In brief, the type of images was first converted into an 8-bit grayscale form. Next, the images' background noise removal was carried out at a threshold value which might distinguish individual mitochondrial fragments in a single cell. Then the photographs were converted into binary images; the number of noncontiguous mitochondrial fragments and the area of these mitochondria were calculated by ImageJ's particle counting subroutine. For each image, the number of mitochondria was normalized by the mitochondrial area and then × 1000 to gain the mitochondrial fragmentation index (MFI), which was proved as a verified index for mitochondrial fragmentation. For each group, 8–25 randomly selected cells were used to calculate the MFI values.

Seahorse XF96 Respirometry

To assess the effects of aconitine on mitochondrial function, the oxygen consumption rate (OCR) and extracellular acidification rate (ECAR) were both analyzed using a Seahorse XF96 extracellular flux analyzer (Seahorse Bioscience, Agilent, TX, United States). Briefly, NRVMs (20,000 cells *per* well) were seeded in XFe96 cell culture microplates (101085-004, Agilent) and repeatedly treated with aconitine (5 μM) for 7 days, with or without CC co-treatment. Before assay, the cells were equilibrated in fresh XF DMEM base medium (103575-100, Agilent) containing 25 mM glucose (103577-100, Agilent), 1 mM sodium pyruvate (103578-100, Agilent), and 2 mM L-glutamine (103579-100, Agilent) for 1 h at 37°C without CO_2. For the Mito Stress test, 2 μM oligomycin A (oligo), 2 μM carbonyl cyanide-p-trifluoromethoxy-phenylhydrazone (FCCP), and 0.5 μM rotenone/antimycin A (A/R) were sequentially injected into each well to perform consecutive OCR measurements. For ATP rate assay, only 2 μM oligo and 0.5 μM A/R were added successively to obtain ECAR value. OCR and ECAR data were used to assess mitochondrial respiratory capacity and ATP production rate according to the manufacturing instructions of Seahorse XF Mito Stress Test Kit (103015-100, Agilent) or the XF Real-Time ATP Rate Assay Kit (103592-100, Agilent), respectively. Finally, cell

counting post the XF metabolic assay was performed using an array of Scan High-Content System (Thermo Fisher Scientific, Waltham, MA, United States) *via* DAPI staining. Mitochondrial respiratory capacity and the ATP production rate were normalized to total cell numbers and showed as pmol/min/10,000 cells.

Blue Native Polyacrylamide Gel Electrophoresis (BN-PAGE)

Mitochondria were firstly isolated from aconitine (5 μM) treated NRVMs using a Mitochondria Isolation Kit (C1260, Applygen) according to the manufacturer's instructions. Briefly, 5×10^7 cells were harvested and resuspended in an ice-cold mito solution, followed by 40 gentle up-and-down grindings in a glass homogenizer. The cellular homogenate was transferred into a 1.5 ml tube, and mitochondria were isolated by gradient centrifugation as reported before (Zhou et al., 2013). Immediately, mitochondrial membrane proteins were homogenized in solubilization buffer before adding 6 μl 20% digitonin and centrifuged at 100,000 g for 15 min. Furthermore, 5 μl of 50% glycerol and 3 μl of 5% Coomassie blue G-250 were added into the supernatants to prevent protein aggregation in the sample gel. Subsequently, purified mitochondrial proteins were separated in 3.5 sample gel and gradient separation gel (4% acrylamide and 13% acrylamide mixture) at 100 V at 4°C. Once the dye marker migrated to the edge of separating gel, electrophoresis was performed with the current less than 15 mA and the voltage less than 500 V. When the blue running front approached 1/3 of the total running distance, the dark blue cathode buffer B was removed, and the electrophoresis was successively run using 10% cathode buffer B. At the end of electrophoresis, the gel was fixed in the solution (50% ddH_2O, 40% methanol, and 10% acetic acid) for 30 min and washed 15 min (× 4), followed by Coomassie staining overnight. The stained gel was scanned and visualized by an automatic exposure system (ImageQuant LAS500).

LC-MS/MS-Based Proteomics Analysis

Two separate LC-MS/MS-based proteomics analyses were performed in control and 5 μM aconitine-treated groups. In brief, the mitochondrial protein extracts were dissolved in lysis buffer, and the concentrations were determined by Bradford assay. Then lyophilized proteins from the two groups were redissolved in the solution (50 μl) containing equal ratios of urea (8 M) and DTT (20 mM) and incubated in a water bath for 4 h at 37°C. An equal volume of IAA (100 mM) was added to each group and then incubated for 1 h in dark. Next, NH_4HCO_3 (50 mM) buffer was added to the samples until the concentration of urea became 1 M. Subsequently, trypsin was added at a 1:50 mass ratio of trypsin: protein and digested at 37°C overnight. Finally, the digested peptides were freeze-dried and redissolved with 0.1% formic acid. The prepared sample was analyzed by a Q Exactive HF spectrometer (Thermo Fisher Scientific) coupled online with a nanoflow liquid chromatography system (Easy-nLC 1200, Thermo Fisher Scientific). All data were acquired using Xcalibur software (Thermo Fisher Scientific). After LC-MS/MS analysis, protein identification was performed by searching against UniProt databases using Mascot software (Matrix Science, London, United Kingdom).

Statistical Analysis

All data were expressed as mean ± SD. And the statistical comparisons between groups were analyzed by one-way ANOVA followed by LSD post hoc pair-wise comparisons test. $p < 0.05$ was considered statistically significant.

RESULTS

Repeated Low Dose of Aconitine Treatment Induced Undetectable Cytotoxicity on NRVMs and Promoted Myocardial Contraction

To examine whether cumulative aconitine administration could cause cytotoxicity on cardiomyocytes, we repeatedly treated purified NRVMs with 0–80 μM aconitine (**Figures 1A,B**) for 7 days. Furthermore, DA (50 μM) was used as a positive control drug (Begieneman et al., 2016). Intriguingly, we found that repeated aconitine (0, 5, and 80 μM) and DA treatment for 7 days did not affect the morphology of the NRVMs (**Figure 1C**). Similarly, 0–10 μM of aconitine and DA did not exert any impact on cell viability and generated no significant enhancement in oxidative stress status (**Figures 1D,E**). During treatment, we observed that aconitine (5 μM) and DA could notably increase the beating rate of cardiomyocytes (**Figure 1F**), accompanying with less beat amplitude (shown in **Supplementary Videos S1, S2**). Meanwhile, we also found that aconitine (20–80 μM) did not induce significant alterations in the morphology of NRVMs, but obvious dysrhythmia, lower contractility, and even beating stop were detected in these groups. To evaluate how cardiomyocytes afford energy supply under the process of aconitine-induced cardiotonic effect, we chose to mainly explore the efficacy of aconitine and underlying mechanisms at a no-toxic-effect dose level (less than 10 μM).

Aconitine Prompted Mitochondrial Turnover in NRVMs at a Certain Dose Range

Mitochondria are highly dynamic organelles; thus, the balance of mitochondrial homeostasis plays a critical role in their function. First, we performed TEM analysis and found that aconitine enhanced the formation of autophagosomes, mitophagy, and obvious lysosomes in neonatal cardiomyocytes (**Figure 2A**). Furthermore, as shown in **Figures 2B,C**, we found that more than 5 μM of aconitine could downregulate the expression of p-mTOR while upregulating mTOR protein levels, resulting in a decrease in the ratio of p-mTOR/mTOR. Meanwhile, the expression levels of beclin1, LC3 lipidation (LC3A was converted to LC3B), and LAMP1 were significantly increased, together with the enhanced content of p62 protein, implying remarkable macroautophagy and the block of autophagic flux caused by repeated treatment with more than 5 μM of aconitine in NRVMs. Also, the proteins participating in mitophagy and biogenesis, such as Parkin, Tom20, and PGC-1α were significantly increased in a dose-dependent manner after aconitine treatment (**Figures 2D,E**). Aconitine-induced PINK1 and fusion-related proteins (OPA1 and Mfn2) peaked at 5 or

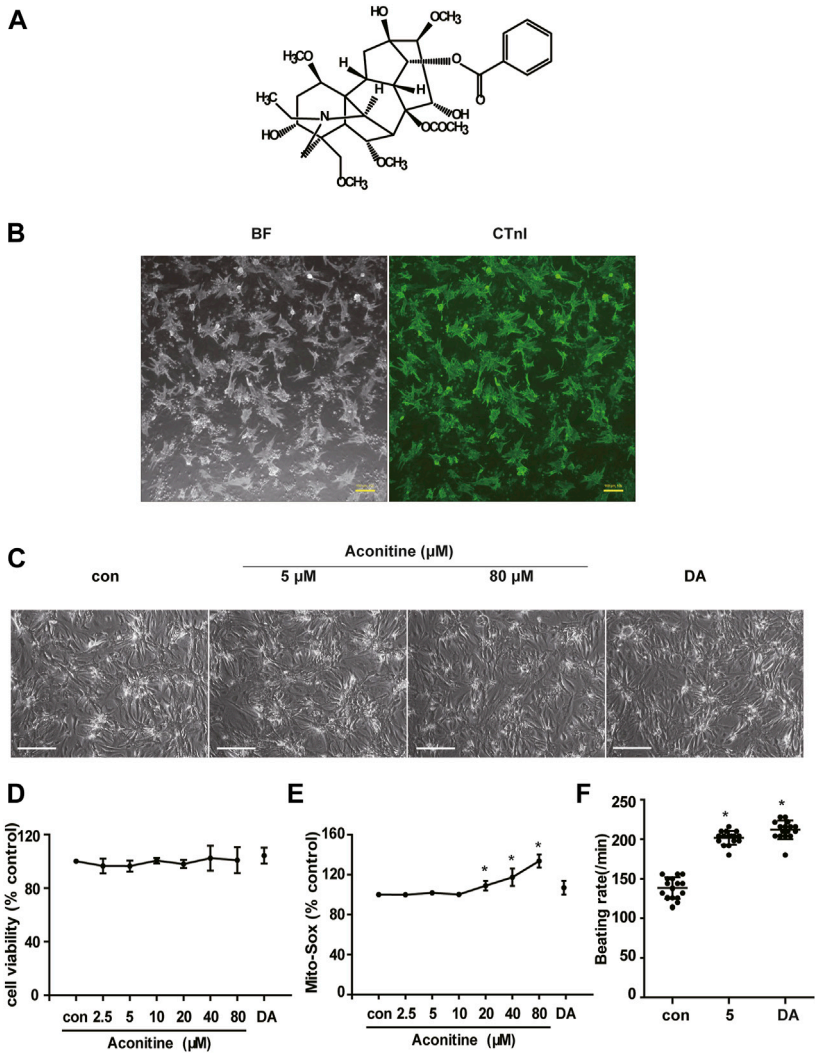

FIGURE 1 | Cytotoxicity of repeated low dose of aconitine on NRVMs. **(A)** Structure formula of aconitine. **(B)** The identification and purity of NRVMs. BF represents the bright field, and the green indicates the fluorescence of CTnI. Scale bars: 100 μm. **(C)** Morphology of NRVMs after treated with different concentrations of aconitine (0, 5, and 80 μM) and DA (50 μM). Scale bars: 200 μm. **(D,E)** The cell viability and mitochondrial superoxide level of NRVMs treated with aconitine or DA for repeated 7 days (n = 3). **(F)** Effects of treatment with aconitine (5 μM) and DA (50 μM) for 7 days on the beating rates of NRVMs (n = 16). ****p < 0.05 vs. control.

10 μM and began to reduce with increased dosage (**Figures 2D,E**). However, repeated doses of aconitine decreased the expression of mitochondrial fission-related proteins (p-Drp1 and p-MFF, **Figures 2D,E**). Altogether, our data suggested that aconitine might promote mito-turnover through mitophagy, mitochondrial fusion, and biogenesis at low levels (less than 10 μM).

Effect of Repeated Aconitine Treatment on the Mitochondrial Fusion in NRVMs

To characterize whether the morphology of mitochondria was altered by repeated 7-day low dose of aconitine (5 μM) exposure, we carried out a TEM assay and presented notable changes in mitochondrial morphologic features that mitochondria exhibited enlarged size and decreased number but no significant abnormal structure in the treated myocytes (**Figure 3A**). And we found that aconitine treatment resulted in an increment (from 0.3022 to 0.5090) in the mitochondrial area compared with that in the control group, which was concerned with a decrease in the number of mitochondrial areas (from 0.5232 to 0.3375) (**Figure 3B**). To further verify this finding, we next quantified the noncontinuous (fragment) mitochondria and calculated the MFI in aconitine-treated NRVMs using immunofluorescence. Also, mitochondria became bigger and the mitochondrial density diminished in the treated NRVMs (**Figure 3C**). Besides, we found that aconitine administration significantly decreased the MFI compared with that of the control group (**Figure 3D**), suggesting that aconitine treatment indeed caused mitochondrial fusion in NRVMs. Consistently, aconitine treatment indeed increased the expressions of Mfn2 and OPA1 but did not exert impact on the content of COX IV (**Figures 3E,F**). Notably, we found that

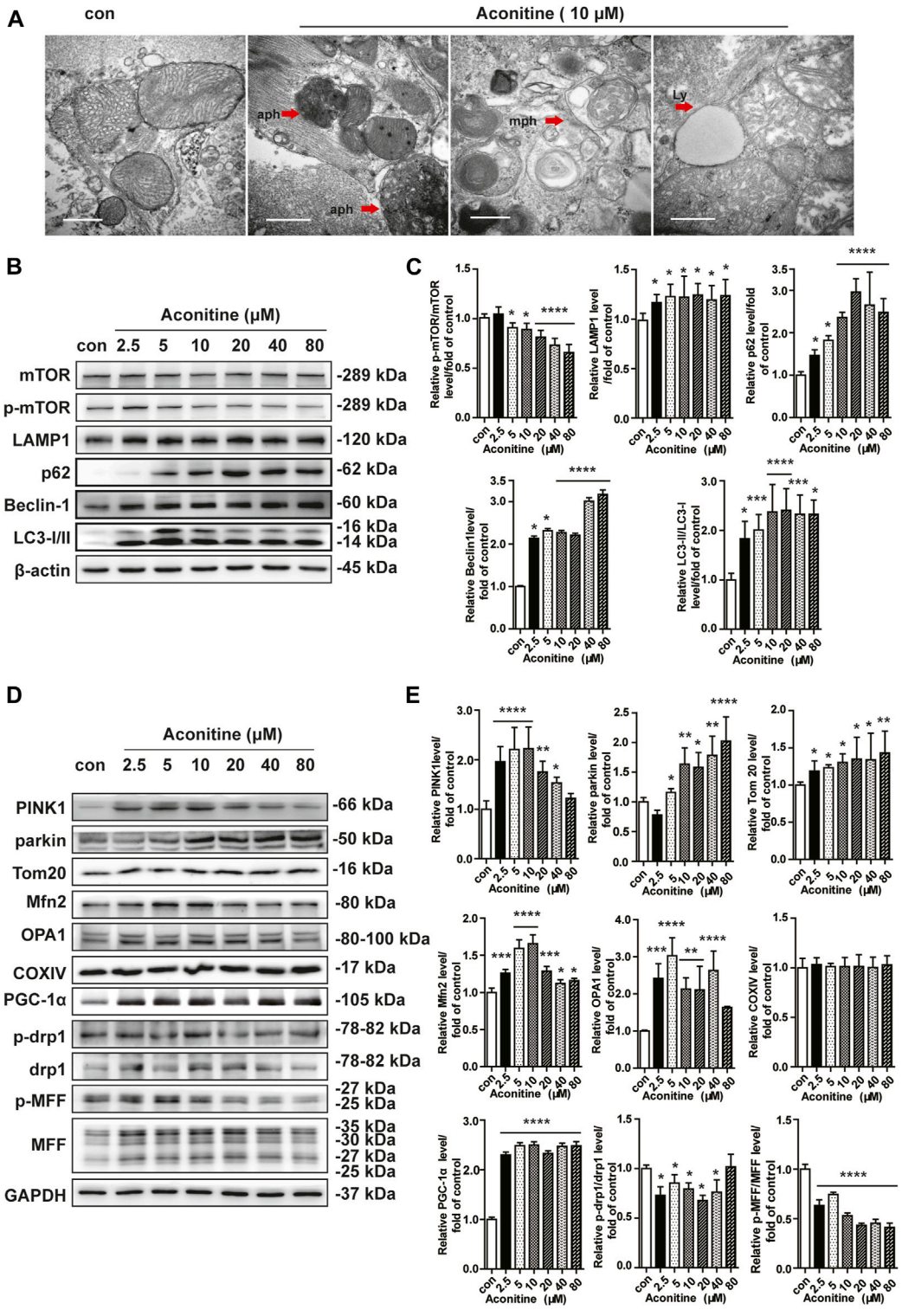

FIGURE 2 | Enhanced mito-turnover in NRVMs induced by repeated treatment with aconitine. **(A)** Representative transmission electron microscopy (TEM) micrographs of NRVMs treated with aconitine (0 and 10 μM). Autophagosomes (aph), mitophagosomes (mph), and lysosome (ly). Scale bars: 1 μm. **(B–E)** Western blot and quantitative analysis of mito-turnover–related proteins. Band intensity was normalized to ß-actin or GAPDH, and presented as fold change relative to control ($n = 3$), $^{*}p < 0.05$, $^{**}p < 0.01$, $^{***}p < 0.001$, $^{****}p < 0.0001$ vs. control.

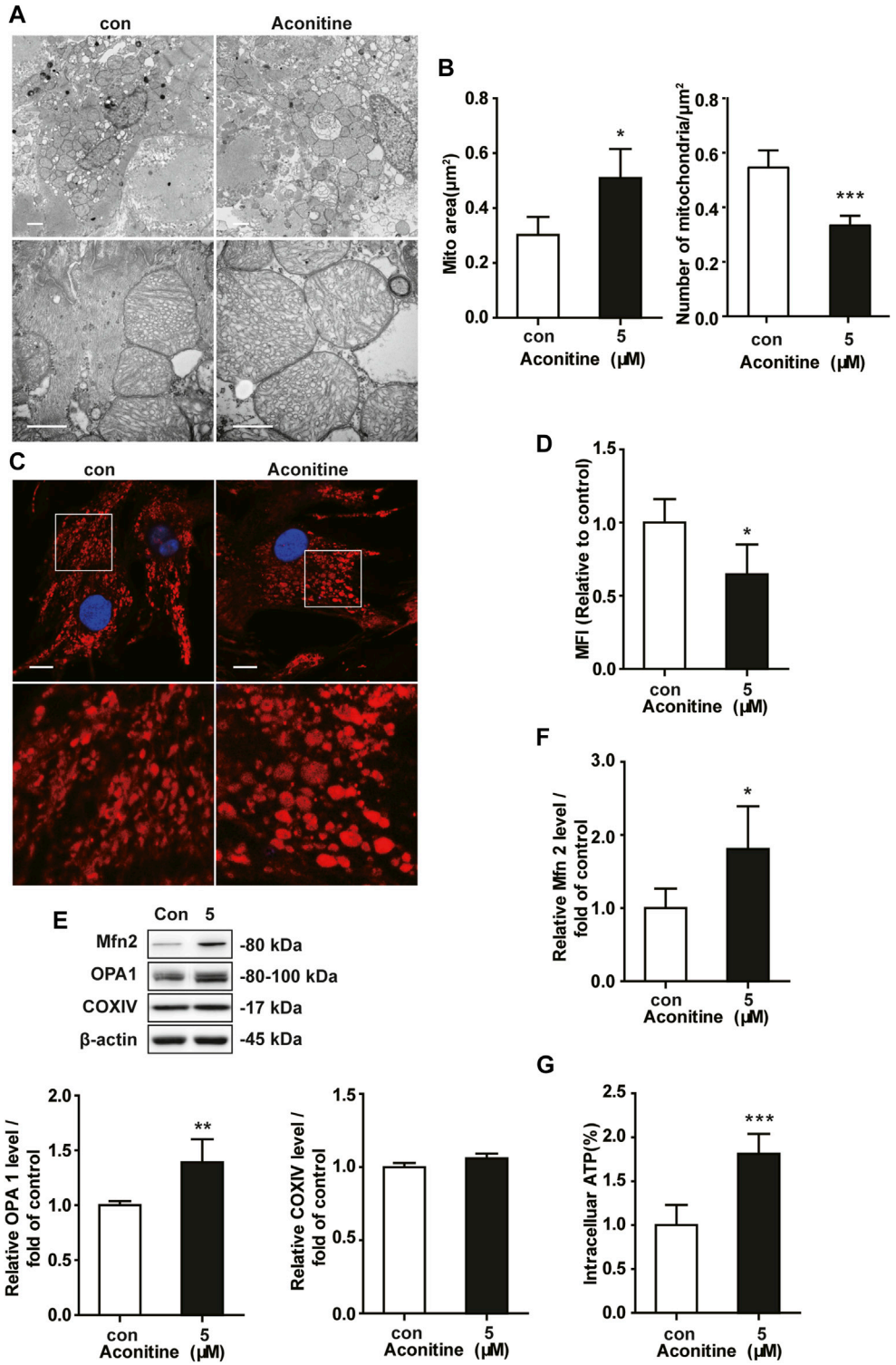

FIGURE 3 | Increment of mitochondrial fusion induced by repeated low dose of aconitine treatment. **(A)** Representative TEM images of NRVMs treated with aconitine (0 and 5 μM). Scale bars: 1 μm. **(B)** The mean values of mitochondrial area (μm^2) and the number of mitochondria per μm^2 ($n = 3$, 100 mitochondria per group) in the two groups. **(C)** Representative confocal images of mitochondrial morphology in control or 5 μM groups. Scale bars: 10 μm. **(D)** Quantification of mitochondrial fragmentation using mitochondrial fragmentation index (MFI) ($n = 20$). **(E, F)** Western blot analysis of the expression of indicated proteins in NRVMs. All data were normalized to ß-actin and expressed as fold-change over control ($n = 3$). **(G)** The levels of intracellular ATP ($n = 5$). $^{*}p < 0.05$, $^{**}p < 0.01$, $^{***}p < 0.001$ vs. control.

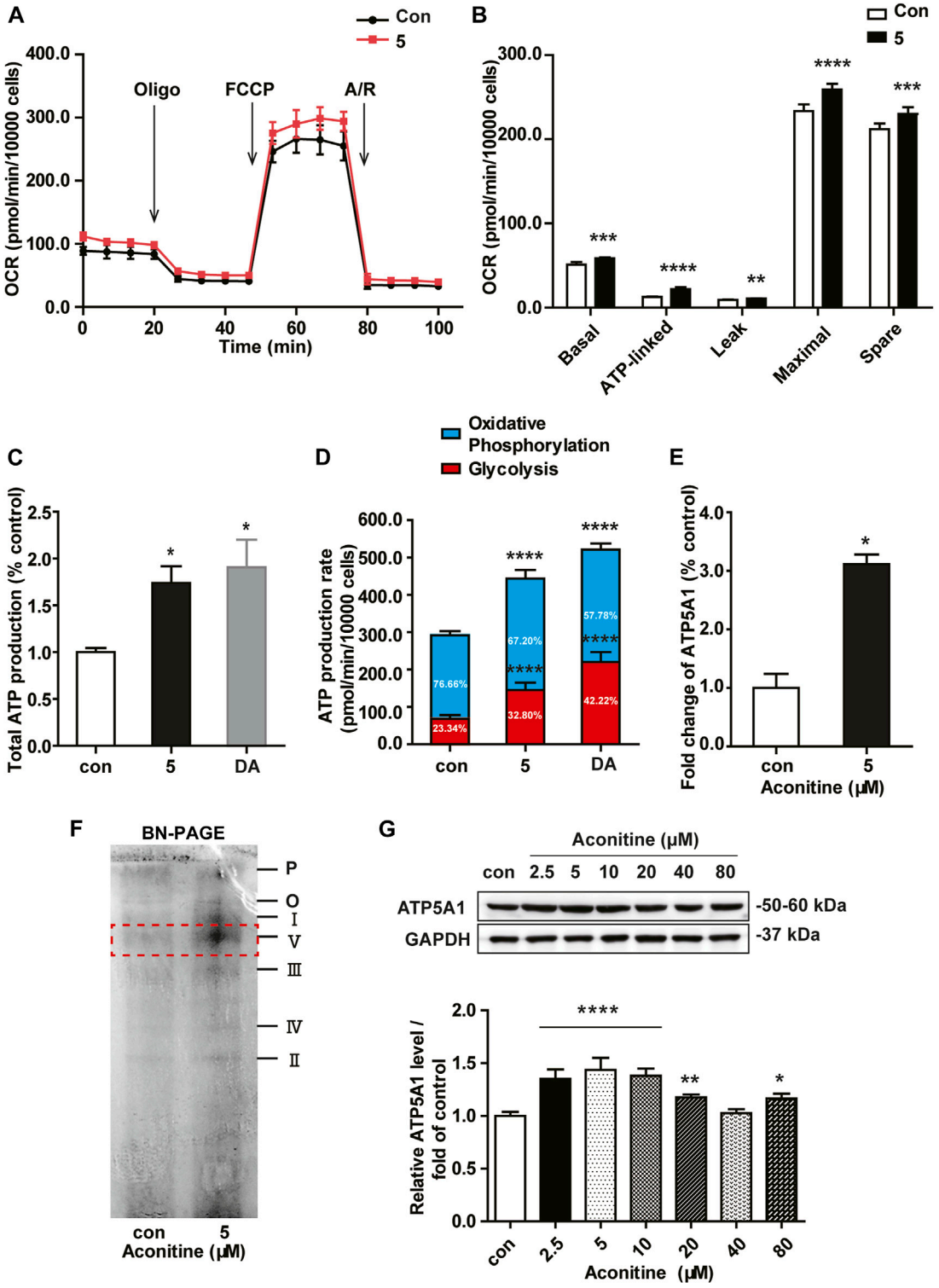

FIGURE 4 | Low dose of aconitine increased mitochondrial respiration by promoting ATP5A1 in NRVMs. **(A)** Mitochondrial function of NRVMs with aconitine (0 and 5 μM) were obtained *via* the Seahorse XF Cell Mito Stress Test, and representative time course data for indicated NRVMs are shown. **(B)** Quantitive analysis of OCRs (n = 8). **(C)** The total ATP production. **(D)** The quantification of ATP production rate in NRVMs (n = 8). **(E)** Aconitine-induced fold change in ATP5A1 obtained by LC-MS/MS-based proteomic analysis (n = 3). **(F)** The content of various respiratory chain complexes in NRVMs treated with aconitine (0 and 5 μM) using BN-PAGE. **(G)** Western blot analysis of ATP5A1 expression in NRVMs treated with aconitine for 7 days. The data represented relative expression to that of control by normalizing to GAPDH (n = 3). $^{*}p < 0.05$, $^{**}p < 0.01$, $^{***}p < 0.001$, $^{****}p < 0.0001$ vs. control.

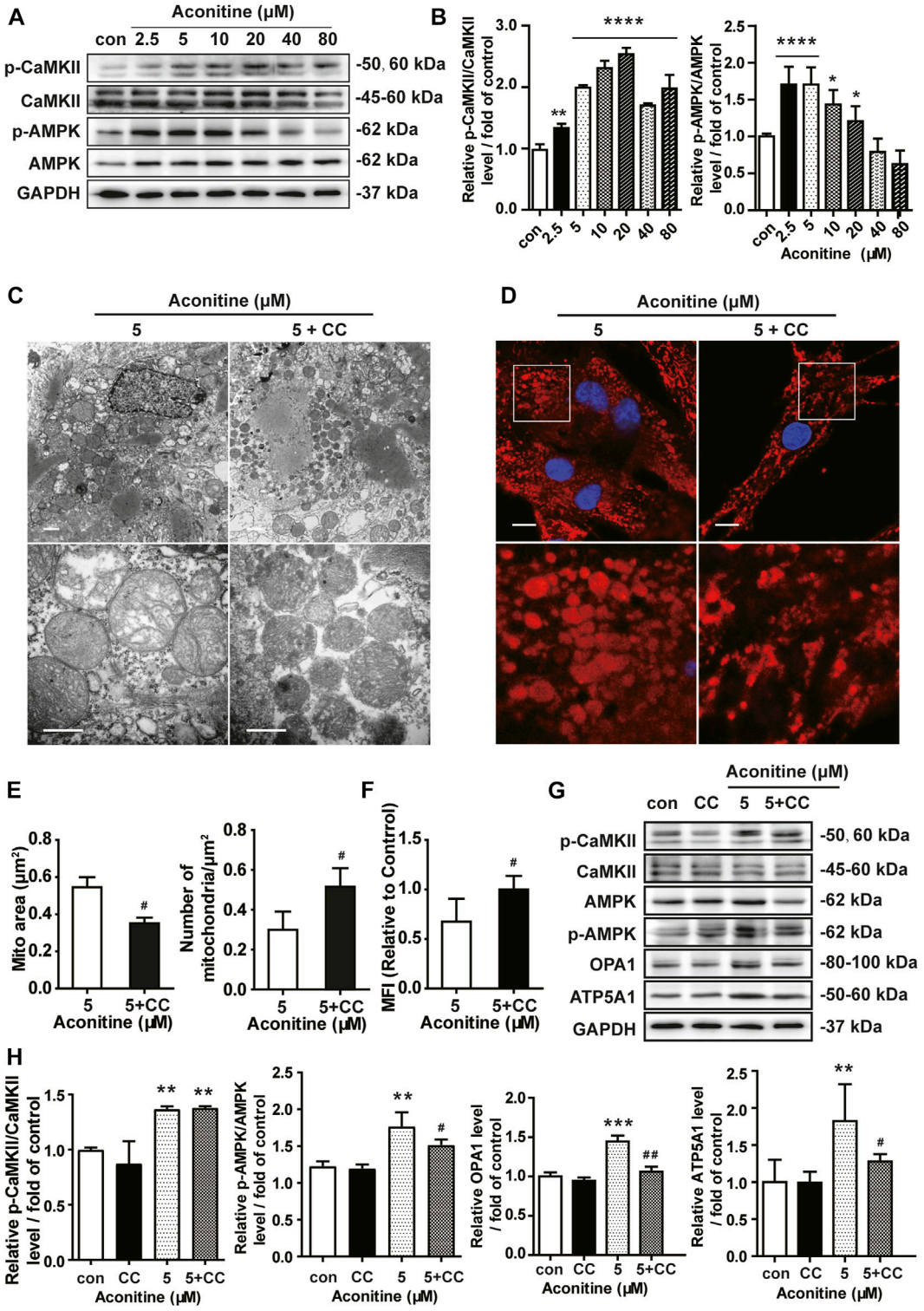

FIGURE 5 | Aconitine increased OPA1-mediated mitochondrial fusion *via* activation of AMPK signaling in NRVMs. **(A, B)** The effects of different treatments on indicated proteins were measured by Western blot. Band intensity was normalized to GAPDH and data presented as fold change relative to control. **(C, D)** Representative TEM and confocal images of mitochondria in aconitine-treated NRVMs with or without compound C (CC) co-treatment. Scales represent 1 μm. **(E)** Quantification of the mitochondrial area (μm^2) and the number of mitochondrial per μm^2 (n = 3, 100 mitochondria per group). **(F)** MFI for mitochondria in the two groups (n = 20). **(G, H)** Western analysis of expression of indicated proteins in NRVMs co-treated with CC and aconitine. All data were normalized to GAPDH and expressed as fold-change over control (n = 3). $^{*}p < 0.05$, $^{**}p < 0.01$, $^{***}p < 0.001$, $^{****}p < 0.0001$ vs. control, $^{\#}p < 0.05$, $^{\#\#}p < 0.01$ vs. 5 μM.

repeated treatment with aconitine and DA both could upregulate cellular ATP content in cardiomyocytes (**Figure 3G**). Therefore, our data implied that 5 μM of aconitine treatment might improve mitochondrial function through enhanced OPA1- or Mfn2-dependent mitochondrial fusion in cardiomyocytes.

Aconitine Increased the Mitochondrial Function by Upregulating ATP5A1 Expression in NRVMs

As shown in **Figure 4A**, OCRs in rat neonatal cardiomyocytes revealed that repeated dosing of aconitine and DA both significantly increased mitochondrial basal respiration, ATP production, maximal respiration, and spare respiratory capacity, suggesting a higher cellular respiratory function in NRVMs (**Figure 4B**). Also, there was no difference in proton leak in aconitine-treated cells, indicating mitochondria were not damaged at this low level. Of note, aconitine and DA induced the increase in ATP content were also evidenced by the following real-time ATP rate assay, and the fractions of ATP produced from OXPHOS in aconitine group were raised by about 1.5 times (**Figures 4C,D**). Next, we found that repeated 5 μM of aconitine markedly enhanced the content of ATP synthase (complex V, **Figure 4F**). Moreover, LC-MS/MS analyses revealed that 5 μM of aconitine induced a significantly increased expression of ATP5A1 in NRVMs (**Figure 4E**). Subsequently, we performed Western blotting and found repeated aconitine treatment increased the expression of ATP5A1 (**Figure 4G**). Together, these results suggested that repeated low dose of aconitine could enhance mitochondrial function *via* ATP5A1-mediated energy synthesis.

Aconitine Regulated OPA1-Mediated Mitochondrial Fusion *via* Activation of AMPK Signaling in NRVMs

Next, we assessed the role of the AMPK signaling in aconitine-induced mitochondrial fusion and found that after repeated 0–80 μM aconitine treatment for 7 days, the ratio of p-CaMKII/CaMKII and p-AMPK/AMPK were firstly upregulated at lower levels but then began to decline with the dose increasing in the NRVMs (**Figures 5A,B**). Interestingly, when we co-treated NRVMs with aconitine and CC, aconitine-induced increasing in the contents of phosphor-AMPK and OPA1 were notably reversed, while there was no inhibition on p-CaMKII (**Figures 5G,H**). As expected, our TEM and confocal results also demonstrated that the alternations in mitochondrial morphology and the MFI caused by 5 μM of aconitine were both attenuated by CC pretreatment (**Figures 5C–F**). Overall, these results illustrated that phosphorylation of the AMPK signaling pathway, activated by aconitine, could contribute to OPA1-mediated mitochondrial fusion. Interestingly, DA induced an increase in the ratio of p-CaMKII/CaMKII without changing the ratio of p-AMPK/AMPK and the expressions of OPA1 and ATP5A1, suggesting the AMPK–OPA1–ATP5A1 signaling pathway did not involve in DA-induced cardiotonic effect on myocytes (**Figures 6A,B**).

Effect of AMPK Inhibitor on Aconitine-Enhanced Mitochondrial Function in NRVMs

Meanwhile, inhibiting AMPK phosphorylation *via* CC caused an evident decline in ATP5A1 content in NRVMs (**Figures 5G,H**), implying that AMPK/OPA1 might be an upstream signaling for aconitine-induced increasing in ATP5A1. The OCRs value associated with mitochondrial function also returned to a similar level compared to that of the control group (**Figures 6C,D**). And as shown in **Figure 6E**, AMPK inhibitor could reverse the increase in cellular ATP content induced by aconitine but could not restore the ratio of OXPHOS to glycolysis in NRVMs (**Figure 6F**). These results demonstrated that repeated aconitine treatment at a low level (5 μM) was responsible for the enhancement of mitochondrial function in NRVMs, and the AMPK signaling pathway could play an important role during this process. Taken together, our data suggested that repeated aconitine (5 μM) treatment facilitated OPA1-mediated mitochondrial fusion and the following mitochondrial function, during which AMPK–OPA1–ATP5A1 signaling could be involved in and play a crucial role in low dose of aconitine-induced cardiotonic effect.

DISCUSSION

In the current study, we first found that repeated treatment with low doses (0–10 μM) of aconitine for 7 days could accelerate the mitochondrial turnover characterized by activating mitophagy, mitochondrial fusion, and biogenesis in cardiomyocytes, all of which eventually contributed to the enhancement of mitochondrial function and ATP production, and induced positive intronic effect. Significantly, the activation of the AMPK–OPA1–ATP5A1 signaling pathway played a crucial role in this process. All of these results may provide a possible mechanism involved in aconitine-induced regulation of energy metabolism, which is necessary to the maintenance of cardiotonic effect induced by medicinal plants containing aconitine.

Since the excellent pharmacological effect, herbs containing aconitine are widely used to treat cardiovascular diseases, such as heart failure, in China and other East Asian countries (Wu et al., 2019). But in the past decades, the studies on aconitine mostly focused on single or short-term administration at extremely high doses and overemphasized the toxicity of these ancient herbs (Jacobs and Haydock, 2019; Peng et al., 2020). However, in disagreement with previous reports (Gao et al., 2018; Ji et al., 2019), we did not find any detectable cytotoxic effects induced by repeated aconitine treatment (0–10 μM). Consistently, this study found that 5 μM of aconitine indeed generated a positive inotropic effect on cardiomyocytes characterized by the increased

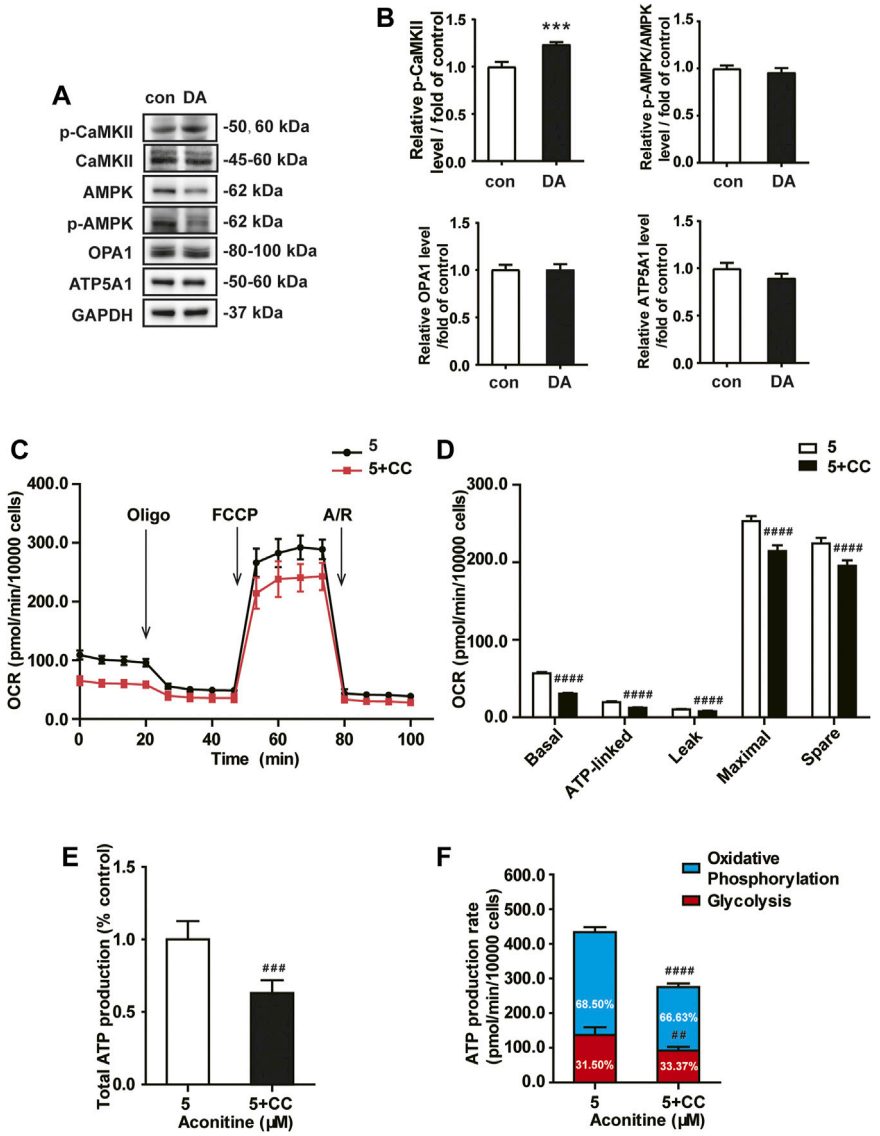

FIGURE 6 | Aconitine-enhanced mitochondrial function was reversed by the AMPK inhibitor in NRVMs. **(A, B)** Western analysis of expression of indicated proteins in NRVMs treated with DA. All data were normalized to GAPDH and expressed as fold-change over control. **(C, D)** Mitochondrial respiratory function in NRVMs co-treated with CC and aconitine ($n = 8$). **(E)** The total ATP production. **(F)** The quantification of ATP production rate in NRVMs co-treated with CC and aconitine ($n = 6$). $^{***}p < 0.001$ vs. control, $^{\#\#}p < 0.01$, $^{\#\#\#}p < 0.001$, $^{\#\#\#\#}p < 0.0001$ vs. 5 μM.

beating rate (Tak et al., 2016; Sun et al., 2018). However, matched energy metabolism supporting such high frequency beating and underlying mechanism remain poorly understood.

Mitochondria, as the main sites of energy metabolism, provide more than 90% of ATP supply through oxidative phosphorylation (Van der Bliek et al., 2017). Also, mitochondria are highly dynamic organelles and always being the homeostasis or named mitochondrial turnover, which consists of biogenesis, mitophagy, and fission/fusion and is critical for mitochondrial function (Liesa et al., 2009; Westermann, 2010). Generally, mitochondrial fission contributes to the redistribution of mitochondria, mitophagy removes damaged or dysfunctional mitochondria, and biogenesis and fusion promote a healthy mitochondrial network, and all of these processes are precisely regulated (Dorn, 2019). In our study, we firstly found that more than 10 μM of aconitine mainly induced autophagy and blockage of autophagic flux, evidenced by a dose-dependent increase in autophagy-related proteins (LC3B, Beclin1, and p62, and LAMP1) and autophagic vacuoles in myocytes. However, in the groups treated with lower doses of aconitine, the enhanced protein content of Parkin and PINK1 and degraded mitochondria in autophagosome or nearby lysosome suggested the PINK1–Parkin system-mediated mitophagy was activated in these groups. Besides, the expression of PGC1α, Mfn2, and

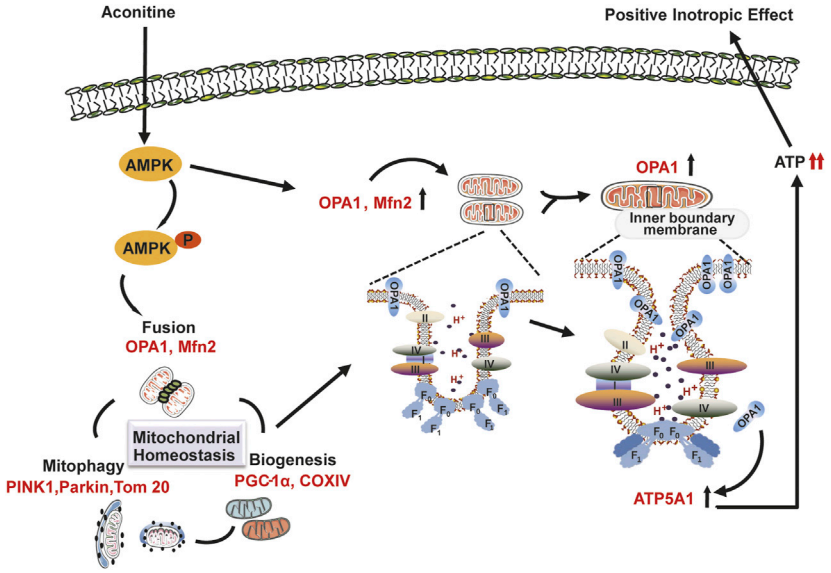

FIGURE 7 | Schematic representation of the possible molecular model of action underlying aconitine-induced cardiotonic effect–related energy metabolism.

OPA1, three important proteins controlling mitochondrial biogenesis and fusion, was increased in lower-dose groups, while aconitine did not cause any changes in the content of fission-related proteins (p-Drp1, Drp1, p-MFF, and MFF). Therefore, we deemed that repeated treatment with low doses of aconitine could promote mitochondrial turnover, particularly mitochondrial fusion.

Moreover, our results showed significant increases in the function of respiratory chain and ATP content in aconitine-treated NRVMs, and compared to DA, 5 μM of aconitine generated the same positive inotropic effect but with less glycolysis, both implying that repeated aconitine caused obvious alterations in mitochondrial energy metabolism. Considering no changes in the content of mitochondria, confirmed by cellular COX IV expression, aconitine-induced enhancement in energy supply might mostly result from alterations in mitochondrial function but not from mitochondrial quantity.

Generally, mitochondrial function is intimately connected with many complexes involved in the tricarboxylic acid cycle and OXPHOS and located in mitochondrial cristae (Cogliati et al., 2013). In other words, the alternations in cristae are related to the stability of respiratory supercomplexes and also affect the efficiency of mitochondrial respiratory function (Enríquez, 2016). OPA1 mainly controls mitochondrial fusion at the inner mitochondrial membrane and has been reported to participate in mitochondrial cristae remodeling by cross-talking with the mitochondrial contact site and cristae organizing system (MICOS) data not shown, a series of key factors responsible for the regulation of cristae morphology (Muñoz-Gómez et al., 2015; Quintana-Cabrera et al., 2018). Subsequently, we performed mitochondrial proteomic analysis and found that the expression of MICOS was remarkably enhanced after 7 days' repeated treatment with 5 μM of aconitine, accompanied with obvious changes in the morphology of mitochondrial cristae in aconitine-treated myocytes, indicating that aconitine treatment could cause reshaping in mitochondrial cristae during OPA1-mediated fusion. Furthermore, OPA1 could also promote ATP synthase oligomerization and preserve mitochondrial function in cardiac tissue (Wai et al., 2015). Remarkable increases in the content of complex V (ATP synthase), ATP5A1, and ADP/ATP translocase 1 (ANT) data not shown also indicated that OPA1-mediated mitochondrial fusion might play an indispensable role in aconitine-induced remodeling in mitochondrial cristae and respiratory chain complexes. Altogether, aconitine-induced OPA1-mediated mitochondrial fusion and following elevated mitochondrial function could be conducive to meeting the increased energy demands of the fast-beating myocytes.

Many studies have confirmed that AMPK played a crucial role in bioenergetic metabolism, for it could quickly sense the changes in cellular ATP levels (Herzig and Shaw, 2018). Usually, AMPK could be phosphorylated by CaMKII, a Ca^{2+}-activated protein kinase to timely regulate mitochondrial homeostasis (Hardie, 2011). Recently, AMPK signaling had been reported to ameliorate drug-induced hepatocyte injury *via* the enhancement of OPA1-related mitochondrial fusion (Ha et al., 2017), possibly for AMPK could inhibit the expression of mitochondrial ATP synthase β-F1 inhibitor protein, which depressed the activity of ATP synthase, resulting in the activity of oxidative respiratory chain and enhanced the ATP production (Vazquez-Martin et al., 2013; Zhang and Ma, 2018). Previous articles had reported that aconitine directly interacted with L-type Ca^{2+} channel on myocardiocytes membrane and increased the containing of cytosolic Ca^{2+}

(Zhou et al., 2017) triggering downstream CaMKII–AMPK signaling (Raney and Turcotte, 2008). Consistent with the previous studies, our study observed the activation of CaMKII–AMPK signaling in aconitine-treated NRVMs (**Supplementary Figure S1**). And inhibiting the phosphorylated activation of AMPK abolished aconitine-increased OPA1 expression mitochondrial fusion, ATP5A1 content, mitochondrial respiratory function, and ATP production, revealing that the AMPK was indeed involved in aconitine-induced elevation in mitochondrial function and energy metabolism by regulating the expression of OPA1 and ATP5A1 in NRVMs after repeated aconitine administration. As shown in **Figure 7**, we also presented a possible molecular model of action of energy metabolism involved in aconitine-induced cardiotonic effect.

LIMITATION

Several limitations existing in our study need to be acknowledged. First, all results acquired from *in vitro* experiments, the effect of low doses of aconitine on the cardiomyocytes should be further validated in animal experiments. Second, we only explored the mechanism underlying the cardiotonic effect induced by aconitine using normal myocardial cells, leading to limited generalizability of cardiac pharmacological effects of aconitine to the disease model. Furthermore, aconitine-induced toxicity is still the chief issue that prevents its wider use and the interpretation of therapeutic potential, and we also found the overlap between dose margin of this efficacy and that of triggering arrhythmia. Optimal therapeutic concentration of aconitine is up for a much wider scrutiny and discussion.

CONCLUSIONS

In conclusion, we found that repeated administration of aconitine could accelerate mitochondrial turnover through mitophagy, mitochondrial biogenesis, and fusion and promote reshaping of mitochondrial cristae and ATP synthase, both of which contributed to aconitine-induced energy metabolism and provide sufficient ATP for the fast-beating myocytes. Furthermore, we first identified that AMPK–OPA1–ATP5A1 signaling pathway played an important role in this process and could be one of the crucial pharmacological mechanisms underlying aconitine-induced cardiotonic effect–related energy metabolism.

DATA AVAILABILITY STATEMENT

The original contributions presented in the study are included in the article/**Supplementary Material**, and further inquiries can be directed to the corresponding author.

ETHICS STATEMENT

The animal study was reviewed and approved by the Ethics Committee of Department of Pharmaceutical Sciences Beijing Institute of Radiation Medicine.

AUTHOR CONTRIBUTIONS

YG, WZ, and L-ZQ designed research together; L-ZQ and WZ performed research; L-ZQ, F-RH, Y-HW, and P-YL analyzed data; L-ZQ, WZ, and YG wrote the paper, L-ZQ, L-XY, WZ, and YG contributed to the critical revision of this manuscript. All data were generated in-house, and no paper mill was used. All authors agree to be accountable for all aspects of work ensuring integrity and accuracy.

FUNDING

This study was supported by the National Natural Science Foundation of China (No. 81803833 and No. 81630102).

ACKNOWLEDGMENTS

Special thanks to the teachers at the Biomedical Analysis Center of Tsinghua University, including Peng Cheng Jiao and Jiao Ji, who provided great help and support for this work.

SUPPLEMENTARY MATERIAL

The Supplementary Material for this article can be found online at: https://www.frontiersin.org/articles/10.3389/fphar.2021.646121/full#supplementary-material

REFERENCES

Baker, M. J., Lampe, P. A., Stojanovski, D., Korwitz, A., Anand, R., Tatsuta, T., et al. (2014). Stress-induced OMA1 activation and autocatalytic turnover regulate OPA1-dependent mitochondrial dynamics. *EMBO J.* 33 (6), 578–593. doi:10.1002/embj.201386474

Begieneman, M. P. V., Ter Horst, E. N., Rijvers, L., Meinster, E., Leen, R., Pankras, J. E., et al. (2016). Dopamine induces lipid accumulation, NADPH oxidase-related oxidative stress, and a proinflammatory status of the plasma membrane in H9c2 cells. *Am. J. Physiology-Heart Circulatory Physiol.* 311 (5), H1097–H1107. doi:10.1152/ajpheart.00633.2015

Chan, T. Y. K. (2009). Aconite poisoning. *Clin. Toxicol.* 47 (4), 279–285. doi:10.1080/15563650902904407

Cogliati, S., Frezza, C., Soriano, M. E., Varanita, T., Quintana-Cabrera, R., Corrado, M., et al. (2013). Mitochondrial cristae shape determines respiratory chain supercomplexes assembly and respiratory efficiency. *Cell* 155 (1), 160–171. doi:10.1016/j.cell.2013.08.032

Dorn, G. W., 2nd (2019). Evolving concepts of mitochondrial dynamics. *Annu. Rev. Physiol.* 81, 1–17. doi:10.1146/annurev-physiol-020518-114358

Enríquez, J. A. (2016). Supramolecular organization of respiratory complexes. *Annu. Rev. Physiol.* 78, 533–561. doi:10.1146/annurev-physiol-021115-105031

Fu, W., Liu, Y., and Yin, H. (2019). Mitochondrial dynamics: biogenesis, fission, fusion, and mitophagy in the regulation of stem cell behaviors. *Stem Cell Int.* 2019, 1. doi:10.1155/2019/9757201

Fuhrmann, D. C., and Brüne, B. (2017). Mitochondrial composition and function under the control of hypoxia. *Redox Biol.* 12, 208–215. doi:10.1016/j.redox.2017.02.012

Gao, X., Zhang, X., Hu, J., Xu, X., Zuo, Y., Wang, Y., et al. (2018). Aconitine induces apoptosis in H9c2 cardiac cells *via* mitochondriamediated pathway. *Mol. Med. Rep.* 17 (1), 284–292. doi:10.3892/mmr.2017.7894

Ha, B. G., Jung, S. S., and Shon, Y. H. (2017). Effects of proton beam irradiation on mitochondrial biogenesis in a human colorectal adenocarcinoma cell line. *Int. J. Oncol.* 51 (3), 859–866. doi:10.3892/ijo.2017.4067

Hardie, D. G. (2011). AMPK and autophagy get connected. *EMBO J.* 30 (4), 634–635. doi:10.1038/emboj.2011.12

Herzig, S., and Shaw, R. J. (2018). AMPK: guardian of metabolism and mitochondrial homeostasis. *Nat. Rev. Mol. Cel Biol* 19 (2), 121–135. doi:10.1038/nrm.2017.95

Jacobs, C. O., and Haydock, S. (2019). ECG changes in acute aconite poisoning. *QJM* 112 (3), 227. doi:10.1093/qjmed/hcy220

Ji, X., Yang, M., Or, K. H., Yim, W. S., and Zuo, Z. (2019). Tissue accumulations of toxic Aconitum alkaloids after short-term and long-term oral administrations of clinically used radix aconiti lateralis preparations in rats. *Toxins* 11 (6), 353. doi:10.3390/toxins11060353

Liesa, M., Palacín, M., and Zorzano, A. (2009). Mitochondrial dynamics in mammalian health and disease. *Physiol. Rev.* 89 (3), 799–845. doi:10.1152/physrev.00030.2008

Liu, Q., Zhou, C., Xin, J. J., Zhao, Y. X., Gao, J. H., and Yu, X. C. (2020). Considerations about β1-adrenergic receptor pathway-mediated efficacy enhancing and toxicity-attenuating effects of acupuncture combined with aconitine for treatment of heart failure. *J. Guangzhou Univ. Traditional Chin. Med.* 37 (7), 1274–1278. doi:10.13359/j.cnki.gzxbtcm.2020.07.013 (Chinese).

Marín-García, J., and Akhmedov, A. T. (2016). Mitochondrial dynamics and cell death in heart failure. *Heart Fail. Rev.* 21 (2), 123–136. doi:10.1007/s10741-016-9530-2

Muñoz-Gómez, S. A., Slamovits, C. H., Dacks, J. B., and Wideman, J. G. (2015). The evolution of MICOS: ancestral and derived functions and interactions. *Communicative Integr. Biol.* 8 (6), e1094593. doi:10.1080/19420889.2015.1094593

Panchal, K., and Tiwari, A. K. (2019). Mitochondrial dynamics, a key executioner in neurodegenerative diseases. *Mitochondrion* 47, 151–173. doi:10.1016/j.mito.2018.11.002

Peng, F., Zhang, N., Wang, C., Wang, X., Huang, W., Peng, C., et al. (2020). Aconitine induces cardiomyocyte damage by mitigating BNIP3-dependent mitophagy and the TNFα-NLRP3 signalling axis. *Cell Prolif* 53 (1), e12701. doi:10.1111/cpr.12701

Quintana-Cabrera, R., Quirin, C., Glytsou, C., Corrado, M., Urbani, A., Pellattiero, A., et al. (2018). The cristae modulator Optic atrophy 1 requires mitochondrial ATP synthase oligomers to safeguard mitochondrial function. *Nat. Commun.* 9 (1), 3399. doi:10.1038/s41467-018-05655-x

Raney, M. A., and Turcotte, L. P. (2008). Evidence for the involvement of CaMKII and AMPK in Ca2+-dependent signaling pathways regulating FA uptake and oxidation in contracting rodent muscle. *J. Appl. Physiol.* 104 (5), 1366–1373. doi:10.1152/japplphysiol.01282.2007

Sun, W., Yan, B., Wang, R., Liu, F., Hu, Z., Zhou, L., et al. (2018). *In vivo* acute toxicity of detoxified Fuzi (lateral root of Aconitum carmichaeli) after a traditional detoxification process. *EXCLI J.* 17, 889–899. doi:10.17179/excli2018-1607

Tak, S., Lakhotia, M., Gupta, A., Sagar, A., Bohra, G., and Bajari, R. (2016). Aconite poisoning with arrhythmia and shock. *Indian Heart J.* 68 (Suppl 2), S207–S209. doi:10.1016/j.ihj.2015.08.010

Upadhyay, M., and Agarwal, S. (2020). Ironing the mitochondria: relevance to its dynamics. *Mitochondrion* 50, 82–87. doi:10.1016/j.mito.2019.09.007

Van der Bliek, A. M., Sedensky, M. M., and Morgan, P. G. (2017). Cell biology of the mitochondrion. *Genetics* 207 (3), 843–871. doi:10.1534/genetics.117.300262

Vazquez-Martin, A., Corominas-Faja, B., Cufi, S., Vellon, L., Oliveras-Ferraros, C., Menendez, O. J., et al. (2013). The mitochondrial H+-ATP synthase and the lipogenic switch. *Cell Cycle* 12 (2), 207–218. doi:10.4161/cc.23352

Wai, T., García-Prieto, J., Baker, M. J., Merkwirth, C., Benit, P., Rustin, P., et al. (2015). Imbalanced OPA1 processing and mitochondrial fragmentation cause heart failure in mice. *Science* 350 (6265), aad0116. doi:10.1126/science.aad0116

Wang, N.-n., Xu, H.-H., Zhou, W., Yang, H.-x., Wang, J., Ma, Z.-c., et al. (2021). Aconitine attenuates mitochondrial dysfunction of cardiomyocytes *via* promoting deacetylation of cyclophilin-D mediated by sirtuin-3. *J. Ethnopharmacology* 270, 113765. doi:10.1016/j.jep.2020.113765

Wang, N. N., Wang, J., Tan, H. L., Wang, Y. G., Gao, Y., and Ma, Z. C. (2019). Aconitine ameliorates cardiomyocyte hypertrophy induced by angiotensin II. *Zhong guo Zhong Yao Za Zhi* 44 (8), 1642–1647. Chinese. doi:10.19540/j.cnki.cjcmm.20190117.002

Wen, S. S., Wan, H. T., Zhang, Y. Y., and Yang, J. H. (2012). Experimental study of aconitine on dose -time -effect relationship in cardiac effect of heart failure cells. *JETCM* 21 (4), 562–564. (Chinese). doi:10.3969/j.issn.1004-745X.2012.04.026

Westermann, B. (2010). Mitochondrial fusion and fission in cell life and death. *Nat. Rev. Mol. Cel Biol* 11 (12), 872–884. doi:10.1038/nrm3013

Wu, H., Liu, X., Gao, Z.-y., Dai, Z.-f., Lin, M., Tian, F., et al. (2019). Anti-myocardial infarction effects of radix Aconiti Lateralis preparata extracts and their influence on small molecules in the heart using matrix-assisted laser desorption/ionization-mass spectrometry imaging. *Ijms* 20 (19), 4837. doi:10.3390/ijms20194837

Xie, X. F., and Peng, C. (2017). Study progress of multidimensional evaluation and integrated analysis between toxicity and efficacy on heart of radix aconiti lateralis praeparata. *WORLD CHINESE MEDICINE* 12 (11), 2555–2562. (Chinese).

Xin, T., Lv, W., Liu, D., Jing, Y., and Hu, F. (2020). Opa1 reduces hypoxia-induced cardiomyocyte death by improving mitochondrial quality control. *Front. Cel Dev. Biol.* 8, 853. doi:10.3389/fcell.2020.00853

Zhang, D., and Ma, J. (2018). Mitochondrial dynamics in rat heart induced by 5-fluorouracil. *Med. Sci. Monit.* 24, 6666–6672. doi:10.12659/MSM.910537

Zhang, M. H., Fang, X. S., Guo, J. Y., and Jin, Z. (2019). Effects of AMPK on apoptosis and energy metabolism of gastric smooth muscle Cells in Rats with Diabetic Gastroparesis. *Erratum Cel Biochem Biophys* 77(2), 165–177. doi:10.1007/s12013-019-00870-9

Zhang, S. Z., and Wu, B. W. (2001). The inotropic effects of combination of aconitine with potassium channel activator on isolated cardiac dysfunctional rat hearts. *Chin. Pharmacol. Bull.* 17 (5), 5570–5572. (Chinese).

Zhou, W., Yuan, X., Zhang, L., Su, B., Tian, D., Li, Y., et al. (2017). Overexpression of HO-1 assisted PM2.5-induced apoptosis failure and autophagy-related cell necrosis. *Ecotoxicology Environ. Saf.* 145, 605–614. doi:10.1016/j.ecoenv.2017.07.047

Zhou, Y.-h., Piao, X.-m., Liu, X., Liang, H.-h., Wang, L.-m., Xiong, X.-h., et al. (2013). Arrhythmogenesis toxicity of aconitine is related to intracellular Ca2+ signals. *Int. J. Med. Sci.* 10 (9), 1242–1249. doi:10.7150/ijms.6541

Conflict of Interest: The authors declare that the research was conducted in the absence of any commercial or financial relationships that could be construed as a potential conflict of interest.

frontiers in Pharmacology

ORIGINAL RESEARCH
published: 14 June 2021
doi: 10.3389/fphar.2021.667102

Piper sarmentosum Roxb. Attenuates Vascular Endothelial Dysfunction in Nicotine-Induced Rats

Muhd Fakh Rur Razi Md. Salleh[1], *Amilia Aminuddin*[1], *Adila A. Hamid*[1], *Norizam Salamt*[1], *Fadhlullah Zuhair Japar Sidik*[2] *and Azizah Ugusman*[1]*

[1]*Department of Physiology, Faculty of Medicine, Universiti Kebangsaan Malaysia, Cheras, Malaysia,* [2]*Department of Pharmacology, Faculty of Medicine, Universiti Kebangsaan Malaysia, Cheras, Malaysia*

Exposure to cigarette smoke is an important risk factor for cardiovascular diseases. Nicotine is an addictive compound in cigarette smoke that triggers oxidative stress, which leads to vascular dysfunction. *Piper sarmentosum* Roxb. is a herb with antioxidant and vascular protective effects. This study evaluated the potential protective effect of the aqueous extract of *P. sarmentosum* leaf (AEPS) on vascular dysfunction in rats induced with prolonged nicotine administration. A total of 22 male Sprague-Dawley rats were divided into control (normal saline, oral gavage [p.o.]), nicotine (0.8 mg/kg/day nicotine, intraperitoneally [i.p.]), and nicotine + AEPS groups (250 mg/kg/day AEPS, p.o. + 0.8 mg/kg/day nicotine, i.p.). Treatment was given for 21 days. Thoracic aortae were harvested from the rats for the measurement of vasorelaxation, vascular nitric oxide (NO) level, and antioxidant level and the assessment of vascular remodeling. Rats treated with AEPS had improved vasorelaxation to endothelium-dependent vasodilator, acetylcholine (ACh), compared with the nicotine-induced rats ($p < 0.05$). The presence of endothelium increased the maximum relaxation of aortic rings in response to ACh. Compared with the nicotine group, AEPS enhanced vascular NO level ($p < 0.001$) and increased antioxidant levels as measured by superoxide dismutase activity ($p < 0.05$), catalase activity ($p < 0.01$), and reduced glutathione level ($p < 0.05$). No remarkable changes in aortic histomorphometry were detected. In conclusion, *P. sarmentosum* attenuates vascular endothelial dysfunction in nicotine-induced rats by improving vasorelaxation and enhancing vascular NO and antioxidant levels.

Keywords: nicotine, nitric oxide, oxidative stress, vascular remodeling, vascular endothelial dysfunction, *Piper sarmentosum* Roxb.

OPEN ACCESS

Edited by:
Mas Rizky A.A Syamsunarno, Padjadjaran University, Indonesia

Reviewed by:
Leonardo Borges, State University of Goiás, Brazil
Maizura Mohd Zainudin, International Islamic University Malaysia, Malaysia

***Correspondence:**
Azizah Ugusman
dr.azizah@ppukm.ukm.edu.my

Specialty section:
This article was submitted to Ethnopharmacology, a section of the journal Frontiers in Pharmacology

Received: *12 February 2021*
Accepted: *02 June 2021*
Published: *14 June 2021*

Citation:
Md. Salleh MFRR, Aminuddin A, Hamid AA, Salamt N, Japar Sidik FZ and Ugusman A (2021) Piper sarmentosum *Roxb. Attenuates Vascular Endothelial Dysfunction in Nicotine-Induced Rats. Front. Pharmacol. 12:667102. doi: 10.3389/fphar.2021.667102*

INTRODUCTION

Tobacco smoking contributes to eight million of annual deaths worldwide. More than seven million deaths are attributed to the direct effects of smoking, and more than 1.2 million premature deaths of adults and children due to exposure to secondhand smoke have been recorded annually (World Health Organization, 2019). Nicotine is the main ingredient in tobacco smoke that causes addiction (Hecht, 2003). In addition, tobacco smoking and exposure to nicotine increase the risk of cardiovascular diseases (CVD), such as atherosclerosis, ischemic heart disease, hypertension, and stroke (Son and Lee, 2020).

The effect of nicotine on the cardiovascular system is mediated by its binding to endogenous nicotinic acetylcholine receptors (nAChRs). NAChRs are expressed by vascular endothelial cells (EC) and vascular smooth muscle cells (VSMC); thus, ECs and VSMCs are the direct targets of nicotine-induced vascular dysfunction (Brüggmann et al., 2003; Moccia et al., 2004). The presentations of nicotine-induced vascular dysfunction include changes in vasoreactivity and vascular remodeling (Whitehead et al., 2021).

Nicotine impacts the survival, proliferation, migration, and matrix production of ECs and VSMCs and leads to vascular remodeling. Acute exposure to nicotine promotes the angiogenic response of the endothelium, whereas chronic exposure blunts pro-angiogenic response. Acute and chronic nicotine exposures lead to fibroblast proliferation, extracellular matrix deposition, VSMC proliferation and migration, and neointima formation (Cucina et al., 2000; Ng et al., 2007; Rodella et al., 2012). In addition, chronic nicotine infusion induces matrix metalloproteinase (MMP)-2 and MMP-9 expression and activity. MMPs cause elastin degradation in the aortic wall and irreversible aortic stiffening (Wagenhauser et al., 2018).

Concerning vascular reactivity, nicotine impairs vasorelaxation through endothelium-dependent and -independent mechanisms. The endothelium secretes various vasoactive substances that move to the underlying VSMC to induce vasoconstriction or vasorelaxation (Wright et al., 2004). Nicotine stimulates the release of the vasoconstrictor, endothelin-1, and inhibits the synthesis of the vasorelaxants, nitric oxide (NO) and prostacyclin, from the endothelium (Su and Wang, 1991; Toda and Toda, 2010; Durand and Gutterman, 2013). As for the endothelium-independent mechanisms, nicotine promotes vasoconstriction by activating voltage-gated potassium channels and enhancing VSMC response to norepinephrine (Mayhan and Sharpe, 2002; Olfert et al., 2018).

Oxidative stress is the underlying pathogenesis of nicotine-induced impaired vasorelaxation (Carnevale et al., 2016). Nicotine stimulates excessive reactive oxygen species (ROS) production and lowers antioxidant levels to cause oxidative stress (Tonnessen et al., 2000). Multiple studies suggested that excessive ROS contributes to the nicotine-induced impairment of NO-mediated, endothelium-dependent vasorelaxation (Jiang et al., 2006; Toda and Toda, 2010). Cells produce a system of endogenous antioxidants to neutralize ROS. Among these antioxidants are superoxide dismutase (SOD), catalase (CAT), and reduced glutathione (GSH) (Aguilar et al., 2016). Nicotine exposure reduces aortic SOD and GSH levels, and this finding is associated with the impairment of the endothelium-dependent vasorelaxation of the aorta (Zainalabidin et al., 2014).

Piper sarmentosum Roxb. is a herbaceous plant that is widely used in Chinese traditional medicine to treat fever, cough, and pleurisy. Pharmacologically, the herb has various vascular protective effects (Peungvicha et al., 1998; Mohd Zainudin et al., 2013). The aqueous extract of *P. sarmentosum* leaf (AEPS) has high antioxidant activity (Ismail et al., 2018) and can stimulate NO production in oxidative stress-induced endothelial cells (Ugusman et al., 2010). AEPS also reduces the formation of atherosclerotic lesions in hypercholesterolemic rabbits (Amran et al., 2010).

Even though AEPS has vascular protective effects in various experimental models, the potential of AEPS in attenuating nicotine-induced vascular dysfunction, including impaired vasorelaxation and vascular remodeling, has not been studied. Nicotine in tobacco smoke causes direct harm to smokers and, unfortunately, has harmful effects on passive smokers or people who are inadvertently exposed to environmental tobacco smoke (World Health Organization, 2019). We hypothesized that AEPS can protect against the vascular dysfunction caused by nicotine. Therefore, this study determined the effect of AEPS on vasorelaxation, vascular NO level, and antioxidant levels, as well as vascular remodeling, in nicotine-induced rats. Findings from this study will support the potential use of AEPS as a supplement to prevent nicotine-induced vascular dysfunction in people who are inadvertently exposed to tobacco smoke.

MATERIALS AND METHODS

Preparation and Analysis of Aqueous extract of *Piper sarmentosum* Roxb. leaf

P. sarmentosum leaves were supplied by Herbagus Sdn. Bhd., Penang, Malaysia and identified by a plant taxonomist in the Herbarium of Universiti Kebangsaan Malaysia (UKM; specimen voucher number: UKMB40240). AEPS was prepared according to a previous method (Ugusman et al., 2011). Fresh *P. sarmentosum* leaves were sun-dried and ground into powder. The powder was mixed with distilled water in a ratio of 1:10 (w/v) and heated at 80°C for 3 h. The extract was filtered and concentrated repeatedly and then freeze-dried and kept at 4°C. Liquid chromatography–mass spectrometry (LCMS)–Orbitrap full-scan analysis was conducted to identify the compounds in AEPS, and the results have been published previously (Sundar et al., 2019).

Animals and Study Design

The study was approved by the Animal Ethics Committee of UKM (approval code: PP/FISIO/2018/AZIZAH/26-SEPT./957-SEPT.-2018-SEPT.-2019). Twenty-two male Sprague-Dawley rats (250–300 g) were obtained from the Animal Resource Unit of UKM. Each rat was kept in a cage and maintained under standard conditions of a 12 h light and 12 h dark cycle. The rats were fed on a standard rat chow diet with water ad libitum. The rats were randomly divided into three groups (n = 6–8 per group): the control group was given normal saline; the nicotine group was given 0.8 mg/kg/day nicotine (Tokyo Chemical Industry, Japan) intraperitoneally (i.p.); and the AEPS group was fed with 250 mg/kg/day AEPS by oral gavage (p.o.) 30 min before treatment with 0.8 mg/kg/day nicotine (i.p.). Treatment was continued daily for 21 days. The dosage and duration of nicotine treatment mimic the exposure of a chronic light smoker and has been proven to cause vascular dysfunction in a previous study (Moon et al., 2014). The dose of AEPS was chosen based on the optimal dose that improved vasorelaxation in nicotine-induced rats (**Supplementary Figure S1**, **Supplementary Table S1**). On day 22, the rats were terminally anaesthetized with intravenous injection of ketamine and xylazine cocktail (0.2 ml/kg BW). The thoracic aortae were then harvested and cleaned from the surrounding fat and connective tissues. Parts of the fresh aortic tissues were immediately used for wire

myography. The remaining aortic tissues were used for vascular NO, antioxidant, and histological analyses.

Measurement of Mean Systolic Blood Pressure

MSBP was measured in conscious rats on day 21 by using the CODA II™ Non-Invasive Blood Pressure System (Kent Scientific Corporation, United States). MSBP values were then used for aortic morphometry analysis.

Wire Myography

The thoracic aortae were cut into 2 mm rings. Some rings were endothelium-denuded, whereas others had intact endothelium. The endothelium was removed by gently rubbing the interior of the vessel around a wire, and removal was confirmed by the lack of a vasodilator response to 10^{-6} M acetylcholine (ACh; Tokyo Chemical Industry, Japan). The aortic rings were mounted on two stainless steel pins in a four-channel wire myograph (Danish Myo Technology, United States). The vessels were bathed in physiological Krebs solution with the following composition: 118 mM NaCl, 4.7 mM KCl, 11 mM glucose, 1.2 mM $MgSO_4$, 25 mM $NaHCO_3$, 1.03 mM KH_2PO_4, and 2.5 mM $CaCl_2$. Then, the vessels were gassed continuously with 95% O_2 and 5% CO_2 at 37°C. The aortic rings were set to an optimum tension of 1 g and allowed to equilibrate for at least 30 min before use (Almabrouk et al., 2018). After the calibration, the viability of the aortic rings was tested by adding 40 mM KCl. The vessels were then contracted with 10^{-6} M phenylephrine (Sigma, United States) before starting experiments. The cumulative concentration–relaxation curves to the endothelium-dependent vasodilator, ACh (10^{-9}–10^{-6} M), and the endothelium-independent vasodilator, sodium nitroprusside (SNP; 10^{-9}–10^{-6} M; Sigma, United States), added at 3 min intervals were constructed. Power-Lab Data Acquisition System (ADInstruments, Australia) was used to measure and record the changes in vessel tension. Vasorelaxation data were expressed as the percentage loss of phenylephrine-induced contraction.

Preparation of Tissue Lysates

Aortic tissue lysates were prepared based on previous methods (Zainalabidin et al., 2014). The tissues were weighed and crushed into powder form using a mortar and pestle in liquid nitrogen. Then, phosphate-buffered saline (PBS; 0.1 M, pH 7.4) was added to the tissue powder in a ratio of 1:9 (w/v) and centrifuged for 10 min at 4°C. The protein concentration in the aortic tissue lysates was measured using Bradford assay (Bradford, 1976).

Measurement of Vascular Nitric Oxide Level

The concentration of NO in the aortic tissue lysates was measured indirectly using Nitrite/Nitrate Colorimetric Assay Kit (Sigma, United States) according to the manufacturer's instructions. The whole aorta was used for this assay without specifically isolating the endothelial layer. The principle of this assay is based on the measurement of total nitrite in the samples. Nitrate reductase was used to reduce nitrate to nitrite. Total nitrite was measured at 540 nm after the addition of Griess reagent.

Measurement of Vascular Antioxidant Levels

SOD activity in the aortic tissue lysates was measured as described previously (Beyer and Fridovich, 1987). Briefly, the tissue lysates were mixed with SOD substrate containing PBS–EDTA, riboflavin, L-methionine, Triton-X, and nitro blue tetrazolium (NBT). SOD activity in the samples was determined on the basis of one unit of an enzyme that inhibited 50% of NBT reduction and expressed as unit per milligram protein. CAT activity in the aortic samples was tested on the basis of a previous method (Aebi, 1984). The samples were mixed into H_2O_2, and the disappearance of H_2O_2 was measured spectrophotometrically at 240 nm. GSH level in the aortic tissue lysates was measured as described previously (Ellman, 1959). The samples were mixed with 5,5-dithio-bis-[2-nitrobenzoic acid] for 15 min. Subsequently, the absorbance values of the samples were measured at 415 nm using a microplate reader.

Histological Analysis

Thoracic aortae were fixed in 10% formalin, dehydrated, and embedded in paraffin wax. Aortic sections were cut on a rotary microtome and stained with hematoxylin and eosin. The sections were photographed using an Olympus SZ61TR-TP051000 microscope (Olympus, Japan), and the images were analyzed using Life Science Olympus cellSens Standard software (Olympus, Japan). The morphometric parameters of the aorta, including intima–media thickness (IMT), intima–media area (IMA), lumen diameter (d), circumference wall tension (CWT), and tensile stress (TS), were measured based on previous protocols (Zainalabidin et al., 2014). The four quadrants of the aortic lumen at 0°, 90°, 180°, and 270° between the layers of the tunica media and tunica intima were measured, and the average readings were recorded as the IMT value. Lumen area (α) was calculated by drawing a circular line over the tunica intima layer. Lumen diameter (d) was calculated using the formula $d = (2\sqrt{\alpha})/\pi$, where π is equivalent to 3.14. IMA was calculated using the formula: $[\pi(d/2 + IMT)^2] - [\pi(d/2)^2]$. MSBP was used in the formula to calculate CWT, where CWT = MSBP × (d/2). Finally, TS was calculated using the formula: TS = CWT/IMT.

Statistical Analysis

The data were analyzed using GraphPad Prism software version 7. The results are presented as mean ± standard error of the mean (SEM). The myography data were analyzed using two-way ANOVA followed by Tukey's post hoc test. For other data, unpaired t-test was used to compare the means. $p < 0.05$ was considered statistically significant.

RESULTS

Effect of Aqueous Extract of *Piper sarmentosum* Roxb. Leaf on Vasorelaxation

The endothelium-intact aortic rings of rats treated with AEPS had higher relaxation response to ACh compared with the nicotine group ($p < 0.05$). The endothelium-intact aortic rings of nicotine-induced rats showed lower relaxation response to ACh compared

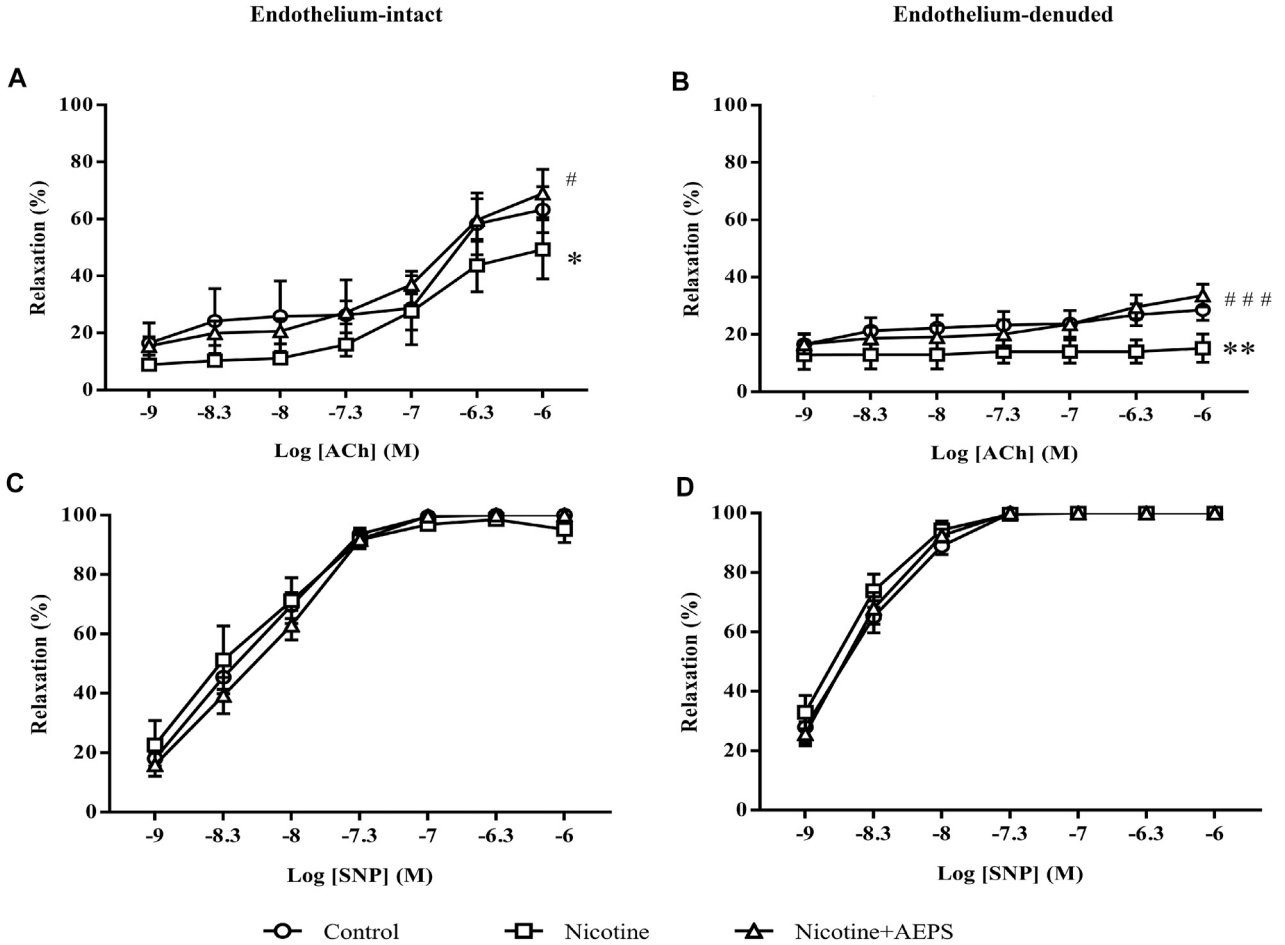

FIGURE 1 | Concentration-relaxation curves to the endothelium-dependent vasodilator ACh **(A, B)** and endothelium-independent vasodilator SNP **(C, D)** in rat aortic rings from each group. The values are given as mean ± SEM, $n = 6–8$ for each group. $^{*}p < 0.05$, $^{**}p < 0.01$ compared with the control group; $^{\#}p < 0.05$, $^{\#\#\#}p < 0.001$ compared with the nicotine group. (See **Table 1** for comparison of maximum relaxation among the groups).

with the control group ($p < 0.05$) (**Figure 1A**). Besides, the endothelium-denuded aortic rings of rats treated with AEPS had higher relaxation response to ACh compared with the nicotine group ($p < 0.001$). Endothelium-denuded aortic rings of nicotine-induced rats showed lower relaxation response to ACh compared with the control group ($p < 0.01$, **Figure 1B**). The maximum relaxation (R_{max}) of the vessels with ACh was remarkably higher in endothelium-intact vessels than in endothelium-denuded vessels in all groups (**Table 1**). No remarkable difference was observed in vasorelaxation toward endothelium-independent vasodilator, SNP, in all groups (**Figures 1C,D**). The presence or absence of endothelium also did not affect the maximum relaxation to SNP in all groups (**Table 1**).

Effect of Aqueous Extract of *Piper sarmentosum* Roxb. Leaf on Vascular Nitric Oxide Level

Rats treated with AEPS had significantly higher vascular NO level compared with nicotine-administered rats ($p < 0.001$). However, nicotine administration did not cause any remarkable change in vascular NO level compared with the control (**Figure 2**).

Effect of Aqueous Extract of *Piper sarmentosum* Roxb. Leaf on Vascular Antioxidant Levels

Treatment with AEPS significantly improved vascular antioxidant levels as shown by the enhanced SOD activity ($p < 0.05$), CAT activity ($p < 0.05$), and GSH level ($p < 0.05$) compared with the nicotine group. Nicotine significantly reduced vascular SOD activity ($p < 0.05$) but not CAT activity and GSH levels compared with the control group (**Figures 3A–C**).

Effect of Aqueous Extract of *Piper sarmentosum* Roxb. Leaf on Vascular Remodeling

The aorta from the control and AEPS groups exhibited normal histology as indicated by the regular arrangement of the elastic

TABLE 1 | Maximum relaxation (R_{max}) of aortic rings in response to ACh and SNP.

	Endothelium-intact			Endothelium-denuded		
	Control	**Nicotine**	**Nicotine + AEPS**	**Control**	**Nicotine**	**Nicotine + AEPS**
ACh						
R_{max} (%)	63.30 ± 8.12**	49.27 ± 10.31*	68.94 ± 8.40**	28.60 ± 3.63	15.24 ± 4.99	33.59 ± 3.94
SNP						
R_{max} (%)	100.00 ± 0.0	100.00 ± 0.0	95.20 ± 4.41	100.00 ± 0.0	100.00 ± 0.0	100.00 ± 0.0

The values are given as mean ± SEM, n = *6–8 for each group.* *p < *0.05,* **p < *0.01 compared with the endothelium-denuded aortic rings from the similar group. ACh, acetylcholine; SNP, sodium nitroprusside; R_{max}, maximum relaxation; AEPS, aqueous extract of* Piper sarmentosum *Roxb. leaf.*

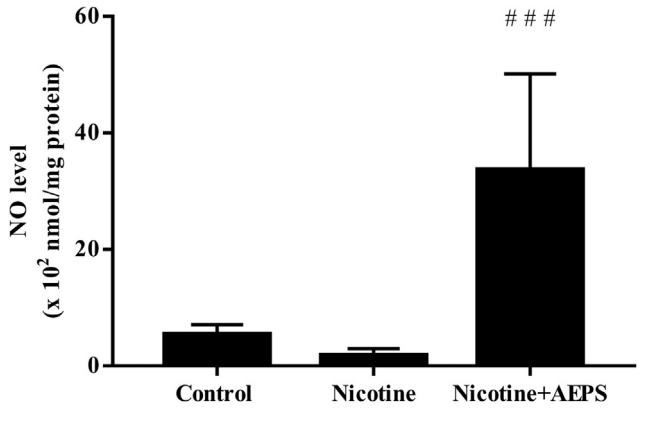

FIGURE 2 | Level of nitric oxide (NO) in rat aortic tissues. The values are given as mean ± SEM, *n* = 6–8 for each group. ###*p* < 0.001 compared with the nicotine group.

lamella in the tunica media layer. The nicotine group displayed disorganized tunica media layer with increased interlamellar space (**Figure 4**). However, the morphometric analysis of the aorta, including IMT, IMA, *d*, CWT, and TS, showed no remarkable changes in all groups, even though the nicotine group showed an increasing trend in IMT (**Table 2**).

DISCUSSION

This study showed that AEPS attenuated nicotine-induced vascular endothelial dysfunction as AEPS improved endothelium-dependent vasorelaxation in rats administered with nicotine. Exposure to nicotine impaired endothelium-dependent vasorelaxation to ACh. Impaired endothelium-dependent vasorelaxation is a functional characteristic of vascular endothelial dysfunction (Daiber et al., 2017). The effects of nicotine and AEPS on vasorelaxation were endothelium dependent because of the remarkable reduction in vasorelaxation in response to ACh but not in response to SNP. Besides, the maximum vasorelaxation to ACh was substantially higher in endothelium-intact vessels.

ACh works by binding to M3 receptors on the endothelium, which leads to calcium release and endothelial nitric oxide synthase (eNOS) activation. eNOS converts L-arginine to NO, which diffuses from the ECs into the adjacent layer of smooth muscle to cause vasorelaxation (Sandoo et al., 2010). By contrast, SNP is a NO donor that acts directly on VSMCs to cause vasorelaxation. The response to SNP is not dependent on the production of NO by ECs (Si et al., 2017).

This study demonstrated that AEPS supplementation to nicotine-induced rats increased vascular NO level. NO is a potent vasodilator; thus, the improved vasorelaxation observed in rats treated with AEPS is most likely contributed by the enhanced NO levels. AEPS also increases NO levels in spontaneously hypertensive rats and L-N^G-nitro arginine methyl ester-induced hypertensive rats (Zainudin et al., 2015; Alwi et al., 2018). AEPS stimulates the synthesis of NO by increasing mRNA expression, protein level, and eNOS activity in ECs (Ugusman et al., 2010). Besides, antioxidants can also protect NO from degradation by free radicals and thus maintain the bioavailability of NO (Ugusman et al., 2010). The antioxidant activity of AEPS is well established (Zainudin et al., 2015; Wang et al., 2017; Yeo et al., 2018) and may also contribute to the enhanced NO level.

Impaired vasorelaxation due to nicotine exposure has been linked to increased vascular oxidative stress (Si et al., 2017). In a previous study, nicotine reduced the relaxation of rat's aortic rings and increased the level of oxidative stress marker, malondialdehyde (Zainalabidin et al., 2014). Oxidative stress reduces endothelial NO production by deactivating eNOS (Ugusman et al., 2010). Nicotine deactivates eNOS by reducing the availability of eNOS essential cofactor, tetrahydrobiopterin (BH_4). BH_4 deficiency causes eNOS to become unpaired and unable to produce NO (Forstermann and Munzel, 2006; Li et al., 2018). Apart from NO, nicotine reduces other endothelium-dependent vasodilators, such as prostaglandins and prostacyclin (Tonnessen et al., 2000). The reduction of NO and other endothelium-dependent vasodilator results in impaired vasorelaxation. However, we did not measure the level of other endothelium-dependent vasodilators in this study.

Nonetheless, in this study, nicotine did not cause a remarkable reduction in NO level. Even though the NO level in nicotine-treated rats was not substantially reduced, the nicotine group had a NO reduction trend. We used the whole aorta for the measurement of NO level without specifically isolating the endothelial layer. This factor might contribute to the non-remarkability of the results. Nevertheless, previous studies related to the effects of nicotine on NO level have shown

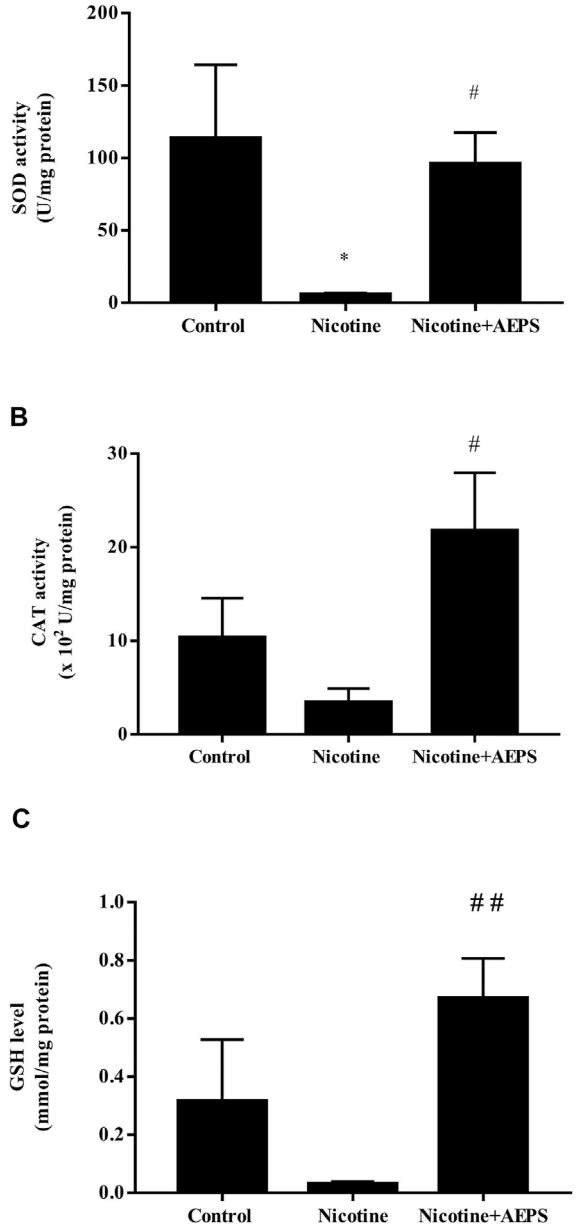

FIGURE 3 | Level of antioxidants **(A)** superoxide dismutase (SOD) activity **(B)** catalase (CAT) activity and **(C)** reduced glutathione (GSH) level in rat aortic tissues from each group. The values are given as mean ± SEM, n = 6–8 for each group. $^{*}p < 0.05$ compared with the control group, $^{\#}p < 0.05$, $^{\#\#}p < 0.01$ compared with the nicotine group.

various inconsistent results. A study showed that nicotine does not cause any change in NO (Moon et al., 2014). Another study showed that nicotine reduces NO level by deactivating eNOS and stimulating the generation of superoxide anions that degrade NO (Kathuria et al., 2013). By contrast, a previous study showed that nicotine increases NO levels by increasing intracellular calcium, which in turn activates eNOS to produce NO (Ijomone et al., 2014). These inconsistent results may be contributed by the difference in the availability of eNOS cofactors, such as BH_4 and NADPH, which are important for eNOS activity (Ugusman et al., 2010), as well as the oxidative degradation of NO by superoxide anion (Tonnessen et al., 2000).

In view of the relationship of nicotine with oxidative stress and NO level, which contributes to vascular endothelial dysfunction, SOD activity, CAT activity, and GSH levels in the aortic tissues were measured. The results showed that supplementation with AEPS enhanced SOD and CAT activities, as well as GSH level, in the aorta of nicotine-induced rats. This result suggests a protective effect of AEPS against oxidative stress induced by nicotine. The results align with previous findings that showed that AEPS enhances the mRNA expression of SOD, CAT, and glutathione peroxidase (GPX) in ECs exposed to H_2O_2 (Ugusman et al., 2011).

The results also demonstrated that nicotine decreased SOD activity, but no considerable differences in CAT activity and GSH level were found. Nicotine stimulates the production of superoxide anion by increasing the expression of NADPH oxidase 4 (NOX4) (Hua et al., 2010). NOX4 is the major source of superoxide anion in blood vessels (Ugusman et al., 2011). SOD is an antioxidant enzyme that acts as the first defense to neutralize superoxide anions into H_2O_2 (Zainalabidin et al., 2016). The excessive usage of SOD to neutralize the superoxide anions produced in response to nicotine has led to reduced SOD activity (Moon et al., 2014; Zainalabidin et al., 2014). Additionally, CAT transforms H_2O_2 to oxygen and water, whereas GSH is needed for GPX to convert H_2O_2 into water (Holben and Smith, 1999). In the present study, nicotine did not reduce the levels of CAT and GSH. This result is probably related to the action of SOD as the first antioxidant enzyme that neutralizes excessive free radicals before the actions of CAT and GSH start (Zainalabidin et al., 2016).

Collectively, this study showed that AEPS attenuates nicotine-induced vascular endothelial dysfunction by improving vasorelaxation and increasing vascular NO and antioxidant levels. The antioxidant activity of AEPS is often associated with its flavonoid content (Lee et al., 2014). Based on the LCMS analysis, the AEPS used in this study contains flavonoids, such as quercetin, naringenin, and vitexin (Sundar et al., 2019). Quercetin and naringenin are potent antioxidants that stimulate endothelial NO production (Yamamoto and Oue, 2006; Qin et al., 2016). Quercetin improves endothelium-dependent vasorelaxation by stimulating eNOS activity and increasing NO bioavailability in endothelial cells (Shen et al., 2012). Another flavonoid found in AEPS, naringenin, restores ACh-induced vasorelaxation in the aorta of diabetic rats. Naringenin reduces diabetic vascular endothelial dysfunction by downregulating oxidative stress and inflammation (Ren et al., 2016). In addition, vitexin improves aortic relaxation to ACh in chronic myocardial ischemia/reperfusion injury rat model (Che et al., 2016). Vitexin activates eNOS via the PI3K/Akt signaling pathway and can therefore regulate NO level (Cui et al., 2019). The present study used crude AEPS and not its purified active compound; thus, we were unable to pinpoint the specific compound of the extract that mediated the positive effects. However, the protective effects of AEPS on vascular

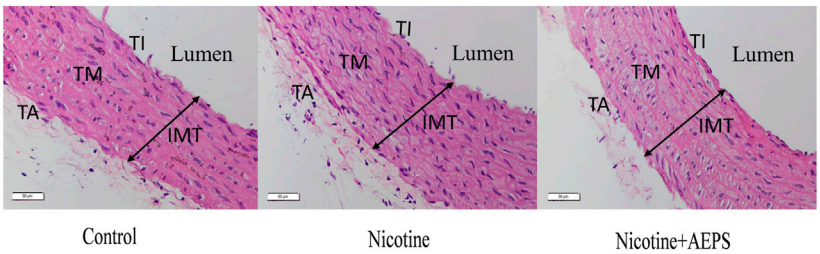

FIGURE 4 | Representative images of haematoxylin and eosin-stained sections of the aortic wall from each group of rats. Control and nicotine + AEPS groups showed normal histological appearance. The nicotine group displayed disorganized tunica media layer (*n* = 6-8 per group, ×400 magnification, scale bar: 50 μm). IMT, intima-media thickness; TI, tunica intima; TM, tunica media; TA, tunica adventitia.

TABLE 2 | Aortic morphometry measurements.

Groups	IMT (μm)	Lumen diameter (mm)	IMA (mm^2)	CWT ($\times 10^4$ dyne/cm)	TS ($\times 10^4$ dyne/cm^2)
Control	153.70 ± 6.12	0.78 ± 0.04	0.45 ± 0.02	4.48 ± 0.34	295.10 ± 27.75
Nicotine	170.00 ± 11.01	0.87 ± 0.03	0.59 ± 0.06	5.13 ± 0.27	310.00 ± 25.89
Nicotine + AEPS	152.80 ± 5.65	0.89 ± 0.03	0.50 ± 0.02	5.45 ± 0.26	361.50 ± 24.99

The values are given as mean ± SEM, n = *6–8 for each group. No significant difference was observed in any group.*
IMT, intima-media thickness; IMA, intima-media area; CWT, circumferential wall tension; TS, tensile stress.

endothelial dysfunction are probably mediated by the abovementioned potential flavonoids.

Apart from impaired vasorelaxation, abnormal vascular remodeling is one of the markers of chronic vascular dysfunction (Zainalabidin et al., 2014). AEPS treatment maintained the normal histological features of the aorta, whereas nicotine disorganized the tunica media layer and increased the interlamellar space. However, the morphometric analysis of the aorta showed no remarkable changes in all groups, even though IMT tend to increase in the nicotine group. The effect of nicotine on vascular remodeling is closely related to its dose and duration (Li et al., 2017). The i.p. injection of 0.6 mg/kg/day nicotine for 28 days causes an increment in IMT and CWT and a narrowing of the aortic lumen in rats (Zainalabidin et al., 2014). Nicotine infusion at 20 mg/kg/day for 40 days results in elastin fragmentation and increased stiffness in mouse aorta (Wagenhauser et al., 2018). The dose and duration of nicotine administration in this study were 0.8 mg/kg/day and 21 days, respectively. The duration of nicotine administration in this study is probably not long enough to cause remarkable structural changes in the aortic wall. Besides, we did not incorporate a special stain, such as the Verhoeff–van Gieson stain, to delineate the elastic fibers in the aortic wall for a better morphological assessment. This factor might also affect our morphometric analysis of the aorta.

Another limitation of this study is the absence of a treatment control group. This study reported the findings from three experimental groups, namely, control, nicotine, and nicotine + AEPS groups. A treatment control group that consists of AEPS alone should be included to affirm the safety and exclude any potential adverse effects of AEPS on healthy vasculature. Nonetheless, our previous studies that incorporated a treatment control group with AEPS alone showed no adverse effect on healthy vasculature in *in vitro* and *in vivo* levels. For instance, AEPS up to 300 μg/ml concentration did not reduce endothelial cell viability (Sundar et al., 2019). In rats, treatment with 500 mg/kg/day AEPS for 28 days did not cause any remarkable change in blood pressure (Alwi et al., 2018; Ugusman et al., 2020; Azmi et al., 2021). Besides, rat aorta displayed normal histology under light and electron microscopic examinations following AEPS treatment (Thent et al., 2012a; Thent et al., 2012b). Overall, previous studies showed that AEPS has no adverse effects on healthy vasculature.

CONCLUSION

P. sarmentosum attenuates nicotine-induced vascular endothelial dysfunction by enhancing vasorelaxation, vascular NO, and antioxidant levels. Thus, *P. sarmentosum* may be beneficial to prevent the vascular endothelial dysfunction caused by nicotine exposure. However, the molecular mechanism underlying the protective effect of *P. sarmentosum* on nicotine-induced vascular endothelial dysfunction needs further investigation. Furthermore, this study is an *in vivo* animal study that investigated some fundamental effects of AEPS on nicotine-induced vascular endothelial dysfunction. Further studies are required to identify and isolate the active compounds in AEPS responsible for the positive effects, as well as to explore their mechanisms of action. In addition, clinical trials that incorporate sufficient sample size and thorough methodology are needed to confirm our conclusions on the efficacy and safety of AEPS as a supplement for nicotine-induced vascular endothelial dysfunction in humans.

DATA AVAILABILITY STATEMENT

The original contributions presented in the study are included in the article/**Supplementary Material**, further inquiries can be directed to the corresponding author.

ETHICS STATEMENT

The animal study was reviewed and approved by Universiti Kebangsaan Malaysia Animal Ethics Committee.

AUTHOR CONTRIBUTIONS

Conceptualization, AA, AH, NS, and AU; methodology, MM, FJ, and AU; formal analysis, MM, FJ and AU; writing: original draft preparation, MM; writing: review and editing, AA, AH, NS, FJ, and AU.; supervision, AA, AH, NS, and AU; funding acquisition, AA, AH, NS, and AU. All authors read and approved the final manuscript.

FUNDING

This research was funded by Ministry of Higher Education Malaysia Fundamental Research Grant Scheme (FRGS/1/2019/SKK08/UKM/02/8) and Universiti Kebangsaan Malaysia Medical Centre Fundamental grant (FF-2018-403).

ACKNOWLEDGMENTS

The authors want to thank Datu Agasi Mohd Kamal, Firdaus Azmi, and all the medical lab technologists in Physiology Department, UKM, for their technical assistance. We also want to extend our gratitude to Satirah Zainal Abidin for her valuable input on the histological interpretation of the aorta.

SUPPLEMENTARY MATERIAL

The Supplementary Material for this article can be found online at: https://www.frontiersin.org/articles/10.3389/fphar.2021.667102/full#supplementary-material

REFERENCES

Aebi, H. (1984). *[13] Catalase* In Vitro. Amsterdam, Netherlands: Elsevier.

Aguilar, T. a. F., Navarro, B. C. H., and Perez, J. a. M. (2016). *Endogenous Antioxidants: A Review of Their Role in Oxidative Stress*. London, UK: IntechOpen. doi:10.5772/65715

Almabrouk, T. A. M., White, A. D., Ugusman, A. B., Skiba, D. S., Katwan, O. J., Alganga, H., et al. (2018). High Fat Diet Attenuates the Anticontractile Activity of Aortic PVAT via a Mechanism Involving AMPK and Reduced Adiponectin Secretion. *Front. Physiol.* 9, 1–14. doi:10.3389/fphys.2018.00051

Alwi, N. a. N. M., Zakaria, Z., Karim, A. a. H., Nordin, N. a. M. M., and Ugusman, A. (2018). Antihypertensive Effect of Piper Sarmentosum in L-NAME-Induced Hypertensive Rats. *Sains Malays*. 47, 2421–2428. doi:10.17576/jsm-2018-4710-18

Amran, A. A., Zakaria, Z., Othman, F., Das, S., Raj, S., and Nordin, N.-A. M. (2010). Aqueous Extract of Piper Sarmentosum Decreases Atherosclerotic Lesions in High Cholesterolemic Experimental Rabbits. *Lipids Health Dis.* 9, 44–46. doi:10.1186/1476-511X-9-44

Azmi, M. F., Aminuddin, A., Jamal, J. A., A Hamid, A., and Ugusman, A. (2021). Quantified Piper Sarmentosum Roxb. Leaves Aqueous Leaf Extract and its Antihypertensive Effect in Dexamethasone-Induced Hypertensive Rats. *Sains Malaysiana*. 50, 171–179. doi:10.17576/jsm-2021-5001-17

Beyer, W. F., and Fridovich, I. (1987). Assaying for Superoxide Dismutase Activity: Some Large Consequences of Minor Changes in Conditions. *Anal. Biochem.* 161, 559–566. doi:10.1016/0003-2697(87)90489-1

Bradford, M. M. (1976). A Rapid and Sensitive Method for the Quantitation of Microgram Quantities of Protein Utilizing the Principle of Protein-Dye Binding. *Anal. Biochem.* 72, 248–254. doi:10.1006/abio.1976.999910.1016/0003-2697(76)90527-3

Brüggmann, D., Lips, K. S., Pfeil, U., Haberberger, R. V., and Kummer, W. (2003). Rat Arteries Contain Multiple Nicotinic Acetylcholine Receptor α-subunits. *Life Sci.* 72, 2095–2099. doi:10.1016/s0024-3205(03)00067-5

Carnevale, R., Sciarretta, S., Violi, F., Nocella, C., Loffredo, L., Perri, L., et al. (2016). Acute Impact of Tobacco vs Electronic Cigarette Smoking on Oxidative Stress and Vascular Function. *Chest*. 150, 606–612. doi:10.1016/j.chest.2016.04.012

Che, X., Wang, X., Zhang, J., Peng, C., Zhen, Y., Shao, X., et al. (2016). Vitexin Exerts Cardioprotective Effect on Chronic Myocardial Ischemia/reperfusion Injury in Rats via Inhibiting Myocardial Apoptosis and Lipid Peroxidation. *Am. J. Transl Res.* 8, 3319–3328.

Cucina, A., Sapienza, P., Corvino, V., Borrelli, V., Mariani, V., Randone, B., et al. (2000). Nicotine-induced Smooth Muscle Cell Proliferation Is Mediated through bFGF and TGF-B1. *Surgery*. 127, 316–322. doi:10.1067/msy.2000.104249

Cui, Y.-h., Zhang, X.-q., Wang, N.-d., Zheng, M.-d., and Yan, J. (2019). Vitexin Protects against Ischemia/reperfusion-Induced Brain Endothelial Permeability. *Eur. J. Pharmacol.* 853, 210–219. doi:10.1016/j.ejphar.2019.03.015

Daiber, A., Steven, S., Weber, A., Shuvaev, V. V., Muzykantov, V. R., Laher, I., et al. (2017). Targeting Vascular (Endothelial) Dysfunction. *Br. J. Pharmacol.* 174, 1591–1619. doi:10.1111/bph.13517

Durand, M. J., and Gutterman, D. D. (2013). Diversity in Mechanisms of Endothelium-dependent Vasodilation in Health and Disease. *Microcirculation*. 20, 239–247. doi:10.1111/micc.12040

Ellman, G. L. (1959). Tissue Sulfhydryl Groups. *Arch. Biochem. Biophys.* 82, 70–77. doi:10.1016/0003-9861(59)90090-6

Förstermann, U., and Münzel, T. (2006). Endothelial Nitric Oxide Synthase in Vascular Disease: from Marvel to Menace. *Circulation*. 113, 1708–1714. doi:10.1161/CIRCULATIONAHA.105.602532

Hecht, S. S. (2003). Tobacco Carcinogens, Their Biomarkers and Tobacco-Induced Cancer. *Nat. Rev. Cancer* 3, 733–744. doi:10.1038/nrc1190

Holben, D. H., and Smith, A. M. (1999). The Diverse Role of Selenium within Selenoproteins. *J. Am. Diet. Assoc.* 99, 836–843. doi:10.1016/S0002-8223(99)00198-4

Hua, P., Feng, W., Ji, S., Raij, L., and Jaimes, E. A. (2010). Nicotine Worsens the Severity of Nephropathy in Diabetic Mice: Implications for the Progression of Kidney Disease in Smokers. *Am. J. Physiology-Renal Physiol.* 299, F732–F739. doi:10.1152/ajprenal.00293.2010

Ijomone, O. M., Olaibi, O. K., and Nwoha, P. U. (2014). Effects of Chronic Nicotine Administration on Body Weight, Food Intake and Nitric Oxide Concentration in Female and Male Rats. *Pathophysiology* 21, 185–190. doi:10.1016/j.pathophys.2014.08.003

Ismail, S. M., Chua, K. H., Aminuddin, A., and Ugusman, A. (2018). Piper Sarmentosum as an Antioxidant: A Systematic Review. *Sains Malaysiana*.

47, 2359–2368. doi:10.1016/j.jtumed.2018.01.00310.17576/jsm-2018-4710-12

Jiang, D.-J., Jia, S.-J., Yan, J., Zhou, Z., Yuan, Q., and Li, Y.-J. (2006). Involvement of DDAH/ADMA/NOS Pathway in Nicotine-Induced Endothelial Dysfunction. *Biochem. Biophysical Res. Commun.* 349, 683–693. doi:10.1016/j.bbrc.2006.08.115

Kathuria, S., Mahadevan, N., and Balakumar, P. (2013). Possible Involvement of PPARγ-Associated eNOS Signaling Activation in Rosuvastatin-Mediated Prevention of Nicotine-Induced Experimental Vascular Endothelial Abnormalities. *Mol. Cel Biochem.* 374, 61–72. doi:10.1007/s11010-012-1505-6

Lee, J. H., Cho, S., Paik, H. D., Choi, C. W., Nam, K. T., Hwang, S. G., et al. (2014). Investigation on Antibacterial and Antioxidant Activities, Phenolic and Flavonoid Contents of Some Thai Edible Plants as an Alternative for Antibiotics. *Asian Australas. J. Anim. Sci.* 27, 1461–1468. doi:10.5713/ajas.2013.13629

Li, J., Liu, S., Cao, G., Sun, Y., Chen, W., Dong, F., et al. (2018). Nicotine Induces Endothelial Dysfunction and Promotes Atherosclerosis via GTPCH1. *J. Cel Mol Med.* 22, 5406–5417. doi:10.1111/jcmm.13812

Li, W., Du, D.-Y., Liu, Y., Jiang, F., Zhang, P., and Li, Y.-T. (2017). Long-term Nicotine Exposure Induces Dysfunction of Mouse Endothelial Progenitor Cells. *Exp. Ther. Med.* 13, 85–90. doi:10.3892/etm.2016.3916

Mayhan, W. G., and Sharpe, G. M. (2002). Acute and Chronic Treatment with Nicotine Impairs Reactivity of Arterioles in Response to Activation of Potassium Channels. *J. Cardiovasc. Pharmacol.* 39, 695–703. doi:10.1097/00005344-200205000-00010

Moccia, F., Frost, C., Berra-Romani, R., Tanzi, F., and Adams, D. J. (2004). Expression and Function of Neuronal Nicotinic ACh Receptors in Rat Microvascular Endothelial Cells. *Am. J. Physiology-Heart Circulatory Physiol.* 286, H486–H491. doi:10.1152/ajpheart.00620.2003

Mohd Zainudin, M., Zakaria, Z., Megat Mohd Nordin, N. A., and Othman, F. (2013). Does Oral Ingestion ofPiper sarmentosumCause Toxicity in Experimental Animals? *Evidence-Based Complement. Altern. Med.* 2013, 1–9. doi:10.1155/2013/705950

Moon, H. K., Kang, P., Lee, H. S., Min, S. S., and Seol, G. H. (2014). Effects of 1,8-cineole on Hypertension Induced by Chronic Exposure to Nicotine in Rats. *J. Pharm. Pharmacol.* 66, 688–693. doi:10.1111/jphp.12195

Ng, M. K. C., Wu, J., Chang, E., Wang, B.-y., Katzenberg-Clark, R., Ishii-Watabe, A., et al. (2007). A central Role for Nicotinic Cholinergic Regulation of Growth Factor-Induced Endothelial Cell Migration. *Arterioscler Thromb Vasc Biol.* 27, 106–112. doi:10.1161/01.ATV.0000251517.98396.4a

Olfert, I. M., Devallance, E., Hoskinson, H., Branyan, K. W., Clayton, S., Pitzer, C. R., et al. (2018). Chronic Exposure to Electronic Cigarettes Results in Impaired Cardiovascular Function in Mice. *J. Appl. Physiol.* 124, 573–582. doi:10.1152/japplphysiol.00713.2017

Peungvicha, P., S. Thirawarapan, S., Temsiririrkkul, R., Watanabe, H., Kumar Prasain, J., and Kadota, S. (1998). Hypoglycemic Effect of the Water Extract of Piper Sarmentosum in Rats. *J. Ethnopharmacology.* 60, 27–32. doi:10.1016/s0378-8741(97)00127-x

Qin, W., Ren, B., Wang, S., Liang, S., He, B., Shi, X., et al. (2016). Apigenin and Naringenin Ameliorate PKCβII-Associated Endothelial Dysfunction via Regulating ROS/caspase-3 and NO Pathway in Endothelial Cells Exposed to High Glucose. *Vasc. Pharmacol.* 85, 39–49. doi:10.1016/j.vph.2016.07.006

Ren, B., Qin, W., Wu, F., Wang, S., Pan, C., Wang, L., et al. (2016). Apigenin and Naringenin Regulate Glucose and Lipid Metabolism, and Ameliorate Vascular Dysfunction in Type 2 Diabetic Rats. *Eur. J. Pharmacol.* 773, 13–23. doi:10.1016/j.ejphar.2016.01.002

Rodella, L. F., Rossini, C., Favero, G., Foglio, E., Loreto, C., and Rezzani, R. (2012). Nicotine-induced Morphological Changes in Rat Aorta: the Protective Role of Melatonin. *Cells Tissues Organs.* 195, 252–259. doi:10.1159/000324919

Sandoo, A., Veldhuijzen Van Zanten, J. J. C. S., Metsios, G. S., Carroll, D., and Kitas, G. D. (2010). The Endothelium and its Role in Regulating Vascular Tone. *Open Cardiovasc Med J.* 4, 302–312. doi:10.2174/1874192401004010302

Shen, Y., Croft, K. D., Hodgson, J. M., Kyle, R., Lee, I.-L. E., Wang, Y., et al. (2012). Quercetin and its Metabolites Improve Vessel Function by Inducing eNOS Activity via Phosphorylation of AMPK. *Biochem. Pharmacol.* 84, 1036–1044. doi:10.1016/j.bcp.2012.07.016

Si, L. Y.-N., Kamisah, Y., Ramalingam, A., Lim, Y. C., Budin, S. B., and Zainalabidin, S. (2017). Roselle Supplementation Prevents Nicotine-Induced Vascular Endothelial Dysfunction and Remodelling in Rats. *Appl. Physiol. Nutr. Metab.* 42, 765–772. doi:10.1139/apnm-2016-0506

Son, Y.-J., and Lee, H.-J. (2020). Association between Persistent Smoking after a Diagnosis of Heart Failure and Adverse Health Outcomes: A Systematic Review and Meta-Analysis. *Tob. Induc. Dis.* 18, 1–11. doi:10.18332/tid/116411

Su, Y. C., and Wang, D. X. (1991). Effects of Cigarette Smoking, Hypoxia and Vasoactive Mediators on the Production of PGI2 and TXA2 in Cultured Pulmonary Artery Endothelial Cells. *J. Tongji Med. Univ.* 11, 6–9. doi:10.1007/bf02893179

Sundar, U. M., Ugusman, A., Chua, H. K., Latip, J., and Aminuddin, A. (2019). Piper Sarmentosum Promotes Endothelial Nitric Oxide Production by Reducing Asymmetric Dimethylarginine in Tumor Necrosis Factor-α-Induced Human Umbilical Vein Endothelial Cells. *Front. Pharmacol.* 10, 1–14. doi:10.3389/fphar.2019.01033

Thent, Z. C., Lin, T. S., Das, S., and Zakaria, Z. (2012a). Histological Changes in the Heart and the Proximal Aorta in Experimental Diabetic Rats Fed with Piper Sarmentsoum. *Afr. J. Tradit Complement. Altern. Med.* 9, 396–404.

Thent, Z. C., Seong Lin, T., Das, S., and Zakaria, Z. (2012b). Effect ofPiper sarmentosumExtract on the Cardiovascular System of Diabetic Sprague-Dawley Rats: Electron Microscopic Study. *Evidence-Based Complement. Altern. Med.* 2012, 1–9. doi:10.1155/2012/628750

Toda, N., and Toda, H. (2010). Nitric Oxide-Mediated Blood Flow Regulation as Affected by Smoking and Nicotine. *Eur. J. Pharmacol.* 649, 1–13. doi:10.1016/j.ejphar.2010.09.042

Tonnessen, B. H., Severson, S. R., Hurt, R. D., and Miller, V. M. (2000). Modulation of Nitric-Oxide Synthase by Nicotine. *J. Pharmacol. Exp. Ther.* 295, 601–606.

Ugusman, A., Md Fadze, N. F., Hamid, A. A., Asmawi, Z., and Aminuddin, A. (2020). Piper Sarmentosum Attenuates Dexamethasone-Induced Hypertension by Stimulating Endothelial Nitric Oxide Synthase. *J. Res. Pharm.* 24, 1–9. doi:10.35333/jrp.2020.122

Ugusman, A., Zakaria, Z., Hui, C. K., and Megat Mohd Nordin, N. A. (2011). Piper Sarmentosum Inhibits ICAM-1 and Nox4 Gene Expression in Oxidative Stress-Induced Human Umbilical Vein Endothelial Cells. *BMC Complement. Altern. Med.* 11, 1–8. doi:10.1186/1472-6882-11-31

Ugusman, A., Zakaria, Z., Hui, C. K., and Nordin, N. A. M. M. (2010). Piper Sarmentosum Increases Nitric Oxide Production in Oxidative Stress: a Study on Human Umbilical Vein Endothelial Cells. *Clinics.* 65, 709–714. doi:10.1590/S1807-59322010000700010

Wagenhäuser, M. U., Schellinger, I. N., Yoshino, T., Toyama, K., Kayama, Y., Deng, A., et al. (2018). Chronic Nicotine Exposure Induces Murine Aortic Remodeling and Stiffness Segmentation-Implications for Abdominal Aortic Aneurysm Susceptibility. *Front. Physiol.* 9, 1–11. doi:10.3389/fphys.2018.01459

Wang, D. F., Zhou, L. L., Zhou, H. L., Hou, G. Y., Zhou, X., and Li, W. (2017). Effects ofPiper Sarmentosumextract on the Growth Performance, Antioxidant Capability and Immune Response in Weaned Piglets. *J. Anim. Physiol. Anim. Nutr.* 101, 105–112. doi:10.1111/jpn.12517

Whitehead, A. K., Erwin, A. P., and Yue, X. (2021). Nicotine and Vascular Dysfunction. *Acta Physiol.* 231, 1–13. doi:10.1111/apha.13631

World Health Organization (2019). *Tobacco* [Online].

Wright, J. L., Tai, H., and Churg, A. (2004). Cigarette Smoke Induces Persisting Increases of Vasoactive Mediators in Pulmonary Arteries. *Am. J. Respir. Cel Mol Biol* 31, 501–509. doi:10.1165/rcmb.2004-0051OC

Yamamoto, Y., and Oue, E. (2006). Antihypertensive Effect of Quercetin in Rats Fed with a High-Fat High-Sucrose Diet. *Biosci. Biotechnol. Biochem.* 70, 933–939. doi:10.1271/bbb.70.933

Yeo, E. T. Y., Wong, K. W. L., See, M. L., Wong, K. Y., Gan, S. Y., and Chan, E. W. L. (2018). Piper Sarmentosum Roxb. Confers Neuroprotection on Beta-Amyloid (Aβ)-Induced Microglia-Mediated Neuroinflammation and Attenuates Tau Hyperphosphorylation in SH-Sy5y Cells. *J. Ethnopharmacology* 217, 187–194. doi:10.1016/j.jep.2018.02.025

Zainalabidin, S., Budin, S. B., Ramalingam, A., and Lim, Y. C. (2014). Aortic Remodelling in Chronic Nicotine-Administered Rat. *Korean J. Physiol. Pharmacol.* 18, 411–418. doi:10.4196/kjpp.2014.18.5.411

Zainalabidin, S., Shahidin, S. N. F. S. N., and Budin, S. B. (2016). Hibiscus sabdariffa Linn.(Roselle) Protects against Nicotine-Induced Heart Damage in Rats. *Sains Malays* 45, 207–21.

Zainudin, M. M., Zakaria, Z., and Nordin, N. a. M. M. (2015). The Use of Piper Sarmentosum Leaves Aqueous Extract (Kadukmy™) as Antihypertensive Agent in Spontaneous Hypertensive Rats. *BMC Complement. Altern. Med.* 15, 1–10. doi:10.1186/s12906-015-0565-z

Conflict of Interest: The authors declare that the research was conducted in the absence of any commercial or financial relationships that could be construed as a potential conflict of interest.

GLOSSARY

ACh acetylcholine
AEPS aqueous extract of *Piper sarmentosum* Roxb. leaf
BH_4 tetrahydrobiopterin
BW body weight
CAT catalase
CVD cardiovascular diseases
CWT circumference wall tension
EC endothelial cell
EDTA ethylenediaminetetraacetic acid
eNOS endothelial nitric oxide synthase
GPX glutathione peroxidase
GSH reduced glutathione
H&E hematoxylin and eosin
H_2O_2 hydrogen peroxide
i.p. intraperitoneally
IMA intima-media area
IMT intima-media thickness
LCMS liquid chromatography mass spectrometry
MMP matrix metalloproteinase
mRNA messenger ribonucleic acid
MSBP mean systolic blood pressure
NAChR nicotinic acetylcholine receptor
NADPH nicotinamide adenine dinucleotide phosphate
NBT nitro blue tetrazolium
NO nitric oxide
NOX4 NADPH oxidase 4
p.o. oral gavage
PBS phosphate-buffered saline
R_{max} maximum relaxation
SEM standard error of the mean
SNP sodium nitroprusside
SOD superoxide dismutase
TS tensile stress
UKM Universiti Kebangsaan Malaysia
VSMC vascular smooth muscle cell
w/v weight/volume

frontiers in Pharmacology

ORIGINAL RESEARCH
published: 02 July 2021
doi: 10.3389/fphar.2021.685948

Extract of Seaweed *Codium fragile* Inhibits Integrin αIIbβ3-Induced Outside-in Signaling and Arterial Thrombosis

*Tae In Kim, Yeon-Ji Kim and Kyungho Kim**

Korean Medicine-Application Center, Korea Institute of Oriental Medicine, Daegu, South Korea

Seaweeds are thought to be promising candidates for functional foods and to help prevent thrombotic and related cardiovascular diseases. *Codium fragile* (Suringer) Hariot has been traditionally used as a culinary ingredient, and it possesses a range of biological activities, including the inhibition of platelet function. However, the mechanism of this inhibition is unclear. The aim of this study was to examine the inhibitory effect of *C. fragile* in platelet function. The antiplatelet activity of *C. fragile* on agonist-activated platelet aggregation, granule secretion, calcium mobilization, platelet spreading, and clot retraction was assessed. The phosphorylation of c-Src, Syk, PLCγ2, and several proteins involving in the αIIbβ3 integrin outside-in signaling pathway were also studied in thrombin and CRP-stimulated platelets. The antithrombotic effect was investigated in mice using ferric chloride-induced arterial thrombus formation *in vivo*. Transection tail bleeding time was used to evaluate whether *C. fragile* inhibited primary hemostasis. The main components and contents of *C. fragile* ethanol extract were confirmed by GC-MS analysis. *C. fragile* significantly impaired agonist-induced platelet aggregation granule secretion, calcium mobilization, platelet spreading, and clot retraction. Biochemical analysis revealed that *C. fragile* inhibited the agonist-induced activation of c-Src, Syk, and PLCγ2, as well as the phosphorylation of PI3K, AKT, and mitogen-activated protein kinases (MAPKs). The inhibitory effect of *C. fragile* resulted from an inhibition of platelet αIIbβ3 integrin outside-in signal transduction during cell activation. Oral administration of *C. fragile* efficiently blocked $FeCl_3$-induced arterial thrombus formation *in vivo* without prolonging bleeding time. GC-MS analysis revealed that phytol was the main constituent and the total content of isomers was 160.8 mg/kg. Our results demonstrated that *C. fragile* suppresses not only the inside-out

OPEN ACCESS

Edited by:
Mas Rizky A. A. Syamsunarno, Padjadjaran University, Indonesia

Reviewed by:
Ali H. Eid, Qatar University, Qatar
Carlos R. Pungitore, Consejo Nacional de Investigaciones Científicas y Técnicas (CONICET), Argentina

***Correspondence:**
Kyungho Kim
jk6012@kiom.re.kr

Specialty section:
This article was submitted to Ethnopharmacology, a section of the journal Frontiers in Pharmacology

Received: *26 March 2021*
Accepted: *11 June 2021*
Published: *02 July 2021*

Citation:
Kim TI, Kim Y-J and Kim K (2021) Extract of Seaweed Codium fragile *Inhibits Integrin αIIbβ3-Induced Outside-in Signaling and Arterial Thrombosis. Front. Pharmacol. 12:685948. doi: 10.3389/fphar.2021.685948*

Abbreviations: ACD, acid-citrate-dextrose solution; ADP, adenosine diphosphate; ATP, adenosine triphosphate; AKT, protein kinase B; ASA, acetylsalicylic acid; BW, body weight; c-Src, sarcoma tyrosine-protein kinase; CMC, carboxymethylcellulose; CRP, collagen-related peptide; DMSO, dimethyl sulfoxide; EGTA, ethylene glycol-bis(β-aminoethyl ether)-N,N,N′,N′-tetraacetic acid; ERK, extracellular signal-regulated kinase; FAK, focal adhesion kinase; FeCl3, ferric chloride; FG, fibrinogen; GC-MS, gas chromatography-mass spectrometry; MAPK, mitogen-activated protein kinase; PI3K, phosphoinositide 3-kinase; PLCγ2, phospholipase Cγ2; PRP, platelet-rich plasma; PPACK, d-Phe-Pro-Arg-chloromethyl ketone; RT, room temperature; SLP-76, SH2 domain-containing leukocyte protein of 76 kDa; Syk, spleen tyrosine kinase; Vav1, Proto-oncogene vav; U46619, thromboxane A2 analogue

signaling of αIIbβ3 integrin but also outside-in signal transmission. Therefore, *C. fragile* could be an effective antiplatelet therapeutic candidate.

Keywords: platelet, thrombosis, outside-in signaling, integrin αIIbβ3, codium fragile

INTRODUCTION

Platelets play crucial roles in thrombosis and hemostasis. Platelet integrin αIIbβ3 is a key mediator of platelet aggregation and is abundantly expressed on the platelet surface (Shen et al., 2013). In resting platelets, integrin αIIbβ3 is maintained in a low-affinity binding state, in which the extracellular domain of αIIbβ3 integrin is in a closed conformation. However, upon the activation of a platelet, αIIbβ3 undergoes a conformational change from a low-affinity state to a high-affinity ligand-binding state, in which it can bind ligands such as fibrinogen (FG) and von Willebrand factor (Takagi et al., 2002; Bennett, 2005; Li et al., 2010). Ligand binding to activated integrin αIIbβ3 induces a cascade of outside-in signaling events, thereby facilitating platelet spreading, aggregation, clot retraction, and thrombosis (Takagi et al., 2002; Gong et al., 2010).

Outside-in signaling *via* platelet integrin αIIbβ3 involves a wide range of enzymes, signaling adaptors, and cytoskeletal components (Estevez et al., 2015). The integrin αIIbβ3-induced platelet outside-in signaling pathway is initiated by members of the sarcoma tyrosine-protein kinase (c-Src) family of kinases (SFKs)-mediated phosphorylation events. Cellular and c-Src is associated with the cytoplasmic tail of β3 integrin and activated by the signaling cascades involved in the recruitment and activation of focal adhesion kinase (FAK), phosphoinositide 3-kinase (PI3K), and protein kinase B (AKT) (Arias-Salgado et al., 2003; Li et al., 2010; Durrant et al., 2017). Ligand binding to integrin αIIbβ3 also triggers the tyrosine phosphorylation of signaling cascades involved in the recruitment and activation of spleen tyrosine kinase (Syk), phospholipase Cγ2 (PLCγ2), and SH2 domain-containing leukocyte protein of 76 kDa (SLP-76), the proto-oncogene vav (Vav1), PI3K, and more, thereby initiating downstream platelet responses, such as granule secretion, platelet spreading, and clot retraction (Law et al., 1999; Phillips et al., 2001; Wonerow et al., 2003; Suzuki-Inoue et al., 2007b).

The ligand-binding function of integrin αIIbβ3 has been considered as a potential target for the development of antithrombotic agents (Estevez et al., 2015; Xu et al., 2016). However, current antithrombotic agents have significant side effects against thrombocytopenia and increase the risk of bleeding (Alexander and Peterson, 2010). These side effects limit the applicability and dosage of the antithrombotic agents, thereby restricting their effectiveness (Wang et al., 2014b; Xu et al., 2016). Recently, studies have suggested that selectively targeting the integrin αIIbβ3-induced platelet outside-in signaling pathway allows for strong inhibition of thrombosis without hemostasis (Estevez et al., 2015). The main advantage of targeting αIIbβ3 integrin-mediated platelet outside-in signaling is that intervention in this pathway does not affect primary platelet adhesion and aggregation, which are important for hemostasis, but limits the size of thrombus formation, which prevents vascular occlusion (Estevez et al., 2015). Thus, selective inhibitors of integrin outside-in signaling could be potential new antithrombotic drugs.

Cardiovascular disease (CVD) is the leading cause of global mortality and morbidity. There are several risk factors associated with CVD, including high cholesterol, diet, hypertension, atherosclerosis, and thrombosis (Falk, 2006; Saleh Al-Shehabi et al., 2016). The healing properties of natural products have long been identified as one of the most important strategies for treating and managing CVD (Al Disi et al., 2015; Shaito et al., 2020). Recently, the interest in natural products including medicinal herbs has been increased based on the effectiveness against CVD (Shaito et al., 2020). Due to the wide range of biological activities, natural products offer a promise to develop novel pharmacological agents that may prove promising in controlling CVD. Edible marine algae are considered to be good sources of nutrients, and the algae have diverse biological activities, including anti-inflammatory, anti-oxidative, anti-cancer, and anti-nociceptive effects (Wang et al., 2014a). *Codium fragile* (Suringer) Hariot is a heavily utilized edible green alga belonging to the family Codiaceae. The algae are widely distributed along the coasts of East Asia, Oceania, and Northern Europe. In Korea, *C. fragile* has been used as a culinary ingredient and traditional medicine to treat enterobiasis, dropsy, and dysuria (Lehnhardt Pires et al., 2013). Several studies have indicated a protective effect of *C. fragile* against pro-inflammatory stimuli, oxidative damage, and tumor progression in experimental models (Kang et al., 2012; Lee et al., 2013; Dilshara et al., 2016). Sterol-based compounds with varying bioactivities were identified as the main components of *C. fragile* extract (Rubinstein and John Goad, 1974; Lee et al., 2013). However, the protective effect and molecular mechanisms underlying the potential inhibitory effects of *C. fragile* on platelet thrombus formation have not been fully elucidated. Therefore, in the present study, we aimed to clarify whether *C. fragile* is involved in the attenuation of platelet function and integrin αIIbβ3 signaling and to identify which compounds produce antiplatelet activity in *C. fragile*.

In the present study, we found that extract of *C. fragile* inhibited thrombus formation *in vivo* and *in vitro*. *C. fragile* specifically inhibited platelet activation and aggregation induced by thrombin, collagen, collagen-related peptide (CRP), adenosine diphosphate (ADP), and U46619 (thromboxane A2 analogue). Using biochemical approaches, we found that the phosphorylation levels of the c-Src/Syk/PLCγ2/PI3K/AKT/MAPK axis were inhibited by treatment with *C. fragile*. GC-MS analysis was conducted to identify and quantify the main constituents of *C. fragile* extract. *C. fragile* inhibited platelet spreading on immobilized FG and clot retraction. These findings suggest that *C. fragile* regulates integrin αIIbβ3-mediated outside-in signaling by the inhibition of platelet activation. Studies using a mouse model of $FeCl_3$-induced arterial thrombosis indicated that *C. fragile* plays a crucial role in arterial thrombosis. The tail bleeding time was not significantly

higher in *C. fragile*-treated mice than in control mice. These results demonstrate that *C. fragile* can potentially exert antiplatelet and antithrombotic effects without affecting hemostasis.

MATERIALS AND METHODS

Reagents. Human thrombin, PGE1, rhodamine-phalloidin, dimethyl sulfoxide (DMSO), ADP, fibrinogen, human fibrinogen, ferric chloride ($FeCl_3$), Acetylsalicylic acid (ASA), and all the reagents were purchased from Sigma (St. Louis, MO, United States). Equine tendon collagen (type I) and ATP luciferin/luciferase reagent were obtained from Chrono-log (Havertown, PA). D-Phe-Pro-Arg-chloromethyl ketone (PPACK) was purchased from EMD Millipore (Billerica, MA, United States). CRP was obtained from Dr Richard Farndale (Department of Biochemistry, University of Cambridge, United Kingdom). Phycoerythrin (PE)-conjugated isotype control IgGs, rat monoclonal antibodies against mouse P-selectin, activated αIIbβ3 (JON/A) were from Emfret Analytics (Eibelstadt, Germany). Antibodies against phospho-c-Src at Tyr416, phospho-Syk at Tyr525/526, phospho-PLCγ2 at Tyr759, phospho-PLCγ2 at Tyr1217, phospho-PI3K p85α/β at Tyr458/p55α/γ at Tyr199, phospho-Akt at Ser473, phospho-p38 at Thr180/Tyr182, phospho-ERK at Thr202/Tyr204, phosphor-FAK at Tyr397, Total c-Src, Total Syk, Total PLCγ2, Total PI3K p85, Total Akt, Total p38, Total ERK, Total FAK, and actin were obtained from Cell Signaling (Danvers, MA, United States). Monoclonal antibodies against phospho-integrin β3 at Tyr 759 and Total integrin β3 were obtained from Santa Cruz (Santa Cruz, CA, United States). Calcium dye (FLIPR Calcium Assay kit) was from Molecular Devices (Sunnyvale, CA, United States). Phytol (a mixture of isomers) was purchased from Sigma (St. Louis, MO, United States). HPLC-grade methanol was obtained from JT Baker (Philipsburg, NJ, United States).

C. fragile preparation. The *C. fragile* was collected from the Wando Island coast of Korea, and its identity was confirmed by Dr Wei Li. A voucher specimen (KIOM-30) was deposited at the Herbarium of Korean Medicine-Application Center, Korea Institute of Oriental Medicine, Republic of Korea. The collected *C. fragile* was soaked in fresh water for a day to remove salt and dry at 65°C. The dried *C. fragile* (50.0 g) was pulverized and extracted with 1 L of 70% EtOH or 1 L of water at room temperature for 2 weeks. The filtrate was evaporated and freeze-dried (22.86 g, yield 45.7%) and the dry extract powder was stored at 4°C until used (**Supplementary Figure S1A**).

Instrumentation. The GC-MS analysis was conducted using the Shimadzu GC-MS-QP2010 Ultra system (GC–Gas Chromatograph GC-2010 Plus, Injector–AOC-20i, Autosampler–AOC-20s). Data acquisition and processing was used (GC-MS Real-Time Analysis).

Preparation of Standard and Sample Solutions. The *C. fragile* ethanol extract was dissolved in methanol (HPLC grade) using an ultrasonicator (JAC Ultrasonic JAC-3010) at 6 mg/ml concentration. After extraction, the solution was filtered with 0.2 μm membrane and the fraction of 1 μL filtrate was analyzed using GC-MS system. A standard curve of the phytol solution was prepared at 1 mg/ml (1,000 ppm) with methanol.

GC-MS analysis condition. GC-MS analysis was performed to identify of contents of phytol in *C. fragile*. GC-MS analysis was conducted using DB-5 column (30 mm × 0.25 mm × 0.25 μm). The carrier gas used helium gas (99.999%) eluted with a flow rate of 0.78 ml/min and the split ratio was 1:20. The injector temperature was set at 250°C, column oven programmed from 110°C (isothermal for 2 min), with an increasing rate of 10°C/min to 200°C, then 5°C/min to 280°C, finishing with a 9 min isothermal at 280°C. Ion source electron voltage with 70 eV and Ion source temperature was set was 280°C. Calibration curves, established by standard solution diluted with solvent at each concentration and the limits of detection (LOD) and quantification (LOQ) under the chromatographic conditions, were determined by injecting a series of standard solutions. Chromatograms of each sample were collected under the same condition.

Mice. Wild-type (WT, C57BL/6 strain, 6–8 weeks old, 18–22 g, BW) male mice were obtained from DooYeol Biotech (Seoul, Korea) and acclimated for 1 week. The WT mice were then divided randomly into four groups of five to ten animals each: 1) vehicle group (orally administrated 0.5% low-viscosity CMC), 2) low dose of *C. fragile* treated group (50 mg/kg, BW), 3) high dose of *C. fragile* treated group (100 mg/kg, BW), and 4) ASA treated group (100 mg/kg, BW). The mice were housed in a conventional animal facility with free access to food and water in a controlled temperature and humidity environment under a 12-h/12-h light/dark schedule. The animals were cared for in accordance with the dictates of the National Animal Welfare Law of Korea. The animal experiments (reference number #D-20–057) were approved by the Animal Care and Use Committee of the Korea Institute of Oriental Medicine (KIOM, Daegu, Korea) and performed in accordance with their guidelines.

Isolation of mouse blood platelets. Mouse blood was drawn from isoflurane-anesthetized WT (6–8 weeks old) mice from the inferior vena cava using a one-ninth volume of citrate-dextrose solution (ACD, Sigma). Mouse whole blood was centrifuged at 300 g for 20 min at room temperature (RT) to obtain platelet-rich plasma (PRP). The mouse and human PRP were collected and re-centrifuged at 700 g for 4 min in the presence of 0.5 μM PGE1. The platelet pellet was suspended in HEPES-Tyrode's buffer containing 10% ACD and centrifuged at 700 g for 5 min. The pellet was re-suspended in HEPES-Tyrode's buffer, and the final suspensions were adjusted to 3×10^8 platelets/ml.

Platelet aggregation and ATP secretion. The platelet aggregation assay was performed as previously described (Kim et al., 2018). Washed platelets were pre-incubated with 0.01% DMSO or various concentrations of *C. fragile* (30, 50, and 100 μg/ml) or ASA (30, 50, and 100 μM) for 10 min at 37°C and then stimulated with numerous agonists. Platelet aggregation was measured in a 4-channel platelet lumi-aggregometer (Chronolog Corp, Havertown, and PA) at 37°C with stirring at 1,000 rpm. Platelet secretion was monitored as ADP/ATP release by addition of luciferin/luciferase reagent (Chrono-log) to the platelet suspension. In some experiments, mouse platelets were incubated with *C. fragile* (100 μg/ml) prior to treatment with 2 mM EGTA for 10 min at 37°C. In some experiments, mouse platelets were incubated with 100 μg/ml of *C. fragile* aqueous

extract for 10 min at 37°C and then stimulated with 0.025 U/ml thrombin or 2 μg/ml Collagen.

TxB_2 generation assay. Washed platelets were pre-incubated with 0.01% DMSO or various concentrations of *C. fragile* (30, 50, and 100 μg/ml) or ASA (100 μM) for 10 min at 37°C and then stimulated with thrombin (0.025 U/ml) or CRP (0.2 μg/ml) in an aggregometer at 37°C with stirring (1,000 rpm). The reaction was stopped after 5 min by the addition of 2 mM EGTA containing 0.1 M KCl and 5 mM indomethacin for 10 min on ice. The mixture was then centrifuged at 6,000 g for 3 min, and the supernatant was stored at −80°C until analysis. Thromboxane B_2 (TxB_2) levels were measured using an enzyme-linked immunosorbent assay kit (Enzo Life Sciences, Farmingdale, NY) according to the manufacturer's protocol.

Flow cytometric analysis. Washed platelets were pre-incubated with 0.01% DMSO or various concentrations of *C. fragile* (30, 50, and 100 μg/ml) for 10 min at 37°C. Platelets were treated with thrombin (0.025 U/ml) or CRP (0.2 μg/ml) for 5 min at 37°C, followed by incubation with PE-conjugated antibodies against P-selectin or activated αIIbβ3 integrin (JON/A) for 15 min. Cells were analyzed by flow cytometry (Gallios, Beckman Coulter).

Ca^{2+} mobilization. Ca^{2+} mobilization was measured as previously described (Kim et al., 2018). Platelets (1×10^8/ml) were suspended in HEPES-Tyrode's buffer, pH 7.4 without $CaCl_2$ and treated with 0.01% DMSO or *C. fragile* (30, 50, and 100 μg/ml) or ASA (100 μM) for 10 min at 37°C. Cells were incubated with a Ca^{2+} dye (FLIPR Calcium five Assay kit) for 30 min at 37°C in the dark, followed by stimulation with thrombin (0.025 U/ml) or CRP (0.2 μg/ml). Cytosolic Ca^{2+} levels were measured using a spectrofluorometer (Spectramax I3, Molecular Devices) with an excitation wavelength of 485 nm and an emission wavelength of 525 nm Ca^{2+} mobilization was quantified by area under the curve (AUC) and expressed in relative fluorescence units.

Platelet spreading assay. Glass coverslips were coated with human fibrinogen (FG), 100 μg/ml, for 1 h at 37°C and then post-coated with 1% fatty acid-free BSA for 1 h at RT. Mouse platelets, 400 μL (2×10^7/ml), were incubated on the coverslip for 2 h at 37°C in the presence of 0.025 U/ml thrombin. After washing, adherent and spread platelets were fixed with 3% paraformaldehyde, permeabilized with 0.1% Triton X-100, blocked with 0.1% BSA, and stained with 0.1 μg/ml rhodamine-conjugated phalloidin (Sigma). Images were obtained using an Olympus microscope (IX73, Seocho, Seoul, Korea) equipped with 100 x/1.3 NA oil objective lens and recorded with a camera (Andor Zyla sCMOS). Care was taken to image a given fluorochrome at the same settings for all experimental permutations using MetaVue (version 7.8.3.0). Adherent and spreading platelets were monitored in an area of 0.006 mm^2 and counted in 10 separate fields. The surface area of spread platelets was measured as pixels using ImageJ (v1.52a).

Immunoblotting. Washed platelets were stimulated with thrombin (0.025 U/ml) or CRP (0.2 μg/ml) in the presence or absence of three different concentrations of *C. fragile* (30, 50, and 100 μg/ml) or ASA (100 μM) under stirring conditions (1,000 rpm) in an aggregometer. To measure kinase phosphorylation, platelets (6×10^8/ml) were lysed in an equal volume of 2 x ice-cold lysis buffer (TBS, pH 7.4, containing 2% Triton X-100, 0.1% SDS, 2 mM EDTA, 2 mM Na_3VO_4, phosphatase inhibitor cocktail, protease inhibitor cocktail, and 2 mM phenylmethylsulfonyl fluoride) and sonicated. An equal amount of protein (30 μg) was electrophoresed under reduced conditions and immunoblotted, followed by re-probing with different antibodies. In some experiment, spreading platelets were lysed in an equal volume of 2 x ice-cold lysis buffer (TBS, pH 7.4, containing 2% Triton X-100, 0.1% SDS, 2 mM EDTA, 2 mM Na_3VO_4, phosphatase inhibitor cocktail, protease inhibitor cocktail, and 2 mM phenylmethylsulfonyl fluoride) into reactions. The band density was measured by densitometry using ImageJ (v1.52a). The level of phosphorylation of each kinase was calculated via normalization of the density of antibodies against the phosphorylated kinases to that of the antibodies against total kinases.

$FeCl_3$-induced *in vivo* thrombosis. Mice (10 mice of each group) were orally administered 0.5% low-viscosity CMC and/or *C. fragile* (50 or 100 mg/kg, BW) or ASA (100 mg/kg, BW) twice a day for 3 days, with the administration occurring 30 min before the experiments on the third day. The left carotid artery was isolated, and then filter paper (2 mm diameter) soaked with 10% (460 mM) $FeCl_3$ was placed on top of the artery for 2 min. Blood flow was then monitored until 10 min after blood occlusion using a blood flowmeter (AD instruments, Blood flowmeter).

Tail bleeding time. Mice (10 mice of each group) were orally administered 0.5% low-viscosity CMC and/or *C. fragile* (50 or 100 mg/kg, BW) or ASA (100 mg/kg, BW) twice a day for 3 days, with the administration occurring 30 min before the experiments on the third day. Body temperature was maintained at 37°C using a heating pad. Using a sharp razor blade, 5 mm of the tail was removed and held in a 15 ml tube containing 13 ml of PBS prewarmed to 37°C. Tail bleeding was monitored and the time to cessation of blood flow was measured, and after 10 min the bleeding was stopped by cauterization. Blood loss was quantified by measuring the hemoglobin content of blood collected into 13 ml of PBS. After centrifugation, the pellet of red blood cells was lysed with 5 ml lysis buffer (8.3 g/L NH_4Cl, 1.0 g/L $KHCO_3$, and 0.037 g/L EDTA), and the absorbance of the sample was measured at 575 nm.

Statistical analysis. Data analysis was performed using GraphPad Prism 5. Statistical significance was assessed by ANOVA and Dunnett's test or Tukey's test for comparisons of multiple groups or Student's *t*-test for comparisons of two groups. A p value of less than 0.05 was considered significant.

RESULTS

Extract of *C. fragile* Inhibits Agonist-Induced Platelet Aggregation, ATP Secretion, and TxB_2 Generation

To investigate the effect of *C. fragile* on platelet function, we first examined platelet aggregation induced by various agonists, including thrombin, CRP, collagen, and ADP. We found that, compared to the vehicle control, platelets treated with *C. fragile*

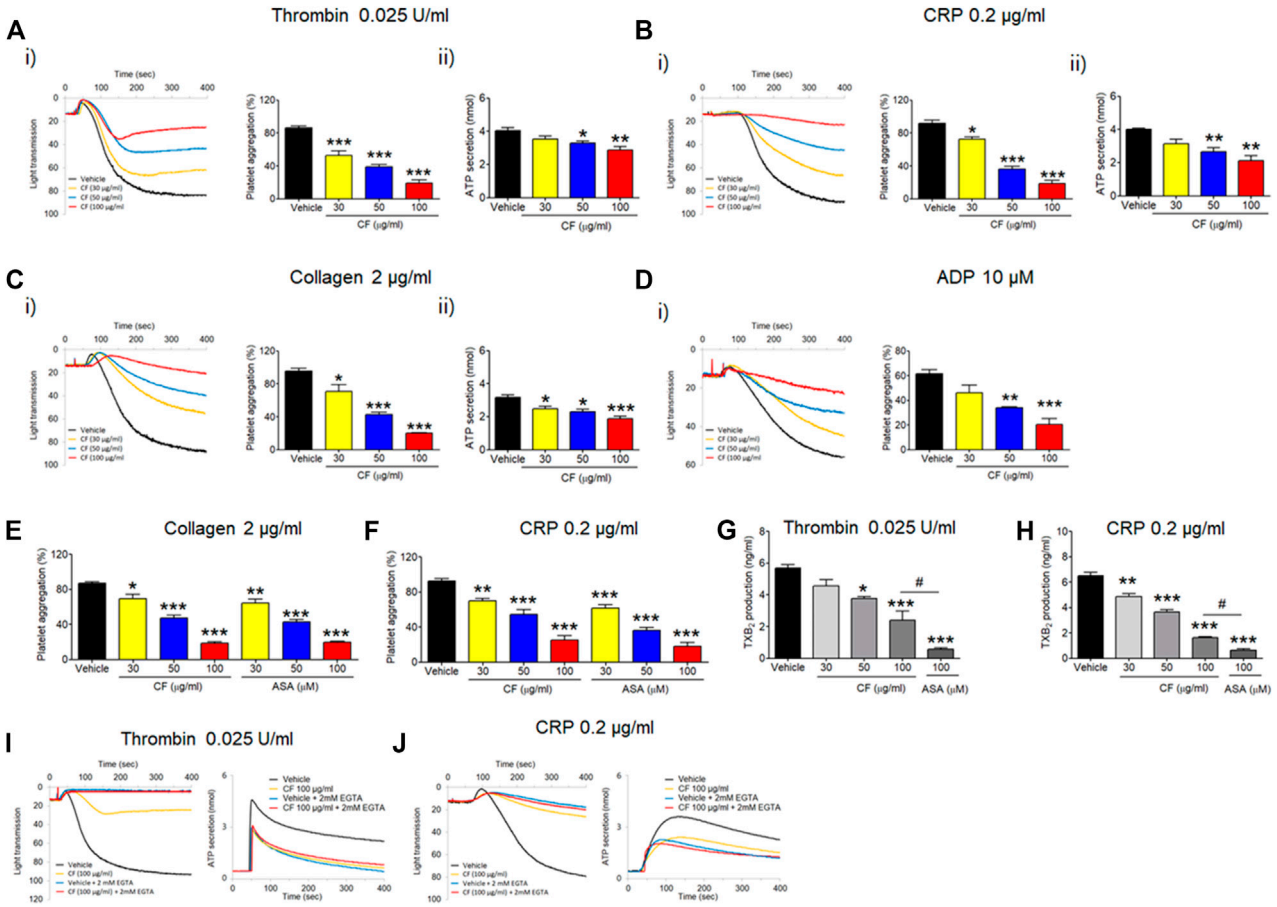

FIGURE 1 | Inhibitory effect of *C. fragile* on platelet aggregation, ATP secretion, and TxB2 production following stimulation with various agonists. Washed mouse platelets were preincubated with various concentrations of *C. fragile* (30, 50, and 100 μg/ml) for 10 min at 37°C and then stimulated with 0.025 U/ml Thrombin **(A)**, 0.2 μg/ml CRP **(B)**, 2 μg/ml Collagen **(C)**, and 10 μM ADP **(D)**. In the ADP-induced aggregation assay, 30 μg/ml of human FG was added to the platelet suspension before ADP stimulation. In some experiments, washed platelets were pretreated with *C. fragile* (30, 50, and 100 μg/ml) or ASA (30, 50, and 100 μM) and then stimulated with 2 μg/ml Collagen **(E)** and 0.2 μg/ml CRP **(F)**. Aggregation was measured for 5 min at 37°C under constant stirring (1,000 rpm) conditions in a platelet aggregometer (Chrono-Log). (i) Platelet aggregation and quantitative graphs. The effect of *C. Fragile* on T_XB2 generation was measured using a TXB2 ELISA assay kit **(G,H)**. In the ADP secretion, washed platelets were preincubated with various concentrations of *C. fragile* (30, 50, and 100 μg/ml) for 10 min at 37°C before adding a luciferin/luciferase reagent. After the luciferin/luciferase reagent added, platelets were stimulated with 0.025 U/ml Thrombin **(A)**, 0.2 μg/ml CRP **(B)**, and 2 μg/ml Collagen **(C)**. (ii) ATP secretion was measured using a luminometer. In other experiments, mouse platelets were preincubated with a high concentration of *C. fragile* (100 μg/ml) and activated with 0.025 U/ml Thrombin **(I)** and 0.2 μg/ml CRP **(J)** in the presence of 20 mM EGTA. Aggregation and ATP secretion were monitored with a platelet aggregometer. All data represent the mean ± SD (n = 5). *:p < 0.05, **:p < 0.01, and ***:p < 0.001 vs. vehicle control after ANOVA and Dunnett's test.

had significantly decreased platelet aggregation induced by the intermediated concentration of thrombin (≤0.025 U/ml), CRP (≤0.2 μg/ml), collagen (≤2 μg/ml), and ADP (≤10 μM), in a concentration-dependent manner (30, 50, and 100 μg/ml) (**Figures 1A–D, i**). The reduced aggregation of *C. fragile*-treated platelets was similar to the inhibition of platelet aggregation by acetylsalicylic acid (ASA; 30, 50, and 100 μM) in response to collagen (**Figure 1E**) and CRP (**Figure 1F**) stimulation. Further, aqueous extraction of *C. fragile* was also investigated to elucidate the inhibitory effect on platelet aggregation. We found that *C. fragile* aqueous extract did not show an inhibitory effect on platelet aggregation (**Supplementary Figure S1B**). To further confirm the effect of *C. fragile* on platelet function, we examined adenosine triphosphate (ATP) secretion. We observed that compared to the vehicle control, *C. fragile* treatment dose-dependently (30, 50, and 100 μg/ml) inhibited ATP secretion induced by thrombin (0.025 U/ml), CRP (0.2 μg/ml), and collagen (2 μg/ml) (**Figures 1A–C, ii**). We assessed TxB_2 generation after stimulation by thrombin (0.025 U/ml) and CRP (0.2 μg/ml). The levels of TxB_2 were dramatically elevated by both agonists, but treatment with *C. fragile* showed potent inhibition of agonist-induced TxB_2 generation (**Figures 1G,H**). These results suggest that *C. fragile* plays a crucial role in stimulating platelet aggregation, ATP secretion, and TxB_2 generation.

To further examine the way in which *C. fragile* regulates ATP secretion, *C. fragile*-pretreated mouse platelets were incubated with 2 mM ethylene glycol-bis(β-aminoethyl ether)-*N*,*N*,*N*′,*N*′-tetraacetic acid (EGTA) to prevent the interaction of FG with activated αIIbβ3 integrin and then stimulated with thrombin

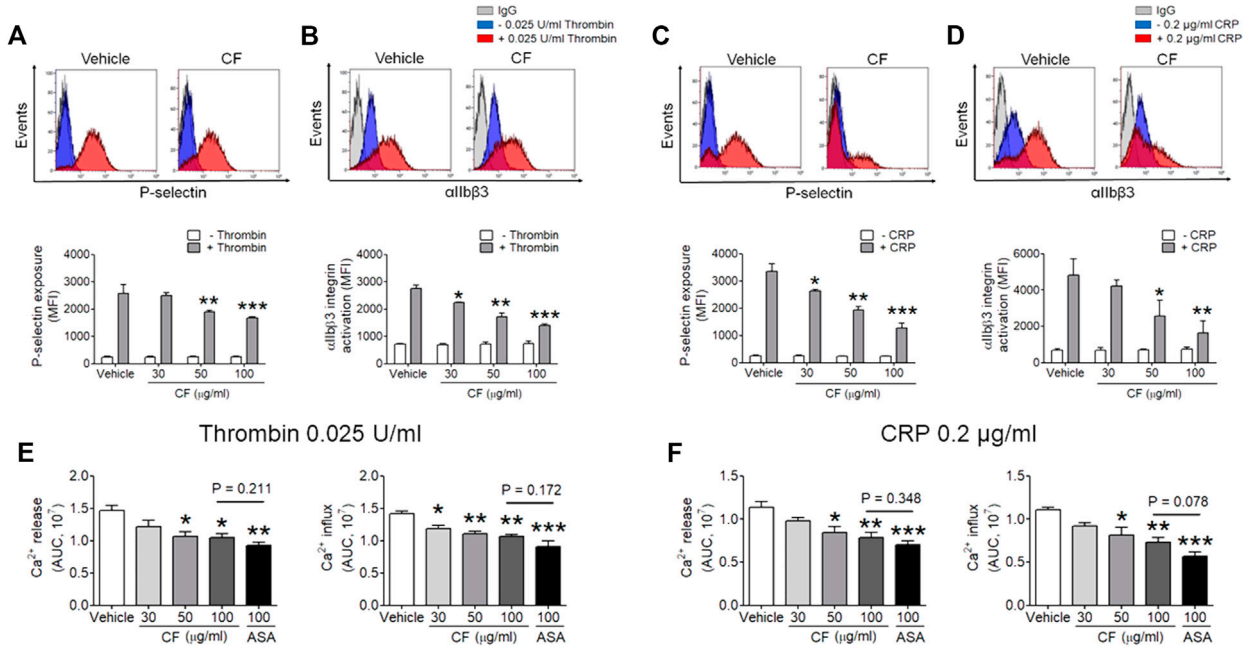

FIGURE 2 | Inhibitory effect of *C. fragile* on P-selectin exposure, αIIbβ3 integrin activation, and Ca^{2+} mobilization during platelet activation. Mouse platelets were pre-treated with the concentration of *C. fragile* (30, 50, and 100 μg/ml), and stimulated with 0.025 U/ml thrombin **(A,B)** or 0.2 μg/ml CRP **(C,D)**. P-selectin exposure and αIIbβ3 integrin activation were analyzed by flow cytometry as described in Methods. The binding of anti-activated αIIbβ3 (JON/A) and anti-P-selectin antibodies to platelets was calculated by the ratio of the geometric mean fluorescence intensity (MFI) value of antibodies to that of control IgG. Data represent mean ± SD ($n = 5$). *:$p < 0.05$, **:$p < 0.01$, and ***:$p < 0.001$ vs vehicle control after ANOVA and Dunnett's test. In Ca^{2+} mobilization assay, mouse platelets were resuspended in HEPES-Tyrode buffer without 1 mM $CaCl_2$ and preincubated with various concentration of *C. fragile* (30, 50, and 100 μg/ml) or ASA (100 μM) for 10 min at 37°C, and then incubated with a calcium-sensitive dye for 30 min at 37°C in the dark. After treatment with a Ca^{2+} dye, platelets were stimulated with platelets were stimulated with 0.025 U/ml Thrombin **(E)** and 0.2 μg/ml CRP **(F)** for 20 min and 2 mM $CaCl_2$ was then added for 20 min and 2 mM $CaCl_2$ was then added. Intracellular Ca^{2+} release and influx were measured and quantified by the AUC (arbitrary units). Data represent the mean ± SD ($n = 5$). *:$p < 0.05$, **:$p < 0.01$, and ***:$p < 0.001$ vs. vehicle control and a p value between two groups after ANOVA and Turkey's test.

(0.025 U/ml) and CRP (0.2 μg/ml). Neither the vehicle nor the *C. fragile-treated* platelets aggregated but released an equal amount of ATP (**Figures 1I,J**). Since ATP secretion is only derived from agonist-induced platelet activation in the presence of EGTA (Kim et al., 2013), these results suggest that *C. fragile* reduces the interaction of FG with activated αIIbβ3 integrin.

C. fragile Inhibits P-Selectin Exposure, αIIbβ3 Integrin Activation, and Ca^{2+} Mobilization During Cell Activation

Next, we sought to investigate whether *C. fragile* plays an important role in platelet activation. We assessed the contribution of *C. fragile* to P-selectin exposure, αIIbβ3 integrin activation, and Ca^{2+} mobilization during cell activation. Treatment with *C. fragile* (30, 50, and 100 μg/ml) significantly inhibited P-selectin exposure (**Figures 2A,C**), αIIbβ3 integrin activation (**Figures 2B,D**), and Ca^{2+} mobilization (**Figures 2E,F**) in response to thrombin (0.025 U/ml) and CRP (0.2 μg/ml) stimulation, in a dose-dependent manner. These results suggest that *C. fragile* plays an important role in regulating platelet activation through its effects on granule secretion, Ca^{2+} mobilization, and αIIbβ3 integrin activation.

Effects of *C. fragile* on Platelet Spreading and Clot Retraction Assay

Since *C. fragile* treatment regulated platelet aggregation and ATP secretion through the regulation of the activation of αIIbβ3 integrin, we further examined whether outside-in signaling events were affected by the treatment of *C. fragile* using platelet spreading assays. We found that compared to the vehicle control, *C. fragile* treatment dose-dependently (30, 50, and 100 μg/ml) prevented platelet spreading on immobilized FG (**Figure 3A**). Although the number of adherent platelets showed a moderate reduction following treatment with a low dose of *C. fragile*, it showed a significant reduction in high-dose *C. fragile* treatment (**Figures 3A–D**). The lamellipodial actin assembly and surface coverage were markedly reduced by *C. fragile* treatment in a concentration-dependent manner (**Figures 3B–D**). Platelet spreading and clot retraction assays reflect the processing of early and late-αIIbβ3 integrin outside-in signaling, respectively (Flevaris et al., 2007). The assessment derived from the earliest event of integrin αIIbβ3 mediated outside-in signaling displayed that the activated integrin such as integrin β3 phosphorylation was significantly suppressed by *C. fragile* treatment. Besides the inhibitory effect on FAK phosphorylation, *C. fragile* treatment also inhibited the outside-in signaling by negatively regulating the Src-AKT signaling pathways (**Figures 3G,H**). Further, we

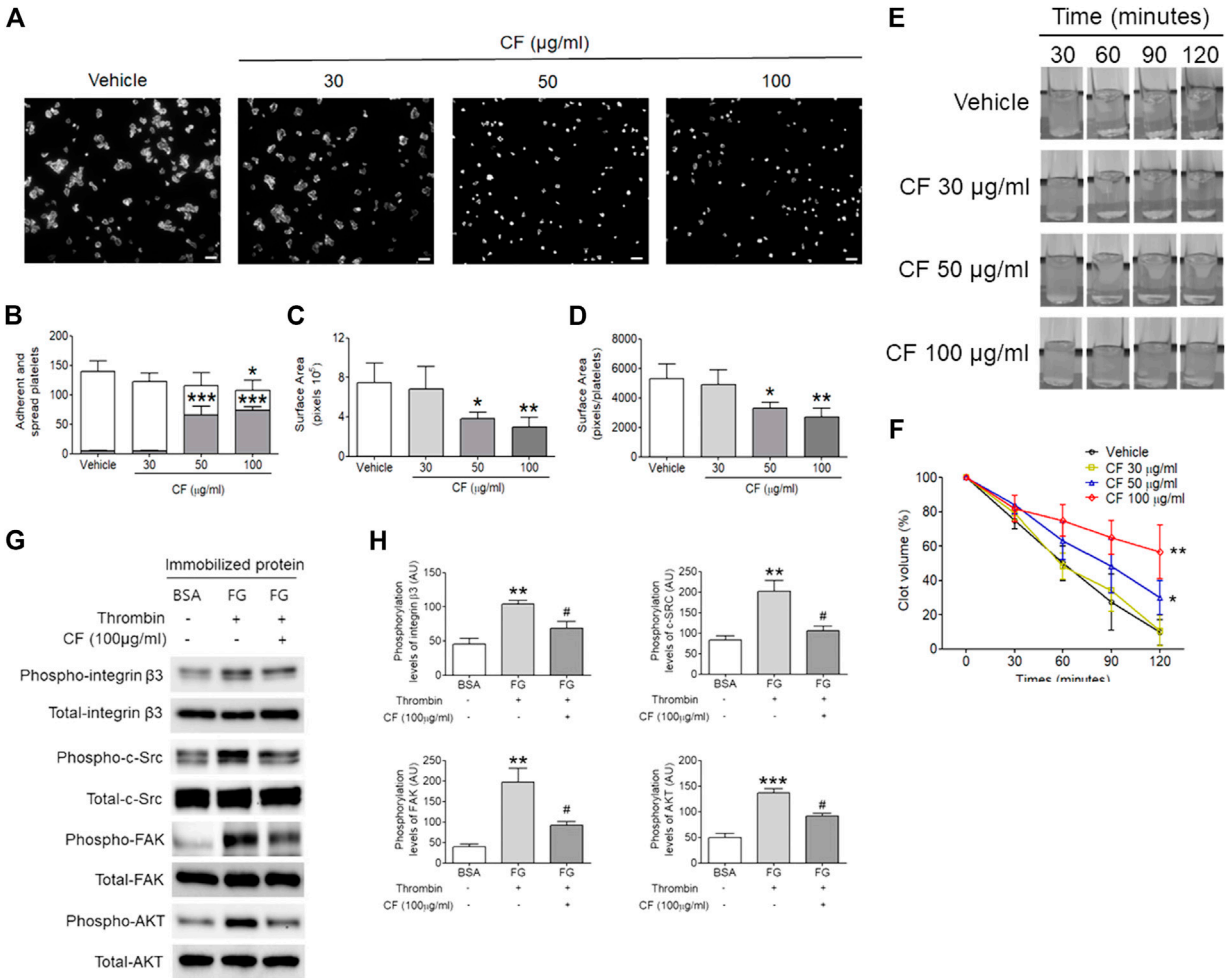

FIGURE 3 | *C. fragile* shows a defective αIIbβ3 integrin-dependent spreading on fibrinogen and fibrin clot retraction. Washed platelets pre-treated with various concentrations of *C. fragile* (30, 50, and 100 μg/ml) or vehicle control (0.01% DMSO) and incubated on FG-coated surfaces for 2 h at 37°C. Adherent and spread platelets were stained with rhodamine-conjugated phalloidin. **(A)** Representative images. Scale bars: 10 μm (white). **(B)** Number of adherents (but not spread, gray bars) and fully spread (white bars). Platelet spreading was analyzed by the surface area **(C)** which was measured by the number of pixels divided by the number of platelets **(D)** in the field. **(E,F)** Mouse platelets were incubated with various concentrations of *C. fragile* (30, 50, and 100 μg/ml) or vehicle control (0.01% DMSO) and fibrin clot retraction was assessed up to 2 h after addition of thrombin, fibrinogen, and $CaCl_2$. **(E)** Representative photographs and **(F)** summary data were presented. **(G,H)** The phosphorylation levels of integrin β3, c-Src, FAK, and AKT in lysed spreading platelet. *:$p < 0.05$, **:$p < 0.01$, and ***:$p < 0.001$ vs. vehicle control and #:$p < 0.05$ after ANOVA and Dunnett's test. Data represent mean ± SD ($n = 5$).

investigated the effect of *C. fragile* on clot retraction. Consistent with the ablated platelet spreading, *C. fragile* showed a significant impairment of clot retraction compared to vehicle control (**Figures 3E,F**). These results suggest that the effects of *C. fragile* are likely limited to early and late-αIIbβ3 integrin outside-in signaling and that these effects may occur through the regulation of the ligand-binding activity of αIIbβ3 integrin.

C. fragile Plays an Important Role in Regulating αIIbβ3 Integrin Outside-in Signaling

The activation of αIIbβ3 integrin outside-in signaling leads to the phosphorylation of Src, Syk, and PLCγ2 (Wonerow et al., 2003; Suzuki-Inoue et al., 2007a; Battram et al., 2017). Therefore, we measured the phosphorylation status of these signaling intermediates. Consistent with the defective platelet spreading and clot retraction, *C. fragile*-treated platelets exhibited a significant reduction of Src, Syk, and PLCγ2 phosphorylation following thrombin (**Figures 4A,B**) and CRP (**Figures 4C,D**) stimulation compared with that of vehicle control-treated platelets. These results demonstrated that *C. fragile* treatment has a specific role in the regulation of platelet functions involving the c-Src-Syk-PLCγ2 signaling pathway.

Members of the PI3K-AKT-mitogen-activated protein kinases (MAPK) family, p38, and extracellular signal-regulated kinase (ERK) have been reported to play a pivotal role in the integrin

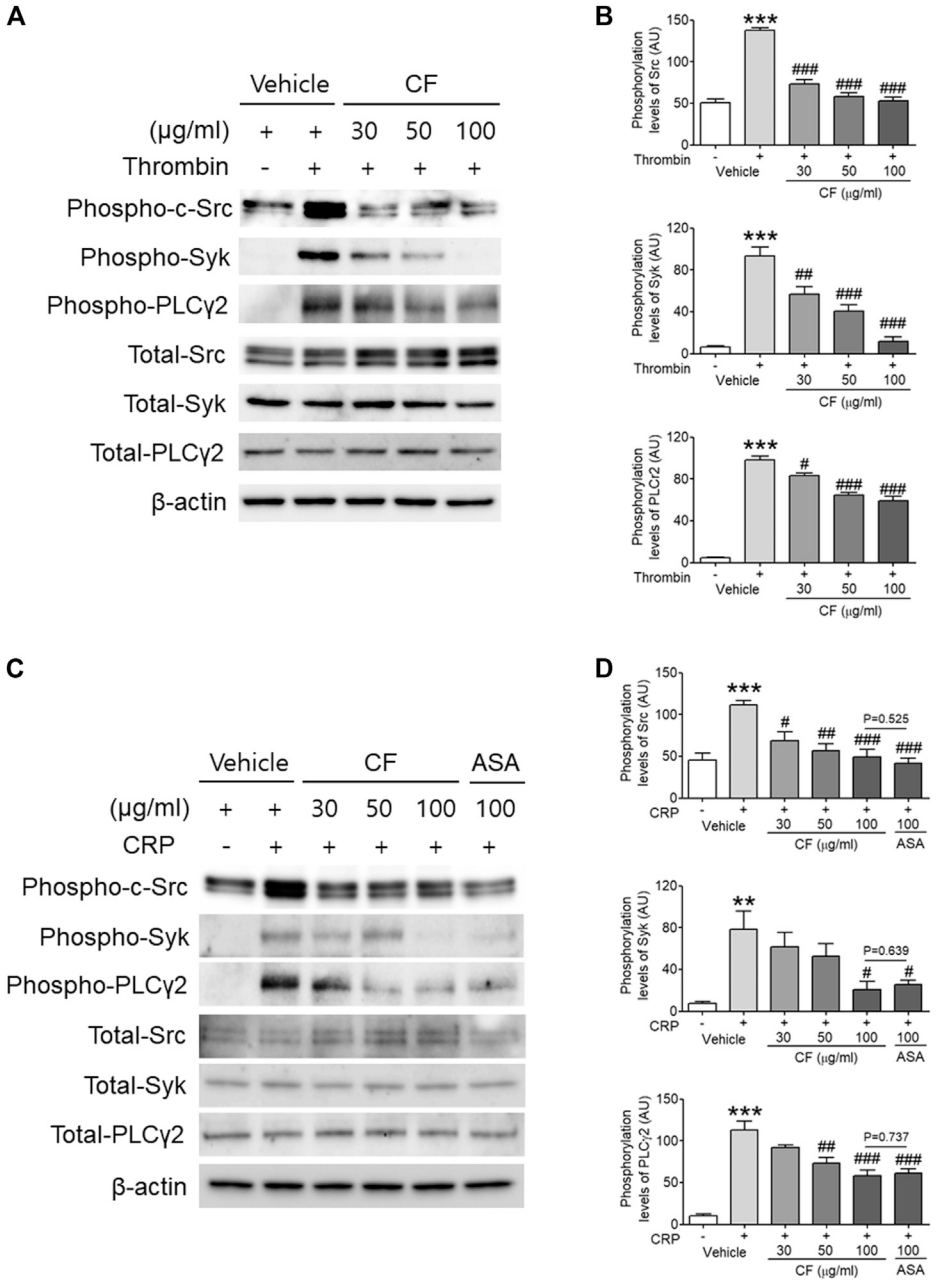

FIGURE 4 | *C. fragile* attenuated phosphorylation of c-Src, Syk, PLC*γ*2, PI3K, AKT, p38, and ERK after thrombin and CRP stimulation. Mouse platelets were pre-treated with various concentrations of *C. fragile* (30, 50, and 100 μg/ml), and stimulated with 0.025 U/ml Thrombin **(A,B)**. In some experiments, washed platelets were pretreated with *C. fragile* (30, 50, and 100 μg/ml) or ASA (100 μM) and then stimulated with 0.2 μg/ml CRP **(C–F)**. Equal amounts (30 μg) of cell lysate protein were immunoblotted to determine specific inhibition of c-Src, Syk, PLCr2, PI3K, AKT, p38, and ERK phosphorylation. Representative blots **(A,C,E)**. Quantitative graphs **(B,D,F)**. Data represent the mean ± SD ($n = 5$). **:$p < 0.01$ and ***:$p < 0.001$ vs. vehicle control (unstimulated) after Student's *t*-test, and. #:$p < 0.05$, ##:$p < 0.01$, and ###:$p < 0.001$ vs. vehicle control (stimulated) after ANOVA and Turkey's test.

outside-in signaling pathway (Watanabe et al., 2003; Flevaris et al., 2009). We, therefore, investigated the underlying molecular mechanism of the inhibitory effect of *C. fragile* on platelet activation. Biochemical analysis using platelet lysates indicated that compared with vehicle control, pretreatment of platelets with *C. fragile* significantly reduced the phosphorylation of PI3K, AKT, p38, and ERK following CRP stimulation (**Figures 4E,F**). These results suggested that *C. fragile* might function as a negative regulator of PI3K-AKT-MAPK signaling, to inhibit agonist-induced platelet activation. These findings support the hypothesis that *C. fragile* has a pivotal role in the regulation of platelet integrin αIIbβ3 outside-in signaling.

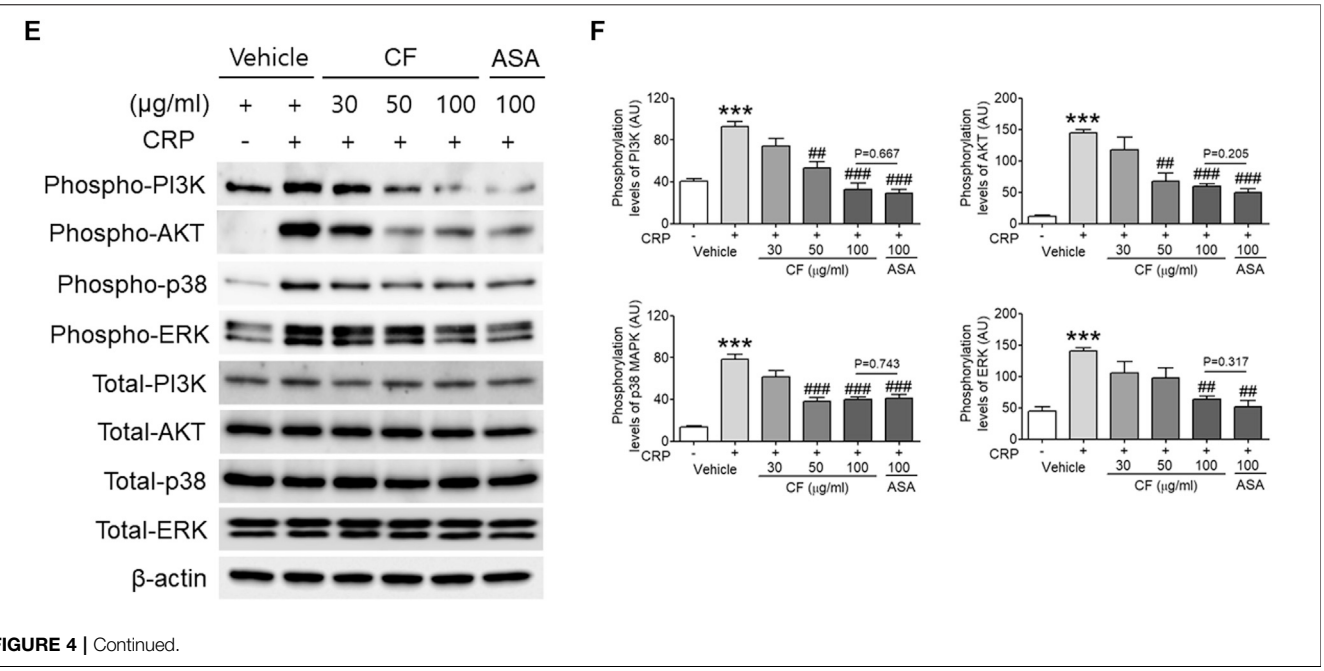

FIGURE 4 | Continued.

C. fragile Inhibits *in vivo* $FeCl_3$-Induced Thrombus Formation, but Not Hemostasis

The $FeCl_3$-induced vascular injury model has been widely used to study thrombogenesis (Eckly et al., 2011). We investigated whether treatment with *C. fragile* had an inhibitory effect on $FeCl_3$-induced thrombus formation. Thrombus formation was evaluated using 10% (460 mM) $FeCl_3$. The carotid artery occlusion time in the oral administration of *C. fragile* (50 and 100 mg/kg, body weight (BW)) was significantly prolonged compared to control (**Figure 5A**). The oral administration of *C. fragile* (100 mg/kg, BW) showed a blood flow prolongation close to that induced by the positive control (ASA, 100 mg/kg, BW). We investigated whether the oral administration of *C. fragile* (50 and 100 mg/kg, BW) influenced hemostatic function. We observed that tail bleeding times were similar between the *C. fragile*- and control-treated groups (**Figure 5B**). Blood collected from the site of amputation and quantified by hemoglobin content revealed no difference in blood loss between the *C. fragile*- and control-treated groups (**Figure 5B**). However, the oral administration of 100 mg/kg ASA led to a much longer bleeding time and increased hemoglobin content than that exhibited in the *C. fragile*-treated mice and the vehicle controls (**Figure 5B**). These results suggest that *C. fragile* inhibits $FeCl_3$-induced arterial thrombosis but not hemostasis *in vivo*.

Content Analysis of Phytol in *C. fragile* Ethanol Extract

The component of the phytol that contributed to the antiplatelet effect in *C. fragile* ethanol extract was determined using GC-MS analysis. Phytol-1 and phytol-2 were successively detected under the GC-MS conditions we described at 15.769 and 16.124 min, respectively, and were found in *C. fragile* ethanol extract at the same retention times, 15.777 and 16.128 min. However, it is not yet clear which peak was *trans*-phytol and which was *cis*-phytol (**Figures 6A,C**). The calibration curve was y = 10.52101x − 1,093.766, with a coefficient of determination of 0.9993 at injected concentrations of 100–5,000 μg/kg (**Figure 6B**). The total phytol isomer content was 160.8 mg/kg; it was one of the most abundant compounds in *C. fragile* ethanol extract.

DISCUSSION

Platelet-derived thrombus formation during vascular damage is the main cause of cardiovascular diseases such as myocardial infarction and ischemic stroke. Although antiplatelet drugs have been widely used in the treatment of thrombotic disorders, these have limited efficacy and concerns have been expressed about their safety (McFadyen et al., 2018). Hence, the development of new antiplatelet drugs is required for the improved treatment of thrombotic disorders. Marine algae could be good therapeutic agents because they are a source of natural derivatives and edible nutrients and a potential source of bioactive compounds, so the risk of adverse effects is reduced. However, few studies have reported on some marine algae and their probable antithrombotic effects (Trento et al., 2001). In the present study, therefore, we evaluated the antithrombotic properties of *Codium fragile* (Suringar) Hariot, which has been used as a therapeutic agent for its anti-inflammatory and antioxidant effects in traditional medicine (Lee et al., 2013; Dilshara et al., 2016). We demonstrated that treatment with *C. fragile* inhibits thrombus formation *in vivo* and *in vitro*. Platelet activation

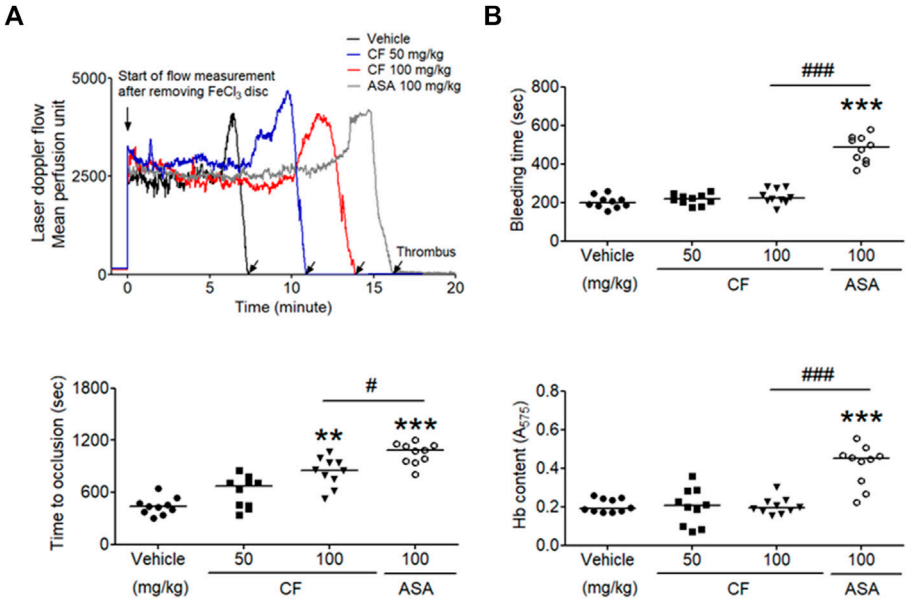

FIGURE 5 | *C. fragile* delayed $FeCl_3$ induced arterial thrombus formation but not hemostasis. $FeCl_3$-induced arterial thrombus formation was performed as described in Methods. After oral administration of 0.5% low-viscosity CMC and/or *C. fragile* (50 or 100 mg/kg, BW) or ASA (100 mg/kg, BW) twice a day for 3 days **(A)**, the mouse carotid artery was treated with 10% $FeCl_3$ for 2 min, and blood flow traces were monitored until stable occlusion took place. Horizontal bars represent the median occlusion time (n = 10). In the bleeding time assay, tails of the vehicle (circle), a low dose of *C. fragile* (50 mg/kg, square), a high dose of *C. fragile* (100 mg/kg, reverse triangle), and ASA (open circle) treated mice were amputated **(B)**, and the bleeding time and Hb content were monitored as described in Methods. Horizontal bars represent the median of occlusion and bleeding times for each group of animals (n = 10). **:p < 0.01 and ***:p < 0.001 vs. vehicle control and #:p < 0.05 and ###:p < 0.001 between two groups after ANOVA and Turkey's test.

and aggregation following stimulation with various agonists have been markedly reduced by treatment with *C. fragile*, in a dose-dependent manner. Thus, this study indicated an important role for *C. fragile* in platelet activation and aggregation.

Integrins are heterodimeric transmembrane proteins expressed on the cell surface. They act as adhesion receptors that trigger intracellular signaling pathways by binding extracellular ligands (Hynes, 2002). On the surface of platelets, integrin αIIbβ3 acts as a bidirectional receptor for inside-out and outside-in signaling and plays a pivotal role in initiating downstream signaling that triggers intracellular processes such as platelet spreading, adhesion, clot retraction, and aggregation, which leads to platelet thrombus formation and stabilization (Hynes, 2002; Huang et al., 2019). There is increasing evidence of the importance of αIIbβ3 integrin-mediated outside-in signaling in thrombotic disorders. The current understanding of thrombogenesis suggested that the inhibition of outside-in

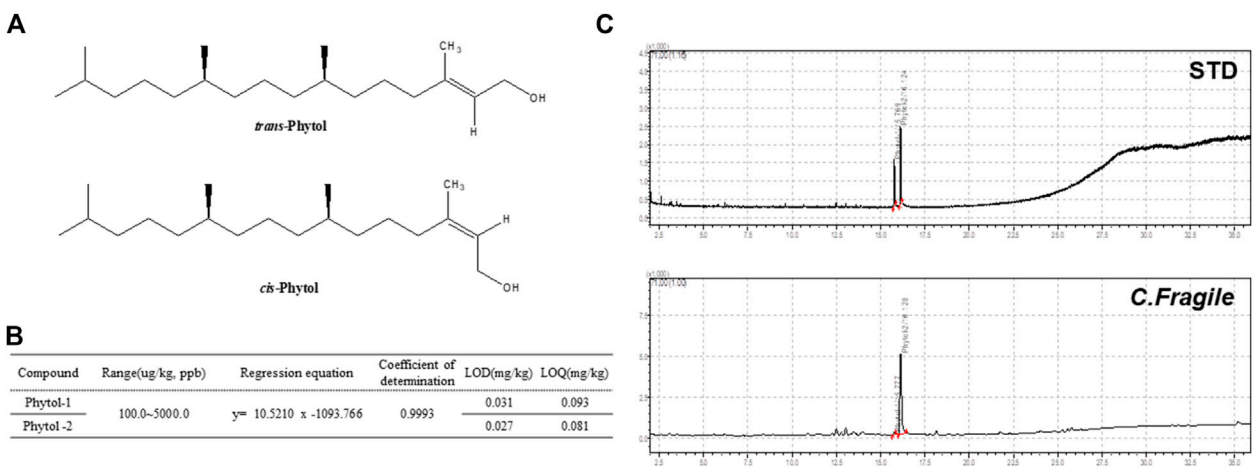

Compound	Range(ug/kg, ppb)	Regression equation	Coefficient of determination	LOD(mg/kg)	LOQ(mg/kg)
Phytol-1	100.0~5000.0	y= 10.5210 x -1093.766	0.9993	0.031	0.093
Phytol -2				0.027	0.081

FIGURE 6 | Analysis of *C. fragile* ethanol extract by using GC-MS **(A)** Structure of *trans*-phytol and *cis*-phytol. **(B)** Regression equations, LODs, and LOQs of phytol-1 and phytol-2. **(C)** GC-MS chromatogram of a mixture of phytol isomers standard and *C. fragile* ethanol extract.

signaling could be a valuable approach to the development of therapeutics with antiplatelet activities, without causing excessive hemorrhage (Shen et al., 2013; Estevez et al., 2015). Our study demonstrated that treatment with *C. fragile* downregulated integrin αIIbβ3 outside-in signaling, thus diminishing platelet spreading on immobilized FG and clot retraction, which may contribute to the effective inhibition of the development of thrombogenesis.

Due to the wide range of biological activities, natural products have long been used as one of the most important strategies for treating and preventing cardiovascular disease (Al Disi et al., 2015; Shaito et al., 2020). However, it is currently difficult to determine to what extent the *in vitro* effects produced can be extrapolated to the *in vivo* situation (Maaliki et al., 2019). In order to investigate, therefore, the effect of oral administration of *C. fragile* on thrombus formation, we used a mouse model of $FeCl_3$-induced arterial thrombosis, which has been widely used as an experimental arterial thrombosis model. *C. fragile* prevented thrombotic occlusion due to $FeCl_3$-induced artery injury. The tail bleeding time was not significantly higher in mice treated with *C. fragile* than in control mice. These results indicate that *C. fragile* can exert antiplatelet and antithrombotic effects without affecting hemostasis.

Although it is unclear how *C. fragile* regulates platelet responses to all agonists, this regulation is probably due to the different key components of *C. fragile*. In this study, we confirmed the content of the major compound in the extract using GC-MS analysis. Phytol was the major component in *C. fragile* extract, with content of 160.8 mg/kg. Phytol is one of the acyclic diterpene alcohols and is a precursor of a synthetic form of vitamin E. Vitamin E is a fat-soluble vitamin and has shown antiplatelet activity when used in conjunction with aspirin (Celestini et al., 2002). Therefore, we suggest that the antiplatelet activity of *C. fragile* ethanol extract was contributed by the high content of phytol in *C. fragile*. Extract of *C. fragile* has been shown to produce anticoagulant properties *via* the fibrinolytic activities of a biofunctional serine protease. Although it is not known which components of *C. fragile* are important for thrombolytic activity *in vitro* and *in vivo*, we speculate that most polyphenolic compounds might play important roles in platelet function. However, the synergy and additive effects of the individual components of *C. fragile* are still unclear. In order to study the pharmacological action of *C. fragile* and its interactions with different targets, a deeper understating of the pharmacokinetics and efficacy of the key components of *C. fragile* is necessary.

In conclusion, our study found that *C. fragile* effectively attenuated platelet activation and thrombus formation by downregulating αIIbβ3 signaling, without affecting hemostasis. Therefore, it may have the potential to be an antithrombotic agent for the treatment of arterial thrombotic disorders and the prevention of thrombotic diseases.

DATA AVAILABILITY STATEMENT

The raw data supporting the conclusion of this article will be made available by the authors, without undue reservation.

ETHICS STATEMENT

The animal study was reviewed and approved by the study was conducted in strict accordance with the recommendations in the Guide for the Care and Use of Laboratory Animals from the National Animal Welfare Law of Korea. All animal operations in this study were approved by the Ethics Committee of the Korea Institute of Oriental Medicine. All animal operations in this study were conducted according to the guidelines of the Animal Management Committee of the Korea Institute of Oriental Medicine.

AUTHOR CONTRIBUTIONS

TK: designed and performed research, collected and analyzed data, and wrote the manuscript; YK: performed research, provided important data; KK: initiated and designed research, analyzed data, and wrote the manuscript; all authors reviewed the manuscript.

FUNDING

This work has been supported by Grant NRN2011120 awarded to Korea Institute of Marine Science and Technology Promotion from the Ministry of Oceans and Fisheries, Republic of Korea. This work has been supported by Grant 20200219 awarded to Korea Institute of Marine Science and Technology Promotion from the Ministry of Oceans and Fisheries, and Grant KSN2021230 awarded to Korea Institute of Oriental Medicine (KIOM) from Ministry of Science and ICT, Republic of Korea.

SUPPLEMENTARY MATERIAL

The Supplementary Material for this article can be found online at: https://www.frontiersin.org/articles/10.3389/fphar.2021.685948/full#supplementary-material

REFERENCES

Al Disi, S. S., Anwar, M. A., and Eid, A. H. (2015). Anti-hypertensive Herbs and Their Mechanisms of Action: Part I. *Front. Pharmacol.* 6, 323. doi:10.3389/fphar.2015.00323

Alexander, K. P., and Peterson, E. D. (2010). Minimizing the Risks of Anticoagulants and Platelet Inhibitors. *Circulation* 121, 1960–1970. doi:10.1161/circulationaha.109.853135

Arias-Salgado, E. G., Lizano, S., Sarkar, S., Brugge, J. S., Ginsberg, M. H., and Shattil, S. J. (2003). Src Kinase Activation by Direct Interaction with the Integrin Cytoplasmic Domain. *Proc. Natl. Acad. Sci.* 100, 13298–13302. doi:10.1073/pnas.2336149100

Battram, A. M., Durrant, T. N., Agbani, E. O., Heesom, K. J., Paul, D. S., Piatt, R., et al. (2017). The Phosphatidylinositol 3,4,5-trisphosphate (PI(3,4,5)P3) Binder Rasa3 Regulates Phosphoinositide 3-kinase (PI3K)-dependent Integrin αIIbβ3 Outside-In Signaling. *J. Biol. Chem.* 292, 1691–1704. doi:10.1074/jbc.m116.746867

Bennett, J. S. (2005). Structure and Function of the Platelet Integrin IIb 3. *J. Clin. Invest.* 115, 3363–3369. doi:10.1172/jci26989

Celestini, A., Pulcinelli, F. M., Pignatelli, P., Lenti, L., Frati, G., Gazzaniga, P. P., et al. (2002). Vitamin E Potentiates the Antiplatelet Activity of Aspirin in Collagen-Stimulated Platelets. *Haematologica* 87, 420–426.

Dilshara, M. G., Jayasooriya, R. G. P. T., Kang, C.-H., Choi, Y.-H., and Kim, G.-Y. (2016). Methanol Extract of Codium Fragile Inhibits Tumor Necrosis Factor-α-Induced Matrix Metalloproteinase-9 and Invasiveness of MDA-MB-231 Cells by Suppressing Nuclear Factor-Kb Activation. *Asian Pac. J. Trop. Med.* 9, 535–541. doi:10.1016/j.apjtm.2016.04.010

Durrant, T. N., Van Den Bosch, M. T., and Hers, I. (2017). Integrin αIIbβ3 Outside-In Signaling. *Blood* 130, 1607–1619. doi:10.1182/blood-2017-03-773614

Eckly, A., Hechler, B., Freund, M., Zerr, M., Cazenave, J.-P., Lanza, F., et al. (2011). Mechanisms Underlying FeCl3-Induced Arterial Thrombosis. *J. Thromb. Haemost.* 9, 779–789. doi:10.1111/j.1538-7836.2011.04218.x

Estevez, B., Shen, B., and Du, X. (2015). Targeting Integrin and Integrin Signaling in Treating Thrombosis. *Arterioscler Thromb. Vasc. Biol.* 35, 24–29. doi:10.1161/atvbaha.114.303411

Falk, E. (2006). Pathogenesis of Atherosclerosis. *J. Am. Coll. Cardiol.* 47, C7–C12. doi:10.1016/j.jacc.2005.09.068

Flevaris, P., Li, Z., Zhang, G., Zheng, Y., Liu, J., and Du, X. (2009). Two Distinct Roles of Mitogen-Activated Protein Kinases in Platelets and a Novel Rac1-MAPK-dependent Integrin Outside-In Retractile Signaling Pathway. *Blood* 113, 893–901. doi:10.1182/blood-2008-05-155978

Flevaris, P., Stojanovic, A., Gong, H., Chishti, A., Welch, E., and Du, X. (2007). A Molecular Switch that Controls Cell Spreading and Retraction. *J. Cel Biol* 179, 553–565. doi:10.1083/jcb.200703185

Gong, H., Shen, B., Flevaris, P., Chow, C., Lam, S. C.-T., Voyno-Yasenetskaya, T. A., et al. (2010). G Protein Subunit G 13 Binds to Integrin IIb 3 and Mediates Integrin "Outside-In" Signaling. *Science* 327, 340–343. doi:10.1126/science.1174779

Huang, J., Li, X., Shi, X., Zhu, M., Wang, J., Huang, S., et al. (2019). Platelet Integrin αIIbβ3: Signal Transduction, Regulation, and its Therapeutic Targeting. *J. Hematol. Oncol.* 12, 26. doi:10.1186/s13045-019-0709-6

Hynes, R. O. (2002). Integrins. *Cell* 110, 673–687. doi:10.1016/s0092-8674(02)00971-6

Kang, C.-H., Choi, Y. H., Park, S.-Y., and Kim, G.-Y. (2012). Anti-inflammatory Effects of Methanol Extract of Codium Fragile in Lipopolysaccharide-Stimulated RAW 264.7 Cells. *J. Med. Food* 15, 44–50. doi:10.1089/jmf.2010.1540

Kim, K., Do, H. J., Oh, T. W., Kim, K. Y., Kim, T. H., Ma, J. Y., et al. (2018). Antiplatelet and Antithrombotic Activity of a Traditional Medicine, Hwangryunhaedok-Tang. *Front. Pharmacol.* 9, 1502. doi:10.3389/fphar.2018.00723

Kim, K., Hahm, E., Li, J., Holbrook, L.-M., Sasikumar, P., Stanley, R. G., et al. (2013). Platelet Protein Disulfide Isomerase Is Required for Thrombus Formation but Not for Hemostasis in Mice. *Blood* 122, 1052–1061. doi:10.1182/blood-2013-03-492504

Law, D. A., Deguzman, F. R., Heiser, P., Ministri-Madrid, K., Killeen, N., and Phillips, D. R. (1999). Integrin Cytoplasmic Tyrosine Motif Is Required for Outside-In αIIbβ3 Signalling and Platelet Function. *Nature* 401, 808–811. doi:10.1038/44599

Lee, C., Park, G. H., Ahn, E. M., Kim, B.-A., Park, C.-I., and Jang, J.-H. (2013). Protective Effect of Codium Fragile against UVB-Induced Pro-inflammatory and Oxidative Damages in HaCaT Cells and BALB/c Mice. *Fitoterapia* 86, 54–63. doi:10.1016/j.fitote.2013.01.020

Lehnhardt Pires, C., Rodrigues, S., Bristot, D., Gaeta, H., De Oliveira Toyama, D., Lobo Farias, W., et al. (2013). Evaluation of Macroalgae Sulfated Polysaccharides on the Leishmania (L.) Amazonensis Promastigote. *Mar. Drugs* 11, 934–943. doi:10.3390/md11030934

Li, Z., Delaney, M. K., O'brien, K. A., and Du, X. (2010). Signaling during Platelet Adhesion and Activation. *Atvb* 30, 2341–2349. doi:10.1161/atvbaha.110.207522

Maaliki, D., Shaito, A. A., Pintus, G., El-Yazbi, A., and Eid, A. H. (2019). Flavonoids in Hypertension: a Brief Review of the Underlying Mechanisms. *Curr. Opin. Pharmacol.* 45, 57–65. doi:10.1016/j.coph.2019.04.014

Mcfadyen, J. D., Schaff, M., and Peter, K. (2018). Current and Future Antiplatelet Therapies: Emphasis on Preserving Haemostasis. *Nat. Rev. Cardiol.* 15, 181–191. doi:10.1038/nrcardio.2017.206

Phillips, D. R., Nannizzi-Alaimo, L., and Prasad, K. S. (2001). Beta3 Tyrosine Phosphorylation in αIIbβ3 (Platelet Membrane GP IIb-IIIa) Outside-In Integrin Signaling. *Thromb. Haemost.* 86, 246–258.

Rubinstein, I., and John Goad, L. (1974). Sterols of the Siphonous marine Alga Codium Fragile. *Phytochemistry* 13, 481–484. doi:10.1016/s0031-9422(00)91238-x

Saleh Al-Shehabi, T., Iratni, R., and Eid, A. H. (2016). Anti-atherosclerotic Plants Which Modulate the Phenotype of Vascular Smooth Muscle Cells. *Phytomedicine* 23, 1068–1081. doi:10.1016/j.phymed.2015.10.016

Shaito, A., Thuan, D. T. B., Phu, H. T., Nguyen, T. H. D., Hasan, H., Halabi, S., et al. (2020). Herbal Medicine for Cardiovascular Diseases: Efficacy, Mechanisms, and Safety. *Front. Pharmacol.* 11, 422. doi:10.3389/fphar.2020.00422

Shen, B., Zhao, X., O'Brien, K. A., Stojanovic-Terpo, A., Delaney, M. K., Kim, K., et al. (2013). A Directional Switch of Integrin Signalling and a New Anti-thrombotic Strategy. *Nature* 503, 131–135. doi:10.1038/nature12613

Suzuki-Inoue, K., Hughes, C. E., Inoue, O., Kaneko, M., Cuyun-Lira, O., Takafuta, T., et al. (2007a). Involvement of Src Kinases and PLCγ2 in Clot Retraction. *Thromb. Res.* 120, 251–258. doi:10.1016/j.thromres.2006.09.003

Suzuki-Inoue, K., Kato, Y., Inoue, O., Kaneko, M. K., Mishima, K., Yatomi, Y., et al. (2007b). Involvement of the Snake Toxin Receptor CLEC-2, in Podoplanin-Mediated Platelet Activation, by Cancer Cells. *J. Biol. Chem.* 282, 25993–26001. doi:10.1074/jbc.m702327200

Takagi, J., Petre, B. M., Walz, T., and Springer, T. A. (2002). Global Conformational Rearrangements in Integrin Extracellular Domains in Outside-In and Inside-Out Signaling. *Cell* 110, 599–611. doi:10.1016/s0092-8674(02)00935-2

Trento, F., Cattaneo, F., Pescador, R., Porta, R., and Ferro, L. (2001). Antithrombin Activity of an Algal Polysaccharide. *Thromb. Res.* 102, 457–465. doi:10.1016/s0049-3848(01)00264-x

Wang, L., Wang, X., Wu, H., and Liu, R. (2014a). Overview on Biological Activities and Molecular Characteristics of Sulfated Polysaccharides from marine green Algae in Recent Years. *Mar. Drugs* 12, 4984–5020. doi:10.3390/md12094984

Wang, X., Palasubramaniam, J., Gkanatsas, Y., Hohmann, J. D., Westein, E., Kanojia, R., et al. (2014b). Towards Effective and Safe Thrombolysis and Thromboprophylaxis. *Circ. Res.* 114, 1083–1093. doi:10.1161/circresaha.114.302514

Watanabe, N., Nakajima, H., Suzuki, H., Oda, A., Matsubara, Y., Moroi, M., et al. (2003). Functional Phenotype of Phosphoinositide 3-kinase P85 -null Platelets Characterized by an Impaired Response to GP VI Stimulation. *Blood* 102, 541–548. doi:10.1182/blood-2002-11-3327

Wonerow, P., Pearce, A. C., Vaux, D. J., and Watson, S. P. (2003). A Critical Role for Phospholipase Cγ2 in αIIbβ3-mediated Platelet Spreading. *J. Biol. Chem.* 278, 37520–37529. doi:10.1074/jbc.m305077200

Xu, X. R., Carrim, N., Neves, M. A., Mckeown, T., Stratton, T. W., Coelho, R. M., et al. (2016). Platelets and Platelet Adhesion Molecules: Novel Mechanisms of Thrombosis and Anti-thrombotic Therapies. *Thromb. J.* 14, 29. doi:10.1186/s12959-016-0100-6

Conflict of Interest: The authors declare that the research was conducted in the absence of any commercial or financial relationships that could be construed as a potential conflict of interest.

frontiers in Pharmacology

ORIGINAL RESEARCH
published: 30 July 2021
doi: 10.3389/fphar.2021.705617

Oroxylin a Attenuates Limb Ischemia by Promoting Angiogenesis *via* Modulation of Endothelial Cell Migration

Lusha Zhang[1,2†], *Lu Chen*[1,2,3,4,5†], *Chunxiao Li*[1,2,3], *Hong Shi*[1,2,3,4,5], *Qianyi Wang*[1,2], *Wenjie Yang*[1,2], *Leyu Fang*[1,2], *Yuze Leng*[1,2], *Wei Sun*[1,2], *Mengyao Li*[1,2], *Yuejin Xue*[1,2], *Xiumei Gao*[1,2,4] *and Hong Wang*[1,2,3,4,6*]

[1]State Key Laboratory of Component-based Chinese Medicine, Tianjin University of Traditional Chinese Medicine, Tianjin, China, [2]Key Laboratory of Pharmacology of Traditional Chinese Medical Formula, Ministry of Education, Tianjin University of Traditional Chinese Medicine, Tianjin, China, [3]Tianjin Key Laboratory of Traditional Chinese Medicine Pharmacology, Tianjin, China, [4]Tianjin State Key Laboratory of Modern Chinese Medicine, Tianjin, China, [5]Institute of Traditional Chinese Medicine, Tianjin University of Traditional Chinese Medicine, Tianjin, China, [6]School of Integrative Medicine, Tianjin University of Traditional Chinese Medicine, Tianjin, China

OPEN ACCESS

Edited by:
Yue Liu,
Xiyuan Hospital, China

Reviewed by:
Shih-Wei Wang,
Mackay Medical College, Taiwan
Bo Yang,
Zhejiang University, China

***Correspondence:**
Hong Wang
wanghongsys@tjutcm.edu.cn

[†]*These authors have contributed equally to this work*

Specialty section:
This article was submitted to Ethnopharmacology, a section of the journal Frontiers in Pharmacology

Received: *05 May 2021*
Accepted: *16 July 2021*
Published: *30 July 2021*

Citation:
Zhang L, Chen L, Li C, Shi H, Wang Q, Yang W, Fang L, Leng Y, Sun W, Li M, Xue Y, Gao X and Wang H (2021) Oroxylin a Attenuates Limb Ischemia by Promoting Angiogenesis via Modulation of Endothelial Cell Migration. Front. Pharmacol. 12:705617. doi: 10.3389/fphar.2021.705617

Oroxylin A (OA) has been shown to simultaneously increase coronary flow and provide a strong anti-inflammatory effect. In this study, we described the angiogenic properties of OA. OA treatment accelerated perfusion recovery, reduced tissue injury, and promoted angiogenesis after hindlimb ischemia (HLI). In addition, OA regulated the secretion of multiple cytokines, including vascular endothelial growth factor A (VEGFA), angiopoietin-2 (ANG-2), fibroblast growth factor-basic (FGF-2), and platelet derived growth factor BB (PDGF-BB). Specifically, those multiple cytokines were involved in cell migration, cell population proliferation, and angiogenesis. These effects were observed at 3, 7, and 14 days after HLI. In skeletal muscle cells, OA promoted the release of VEGFA and ANG-2. After OA treatment, the conditioned medium derived from skeletal muscle cells was found to significantly induce endothelial cell (EC) proliferation. OA also induced EC migration by activating the Ras homolog gene family member A (RhoA)/Rho-associated coiled-coil kinase 2 (ROCK-II) signaling pathway and the T-box20 (TBX20)/prokineticin 2 (PROK2) signaling pathway. In addition, OA was able to downregulate the number of macrophages and neutrophils, along with the secretion of interleukin-1β, at 3 days after HLI. These results expanded current knowledge about the beneficial effects of OA in angiogenesis and blood flow recovery. This research could open new directions for the development of novel therapeutic intervention for patients with peripheral artery disease (PAD).

Keywords: oroxylin A, hind limb ischemia, angiogenesis, endothelial cells, migration, inflammation

INTRODUCTION

Ischemia after artery obstruction that occurs during PAD is estimated to affect approximately 202 million adults worldwide (Gerhard-Herman et al., 2017; McDermott and Kibbe, 2017). The enhancement of angiogenesis and the resulting improvement of blood flow to the limb are the key restorative mechanisms in response to ischemia (Cooke and Losordo, 2015; Suzuki et al., 2016; Albrecht-Schgoer et al., 2017; Fan et al., 2018). At this point, treatments have not been fully effective

at improving blood flow through angiogenesis in PAD (Suzuki et al., 2016; Gorenoi et al., 2017). Therefore, a better understanding of the underlying mechanisms involved in ischemic revascularization may help to optimize future clinical interventions.

Angiogenesis is a tightly regulated, multi-step process. When quiescent vessels sense angiogenic signals, such as guanosine triphosphatase (GTPase), vascular endothelial growth factor (VEGF), angiopoietin-2 (ANG-2), and fibroblast growth factor (FGFs), pericytes detach from the vessel wall and liberate themselves from the basement membrane *via* proteolytic degradation. Endothelial cells (ECs) loosen their junctions and the nascent vessel dilates (Carmeliet and Jain, 2011; Sun et al., 2017; Lee and Kang, 2018). In the early stage of angiogenesis, secretion of VEGF is closely related to inflammation, which can promote aggregation of neutrophils and production of inflammatory factor IL-1β (Saleh et al., 2015; Rajasagi et al., 2017). For therapeutic angiogenesis, it is not enough to identify pivotal regulators of angiogenesis as therapeutic targets to promote blood flow recovery. The surrounding inflammatory microenvironment should be considered at the same time to assess functional vasculature establishment in ischemic tissues (Liu et al., 2018; Minoshima et al., 2018). Previous research has shown that promoting angiogenesis while reducing inflammation can improve the prognosis of PAD (Zhang et al., 2016; Liu et al., 2018).

Oroxylin A (OA) (PubChem CID: 5320315) is one of the main bioactive compounds that is purified from the root of the medicinal herb *Scutellaria baicalensis* Georgi. This herb has been reported to have strong anti-inflammatory effects (Liu et al., 2012; Tseng et al., 2012; Wang et al., 2013). OA ameliorated some cardiac functions by increasing coronary flow (Liu et al., 2012; Tseng et al., 2016). These anti-inflammatory and pro-angiogenic effects of OA suggest that OA is most likely to establish functional vasculature in ischemic tissues and improve the prognosis of PAD. In this study, we investigated the therapeutic efficacy of OA for treating PAD and identified the molecular signaling pathways involved in the pro-angiogenic response both *in vivo* and *in vitro*.

MATERIALS AND METHODS

Reagents

Avertin, simvastatin (Sim), collagenase II (C6885), and dispase II (D4693) were purchased from Sigma-Aldrich (MO, United States). Mouse XL Cytokine Array Kit (ARY028) and Mouse Angiogenesis Array Kit (ARY015) were purchased from R and D (MN, United States). α-SMA antibody (ab32575) was purchased from Abcam (Cambridge, United Kingdom). One Step TUNEL Apoptosis Assay Kit (C1089) was purchased from Beyotime Biotechnology (Shanghai, China). PE anti-F4/80 (565410), APC-Cy^{TM}7 anti-Ly-6G (560600), PerCP anti-CD45 (561047) and matrigel (354234) were purchased from BD Company (NY, United States). Antibodies of VEGFA (ab51745), T-box20 (TBX20) (ab197386), and Prokineticin 2 (PROK2) (ab128293) were obtained from Abcam (Cambridge, United Kingdom). Antibodies for glyceraldehyde-3-phosphate dehydrogenase (GAPDH) (2118S), vascular endothelial growth factor receptor 2 (VEGFR2) (9698), Rho-associated coiled-coil kinase 2 (ROCK-II) (9029), Cofilin (5175), *p*-Cofilin (3313), β-actin (4970) were bought from Cell Signaling Technology (MA, United States). VEGFA (E-EL-M1292c), ANG-2 (E-EL-M0098c), PDGF-BB (E-EL-M0632c), IL-1β (E-EL-M0037c) mouse ELISA kits were obtained from Elabscience® (Wuhan, China). FGF basic mouse ELISA kit (MFB00) and $VEGFA_{165}$ (293-VE-010) were obtained from R and D (MN, United States). Human umbilical vein endothelial cells (HUVECs, HUVEC-20001), endothelial cell growth medium (EGM) and fatal bovine serum (FBS) were obtained from Cyagen Biosciences Inc. (Guangzhou, China). Skeletal muscle cells (CP-H095) and skeletal muscle cells growth medium (CM-H095) were purchased from Procell Life Science & Technology Co., Ltd. (Wuhan, China). RhoA/Rac1/Cdc42 activation assay combo biochem kit™ (#BK030) was bought from Cytoskeleton (CO, United States). ROCK-II small interfering RNA (siRNA) (sc-29474), scrambled siRNA (sc-37007), and siRNA transfection reagent (sc-29528) were obtained from Santa Cruz Biotechnology (TX, United States).

Animals

Male C57BL/6 mice of specific pathogen free, 22–25 g, were purchased from Beijing Weitong Lihua Experimental Animal Technology Co. Ltd. and maintained at the Animal Center of Institute of Biomedical Engineering, Chinese Academy of Medical Sciences (Tianjin, China). All animals were kept under 22–25°C and a 12 h light/dark cycle with standard food pellets and free access to tap water. All animal care and experimental procedures were approved by the Animal Ethics Committee of Tianjin University of Traditional Chinese Medicine and performed in accordance with the approved guidelines on the use of laboratory animals. The reference number of Institutional Animal Care and Use Committee (IACUC) is TCM-LAEC2019078.

Surgical Hind Limb Ischemia Model

Mice were anesthetized with injection of Avertin (0.33 ml/20 g) into the abdominal cavity and maintained on a temperature-controlled water blanket at 37°C. Depilatory cream was applied to the limbs and the area was sterilized by 70% ethanol applications. A 5-mm vertical skin incision was made lateral to the abdomen and superficial to the inguinal ligament. The inguinal fat pad was separated from the peritoneal lining to reveal the proximal femoral artery branching from the internal iliac artery. The femoral artery and vein were then separated from the membrane sheath and two ligatures were tied around both vessels approximately 2-mm apart. Vessels were transected between the ligatures and the skin incision was closed with two discontinuous 6–0 silk sutures. Limb in sham mice were opened, dissected, and closed without vessel ligature and excision. After surgery the mice were sub-divided into four groups: 1. sham group (not HLI + saline); 2. saline group (HLI + saline); 3. OA group (HLI + OA, 10 mg/kg/d); 4. Sim group (HLI + Sim, 10 mg/kg/d). Treatments were given daily until euthanasia.

Perfusion Imaging

The blood flow perfusion was measured by laser doppler perfusion imaging system both pre- and post-operatively and 3, 7, 14, 28 days after excision of the femoral artery in three groups. The blood flow images were collected by laser doppler high resolution imaging system (moor instruments, United States) and stored in the form of two-dimensional images of the whole area of the lower limbs. The ratio of blood flow in the ischemic (right) to the control (left) limb was calculated by moorLDI laser doppler imager review V 6.0 analysis software to show the recovery rate of ischemic hindlimb blood flow.

Histological Analysis

The ischemic hindlimb muscle tissues were obtained 28 days after operation and fixed with 4% paraformaldehyde. The muscles were dehydrated, embedded, and transversely sectioned into 5 μm pieces. Gross examination of tissue injury was performed on hematoxylin and eosin (H and E) stained sections.

Terminal Deoxynucleotidyl Transferase-Mediated dUTP Nick End-Labeling Assay

TUNEL staining was performed following the manufacturers' instructions in paraffin sections. DAPI staining was used to count the total number of nuclei. Apoptotic myocytes were quantified and classified as $TUNEL^+$ cells.

Immunofluorescence

For immunofluorescent labeling, the mice were intravenously injected with 50 μL Griffonia (Bandeiraea) Simplicifolia Lectin I 30 min before sacrifices. The paraffin sections were incubated with Griffonia (Bandeiraea) Simplicifolia Lectin I and α-SMA antibodies overnight at 4°C. The following day, the tissue sections were incubated with DyLight® 594 ANTI-GOAT IgG (H + L) and FITC mouse anti-rabbit (1:200) for 1 h in the dark at room temperature. All sections were counterstained with DAPI.

Proteome Antibody Array Analysis

To determine the regulated proteins in the gastrocnemius muscle after ischemia, mice were euthanized after 3, 7, and 14 days. After adding Triton X-100 to a final concentration of 1%, tissue homogenates were frozen at −80°C for 2 h, then quickly thawed and centrifuged at 10,000 g for 5 min to remove cellular debris. The upper aqueous phase was transferred to a new tube for proteome antibody array analysis, which included Mouse XL Cytokine Array Kit for 3 days and Mouse Angiogenesis Array Kit for 7, 14 days after surgery.

Flow Cytometry Analysis

The ischemic gastrocnemius muscles were digested in 1.8 ml Hanks Balanced Salt Solution with 7.2 mg collagenase II and 9 mg dispase II at 37°C for 1.5 h using GentleMACS™ Dissociator (MACS, German). The strained cells were stained with PE anti-F4/80, APC-Cy™7 anti-Ly-6G, and PerCP anti-CD45. Single-cell suspensions were examined on a FACS Aria III flow cytometer.

Western Blotting

For this experiment, frozen skeletal samples from hindlimbs were homogenized in lysis buffer. Protein concentration was measured by BCA method. Nine primary antibodies were used in the experiments: GAPDH, VEGFA, VEGFR2, ROCK2 (ROCK-II), TBX20, PROK2, Cofilin, *p*-Cofilin (Ser3), β-Actin. The reactive bands were developed using chemiluminescence according to the manufacturer's instruction. A semi-quantitative estimation can be derived from the size and color intensity of the band on the blot membrane.

Enzyme-Linked Immunosorbent Assay

Secreted VEGFA, ANG-2, FGF-2, PDGF-BB, and IL-1β in tissue lysates or serum were determined by ELISA according to the manufacturer's instructions.

Cell Culture

We obtained HUVECs from Cyagen Biosciences Inc. (HUVEC-20001) and skeletal muscle cells from Procell Life Science and Technology Co., Ltd. (CP-H095). Endothelial cell growth medium (EGM) contains endothelial cell basal medium (EBM), fetal bovine serum (10%), penicillin-streptomycin (1%), glutamine (1%), ECGS (1%), heparin (1%). EGM was used to culture HUVECs and skeletal muscle cells growth medium (CM-H095) was used to culture skeletal muscle cells in a cell incubator consisting of 5% humidified CO_2 at 37°C.

Preparation of Conditioned Medium

Skeletal muscle cells within a range of three passages were seeded in skeletal muscle cells growth medium in 6-well plate at a density of 1×10^4 cells per well. HUVECs within a range of five passages were seeded in EGM in 96-well plate at a density of 3×10^3 cells per well. When skeletal muscle cells density reached 60%, OA or DMSO (control) was given to intervene skeletal muscle cells for 24 h and then the medium of skeletal muscle cell was centrifuged at 1000 rpm for 5 min, and the supernatant was collected, aliquoted and stored in a refrigerator at −80°C (to detect secreted cell growth factors) or used for the culture of HUVECs. After OA or DMSO acted on skeletal muscle cells, the supernatants were the conditioned medium containing growth factors. The medium of HUVECs was removed and the skeletal muscle cells-conditioned medium were added to HUVECs for 24 h and then cell proliferation was measured using a BrdU kit.

Tube Formation Assay

Chilled Matrigel (50 μL) was added to each well of a 96-well plate and allowed to polymerize for 30 min at 37°C. Cell suspension was added per well and incubated for 18 h. Brightfield images were taken using a Nikon microscope and quantified using Photoshop CS5 software (Adobe Systems, United States).

Scratch Assays

With the use of WOUNDMAKER 96 (ESSEN BIOSCIENCE, United States), horizontal scratches were made across the culture dish. The scratches were imaged using IncuCyte Zoom (ESSEN, United States).

Cell Proliferation Assays

Cell proliferation was measured using a BrdU kit (Roche, United States) and quantitated on a microplate reader, whereas viability and total cell number were determined in separate assays using an MTT assay kit (Invitrogen, United States).

RNA Interference

For ROCK-II knock-down, HUVECs were transfected with ROCK-II siRNA (10 μM) or scrambled siRNA (10 μM) using siRNA transfection reagent according to the manufacturer's instructions. Knockdown efficiency was assessed by quantitative reverse transcriptase polymerase chain reaction (qRT-PCR) 48 h later.

Quantitative Reverse Transcriptase Polymerase Chain Reaction

qRT-PCR was performed in QuantStudio six Flex. The following human primers were used:

GAPDH:
Forward CAACGTGTCAGTGGTGGACCTG.
Reverse GTGTCGCTGTTGAAGTCAGAGGAG.
VEGFR2:
Forward CGGACAGTGGTATGGTTCTTGCC.
Reverse GTGGTGTCTGTGTCATCGGAGTG.
ROCK-II:
Forward TCGTCACAAGGCATCGCAGAAG.
Reverse CCACCAGGCATGTACTCCATTACC.
TBX20:
Forward ACCAGCACAGCATCCATAGCAAC.
Reverse GCAATGGCCGATGGTGTCAGAG.
PROK2:
Forward ACTCCTGCTCCTCTTGCTGCTG.
Reverse GCACATGCCTCCACCACATTGG.

Transwell

A chemotactic migration assay was performed using transwell plates with 6.5 mm diameter polycarbonate filters (8 μm pore size). The upper and lower surfaces of the chamber were coated with fibronectin. EGM medium was placed in the lower wells. Cells were loaded into upper wells. The chamber was incubated at 37°C for 4 h. Migrated cells were stained with crystal violet and quantified using an optical microscope.

Statistical Analysis

Statistical analysis was performed using SPSS software (version 17.0). Data were expressed as mean ± standard deviation (SD). Differences between two groups were estimated with Student's *t*-test. Values of $p < 0.05$ were considered statistically significant.

RESULTS

Oroxylin A Ameliorated Hindlimb Ischemia in Hind Limb Ischemia Mouse Model

Mice undergoing HLI showed a time-dependent increase in tissue perfusion that reached about 30% restoration of blood flow by day 14 post-HLI. The mean ratios of ischemic to non-ischemic perfusion in the OA group (0.59 ± 0.14) and Sim-treated mice (0.52 ± 0.13) were significantly higher than that of saline group (0.33 ± 0.10). The recovery was more pronounced by day 28. OA treatment significantly accelerated perfusion recovery as compared with saline (0.71 ± 0.16 versus 0.45 ± 0.10), similar with the effect of Sim (0.63 ± 0.13), which showed that OA improved hindlimb ischemia in limb ischemic mice (**Figures 1A,B**). The H and E-stained sections of the gastrocnemius muscle shown in **Figures 1C,D** were used for the analysis of skeletal muscle remodeling, damage, and necrosis. Muscle regeneration was assessed by the number of myocytes with centrally located nuclei. The histopathological features of necrosis were defined by the presence of multi-cellular infiltrates and hyper-eosinophilic muscle cells that were devoid of nuclei. In the model mice treated with saline, the myofibers were shrunken and the intermuscular gaps were large. In the OA-treated groups, the muscles had repopulated with intensely staining myocytes and no obvious infiltration of inflammatory cells, indicating that OA reduced tissue injury and made skeletal myocytes regenerated. The TUNEL results showed that OA significantly reduced the gastrocnemius muscle cell apoptosis. This further demonstrated that OA could protect the muscle tissue surrounding the ischemic site (**Figures 1E,F**). In addition, the histological findings correlated with vascular and functional outcomes. The capillary density was assessed by quantification of lectin positive vessels observed in the interface between the skeletal muscles at day 28 post-ischemia. The level of capillary density was higher in the OA-treated mice compared with saline (**Figures 1G,H**). To determine the collateral formation and demonstrate the arterial nature of the newly formed vessels in the adductor muscle, we co-stained α-SMA and examined the number of tube-like structures, as shown in **Figures 1I,J**. Remarkably, the level of mature vessels was higher in the OA-treated mice compared with saline. Collectively, these results demonstrated that OA accelerated perfusion recovery, reduced tissue injury, and promoted angiogenesis after HLI.

Oroxylin A Regulated the Secretion of Vascular Endothelial Growth Factor A, Angiopoietin-2, Fibroblast Growth Factor-2, and Platelet Derived Growth Factor BB at Distinct Time Points After Hind Limb Ischemia

The formation of a mature vascular network requires the precise spatial and temporal regulation of many angiogenic factors, including VEGF, ANG-2, FGF-2, and PDGF. VEGF aids in vascular permeability and the recruitment of ECs, FGF-2 activates ECs proliferation and migration, while PDGF stimulates vascular stability (Carmeliet and Jain, 2011; Bai et al., 2018). To define the molecular mediators of angiogenesis secreted from ischemic tissue; the proteome antibody array was used to detect the regulated proteins in the gastrocnemius muscle post ischemia. OA modulated several secreted factors, including VEGFA, ANG-2, FGF-2, and PDGF-BB (**Supplementary Figure S1A-C,S2**). These regulated factors were correlated with

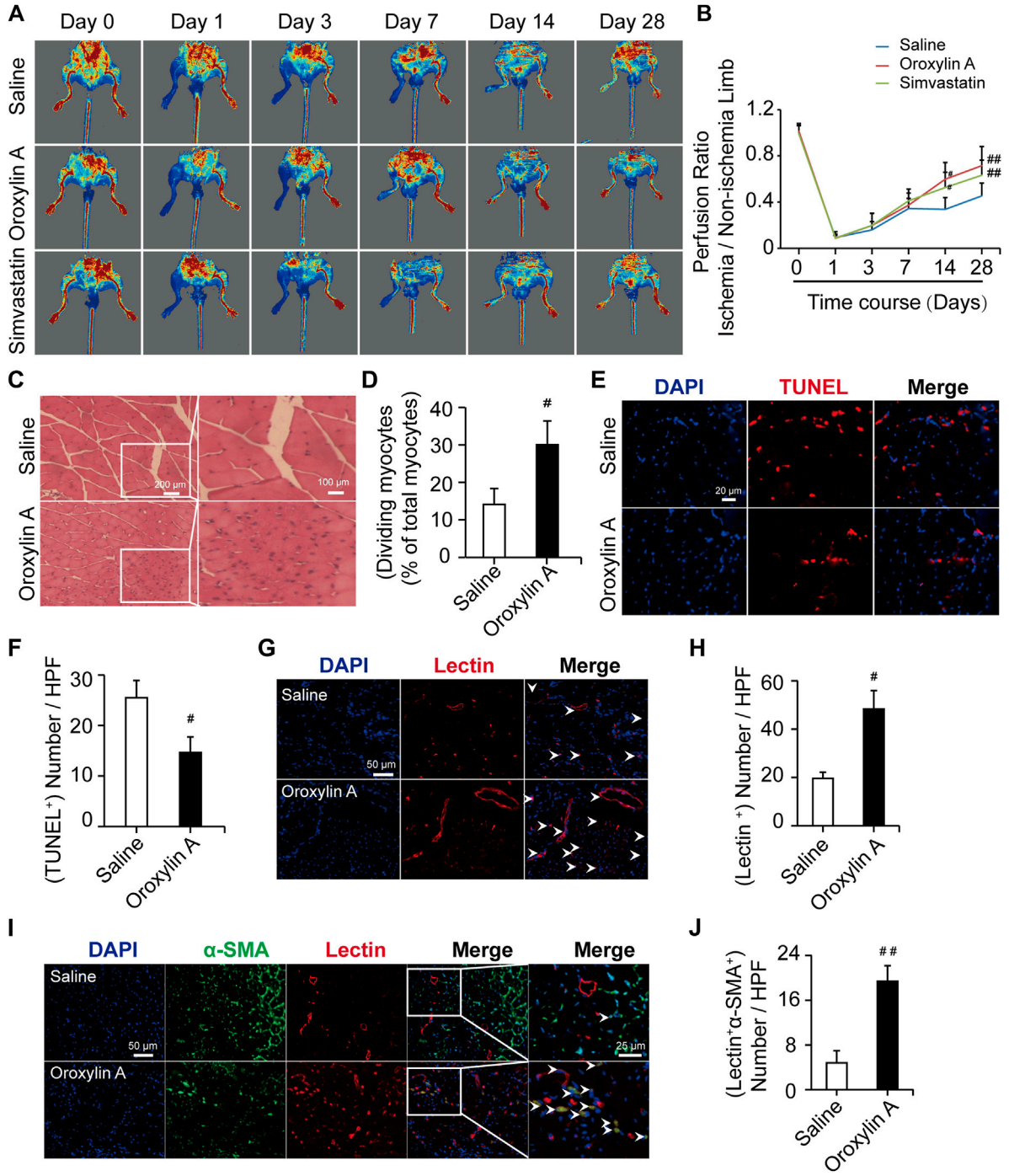

FIGURE 1 | OA ameliorated hindlimb ischemia in a mouse model of HLI. **(A)** Typical blood flow perfusion photographs at different time (pre- and post-operatively, as well as 3, 7, 14, and 28 days after excision of the femoral artery) in three groups were presented. **(B)** Quantification of blood perfusion at different times was performed. Data are mean ± SD; n = 5–8/group. **(C,D)** H and E staining of muscle tissue in hindlimb confirmed the number of myocytes with centrally-located nuclei were increased by OA therapy. The scale bar represented 200 μm (left) and the scale bar represented 100 μm (right). **(E,F)** TUNEL staining was used for detecting apoptosis (red) of myocytes and DAPI (blue) was for nuclear staining. OA could significantly reduce the myocytes apoptosis. The scale bar represented 20 μm. Data are mean ± SD; n = 3–4/group. **(G)** Representative immunofluorescent images were presented to determine capillary density in ischemic muscles on day 28. Capillaries were stained with lectin (red) and nuclei were stained with DAPI (blue). The white arrowheads showed the region of blood vessels. The scale bar represented 50 μm. **(H)** Quantification of capillary density was expressed as lectin positive number per randomly chosen high-power field (HPF). n = 3/group. **(I)** Capillaries were stained with lectin (red), α-SMA (green), and nuclei were stained with DAPI (blue). The white arrowheads showed the region of mature, functional blood vessels. The scale bar represented 25 μm. **(J)** Quantification of the mature, functional blood vessels in the adductor muscle was expressed as lectin, α-SMA double-positive number per randomly chosen HPF. Data are mean ± SD; n = 5/group, $^{\#}p < 0.05$, $^{\#\#}p < 0.01$ *vs*. saline.

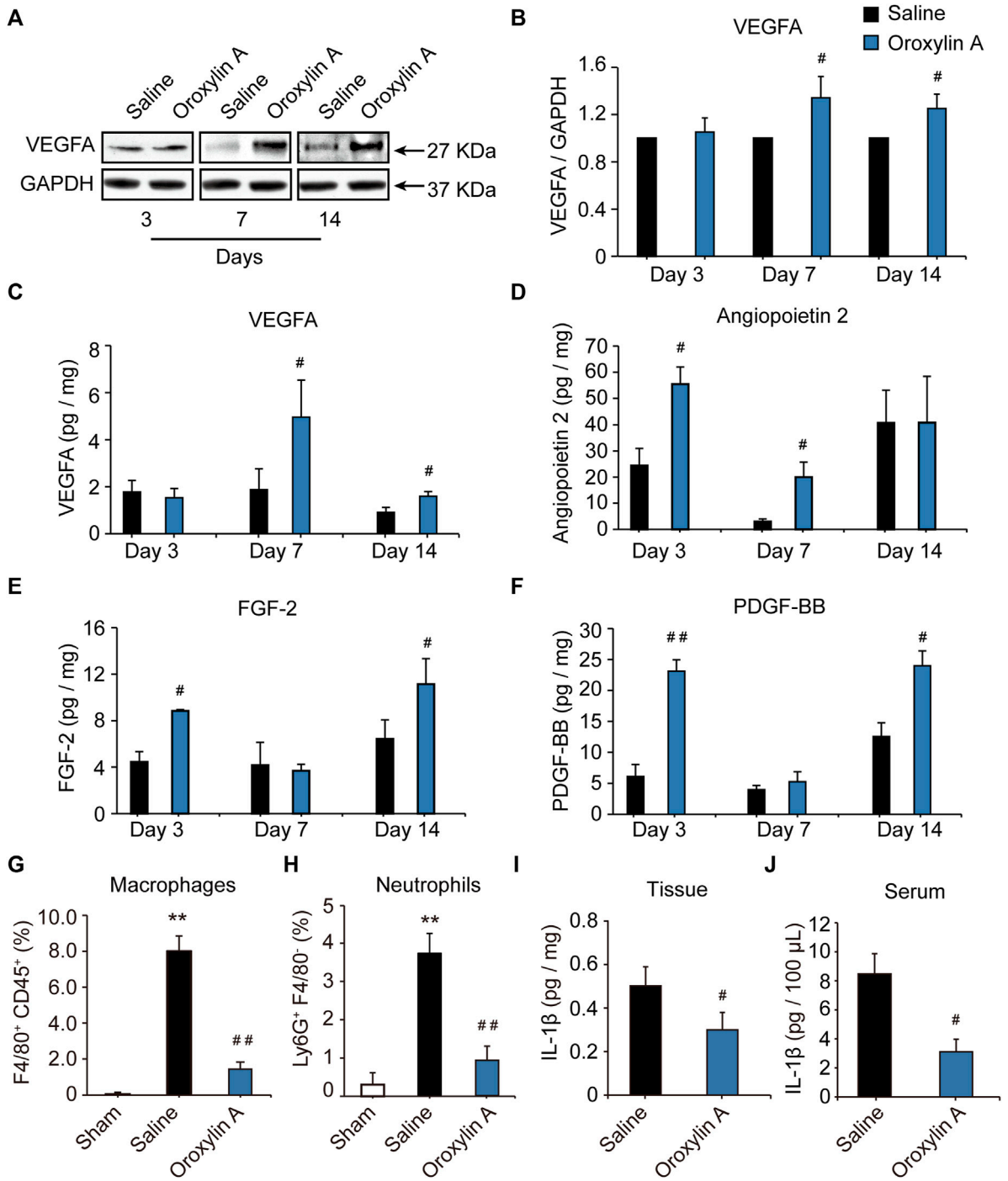

FIGURE 2 | OA regulated the secretion of VEGFA, ANG-2, FGF-2, and PDGF-BB at distinct time points during angiogenesis after HLI and resolved inflammation during HLI. Lysates were immunoblotted with VEGF antibody, and detected with an enhanced chemiluminescence kit. Blots were normalized by densities for GAPDH as an internal control **(A,B)**. Quantitative VEGFA **(C)**, ANG-2 **(D)**, FGF-2 **(E)**, and PDGF-BB **(F)** in ischemic tissue at 3, 7 and 14 days after HLI in the presence of OA or saline were detected by ELISA. Values were represented as means ± SD (n = 3–4). Quantification by flow cytometry of $F4/80^+CD45^+$ macrophages **(G)** and $Ly6G^+F4/80^-$ neutrophils **(H)** in skeletal muscle isolated from mice undergoing HLI (day 3) and treated with saline or OA was presented. Tissue **(I)** and Serum **(J)** levels of IL-1β in mice undergoing HLI and treated with saline or OA were detected. Data were represented as mean ± SD (n = 5). $^{**}p < 0.01$ *vs*. sham; $^{\#}p < 0.05$, $^{\#\#}p < 0.01$ *vs*. saline.

the immune system and functions of cell migration, cell proliferation, and angiogenesis. (**Supplementary Figure S1D-I**). Further experiments were performed to identify the array results. Results showed that VEGFA levels were comparable between groups at the 3-days time point, while OA improved VEGFA levels at day 7 and 14 after HLI, when compared with the respective

saline group (**Figures 2A–C**). This facilitated vessel sprouting and lumen elongation during angiogenesis (Potente et al., 2011). In addition, OA significantly increased ischemia-induced decreases in ANG-2 at days 3 and 7 after HLI (**Figure 2D**). These results were consistent with the defined role of OA in regulating pericytes that detach from the vessel wall to enlarge the size of the lumen (Carmeliet and Jain, 2011). ANG-2 levels were comparable between groups at the day 14 time point. FGF is critical for maintaining vascular integrity, because inhibition of FGFR signaling in ECs leads to vascular disintegration (Murakami et al., 2008). After HLI, FGF was increased in the OA group at days 3 and 14, as compared with saline group. However, there was no significant difference between the two groups 7 days after HLI (**Figure 2E**). Damaged PDGF-BB might lead to vascular leakage, tortuosity, microaneurysm formation, and bleeding due to lack of pericytes, which is not conducive to the repair of ischemic injury. PDGF-BB plays a key role in the mature stage of angiogenesis (Skovseth et al., 2005; Mittermayr et al., 2016). Like FGF, PDGF-BB was also increased in the early and late stages of angiogenesis when compared with the respective saline group and PDGF-BB levels were comparable between groups at 7 days (**Figure 2F**). Current research revealed that angiogenic factors go through a dynamic progression in this multi-step angiogenesis process, in which tubular structures are created, elongated, and then matured during angiogenesis after HLI. In addition, OA promoted angiogenesis by regulating VEGFA, ANG-2, FGF-2, and PDGF-BB at distinct time points after HLI.

Oroxylin A Resolved Inflammation During Hind Limb Ischemia

The inflammatory response is an integral part of the ischemic microenvironment, which is tightly coupled to angiogenesis. OA has been reported to have strong anti-inflammatory effects in macrophages *in vitro*. Next, we sought to determine how OA modulated the inflammatory microenvironment *in vivo*. In comparison with sham group, levels of $CD45^{+}F4/80^{+}$ macrophages (**Figure 2G**) and $Ly6G^{+}F4/80^{-}$ neutrophils (**Figure 2H**) increased significantly in skeletal muscle of mice undergoing HLI. This increase was prevented in mice treated with OA. Meanwhile, OA significantly decreased the ischemia-induced increase in pro-inflammatory cytokine IL-1β (**Figures 2I,J**). These results indicated that OA resolved inflammation by reducing macrophage and neutrophil recruitment and proinflammatory cytokine production, which will have a positive effect on promoting blood flow recovery.

Oroxylin A Promoted Release of Vascular Endothelial Growth Factor A and Angiopoietin-2 in Skeletal Muscle Cells

Skeletal muscle is a secretory organ that can secrete various angiogenic factors, and is very crucial for angiogenesis. We examined the effect of the OA-treated secretome of skeletal muscle cells on vascular endothelial cells. OA (2.5 μM) significantly promoted the release of VEGFA (**Figure 3A**) and ANG-2 (**Figure 3B**) in skeletal muscle cells. After OA treatment, the conditioned medium derived from skeletal muscle cells was added to HUVEC in culture for 24 h. There was a statistically significant increase in the pro-proliferative activity of ECs as compared to conditioned medium after DMSO intervention (**Figure 3C**). This study demonstrated that OA-mediated angiogenesis was associated with increase of angiogenic factors within the skeletal muscle microenvironment.

Oroxylin A Induced Tube Formation and Migration in Human Umbilical Vein Endothelial Cells

In vitro angiogenesis assays were conducted. EC proliferation and migration contributes to dissemination of pre-existing vessels to form new vessels. OA also significantly induced the formation of capillary-like structures (**Figures 3D,E**). OA did not stimulate EC proliferation, which was robustly stimulated by $VEGFA_{165}$ (100 ng/ml). This lack of effect on proliferation was not due to a decrease in cell viability (**Figures 3F,G**; **Supplementary Figure S3**). We further investigated the effect of OA on cell migration and it was observed that OA directly enhanced EC migration following a scrape injury (**Figures 3H,I**). OA-induced rearrangement of the actin cytoskeleton and enhanced the formation of stress fibers. These stress fibers terminated at pointed edges and were a typical morphological feature in migrating cells (**Figure 3J**). These results indicated that OA stimulated the migration of HUVECs.

Oroxylin A Induced Endothelial Cell Migration Through the Ras Homolog Gene Family Member A/Rho-Associated Coiled-Coil Kinase II Pathway

To identify the mechanism of OA, we examined Rho GTPases, which play a fundamental role in EC migration (Warner et al., 2019). OA increased the amount of active, GTP-bound RhoA, but did not increase the amount of Cdc42 or Rac1. In addition, OA induced the formation of stress fiber mediated by RhoA (**Figures 4A–D**). Previous studies have demonstrated that VEGFR2 activation induced the stimulation of RhoA and its major downstream effector, Rho-associated protein kinase ROCK-II, to regulate stress fiber formation and cell migration in ECs (Bryan et al., 2010; Liu et al., 2018). In addition, Cofilin has been previously shown to regulate cell migration (Li et al., 2015). Our data showed that OA increased the expression of VEGFR2, ROCK-II, and increased the phosphorylation of Cofilin in HUVECs in a time-dependent manner (**Figures 4E–J**).

ROCK-II is the downstream of VEGFR2. It is estimated that knockdown of ROCK-II will not alter the expression of VEGFR2. We tested the level of VEGFR2 after siROCK-II. **Figures 5A–D** showed that the transfection of ROCK-II siRNA resulted in a marked reduction in ROCK-II. After siROCK-II treatment, the level of VEGFR2 was significantly increased for 30 min after OA treatment, while after 60 min of OA treatment, the level of VEGFR2 was not altered, which is not in line with the expected results. Furthermore, the results showed that the concurrent cell migrations and capillary-like structures of HUVECs that were induced by OA treatments were able to be

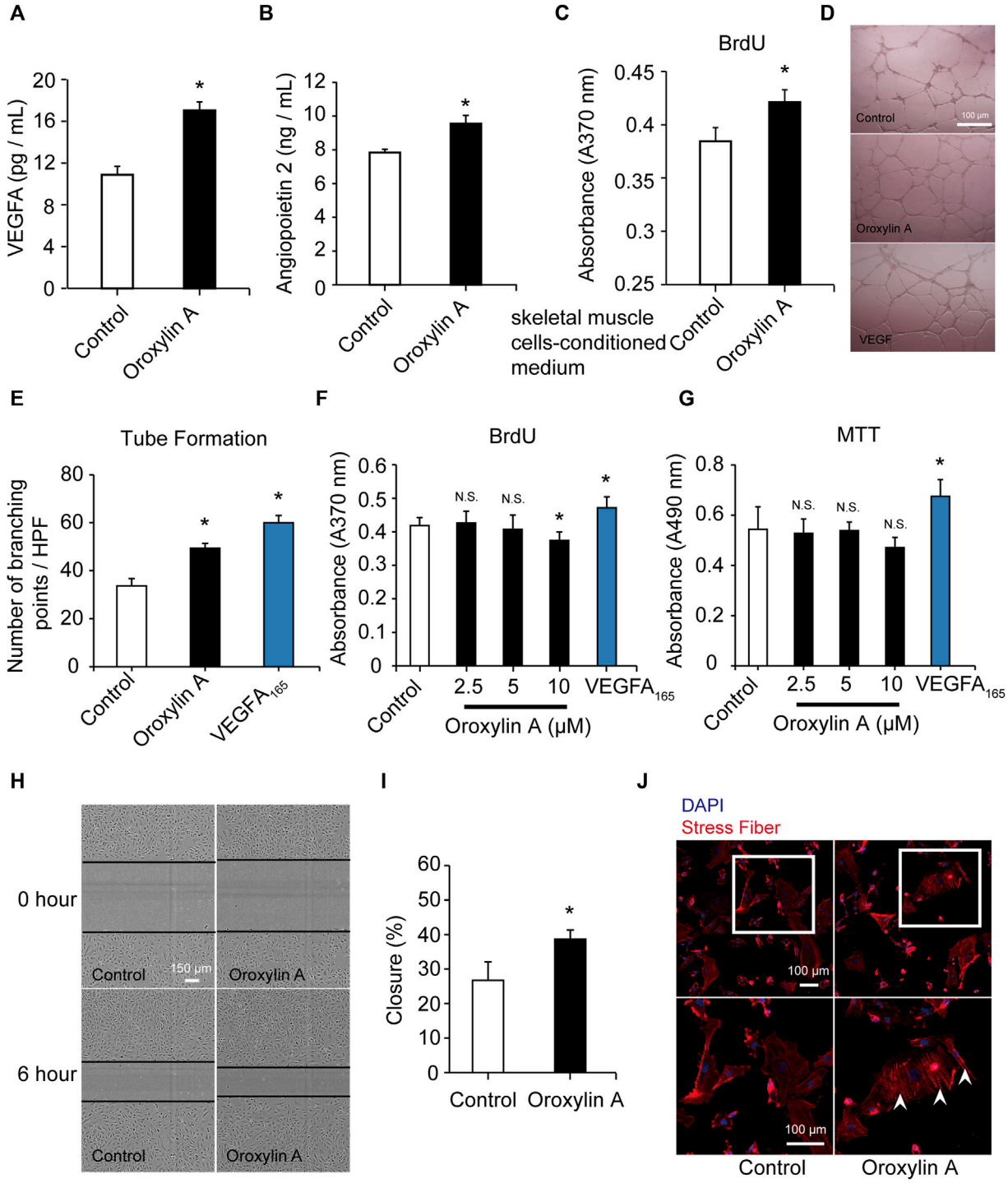

FIGURE 3 | OA promoted the secretion of VEGFA and ANG-2 in skeletal muscle cells and induced tube formation and migration in HUVECs. Skeletal muscle cells were cultured with DMSO or OA (2.5 μM) for 24 h, and then the contents of VEGFA **(A)** and ANG-2 **(B)** in the supernatant were quantified by ELISA. After DMSO or OA treatment, medium derived from skeletal muscle cells was added to HUVEC in culture for 24 h, and then assayed by a BrdU kit **(C)**. Data were represented as mean ± SD ($n = 6$). Tube formation of HUVECs were performed on Matrigel in response to DMSO, OA (2.5 μM) or $VEGFA_{165}$ for 18 h, with $VEGFA_{165}$ as a positive control. The scale bars represented 100 μm **(D)**. Quantification of tube formation were presented as several branching points **(E)**. HUVECs were cultured with DMSO or OA (2.5, 5, 10 μM) for 24 h, and then assayed by a BrdU kit **(F)** and MTT assay **(G)**. $VEGFA_{165}$ was acted as a positive control. Representative images and quantification of ECs migration following scrape injury in response to DMSO or OA (2.5 μM) were shown in **H and I**. The scale bars represented 150 μm. Actin cytoskeleton rearrangement in HUVECs was shown in **(J)**. Below is a higher magnification of the white-boxed area. Formation of stress fibers terminated at pointed edges (white arrowhead). The scale bars represented 100 μm. Data were represented as mean ± SD ($n = 5$). *$p < 0.05$, N.S. not significant, *vs.* control.

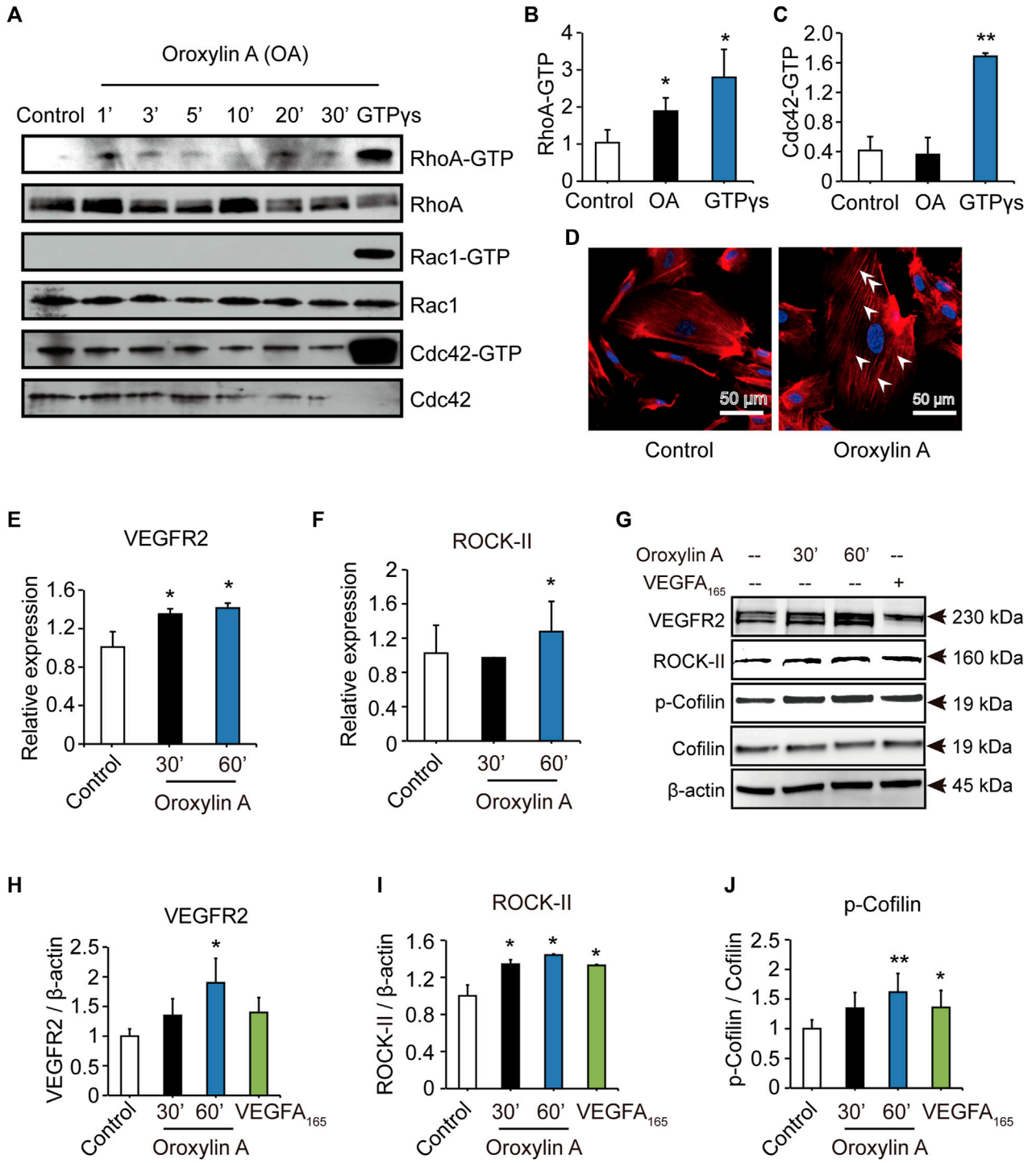

FIGURE 4 | OA induced stress fiber formation and cell migration in HUVECs through RhoA/ROCK-II pathway. The amounts of active GTP-bound RhoA (RhoA-GTP, rhotekin-RBD), Rac1 (Rac1-GTP, PAK-PBD), Cdc42 (Cdc42-GTP, PAK-PBD) were determined by a pull-down assay, in non-stimulated (control) or OA-stimulated (2.5 μM) HUVECs for 1 min (1′), 3′, 5′, 10′, 20′ or 30'. Total RhoA, Rac1, Cdc42 in total cell extracts were also detected **(A)**. Quantification of active, GTP-bound state was presented as RhoA-GTP (20′) **(B)** and Cdc42-GTP (3′) **(C)**. HUVECs treated for 20 min with 2.5 μM OA after serum were starved and subsequently stained with rhodamine-phalloidin and with DAPI for nuclei. RhoA induced actin stress fibers were visible **(D)**. *VEGFR2* **(E)** and *ROCK-II* **(F)** mRNA expression in HUVECs were stimulated with 2.5 μM OA for 30, 60 min. HUVECs stimulated with DMSO, 2.5 μM OA for 30, 60 min and $VEGFA_{165}$ for 60 min. Western blotting analysis of VEGFR2, ROCK-II or *p*-Cofilin and total Cofilin in HUVECs were performed. β-actin expression was presented as an internal control of protein loading. $VEGFA_{165}$ was acted as a positive control **(G)**. Quantitative data included VEGFR2 **(H)**, ROCK-II **(I)** and *p*-Cofilin **(J)**. Data were represented as mean ± SD ($n = 3$). $^{*}p < 0.05$; $^{**}p < 0.01$ *vs.* control.

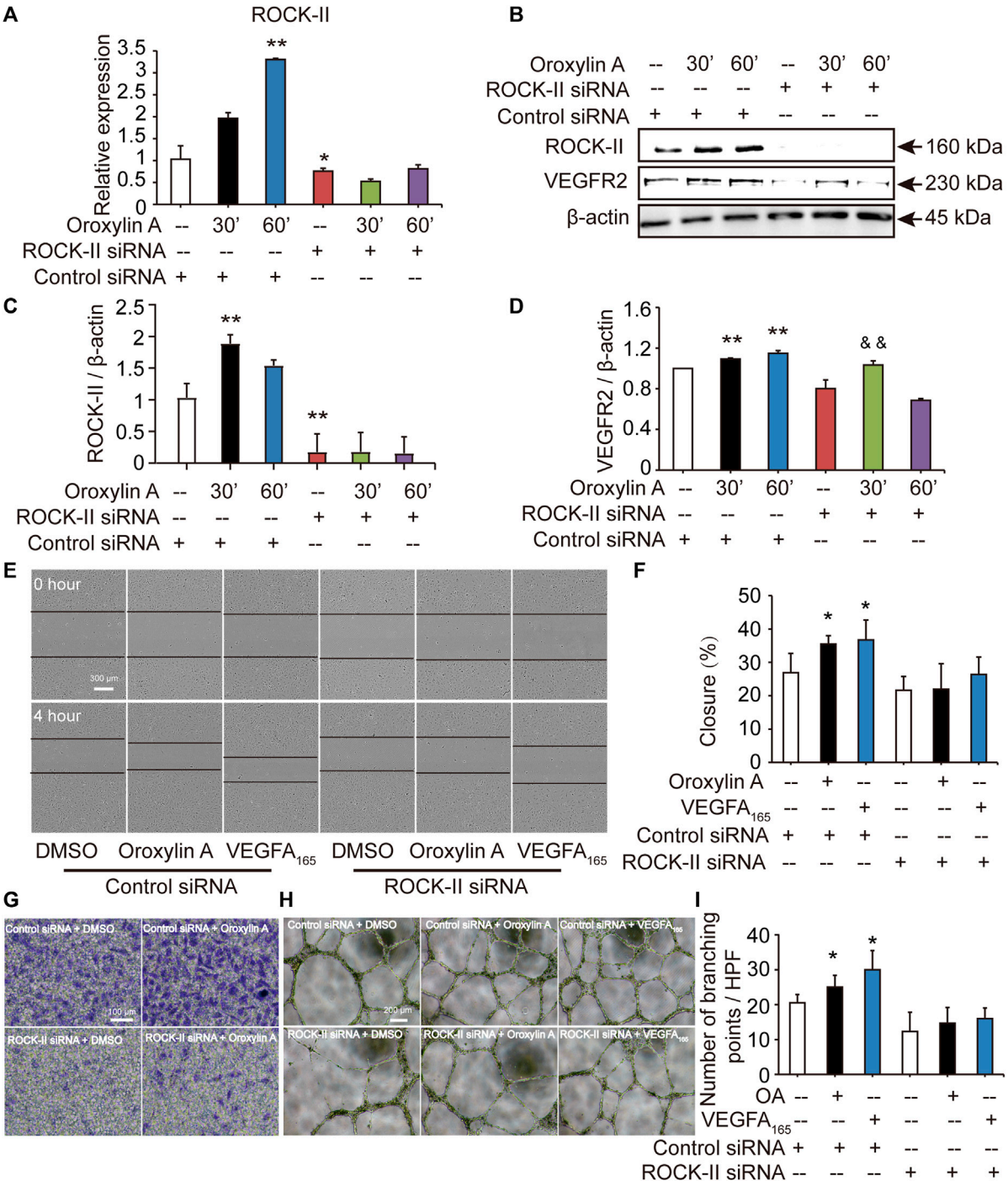

FIGURE 5 | Cell migrations and capillary-like structures of HUVECs induced by OA were decreased by silencing ROCK-II with siRNA. HUVECs were transfected with non-specific siRNA or ROCK-II siRNA and stimulated with DMSO or 2.5 μM OA for 30, 60 min and analyzed using qRT-PCR **(A)**. Western blotting analysis of ROCK-II and VEGFR2 in HUVECs transfected with non-specific siRNA or ROCK-II siRNA and stimulated with DMSO or 2.5 μM OA for 30, 60 min were performed in **(B)**. Quantitative data included ROCK-II **(C)** and VEGFR2 **(D)**. The mobility of HUVECs was analyzed by using scrape injury, with $VEGFA_{165}$ as a positive control. HUVECs were transfected with control siRNA or ROCK-II siRNA and stimulated with DMSO, 2.5 μM OA or $VEGFA_{165}$ for 4 h **(E)**. Quantitative data were shown in **(F)**. Performed Transwell invasion of HUVECs transfected with control siRNA or ROCK-II siRNA and stimulated with DMSO or 2.5 μM OA were presented in **(G)**. Representative images of tube formation of HUVECs transfected with control siRNA or ROCK-II siRNA and stimulated with DMSO, 2.5 μM OA or $VEGFA_{165}$ were presented, with $VEGFA_{165}$ as a positive control **(H)**. Quantitative data were shown in **(I)**. Data were represented as mean ± SD ($n = 3$). $^{*}p < 0.05$; $^{**}p < 0.01$ *vs*. control siRNA, $^{\&\&}p < 0.01$ *vs*. ROCK-II siRNA.

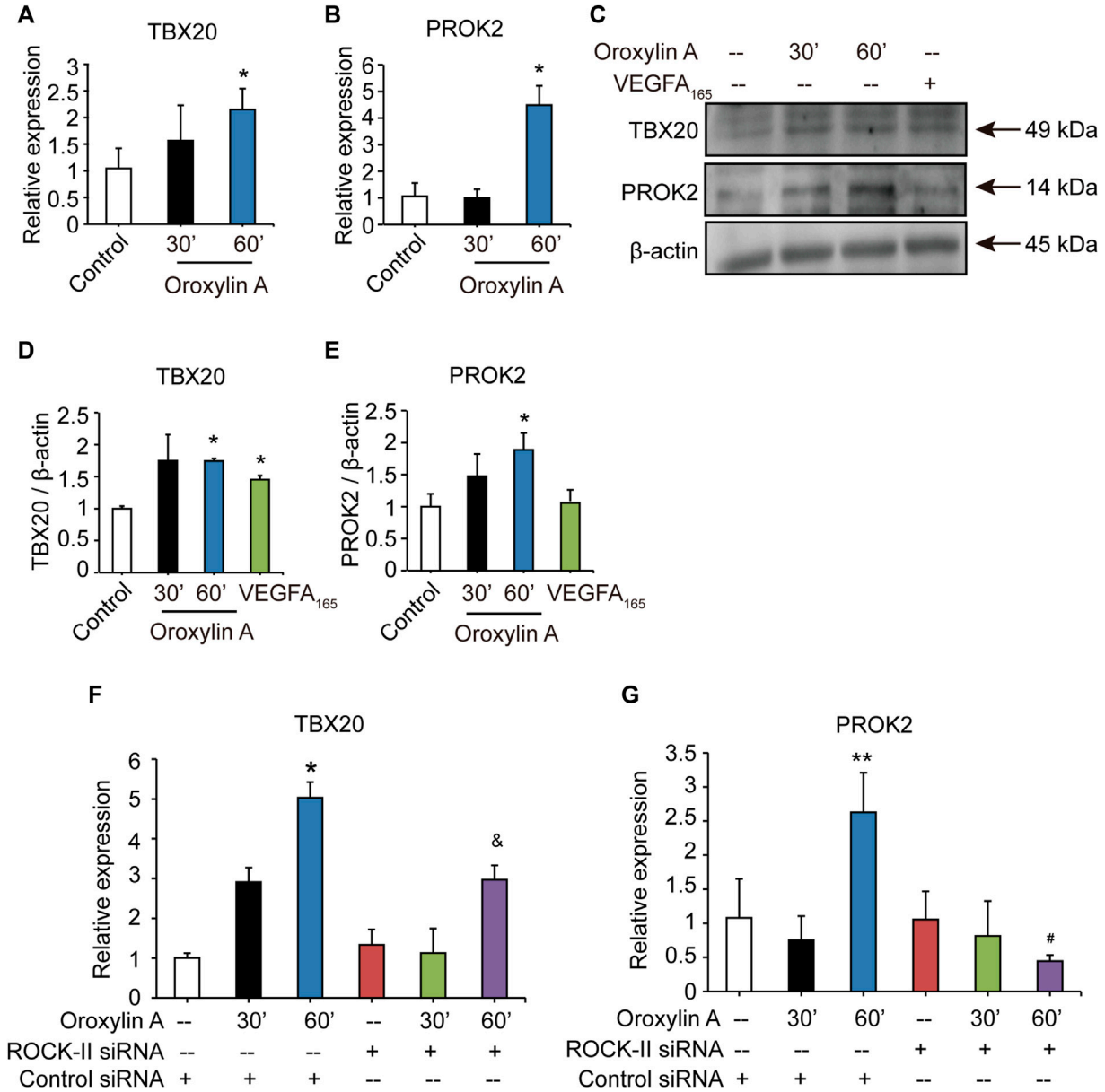

FIGURE 6 | OA regulated TBX20/PROK2 signaling pathway. Western blotting analysis of TBX20 or PROK2 in HUVECs stimulated with DMSO, 2.5 μM OA (30, 60 min) and $VEGFA_{165}$ (100 ng/ml), β-actin expression an internal control of protein loading was performed, with $VEGFA_{165}$ as a positive control **(A)**. Quantitative data included TBX20 **(B)** and PROK2 **(C)**. *TBX20* **(D)** and *PROK2* **(E)** mRNA expression in HUVECs treated with DMSO or 2.5 μM OA for 30, 60 min were analyzed using qRT-PCR. Statistical analysis of *TBX20* **(F)** and *PROK2* **(G)** mRNA of HUVECs transfected with non-specific siRNA or ROCK-II siRNA and stimulated with DMSO or 2.5 μM OA for 30, 60 min were presented. Data were represented as mean ± SD ($n = 3$). $^{*}p < 0.05$, $^{**}p < 0.01$ *vs*. control siRNA; $^{\&}p < 0.05$ *vs*. ROCK-II siRNA; $^{\#}p < 0.05$ *vs*. control siRNA + OA 60 min.

decreased by silencing ROCK-II (**Figures 5E–I**). This indicated that ROCK-II played an important role in OA-induced stress fiber formation and EC migration.

Oroxylin A Regulated the T-Box20/ Prokineticin 2 Signaling Pathway

After silencing ROCK-II with siRNA, we observed that the concurrent cell migrations and capillary-like structures of HUVECs were significantly decreased, but still existed. Therefore, we speculated that OA may regulate other key pathways to promote angiogenesis. Previous studies have shown that loss of TBX20-PROK2 hindered tube formation and EC migration in HUVECs (Meng et al., 2018). To verify the hypothesis, we explored the role of OA on the TBX20/PROK2 signaling pathway. Both qRT-PCR and Western blot analysis showed that OA significantly increased TBX20 and PROK2 expression in HUVECs (**Figures 6A–E**). These results

indicated that OA regulated the TBX20/PROK2 signaling pathway. Transfection of ROCK-II siRNA did not affect TBX20 and PROK2 expression when compared with the control siRNA, while PROK2 was robustly decreased by OA after silencing ROCK-II with siRNA (**Figures 6F,G**). These results confirmed that PROK2 functions downstream of ROCK-II. The above results suggest that these two pathways may play essential roles in promoting EC migration and that OA could promote EC migration through these two pathways to promote angiogenesis. Further investigation is required to fully understand this detailed mechanism.

DISCUSSION

In this study, we investigated the therapeutic efficacy of OA for the treatment of PAD. OA treatment significantly accelerated perfusion recovery following 14 days of therapy. In addition, OA treatment enhanced angiogenesis by inducing EC migration, promoted the secretion of VEGFA and ANG-2 in skeletal muscle cells, and modulated the inflammatory microenvironment. These results suggest that OA is emerging as a novel approach for patients with PAD.

In recent research, pivotal regulators of angiogenesis have been tested in human clinical trials to promote angiogenesis; however therapeutic outcomes remain far from satisfactory. Clinical designs for these trials have been single-targeted and have not considered the entire mechanism of angiogenesis, like the sprouting of ECs and further vascular maturation (Roncalli et al., 2008; Minoshima et al., 2018). VEGFA promotes tip cell selection, stalk elongation, and vascular maintenance (Carmeliet and Jain, 2011). FGF is critical for maintaining vascular integrity (Carmeliet and Jain, 2011). PDGF-BB plays a key role in the mature stage of angiogenesis (Carmeliet and Jain, 2011). Sequential delivery of VEGF and PDGF-BB improves revascularization and heart function after myocardial infarction (Awada et al., 2015). FGF-2 and PDGF-BB alone may cause vascular degeneration, while the combination of the two is more conducive to vascular stability and maturation (de Paula et al., 2009; Li et al., 2010). Sequential delivery of VEGF, FGF-2, and PDGF resulted in significant angiogenic differentiation of HUVECs and rapid formation of mature vascular networks in the chorioallantoic membrane (Bai et al., 2018). Nintedanib, co-targeting PDGFRs, VEGFRs, and FGFR, have been used in phase 3 trials (Scagliotti et al., 2019). In this study, OA promoted angiogenesis by regulating VEGFA, ANG-2, FGF-2, and PDGF-BB at distinct time points during angiogenesis. This implies that OA therapy could be exploited as a promising strategy to promote angiogenesis in clinic.

In this study, murine HLI model was performed on C57BL/6 mice as previously described (Limbourg et al., 2009; Brenes et al., 2012; Zhang et al., 2016; Ministro et al., 2017; Aref et al., 2019; Chang et al., 2019). Although there is minimal variation of the gross vascular anatomy of the femoral artery and its main branches in all mouse strains, the murine genetic background greatly influences the vascular response and the recovery of perfusion after femoral artery ligation. C57BL/6 mice are known to recover quickly from ischemia, as compared with the slow recovering Balb/C mice. It is critical to choose the optimal timing for perfusion imaging and tissue harvest. In our research, mice undergoing HLI showed a time-dependent increase in perfusion ratio that reached about 30% restoration of blood flow by day 14 post-HLI. The mean ratios of ischemic to non-ischemic perfusion in the OA group (0.59 ± 0.14) were significantly higher than that of saline group (0.33 ± 0.10), indicating OA improved perfusion in HLI mice. To further confirm that OA is an effective compound for treating HLI, animal experiments using other mouse strains will be performed in the future studies.

In the traditional Chinese medicinal practice, most crude drugs or compound formulas are prepared as decoctions and taken orally. Pharmacokinetic studies of OA after intragastrical administration in rats indicated that OA can be absorbed from the gastrointestinal tract in its native form and the concentration of OA in the plasma increased with time (Li et al., 2011; Cai et al., 2016; Ren et al., 2020). OA has two metabolites: oroxylin A 7-O-glucuronide (OG) and oroxylin A sodium sulfonate (OS). After the oral administration of OA, this molecule was more widely distributed in tissue than its metabolites and the tissue concentration level of OA was the highest. The C_{max} of OA was lower and the elimination rate was slower than intravenous administration. The angiogenic effects of active metabolites of OA will be further investigated in future studies.

Several therapeutic strategies have been tested to increase angiogenesis, including the use of growth factors and mononuclear cells. These approaches have had limited success in large clinical trials, which could be related to the chronic inflammatory environment typically encountered in patients with PAD (Cooke and Losordo, 2015; Zhang et al., 2016). Biopsies from patients with PAD showed clear signs of inflammation, with a significantly higher density of macrophages (Caradu et al., 2018). The inflammatory response is an integral part of the ischemic microenvironment, which is tightly coupled to angiogenesis (Jalkanen et al., 2016). Inflammatory cells multitask at the ischemic site by facilitating cellular debris removal and producing chemokines, metabolites, and growth factors. These molecules are helpful for the repair of ischemic tissue damage. Unfortunately, this well-orchestrated response becomes dysregulated in PAD. The ischemic tissue can produce a continuous inflammatory response, resulting in impaired tissue function. Previous studies have shown that OA had strong anti-inflammatory effects on macrophages *in vitro* (Wang et al., 2013). Our data revealed that, levels of neutrophils and macrophages increased significantly in the skeletal muscle of mice undergoing HLI. In addition, OA resolved inflammation by reducing neutrophil and macrophage recruitment and down-regulating pro-inflammatory cytokine IL-1β production in serum and tissue. OA could also promote ischemic tissue repair by promoting angiogenesis and downregulating the number of inflammatory cells and the secretion of inflammatory factors. These findings offered a novel beneficial mechanism of OA regarding PAD protection.

Angiogenesis requires EC proliferation and migration. Unlike growth factors, OA selectively controlled EC migration, but did not stimulate EC proliferation. Since we utilized VEGF as positive control, cell proliferation was significantly enhanced in VEGF group, indicating the experimental system is credible. There are several possible explanations for this unexpected result. First, the

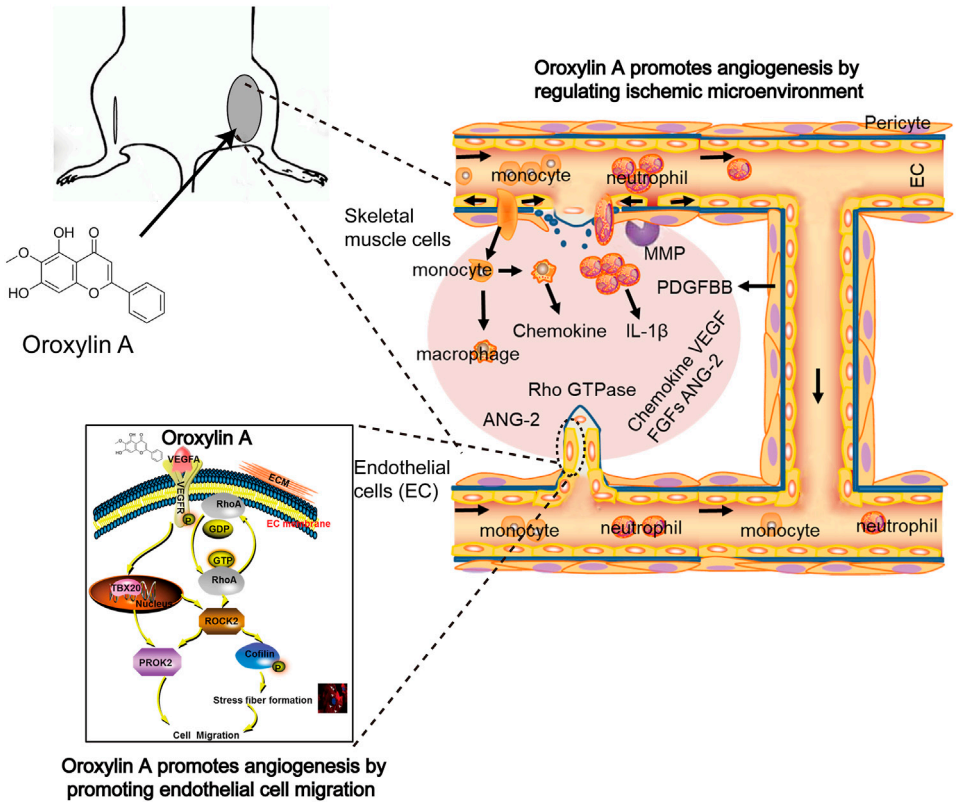

FIGURE 7 | OA increased angiogenesis through multiple mechanisms involving enhanced EC migration, elevated angiogenic factors release, and induced stabilization and growth of blood vessels.

OA-mediated elevated expression of VEGF in HUVEC was not sufficient to promote proliferation of ECs. Second, OA may inhibit proliferation of HUVEC through undiscovered mechanisms. This inhibitory effect counteracted the mitogenic effects of OA mediated by VEGF upregulation. Third, the concentrations, duration of drug delivery, and observation time may be responsible for the property of OA revealed in the present study. Further investigation is needed to unravel the detailed mechanisms of OA's effects.

Other preclinical studies have showed that inhibition of RhoA could prevent VEGF-enhanced EC migration in response to vascular injury (Van Nieuw Amerongen et al., 2003). Our study demonstrated that OA induced stress fiber formation and EC migration associated with an increase in RhoA activation, implying that RhoA may act as a possible therapeutic target of OA for inducing EC migration. ROCK-II is a downstream effector of RhoA. In response to VEGF, ECs with ROCK-II knockdown exhibit a drastic reduction in migration and tube formation (Liu et al., 2018). OA was found to stimulate ROCK-II expression. In HUVECs lacking ROCK-II, the beneficial effects of OA were abrogated. These data indicated that OA promoted tube formation through a ROCK-II-dependent mechanism. ROCK-activated LIMK then phosphorylates Cofilin and inactivates its actin-depolymerization activity, leading to stabilization of actin filaments (Li et al., 2005; Li et al., 2015). OA can upregulate the phosphorylation at serine-3 of Cofilin, which suggests that OA might promote stabilization of actin filaments by phosphorylating Cofilin. Therefore, it is reasonable to assume that the enhanced RhoA/ROCK-II/p-Cofilin signaling pathway induced by OA is associated with stress fiber formation and therefore improves tube formation in HUVECs.

During EC migration, in addition to the RhoA/ROCK-II signaling pathway, the TBX20/PROK2 signaling pathway acts as a "biological capacitor" to relay and sustain the pro-angiogenic effect of VEGF. This may be an aspect worth exploring for the treatment of PAD (Meng et al., 2018). TBX20 encodes a key transcription factor that is expressed in the heart, eyes, ventral neural tube, and limbs during embryonic development (Meins et al., 2000). PROK2 is a secreted protein that functions downstream of TBX20 and helps to regulate angiogenesis. A recent study showed that TBX20-regulated tube formation and cell migration in ECs, along with intramuscular injection of recombinant PROK2 protein increased blood perfusion recovery in the ischemic limb (Meng et al., 2018). Our present study validated the upregulation of TBX20 and PROK2 after treatment with OA in HUVECs, indicating that OA may promote EC migration and tube formation by promoting the TBX20/PROK2 signaling pathway. Previous work demonstrated that the regulation of GTPase activity is implicated in the modulation E-cadherin expression through a pathway involving TBX (Yano et al., 2011). ROCK inhibition resulted in a drastic change in

colony morphology, accompanied by the loss of TBX20 in murine embryonic stem cells and the induction of pluripotent stem cells (Cheng et al., 2015). We evaluated whether ROCK-II regulates the TBX20/PROK2 signaling pathway after OA treatment. The results showed that transfection of ROCK-II siRNA did not affect TBX20 and PROK2 expression; however, PROK2 was robustly decreased by OA after silencing ROCK-II. For the first time, we observed that PROK2 may be regulated by ROCK-II during angiogenesis *in vitro* after OA treatment. Further studies will be performed to determine whether ROCK-II affects PROK2 expression in the OA-treated group during angiogenesis after HLI. These results provide new drug targets to treat diseases with dysregulated angiogenesis.

Previous studies have shown that pathologic neovascularization is inhibited by OA (Gao et al., 2010; Song et al., 2012; Zhang et al., 2018; Zhao et al., 2018). The effect of OA differs between different studies due to different concentrations and the complexity of various tissue microenvironment. Previous studies have shown that HUVECs cultured in medium 199 containing FBS, EGF and endothelial cell growth supplement, which were treated with OA for 1 h at concentrations of 1, 10, and 100 μM, were able to suppress the VEGF and LPS-stimulated migration and tube formation. And OA (1 μM) suppressed the VEGF-stimulated migration and tube formation through blocking MAPK signaling pathway induced by VEGF. In murine primary liver sinusoidal endothelial cells (LSECs), concentrations of 20, 30, and 40 μM of OA inhibited hypoxia-induced angiogenesis as indicated by MTT and tube formation assays. For 24 h of treatment with oroxylin A-7-glucuronide (Oroxyloside), a main metabolite of OA, inhibited the proliferation, migration, and tube formation of human endothelial cells at concentrations of 40, 80, and 160 μM. Compared with previous studies, we explored the direct effect of OA on endothelial cells. The concentrations we chose are 2.5, 5, 10 and 20 μM. The treatment time is 24 h. The results showed that OA inhibited the viability of endothelial cells at 20 μM and inhibited endothelial cell proliferation at 10 μM after 24 h of treatment. A concentration of 2.5 μM OA was found to significantly induce tube formation in HUVECs. We selected 2.5 μM as the concentration of OA in subsequent experiments. OA promoted endothelial cell migration through the GTPases signaling pathway. The above results indicated that OA may play a dual role: low concentration of OA promotes angiogenesis, while high concentration of OA possesses anti-angiogenic effects. This is not uncommon, and a similar phenomenon took place in tetramethyl pyrazine (TMP), *panax ginseng*, rhubarb, and danshensu (Zhang et al., 2010; Qin et al., 2011; Chen et al., 2012; Zhang et al., 2014; Yin et al., 2017), implying that drug dose is an important parameter for the efficacy of drugs and that the same drug may play a diametrically opposite and context-dependent role in different pathological states. This property of OA could be particularly beneficial in the context of atherosclerosis and cancer, where angiogenesis could fuel disease progression.

In conclusion, the data suggested that OA increased angiogenesis through multiple mechanisms (**Figure 7**). First, OA could act on ECs to stimulate endothelial migration. Second, OA treatment increased the expression of several angiogenic factors, including VEGFA, ANG-2, PDGF-BB, and FGF-2 in ischemic muscle at distinct time points post ischemia. Third, OA promoted the release of VEGFA and ANG-2 in skeletal muscle cells, which induced proliferation of ECs. Finally, OA promoted the formation of smooth, muscle-covered, mature blood vessels. The maturation of blood vessels into multilayer structures is essential for their persistence. These results uncovered a new role of OA in tissue revascularization following ischemic injury and could open up new directions for the development of novel therapeutic interventions for patients with PAD.

DATA AVAILABILITY STATEMENT

The original contributions presented in the study are included in the article/**Supplementary Material**, further inquiries can be directed to the corresponding author.

ETHICS STATEMENT

The animal study was reviewed and approved by Animal Ethics Committee of Tianjin University of Traditional Chinese Medicine.

AUTHOR CONTRIBUTIONS

HW and LC conceived and designed the study and wrote the manuscript; LZ and CL performed major experiments and analyzed data; HS, QW, and LF performed part of Western blotting experiments; WY, YL, WS, ML, and YX performed part of animal and cell culture experiments. XG made the final approval of the version to be published. All authors had contributed and approved the manuscript.

FUNDING

This work was supported by the Program of International S and T Cooperation Project of China (Grant No 2015DFA30430); the National Natural Science Foundation of China (Grant No 81603329); and Natural Science Foundation of Tianjin Municipal Government (Grant No 16JCZDJC36300).

ACKNOWLEDGMENTS

We thank LetPub (www.letpub.com) for its linguistic assistance during the preparation of this manuscript.

SUPPLEMENTARY MATERIAL

The Supplementary Material for this article can be found online at: https://www.frontiersin.org/articles/10.3389/fphar.2021.705617/full#supplementary-material

REFERENCES

Albrecht-Schgoer, K., Barthelmes, J., Schgoer, W., Theurl, M., Nardin, I., Lener, D., et al. (2017). Nanoparticular Delivery System for a Secretoneurin Derivative Induces Angiogenesis in a Hind Limb Ischemia Model. *J. Controlled Release* 250, 1–8. doi:10.1016/j.jconrel.2017.02.004

Aref, Z., de Vries, M. R., and Quax, P. H. A. (2019). Variations in Surgical Procedures for Inducing Hind Limb Ischemia in Mice and the Impact of These Variations on Neovascularization Assessment. *Ijms* 20 (15), 3704. doi:10.3390/ijms20153704

Awada, H. K., Johnson, N. R., and Wang, Y. (2015). Sequential Delivery of Angiogenic Growth Factors Improves Revascularization and Heart Function after Myocardial Infarction. *J. Controlled Release* 207, 7–17. doi:10.1016/j.jconrel.2015.03.034

Bai, Y., Bai, L., Zhou, J., Chen, H., and Zhang, L. (2018). Sequential Delivery of VEGF, FGF-2 and PDGF from the Polymeric System Enhance HUVECs Angiogenesis *In Vitro* and CAM Angiogenesis. *Cell Immunol.* 323, 19–32. doi:10.1016/j.cellimm.2017.10.008

Brenes, R. A., Jadlowiec, C. C., Bear, M., Hashim, P., Protack, C. D., Li, X., et al. (2012). Toward a Mouse Model of Hind Limb Ischemia to Test Therapeutic Angiogenesis. *J. Vasc. Surg.* 56 (6), 1669–1679. doi:10.1016/j.jvs.2012.04.067

Bryan, B. A., Dennstedt, E., Mitchell, D. C., Walshe, T. E., Noma, K., Loureiro, R., et al. (2010). RhoA/ROCK Signaling Is Essential for Multiple Aspects of VEGF-mediated Angiogenesis. *FASEB j.* 24, 3186–3195. doi:10.1096/fj.09-145102

Cai, Y., Li, S., Li, T., Zhou, R., Wai, A. T.-S., and Yan, R. (2016). Oral Pharmacokinetics of Baicalin, Wogonoside, Oroxylin A 7- O -β- D -glucuronide and Their Aglycones from an Aqueous Extract of Scutellariae Radix in the Rat. *J. Chromatogr. B* 1026, 124–133. doi:10.1016/j.jchromb.2015.11.049

Caradu, C., Couffinhal, T., Chapouly, C., Guimbal, S., Hollier, P.-L., Ducasse, E., et al. (2018). Restoring Endothelial Function by Targeting Desert Hedgehog Downstream of Klf2 Improves Critical Limb Ischemia in Adults. *Circ. Res.* 123, 1053–1065. doi:10.1161/circresaha.118.313177

Carmeliet, P., and Jain, R. K. (2011). Molecular Mechanisms and Clinical Applications of Angiogenesis. *Nature* 473, 298–307. doi:10.1038/nature10144

Chang, T.-T., Lin, L.-Y., and Chen, J.-W. (2019). Inhibition of Macrophage Inflammatory Protein-1β Improves Endothelial Progenitor Cell Function and Ischemia-Induced Angiogenesis in Diabetes. *Angiogenesis* 22 (1), 53–65. doi:10.1007/s10456-018-9636-3

Chen, I.-J., Chang, M.-Y., Chiao, S.-L., Chen, J.-L., Yu, C.-C., Yang, S.-H., et al. (2012). Korean Red Ginseng Improves Blood Pressure Stability in Patients with Intradialytic Hypotension. *Evidence-Based Complement. Altern. Med.* 2012, 1–9. doi:10.1155/2012/595271

Cheng, Y.-T., Yeih, D.-F., Liang, S.-M., Chien, C.-Y., Yu, Y.-L., Ko, B.-S., et al. (2015). Rho-associated Kinase Inhibitors Promote the Cardiac Differentiation of Embryonic and Induced Pluripotent Stem Cells. *Int. J. Cardiol.* 201, 441–448. doi:10.1016/j.ijcard.2015.08.118

Cooke, J. P., and Losordo, D. W. (2015). Modulating the Vascular Response to Limb Ischemia. *Circ. Res.* 116 (9), 1561–1578. doi:10.1161/CIRCRESAHA.115.303565

de Paula, E. V., Flores-Nascimento, M. C., Arruda, V. R., Garcia, R. A., Ramos, C. D., Guillaumon, A. T., et al. (2009). Dual Gene Transfer of Fibroblast Growth Factor-2 and Platelet Derived Growth Factor-BB Using Plasmid Deoxyribonucleic Acid Promotes Effective Angiogenesis and Arteriogenesis in a Rodent Model of Hindlimb Ischemia. *Translational Res.* 153, 232–239. doi:10.1016/j.trsl.2009.02.002

Fan, Y., Lu, H., Liang, W., Garcia-Barrio, M. T., Guo, Y., Zhang, J., et al. (2018). Endothelial TFEB (Transcription Factor EB) Positively Regulates Postischemic Angiogenesis. *Circ. Res.* 122 (7), 945–957. doi:10.1161/CIRCRESAHA.118.312672

Gao, Y., Lu, N., Ling, Y., Chen, Y., Wang, L., Zhao, Q., et al. (2010). Oroxylin A Inhibits Angiogenesis through Blocking Vascular Endothelial Growth Factor-Induced KDR/Flk-1 Phosphorylation. *J. Cancer Res. Clin. Oncol.* 136 (5), 667–675. doi:10.1007/s00432-009-0705-2

Gerhard-Herman, M. D., Gornik, H. L., Barrett, C., Barshes, N. R., Corriere, M. A., Drachman, D. E., et al. (2017). 2016 AHA/ACC Guideline on the Management of Patients with Lower Extremity Peripheral Artery Disease: Executive Summary: A Report of the American College of Cardiology/American Heart Association Task Force on Clinical Practice Guidelines. *Circulation* 135, e686–e725. doi:10.1161/cir.0000000000000470

Gorenoi, V., Brehm, M. U., Koch, A., and Hagen, A. (2017). Growth Factors for Angiogenesis in Peripheral Arterial Disease. *Cochrane Database Syst. Rev.* 6, CD011741. doi:10.1002/14651858.CD011741.pub2

Jalkanen, J., Maksimow, M., Hollmén, M., Jalkanen, S., and Hakovirta, H. (2016). Compared to Intermittant Claudication Critical Limb Ischemia Is Associated with Elevated Levels of Cytokines. *PLoS One* 11 (9), e0162353. doi:10.1371/journal.pone.0162353

Lee, H., and Kang, K.-T. (2018). Advanced Tube Formation Assay Using Human Endothelial Colony Forming Cells for *In Vitro* Evaluation of Angiogenesis. *Korean J. Physiol. Pharmacol.* 22 (6), 705–712. doi:10.4196/kjpp.2018.22.6.705

Li, C., Zhang, L., Lin, G., and Zuo, Z. (2011). Identification and Quantification of Baicalein, Wogonin, Oroxylin A and Their Major Glucuronide Conjugated Metabolites in Rat Plasma after Oral Administration of Radix Scutellariae Product. *J. Pharm. Biomed. Anal.* 54 (4), 750–758. doi:10.1016/j.jpba.2010.10.005

Li, J., Wei, Y., Liu, K., Yuan, C., Tang, Y., Quan, Q., et al. (2010). Synergistic Effects of FGF-2 and PDGF-BB on Angiogenesis and Muscle Regeneration in Rabbit Hindlimb Ischemia Model. *Microvasc. Res.* 80, 10–17. doi:10.1016/j.mvr.2009.12.002

Li, S., Dang, Y., Zhou, X., Huang, B., Huang, X., Zhang, Z., et al. (2015). Formononetin Promotes Angiogenesis through the Estrogen Receptor Alpha-Enhanced ROCK Pathway. *Sci. Rep.* 5, 16815. doi:10.1038/srep16815

Li, S., Guan, J.-L., and Chien, S. (2005). Biochemistry and Biomechanics of Cell Motility. *Annu. Rev. Biomed. Eng.* 7, 105–150. doi:10.1146/annurev.bioeng.7.060804.100340

Limbourg, A., Korff, T., Napp, L. C., Schaper, W., Drexler, H., and Limbourg, F. P. (2009). Evaluation of Postnatal Arteriogenesis and Angiogenesis in a Mouse Model of Hind-Limb Ischemia. *Nat. Protoc.* 4 (12), 1737–1748. doi:10.1038/nprot.2009.185

Liu, C.-H., Chen, M.-F., Tseng, T.-L., Chen, L.-G., Kuo, J.-S., and Lee, T. J.-F. (2012). Oroxylin A, but Not Vasopressin, Ameliorates Cardiac Dysfunction of Endotoxemic Rats. *Evidence-Based Complement. Altern. Med.* 2012, 1–12. doi:10.1155/2012/408187

Liu, J., Wada, Y., Katsura, M., Tozawa, H., Erwin, N., Kapron, C. M., et al. (2018). Rho-Associated Coiled-Coil Kinase (ROCK) in Molecular Regulation of Angiogenesis. *Theranostics* 8, 6053–6069. doi:10.7150/thno.30305

McDermott, M. M., and Kibbe, M. R. (2017). Improving Lower Extremity Functioning in Peripheral Artery Disease. *JAMA* 317 (7), 689–690. doi:10.1001/jama.2016.20673

Meins, M., Henderson, D. J., Bhattacharya, S. S., and Sowden, J. C. (2000). Characterization of the Human TBX20 Gene, a New Member of the T-Box Gene Family Closely Related to the Drosophila H15 Gene. *Genomics* 67, 317–332. doi:10.1006/geno.2000.6249

Meng, S., Gu, Q., Yang, X., Lv, J., Owusu, I., Matrone, G., et al. (2018). TBX20 Regulates Angiogenesis through the Prokineticin 2-Prokineticin Receptor 1 Pathway. *Circulation* 138, 913–928. doi:10.1161/circulationaha.118.033939

Ministro, A., de Oliveira, P., Nunes, R. J., Dos Santos Rocha, A., Correia, A., Carvalho, T., et al. (2017). Low-dose Ionizing Radiation Induces Therapeutic Neovascularization in a Pre-clinical Model of Hindlimb Ischemia. *Cardiovasc. Res.* 113 (7), 783–794. doi:10.1093/cvr/cvx065

Minoshima, A., Kabara, M., Matsuki, M., Yoshida, Y., Kano, K., Tomita, Y., et al. (2018). Pericyte-specific Ninjurin1 Deletion Attenuates Vessel Maturation and Blood Flow Recovery in Hind Limb Ischemia. *Atvb* 38 (10), 2358–2370. doi:10.1161/ATVBAHA.118.311375

Mittermayr, R., Slezak, P., Haffner, N., Smolen, D., Hartinger, J., Hofmann, A., et al. (2016). Controlled Release of Fibrin Matrix-Conjugated Platelet Derived Growth Factor Improves Ischemic Tissue Regeneration by Functional Angiogenesis. *Acta Biomater.* 29, 11–20. doi:10.1016/j.actbio.2015.10.028

Murakami, M., Nguyen, L. T., Zhang, Z. W., Moodie, K. L., Carmeliet, P., Stan, R. V., et al. (2008). The FGF System Has a Key Role in Regulating Vascular Integrity. *J. Clin. Invest.* 118, 3355–3366. doi:10.1172/jci35298

Potente, M., Gerhardt, H., and Carmeliet, P. (2011). Basic and Therapeutic Aspects of Angiogenesis. *Cell* 146, 873–887. doi:10.1016/j.cell.2011.08.039

Qin, Y., Wang, J.-b., Kong, W.-j., Zhao, Y.-l., Yang, H.-y., Dai, C.-m., et al. (2011). The Diarrhoeogenic and Antidiarrhoeal Bidirectional Effects of Rhubarb and its

Potential Mechanism. *J. Ethnopharmacology* 133, 1096–1102. doi:10.1016/j.jep.2010.11.041

Rajasagi, N. K., Bhela, S., Varanasi, S. K., and Rouse, B. T. (2017). Frontline Science: Aspirin-Triggered Resolvin D1 Controls Herpes Simplex Virus-Induced Corneal Immunopathology. *J. Leukoc. Biol.* 102 (5), 1159–1171. doi:10.1189/jlb.3hi1216-511rr

Ren, G., Chen, H., Zhang, M., Yang, N., Yang, H., Xu, C., et al. (2020). Pharmacokinetics, Tissue Distribution and Excretion Study of Oroxylin A, Oroxylin A 7-O-Glucuronide and Oroxylin A Sodium Sulfonate in Rats after Administration of Oroxylin A. *Fitoterapia* 142, 104480. doi:10.1016/j.fitote.2020.104480

Roncalli, J., Tongers, J., Renault, M.-A., and Losordo, D. W. (2008). Biological Approaches to Ischemic Tissue Repair: Gene- and Cell-Based Strategies. *Expert Rev. Cardiovasc. Ther.* 6 (5), 653–668. doi:10.1586/14779072.6.5.653

Saleh, A., Stathopoulou, M. G., Dadé, S., Ndiaye, N. C., Azimi-Nezhad, M., Murray, H., et al. (2015). Angiogenesis Related Genes NOS3, CD14, MMP3 and IL4R Are Associated to VEGF Gene Expression and Circulating Levels in Healthy Adults. *BMC Med. Genet.* 16, 90. doi:10.1186/s12881-015-0234-6

Scagliotti, G. V., Gaafar, R., Nowak, A. K., Nakano, T., van Meerbeeck, J., Popat, S., et al. (2019). Nintedanib in Combination with Pemetrexed and Cisplatin for Chemotherapy-Naive Patients with Advanced Malignant Pleural Mesothelioma (LUME-Meso): a Double-Blind, Randomised, Placebo-Controlled Phase 3 Trial. *Lancet Respir. Med.* 7 (7), 569–580. doi:10.1016/S2213-2600(19)30139-0

Skovseth, D. K., Veuger, M. J. T., Sorensen, D. R., De Angelis, P. M., and Haraldsen, G. (2005). Endostatin Dramatically Inhibits Endothelial Cell Migration, Vascular Morphogenesis, and Perivascular Cell Recruitment *In Vivo*. *Blood* 105, 1044–1051. doi:10.1182/blood-2004-03-1164

Song, X., Chen, Y., Sun, Y., Lin, B., Qin, Y., Hui, H., et al. (2012). Oroxylin A, a Classical Natural Product, Shows a Novel Inhibitory Effect on Angiogenesis Induced by Lipopolysaccharide. *Pharmacol. Rep.* 64 (5), 1189–1199. doi:10.1016/s1734-1140(12)70915-5

Sun, H.-J., Cai, W.-W., Gong, L.-L., Wang, X., Zhu, X.-X., Wan, M.-Y., et al. (2017). FGF-2-mediated FGFR1 Signaling in Human Microvascular Endothelial Cells Is Activated by Vaccarin to Promote Angiogenesis. *Biomed. Pharmacother* 95, 144–152. doi:10.1016/j.biopha.2017.08.059

Suzuki, J.-i., Shimamura, M., Suda, H., Wakayama, K., Kumagai, H., Ikeda, Y., et al. (2016). Current Therapies and Investigational Drugs for Peripheral Arterial Disease. *Hypertens. Res.* 39, 183–191. doi:10.1038/hr.2015.134

Tseng, T.-L., Chen, M.-F., Liu, C.-H., Pang, C.-Y., Hsu, Y.-H., and Lee, T. J. F. (2016). Induction of Endothelium-dependent Constriction of Mesenteric Arteries in Endotoxemic Hypotensive Shock. *Br. J. Pharmacol.* 173 (7), 1179–1195. doi:10.1111/bph.13415

Tseng, T.-L., Chen, M.-F., Tsai, M.-J., Hsu, Y.-H., Chen, C.-P., and Lee, T. J. F. (2012). Oroxylin-A Rescues LPS-Induced Acute Lung Injury via Regulation of NF-κB Signaling Pathway in Rodents. *PLoS One* 7 (10), e47403. doi:10.1371/journal.pone.0047403

Van Nieuw Amerongen, G. P., Koolwijk, P., Versteilen, A., and Van Hinsbergh, V. W. M. (2003). Involvement of RhoA/Rho Kinase Signaling in VEGF-Induced Endothelial Cell Migration and Angiogenesis *In Vitro*. *Atvb* 23 (2), 211–217. doi:10.1161/01.ATV.0000054198.68894.88

Wang, H., Guo, Y., Zhao, X., Li, H., Fan, G., Mao, H., et al. (2013). An Estrogen Receptor Dependent Mechanism of Oroxylin A in the Repression of Inflammatory Response. *PLoS One* 8, e69555. doi:10.1371/journal.pone.0069555

Warner, H., Wilson, B. J., and Caswell, P. T. (2019). Control of Adhesion and Protrusion in Cell Migration by Rho GTPases. *Curr. Opin. Cell Biol.* 56, 64–70. doi:10.1016/j.ceb.2018.09.003

Yano, T., Yamazaki, Y., Adachi, M., Okawa, K., Fort, P., Uji, M., et al. (2011). Tara Up-Regulates E-Cadherin Transcription by Binding to the Trio RhoGEF and Inhibiting Rac Signaling. *J. Cell Biol.* 193, 319–332. doi:10.1083/jcb.201009100

Yin, Y., Duan, J., Guo, C., Wei, G., Wang, Y., Guan, Y., et al. (2017). Danshensu Accelerates Angiogenesis after Myocardial Infarction in Rats and Promotes the Functions of Endothelial Progenitor Cells through SDF-1α/CXCR4 axis. *Eur. J. Pharmacol.* 814, 274–282. doi:10.1016/j.ejphar.2017.08.035

Zhang, C., Bian, M., Chen, X., Jin, H., Zhao, S., Yang, X., et al. (2018). Oroxylin A Prevents Angiogenesis of LSECs in Liver Fibrosis via Inhibition of YAP/HIF-1α Signaling. *J. Cell. Biochem.* 119 (2), 2258–2268. doi:10.1002/jcb.26388

Zhang, L.-j., Chen, L., Lu, Y., Wu, J.-m., Xu, B., Sun, Z.-g., et al. (2010). Danshensu Has Anti-tumor Activity in B16F10 Melanoma by Inhibiting Angiogenesis and Tumor Cell Invasion. *Eur. J. Pharmacol.* 643 (2-3), 195–201. doi:10.1016/j.ejphar.2010.06.045

Zhang, M., Gao, F., Teng, F., and Zhang, C. (2014). Tetramethylpyrazine Promotes the Proliferation and Migration of Brain Endothelial Cells. *Mol. Med. Rep.* 10, 29–32. doi:10.3892/mmr.2014.2169

Zhang, M. J., Sansbury, B. E., Hellmann, J., Baker, J. F., Guo, L., Parmer, C. M., et al. (2016). Resolvin D2 Enhances Postischemic Revascularization while Resolving Inflammation. *Circulation* 134, 666–680. doi:10.1161/circulationaha.116.021894

Zhao, K., Li, X., Lin, B., Yang, D., Zhou, Y., Li, Z., et al. (2018). Oroxyloside Inhibits Angiogenesis through Suppressing Internalization of VEGFR2/Flk-1 in Endothelial Cells. *J. Cell. Physiol.* 233 (4), 3454–3464. doi:10.1002/jcp.26198

Conflict of Interest: The authors declare that the research was conducted in the absence of any commercial or financial relationships that could be construed as a potential conflict of interest.

Publisher's Note: All claims expressed in this article are solely those of the authors and do not necessarily represent those of their affiliated organizations, or those of the publisher, the editors and the reviewers. Any product that may be evaluated in this article, or claim that may be made by its manufacturer, is not guaranteed or endorsed by the publisher.

frontiers in Pharmacology

ORIGINAL RESEARCH
published: 13 August 2021
doi: 10.3389/fphar.2021.722530

Huangqi Shengmai Yin Ameliorates Myocardial Fibrosis by Activating Sirtuin3 and Inhibiting TGF-β/Smad Pathway

*Jianheng Pan[1], Zhanhong Cao[1], Chunqiu Fang[1], Yuting Lei[1], Jiaming Sun[2], Xiaowei Huang[1] and Dong Han[1]**

[1]Department of Pharmacy, Changchun University of Chinese Medicine, Changchun, China, [2]Jilin Ginseng Academy, Changchun University of Chinese Medicine, Changchun, China

Myocardial fibrosis (MF) is an important pathological process in which a variety of cardiovascular diseases transform into heart failure. The main manifestation of MF is the excessive deposition of collagen in the myocardium. Here, we explored whether Huangqi Shengmai Yin (HSY) can inhibit isoprenaline (ISO)-induced myocardial collagen deposition in rats, thereby reducing the cardiac dysfunction caused by MF. The results of echocardiography showed that HSY upregulated fractional shortening and ejection fraction, and reduced the left ventricular systolic dysfunction in the rats with MF. Pathological results showed that HSY protected myocardium, inhibited apoptosis, and effectively reduced collagen deposition. HSY also inhibited the expression of collagen I and III and α-smooth muscle actin (α-SMA) in the heart tissue. HSY increased the expression of Sirtuin 3 (Sirt3) and inhibited the protein levels of the components in the transforming growth factor-β (TGF-β)/Smad pathway. At the same time, it also regulated the expression of related proteins in the matrix metalloproteinases family. In summary, HSY played a therapeutic role in rats with ISO-induced MF by protecting myocardium and inhibiting collagen deposition. Therefore, HSY is a potential therapeutic agent for ameliorating MF.

Keywords: Huangqi Shengmai Yin, myocardial fibrosis, isoprenaline, sirtuin 3, TGF-β/Smad pathway

OPEN ACCESS

Edited by:
Yusof Kamisah, Universiti Kebangaan Malaysia, Malaysia

Reviewed by:
Satirah Zainalabidin, Universiti Kebangsaan Malaysia (UKM), Malaysia
Ying-Yong Zhao, Northwest University, China

****Correspondence:***
Dong Han
handong01@ccucm.edu.cn

Specialty section:
This article was submitted to Ethnopharmacology, a section of the journal Frontiers in Pharmacology

Received: *08 June 2021*
Accepted: *06 August 2021*
Published: *13 August 2021*

Citation:
Pan J, Cao Z, Fang C, Lei Y, Sun J, Huang X and Han D (2021) Huangqi Shengmai Yin Ameliorates Myocardial Fibrosis by Activating Sirtuin3 and Inhibiting TGF-β/Smad Pathway. Front. Pharmacol. 12:722530. doi: 10.3389/fphar.2021.722530

INTRODUCTION

Despite the increasing development of medicine and living standards, cardiovascular diseases are still currently the main cause of death (Oka et al., 2014). Many diseases, such as dilated cardiomyopathies, diabetic cardiomyopathies, and acute myocardial infarctions, are associated with myocardial fibrosis (MF) (McDonald et al., 2018; Yuan et al., 2018; Zhang et al., 2018). Delaying the development of MF is thus an effective strategy to reduce the risk of death from cardiovascular disease.

MF is caused by excessive accumulation of extracellular matrix proteins, which contributes to systolic and diastolic dysfunction, ultimately leading to the heart failure. It has been reported that the Renin-Angiotensin-Aldosterone System (RAAS) is involved in MF through transforming growth factor-β (TGF-β) (Gourdie et al., 2016), angiotensin II(Ang II) (He and Ou 2020), and other factors. After myocardial infarction occurs in the body, the process of MF is activated, a large amount of collagen is secreted, and scar tissue is formed by deposition. On the one hand, the formation of scar tissue ensures the integrity of the myocardial tissue; however, on the other hand, the scar tissue that is formed due to excessive MF reduces myocardial elasticity, leading to a systolic and diastolic

TABLE 1 | Composition of HSY.

Component	Family	Concentrations (g/100 ml)
Astragalus mongholicus Bunge	Leguminosae	30
Codonopsis pilosula (Franch.) Nannf	Campanulaceae	20
Ophiopogon japonicus (Thunb.) Ker Gawl	Liliaceae	20
Schisandra chinensis (Turcz.) Baill	Magnoliaceae	10

dysfunction (Leask 2015). At the same time, some related cytokines that promotes cardiomyocyte hypertrophy are also secreted, resulting in heart failure and even death (Mohammed et al., 2015; Stuart et al., 2016). Therefore, many researchers have been exploring safe and effective methods to ameliorate MF. In recent years, many studies have shown that Traditional Chinese medicine (TCM) has a significant effect in the alleviation of MF (Lv et al., 2020).

Huangqi Shengmai Yin (HSY) is a Chinese medicine compound prescriptions which is evolved from the basic prescription of Sheng mai power and composed of *Astragalus mongholicus* Bunge, *Codonopsis pilosula* (Franch.) Nannf., *Ophiopogon japonicus* (Thunb.) Ker Gawl., and *Schisandra chinensis* (Turcz.) Baill. (**Table 1**). HSY is traditionally used to treat cardiovascular diseases, respiratory diseases and improve immunity (Liu et al., 2009). Modern pharmacological studies have shown that HSY has pharmacological effects such as dilating blood vessels, increasing myocardial contractility and anti-virus. Clinically, HSY is mainly used to treat viral myocarditis, coronary heart disease and heart failure (Jiang et al., 2021). In addition, some studies have shown HSY can alleviate radiation-induced MF (Gu et al., 2019). However, the protective effects of HSY against MF after myocardial infarction have not yet been reported. In this study, we aimed to examine the hypothesis that HSY exerts its cardioprotective effect by inhibiting collagen deposition in a rat model of isoprenaline (ISO)-induced MF. Considering the fact that captopril, an angiotensin-converting enzyme inhibitor, has antifibrotic activity by diminishing MF associated with enhanced collagen degradation, the drug was used as a positive control in this study (Brilla et al., 2003; Guo et al., 2010; Wang, Shen, et al., 2019).

MATERIALS AND METHODS

Preparation of Huangqi Shengmai Yin

The HSY (batch no. 190916) was purchased from the Nan Chang Ji Sheng Pharmaceutical Factory (Nanchang, China). HSY (GB (2014)Z-0058)) was routinely prepared according to Chinese standard (No. WS3-B-3102-98-1). *Codonopsis pilosula* (Franch.) Nannf. (200 g), *Ophiopogon japonicus* (Thunb.) Ker Gawl. (200 g) and *Schisandra chinensis* (Turcz.) Baill. (100 g) were extracted twice by boiling water, and the two decoctions were combined, filtered, concentrated, and precipitated by ethanol to remove the impurities. Ethanol was recovered from the supernatant by evaporation, and then the supernatant was suspended in water, and medicinal charcoal was added, and then the filtrate was filtered to form extract A. *Astragalus mongholicus* Bunge (300 g) was extracted by boiling water twice, and the two decoctions were combined, then filtered, concentrated, and then precipitated by ethanol. The precipitate was dissolved with ethanol, filtered, and ethanol was removed. Then it was combined with the above-mentioned extract A. Steviosin (0.2 g) and sodium benzoate(3 g) were added, and water was added to 1000ml, and then the pH was adjusted, stirred, sealed, and sterilized. Finally, HSY was obtained. In the final preparation solution, the concentration of *Codonopsis pilosula* (Franch.) Nannf. was 0.2 g/ml, the concentration of *Ophiopogon japonicus* (Thunb.) Ker Gawl. was 0.2 g/ml, the concentration of *Schisandra chinensis* (Turcz.) Baill. was 0.1 g/ml, the concentration of *Astragalus mongholicus* Bunge was 0.3 g/ml.

Reagents and Drugs

The ISO was obtained from Sigma-Aldrich (St. Louis, MO, United States). The captopril was purchased from the PURCON Pharmaceutical Factory (Shanghai, China). The creatine kinase (CK), hydroxyproline (HYP), and lactate dehydrogenase (LDH) kits were purchased from Nanjing Jiancheng Bioengineering Institute (Nanjing, China). The creatine kinase-MB (CK-MB), procollagen type I carboxy-terminal peptide (PICP), and type I collagen carboxyl terminal peptide (ICTP) ELISA kits were purchased from Meimian Biotechnology Institute (Shenyang, China). The primary antibodies against Sirt3, Smad2, Smad4, Smad7, GAPDH, Matrix Metalloproteinase (MMP) 2, and MMP9 were purchased from Proteintech Group, Inc. (Wuhan, China). The primary antibodies against TGF-β and Smad3 were purchased from Bioss Co. (Beijing, China). The primary antibody against Tissue Inhibitors of Metalloproteinase (TIMP)-1 was purchased from Shanghai Bowan Biotechnology Co., Ltd. (Shanghai, China).

UPLC-ESIQ-Exactive Orbitrap/MS Analysis

The chemical compositions of HSY were identified by UPLC-ESIQ-Exactive Orbitrap/MS according to the previous study (Xin and Bai 2021). The chromatographic method was achieved adopting ACQUTIY UPLC BEH C18 (50 mm × 2.1 mm × 1.7 μm) as a stationary phase and 0.1% formic acid (A)/ 100% acetonitrile (B) as mobile phase with gradient elution at a constant flow rate of 0.25 ml/min. The elution order was as follows: maintained with 10% B in 3 min, linear gradient from 10% B to 30% B in 3 min, 30% B to 50% B in 3 min, 50% B to 70% B in 3 min, 70% B to 80% B in 3 min, 80% B to 95% B in 3 min, maintained with 95% B in 4 min, 95% B to 10% B in 0.1 min, maintained with 10% B in 2.9 min. Mass spectrometric detection was carried out on a Q-Exactive quadrupole electrostatic field orbitrap high resolution mass spectrometry (Thermo Fisher

Scientific, MA, United States). The electrospray ionization source in both positive (ESI+) and negative (ESI−)ion modes was used with scanning range of m/z 100~1,500. The MS source parameters were set as follows: sheath gas flow of 20 arbitrary units, aux gas (Nitrogen) flow of 5.7 arbitrary units. The capillary voltage was set to +3.5 kV and −2.8kV at the capillary temperature of 200°C and aux gas heater temperature of 350°C. The scan mode was Full MS, of which the resolution was 70,000 (Full MS). Data are recorded and analyzed using the Xcalibur software (Version 2.2.42, Thermo Fisher Scientific, MA, United States).

Experimental Animals and Protocols

Male Sprague-Dawley rats (weighing 200–230 g) were purchased from Changchun Yisi Laboratory Animal Technology Co., Ltd. (Jilin, China). All the animals were housed in a room according to a 12 h light/dark cycle and had free access to a standard diet and drinking water. Fifty rats were assigned randomly into five groups: the control group (Con, n = 10), ISO group (ISO, n = 10), captopril group (Cap, n = 10, 13.5 mg/kg/d), low-dose HSY group (HSY-L, n = 10, 2.7 ml/kg/d), and high-dose HSY group (HSY-H, n = 10, 5.4 ml/kg/d). Based on the doses used in previous studies (Wang, Yu, et al., 2019), ISO (5 mg/kg, IH.) was injected once daily for 7 days to induce MF. The rats were injected with the same volume of normal saline in the control group. The dose and duration of use of HSY and captopril were calculated based on the equivalent dose ratio (approximately 6.3) between humans and rats in terms of body surface area. The dose of HSY-L group and captopril group were equivalent to human dose, and the dose of HSY-H group was twice the dose of HSY-L group. The rats in the HSY and captopril groups were given HSY and captopril respectively for 4 weeks, while the rats were administered the same volume of distilled water in the control and ISO groups. Four weeks later, all rats were performed by echocardiography. All the experiments were approved by the Experimental Animal Ethics Committee of Changchun University of Chinese Medicine (Approval Number: 2020319) and were performed in accordance with the guidelines of the National Institute of Health Guide for the Care and Use of Laboratory Animals.

Echocardiography Measurements and Determination of Serum Biomarkers

At the end of the 4th week, the rats in each group were anesthetized with 40 mg/kg of pentobarbital, and the chest hair was removed with an electric hair shaver. Cardiac function was evaluated by echocardiography with a vivid-I ultrasound machine (General Electric Company, America) with a 10 s sensor. The ejection fraction (EF) and fractional shortening (FS) were measured. The blood was collected from the abdominal aorta and centrifuged at 3,000 rpm/min (4°C) for 15 min. The serum was then collected and stored at −80°C until analysis. The serum levels of CK, LDH, and HYP were measured according to the manufacturer's instructions. In addition, the serum CK-MB, PICP and ICTP were quantified by ELISA kit according to the manufacturer's instructions.

Hematoxylin-Eosin Staining and Masson Staining

The heart was embedded in paraffin with a section thickness of 5 μm. Hematoxylin-eosin (HE) was performed after routine dewaxing and hydration. The morphological characteristics of the injured myocardial tissue were observed by HE staining.

The progress degree of MF was observed by Masson staining. The sections were incubated with Masson's trichrome stain following routine methods. The cardiomyocytes were visualized as red-stained areas and collagen was visualized as blue-stained areas. The collagen volume fraction (CVF) of the cardiac tissue was quantified using Image J software (National Institutes of Health, America). The formula used to calculate the CVF was myocardial interstitial collagen area/total visual field area.

Immunohistochemistry

The paraffin sections were deparaffinized in water. The endogenous peroxidase blocker was dropped onto the tissue, incubated for 10 min, and rinsed with double-distilled water. The antigen was then repaired with microwave heating. The sections were blocked with BSA for 30 min. Subsequently, the sections were incubated with collagen I, collagen III, and α-Smooth Muscle Actin (α-SMA) (1:100) antibodies at 4°C overnight. Goat anti-rabbit/mouse IgG was then added dropwise, and the sections were incubated for 30 min. After 30 min with streptavidin/peroxidase complex, 3,3′-diaminobenzidine hydrochloride color culture was added dropwise to the slice. Subsequently, hematoxylin restaining was performed for 2 min. The histochemical score (H-Score) was calculated using the Image-Pro Plus software 6.0 (Media Cybernetics, Inc. America) according to the equation: H-Score = Ratio of Strong-Positive*3 + Ratio of Moderate-Positive*2 + Ratio of Weak-Positive*3.

Western Blotting

The total protein from the left ventricular tissue was extracted by a RIPA lysis buffer (Beijing Ding Guo Chang Sheng Biotechnology Co., Ltd. China), and protein concentration is determined via bicinchoninic acid (BCA) Protein Assay kit. Equal amounts of protein were separated using SDS-PAGE. Proteins on the gel were transferred to a polyvinylidene fluoride (PVDF) membrane (Millipore Co., Ltd. NJ, United States) and blocked with 5% non-fat milk for 2 h. The membrane was then incubated with the primary antibodies overnight at 4°C. The primary antibodies were: anti-TGF-β (1:500), anti-Sirt3 (1:500), anti-Smad2 (1:1,000), anti-Smad3 (1:500), anti-Smad4 (1:500), anti-Smad7 (1:500), anti-MMP2 (1:500), anti-MMP9 (1:500), anti-TIMP1 (1:500), and anti-GAPDH (1:20000). After the membranes were washed, the membranes were incubated with HRP-conjugated secondary antibodies, and target proteins were developed by an enhanced chemiluminescence imager. Image J software was used to analyze the band intensity of the immune response quantitatively and to calculate the content of the target protein.

Statistical Analysis

All data have been tested for normality and presented as mean ± SD and analyzed using GraphPad Prism 8 software (GraphPad Software, San Diego, CA, United States). Student's t-tests were

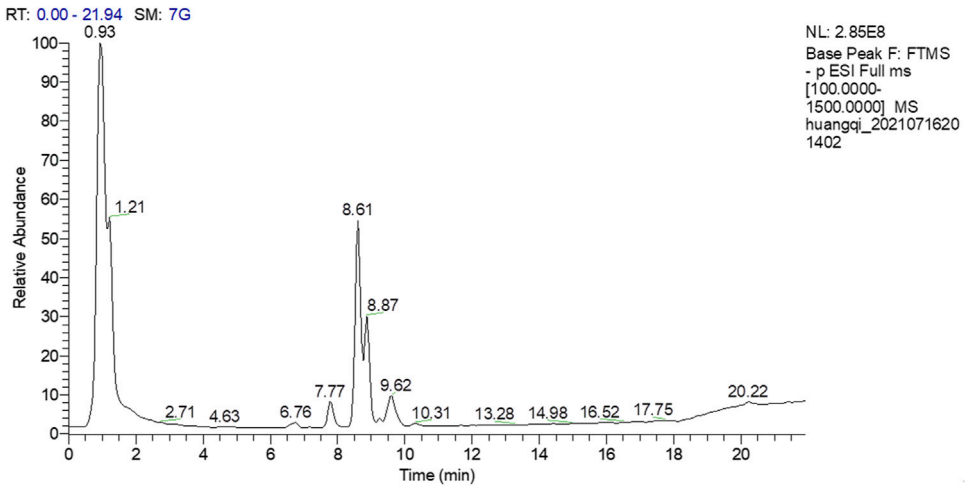

FIGURE 1 | Total ion chromatogram of HSY by UPLC-ESIQ-Exactive Orbitrap/MS.

TABLE 2 | The chemical components identified from HSY.

NO	RT (min)	Formula	Molecular weight	ppm	Compounds
1	6.62	$C_{22}H_{22}O_{10}$	446.40408	2.17	Calycosin-7-glucoside
2	7.77	$C_{20}H_{28}O_8$	396.43152	1.85	Lobetyolin
3	8.01	$C_{22}H_{22}O_9$	430.40468	2.28	Ononin
4	8.43	$C_{23}H_{28}O_{10}$	464.46242	2.69	Isomucronulatol 7-O-Glucoside
5	8.48	$C_{17}H_{18}O_5$	302.32182	3.06	Isomucronulatol
6	8.59	$C_{18}H_{32}O_3$	296.44488	3.24	9-hydroxy-10,12-octadecadienoic acid
7	8.64	$C_{16}H_{12}O_5$	284.26348	2.61	7-hydroxy-3-(3-hydroxy-4-methoxyphenyl)-4H-chromen-4-one
8	9.38	$C_{18}H_{32}O_5$	328.44368	3.42	9,12,13-Trihydroxy-10,15-octadecadienoic acid
9	9.70	$C_{30}H_{46}O_3$	454.68444	-3.10	Schisandronic acid
10	9.73	$C_{41}H_{68}O_{14}$	784.97022	2.54	Astragaloside IV
11	9.78	$C_{18}H_{34}O_5$	330.45956	3.28	9,10,13-Trihydroxy-11-Octadecenoic Acid
12	10.18	$C_{16}H_{12}O_4$	268.26408	3.99	Formononetin
13	10.20	$C_{44}H_{70}O_{18}$	887.0158	1.30	Ophiopogonin C
14	10.95	$C_{43}H_{70}O_{15}$	827.0069	2.57	Astragaloside II
15	11.72	$C_{45}H_{72}O_{16}$	869.04358	3.52	Astragaloside I
16	12.04	$C_{23}H_{28}O_7$	416.46422	-3.65	Gomisin A
17	12.59	$C_{44}H_{70}O_{16}$	855.017	2.68	Ophiopogonin D
18	12.85	$C_{18}H_{34}O_4$	314.46016	4.13	9,10-Dihydroxy-12-Octadecenoic Acid

used to compare the differences between two groups. One way analysis of variance (ANOVA) followed by Tukey's multiple comparison test were used to compare more than two groups. $p < 0.05$ was considered to be statistically significant.

RESULTS

Identification of Main Bioactive Compounds in Huangqi Shengmai Yinby UPLC-ESIQ-Exactive Orbitrap/MS Analysis

A total of 18 chemical compounds were identified in HSY, namely calycosin-7-glucoside, lobetyolin, ononin, isomucronulatol 7-O-glucoside, isomucronulatol, 9-hydroxy-10,12-octadecadienoic acid, 7-hydroxy-3-(3-hydroxy-4-methoxyphenyl)-4H-chromen-4-one, 9,12,13-trihydroxy-10,15-octadecadienoic acid, schisandronic acid, astragaloside IV, 9,10,13-trihydroxy-11-octadecenoic acid, formononetin, ophiopogonin C, astragaloside II, astragaloside I, gomisin A, ophiopogonin D and 9,10-dihydroxy-12-octadecenoic acid (**Figure 1**; **Table 2**).

Huangqi Shengmai Yin Prevents Cardiac Dysfunction in the Rat Myocardial Fibrosis Model Induced by Isoprenaline

We used echocardiogram to determine the cardiac function effect of HSY on rats. As shown in **Figure 2**, the EF and FS of rats were reduced significantly in the ISO group, indicating severe ventricular systolic dysfunction and reduced cardiac output. After 4 weeks of treatment, the EF and FS of rats were improved in the HSY groups or captopril group.

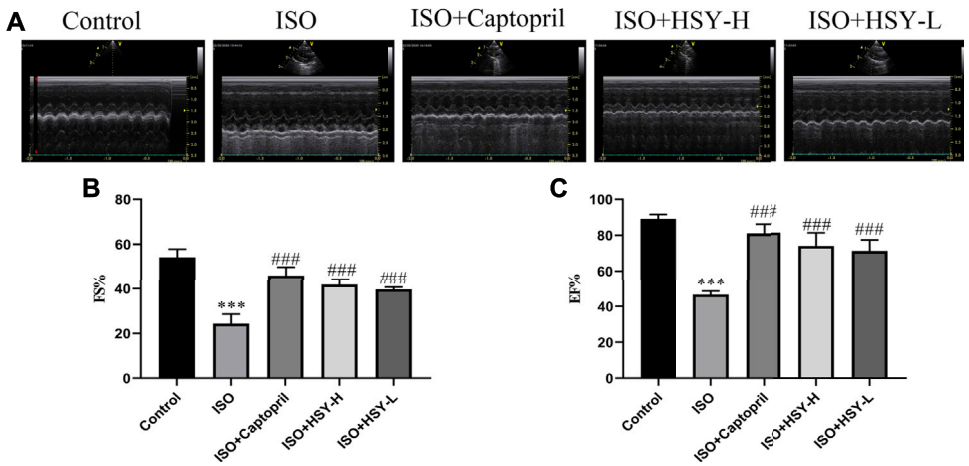

FIGURE 2 | The effect of HSY on the echocardiography of ISO-induced MF in rats. **(A)** Representative images of ultrasound in different groups. **(B–C)** Fractional shortening (FS) and ejection fraction (EF) was used to evaluate left ventricular systolic function. (n = 6). Data are shown as the mean ± SD. Significance: $^{***}p < 0.005$ vs control group; $^{###}$<0.005 vs ISO group.

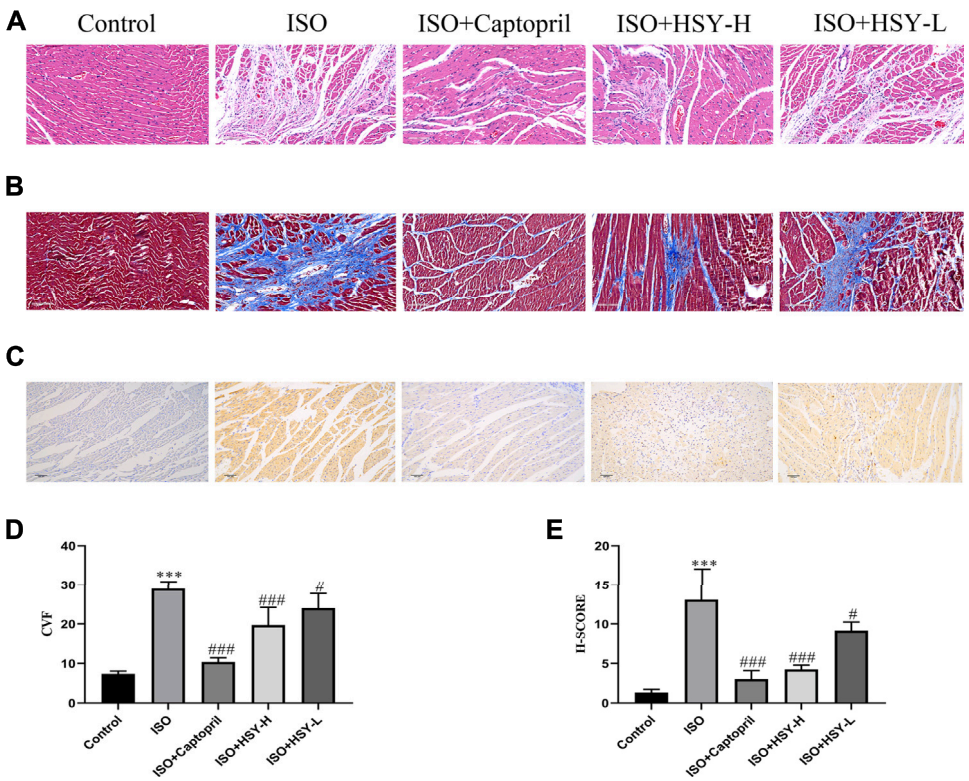

FIGURE 3 | Effect of HSY on histopathological changes in rat heart tissue. **(A)** Representative images of HE staining of left ventricular tissue in different groups. **(B)** Representative images of Masson trichrome staining of left ventricular tissue in different groups. **(C)** Representative images of Tunel staining of left ventricular tissue in different groups. **(D)** The quantitative analyses of area percentage of collagen deposition (n = 6). **(E)** The H-SCORE of Tunel staining of different groups (n = 6). Data are shown as the mean ± SD. Significance: $^{***}p < 0.005$ vs control group; $^{#}p < 0.05$ vs ISO groups; $^{##}p < 0.01$ vs ISO group; $^{###}p < 0.005$ vs ISO group.

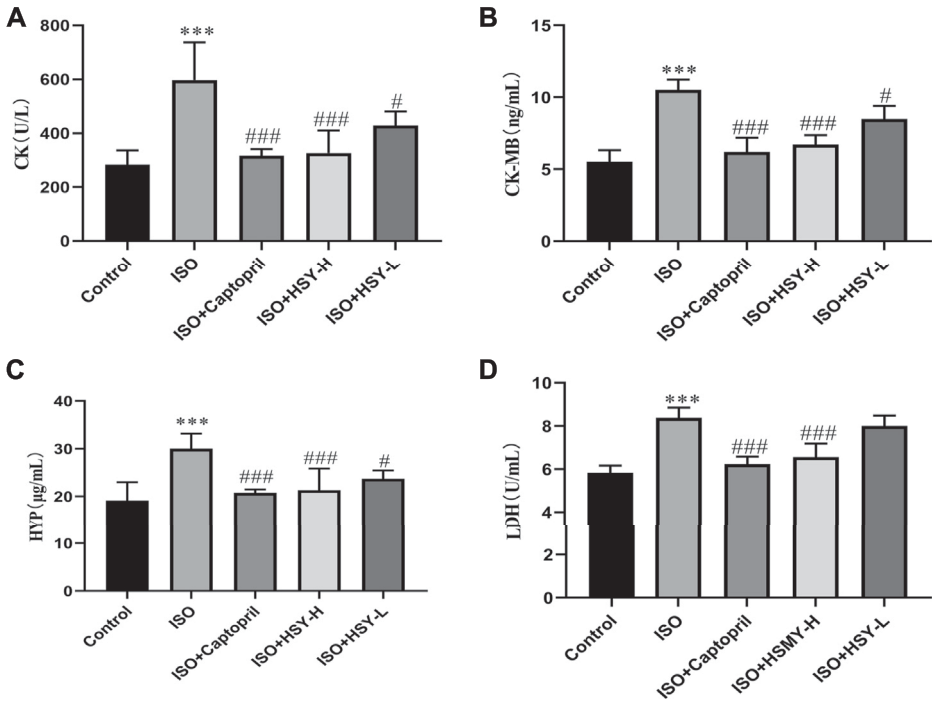

FIGURE 4 | HSY significantly reduced myocardial injury in ISO-induced cardiac fibrosis rats. **(A–D)** Serum CK, CK-MB, HYP and LDH of each group was determined using kits. Data are shown as the mean ± SD. Significance: $^{***}p < 0.005$ vs control group; $^{\#}p < 0.05$ vs ISO groups; $^{\#\#\#}p < 0.005$ vs ISO group.

Effects of Huangqi Shengmai Yin on Myocardial Injury on the Rat Myocardial Fibrosis Model Induced by Isoprenaline

Pictures of hematoxylin-eosin (HE)-stained myocardial tissue are shown in **Figure 3A**. Compared with the control group, ISO group showed severe myocardial structural alterations, including inflammatory infiltration, and nuclear lysis. There were less inflammatory infiltration and nuclear lysis of the cardiomyocytes in the HSY-L group. There was a significant improvement in the myocardium in the HSY-H or captopril group, with a neat arrangement and only a small number of inflammatory infiltrates. The myocardial enzymes were also evaluated (**Figure 4**). The CK, CK-MB, LDH, and HYP levels of rats in the ISO group were significantly higher than those in the control group. With HSY or captopril intervention, the above myocardial enzymes were reduced significantly.

Through TUNEL staining of the myocardial tissue of each group, there are a large number of apoptotic cells in the ISO group (**Figures 3C,E**). After the intervention of HSY or captopril, the number of apoptotic cells was reduced significantly, which suggested that HSY or captopril could inhibit the apoptosis of cardiomyocytes.

Effect of Huangqi Shengmai Yin on the Expression of Collagen and α-Smooth Muscle Actin in the Rat Myocardial Fibrosis Model Induced by Isoprenaline

Masson staining was used to evaluate the amount of collagen deposition in the myocardium (**Figures 3B,D**). The results showed that with ISO intervention, there was a large amount of blue collagen deposition in the myocardium. HSY or captopril reduced the collagen deposition in the myocardium, significantly. The ELISA results showed that the ratio of PICP/ICTP was increased significantly in the ISO group, while the ratio of PICP/ICTP was decreased in the HSY groups or captopril group. (**Figure 5G**).

To further confirm the inhibitory effect of HSY on the MF induced by ISO, immunohistochemical staining was used to evaluate the content of collagen I and collagen III, which are the two main components of the extracellular matrix. The α-SMA expression was also evaluated with immunohistochemistry. The immunohistochemical results showed that compared with the control group, the expression of myocardial collagen I and collagen III were increased significantly in myocardial tissue in the ISO group (**Figures 5A,B,D,E**). Compared with the ISO group, the expression of myocardial collagen I and collagen III was decreased with HSY or captopril intervention. The immunohistochemical results of the α-SMA showed that compared with the control group, more brown particles were seen in the ISO group, while that HSY or captopril reduced the intensity of the positive staining (**Figures 5C,F**).

Effect of Huangqi Shengmai Yin on Sirtuin 3, Transforming Growth Factor-β/Smad Signaling Pathway and Matrix Metalloproteinase-Related Proteins Expression

In order to clarify the molecular mechanisms of HSY in the treatment of ISO-induced MF, western blot experiments

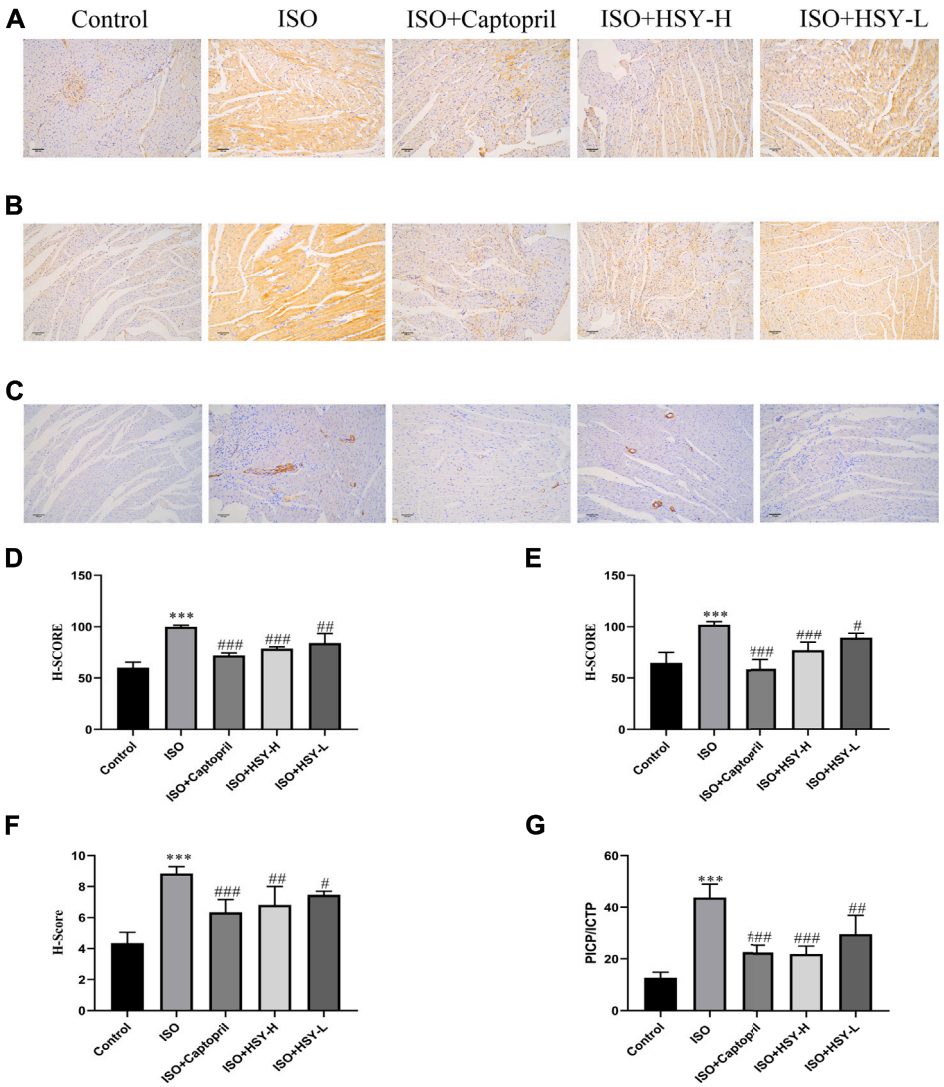

FIGURE 5 | The effect of HSY on the expression of collagen and α-SMA in each group. **(A–C)** Representative images of different groups of collagen I, III and α-SMA immunohistochemistry. **(D–F)** The H-SCORE of collagen I, III and α-SMA in different groups (n = 6). **(G)** The ratio of the content of PICP and ICTP in each group of serum. Data are shown as the mean ± SD. Significance: $^{***}p < 0.005$ vs control group; $^{\#}p < 0.05$ vs ISO groups; $^{\#\#}p < 0.01$ vs ISO group; $^{\#\#\#}p < 0.005$ vs ISO group.

were performed to detect the Sirt3, TGF-β/Smad signaling pathways, and the related protein expressions of MMPs (**Figure 6A**). As shown in **Figures 6B–D**, compared with the control group, the expressions of TGF-β, Smad2, 3, and 4 were increased, while the expressions of Sirt3 and Smad7 were decreased in the ISO group. Among the MMP-related proteins, the expressions of MMP2 and 9 were decreased, while the expression of TIMP-1 was increased in the ISO group. Compared with the ISO group, HSY or captopril upregulated the expressions of Sirt3 and Smad7 and downregulated the expressions of TGF-β and Smad2, 3, and 4. In addition, HSY or captopril also upregulated the protein expressions of MMP2 and MMP9 in the MMP family and inhibited the expression of TIMP-1.

DISCUSSION

With the intensification of global aging, cardiovascular diseases have become the main cause of death (Arnett et al., 2019). MF is an important pathological feature of cardiovascular diseases because it can lead to ventricular remodeling (Hughes et al., 2019). Many cardiovascular diseases, such as hypertension, myocarditis, and myocardial infarction, can cause MF. (Dixon and Spinale 2010; Masci et al., 2013). The effective prevention of MF is of great significance for prolonging lives of patients with cardiovascular diseases.

MF is an abnormal deposition of the extracellular matrix (ECM) in the myocardium, which is characterized by collagen deposition increasing in the gap. Collagen I and III are the main

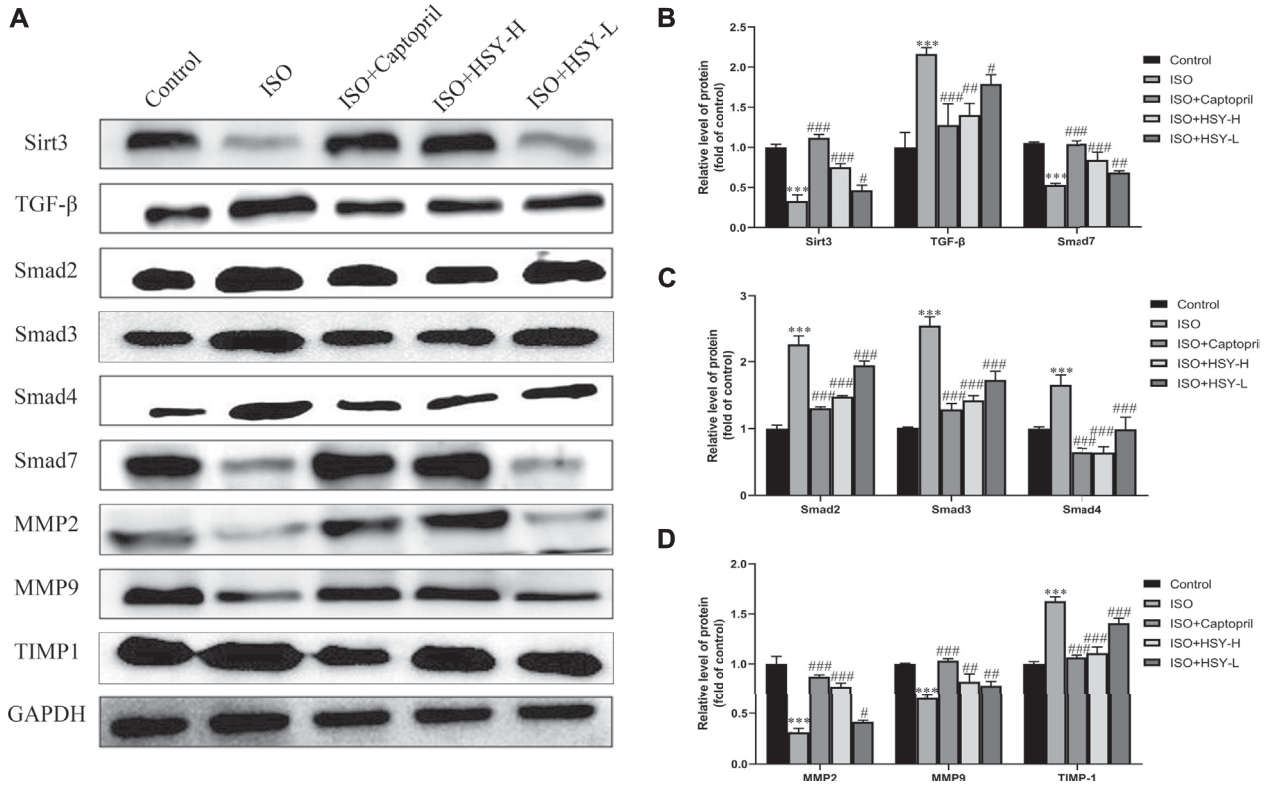

FIGURE 6 | Effect of HSY on the Sirt3/TGF-β/Smad signaling pathway in rats. **(A)** The level of Sirt3/TGF-β/Smad signaling pathway and MMPs in each group.**(B–D)** Quantified protein bands of Sirt3/TGF-β/Smad signaling pathway and MMPs with GAPDH as control. Data are shown as the mean ± SD. Significance: $^{*}p < 0.05$ vs control group; $^{***}p < 0.005$ vs control group; $^{\#}p < 0.05$ vs ISO group; $^{\#\#}p < 0.01$ vs ISO group; $^{\#\#\#}p < 0.005$ vs ISO group.

components of the cardiac ECM (Essick and Sam 2011; Li et al., 2018). This excessive deposition of collagen reduces the elasticity of the myocardium, causing disorders in the diastolic and systolic function of the heart leading to heart failure and even sudden cardiac death (Czubryt 2012; Raman et al., 2019). We assessed the cardiac function of the rats in each group by echocardiography and found the rats developed severe heart failure, and their EF and FS decreased significantly, suggesting that the rats had left ventricular systolic dysfunction in the ISO group. Compared with the ISO group, the EF and FS of the rats were increased in the HSY-H group and HSY-L group, indicating that the left ventricular systolic disorder was relieved, which suggested that HSY could improve heart function.

Myocardial enzymes have been widely used as a biomarker for the clinical diagnosis of myocardial injuries (Yu and Wang 2018). When cardiomyocytes are inflamed (myocarditis) or necrotized (myocardial infarction) for various reasons, the enzymes contained in the cardiomyocytes can enter the blood, so the contents of these enzymes in the blood will increase. Myocardial enzymes such as LDH, CK and CK-MB are the most common biomarkers for myocardial ischemia and HF (Mallick and Januzzi 2015). After testing, it was found that HSY can significantly reduce the increase in CK, CK-MB, LDH and HYP caused by ISO. In order to further examine the myocardial injury, we performed HE staining to observe the morphology of rats in each group and Tunel staining to observe the apoptosis in the myocardium of rats in each group. The results of HE staining showed that there was a large amount of inflammatory infiltration in the myocardial tissue of the ISO group, the nucleus was dissolved or disappeared, and the arrangement of myocardial cells was disordered. Compared with the ISO group, inflammatory infiltration and a small amount of nuclear dissolution or disappearance were seen in the myocardial tissue of the HSY-L group, while the rat cardiomyocytes were arranged in an orderly manner with only partial inflammatory infiltration in the HSY-H group. Tunel staining results showed that HSY effectively reduced ISO-induced apoptosis in the myocardium of MF rats. Combined with myocardial enzymes, HE staining and Tunel staining results show that HSY has a protective effect on ISO-induced MF rat cardiomyocytes.

The Masson staining and immunohistochemical results showed that HSY can effectively reduce the collagen deposition in the myocardial tissue of rats with MF. PICP and ICTP are serum biochemical markers of cardiac ECM (Sun et al., 2017). These results showed that the ratio of PICP/ICTP in the ISO group was significantly higher than that in the control group. The PICP/ICTP ratio of the HSY groups was effectively decreased. The combined results of Masson and collagen I and III immunohistochemistry showed that HSY may reduce collagen deposition by regulating the rate of collagen production/

degradation. In summary, these results showed that HSY could reduce the formation of collagen and increase its degradation, thereby reducing the deposition of collagen in myocardial tissue.

Previous studies have shown that Sirt3 may be a negative regulator of MF (Chen et al., 2015). Su et al. confirm that Sirt3 has a critical role in Ang-II-induced cardiac fibrosis and remodeling through pericyte transition and ROS-TGF-β pathway (Su et al., 2020). TGF-β has a strong inducing effect on the proliferation of ECM and plays a key role in the development of MF. TGF-β promotes phosphorylation of the Smad2, 3 complex by binding to the receptor (Dobaczewski et al., 2011). The complex form hetero-oligomeric complexes with Smad4 and enter the nucleus, promote the conversion of fibroblasts into myofibroblasts in the heart, and then increase collagen production (Xie et al., 2017). As an inhibitory Smad protein, Smad7 can bind to the activated type I receptors to inhibit signal transduction in the TGF-β family. The results of western blot indicated that HSY could increase the expression of SIRT3 and Smad7, inhibit the TGF-β/Smad signaling pathway, and suppress the conversion of fibroblasts to myofibroblasts and the production of collagen.

Matrix metalloproteinases (MMPs) are zinc-dependent endopeptidases that can degrade various ECM proteins (Laronha and Caldeira 2020). MMP activity can be inhibited by the molecular family of tissue inhibitors of metalloproteinases (TIMPs). Under physiological conditions, a dynamic balance is maintained between the MMPs/TIMP to maintain the ECM content. When MF occurs, this balance is disrupted. Through HSY intervention, the expression of MMP2, MMP9, and TIMP-1 tended to be normal. These results suggested that HSY could increase the degradation of collagen and reduce ECM deposition by regulating MMPs and TIMP-1.

In this study, we successfully established a rat model of MF induced by ISO. Compared to other animal models, the ISO-induced MF model was found to be more stable and more consistent with clinical pathology (Krenek et al., 2009). In addition, a total of 18 different kinds of compounds of HSY were identified using UPLC-ESIQ-Exactive Orbitrap/MS (**Table 2**). Synchronously, there was evidence that Calycosin-7-glucoside (He et al., 2013), Astragaloside IV(Wei et al., 2020), Calycosin-7-glucoside (He, Liu, Peng, Huang and Wu 2013), Schisandronic acid (Zhang et al., 2020) had inhibitory effects on MF, anti-inflammatory and anti-tumor activities. These may be the main effective ingredients in HSY to treat MF, and we will verify them in subsequent experiments.

Overall, we verified that HSY can protect myocardium, ameliorate ISO-induced MF, and improve cardiac function. This protective effect may occur in two ways. One is the activation of Sirt3, the inhibition of the TGF-β/Smad signaling pathway and prevent the transformation of fibroblasts into myofibroblasts, thereby inhibiting the production of collagen, and the other is to regulate MMPs, thereby increasing collagen degradation. In addition, in this study, we explored the blocking effect of HSY on ISO-induced MF, and the synergy between the main components of HSY will be carried out in subsequent studies.

DATA AVAILABILITY STATEMENT

The raw data supporting the conclusions of this article will be made available by the authors, without undue reservation.

ETHICS STATEMENT

The animal study was reviewed and approved by Experimental Animal Ethics Committee of Changchun University of Chinese Medicine (approval number: 2020319).

AUTHOR CONTRIBUTIONS

JP and DH conceived and designed the research. JP and ZC performed the *in vivo* experiments. CF and YL carried out the statistical analysis. JP worte the paper. JS XH and DH revision the manuscript. All authors contributed to the article and approved the submitted version.

FUNDING

This work was supported by Jilin Province Traditional Chinese Medicine Science and Technology Project (2021011); the "Twelfth Five-Year" Science and Technology Research Planning Project of the Education Department of Jilin Province (Jijiaoke Hezi (2015) No. 340); Jilin Province Health and Family Planning Youth Scientific Research Project, 2015Q037; the Doctoral Fund of the Ministry of Education (20132227120004); the National Natural Science Foundation of China (82074127); Innovation Capacity Building Project of Jilin Provincial Development and Reform Commission (2021C011); 2020 Jilin Province "College Students Innovation and Entrepreneurship Training Program" Project (202010199014).

REFERENCES

Arnett, D. K., Blumenthal, R. S., Albert, M. A., Buroker, A. B., Goldberger, Z. D., Hahn, E. J., et al. (2019). 2019 ACC/AHA Guideline on the Primary Prevention of Cardiovascular Disease: Executive Summary: A Report of the American College of Cardiology/American Heart Association Task Force on Clinical Practice Guidelines. *J. Am. Coll. Cardiol.* 74, 1376–1414. doi:10.1016/j.jacc.2019.03.009

Brilla, C. G., Rupp, H., and Maisch, B. (2003). Effects of ACE Inhibition versus Non-ACE Inhibitor Antihypertensive Treatment on Myocardial Fibrosis in Patients with Arterial Hypertension. Retrospective Analysis of 120 Patients with Left Ventricular Endomyocardial Biopsies. *Herz* 28, 744–753. doi:10.1007/s00059-003-2524-6

Chen, T., Li, J., Liu, J., Li, N., Wang, S., Liu, H., et al. (2015). Activation of SIRT3 by Resveratrol Ameliorates Cardiac Fibrosis and Improves Cardiac Function via the TGF-β/Smad3 Pathway. *Am. J. Physiol. Heart Circ. Physiol.* 308, H424–H434. doi:10.1152/ajpheart.00454.2014

Czubryt, M. P. (2012). Common Threads in Cardiac Fibrosis, Infarct Scar Formation, and Wound Healing. *Fibrogenesis Tissue Repair* 5, 19–11. doi:10.1186/1755-1536-5-19

Dixon, J. A., and Spinale, F. G. (2010). Pathophysiology of Myocardial Injury and Remodeling: Implications for Molecular Imaging. *J. Nucl. Med.* 51 (1), 102S–106S. doi:10.2967/jnumed.109.068213

Dobaczewski, M., Chen, W., and Frangogiannis, N. G. (2011). Transforming Growth Factor (TGF)-β Signaling in Cardiac Remodeling. *J. Mol. Cel Cardiol* 51, 600–606. doi:10.1016/j.yjmcc.2010.10.033

Essick, E. E., and Sam, F. (2011). Cardiac Hypertrophy and Fibrosis in the Metabolic Syndrome: a Role for Aldosterone and the Mineralocorticoid Receptor. *Int. J. Hypertens.* 2011, 346985. doi:10.4061/2011/346985

Francis Stuart, S. D., De Jesus, N. M., Lindsey, M. L., and Ripplinger, C. M. (2016). The Crossroads of Inflammation, Fibrosis, and Arrhythmia Following Myocardial Infarction. *J. Mol. Cel Cardiol* 91, 114–122. doi:10.1016/j.yjmcc.2015.12.024

Gourdie, R. G., Dimmeler, S., and Kohl, P. (2016). Novel Therapeutic Strategies Targeting Fibroblasts and Fibrosis in Heart Disease. *Nat. Rev. Drug Discov.* 15, 620–638. doi:10.1038/nrd.2016.89

Gu, J., Liu, Y., Wu, H., Li, H., and Liu, K. (2019). Huangqi Shengmai Yin Protects against Radiation-Induced Cardiac Fibrosis Injury by Regulating the TGF-β1/Smads and MMPs. *Evid. Based Complement. Alternat Med.* 2019, 1358469. doi:10.1155/2019/1358469

Guo, C., Wang, Y., Liang, H., and Zhang, J. (2010). ADAMTS-1 Contributes to the Antifibrotic Effect of Captopril by Accelerating the Degradation of Type I Collagen in Chronic Viral Myocarditis. *Eur. J. Pharmacol.* 629, 104–110. doi:10.1016/j.ejphar.2009.12.009

He, X., and Ou, C. (2020). CircRNA circHIPK3: A Novel Therapeutic Target for Angiotensin II-Induced Cardiac Fibrosis. *Int. J. Cardiol.* 312, 98. doi:10.1016/j.ijcard.2020.03.034

He, X. Y., Liu, Q. C., Peng, W., Huang, Y. L., and Wu, C. J. (2013). Bioactivities and Serum Pharmacochemistry of Qi-Wei-Xiao-Yan-Tang. *Pharm. Biol.* 51, 629–634. doi:10.3109/13880209.2012.761243

Hughes, A., Okasha, O., Farzaneh-Far, A., Kazmirczak, F., Nijjar, P. S., Velangi, P., et al. (2019). Myocardial Fibrosis and Prognosis in Heart Transplant Recipients. *Circ. Cardiovasc. Imaging* 12, e009060. doi:10.1161/circimaging.119.009060

Jiang, j., Du, X., Yao, Y., Tang, Z., Wang, X., Shen, X., et al. (2021). Effects of Huangqishengmaiyin on Cardiac Function, Immune Function and Expression of Plasma miRNA-155 in Patients with Coronary Heart Disease and Heart Failure. *J. Electrocardiol. Circ.* 40, 262–266.

Krenek, P., Kmecova, J., Kucerova, D., Bajuszova, Z., Musil, P., Gazova, A., et al. (2009). Isoproterenol-induced Heart Failure in the Rat Is Associated with Nitric Oxide-dependent Functional Alterations of Cardiac Function. *Eur. J. Heart Fail.* 11, 140–146. doi:10.1093/eurjhf/hfn026

Laronha, H., and Caldeira, J. (2020). Structure and Function of Human Matrix Metalloproteinases. *Cells* 9, 1–18. doi:10.3390/cells9051076

Leask, A. (2015). Getting to the Heart of the Matter: New Insights into Cardiac Fibrosis. *Circ. Res.* 116, 1269–1276. doi:10.1161/circresaha.116.305381

Li, L., Zhao, Q., and Kong, W. (2018). Extracellular Matrix Remodeling and Cardiac Fibrosis. *Matrix Biol.* 68-69, 490–506. doi:10.1016/j.matbio.2018.01.013

Liu, Y., Wang, F., Hao, J., Liu, Y., and Sun, B. (2009). The Clinical Application and Basic Research Progress of Huangqi Shengmaiyin. *Mod. J. Integrated Traditional Chin. West. Med.* 18, 1961–1963.

Lv, S., Yuan, P., Dong, J., Lu, C., Li, M., Qu, F., et al. (2020). QiShenYiQi Pill Improves the Reparative Myocardial Fibrosis by Regulating Autophagy. *J. Cel Mol Med* 24, 11283–11293. doi:10.1111/jcmm.15695

Mallick, A., and Januzzi, J. L. (2015). Biomarkers in Acute Heart Failure. *Rev. Esp Cardiol. (Engl Ed.* 68, 514–525. doi:10.1016/j.rec.2015.02.009

Masci, P. G., Schuurman, R., Andrea, B., Ripoli, A., Coceani, M., Chiappino, S., et al. (2013). Myocardial Fibrosis as a Key Determinant of Left Ventricular Remodeling in Idiopathic Dilated Cardiomyopathy: a Contrast-Enhanced Cardiovascular Magnetic Study. *Circ. Cardiovasc. Imaging* 6, 790–799. doi:10.1161/CIRCIMAGING.113.000438

McDonald, H., Peart, J., Kurniawan, N., Galloway, G., Royce, S., Samuel, C. S., et al. (2018). Hexarelin Treatment Preserves Myocardial Function and Reduces Cardiac Fibrosis in a Mouse Model of Acute Myocardial Infarction. *Physiol. Rep.* 6, e13699. doi:10.14814/phy2.13699

Mohammed, S. F., Hussain, S., Mirzoyev, S. A., Edwards, W. D., Maleszewski, J. J., and Redfield, M. M. (2015). Coronary Microvascular Rarefaction and Myocardial Fibrosis in Heart Failure with Preserved Ejection Fraction. *Circulation* 131, 550–559. doi:10.1161/circulationaha.114.009625

Oka, T., Akazawa, H., Naito, A. T., and Komuro, I. (2014). Angiogenesis and Cardiac Hypertrophy: Maintenance of Cardiac Function and Causative Roles in Heart Failure. *Circ. Res.* 114, 565–571. doi:10.1161/CIRCRESAHA.114.300507

Raman, B., Ariga, R., Spartera, M., Sivalokanathan, S., Chan, K., Dass, S., et al. (2019). Progression of Myocardial Fibrosis in Hypertrophic Cardiomyopathy: Mechanisms and Clinical Implications. *Eur. Heart J. Cardiovasc. Imaging* 20, 157–167. doi:10.1093/ehjci/jey135

Su, H., Zeng, H., Liu, B., and Chen, J. X. (2020). Sirtuin 3 Is Essential for Hypertension-Induced Cardiac Fibrosis via Mediating Pericyte Transition. *J. Cel Mol Med* 24, 8057–8068. doi:10.1111/jcmm.15437

Sun, R., Wang, J., Zheng, Y., Li, X., Xie, T., Li, R., et al. (2017). Traditional Chinese Medicine Baoxin Decoction Improves Cardiac Fibrosis of Rats with Dilated Cardiomyopathy. *EXP. Ther. Med.* 13, 1900–1906. doi:10.3892/etm.2017.4223

Wang, J., Shen, W., Zhang, J. Y., Jia, C. H., and Xie, M. L. (2019a). Stevioside Attenuates Isoproterenol-Induced Mouse Myocardial Fibrosis through Inhibition of the Myocardial NF-Kb/tgf-β1/Smad Signaling Pathway. *Food Funct.* 10, 1179–1190. doi:10.1039/c8fo01663a

Wang, Q. W., Yu, X. F., Xu, H. L., Zhao, X. Z., and Sui, D. Y. (2019b). Ginsenoside Re Improves Isoproterenol-Induced Myocardial Fibrosis and Heart Failure in Rats. *Evid. Based Complement. Alternat Med.* 2019, 3714508. doi:10.1155/2019/3714508

Wei, Y., Wu, Y., Feng, K., Zhao, Y., Tao, R., Xu, H., et al. (2020). Astragaloside IV Inhibits Cardiac Fibrosis via miR-135a-TRPM7-TGF-β/Smads Pathway. *J. Ethnopharmacol* 249, 112404–112419. doi:10.1016/j.jep.2019.112404

Xie, J., Tu, T., Zhou, S., and Liu, Q. (2017). Transforming Growth Factor (TGF)-β1 Signal Pathway: A Promising Therapeutic Target for Attenuating Cardiac Fibrosis. *Int. J. Cardiol.* 239, 9. doi:10.1016/j.ijcard.2017.02.032

Xin, Y., and Bai, J. (2021). Analysis of Chemical Constituents in Compound Huangqi Shengmai Decoction by UPLC-Q-TOF/MS. *J. Harbin Univ. Commerce(Natural Sci. Edition)* 37, 21–25+78.

Yu, B., and Wang, W. (2018). Cardioprotective Effects of Morroniside in Rats Following Acute Myocardial Infarction. *Inflammation* 41, 432–436. doi:10.1007/s10753-017-0699-x

Yuan, J., Liu, H., Gao, W., Zhang, L., Ye, Y., Yuan, L., et al. (2018). MicroRNA-378 Suppresses Myocardial Fibrosis through a Paracrine Mechanism at the Early Stage of Cardiac Hypertrophy Following Mechanical Stress. *Theranostics* 8, 2565–2582. doi:10.7150/thno.22878

Zhang, K.-X., Qian, X.-J., Wei-Zheng, W., Cai, M.-C., Ma, Y., Zhang, D.-Z., et al. (2020). Synthesis and *In Vitro* Anti-HCV and Antitumor Evaluation of Schisan-Dronic Acid Derivatives. *Med Chem* 16, 1–9. doi:10.2174/1573406416999200818150053

Zhang, Y., Cui, L., Guan, G., Wang, J., Qiu, C., Yang, T., et al. (2018). Matrine Suppresses Cardiac Fibrosis by Inhibiting the TGF-β/Smad P-athway in E-xperimental D-iabetic C-ardiomyopathy. *Mol. Med. Rep.* 17, 1775–1781. doi:10.3892/mmr.2017.8054

Conflict of Interest: The authors declare that the research was conducted in the absence of any commercial or financial relationships that could be construed as a potential conflict of interest.

Publisher's Note: All claims expressed in this article are solely those of the authors and do not necessarily represent those of their affiliated organizations, or those of the publisher, the editors and the reviewers. Any product that may be evaluated in this article, or claim that may be made by its manufacturer, is not guaranteed or endorsed by the publisher.

frontiers in Pharmacology

ORIGINAL RESEARCH
published: 08 September 2021
doi: 10.3389/fphar.2021.724670

Danlou Tablets Inhibit Atherosclerosis in Apolipoprotein E-Deficient Mice by Inducing Macrophage Autophagy: The Role of the PI3K-Akt-mTOR Pathway

Chunping Liu[1,2,3†], Guiling Chen[1,4†], Yanfen Chen[5†], Yue Dang[6], Guangning Nie[1], Dinghong Wu[1], Jinhua Li[1], Zide Chen[7], Hailong Yang[2], Dongyue He[2], Xiong Li[1], Jingbo Sun[8], Jiahong Lu[3] and Lei Wang[1,2]**

[1]State Key Laboratory of Dampness Syndrome of Chinese Medicine, The Second Affiliated Hospital of Guangzhou University of Chinese Medicine, Guangzhou, China, [2]Department of Cardiovascular Medicine, Guangdong Provincial Hospital of Chinese Medicine, Guangzhou, China, [3]State Key Laboratory of Quality Research in Chinese Medicine, Institute of Chinese Medical Sciences, University of Macau, Macau, China, [4]Department of National Institute of Stem Cell Clinical Research, Guangdong Provincial Hospital of Chinese Medicine, Guangzhou, China, [5]Puning Hospital of Traditional Chinese Medicine, Puning, China, [6]College of Traditional Chinese Medicine, Shenyang Pharmaceutical University, Shenyang, China, [7]Department of Interventional Radiology, Cancer Center, Guangdong Provincial People's Hospital, Guangdong Academy of Medical Sciences, South China University of Technology, Guangzhou, China, [8]Guangdong Provincial Key Laboratory of Research on Emergency in TCM, Guangzhou, China*

OPEN ACCESS

Edited by:
Yue Liu,
Xiyuan Hospital, China

Reviewed by:
Yanfei Liu,
China Academy of Chinese Medical Sciences, China
Min Wu,
China Academy of Chinese Medical Sciences, China

***Correspondence:**
Jiahong Lu
jiahonglu@um.edu.mo
Lei Wang
Dr.wanglei@gzucm.edu.cn

†These authors contributed equally to this work

Specialty section:
This article was submitted to Ethnopharmacology, a section of the journal Frontiers in Pharmacology

Received: *14 June 2021*
Accepted: *25 August 2021*
Published: *08 September 2021*

Citation:
Liu C, Chen G, Chen Y, Dang Y, Nie G, Wu D, Li J, Chen Z, Yang H, He D, Li X, Sun J, Lu J and Wang L (2021) Danlou Tablets Inhibit Atherosclerosis in Apolipoprotein E-Deficient Mice by Inducing Macrophage Autophagy: The Role of the PI3K-Akt-mTOR Pathway. Front. Pharmacol. 12:724670. doi: 10.3389/fphar.2021.724670

Atherosclerosis (AS) is a type of chronic vascular disease, and its etiology is not yet fully understood. AS is characterized by lipid deposition, atherosclerotic plaque formation, vascular stenosis or even complete blockage of the blood vessel wall. Clinical studies have shown that Danlou tablets (DLTs) can improve the heart function, quality of life, and prognosis of patients with coronary heart disease and myocardial infarction. However, its mechanism of action remains unknown. Our study revealed that DLTs ameliorated ApoE$^{-/-}$AS mouse aortic atherosclerotic plaques [hematoxylin-eosin (HE) staining and small animal ultrasound] and reduced CD68^{+} macrophage infiltration, the expression of the inflammatory factor interferon-gamma (IFN-γ), vascular smooth muscle α-actin, and serum lipid levels. *In vitro*, in the macrophage foaming model, DLTs partially restored the activity of RAW264.7 cells, reduced the uptake of lipid droplets, and inhibited lipid droplet accumulation and apoptosis within BMDMs. We also found that Torin1, an autophagy agonist, reduced intracellular lipid deposition in BMDMs, as did DLTs. Moreover, DLTs upregulated the expression of the autophagy-related protein LC3II and decreased p62 accumulation in RAW264.7 cells. DLTs also inhibited the phosphorylation of p-PI3K, p-Akt, and p-mTOR, leading to upregulated autophagy in RAW264.7 cells. In summary, our results suggested that DLTs can promote autophagy in macrophages by inhibiting the PI3K/Akt/mTOR signaling pathway, thereby reducing foam cell formation and improving atherosclerosis.

Keywords: atherosclerosis, danlou tablets, apolipoprotein E deficient mice, macrophage, autophagy, PI3K/Akt/mTOR signaling pathway

INTRODUCTION

Atherosclerosis is a progressive disease characterized by the accumulation of lipid-rich macrophages on the inner wall of the artery, accompanied by the proliferation of vascular smooth muscle cells and fibrous matrix, forming asymmetric focal thickening of the intima, and gradually developing into the formation of atherosclerotic plaques. Arterial plaque can cause vascular stenosis or even complete blockage and ultimately cause ischemia or infarction of the corresponding organ. In addition, atherosclerotic plaques rupture and trigger thrombosis (Stary, Chandler et al., 1995; Nanchen and Raggi 2017). At present, the treatments of atherosclerosis mainly depend on statins, antithrombotic drugs and surgical intervention. Statins are currently the most effective drugs to prevent and treat cardiovascular events (Horodinschi, Stanescu et al., 2019). However, high-dose statin administration has been associated with severe side effects, including an increased risk of new-onset diabetes, liver damage, rhabdomyolysis, etc.

In China, a proprietary medicine named Danlou tablets (DLTs) has long been considered a common therapy for cardiovascular diseases (Mao, Wang et al., 2016). DLTs have the characteristics of good curative effects, inducing an obvious improvement of symptoms, and mild adverse reactions, which have been widely recognized in long-term clinical practice. DLTs are composed of 10 types of Chinese herbs: *Trichosanthes kirilowii Maxim. [Cucurbitaceae; Pericarpium Trichosanthis]; Allium macrostemon Bge [Liliaceae; Bulbus allii macrostemonis] Pueraria lobata (Willd.) Ohwi [Leguminosae; Radix puerariae]; Ligusticum chuanxiong hort [Umbelliferae; Rhizoma chuanxiong]; Salvia miltiorrhiza Bunge [Lamiaceae; Salviae miltiorrhizae radix et rhizoma]; Paeonia lactiflora Pall [Ranunculaceae; Radix paeoniae rubra]; Alisma orientalis (Sam.) Juzep [Alismataceae; Rhizoma alismatis]; Astragalus membranaceus (Fisch.) Bge [Leguminosae; Radix astragali]; Drynaria fortunei (Kunze) J. Sm.[Davalliaceae; Rhizoma drynariae] and Curcuma wenyujin Y.H. Chen et C. Ling [Zingerberaceae; Radix curcumae]*. Randomized controlled trials of 219 patients undergoing percutaneous coronary intervention (PCI) with non-ST elevation acute coronary syndrome (NSTE-ACS) showed that the DLT group could reduce the incidence of periprocedural myocardial infarction in patients with ACS undergoing PCI. The incidence of major adverse cardiac events (MACEs) at the 90 day follow-up was significantly decreased in the DLT group compared with the placebo group, and the incidence of nonfatal myocardial infarction at 90 days was reduced in the DLT group (Wang, Zhao et al., 2016). *In vivo*, several studies have shown that DLTs can improve dyslipidemia and atherosclerosis (Liu, Lin et al., 2013; Gao, Xue et al., 2020; Tang, Li et al., 2020). In apolipoprotein E (ApoE)-knockout mouse models of myocardial ischemia, DLTs could regulate the NF-κB signaling pathway related to inflammatory factors, including TNF-α, IL-6, IL-1β, IL-8, MMP-1 and MMP-2, to alleviate atherosclerosis (Gao, Xue et al., 2020). Tang et al. predicted that DLTs can improve the TG and TC levels of $ApoE^{-/-}$ mice treated with chronic intermittent hypoxia through the HIF-1α-Angptl4 mRNA signaling pathway, as well as the area of atherosclerotic plaques (Tang, Li et al., 2020).

Macrophages play important roles in all stages of atherosclerosis, including plaque formation and rupture. In the early stage, oxidized LDL (ox-LDL), aggregated lipoproteins, and other substances are internalized by macrophages, which transform into foam cells. These foam cells enter the inner membrane and release inflammatory mediators to increase the permeability of the endothelium and damage the cells and mononuclear macrophages, thus forming a vicious cycle and inducing the progression of atherosclerosis. A study by Deng et al. indicated that ethanol extracts of DLTs attenuate atherosclerosis through anti-inflammation and prevent lipid deposition in macrophages by suppressing NF-κB signaling and triggering the PPARα/ABCA1 signaling pathway (Hao, Danbin et al., 2019).

Autophagy is a self-protective process mediated by the degradation and recycling of cytoplasmic products to maintain cell homeostasis. Autophagy has been proven to be involved in lipid metabolism, termed macrolipophagy, and is considered a protective mechanism during atherosclerosis (Martinet and De Meyer 2009; Singh, Kaushik et al., 2009; Sergin, Evans et al., 2017; Miao, Zang et al., 2020). Impaired autophagy accelerates atherosclerosis by regulating the dysfunction of lipid metabolism in macrophages (Li W. et al., 2016; Evans, Jeong et al., 2018).

Although DLTs are commonly used for patients with coronary heart disease in China, their mechanism of action has not yet been elucidated. In this study, we used an $ApoE^{-/-}$ mouse model and *in vitro* cell lines, including RAW264.7 cells and BMDMs, to explore the mechanisms of DLTs in treating atherosclerosis. The findings indicated that DLTs improved atherosclerosis by enhancing autophagy in macrophages.

MATERIALS AND METHODS

Ultrahigh-Performance Liquid Chromatography Analysis

Five different batches of DLTs were monitored for quality control by UHPLC. Briefly, DLTs and 4 standards (danshensu; salvianolic acid A; cryptotanshinone; tanshinone ⅡA) were dissolved in methanol-0.1% formic acid. Chromatographic separation was performed using an Accela™ UHPLC system, which was comprised of a UHPLC pump and a PDA detector with scanning from 200 to 400 nm and recorded at 214 nm. The HPLC conditions were set as follows: column: KintexR C18, 150 mm × 2.1 mm, 2.6 μm particle size (Phenomenax, United States); mobile phase components: A was water with 0.1% formic acid and B was methanol; flow rate: 250 μl/min; injection volume: 10 μl; gradient: 0–45 min, linear gradient of 10–35% A, 45–50 min, 35–46% A, 50–60 min, 46–85% A.

Ethics Statement

All experimental animals were treated responsibly and humanely, and all animal experiments and breeding programs complied with the Animal Handling Regulations of the People's Republic of China (Ministry of Health, People's Republic of China,

Regulation No.: 552001). The protocol was approved by the Ethics Committee at Guangdong Provincial Hospital of Chinese Medicine and was conducted in accordance with the 1989 Declaration of Helsinki.

Animals and Models

ApoE$^{-/-}$ mice (male, 8 weeks) were purchased from Vital River Laboratory Animal Technology Co., Ltd. (Beijing, China) and housed in specific pathogen-free (SPF) environments in climate-controlled conditions (20–23°C, 45–65% humidity) and illumination (12 h light/dark cycles) with access to food and water ad libitum. The light period was 7 am to 7 pm, and adaptive feeding was performed for 7 days before the experiment. ApoE$^{-/-}$ mice were randomly divided into six groups: the control group; the model group; the DLT-low group (120 μg/kg); the DLT-middle group (240 μg/kg); the DLT-high group (480 μg/kg) (provided by Connell Pharmaceutical Co., Ltd. [Jilin, China], batch number: 20191204) (Lin, Wang et al., 2020); and the atorvastatin group (2 mg/kg) (purchased from Pfizer [United States]). The control and model groups were administered the same volume of 0.9% normal saline (normal saline 1.5 ml/kg/d) every day. All treatments were administered orally by gavage. The control group was fed a normal diet for 16 weeks; the model group and other groups were fed a high-fat diet for 16 weeks. There were $n = 7$ mice in each group.

Hematoxylin-Eosin Staining and Oil Red O Staining of Tissue Slices

Hematoxylin-eosin (HE) staining and oil red O staining were conducted to evaluate left carotid or aortic structure atherosclerosis. Tissue isolated from all groups was fixed (4% paraformaldehyde for 24 h), dehydrated, transparentized, waxed, embedded, sectioned, and then stained with HE and oil red O.

High-Frequency Ultrasound

Sonographic evaluation of carotid arteries was conducted using a high-resolution ultrasound device (Vevo2100, FUJIFILM VisualSonics Inc.) and a high-frequency transducer probe (VisualSonics MS-550D, FUJIFILM VisualSonics Inc.). The transducer probe with a frequency of 22–50 MHz provided a characteristic resolution of 13.9 μm and a maximum imaging depth of 0–10 mm.

Immunohistochemistry

The paraffin tissue sections were dewaxed and then treated with 0.3% hydrogen peroxide solution for 10 min. Then, the sections were immersed in 0.01 mol/L citric acid buffer and heated to boiling in an autoclave 3 min 3 times. Next, the sections were blocked with 5% bovine serum albumin (BSA) for 1 h at room temperature. Then, the samples were washed three times with phosphate-buffered saline (PBS) and incubated with primary antibodies (rat anti-mouse α-actin [dilution 1:100], rabbit anti-mouse IFN-γ [dilution 1:100] and rabbit anti-mouse CD68 [dilution 1:50], all purchased from Abcam, United Kingdom) for 1 h at 37°C. The sections were then rinsed three times with PBS, treated with appropriate horseradish peroxidase (HRP)-conjugated secondary antibodies for 30 min at 37°C and washed 3 times with PBS again. Antigen-antibody reactions were stained with diaminobenzidine (DAB) for 5–10 min, and all sections were counterstained with hematoxylin. The expression levels of CD68, IFN-γ and α-actin were observed with a Nikon E400 microscope under high-power (400×) fields.

Real-Time PCR

Total RNA was extracted from fresh frozen aortae with a FastPure Cell/Tissue total RNA isolation kit (Vazyme, China) according to the manufacturer's instructions. Total RNA (1 μg) was reverse transcribed to cDNA with a HiScript III RT SuperMix for use in a qPCR kit (Vazyme, China) at 37°C for 15 min and 85°C for 5 s. Extracted mRNA was then reverse transcribed into cDNA using the iScript cDNA synthesis kit (Bio-Rad, United States). Real-time PCR analysis was performed using ChamQ Universal SYBR qPCR master mix (Vazyme, China) and an Applied Biosystems Quant Studio 3 Detection System according to the manufacturer's recommendations (Thermo Fisher Scientific, United States). Specific primers for IFN-γ, TNF-α, oxidized low-density lipoprotein receptor 1 (LOX-1), IL-10, PI3K, AKT and mTOR were designed using Primer 3 software (**Table 1**). A melting curve analysis was performed to confirm the specificity of qPCR products. Fold-changes were calculated using the $2^{-\Delta\Delta Ct}$ method and were normalized to β-actin expression. All reactions were performed in triplicate and repeated three times.

Serum Chemistry Analysis

All ApoE$^{-/-}$ mice were fasted overnight before being anesthetized and sacrificed. All blood samples were placed at 4°C overnight and then centrifuged at 3,000 rpm for 10 min to obtain the upper serum. Total cholesterol (TC), triglycerides (TGs), high-density lipoprotein cholesterol (HDL-C) and low density lipoprotein cholesterol (LDL-C) were measured by an automatic animal biochemistry analyzer (Catalyst One, IDEXX, United States).

Network Target Prediction

First, the compounds meeting the Lipinski "rule of five" and drug-likeness (DL) ≥0.18 criteria in DLTs were searched using 3 databases: the Lab of Systems Pharmacology database; the TCM Database @ Taiwan; and BATMAN-TCM. Autophagy-related targets were obtained by using known autophagy-related targets from two existing databases: the TTD database (http://database.idrb.cqu.edu.cn/TTD/) and the DrugBank database (http://www.drugbank.ca/). Then, we used MOE software for molecular docking of the compounds to the major autophagy-related targets. The component-target network was established using Cytoscape 3.6.1 software (Bethesda, MD, United States).

Cell Culture and Treatment

RAW264.7 macrophages (Xiangya Central Laboratory Cell Bank, Central South University, Changsha, China) were cultured in high-glucose Dulbecco's modified Eagle's medium (DMEM) (HyClone, United States) supplemented with 10% heat-inactivated fetal bovine serum (FBS) (Gibco, United States), 100 U/mL penicillin, and 100 μg/ml streptomycin (Gibco, United States) at 37°C in a humidified incubator containing 5% CO_2.

TABLE 1 | qPCR primer sequences used in this study.

Target gene	Primer sequence (forward)	Primer sequence (reverse)
IFN-γ	AGTGGCATAGATGTGGAA	CAATGACGCTTATGTTGT
TNF-α	CCCCAGTCTGTATCCTTCTAA	TCGAGGCTCCAGTGAATT
LOX-1	TCTTCCATGGGCCCTTTAGCTG	TTCCGATGCAATCCAATCCAGA
IL-10	ACCTGCTCCACTGCCTTGCT	GGTTGCCAAGCCTTATCGGA
PI3K	CTTGCCTCCATTCACCACCTCT	GCCTCTAATCTTCTCCCTCTCCTTC
AKT	TGTCTCGTGAGCGCGTGTTTTT	CCGTTATCTTGATGTGCCCGTC
mTOR	AGTGAAGCCGAGAGCAATGAGA	GCCAAGGAGATAGAACGGAAGAAGC
β-actin	AACACCACCCAGTTGCTGTA	TCCACCACCCAGTTGCTGTA

Mouse BMDMs were obtained by flushing the femurs of C57BL/6 mice and cultured with DMEM containing 10% heat-inactivated FBS. To obtain differentiated macrophages, 5 ng/ml macrophage colony-stimulating factor (R&D Systems) was added every 2 days for 7 days.

After 24 h of seeding in a 6-well plate (3506, Corning, United States), these cells were randomly divided into different groups: control; Torin1; Model (oxLDL); DLT^{low} (7.5 μg/ml); DLT^{middle} (75 μg/ml) and DLT^{high} (750 μg/ml).

MTT Assay

The effect of DLTs (Connell, Jilin, China) on RAW264.7 macrophage viability was assessed by measuring the absorbance of 3-(4.5-dimethylthiazol-2-yl)-2, 5-diphenyl tetrazolium bromide (MTT) dye in the cells. RAW264.7 cells (5×10^3, 4×10^3 and 3×10^3) were seeded in 96-well culture plates (Corning, United States) and treated with DLTs (0, 30, 60, 90, 120, 180, 210, 240, 270 and 300 μg/ml) for 24, 48, and 72 h, respectively. Subsequently, 100 μl of MTT solution (0.5 mg/ml) was added to each well and incubated at 37°C for another 4 h. Then, the supernatant was discarded and replaced with 100 μl of DMSO. The optical density was read on a PerkinElmer VICTOR X5 (PerkinElmer, United States) with a monochromatic microplate reader at a wavelength of 490 nm.

Cell Index Evaluation Using the xCELLigence System

Experiments were performed using the xCELLigence real-time cell analysis (RTCA) DP instrument (ACEA Biosciences Inc., San Diego, CA, United States) at 37°C with 5% CO_2. To measure the CI of RAW264.7 cells on oxLDL and DLTs in real time, RAW264.7 cells were seeded on gold microelectrodes embedded at the bottom of 16-well microplates (E-plates; ACEA Biosciences Inc., San Diego, CA, United States) at a density of 7.0×10^3 cells/well. After the baseline measurement was calibrated, the cell index was measured every 15 min. Then, 24 h after seeding, 50 μg/ml oxLDL and 12, 120, 210, 240, 270 and 300 μg/ml DLTs were added to the culture system every 1 min for 2 h and every 15 min for 249 h to observe the short-term and long-term effects of the drug, respectively.

Phagocytosis of DiI-oxLDL by RAW264.7 Cells

RAW264.7 cells were inoculated in 24-well plates, 10 μg/ml DiI-oxLDL was added to induce the formation of foam cells, and different concentrations of DLTs were applied to intervene in the process. The control group was supplemented with culture medium without DiI-oxLDL or DLTs. Flow cytometry was used to analyze the content of DiI-oxLDL phagocytosed by the cells of each group by measuring the median fluorescence intensity (MFI).

Oil Red O Staining of BMDMs

BMDMs were cultured in 6-well culture plates, and the corresponding drugs were added for 24 h of treatment. Cells were gently rinsed twice with PBS solution and fixed with 4% paraformaldehyde for 30 min. Cells were rinsed with PBS solution for 1 min, stained with oil red O working solution for 30 min at room temperature, and washed twice with distilled water for 1–2 min. Red intracellular lipid droplets were subsequently observed under a microscope.

DAPI-PI Staining of BMDMs

BMDMs were seeded in 6-well plates. After treatment with DLTs and/or ox-LDL, cells were rinsed 2 times with PBS and then incubated with DAPI staining solution for 15 min at room temperature in the dark. The solution was discarded and stained with PI dye solution for 10 min after rinsing 2 times with PBS. Cells were observed under an immunofluorescence microscope.

Western Blotting

RAW264.7 cell protein was extracted using RIPA buffer. Protein concentration was measured using the BCA Kit (Beyotime Biotechnology, China). The protein samples (10 μg/well) were separated by 10–15% sodium dodecyl sulfate (SDS)-polyacrylamide gel electrophoresis and then transferred to a polyvinylidene difluoride (PVDF) membrane (Millipore, United States). Each PVDF membrane was incubated with primary monoclonal antibodies against p-PI3K (17366), p-Akt (4060), p-mTOR (5536), Akt (4691), mTOR (2983), LC3 (12741), p62 (23214) and GAPDH (5174) (Cell Signaling Technology, United States) overnight at 4°C. Then, the cells were blotted with a secondary antibody conjugated with horseradish peroxidase for 1 h at a dilution of 1:5000. Finally, the bands were visualized by enhanced chemiluminescence staining. The intensities of the bands were quantified with ImageJ software. (NIH Image, United States)

Statistical Analysis

Statistical analysis was performed using SPSS 17.0 (SPSS, Inc., United States). The data were expressed as the mean ± SD. When the data conformed to normality and homogeneity of variance,

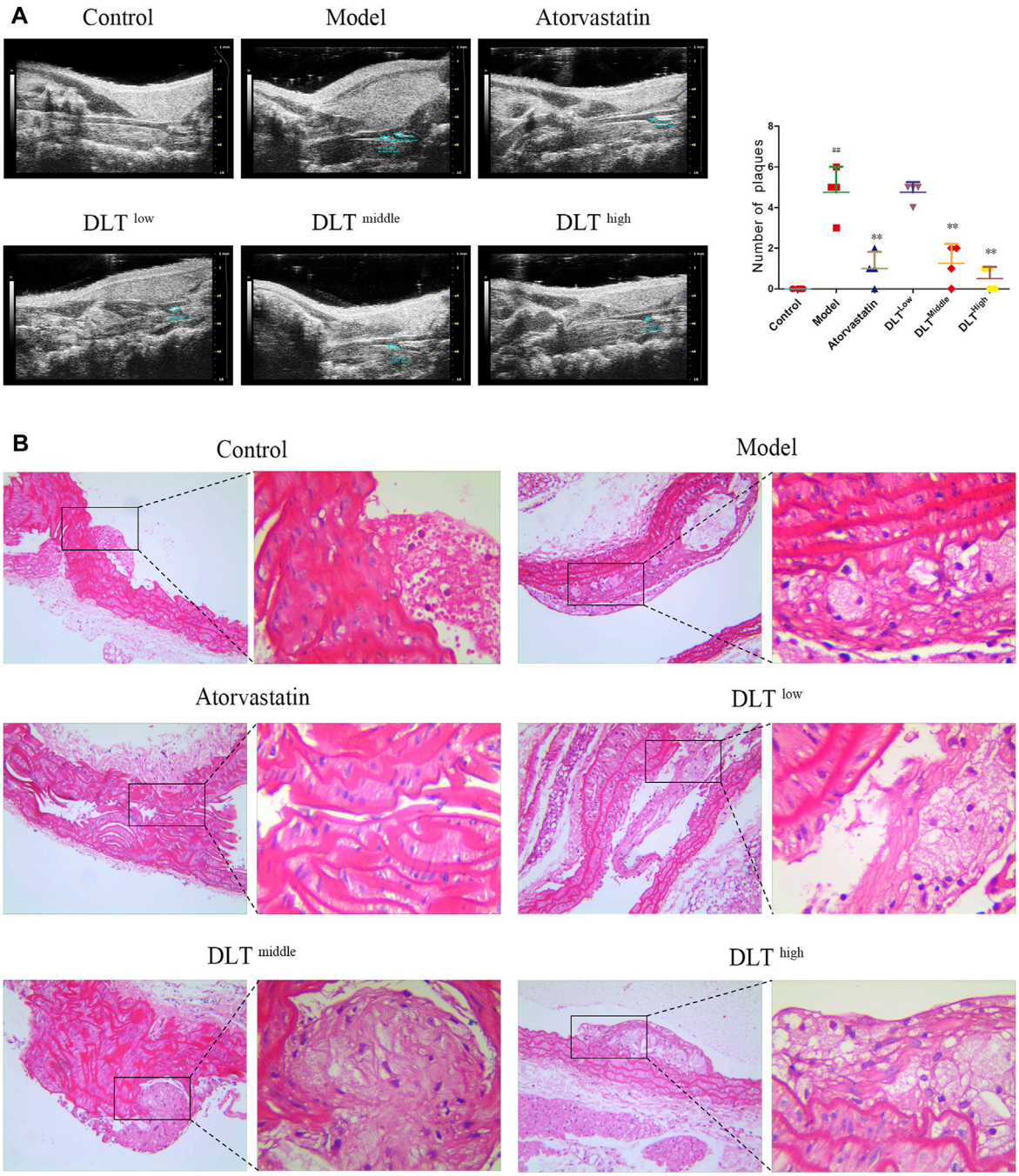

FIGURE 1 | DLTs reduced atherosclerotic plaque formation of the aorta and carotid artery in ApoE$^{-/-}$ AS mice. Plaques were observed by **(A)** vascular ultrasound of the carotid artery and **(B)** HE staining of aortic tissue sections. **(A)** The control group showed the uniformly continuous vascular acoustic shadow of the carotid artery, and no abnormal acoustic shadow was observed in the lumen; most mice in the model group had an uneven continuous sound shadow in the carotid artery, some of the vessel walls had a hyperechoic shadow, and an abnormal sound shadow was present in the vessel wall (plaques, see circled); inhomogeneous and continuous hyperechoic lights were also observed in the carotid arteries of the DLT-low group; the phenomenon was effectively restrained in DLT-middle and DLT-high groups and the atorvastatin group. The number of plaques is indicated in graphs. **(B)** In the model group, the endothelial layer was sloughed off, with more plaques attached to the vessel wall, intimal hyperplasia was severe, many foam cells could be observed; compared with the model group, the area of plaques in the DLT groups and the atorvastatin group was smaller, the foam cell infiltration was reduced and the effect was dose-dependent in the DLT groups. The high-dose DLT group and the atorvastatin group showed continuous vascular endothelial cells. The data are presented as the mean ± SD ($n = 4$). $^{\#\#}p < 0.01$ vs the control group, and $^{**}p < 0.01$ vs the model group.

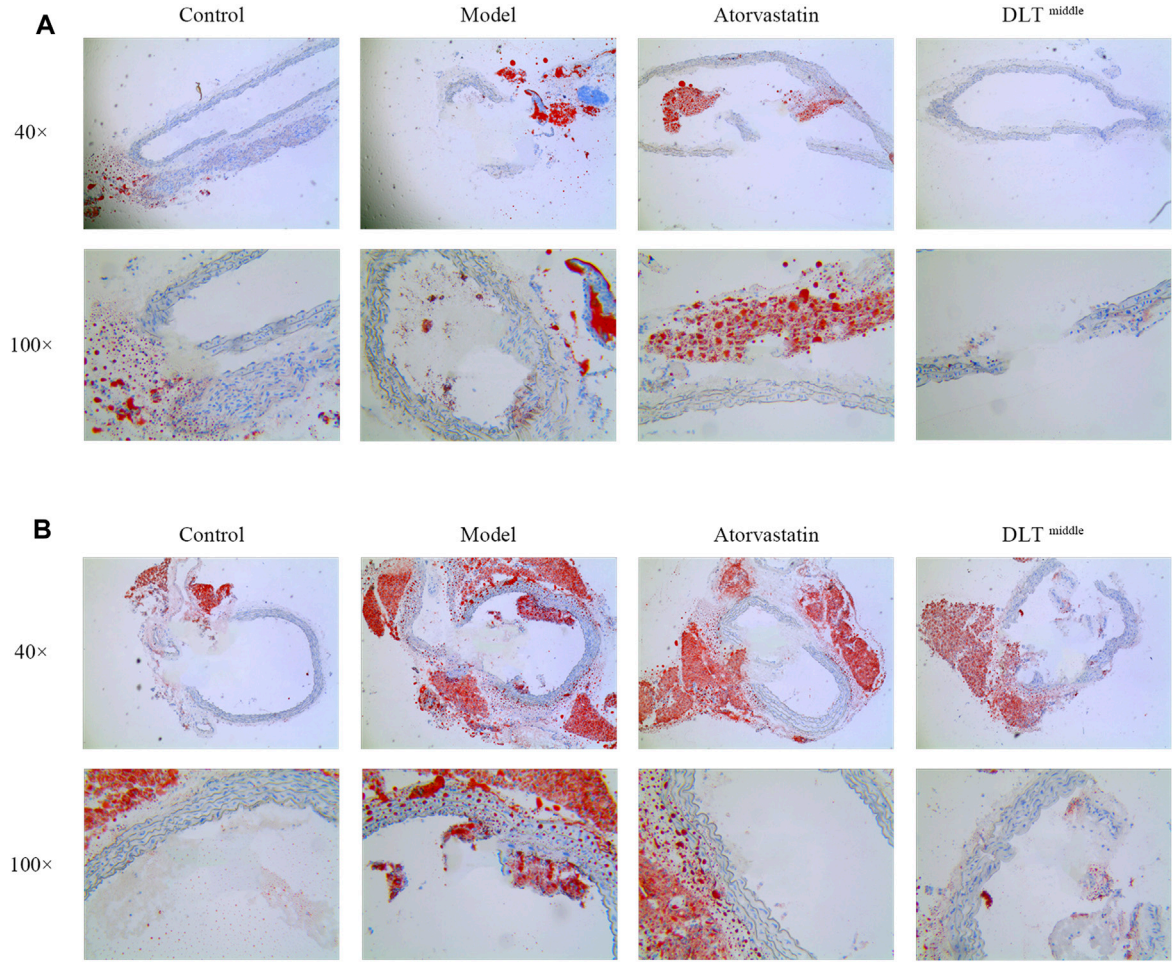

FIGURE 2 | DLTs reduced intracellular lipid droplet accumulation in the aorta and left carotid artery of ApoE$^{-/-}$ mice. Intracellular lipid droplet accumulation was observed by oil red O staining in the carotid **(A)** and aortic **(B)** arteries. Images revealed the most severe intracellular lipid droplet deposition (in red) in the vessel wall of the model groups, while it was markedly reduced in the DLT-middle group in aortic tissue and carotid tissue compared with the model group, so did the atorvastatin group in aortic tissue. No significant difference in lipid droplet deposition was seen between the atorvastatin group and the model group in carotid tissue.

one-way ANOVA was used to analyze the data. Otherwise, the Kruskal-Wallis method was used for analysis. Values of $p < 0.05$ were considered significant.

RESULTS

Chemical Profiles of Danlou Tablets

For the quality control of DLTs, we detected the main chemical compositions of DLTs by UHPLC analysis. UHPLC fingerprints of five batches of DLTs were obtained (**Supplementary Figure S1** in the Supplementary Material).

Danlou Tablets Reduced the Formation and Number of Atherosclerotic Plaques

A small animal ultrasound machine was used to acquire and evaluate the effects of DLTs on atherosclerotic plaques in ApoE$^{-/-}$ mice after 16 weeks with high fat diets (**Figure 1A**). The results revealed middle- and high-dose DLTs and atorvastatin reduced the number of atherosclerotic plaques compared with the model group ($p < 0.01$), whereas there is no significant difference between the low-dose DLT group and the model group in the number of plaques ($p > 0.05$). The ultrasound image in the control group showed smooth carotid arteries without plaque formation.

After HE staining, the plaque structure of atherosclerosis mice in each group was observed under a 200× optical microscope, as shown in **Figure 1B**. In the model group, the endothelial layer was sloughed off, with a large number of plaques attached to the inner wall of the vessel, severe intimal hyperplasia and massive foam cell infiltration. Compared with the model group, the area of plaques in the DLT groups and the atorvastatin group was smaller, the foam cell infiltration was reduced with a dose-dependent effect in the DLT groups. The high-dose DLT group and the atorvastatin group showed continuous vascular

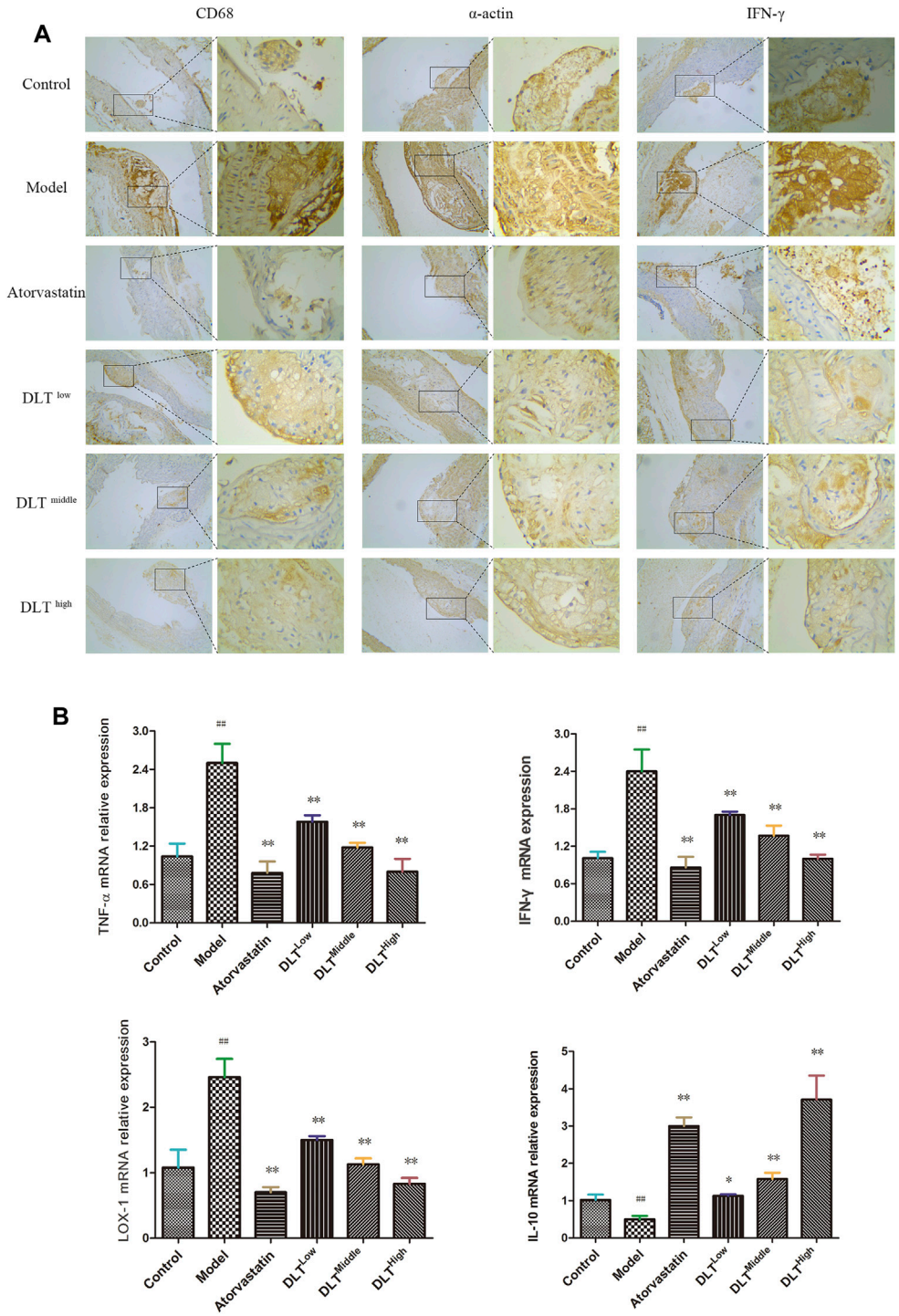

FIGURE 3 | Changes in macrophage (CD68) infiltration and the expression of LOX-1, the inflammatory factors TNF-α, IFN-γ, IL-10 and smooth muscle (α-actin) in the aorta of ApoE$^{-/-}$ mice. Macrophage (CD68) infiltration, the inflammatory molecule IFN-γ and smooth muscle (α-actin) were evaluated by immunohistochemical staining **(A)**, and the mRNA expression levels of LOX-1, TNF-α, IFN-γ and IL-10 were analyzed by RT-PCR (B). **(A)** CD68, α-actin, and IFN-γ immunohistochemical staining showed brown-yellow granules atherosclerotic lesions of the aorta in each group. Among all groups, the brown-yellow granules in the model group were the most abundant and were decreased gradually in a dose-dependent manner in the DLT groups; the atorvastatin group also exhibited fewer yellow granules compared with the model group. **(B)** mRNA levels of the proinflammatory factors IFN-γ and TNF-α and oxidized low-density lipoprotein receptor LOX-1in the model group were significantly higher than those in the control group. The atorvastatin group and the DLT groups treated with low, middle, and high doses exhibited reduced expression of IFN-γ, TNF-α and LOX-1 mRNA. The mRNA expression of the anti-inflammatory factor IL-10 was significantly increased in the atorvastatin group and DLT groups. The data are presented as the mean ± SEM (n = 7). $^{\#\#}p < 0.01$ vs the control group, and $^{*}p < 0.05$, $^{**}p < 0.01$ vs the model group.

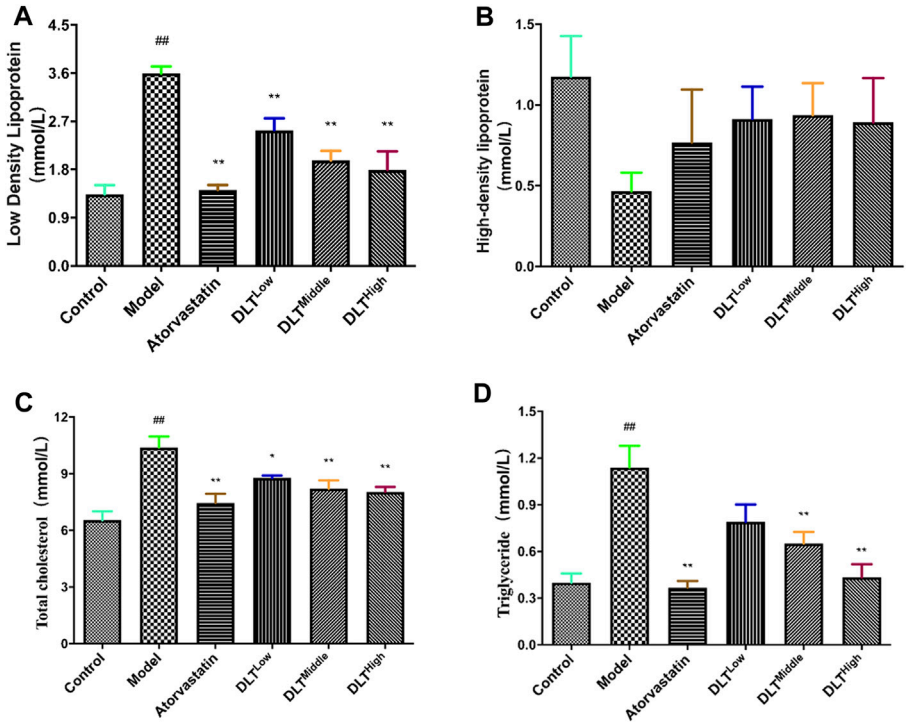

FIGURE 4 | DLTs influenced plasma lipids following a 16 week high-fat diet in AS APOE$^{-/-}$ mice. **(A)** Low-density lipoprotein. **(B)** High-density lipoprotein. **(C)** Total cholesterol. **(D)** Triglyceride. The data are presented as the mean ± SD (n = 7). $^{\#\#}p < 0.01$ vs the control group, and $^{*}p < 0.05$, $^{**}p < 0.01$ vs the model group.

endothelial cells. HE staining results showed that DLTs can reduce plaque formation and foam cell infiltration.

In addition, oil red O-stained areas in sections of the left carotid and aorta artery tissue in the model groups were larger than them in the control groups. The administration of middle-dose DLTs markedly decreased the area of lipid deposition in the left carotid and the aorta vessel. Similarly, lipid droplet accumulation was reduced in aortic tissue in the atorvastatin group compared with the model group whereas there was no difference in the accumulation of lipid droplets in the left carotid artery tissue between two groups (**Figure 2**).

Immunohistochemical Observation of Macrophage (CD68) Infiltration, Inflammatory Molecule IFN-γ and Vascular Smooth Muscle (α-actin) in the Aorta of ApoE$^{-/-}$ Mice

Under a light microscope, CD68, α-actin and IFN-γ (brown-yellow particles) were observed in the atherosclerotic lesions of the aorta (**Figure 3A**). Compared with the control group, the expression of CD68, IFN-γ and α-actin in the atherosclerotic plaques of ApoE$^{-/-}$ mice was significantly increased in the model group; compared with the model group, the expression of CD68, IFN-γ and α-actin in the atherosclerotic plaques of the aorta in the DLT groups of different doses were reduced in a dose-dependent manner. Similarly, the expression of CD68, IFN-γ and α-actin in ApoE$^{-/-}$ mice in the atorvastatin group was markedly reduced, suggesting that DLTs inhibited macrophage (CD68) infiltration, the expression of inflammatory molecule IFN-γ and vascular smooth muscle (α-actin) in the aorta of ApoE$^{-/-}$ mice fed with a high-fat diet.

TABLE 2 | The number of active ingredients in herbs of DLTs and their main autophagy-related targets.

Herbs	Number of active ingredients	Target genes
Danshen	59	ATG1, ATG5, mTOR, PI3K
Yujin	48	GSK3b, ATG1, ATG5, mTOR, PI3K
Chuanxiong	39	ATG1, ATG5, mTOR, PI3K
Huangqi	31	GSK3b, ATG1, ATG5, mTOR, PI3K
Gegen	26	GSK3b, ATG1, ATG5, mTOR, PI3K
Gualoupi	16	ATG1, ATG5, mTOR, PI3K
Chishao	13	ATG1, ATG5, mTOR, PI3K
Zexie	12	GSK3b, ATG1, ATG5, mTOR, PI3K
Xiebai	6	GSK3b, ATG1, ATG5, mTOR, PI3K
Gusuibu	3	ATG5, mTOR, PI3K

Effect of Danlou Tablets on the mRNA Expression of IFN-γ, TNF-α, LOX-1 and IL-10 in the Atherosclerosis Model of ApoE$^{-/-}$ Mice

To observe the effects of DLTs on the expression of pro- and anti-inflammatory factors, as well as lipid metabolism in vascular tissue, the expressions of the inflammatory factors IFN-γ, TNF-α (proinflammatory) and IL-10 (anti-inflammatory) and LOX-1

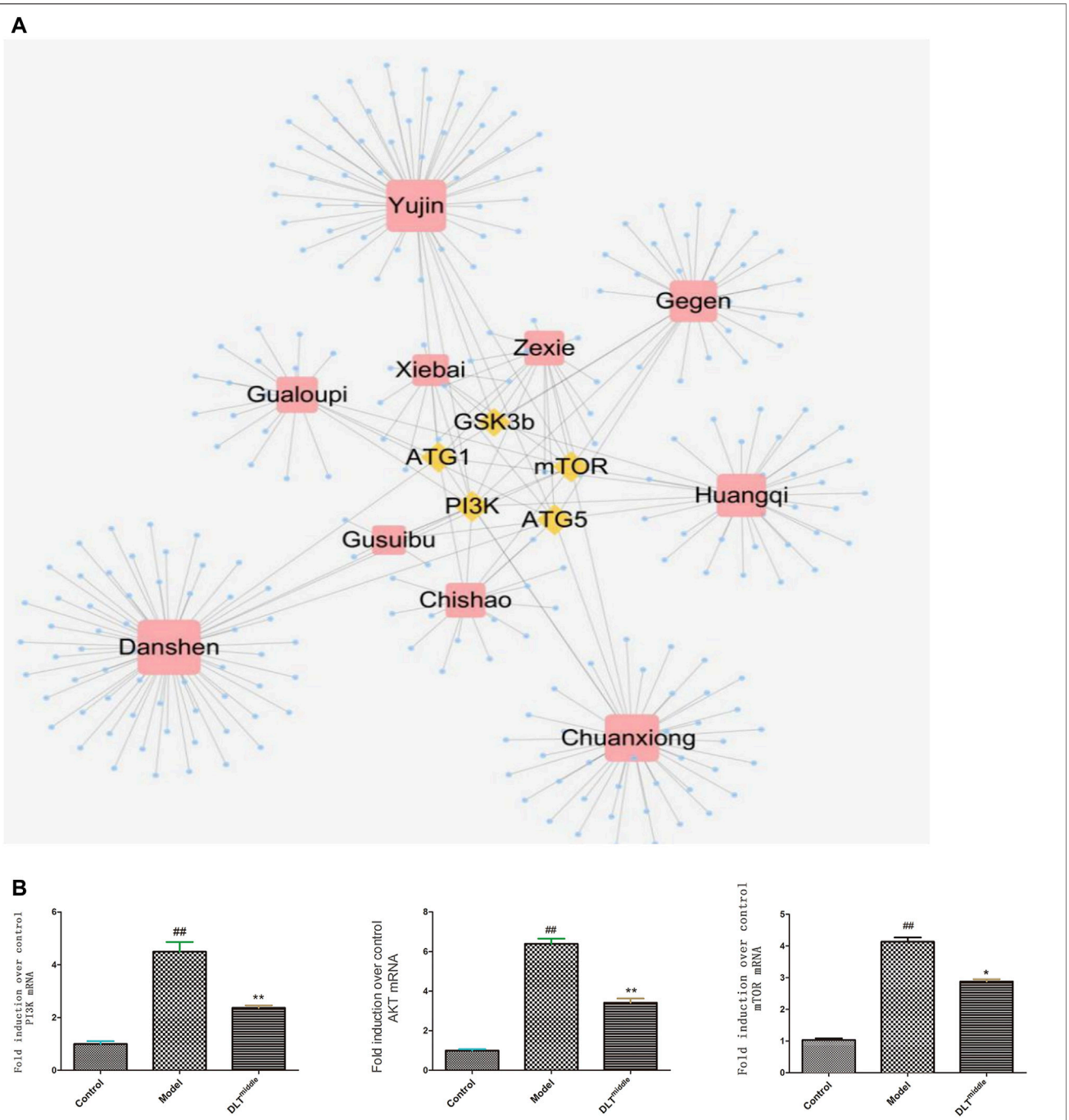

FIGURE 5 | DLTs regulated autophagy through the PI3K/Akt/mTOR signaling pathway in AS APOE$^{-/-}$ mice. **(A)** Compound-target network for DLTs. The yellow nodes represent potential autophagy-related targets, and the blue nodes represent active compounds. **(B)** mRNA expression of PI3K/AKT/mTOR in aorta tissues. The data are presented as the mean ± SD (n = 3). $^{\#\#}p < 0.01$ vs the control group, and $^{*}p < 0.05$, $^{**}p < 0.01$ vs the model group.

were determined by real-time PCR in aortic tissues of mice in each group (**Figure 3B**). The results showed that the IFN-γ, TNF-α and LOX-1 mRNA levels of the model group were significantly higher than those of the control group ($p < 0.01$). Atorvastatin and DLTs at low, middle, and high doses reduced the mRNA expression of IFN-γ, TNF-α and LOX-1 ($p < 0.01$). The expression of IL-10 mRNA was significantly increased in the atorvastatin group and DLT groups vs the model group ($p < 0.05$ or $p < 0.01$).

Changes in Blood Lipid Levels of ApoE$^{-/-}$ Mice

Serum lipid levels were measured at the end of the experiment. The results showed that the serum LDL-C, TC, and TG levels of the model

group were increased compared with those of the control group ($p < 0.01$). In terms of HDL-C levels, no difference was observed among all groups ($p > 0.05$). Significant differences were respectively observed in the levels of LDL-C and TC between the low-, middle-, and high-dose DLT groups and the model group. It was indicated that compared with the model group, DLT decreased the serum levels of LDL-C and TC ($p < 0.05$ or $p < 0.01$). As for the serum level of TG, there is no significant difference between low-dose DLT group and the model group ($p > 0.05$). However, in the middle- and high-dosage of DLT groups, TG levels were sharply lower than those of the model group ($p < 0.01$). The serum levels of LDL-C, TC and TG in the positive control group (atorvastatin) mice were significantly lower than those in the model group ($p < 0.01$). Experiments showed that the blood lipid levels of mice in each group of DLTs gradually decreased in a dose-dependent manner (**Figure 4**).

Network Pharmacology Results

Active ingredients in DLTs were preliminarily screened according to "Lipinski's rule of five" and drug-likeness (DL) ≥ 0.18 criteria. The component-target network indicated that five target genes-GSK3b, ATG1, ATG5, PI3K and mTOR in autophagy pathways were closely associated with 253 active components of DLTs after molecular docking (**Table 2**). The results of the molecule-herb-target network are shown in **Figure 5**A. The RT-PCR results showed that the mRNA levels of PI3K, Akt and mTOR were upregulated in the aortic tissues of ApoE$^{-/-}$ mice ($p < 0.01$) and were downregulated by the middle doses of DLTs ($p < 0.01$) (**Figure 5B**), which suggested that DLTs were involved in regulating the PI3K/Akt/mTOR pathway to enhance autophagy.

Danlou Tablets Inhibited the Growth of RAW264.7 Cells

The MTT assay was performed to evaluate the inhibitory effects of DLTs on RAW264.7 cells. As shown in **Figure 6A**, DLT concentrations from 30 to 300 μg/ml significantly inhibited the proliferation of RAW264.7 cells at different time points (24, 48, and 72 h) in a dose-dependent manner ($p < 0.01$).

Danlou Tablets Increased the Cell Index of RAW264.7 Cells Stimulated by oxLDL

The xCELLigence system was used to evaluate the effect of DLT concentration on RAW264.7 cells transforming to foam cells induced by 50 μg/ml oxLDL. The cell index of the model group was lower than that of the control group, indicating that foam cells could cause cell index decline. In addition, the cell index decreased after 80 h of cell inoculation (**Figure 6B**). The cell index of the DLT groups at different concentrations was significantly higher than that of the model group, which indicated that DLTs significantly inhibited the formation of foam cells. The cell growth index curve was higher than that of the control group when the DLT concentration increased; indicating that DLTs could enhance the oxLDL-induced growth activity of RAW264.7 cells (**Figure 6C**).

Danlou Tablets Inhibited RAW264.7 Macrophage Phagocytosis of oxLDL

The median fluorescence intensity (MFI) was measured by flow cytometry to analyze the content of Dil-oxLDL in RAW264.7 macrophages. After treatment with Dil-oxLDL and various concentrations of DLTs, the cells were collected at 2, 4, 6 and 24 h for flow cytometry analysis. After 2 h of incubation, the MFI values of the DLT groups treated with 60–300 μg/ml DLTs were markedly lower than those of the model group ($p < 0.05$) (**Figures 6D–F**). 24 h later, the MFI of the groups treated with 240 and 300 μg/ml DLTs was significantly decreased ($p < 0.05$) (**Figure 6G**).

Danlou Tablets Alleviated the Apoptosis of BMDMs Induced by Ox-LDL

To examine the effects of DLTs on ox-LDL-induced apoptosis in BMDMs, we stained the cells in each group with DAPI and PI to observe the morphology of the nuclei under an immunofluorescence microscope (**Figure 7**). Apoptotic cells showed nuclear condensation with deepening of staining or nuclear fragments. The results showed more cells with deepened nuclear staining in the ox-LDL-induced BMDM group than in the control group, and the DAPI-PI dye-treated cells were significantly reduced after DLT treatment.

Danlou Tablets Might Alleviate Intracellular Lipid Accumulation Through Autophagy

To observe the inhibitory effects of autophagy on BMDMs transformation into foam cells, oil red O staining was performed, and the differences between Torin1 and DLT treatments were compared. Torin1 is an inhibitor of mTOR, which is a key molecule inducer of autophagy. Our results showed that Torin1 treatment significantly reduced intracellular lipid droplet accumulation as did DLT treatment; that is, promoting autophagy also inhibited macrophage transition into foam cells (**Figure 8**). Moreover, the expression of the autophagy indicators LC3II and P62 suggested enhanced autophagy in DLT-treated RAW264.7 Macrophages induced by oxLDL (**Figure 9A**).

Danlou Tablets Might Alleviate Intracellular Lipid Accumulation Through an Autophagy-Related PI3K/Akt/mTOR Signaling Pathway in RAW264.7 Cells

Because our network pharmacology results indicated that DLTs affected PI3K, ATG5, ATG1 and mTOR targets, we evaluated whether the PI3K/Akt/mTOR pathway was involved in the regulation of DLTs in RAW264.7 cells induced by oxLDL. The data showed that similar to Torin1, p-PI3K, p-Akt and p-mTOR were inhibited in DLT-treated RAW264.7 cells (**Figure 9B**), which suggested that DLTs inhibited the autophagy-related PI3K/Akt/mTOR signaling pathway to alleviate intracellular lipid accumulation in RAW264.7 cells.

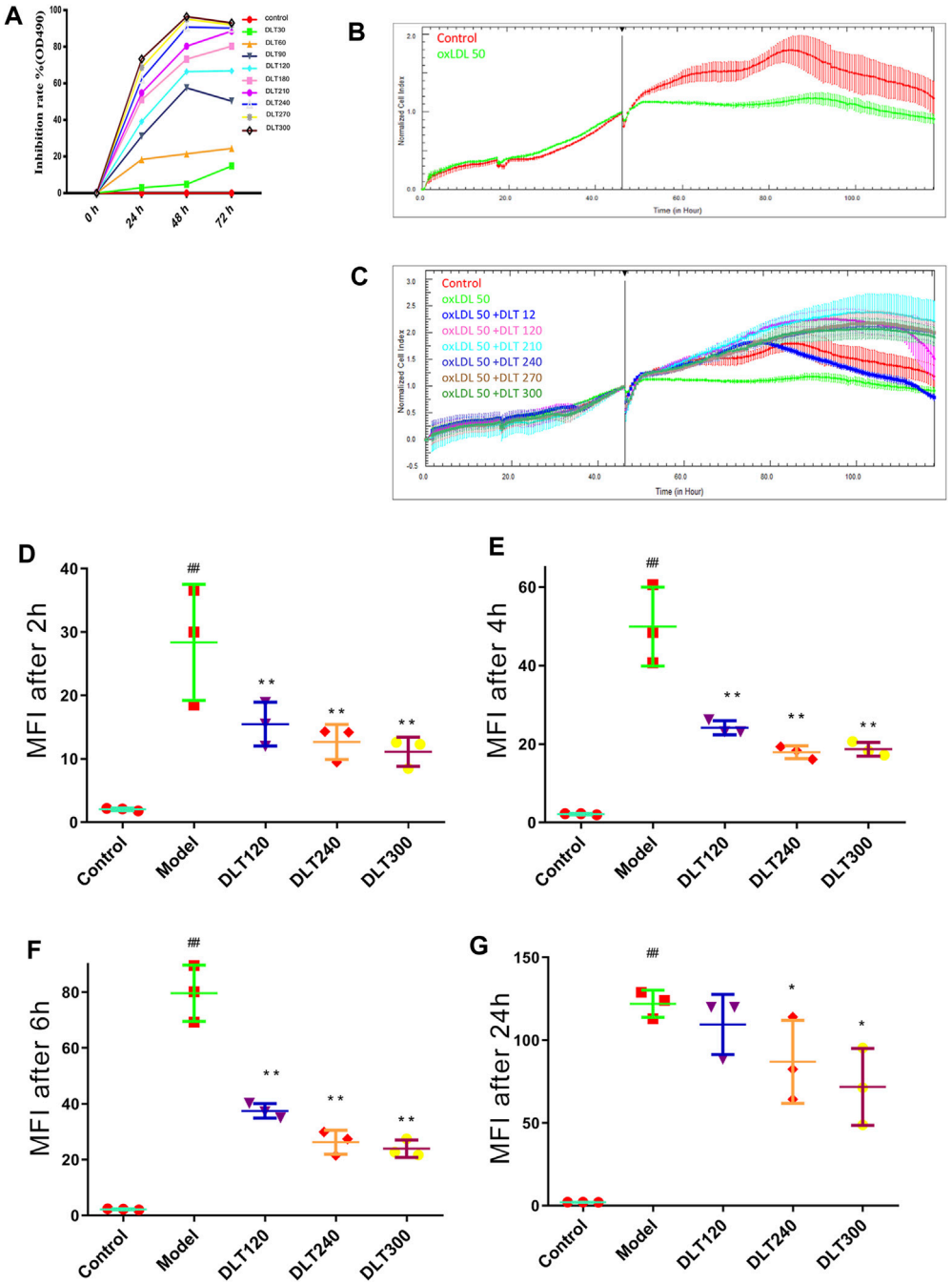

FIGURE 6 | DLTs affected the viability and phagocytosis of Dil-oxLDL in RAW264.7 cells. **(A)** Viability of RAW264.7 cells treated with DLTs. **(B)** CI of RAW264.7 cells treated with ox-LDL. **(C)** CI of RAW264.7 cells treated with DLTs and ox-LDL. **(D–G)** The extent of Dil-oxLDL uptake (MFI) by RAW264.7 cells after treatment with DLTs for 2, 4, 6 and 24 h was determined by flow cytometry, and the results are shown as bar graphs. The data are presented as the mean ± SD, $^{\#\#}p < 0.01$ vs the control group, and $^{*}p < 0.05$, $^{**}p < 0.01$ vs the model group.

DISCUSSION

Atherosclerosis is a progressive disease that occurs in the intima of large and medium-sized arteries (Ahmed, Ameen et al., 2021); it is characterized by the buildup and fusion of scattered plaques in the arterial intima. Dyslipidemia is the main risk factor for atherosclerosis (Ma, Leng et al., 2019). Macrophage uptake and phagocytosis of lipid proteins, such as ox-LDL, result in the accumulation of intracellular cholesterol ester and transformation into foam cells, which is a key link in the progression and outcome of atherosclerosis (Orekhov, Nikiforov et al., 2020).

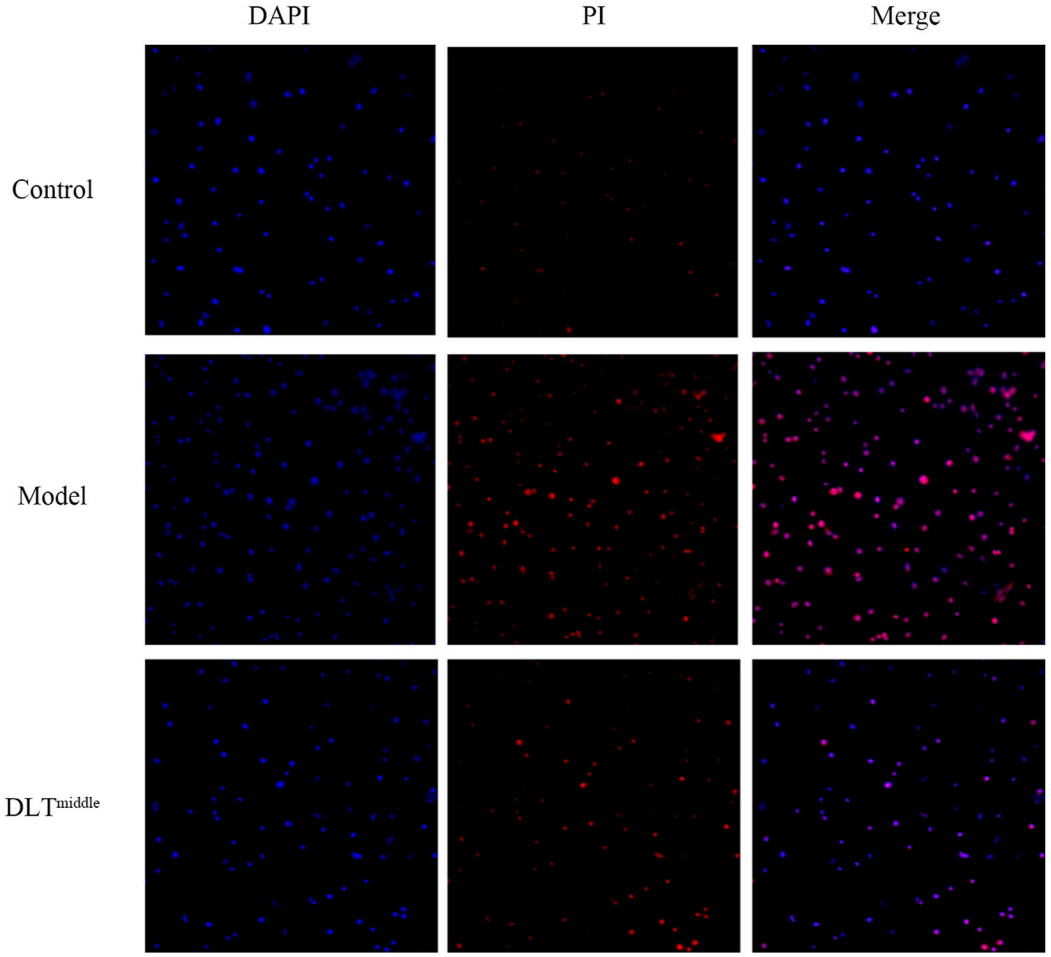

FIGURE 7 | DLTs suppressed apoptosis of BMDMs *in vitro*. Apoptotic cells were stained with DAPI and PI and observed by fluorescence microscopy (magnification ×100) after treatment with ox-LDL and DLT^{middle}. More cells with deepened nuclear staining (merge) were seen in the ox-LDL-induced BMDM group than in the control group, cells with deepened nuclear staining were significantly reduced after DLT treatment.

Traditional Chinese medicine (TCM) holds that the basic disease mechanism of atherosclerosis is a deficiency in origin and excess in superficiality with phlegm and blood stasis. Therefore, "cotreatment of phlegm and stasis" would be an effective treatment for atherosclerosis. DLTs are a representative prescription for the "cotreatment of phlegm and blood stasis", which has been approved by the national CFDA for clinical use and has achieved good clinical efficacy.

Knockout of the ApoE gene in mice caused low-density lipoprotein metabolism disorders with low-density lipoproteins oxidized and deposited in blood vessels, ultimately leading to severe hyperlipidemia and atherosclerotic lesions (Bobryshev 2006; Li Y. et al., 2016). In this study, $ApoE^{-/-}$ mice were fed a high-fat diet for 16 weeks to establish an atherosclerosis model, and the effects of DLTs on the occurrence and development of atherosclerosis were observed. The results showed that DLTs significantly decreased the serum levels of TC, TG, and LDL in AS mice and inhibited the formation of atherosclerotic plaques, arterial intimal hyperplasia and foam cell formation in a dose-dependent manner. These results indicated good antiatherosclerotic effects of DLTs.

Atherosclerosis is also a chronic inflammatory disease affecting the aorta. Inflammatory cytokines, such as TNF-α and IFN-γ, have a role in enhancing VCAM-1 expression and monocyte recruitment to the vessel wall (Zhang, Alcaide et al., 2011; Lee, Ha et al., 2020) and mediating endothelial cell death (Pober and Sessa 2007). IFN-γ signaling mediates the upregulation of LDL scavenger receptor expression and therefore enhances foam cell formation. Both TNF-α and IFN-γ resulted in the remarkably increased accumulation of subintimal macrophages and accelerated atherosclerosis. While IL-10 inhibits monocytes to release proinflammatory cytokines, including IL-1β, TNF-α, and IL-8, and promotes macrophage polarization toward the M2 phenotype (Han and Boisvert 2015), it inhibits the expression of metalloproteinase (MMP), proinflammatory cytokines and cyclooxygenase-2 in lipid-engulfed activated macrophages. In our study, the mRNA levels of TNF-α and IFN-γ were abundantly expressed in the atherosclerotic lesions of the aorta in atherosclerosis mice, while the levels of IL-10 were the opposite. DLTs reversed this trend.

Foam cell formation plays a pivotal role during atherogenesis and progression (Yu, Fu et al., 2013; Maguire, Pearce et al., 2019).

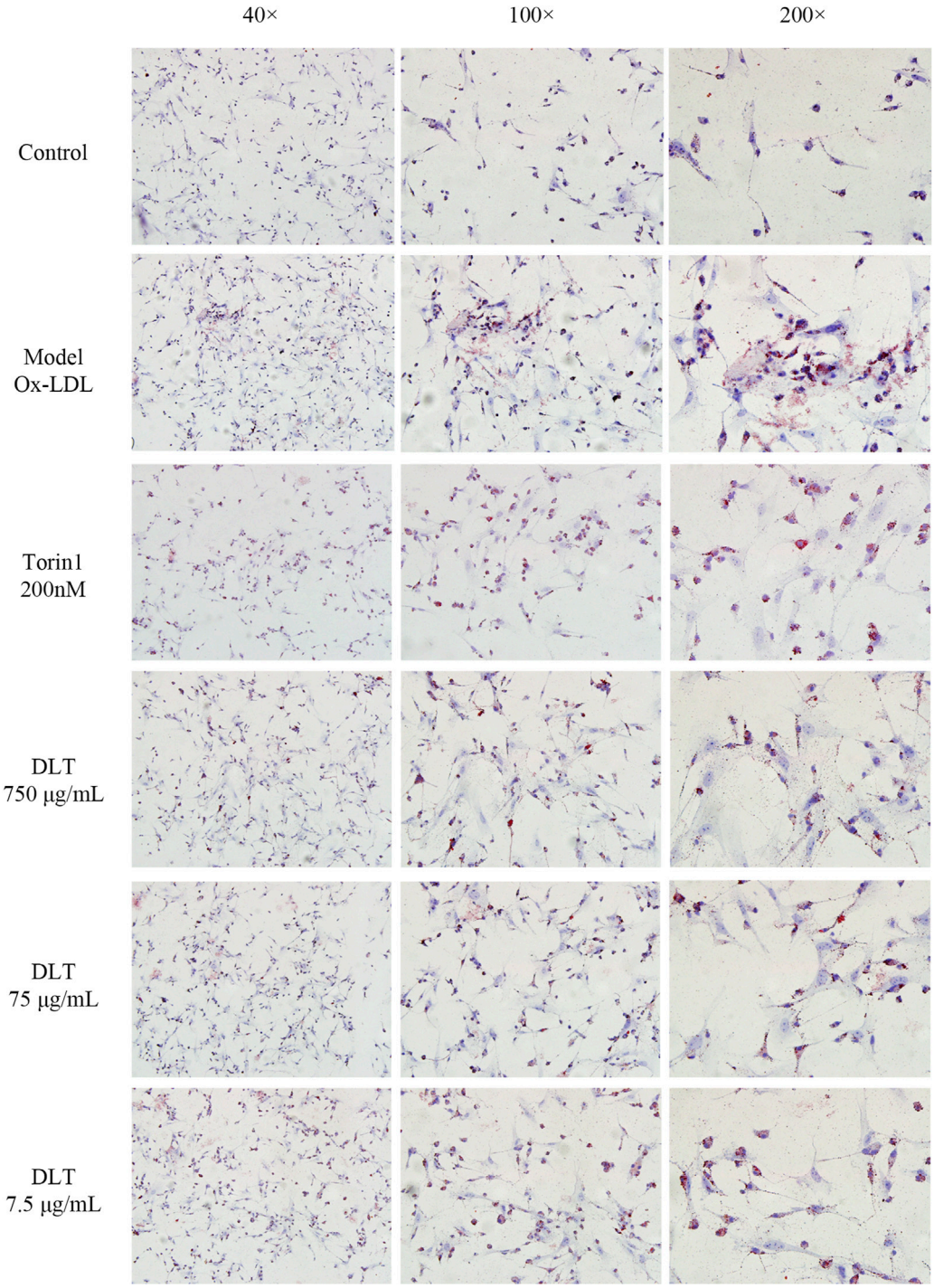

FIGURE 8 | DLTs reduced the accumulation of intracellular lipids in BMDMs. Representative images of oil red O staining are presented (magnification ×40, ×100, ×200). Ox-LDL-induced BMDM group showed more red lipid droplets, while the Torin 1 group and the DLT groups exhibited less red lipid droplets.

Macrophages phagocytose large amounts of oxLDL *via* a scavenger receptor (SR) on their surface, resulting in the formation of foam cells (Bobryshev 2006), which induce a vascular local inflammatory response that exacerbates plaque formation. Macrophagic foam cell formation is thought to be the result of an imbalance in intracellular lipid metabolism, i.e., cholesterol influx and efflux (Sukhorukov and Khotina, 2020). Our results showed that DLTs could obviously alleviate macrophage transformation into foam cells (MFI), accumulation of lipid droplets (oil red O staining) and infiltration (CD68) in arterial tissues.

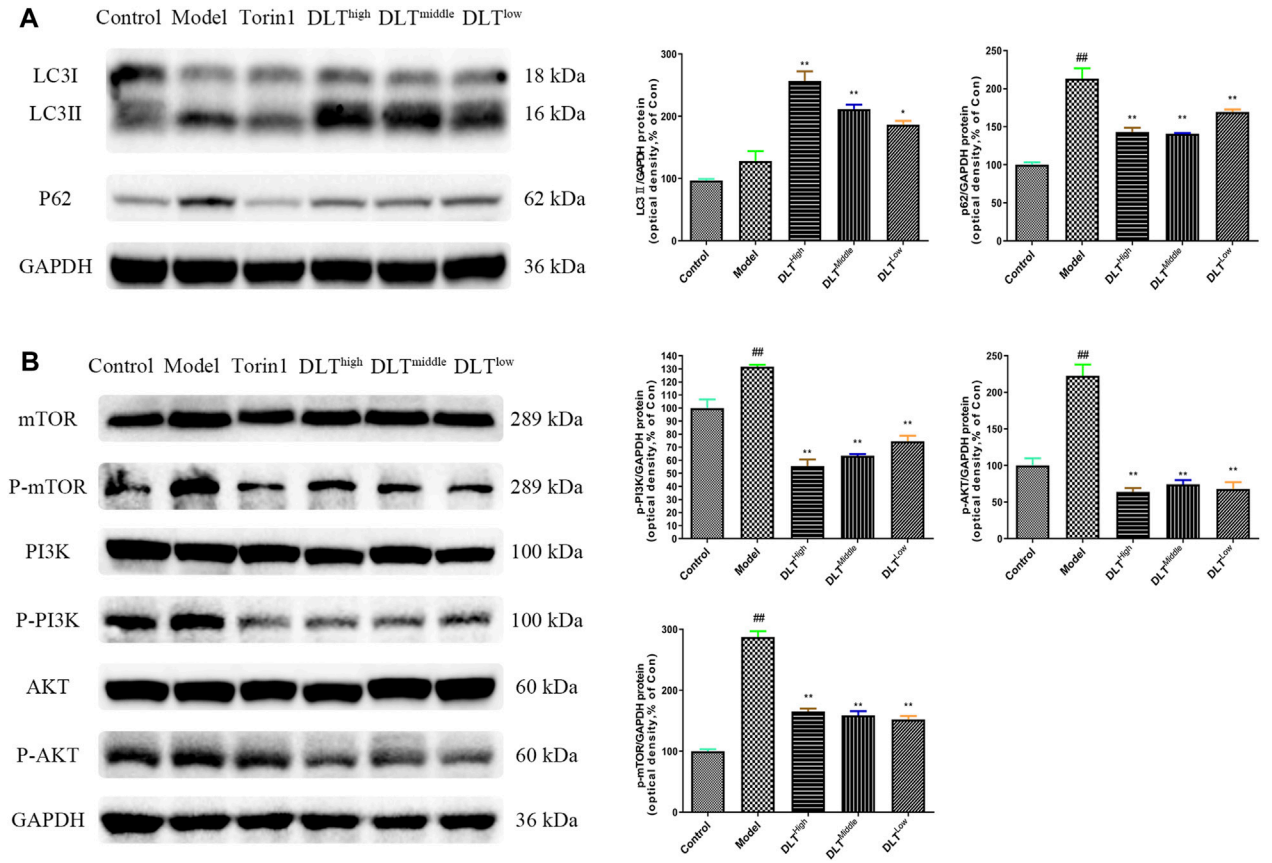

FIGURE 9 | DLTs enhanced autophagy in oxLDL-induced RAW264.7 cells via the PI3K/Akt/mTOR pathway. **(A)** DLTs upregulated the expression of the autophagy-related protein LC3II and decreased P62 accumulation. **(B)** DLTs downregulated the expression of the autophagy-related signaling molecules p-PI3K, p-Akt, and p-mTOR. The bar graphs show the quantification of the indicated proteins. Mean ± SD, $n = 3$. $^{\#\#}p < 0.01$ vs the control group, and $^{*}p < 0.05$, $^{**}p < 0.01$ vs the model group.

The role of autophagy in macrophage lipid metabolism has been highlighted by many researchers (Sun, Fan et al., 2018; Cao, Jia et al., 2019; Zhou, Ren et al., 2019). MD Khurshidul Zahid et al. found that enhancing autophagy could drive cholesterol efflux and inhibit macrophagic foam cell formation in RAW264.7 cells (Zahid, Rogowski et al., 2020). Liu et al. proved that the autophagy activator rapamycin markedly decreased intracellular lipid content and prevented transformation into foam cells, while the autophagy inhibitor 3-MA considerably increased intracellular lipid droplet accumulation. *In vivo* experiments showed that rapamycin administration in ApoE$^{-/-}$ mice reduced the death rate of macrophages and delayed plaque progression (Liu, Tang et al., 2016).

To further explore the mechanism of DLTs acting on atherosclerosis mice, we established a model of BMDMs induced by oxLDL *in vitro* and observed the effects of autophagy on foam cell formation, as well as autophagy-related pathways involved in the regulation of DLTs on BMDMs. The results showed that lipid droplet accumulation within macrophages can be reduced by promoting autophagy when using the autophagy activator Torin1. Enhanced autophagy by DLTs was confirmed by Western Blotting, which showed enhanced LC3II expression and attenuated p62 accumulation. In addition, based on the network pharmacology results of DLTs with autophagy, as well as the animal experimental results, we also validated that DLTs regulated autophagy *via* the PI3K/Akt/mTOR signaling pathway in oxLDL-induced RAW264.7 cells.

In short, we conducted systematic research on DLTs, including component analysis, *in vivo* and *in vitro* studies, and network pharmacological target prediction. We confirmed that DLTs indeed ameliorated atherosclerosis in ApoE$^{-/-}$ mice. In addition, we explored the mechanism of DLTs in atherosclerosis. DLTs may promote autophagy by inhibiting the PI3K/Akt/mTOR signaling pathway, thereby reducing the uptake of ox-LDL by macrophages, which in turn results in the formation of foam cells and the inhibition of atherosclerosis.

DATA AVAILABILITY STATEMENT

The original contributions presented in the study are included in the article/**Supplementary Material**, further inquiries can be directed to the corresponding authors.

ETHICS STATEMENT

The animal study was reviewed and approved by the Ethics Committee at Guangdong Provincial Hospital of Chinese Medicine.

AUTHOR CONTRIBUTIONS

CL, GC and YC designed and conducted the study with equal contribution. YD, GN and DW conducted part of the study. JHL and ZC analyzed the data and interpreted the results. XL, JS, HY and DH polished the manuscript. LW and JHL provided the technical support and advices for the study and supervised the study. All authors listed have made a substantial, direct, and intellectual contribution to the work and approved it for publication.

FUNDING

This work was supported by the National Natural Science Foundation of China (82174161, 82104495, 81804132 & 82174161), Science and Technology Foundation of Guangzhou City (202102010257), Scientific research projects of Guangdong Bureau of traditional Chinese Medicine (No.20200513093851), Guangdong Basic and Applied Basic Research Foundation (2021A1515012573 & 2019A1515111108), the TCM Research Fund of Guangdong Provincial Hospital of Chinese Medicine (YN2019MJ15), the Research Fund of State Key Laboratory of Dampness Syndrome of Chinese Medicine (SZ2021ZZ21), the Research Fund of Guangdong Provincial Key Laboratory of Research on Emergency in TCM (2019-40).

SUPPLEMENTARY MATERIAL

The Supplementary Material for this article can be found online at: https://www.frontiersin.org/articles/10.3389/fphar.2021.724670/full#supplementary-material

Supplementary Figure S1 | UHPLC fingerprints of 5 batches of DLT. 2:danshensu; 9:Salvianolic acid A; 10:Cryptotanshinone; 11:tanshinone IIA.

REFERENCES

Ahmed, H. M., Ameen, E. E., Awad, M. S., and Botrous, O. E. (2021). Assessment of Carotid Intima Media Thickness and Left Ventricular Mass Index in Children with Idiopathic Nephrotic Syndrome. *Vasc. Health Risk Manag.* 17, 349–356. doi:10.2147/VHRM.S295868

Bobryshev, Y. V. (2006). Monocyte Recruitment and Foam Cell Formation in Atherosclerosis. *Micron* 37 (3), 208–222. doi:10.1016/j.micron.2005.10.007

Cao, H., Jia, Q., Yan, L., Chen, C., Xing, S., and Shen, D. (2019). Quercetin Suppresses the Progression of Atherosclerosis by Regulating MST1-Mediated Autophagy in Ox-LDL-Induced RAW264.7 Macrophage Foam Cells. *Int. J. Mol. Sci.* 20 (23). doi:10.3390/ijms20236093

Evans, T. D., Jeong, S. J., Zhang, X., Sergin, I., and Razani, B. (2018). TFEB and Trehalose Drive the Macrophage Autophagy-Lysosome System to Protect against Atherosclerosis. *Autophagy* 14 (4), 724–726. doi:10.1080/15548627.2018.1434373

Gao, S., Xue, X., Yin, J., Gao, L., Li, Z., Li, L., et al. (2020). Danlou Tablet Inhibits the Inflammatory Reaction of High-Fat Diet-Induced Atherosclerosis in ApoE Knockout Mice with Myocardial Ischemia via the NF-Kb Signaling Pathway. *J. Ethnopharmacol.* 263, 113158. doi:10.1016/j.jep.2020.113158

Han, X., and Boisvert, W. A. (2015). Interleukin-10 Protects against Atherosclerosis by Modulating Multiple Atherogenic Macrophage Function. *Thromb. Haemost.* 113 (3), 505–512. doi:10.1160/TH14-06-0509

Hao, D., Danbin, W., Maojuan, G., Chun, S., Bin, L., Lin, Y., et al. (2019). Ethanol Extracts of Danlou Tablet Attenuate Atherosclerosis via Inhibiting Inflammation and Promoting Lipid Effluent. *Pharmacol. Res.* 146, 104306. doi:10.1016/j.phrs.2019.104306

Horodinschi, R. N., Stanescu, A. M. A., Bratu, O. G., Pantea Stoian, A., Radavoi, D. G., and Diaconu, C. C. (2019). Treatment with Statins in Elderly Patients. *Medicina (Kaunas)* 55 (11), 1. doi:10.3390/medicina55110721

Lee, J., Ha, S. J., Park, J., Kim, Y. H., Lee, N. H., Kim, Y. E., et al. (2020). Arctium Lappa Root Extract Containing L-Arginine Prevents TNF-α-Induced Early Atherosclerosis *In Vitro* and *In Vivo*. *Nutr. Res.* 77, 85–96. doi:10.1016/j.nutres.2020.03.003

Li, W., Sultana, N., Siraj, N., Ward, L. J., Pawlik, M., Levy, E., et al. (2016a). Autophagy Dysfunction and Regulatory Cystatin C in Macrophage Death of Atherosclerosis. *J. Cell Mol. Med.* 20 (9), 1664–1672. doi:10.1111/jcmm.12859

Li, Y., Zhang, C. G., Wang, X. H., and Liu, D. H. (2016b). Progression of Atherosclerosis in ApoE-Knockout Mice Fed on a High-Fat Diet. *Eur. Rev. Med. Pharmacol. Sci.* 20 (18), 3863–3867. Available at: https://pubmed.ncbi.nlm.nih.gov/24791505/

Lin, P., Wang, Q., Liu, Y., Qin, Z., Gao, H., Ye, M., et al. (2020). Characterization of Chemical Profile and Quantification of Representative Components of DanLou Tablet, a Traditional Chinese Medicine Prescription, by UHPLC-Q/TOF-MS Combined with UHPLC-TQ-MS. *J. Pharm. Biomed. Anal.* 180, 113070. doi:10.1016/j.jpba.2019.113070

Liu, J. X., Lin, C. R., Ren, J. X., Li, L., Ren, J. G., Fu, J. H., et al. (2013). Experimental Study on Pathogenetic Evolvement Regularity of Phlegm, Toxin and Blood-Stasis Syndromes in Chinese Miniswine with Phlegm-Stasis Cementation Syndrome of Coronary Heart Disease. *Zhongguo Zhong Yao Za Zhi* 38 (23), 4138–4143. Available at: https://pubmed.ncbi.nlm.nih.gov/27735029/.

Liu, X., Tang, Y., Cui, Y., Zhang, H., and Zhang, D. (2016). Autophagy Is Associated with Cell Fate in the Process of Macrophage-Derived Foam Cells Formation and Progress. *J. Biomed. Sci.* 23 (1), 57. doi:10.1186/s12929-016-0274-z

Ma, Y. H., Leng, X. Y., Dong, Y., Xu, W., Cao, X. P., Ji, X., et al. (2019). Risk Factors for Intracranial Atherosclerosis: A Systematic Review and Meta-Analysis. *Atherosclerosis* 281, 71–77. doi:10.1016/j.atherosclerosis.2018.12.015

Maguire, E. M., Pearce, S. W. A., and Xiao, Q. (2019). Foam Cell Formation: A New Target for Fighting Atherosclerosis and Cardiovascular Disease. *Vascul Pharmacol.* 112, 54–71. doi:10.1016/j.vph.2018.08.002

Mao, S., Wang, L., Ouyang, W., Zhou, Y., Qi, J., Guo, L., et al. (2016). Traditional Chinese Medicine, Danlou Tablets Alleviate Adverse Left Ventricular Remodeling after Myocardial Infarction: Results of a Double-Blind, Randomized, Placebo-Controlled, Pilot Study. *BMC Complement. Altern. Med.* 16 (1), 447. doi:10.1186/s12906-016-1406-4

Martinet, W., and De Meyer, G. R. (2009). Autophagy in Atherosclerosis: a Cell Survival and Death Phenomenon with Therapeutic Potential. *Circ. Res.* 104 (3), 304–317. doi:10.1161/CIRCRESAHA.108.188318

Miao, J., Zang, X., Cui, X., and Zhang, J. (2020). Autophagy, Hyperlipidemia, and Atherosclerosis. *Adv. Exp. Med. Biol.* 1207, 237–264. doi:10.1007/978-981-15-4272-5_18

Nanchen, D., and Raggi, P. (2017). Is Atherosclerosis Imaging the Most Sensitive Way to Assess Patients' Risk and the Best Way to Conduct Future Drug Trials? A Pros-And-Cons Debate. *Atherosclerosis* 266, 229–233. doi:10.1016/j.atherosclerosis.2017.08.024

Orekhov, A. N., Nikiforov, N. G., Sukhorukov, V. N., Kubekina, M. V., Sobenin, I. A., Wu, W. K., et al. (2020). Role of Phagocytosis in the Pro-inflammatory Response in LDL-Induced Foam Cell Formation; a Transcriptome Analysis. *Int. J. Mol. Sci.* 21 (3). doi:10.3390/ijms21030817

Pober, J. S., and Sessa, W. C. (2007). Evolving Functions of Endothelial Cells in Inflammation. *Nat. Rev. Immunol.* 7 (10), 803–815. doi:10.1038/nri2171

Sergin, I., Evans, T. D., Zhang, X., Bhattacharya, S., Stokes, C. J., Song, E., et al. (2017). Exploiting Macrophage Autophagy-Lysosomal Biogenesis as a Therapy for Atherosclerosis. *Nat. Commun.* 8, 15750. doi:10.1038/ncomms15750

Singh, R., Kaushik, S., Wang, Y., Xiang, Y., Novak, I., Komatsu, M., et al. (2009). Autophagy Regulates Lipid Metabolism. *Nature* 458 (7242), 1131–1135. doi:10.1038/nature07976

Stary, H. C., Chandler, A. B., Dinsmore, R. E., Fuster, V., Glagov, S., Insull, W., Jr., et al. (1995). A Definition of Advanced Types of Atherosclerotic Lesions and a Histological Classification of Atherosclerosis. A Report from the Committee on Vascular Lesions of the Council on Arteriosclerosis, American Heart Association. *Arterioscler Thromb. Vasc. Biol.* 15 (5), 1512–1531. doi:10.1161/01.atv.15.9.1512

Sukhorukov, V. N., and Khotina, V. A. (2020). Lipid Metabolism in Macrophages: Focus on Atherosclerosis. *Biomedicines* 8 (8), 262. doi:10.3390/biomedicines8080262

Sun, R. Z., Fan, Y., Liang, X., Gong, T. T., Wang, Q., Liu, H., et al. (2018). Rapamycin and FTY720 Alleviate Atherosclerosis by Cross Talk of Macrophage Polarization and Autophagy. *Biomed. Res. Int.* 2018, 1010248. doi:10.1155/2018/1010248

Tang, J. J., Li, G. X., Liu, Z. G., Yi, R., Yu, D., Zhang, Y. B., et al. (2020). Danlou Tablet Improves Chronic Intermittent Hypoxia-induced Dyslipidemia and Arteriosclerosis by HIF-1 α-Angptl4 mRNA Signaling Pathwa. *Chin. J. Integr. Med.* doi:10.1007/s11655-020-3255-8

Wang, L., Zhao, X., Mao, S., Liu, S., Guo, X., Guo, L., et al. (2016). Efficacy of Danlou Tablet in Patients with Non-ST Elevation Acute Coronary Syndrome Undergoing Percutaneous Coronary Intervention: Results from a Multicentre, Placebo-Controlled, Randomized Trial. *Evid. Based Complement. Alternat Med.* 2016, 7960503. doi:10.1155/2016/7960503

Yu, X. H., Fu, Y. C., Zhang, D. W., Yin, K., and Tang, C. K. (2013). Foam Cells in Atherosclerosis. *Clin. Chim. Acta* 424, 245–252. doi:10.1016/j.cca.2013.06.006

Zahid, M. D. K., Rogowski, M., Ponce, C., Choudhury, M., Moustaid-Moussa, N., and Rahman, S. M. (2020). CCAAT/enhancer-binding Protein Beta (C/EBPβ) Knockdown Reduces Inflammation, ER Stress, and Apoptosis, and Promotes Autophagy in oxLDL-Treated RAW264.7 Macrophage Cells. *Mol. Cell Biochem.* 463 (1-2), 211–223. doi:10.1007/s11010-019-03642-4

Zhang, J., Alcaide, P., Liu, L., Sun, J., He, A., Luscinskas, F. W., et al. (2011). Regulation of Endothelial Cell Adhesion Molecule Expression by Mast Cells, Macrophages, and Neutrophils. *PLoS One* 6 (1), e14525. doi:10.1371/journal.pone.0014525

Zhou, M., Ren, P., Zhang, Y., Li, S., Li, M., Li, P., et al. (2019). Shen-Yuan-Dan Capsule Attenuates Atherosclerosis and Foam Cell Formation by Enhancing Autophagy and Inhibiting the PI3K/Akt/mTORC1 Signaling Pathway. *Front. Pharmacol.* 10, 603. doi:10.3389/fphar.2019.00603

Conflict of Interest: The authors declare that the research was conducted in the absence of any commercial or financial relationships that could be construed as a potential conflict of interest.

Publisher's Note: All claims expressed in this article are solely those of the authors and do not necessarily represent those of their affiliated organizations, or those of the publisher, the editors and the reviewers. Any product that may be evaluated in this article, or claim that may be made by its manufacturer, is not guaranteed or endorsed by the publisher.

frontiers in Pharmacology

REVIEW
published: 15 September 2021
doi: 10.3389/fphar.2021.725745

Protective Effects of *Caesalpinia sappan* Linn. and Its Bioactive Compounds on Cardiovascular Organs

Mas Rizky AA Syamsunarno[1], *Ratu Safitri*[2] *and Yusof Kamisah*[3]*

[1]Department of Biomedical Sciences, Faculty of Medicine, Universitas Padjadjaran, Jatinangor, Indonesia, [2]Faculty of Mathematics and Natural Sciences, Universitas Padjadjaran, Jatinangor, Indonesia, [3]Department of Pharmacology, Faculty of Medicine, Universiti Kebangsaan Malaysia, Kuala Lumpur, Malaysia

Cardiovascular diseases are the leading cause of death worldwide. The long-term aim of cardiovascular disease therapy is to reduce the mortality rate and decelerate the progression of cardiovascular organ damage. Current therapies focus on recovering heart function and reducing risk factors such as hyperglycemia and dyslipidemia. However, oxidative stress and inflammation are important causes of further damage to cardiovascular organs. *Caesalpinia sappan* Linn. (Fabaceae), a flowering tree native to tropical Asia, has antioxidant and anti-inflammatory properties. It is used as a natural dye to color food and beverages and as a traditional treatment for diarrhea, diabetes, and blood stasis. The phytochemical compounds in *C. sappan*, mainly the homoisoflavonoids brazilin, sappanone A, protosappanin, and hematoxylin, can potentially be used to protect cardiovascular organs. This review aims to provide updates on recent developments in research on *C. sappan* in relation to treatment of cardiovascular diseases. Many studies have reported protective effects of the plant's bioactive compounds that reduce cardiac damage and enhance vasorelaxation. For example, brazilin and sappanone A have an impact on molecular and cellular changes in cardiovascular disease pathogenesis, mainly by modulating oxidative, inflammatory, and apoptotic signaling pathways. Therefore, bioactive compounds of *C. sappan* have the potential to be developed as therapeutic agents to combat cardiovascular diseases like myocardial infarction and vascular disease. This review could help further the understanding of the possible modulatory role of the compounds in cardiovascular diseases, thereby facilitating future studies.

Keywords: *Caesalpinia sappan*, brazilin, sappanone A, brazilein, ischemia/reperfusion injury, vasorelaxation, heart, vascular

OPEN ACCESS

Edited by:
Andrés Navarrete, Universidad Nacional Autónoma de México, Mexico

Reviewed by:
Elizabeth Arlen Pineda Peña, National Autonomous University of Mexico, Mexico
Priyia Pusparajah, Monash University Malaysia, Malaysia

***Correspondence:**
Yusof Kamisah
kamisah_y@yahoo.com

Specialty section:
This article was submitted to Ethnopharmacology, a section of the journal Frontiers in Pharmacology

Received: *15 June 2021*
Accepted: *31 August 2021*
Published: *15 September 2021*

Citation:
Syamsunarno MRAA, Safitri R and Kamisah Y (2021) Protective Effects of Caesalpinia sappan *Linn. and Its Bioactive Compounds on Cardiovascular Organs. Front. Pharmacol. 12:725745. doi: 10.3389/fphar.2021.725745*

INTRODUCTION

Cardiovascular disease is a leading cause of morbidity and mortality globally, with heart attack and stroke accounting for about 85% of these deaths, the majority occurring in middle- and low-income countries (WHO, 2017). Cardiovascular disease includes disorders of the heart and blood vessels, such as ischemic heart attack or myocardial infarction, heart failure, hypertension, and cerebrovascular disease (Leong et al., 2017). The pathogenesis of these disorders involves oxidative stress and inflammation (Siti et al., 2015).

Therefore, intervention with medicinal plants possessing antioxidant and anti-inflammatory properties may alleviate the severity of the disease. Numerous studies have investigated medicinal plants for their potential pharmacological activities in cardiovascular organs, and many have shown promising effects. *Parkia speciosa* Hassk. alleviated cardiac damage in hypertensive rats (Kamisah et al., 2017), *Hibiscus sabdariffa* L. showed cardioprotective effects in myocardial infarction-induced rats (Si et al., 2019), and *Caesalpinia sappan* Linn. extract demonstrated a vasorelaxant effect on rat arteries (Sasaki et al., 2010).

Caesalpinia sappan is a medicinal plant that possesses antioxidant (Suwan et al., 2018) and anti-inflammatory (Tewtrakul et al., 2015) properties. It exerts protective effects on the cardiac (Nugraheni and Saputri, 2017) and vascular (Sasaki et al., 2010) systems. Investigations of this plant have progressed to isolation of the active metabolites, such as brazilin, sappanchalcone, and protosappanin D (Sasaki et al., 2010), that might be responsible for the protective effects, but these studies are still at the initial phase. Therefore, this review aims to gather information on recent updates to studies on *C. sappan* extract and the effects of its metabolites on cardiovascular organs. Our findings could accelerate future research on the plant and the development of its metabolites as alternatives to modern medicine.

CAESALPINIA SAPPAN AND ITS BIOACTIVE METABOLITES

Caesalpinia sappan Linn. (synonymous with *Biancaea sappan*), commonly known as sappanwood, grows abundantly in Southeast Asia, southern China (Li et al., 2020) and the Indian subcontinent, either in the wild or as a cultivated tree (Mariappan et al., 2014). It is known locally as secang or sekang in Indonesia, *pokok sepang* in Malaysia (Nugraheni and Saputri, 2017), and pattanga in India (Chellappan et al., 2017). The plant belongs to the family Fabaceae (subfamily Caesalpinioideae), and is a shrubby tree that grows to 10 m tall, with a ca. 14 cm diameter trunk and alternate bipinnate leaves (Mariappan et al., 2014). It bears clusters of flat, oblong pods that contain brown flattened and ellipsoid seeds (Warriers et al., 1993). Its wood is hard and orange red. Its heartwood has been traditionally used to treat bleeding gums, anemia, diabetes, cardiac problem and blood stasis and as a post-partum tonic to reduce uterine bleeding; it is also known for its antidiarrheal, sedative, and diuretic properties (Badami et al., 2004; Mekala and Radha, 2015; Li et al., 2020). In Vietnam, *C. sappan* is used to decrease the symptoms of rheumatism and inflammatory diseases (Do, 2001). It is also an ingredient in several Ayurvedic preparations (Mekala and Radha, 2015).

Many bioactive compounds have been isolated from *C. sappan*. Some of the most abundant phytochemicals present in the plant are homoisoflavonoids, of which brazilin—a natural red dye—is the major active compound (Settharaksa et al., 2019; Uddin et al., 2015), along with its oxidized form, brazilein (Dapson and Bain, 2015), in the heartwood. Other homoisoflavonoids present in the plant are sappanol, episappanol, protosappanin B and C (Mueller et al., 2016; Uddin et al., 2015), caesappin A and B (Wang et al., 2014), sappanone A (Zhao et al., 2020), sappanone B, (E)-3-(3,4-dihydroxybenzylidene)-7-hydroxychroman-4-one (He et al., 2009), deoxysappanone B (Zeng et al., 2015), neosappanone A, neoprotosappanin (Nguyen et al., 2005), and caesalpin P and J (Shimokawa et al., 1985) (**Table 1**). The chemical structures of the key metabolites in *C. sappan* are presented in **Figure 1**. These homoisoflavonoids have antioxidant (Uddin et al., 2015), antibacterial (Settharaksa et al., 2019), anti-inflammatory (Choo et al., 2017) and neuroprotective (Zeng et al., 2015) properties. The heartwood also contains the following phenols: caesalpiniaphenol A–H (Cuong et al., 2012; Min et al., 2012; Hung et al., 2013), epicaesalpin J, and 7,10,11-trihydroxydracaenone (Zhao et al., 2014). The latter two compounds do not show significant inhibitory activity against nitric oxide (Zhao et al., 2014), a vasodilator found in blood vessels. The seeds of *C. sappan* are rich in diterpenoids, including caesalsappanin A–N, R and S (Ma et al., 2015; Bao et al., 2016; Zhu et al., 2017; Wang et al., 2020); phanginin A–K and R–T (Yodsaoue et al., 2008; Bao et al., 2016); and ester glycosides, namely caesateroside A–C (Wang et al., 2020). Oleanolic acid, a triterpenoid, has also been isolated from the plant (Zheng et al., 2020). These diterpenoids exhibit antiplasmodial (Zhu et al., 2017) and antitumor (Bao et al., 2016; Wang et al., 2020) activity.

PHARMACOKINETICS AND TOXICITY OF *CAESALPINIA SAPPAN* AND ITS BIOACTIVE COMPOUNDS

Pharmacokinetics

Studies on the pharmacokinetic properties of the *C. sappan* metabolites are still lacking. Only brazilin has been studied extensively. Oral and intravenous administration of brazilin resulted in the incorporation of a similar amount of the phytochemical into the plasma (Jia et al., 2013), indicating its almost complete oral absorption. When brazilin was injected into the tail vein of rats at 50 mg/kg body weight, the plasma area under the curve (AUC) showed that it was absorbed at approximately 1,500 ng h/mL. It has a half-life ($t_{½}$) of 4.4 h, a peak plasma concentration (C_{max}) of approximately 1,600 ng/ml, and a time to reach maximum concentration (T_{max}) of approximately 2 min (Jia et al., 2013), which suggests a rapid absorption process. Brazilin also demonstrated linear pharmacokinetics in rats, according to the C_{max} and AUC values, which increased with increasing dosage (Yan-yan et al., 2014). On the other hand, when *C. sappan* extract that contained 52.25 mg/kg of brazilin was orally administered at 2.83 g/kg body weight, a similar AUC was observed, but the T_{max} was tenfold longer and the $t_{½}$ was shorter (2.21 h) (Tong et al., 2013) than that of brazilin in a previous study (Jia et al., 2013). This may have been due to other bioactive compounds present in the extract affecting the absorption and/or elimination of brazilin. The compound was dispersed into almost all organs, with the highest concentrations found in the kidneys, followed by the liver and lungs (Jia et al., 2013).

TABLE 1 | Phytochemicals isolated from *Caesalpinia sappan*.

Parts of plant	Type	Compound	References
Heartwood	Homoisoflavonoids	Brazilin	Settharaksa et al. (2019)
		Brazilein	Dapson and Bain, (2015)
		Sappanol	Uddin et al. (2015)
		Episappanol	Mueller et al. (2016)
		Protosappanin B–C	Mueller et al. (2016)
		Caesappin A–B	Wang et al. (2014)
		Sappanone A	Zhao et al. (2020)
		Deoxysappanone B	Zeng et al. (2015)
		Neosappanone A	Nguyen et al. (2005)
		Neoprotosappanin	Nguyen et al. (2005)
		Sappanone B	He et al. (2009)
		(E)-3-(3,4-dihydroxybenzylidene)-7-hydroxychroman-4-one	He et al. (2009)
		3′-Deoxy-4-O-methylepisappanol	Fu et al. (2008)
		Caesalpin J and P	Shimokawa et al. (1985)
		Hematoxylin	Xie et al. (2000)
	Phenols	Caesalpiniaphenol A–F	Cuong et al. (2012)
		Caesalpiniaphenol G–H	Hung et al. (2013)
		Epicaesalpin J	Zhao et al. (2014)
		7,10,11-Trihydroxydraca-enone	Zhao et al. (2014)
Seeds	Diterpenoids	Caesalsappanin A–L	Ma et al. (2015)
		Caesalsappanin M–N	Bao et al. (2016)
		Caesalsappanin R and S	Zhu et al. (2017)
		Phanginins A–K	Yodsaoue et al. (2008)
		Phanginins R–T	Bao et al. (2016)
	Triterpenoid	Oleanolic acid	Zheng et al. (2020)
	Ester glycosides	Caesateroside A–C	Wang et al. (2020b)

Oral administration of *C. sappan* extract (at 2.83 g/kg body weight) that contained 35.56 mg/kg protosappanin B resulted in a $t_{½}$ and a T_{max} similar to those of brazilin (Tong et al., 2013). Diabetes affected the pharmacokinetics of protosappanin B and brazilin similarly, observed as augmentation of C_{max}, AUC, and $t_{½}$. However, diabetes reduced the T_{max} of protosappanin B, but did not affect of that of brazilin (Tong et al., 2013). Taken together, these results suggest that brazilin has an almost complete and fast oral absorption as well as distribution. This property makes the compound a promising candidate for further study.

Toxicity

A single oral dose of *C. sappan* at 5,000 mg/kg body weight, and repeated at doses of 250, 500 and 1,000 mg/kg for 30 days yielded no toxic effects in male and female Wistar rats. No apparent changes in body weight, the gross appearance of internal organs—the heart, liver, brain, lungs, pancreas, spleen, adrenal glands, kidneys, and sex organs—or general behavior were noted compared to control (Sireeratawong et al., 2010). An aqueous extract of natural dye from *C. sappan* (100–2000 mg/kg) was demonstrated to be safe and did not cause any abnormalities or mortality during 14 days of observation. Similarly, the dye did not have significant subacute toxicity up to 5,000 mg/kg body weight (Athinarayanana et al., 2017). In an *in vitro* study, a *C. sappan* ethanol extract at 10 μg/ml did not significantly reduce the percentage of viable cells with intact morphology in H9c2 cardiomyocytes, but this percentage decreased after the cells were exposed to the extract at 50 μg/ml (Sulistiyorini et al., 2020). These results indicate that the acute administration of *C. sappan* extract in rats is likely safe. However, other toxicity studies, such as chronic and carcinogenic toxicity studies, should be performed to ascertain safety for long-term use. Nevertheless, in the study (Sulistiyorini et al., 2020), the plant was not authentically validated by a botanist, therefore the reproducibility of the findings could not be ascertained.

Previous toxicity studies on the bioactive compounds of *C. sappan* heartwood have only addressed brazilein (Yuan et al., 2016). In a study with ICR mice, brazilein was administered intravenously (at 5, 10, and 20 mg/kg) to non-pregnant females for 14 days and to males for 30 days before mating, and brazilein administration was continued in females after successful mating until 13 days of gestation. This resulted in an increased ratio of resorbed fetuses compared to control, although no deformed fetuses were observed. In addition, the live fetus ratio decreased, and the dead fetus ratio increased after brazilein treatment. No other gravid parameters were affected, and the mating process of the mice was not influenced. At all doses tested, brazilein did not have toxic effects on males, as demonstrated by the weight of the reproductive organs, vitality, and abnormal sperm levels (Yuan et al., 2016). These findings suggest that brazilein should be taken with caution by pregnant women, as it may have a significant impact on embryo development and growth after implantation.

EFFECTS ON MYOCARDIAL INJURY

Caesalpinia sappan Extract

Only one study to date (Nugraheni and Saputri, 2017) investigated the effects of *C. sappan* crude extract using a

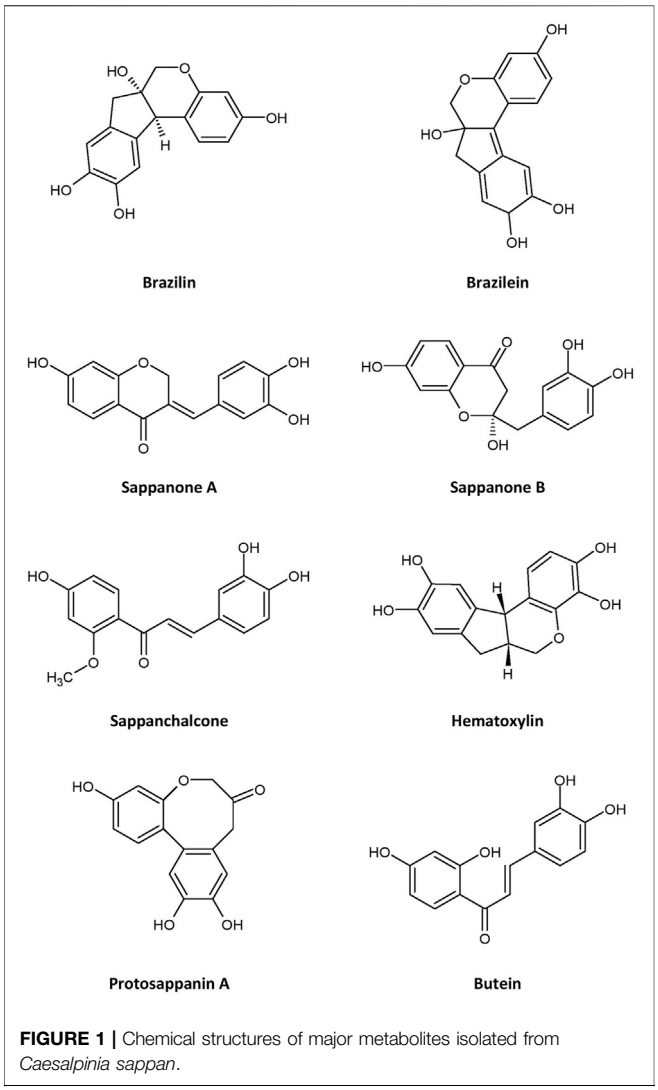

FIGURE 1 | Chemical structures of major metabolites isolated from *Caesalpinia sappan*.

myocardial injury model. However, the plant taxonomy could not be confirmed as it was not validated by a botanist. The study investigated the preventive effect of oral *C. sappan* extract as claimed, at doses of 50, 100, and 200 mg/kg for 30 days on isoproterenol-induced myocardial infarction in rats (**Table 2**). The extract did not reverse the increase in heart weight induced by isoproterenol. However, qualitative observations of the heart infarct area suggested that the extract reduced size or the area with increasing doses. Histologically, the extract significantly reduced myocardial interstitial edema at all experimental doses, and the severity of myocardial necrosis and inflammatory cell infiltration was significantly alleviated at 100 and 200 mg/kg doses of the extract (Nugraheni and Saputri, 2017). These findings demonstrate potential positive effects of *C. sappan* extract that protect against myocardial injury, likely afforded by the presence of bioactive compounds in the extract that was unfortunately not determined in the study. However, in terms of experimental design, the study was not properly outlined with a positive control, which could determine any experimental flaw. It also did not indicate the type of the extract used. An elevation in oxidative stress and inflammation has been reported in isoproterenol-induced myocardial injury (Kumari et al., 2020; Younis et al., 2020). Therefore, the extract most likely elicits protective effects through its antioxidant and anti-inflammatory properties, as previously reported (Tewtrakul et al., 2015; Suwan et al., 2018). The property of the plant extract may support its traditional use in reducing heart problems (Mekala and Radha, 2015). Further *in vivo* studies are necessary to obtain more conclusive evidence of the protective effects of the extract. Heart function should be examined to measure the extent of improvement due to the extract. Other aspects that can be studied are pathways related to myocardial fibrosis, such as the transforming growth factor-β/Smads (TGF-β/Smads) pathway and other pathways linked to oxidative stress, inflammation, apoptosis, and mitogen-activated protein kinase (MAPK) activation.

Stem extract of *C. sappan* (100 μg/ml) has been found to inhibit phosphodiesterase (PDE) activity in *in vitro*, with ethanol extracts demonstrating greater activity against PDE-1 than hexane and chloroform extracts (Helmi et al., 2020). Although the expression of this enzyme was reported to be elevated in heart failure (Chen et al., 2020), the potential effects of *C. sappan* extract on heart failure have not been studied. Recent evidence suggests that PDE5 and PDE10A inhibition is cardioprotective in patients with systolic heart failure and left ventricular hypertrophy (Lawless et al., 2019; Chen et al., 2020). Inhibition of the enzyme increases the intracellular level of cyclic adenosine monophosphate (cAMP) (Chen et al., 2020), which then boosts Ca^{2+} influx leading to increased myocardial contractility (Irie et al., 2009). Therefore, the extract should be further studied to explore its potential inhibitory regulation of isoenzymes, which could have beneficial effects by improving heart function. The effects of the extract on myocardial contractile function, intracellular calcium concentration, and cAMP should also be explored.

Brazilin

The effects of brazilin on myocardial ischemia/reperfusion (I/R) injury have been investigated through *in vitro* and *ex vivo* models for acute myocardial infarction in humans. In rat cardiomyocytes exposed to hypoxia/reoxygenation (H/R), brazilin (5–50 μM) reduced the release of creatine kinase MB (CK-MB) and lactate dehydrogenase (LDH) in a dose-dependent manner (**Table 2**). It also decreased H/R-induced apoptosis, observed as a reduction in cleaved caspase 3 (Qi et al., 2021). In the *ex vivo* study, brazilin pretreatment (at 12.5–50 mg/kg intraperitoneally) reduced myocardial infarct size, CK-MB and LDH release, and myocardial apoptosis (at 25 mg/kg) in isolated hearts subjected to I/R injury. It preserved myocardial function by reversing the detrimental effects of I/R on left ventricular (LV) developed pressure (LVDP), the rate of LV pressure increase (+dp/dt), and the rate of LV pressure reduction (−dp/dt) (Qi et al., 2021). No positive control was adopted in both models. Therefore, comparative protective effects with the brazilin-treated group could not be appreciated. The protective effects of brazilin are believed to be mediated by nuclear factor erythroid 2-related factor 2 (Nrf2), a gene involved in the modulation of

TABLE 2 | Effects of *C. sappan* crude extract and its bioactive compounds on myocardial parameters.

	Model	Dose and duration of bioactive compounds	Effects on cardiac parameters			
			Function	Structure	Injury index	Infarct size
Nugraheni and Saputri, (2017)	I/R (*in vivo*)	Crude extract (50, 100 and 200 mg/kg) pretreatment for 30 days	-	↔ HW/BW All doses ↓ interstitial edema 100 and 200 mg/kg ↓ necrosis ↓ inflammatory cell infiltration	-	↓ Infarct size
Qi et al. (2021)	I/R (*ex vivo*)	Brazilin (12.5–50 mg/kg, ip) pretreatment for 1 h	↑ LVDP, +dp/dt, –dp/dt ↔ HR	-	↓ CK-MB ↓ LDH	↓ Infarct size
Zhao et al. (2006)	*Ex vivo*	Brazilein (0.4–10 mM) concurrently for 2 h	↑ contractility, ↔ HR ↔ coronary perfusion rate	-	-	-
Shi et al. (2020b)	I/R (*ex vivo*)	Sappanone A (20 mg/kg, ip) pretreatment for 1 h	↔ HR ↓ +dp/dt, –dp/dt, LVDP	-	↓ CK-MB ↓ LDH	↓ Infarct size
Jo et al. (2020)	LAD-induced I/R (*in vivo*)	Sappanone A (50 mg/kg, po) for 5 days (day 0 to day 4 post-I/R)	Day 1 ↔ EF, FS, E/A, SV, CO, HR, ↑ E′, ↓ E/E′ ↔ Day 4: ↔ EF, FS, E/A, SV, E′, CO, HR ↓ E/E′	↔ Cardiac structure ↓ Fibrosis in PM ↓ Inflammatory cells in PM and apex	↔ CK-MB ↓ LDH ↓ AST	↓ Infarct size in distal medial, apex and total region
Qi et al. (2021)	H/R in cardio-myocytes	Brazilin (5–50 μM) pretreatment for 1 h	-	-	↓ CK-MB ↓ LDH ↑ cell viability ↓ apoptosis	-
Shi et al. (2020a)	H/R in cardio-myocytes	Sappanone A (5–50 μM) pretreatment for 1 h	-		↓ CK-MB ↓ LDH ↑ cell viability ↓ apoptosis ↓ cTn1	

Abbreviations: AST, Aspartate transaminase; CO, cardiac output; CK-MB, creatine kinase MB; cTn1, cardiac troponin 1; +dp/dt, rate of the rise in left ventricular pressure; –dp/dt; rate of the fall of left ventricular pressure; E′, early relaxation velocity on tissue Doppler; E/A, the ratio of the early (E) to late (A) ventricular filling velocities; E/E′; ratio of transmitral Doppler early filling velocity to tissue Doppler early diastolic mitral annular velocity; FS, fractional shortening; HR, heart rate; ip, intraperitoneum; H/R, hypoxia/reoxygenation; HW/BW, heart weight to body weight ratio; I/R, ischemia/reperfusion; LAD, ligation of the left anterior descending coronary artery; LDH, lactate dehydrogenase; LVDP, Left ventricular developed pressure; po, per oral; PM, papillary muscle; SV, stroke volume; ↔, no change; ↑, increased; ↓, reduced.

oxidative stress (**Figure 2**). Kelch-like ECH-associated protein 1 (Keap1), a substrate adaptor, suppresses Nrf2 transcriptional activity through the formation of a complex between the domains of Nrf2 and Keap1. Upon stimulation of oxidative stress, Nrf2 is dissociated from Keap1 and translocated into the nucleus (Ahmed et al., 2017). Brazilin enhances the nuclear translocation of Nrf2 via the protein kinase C pathway, thus promoting the expression of its target proteins—heme oxygenase-1 (HO-1) and NAD(P)H:quinone oxidoreductase 1(NQO1), which have inhibitory effects on proinflammatory genes (Qi et al., 2021). These findings suggest that brazilin is a promising candidate for protecting against myocardial injury. Additionally, brazilin may confer protection through other mechanisms; for example, it may inhibit the expression of nuclear factor-κB (NF-κB) and its inflammatory signaling pathway. Blockade of NF-κB improved cardiac function and attenuated cardiac remodeling in a myocardial infarct mouse model (Kawano et al., 2006). Brazilin has also been demonstrated to possess PDE-1 inhibitory activity *in vitro* (Helmi et al., 2020), leading to an augmented level of cAMP, which also functions as a fibrotic response modulator (Delaunay et al., 2019). The inhibition of this enzyme led to a decreased fibrotic response in cardiomyocytes (Chen et al., 2020), which may be useful for the therapeutic management of heart failure. However, further studies are needed to confirm this activity *in vivo* and to explore other potentially related mechanisms of brazilin, such as myocardial protein synthesis, fibrosis, autophagy, and hypertrophic signaling.

Sappanone A

Two studies have investigated the effects of sappanone A on myocardial I/R injury (Shi et al., 2020b; Jo et al., 2020). In rats with ligated left anterior descending coronary artery, oral administration of sappanone A at 50 mg/kg for 5 days starting on the day of ischemia induction, significantly reduced the infarct size, particularly in the distal medial and apical myocardial areas, better than that of curcumin, a positive control (Jo et al., 2020). However, the use of curcumin as the positive control was less

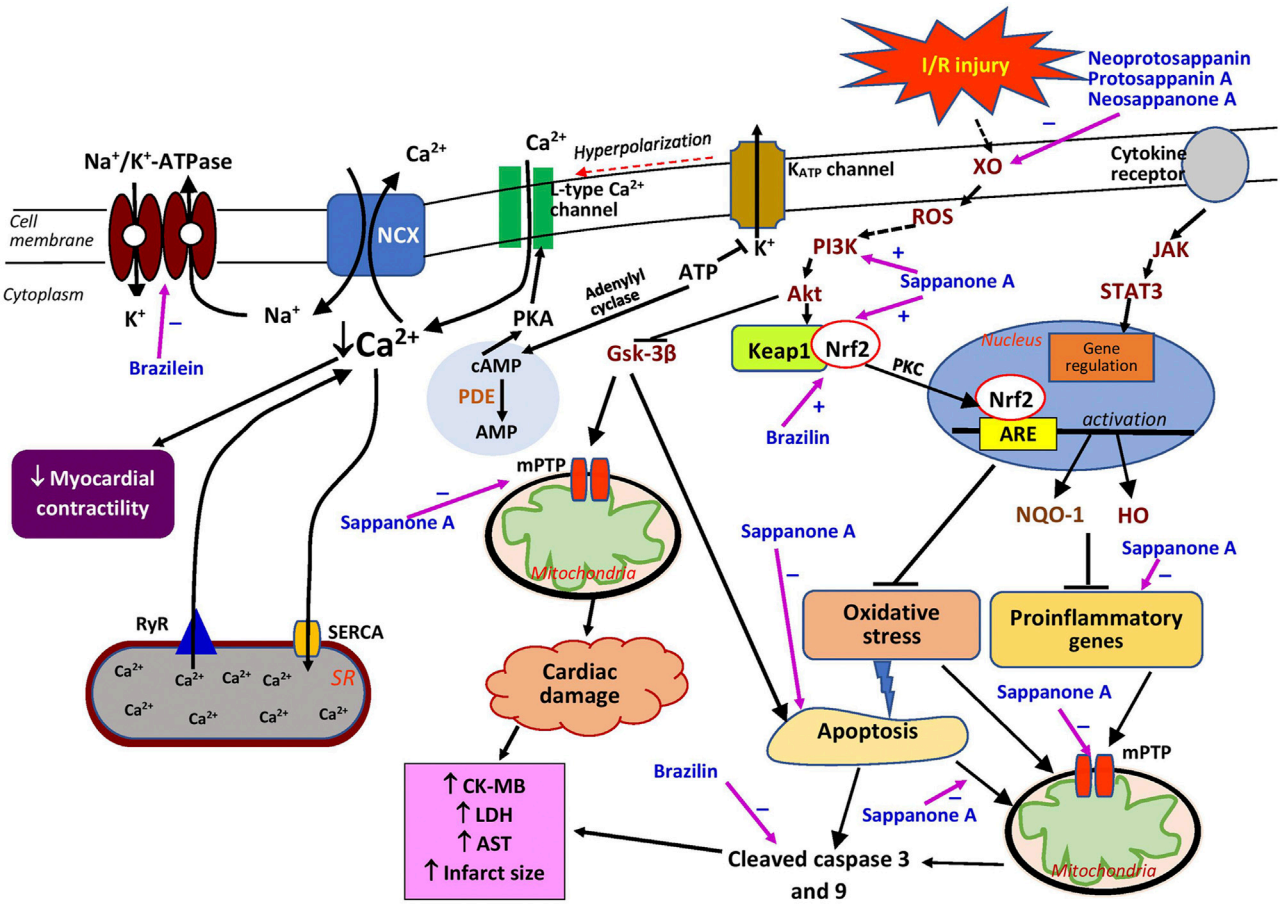

FIGURE 2 | Possible sites of action of *Caesalpinia sappan* bioactive compounds in myocardial injury. Akt, protein kinase B; AMP, adenosine monophosphate; ARE, antioxidant responsive element; AST, aspartate transaminase; ATP, adenosine triphosphate; cAMP, cyclic adenosine monophosphate; CK-MB, creatin kinase MB; GSK-3β, glycogen synthase kinase-3β; HO, heme oxygenase; JAK, Janus kinase; Keap1, Kelch-like ECH-associated protein 1; LDH, lactate dehydrogenase; mPTP, mitochondrial permeability transition pore; Na^+/K^+-ATPase, sodium potassium ATPase; NCX, sodium-calcium exchanger; Nrf2, nuclear factor erythroid 2-related factor 2; NQO1, NAD(P)H quinone oxidoreductase 1; PDE, phosphodiesterase; PI3K, phosphatidylinositol 3-kinase; PKA, protein kinase A; PKC, protein kinase C; ROS, reactive oxygen species; RyR, ryanodine receptor; SERCA, sarcoplasmic/endoplasmic reticulum Ca^{2+} ATPase; STAT3, signal transducer and activator of transcription 3; XO, xanthine oxidase; ⊥, suppression; +, stimulates; –, inhibits.

appropriate since it is not used clinically for heart diseases. In addition, histological analysis revealed that the homoisoflavonoid treatment diminished inflammatory cell infiltration, with larger effects on lymphocytes in all medial myocardial and epicardial regions. It also reduced fibrosis in papillary muscle, comparable to curcumin (Jo et al., 2020). Furthermore, the results indicated that sappanone A reduced fibrosis in the papillary muscle. The positive effects of the compound were supported by decreases in serum CK-MB, LDH, and aspartate transaminase (Jo et al., 2020), indicators of myocardial injury. Shi et al. (2020b) demonstrated that intraperitoneal administration of sappanone A at 20 mg/kg per hour prior to I/R injury induction exerted protective effects in isolated Langendorff hearts, as indicated by a reduction in the myocardial infarct size and a release of myocardial enzymes (CK-MB and LDH). The cardioprotective effects of the compound could also be attributable to its anti-inflammatory properties (Wang et al., 2021).

Both the above studies demonstrated that sappanone A improved cardiac function after I/R (Jo et al., 2020; Shi et al., 2020b) (**Table 2**). LVDP, +dp/dt, and −dp/dt increased in the sappanone A-treated group, as measured in isolated hearts (Shi et al., 2020b), suggesting improvement in LV function. In the *in vivo* study (Jo et al., 2020), sappanone A did not significantly affect LV fractional shortening (FS) or the ejection fraction (EF), two indicators of LV systolic function, although a tendency for a reversal effect was observed. Tissue Doppler imaging revealed that the treatment improved the early relaxation velocity (E′), an indicator of LV diastolic function, on day 1 post-I/R induction but not on day 4. Moreover, positive effects of the compound on the ratio of transmitral Doppler early filling velocity to tissue Doppler early diastolic mitral annular velocity (E/E′), another indicator of LV diastolic function, were noted on both day 1 and day 4 (Jo et al., 2020). The findings of these studies strongly suggest that sappanone A from *C. sappan* affords better

cardioprotection in the early stage of myocardial infarction, resulting in the mitigation of LV dysfunction. It is possible that the preservation of the cardiac function by sappanone A due to its inhibitory effect on fibrosis in the heart (Jo et al., 2020). However, the detailed mechanisms of the antifibrotic property of the compound have yet to be studied.

Treatment with sappanone A resulted in the alteration of the mRNA expression of 2020 genes, including 66 proinflammatory-related genes believed to be involved in myocardial infarction. Sappanone A may exert positive effects by restoring the genes involved in inflammatory responses. It downregulates the expression of the proinflammatory genes Tgfb1, Tgfb2, Tnfrsf1a, Il18, Pik3cd, Cd4, and Cd8a, as well as the apoptotic gene Casp3, which are activated by myocardial infarction (Jo et al., 2020). In cardiomyocytes, sappanone A alleviated H/R-induced injury by inhibiting mitochondrial apoptosis, observed as repressed caspase-3 and caspase-9 cleavage, leading to increased cell viability. The compound also mitigated mitochondrial permeability transition pore (mPTP) opening and transmembrane potential ($\Delta\psi m$) release (Shi et al., 2020a), possibly because of its antioxidant and anti-inflammatory activities (**Figure 2**) that reduce reactive oxygen species (ROS), which stimulate the opening of mPTPs, increase the permeability of mitochondria, and subsequently rupture the organelles (Zhang et al., 2016). Sappanone A is reported to provide cardioprotection against I/R-induced injury by activating the phosphatidylinositol 3-kinase/protein kinase B/glycogen synthase kinase-3β (PI3K/Akt/GSK-3β) signaling pathway without affecting the survivor activating factor enhancement (SAFE) pathway, which can be explained by its lack of effect on signal transducer and activator of transcription 3 (STAT3) phosphorylation in cardiomyocytes (Shi et al., 2020a). As a substitute pathway for cardioprotection against I/R injury, the latter pathway is involved in promoting cardiomyocyte survival (Hadebe et al., 2018). The effects of sappanone A on the activation of Akt and Gsk-3β have also been reported in PC-12 cells obtained from pheochromocytomas of the adrenal glands (Kang et al., 2019). The PI3K/Akt/GSK-3β signaling pathway is activated by an increased ROS level which is partly due to the increased activity of xanthine oxidase (**Figure 2**). The activation of the pathway leads to inhibition of mitochondrial apoptosis and mPTP opening, resulting in decreased cardiac damage. Sappanone A also activates the Keap1/Nrf2 signaling pathway (Shi et al., 2020b), which is one of the crucial signaling pathways controlling the activity of Nrf2, a protein that regulates antioxidant proteins (Tu et al., 2019). Together, these effects suggest that sappanone A could be a potential therapeutic agent for alleviating myocardial I/R injury by targeting mitochondria through the mitigation of the inflammatory, oxidative stress, and apoptosis signaling pathways.

Brazilein

At 0.4–10 mM concentrations, brazilein had a concentration-dependent cardiotonic effect with negligible impacts on coronary perfusion and heart rate in normal isolated guinea pig hearts, better than its positive control, noradrenaline (30 μM); this effect may not involve the stimulation of the β-adrenoceptor because the addition of propranolol, a β-adrenoceptor blocker, had no effect (Zhao et al., 2006). However, the concentrations used were larger than the ones proposed (30–50 μM) for *in vitro* studies (Heinrich et al., 2020). It is quite difficult to translate high concentrations of pure compounds employed *in vitro* for a therapeutic use in humans, as it may pose toxicity.

Brazilein inhibited Na^+/K^+-ATPase (the sodium–potassium pump) (**Figure 2**) but this effect was not modified by increasing concentrations of potassium (Zhao et al., 2006). This finding suggests that the inhibitory effect of brazilein may not be associated with its binding to E2P (Zhao et al., 2006), which in turn prevents E2P from binding to potassium resulting in the inhibition of the sodium–potassium pump. High concentrations of potassium can reverse the inhibitory effects of cardiac glycosides on the sodium–potassium pump and promote the dissociation of E2P and inhibitors (Kanai et al., 2020), suggesting that brazilein has a different mechanism from that of cardiac glycosides. The sodium–potassium pump indirectly regulates the intracellular calcium level in the heart. Its inhibition elevates the myocardial intracellular calcium level by decreasing the calcium efflux through the Na^+/Ca^{2+} exchanger, which then increases myocardial contractility (Salim et al., 2020). Brazilein may modulate other calcium regulators, such as ryanodine receptor 2 (RyR2), L-type calcium channel, and sarcoplasmic/endoplasmic reticulum calcium ATPase (SERCA). It was reported that the vasocontraction effects of brazilein depend on the extracellular calcium level (Shen et al., 2008). In terms of its toxicity, brazilein (at 4–48 mg/kg) is less likely to cause cardiac arrythmias than deslanoside (at 400–560 μg/kg), a sodium–potassium pump inhibitor (Zhao et al., 2006), implying a higher therapeutic index for the former. Therefore, brazilein has the potential to be developed as an inotropic drug with Na^+/K^+-ATPase inhibition as the therapeutic target. Its effects on other calcium regulatory proteins—Na^+/Ca^{2+} exchanger, RyR2, and SERCA—should also be studied.

Other Compounds

The bioactive compounds, neoprotosappanin, protosappanin A, protosappanin A dimethyl acetal, protosappanin E-2, neosappanone A, sappanol, deoxysappanone B, sappanone B, and sappanchalcone isolated from *C. sappan* extract and its methanol ethyl acetate fraction have been reported to possess xanthine oxidase-inhibiting activity (Nguyen et al., 2004, 2005), which could be beneficial in alleviating myocardial injury. Among these compounds, sappanchalcone demonstrated the most potent activity, comparable to allopurinol (Nguyen et al., 2004, 2005). The protective effect is most likely due to these compounds' antioxidant properties. Previous research indicated that some of these compounds possess antioxidant properties (Sasaki et al., 2007). However, no studies investigating these compounds have considered their effects on the heart. The serum xanthine oxidase level is reported to be elevated in patients with myocardial infarction (Ali et al., 2014). This enzyme produces abundant ROS during cardiac ischemia (**Figure 2**), which causes further damage to the heart (Bagheri et al., 2016). A meta-analysis of randomized clinical trials reported that purine-like xanthine oxidase inhibitors, such as allopurinol, reduced in the incidence of adverse cardiovascular outcomes (Bredemeier

et al., 2018). Further investigations of *C. sappan* phytochemicals should be undertaken to explore their potential cardioprotective effects that could be attributed to xanthine oxidase inhibition, such as the expression of extracellular matrix proteins (collagen and fibronectin), growth factors, and inflammatory and oxidative stress biomarkers.

Numerous studies have demonstrated that *C. sappan* extract and its bioactive compounds can reduce heart transplant and allograft rejection. The extract itself was reported to reduce cell ultrastructural damage and pathological morphology in transplanted hearts by reducing perforin mRNA expression (Zhou et al., 2003), whereas the ethyl acetate extract decreased granzyme B (GrB) mRNA expression, comparable to its positive control, cyclosporine A (Zheng et al., 2008). However, both studies lacked a negative control, a group without any treatment for a comparison. Both perforin and GrB are involved in target cell apoptosis (Voskoboinik et al., 2015), indicating that the compounds exert their beneficial effects by diminishing cell apoptosis. The aqueous extract also suppresses T-lymphocyte activation and increases $CD4^+$ $CD25^+$ T cells (Yu et al., 2004; Li et al., 2015), contributing to its immunosuppressive effect, hence reducing the rejection rate. The cardioprotective effects could also be attributed to the presence of protosappanin A. At a dose of 25 mg/kg, the compound prolonged heart allograft survival and decreased pathological damage, leading to reduced graft rejection, comparable to cyclosporine A (Wu et al., 2008). The antirejection property of the compound may be due to the diminished inflammation, observed as reduced mRNA expression of NF-κB; suppressed immune response, indicated by decreased interferon-gamma (IFN-γ), interferon-gamma-inducible protein 10 (IP10), and the $CD4^+/CD8^+$ ratio; and lower levels of apoptosis, demonstrated by downregulated GrB and perforin mRNA expression (Wu et al., 2008; Wu et al., 2010). In conclusion, protosappanin A may promote immunosuppression in recipients by targeting the graft's T cells through inhibition of the NF-κB pathway activation and apoptosis. Further studies should be undertaken to extensively investigate the antirejection effects of protosappanin A, which has the potential to be employed clinically.

EFFECTS ON VASCULAR FUNCTION AND INJURY

Caesalpinia sappan Extract

Endothelial dysfunction promotes vascular injury by disrupting vascular tone and redox balance, and activating inflammatory responses (Sun et al., 2020). Studies investigating the effects of *C. sappan* extract on vascular function and injury are still lacking, although the extract was demonstrated to protect against brain I/R injury (Wan et al., 2019).

Caesalpinia sappan crude extract (10 and 30 μg/ml) had a vasorelaxant effect on precontracted intact rat aortic rings but not denuded rings (Hu et al., 2003). The effects were reduced by N(G)-nitro-L-arginine methyl ester (L-NAME), a nitric oxide synthase (NOS) inhibitor. However, at higher concentrations of the extract (100 μg/ml), the vasorelaxant effect was not affected by denudation or L-NAME treatment (Xie et al., 2000), implying that the effects are both dependent on and independent of the functional endothelium. It is possible that at higher concentrations, the extract may exert its effects by directly stimulating smooth muscle cells rather than by activating the release of nitric oxide, which is primarily synthesized in the endothelium (Cyr et al., 2020). A drawback of the studies (Xie et al., 2000; Hu et al., 2003) was no validated identification of the dried heartwood sappanwood which was obtained from a local store. Therefore, reproducibility of the findings could be questioned.

Brazilin

Similar to the crude extract, brazilin exhibited vasorelaxant properties that were dependent on the endothelium at lower concentrations (30 μM) (Hu et al., 2003) but independent of the endothelium at higher concentrations (100 μM) in precontracted intact rat aortic rings (Xie et al., 2000; Yan et al., 2015). However, Hu et al. (2003) demonstrated that the effect of brazilin was only endothelium-dependent and suggested that the relaxing property of the extract at higher concentrations was possibly attributable to the presence of brazilin, which was similar to histamine (50 μM). In the endothelium-dependent vasorelaxation mechanism, brazilin may induce relaxation by decreasing the influx of Ca^{2+} through L-type calcium channels and its release from the sarcoplasmic reticulum via the compound's effects on RyR2 and inositol trisphosphate (IP_3) receptors, thus enhancing SERCA activity (Yan et al., 2015), but unfortunately these effects could not be compared with a positive control which was not included in the study (**Figure 3**). The vasodilating effect of the compound is notably deterred by L-NAME and hemoglobin (a nitric oxide scavenger), indicating that its effect involves the presence of nitric oxide (Hu et al., 2003; Yan et al., 2015). This is further confirmed by its positive effects on nitric oxide synthesis via activation of endothelial NOS (eNOS) (Hu et al., 2003). Following this activation, cyclic guanosine monophosphate (cGMP) is generated from guanosine-5′-triphosphate (GTP) by the action of soluble guanylate cyclase (sGC) in vascular smooth muscle. Brazilin is reported to augment the accumulation of sGC in the rat aorta, and pretreatment with methylene blue, an sGC inhibitor, markedly diminishes the vasodilating effect of brazilin, suggesting a crucial role of sGC in brazilin's mechanisms of action (Hu et al., 2003; Yan et al., 2015). The increase in cGMP level would enhance the level of cAMP, causing a decline in Ca^{2+} level and finally subsiding the constraction of the blood vessels.

The vasorelaxant effect of brazilin may also involve prostaglandin synthesis, as suggested by its reduced effect with indomethacin, a cyclooxygenase inhibitor, as well as its inhibition of extracellular signal-regulated kinase (ERK) and myosin light chain (MLC) activation (Yan et al., 2015). Cyclooxygenase is an enzyme that synthesizes prostaglandin from arachidonic acid. Prostaglandin itself is a strong vasodilator, which is also converted into products such as thromboxane, a vasoconstrictor, and prostacyclin, a vasodilator (Rouzer and Marnett, 2020). Therefore, brazilin may augment the

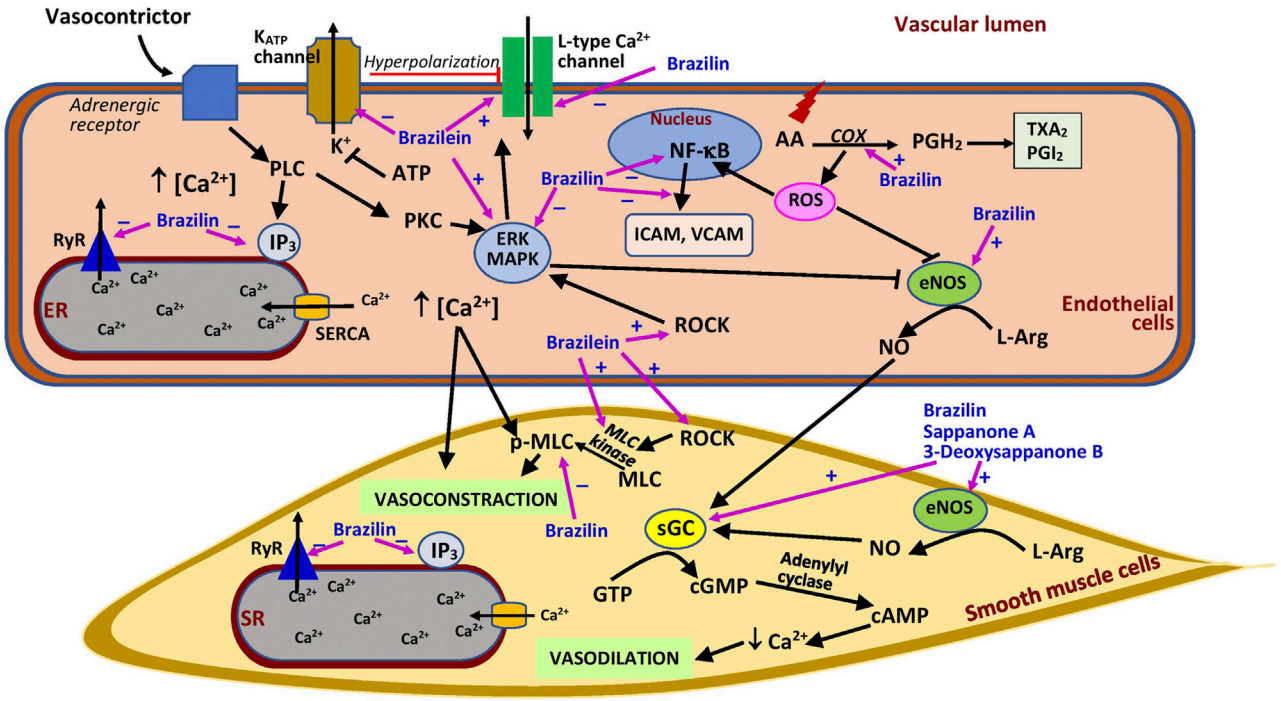

FIGURE 3 | Possible sites of action of *Caesalpinia sappan* bioactive compounds in vascular.AA, arachidonic acid; ATP, adenosine triphosphate; cAMP, cyclic adenosine monophosphate; COX, cyclooxygenase; eNOS, endothelial nitric oxide synthase; ER, endoplasmic reticulum; ERK, extracellular signal-regulated kinase; GTP, guanosine-5′-triphosphate; ICAM, intercellular adhesion molecule; IP3, inositol trisphosphate; K_{ATP} channel, ATP-sensitive potassium channel; L-Arg, L-arginine; MAPK, mitogen activated protein kinase; MLC, myosin light chain kinase; pMLC, phosphorylated myosin light chain; NF-κB, nuclear factor-κB; NO, nitric oxide; PGH_2, prostaglandin H_2; PGI_2, prostacyclin; PKC, protein kinase C; PLC, phospholipase C; ROCK, Rho kinase; ROS, reactive oxygen species; RyR, ryanodine receptor; SERCA, sarcoplasmic/endoplasmic reticulum Ca^{2+} ATPase; sGC, soluble guanylate cyclase; SR, sarcoplasmic reticulum; TXA_2, thromboxane A_2; VCAM, vascular cell adhesion molecule; ⊥, suppression; +, stimulates; –, inhibits.

production of prostaglandin which then promotes vasodilation. By contrast, ERK has an inhibitory effect on eNOS, impairing vasodilation, and MLC causes vasocontraction (**Figure 3**). Thus, the activation of ERK and MLC plays a crucial role in vascular smooth muscle cell contractile function (Roberts, 2012; Liu and Khalil, 2018). However, it was postulated that the brazilin vasodilatory effect is not mediated by Ca^{2+}-dependent K^+ channel activation (Yan et al., 2015), which is responsible for blood vessel dilation (Hasan and Jaggar, 2018). All these results suggest that brazilin has the potential to act as an agent that promotes vasorelaxation and as a calcium antagonist. However, further studies should explore this potential in depth, especially through *in vivo* investigations in hypertensive animals to ascertain its effects on blood pressure. Future studies should also focus on the ability of brazilin to block calcium channels, and well-designed studies are necessary to compare the activity of brazilin with that of existing calcium channel blockers. Through further research, brazilin has the potential to be developed as a blood pressure-lowering agent.

Brazilin pretreatment (at 50 and 100 μM) also ameliorates vascular inflammation and oxidative stress induced by high glucose in human umbilical vein endothelial cells (HUVEC). High glucose enhances the formation of cell adhesion molecules, i.e., intercellular (ICAM) and vascular adhesion molecules (VCAM) in the cells, which are reduced by brazilin (Jayakumar et al., 2014) (**Figure 3**). High glucose promotes NF-κB activation, which mediates the inflammatory response by upregulating cell surface expression of adhesion molecules (Morigi et al., 1998). The beneficial effects of the compound are believed to be mediated by its ability to inhibit the activation of ERK, NF-κB, and eNOS triggered by exposure to high glucose (Jayakumar et al., 2014). These findings suggest that brazilin may be useful in the management of diabetes involving microangiopathy. *C. sappan* crude extract has been used to control diabetes in folk medicines (Mekala and Radha, 2015). However, more in-depth research should be carried out for conclusive evidence. Brazilin was also reported to be protective against renal I/R injury by suppressing the NF-κB signaling pathway (Jia et al., 2016).

Platelets are a blood component involved in blood coagulation in response to bleeding due to vascular injury. Brazilin exerted antiplatelet activity in mouse platelets *in vitro* (Ji et al., 2019), whereas Chang et al. (2013) reported brazilin's ability to stimulate platelet aggregation in human platelets *in vitro*. The discrepancy in these findings could be due to the difference in the platelet source species. Further study is needed to clarify this issue. Chang et al. (2013) demonstrated that brazilin potentiated collagen-induced platelet aggregation *in vitro* at lower concentrations (1–10 μM), whereas at higher concentrations (20–50 μM), it had a direct effect on platelet aggregation. This property

associates with its traditional use in treating bleeding gums and uterine bleeding (Mekala and Radha, 2015). The addition of yohimbine (an adrenoceptor antagonist) and a thrombin protease-activated receptor antagonist had no significant effect on brazilin's properties. However, the addition of caffeic acid phenethyl ester (a collagen receptor antagonist) reduced platelet aggregation. These observations suggest that the platelet-activating property of brazilin does not involve adrenoceptor or protease-activated receptor stimulation; instead, it may be due to the direct activation of collagen receptors. By contrast, it was suggested that brazilin exerts its antiplatelet activity by stimulating protease-activated receptor 4 (Ji et al., 2019). Brazilin is a promising candidate for further research on its potential as a collagen receptor agonist. This property is beneficial in the clinical management of vascular injury that involves blood coagulation.

Other favorable properties of brazilin are the prevention of vascular smooth muscle cell migration and proliferation which was demonstrated in an *in vitro* study (Guo et al., 2013). These vascular events can enhance vascular diseases, such as restenosis and atherosclerosis (Louis and Zahradka, 2010). Brazilin (at 3, 10, and 30 μM) inhibited platelet-derived growth factor (PDGF)-induced vascular smooth muscle cell proliferation by inducing G_0/G_1 cell cycle arrest without affecting cell viability. It also downregulated G_0/G_1 phase regulatory proteins, namely cyclin E and cyclin-dependent kinase 2 (CDK2), and upregulated p27, but it had no effect on cyclin D. Cyclins D and E, and CDK2 are positive regulators for the G_0/G_1 transition, whereas p27 is a negative regulator (Guo et al., 2013). Inhibition of cell migration by brazilin is associated with reduced cellular expression of adhesion molecules (ICAM-1 and VCAM-1) and matrix metalloproteinase-9 (MMP-9). MMPs are mediators of the progression of vascular lesions (Suh et al., 2006). The inhibitory effects of brazilin on both cell proliferation and migration are believed to be linked to the suppression of PDGF receptor β activation, thereby preventing the signaling cascade and leading to the inhibition of ERK1/2, Src, and Akt activation (Guo et al., 2013). ERK1/2 activation promotes cell growth and migration, events that are important in the commencement and development of vascular lesions (Suh et al., 2006), whereas the activation of Src kinases and PI3K/Akt are associated with various cellular events, such as cellular differentiation, proliferation, and cytoskeletal reorganization (Sayeski and Ali, 2003; Zhang et al., 2020). Despite its good findings, a shortcoming of the study (Guo et al., 2013) is an absence of a positive control group. Taken together, brazilin has the potential to prevent atherosclerosis and restenosis, and these effects warrant further *in vivo* studies.

Brazilein

Different from brazilin, its oxidized form, brazilein (at 100 μM), promotes vasocontraction in rat thoracic aortic rings, comparable to caffeine (20 mM) but lesser than phenylephrine (10 μM). The effect is not endothelial-dependent and does not involve the stimulation of α- and β-adrenoceptors, muscarinic receptors, or angiotensin II type 1 receptors (Shen et al., 2008). However, its effects are significantly weakened by the addition of nimodipine and diltiazem (L-type Ca^{2+} channel blockers) and pinacidil (a potassium channel opener), indicating that the vasocontraction effect of brazilein is dependent on Ca^{2+} influx (Shen et al., 2008). Extracellular Ca^{2+} entry is required for the contraction of vascular smooth muscle cells. Pinacidil increased potassium efflux, leading to hyperpolarization, which then reduced Ca^{2+} influx (Tinker et al., 2018) (**Figure 3**). The reduction in Ca^{2+} entry diminishes the effects of brazilein. The effect of brazilein on blood vessels was not associated with the activation of protein kinase C (PKC) or IP_3 receptor, demonstrated by the lack of effect observed with the addition of their respective inhibitors (Shen et al., 2008). However, the co-administration of inhibitors of MLC kinase (MLCK), Rho-kinase (ROCK), and ERK decreased the vasocontraction property of the compound. Collectively, these findings suggest that brazilein most likely exerts vasocontraction via the activation of the L-type calcium channel and the involvement of ROCK, MLCK, and ERK. More studies, especially *in vivo* studies, are needed to confirm the effects seen in the *in vitro* setting.

Other Compounds

Few studies to date have investigated other bioactive compounds isolated from *C. sappan* for their potential role in vascular injury. Hematoxylin (at 10, 30, and 100 μM) from the heartwood also demonstrated vasorelaxant activity in precontracted intact rat aortic rings, but the effects were reduced in denuded rings and these observations were not compared with a positive control (Xie et al., 2000). The effects were also diminished by L-NAME, suggesting the involvement of nitric oxide in its effect. He et al. (2009) reported vasorelaxant effects of (E)-3-(3,4-dihydroxybenzylidene)-7-hydroxychroman-4-one, sappanone B, and 3-deoxysappanone B in endothelium-intact and endothelium-denuded aortic rings, suggesting an independent effect of the presence of endothelium (**Figure 3**). However, the vasorelaxant activity of the compounds was diminished in the presence of an eNOS inhibitor and an sGC inhibitor, indicating that the compounds exerted their effects via the nitric oxide-cGMP pathway (He et al., 2009). Nonetheless, it is not yet confirmed whether these compounds elicit the effect by acting directly or indirectly on the vascular muscarinic receptors. Further studies should be conducted to clarify this. On the other hand, 1-hydroxy-7-methylxanthone, 1,7-dihydroxyxanthone, butein, and sappanone A were demonstrated to significantly inhibit lipopolysaccharide-induced nitric oxide production *in vitro* (Zhao et al., 2014). A high level of nitric oxide in blood vessels is beneficial because of its vasodilating effect (Kamisah et al., 2017), but its synthesis is also enhanced under oxidative stress, which could be harmful because of its ability to form peroxynitrite radicals (Kamisah et al., 2016). Therefore, the ability of these *C. sappan* phytochemicals to suppress nitric oxide production following exposure to stress is advantageous.

Sappanchalcone also possesses antiplatelet activity. Other compounds, such as 3-deoxysappanone B, caesalpin J. epicaesalpin J, episyringaresinol, methylesappanol, and protosappanin A isolated from the plant were also screened and found to have negligible effects (Ji et al., 2019). However, the possible mechanism of action of the

sappanchalcone was not elucidated in the study. The compound may manifest its property via the same mechanism as brazilin, but this postulation has yet to be confirmed. Its effects on other clotting factors, such as prothrombin, activated factor IX, and plasminogen activator, should also be studied.

CONCLUSION AND DIRECTIONS FOR FUTURE STUDY

This review shows that *C. sappan* Linn. contains many bioactive compounds, such as brazilin, brazilein, and sappanone A, that should be further studied and developed as potential candidates for treating cardiovascular problems, particularly myocardial infarction, cardiac remodeling, and hypertension. However, well-designed studies with appropriate controls (negative and positive) and a good range of doses to date are still at a preliminary stage. *In vivo* studies to confirm the activities seen in *ex vivo* and *in vitro* studies are still lacking. The effects of *C. sappan* bioactive compounds on myocardial calcium handling proteins, mitochondrial function, PI3K/Akt/mammalian target of rapamycin (mTOR), and cellular mechanotransduction, as well as the renin–angiotensin–aldosterone system, should be explored to better understand their mechanistic pathways. Certain genes involved in the pathogenesis of hypertension—Alb, Chrm2, Xirp1, Kcnq1, Slc5a7, Kcnh1, Ache, Crlf1 and Galr2— should also be studied. To progress to clinical trials, the safety of the compounds for administration to humans should also be determined.

AUTHOR CONTRIBUTIONS

MS and YK wrote and revised the manuscript. RS contributed to manuscript writing and editing.

FUNDING

This research was supported by the Faculty of Medicine, Universiti Kebangsaan Malaysia Matching Grant (FF-2019-480 and FF-2019–480/1) and University Research Grant from the Ministry of Research and Technology of the Republic of Indonesia (Number: 1827/UN6.3.1/LT/2020).

REFERENCES

Ahmed, S. M., Luo, L., Namani, A., Wang, X. J., and Tang, X. (2017). Nrf2 Signaling Pathway: Pivotal Roles in Inflammation. *Biochim. Biophys. Acta Mol. Basis Dis.* 1863 (2), 585–597. doi:10.1016/j.bbadis.2016.11.005

Ali, O. S., Abdelgawad, H. M., Mohammed, M. S., and El-Awady, R. R. (2014). Ischemic Heart Diseases in Egypt: Role of Xanthine Oxidase System and Ischemia-Modified Albumin. *Heart Vessels* 29 (5), 629–637. doi:10.1007/s00380-013-0413-3

Badami, S., Moorkoth, S., and B, S. (2004). *Caesalpinia Sappan* – A Medicinal and Dye Yielding Plant. *Indian J. Nat. Prod. Resour.* 3 (2), 75–82.

Bagheri, F., Khori, V., Alizadeh, A. M., Khalighfard, S., Khodayari, S., and Khodayari, H. (2016). Reactive Oxygen Species-Mediated Cardiac-Reperfusion Injury: Mechanisms and Therapies. *Life Sci.* 165, 43–55. Elsevier B.V. doi:10.1016/j.lfs.2016.09.013

Bao, H., Zhang, L. L., Liu, Q. Y., Feng, L., Ye, Y., Lu, J. J., et al. (2016). Cytotoxic and Pro-apoptotic Effects of Cassane Diterpenoids from the Seeds of *Caesalpinia Sappan* in Cancer Cells. *Molecules* 21 (6), 791. doi:10.3390/molecules21060791

Bredemeier, M., Lopes, L. M., Eisenreich, M. A., Hickmann, S., Bongiorno, G. K., d'Avila, R., et al. (2018). Xanthine Oxidase Inhibitors for Prevention of Cardiovascular Events: A Systematic Review and Meta-Analysis of Randomized Controlled Trials. *BMC Cardiovasc. Disord.* 18 (1), 24–11. doi:10.1186/s12872-018-0757-9

Chang, Y., Huang, S. K., Lu, W. J., Chung, C. L., Chen, W. L., Lu, S. H., et al. (2013). Brazilin Isolated from *Caesalpinia Sappan* L. Acts as a Novel Collagen Receptor Agonist in Human Platelets. *J. Biomed. Sci.* 20 (1), 4. doi:10.1186/1423-0127-20-4

Chellappan, D. R., Purushothaman, A. K., and Brindha, P. (2017). Gastroprotective Potential of Hydro-Alcoholic Extract of Pattanga (*Caesalpinia Sappan* Linn.). *J. Ethnopharmacol.* 197, 294–305. doi:10.1016/j.jep.2016.07.081

Chen, S., Zhang, Y., Lighthouse, J. K., Mickelsen, D. M., Wu, J., Yao, P., et al. (2020). A Novel Role of Cyclic Nucleotide Phosphodiesterase 10A in Pathological Cardiac Remodeling and Dysfunction. *Circulation* 141 (3), 217–233. doi:10.1161/CIRCULATIONAHA.119.042178

Choo, Y. Y., Tran, P. T., Min, B. S., Kim, O., Nguyen, H. D., Kwon, S. H., et al. (2017). Sappanone A Inhibits RANKL-Induced Osteoclastogenesis in BMMs and Prevents Inflammation-Mediated Bone Loss. *Int. Immunopharmacol.* 52, 230–237. doi:10.1016/j.intimp.2017.09.018

Cuong, T. D., Hung, T. M., Kim, J. C., Kim, E. H., Woo, M. H., Choi, J. S., et al. (2012). Phenolic Compounds from *Caesalpinia Sappan* Heartwood and Their Anti-inflammatory Activity. *J. Nat. Prod.* 75 (12), 2069–2075. doi:10.1021/np3003673

Cyr, A. R., Huckaby, L. V., Shiva, S. S., and Zuckerbraun, B. S. (2020). Nitric Oxide and Endothelial Dysfunction. *Crit. Care Clin.* 36 (2), 307–321. doi:10.1016/j.ccc.2019.12.009

Dapson, R. W., and Bain, C. L. (2015). Brazilwood, Sappanwood, Brazilin and the Red Dye Brazilein: From Textile Dyeing and Folk Medicine to Biological Staining and Musical Instruments. *Biotech. Histochem.* 90 (6), 401–423. doi:10.3109/10520295.2015.1021381

Delaunay, M., Osman, H., Kaiser, S., and Diviani, D. (2019). The Role of Cyclic AMP Signaling in Cardiac Fibrosis. *Cells* 9 (1), 69. doi:10.3390/cells9010069

Do, T. L. (2001). *Vietnamese Medicinal Plants*. Hanoi: Medicine Publisher.

Fu, L. C., Huang, X. A., Lai, Z. Y., Hu, Y. J., Liu, H. J., and Cai, X. L. (2008). A New 3-benzylchroman Derivative from Sappan Lignum (*Caesalpinia Sappan*). *Molecules* 13 (8), 1923–1930. doi:10.3390/molecules13081923

G., A., A.J.A., R., A.Usha Raja, U. R. N., and Padmalatha, C. (2017). Toxicological Studies of *Caesalpinia Sappan* wood Derived Dye in Wister Albino Rats. *Food Sci. Hum. Wellness* 6 (1), 34–38. doi:10.1016/j.fshw.2016.10.004

Guo, J., Li, L., Wu, Y. J., Yan, Y., Xu, X. N., Wang, S. B., et al. (2013). Inhibitory Effects of Brazilin on the Vascular Smooth Muscle Cell Proliferation and Migration Induced by PDGF-BB. *Am. J. Chin. Med.* 41 (6), 1283–1296. doi:10.1142/S0192415X13500869

Hadebe, N., Cour, M., and Lecour, S. (2018). The SAFE Pathway for Cardioprotection: Is This a Promising Target? *Basic Res. Cardiol.* 113 (2), 9. doi:10.1007/s00395-018-0670-5

Hasan, R., and Jaggar, J. H. (2018). KV Channel Trafficking and Control of Vascular Tone. *Microcirculation* 25 (1), 1–11. doi:10.1111/micc.12418

He, W., Fang, T., Zhang, K., and Tu, P. (2009). [Vasorelaxation Effects of Homoisoflavonoids from Caesalpinia Sappan in Rat Thoracic Aortic Rings]. *Zhongguo Zhong Yao Za Zhi* 34 (6), 731–734.

Heinrich, M., Appendino, G., Efferth, T., Fürst, R., Izzo, A. A., Kayser, O., et al. (2020). Best Practice in Research - Overcoming Common Challenges in Phytopharmacological Research. *J. Ethnopharmacol.* 246, 112230. doi:10.1016/j.jep.2019.112230

Helmi, N., Fakhrudin, A., Sudarmanto, B. S. A., and Ikawati, Z. (2020). *In Vitro* and In Silico Studies of Secang wood (*Caesalpinia Sappan* L.) Extracts and Brazilin as Natural Phosphodiesterase-1 (PDE1) Inhibitor for Herbal Cognitive

Enhancer Development. *Rese. Jour. Pharm. Technol.* 13 (5), 2269–2274. doi:10.5958/0974-360X.2020.00409.6

Hu, C. M., Kang, J. J., Lee, C. C., Li, C. H., Liao, J. W., and Cheng, Y. W. (2003). Induction of Vasorelaxation through Activation of Nitric Oxide Synthase in Endothelial Cells by Brazilin. *Eur. J. Pharmacol.* 468 (1), 37–45. doi:10.1016/S0014-2999(03)01639-X

Hung, T. M., Hai, N. X., Nhan, N. T., Quang, T. T., Quan, T. L., Cuong, T. D., et al. (2013). Cytotoxic Activity of New Phenolic Compounds from Vietnamese *Caesalpinia Sappan*. *Biosci. Biotechnol. Biochem.* 77 (12), 2378–2382. doi:10.1271/bbb.130493

Irie, K., Sato, T., Tanaka, I., Nakajima, J., Kawaguchi, M., and Himi, T. (2009). Cardiotonic Effect of *Apocynum Venetum* L. Extracts on Isolated guinea Pig Atrium. *J. Nat. Med.* 63 (2), 111–116. doi:10.1007/s11418-008-0296-2

Jayakumar, T., Chang, C. C., Lin, S. L., Huang, Y. K., Hu, C. M., Elizebeth, A. R., et al. (2014). Brazilin Ameliorates High Glucose-Induced Vascular Inflammation via Inhibiting ROS and CAMs Production in Human Umbilical Vein Endothelial Cells. *Biomed. Res. Int.* 2014, 403703. doi:10.1155/2014/403703

Ji, Y., Zhang, Y.-q., Liu, T.-d., Xia, M.-y., Long, C.-l., Wang, L., et al. (2019). Chemical Constituents from Heartwoods of Caesalpinia Sappan with Antiplatelet Aggregation Activities. *Chin. Herbal Medicines* 11, 423–428. doi:10.1016/j.chmed.2019.09.001

Jia, Y., Wang, H., Song, Y., Liu, K., Dou, F., Lu, C., et al. (2013). Application of a Liquid Chromatography-Tandem Mass Spectrometry Method to the Pharmacokinetics, Tissue Distribution and Excretion Studies of Brazilin in Rats. *J. Chromatogr. B Analyt Technol. Biomed. Life Sci.* 931, 61–67. doi:10.1016/j.jchromb.2013.05.017

Jia, Y., Zhao, J., Liu, M., Li, B., Song, Y., Li, Y., et al. (2016). Brazilin Exerts Protective Effects against Renal Ischemia-Reperfusion Injury by Inhibiting the NF-Kb Signaling Pathway. *Int. J. Mol. Med.* 38 (1), 210–216. doi:10.3892/ijmm.2016.2616

Jo, W., Min, B. S., Yang, H. Y., Park, N. H., Kang, K. K., Lee, S., et al. (2020). Sappanone a Prevents Left Ventricular Dysfunction in a Rat Myocardial Ischemia Reperfusion Injury Model. *Int. J. Mol. Sci.* 21 (18), 1–17. doi:10.3390/ijms21186935

Kamisah, Y., Ang, S. M., Othman, F., Nurul-Iman, B. S., and Qodriyah, H. M. (2016). Renoprotective Effect of virgin Coconut Oil in Heated palm Oil Diet-Induced Hypertensive Rats. *Appl. Physiol. Nutr. Metab.* 41 (10), 1033–1038. doi:10.1139/apnm-2016-0029

Kamisah, Y., Zuhair, J. S. F., Juliana, A. H., and Jaarin, K. (2017). *Parkia Speciosa* Empty Pod Prevents Hypertension and Cardiac Damage in Rats Given N(G)-nitro-L-arginine Methyl Ester. *Biomed. Pharmacother.* 96, 291–298. doi:10.1016/j.biopha.2017.09.095

Kanai, R., Cornelius, F., Ogawa, H., Motoyama, K., Vilsen, B., and Toyoshima, C. (2020). Binding of Cardiotonic Steroids to Na+,K+-ATPase in the E2P State. *Proc. Natl. Acad. Sci. USA* 118 (1), e2020438118–12. doi:10.1073/pnas.2020438118

Kang, C., Gao, J., Kang, M., Liu, X., Fu, Y., and Wang, L. (2019). Sappanone A Prevents Hypoxia-Induced Injury in PC-12 Cells by Down-Regulation of miR-15a. *Int. J. Biol. Macromol.* 123, 35–41. doi:10.1016/j.ijbiomac.2018.11.002

Kawano, S., Kubota, T., Monden, Y., Tsutsumi, T., Inoue, T., Kawamura, N., et al. (2006). Blockade of NF-kappaB Improves Cardiac Function and Survival after Myocardial Infarction. *Am. J. Physiol. Heart Circ. Physiol.* 291 (3), H1337–H1344. doi:10.1152/ajpheart.01175.2005

Kumari, S., Katare, P. B., Elancheran, R., Nizami, H. L., Paramesha, B., Arava, S., et al. (2020). *Musa Balbisiana* Fruit Rich in Polyphenols Attenuates Isoproterenol-Induced Cardiac Hypertrophy in Rats via Inhibition of Inflammation and Oxidative Stress. *Oxid. Med. Cel. Longev.* 2020, 7147498. doi:10.1155/2020/7147498

Lawless, M., Caldwell, J. L., Radcliffe, E. J., Smith, C. E. R., Madders, G. W. P., Hutchings, D. C., et al. (2019). Phosphodiesterase 5 Inhibition Improves Contractile Function and Restores Transverse Tubule Loss and Catecholamine Responsiveness in Heart Failure. *Sci. Rep.* 9 (1), 6801–6817. doi:10.1038/s41598-019-42592-1

Leong, D. P., Joseph, P. G., McKee, M., Anand, S. S., Teo, K. K., Schwalm, J. D., et al. (2017). Reducing the Global burden of Cardiovascular Disease, Part 2: Prevention and Treatment of Cardiovascular Disease. *Circ. Res.* 121 (6), 695–710. doi:10.1161/CIRCRESAHA.117.311849

Li, C., Zhang, H., Gao, D., Ma, Q., Li, Z., Dai, J., et al. (2015). Aqueous Extract of Caesalpinia Sappan Decelerates Allograft Rejection by Inducing Imbalance between CD4(+) CD25(+) T Cells and Th17 Cells. *Int. J. Clin. Exp. Med.* 8 (5), 7107–7115.

Li, L. M., Fu, J. X., and Song, X. Q. (2020). Complete Plastome Sequence of *Caesalpinia Sappan* Linnaeus, a Dyestuff and Medicinal Species. *Mitochondrial DNA B Resour.* 5 (3), 2535–2536. doi:10.1080/23802359.2020.1778579

Liu, Z., and Khalil, R. A. (2018). Evolving Mechanisms of Vascular Smooth Muscle Contraction Highlight Key Targets in Vascular Disease. *Biochem. Pharmacol.* 153, 91–122. doi:10.1016/j.bcp.2018.02.012

Louis, S. F., and Zahradka, P. (2010). Vascular Smooth Muscle Cell Motility: From Migration to Invasion. *Exp. Clin. Cardiol.* 15, e75–85.

Ma, G., Wu, H., Chen, D., Zhu, N., Zhu, Y., Sun, Z., et al. (2015). Antimalarial and Antiproliferative Cassane Diterpenes of *Caesalpinia Sappan*. *J. Nat. Prod.* 78 (10), 2364–2371. doi:10.1021/acs.jnatprod.5b00317

Mekala, K., and Radha, R. (2015). A Review on Sappan Wood-A Therapeutic Dye Yielding Tree. *Rese. Jour. Pharmac. Phytoch.* 7 (4), 227–231. doi:10.5958/0975-4385.2015.00035.7

Min, B. S., Cuong, T. D., Hung, T. M., Min, B. K., Shin, B. S., and Woo, M. H. (2012). Compounds from the Heartwood of *Caesalpinia Sappan* and Their Anti-inflammatory Activity. *Bioorg. Med. Chem. Lett.* 22 (24), 7436–7439. doi:10.1016/j.bmcl.2012.10.055

Morigi, M., Angioletti, S., Imberti, B., Donadelli, R., Micheletti, G., Figliuzzi, M., et al. (1998). Leukocyte-endothelial Interaction Is Augmented by High Glucose Concentrations and Hyperglycemia in a NF-kB-dependent Fashion. *J. Clin. Invest.* 101 (9), 1905–1915. doi:10.1172/JCI656

Mueller, M., Weinmann, D., Toegel, S., Holzer, W., Unger, F. M., and Viernstein, H. (2016). Compounds from *Caesalpinia Sappan* with Anti-inflammatory Properties in Macrophages and Chondrocytes. *Food Funct.* 7 (3), 1671–1679. doi:10.1039/c5fo01256b

Nguyen, M. T., Awale, S., Tezuka, Y., Tran, Q. L., and Kadota, S. (2005). Xanthine Oxidase Inhibitors from the Heartwood of Vietnamese *Caesalpinia Sappan*. *Chem. Pharm. Bull. (Tokyo)* 53 (8), 984–988. doi:10.1248/cpb.53.984

Nguyen, M. T. T., Awale, S., Tezuka, Y., Tran, Q. L., and Kadota, S. (2004). Neosappanone A, a Xanthine Oxidase (XO) Inhibitory Dimeric Methanodibenzoxocinone with a New Carbon Skeleton from *Caesalpinia Sappan*. *Tetrahedron Lett.* 45 (46), 8519–8522. doi:10.1016/j.tetlet.2004.09.107

N., M., Krishnakumar, S., Kumar, S. R., and Surendar, K. K. (2014). *Caesalpinia Sappan* L.: Comprehensive Review on Seed Source Variation and Storability. *pgt* 5 (2), 11–21. doi:10.5376/pgt.2014.05.0002

Nugraheni, K., and Saputri, F. C. (2017). The Effect of Secang Extract (Caesalpinia Sappan Linn) on the Weight and Histology Appearance of White Male Rats' Hearts Induced by Isoproterenol. *Int. J. App Pharm.* 9, 59–61. doi:10.22159/ijap.2017.v9s1.35_41

Qi, B., Zhang, X., Yu, H., Bao, Y., Wu, N., and Jia, D. (2021). Brazilin Prevents against Myocardial Ischemia-Reperfusion Injury through the Modulation of Nrf2 via the PKC Signaling Pathway. *Ann. Transl. Med.* 9 (4), 312. doi:10.21037/atm-20-4414

Roberts, R. E. (2012). The Extracellular Signal-Regulated Kinase (ERK) Pathway: a Potential Therapeutic Target in Hypertension. *J. Exp. Pharmacol.* 4, 77–83. doi:10.2147/jep.s28907

Rouzer, C. A., and Marnett, L. J. (2020). Structural and Chemical Biology of the Interaction of Cyclooxygenase with Substrates and Non-steroidal Anti-inflammatory Drugs. *Chem. Rev.* 120 (15), 7592–7641. doi:10.1021/acs.chemrev.0c00215

Salim, S. M., Yunos, N. M., Jauri, M. H., and Kamisah, Y. (2020). Cardiotonic Effects of Cardiac Glycosides from Plants of Apocynaceae Family. *Chula. Med. J.* 64 (4), 449–456. doi:10.14456/clmj.2020.58

Sasaki, Y., Hosokawa, T., Nagai, M., and Nagumo, S. (2007). *In Vitro* study for Inhibition of NO Production about Constituents of Sappan lignum. *Biol. Pharm. Bull.* 30 (1), 193–196. doi:10.1248/bpb.30.193

Sasaki, Y., Suzuki, M., Matsumoto, T., Hosokawa, T., Kobayashi, T., Kamata, K., et al. (2010). Vasorelaxant Activity of Sappan lignum Constituents and Extracts on Rat Aorta and Mesenteric Artery. *Biol. Pharm. Bull.* 33 (9), 1555–1560. doi:10.1248/bpb.33.1555

Sayeski, P. P., and Ali, M. S. (2003). The Critical Role of C-Src and the Shc/Grb2/ERK2 Signaling Pathway in Angiotensin II-dependent VSMC Proliferation. *Exp. Cel Res.* 287 (2), 339–349. doi:10.1016/s0014-4827(03)00154-x

Settharaksa, S., Monton, C., and Charoenchai, L. (2019). Optimization of Caesalpinia Sappan L. Heartwood Extraction Procedure to Obtain the Highest Content of Brazilin and Greatest Antibacterial Activity. *J. Integr. Med.* 17 (5), 351–358. doi:10.1016/j.joim.2019.05.003

Shen, J., Yip, S., Wang, Z., Wang, W., Xing, D., and Du, L. (2008). Brazilein-induced Contraction of Rat Arterial Smooth Muscle Involves Activation of Ca2+ Entry and ROK, ERK Pathways. *Eur. J. Pharmacol.* 580 (3), 366–371. doi:10.1016/j.ejphar.2007.11.012

Shi, X., Tao, G., Ji, L., and Tian, G. (2020a). Sappanone A Alleviates Hypoxia/reoxygenation-Induced Cardiomyocytes Injury through Inhibition of Mitochondrial Apoptosis and Activation of PI3K-Akt-Gsk-3β Pathway. *Biosci. Rep.* 40 (2), 1–10. doi:10.1042/BSR20192442

Shi, X., Tao, G., Ji, L., and Tian, G. (2020b). Sappanone a Protects against Myocardial Ischemia Reperfusion Injury by Modulation of Nrf2. *Drug Des. Devel. Ther.* 14, 61–71. doi:10.2147/DDDT.S230358

Shimokawa, T., Kinjo, J., Yamahara, J., Yamasaki, M., and Nohara, T. (1985). Two Novel Aromatic Compounds from *Caesalpinia Sappan*. *Chem. Pharm. Bull.* 33 (8), 3545–3547. doi:10.1248/cpb.33.3545

Si, L. Y., Ramalingam, A., Ali, S. S., Aminuddin, A., Ng, P. Y., Latip, J., et al. (2019). Roselle Attenuates Cardiac Hypertrophy after Myocardial Infarction *In Vivo* and *In Vitro*. *EXCLI J.* 18, 876–892. doi:10.17179/excli2019-1792

Sireeratawong, S., Piyabhan, P., Singhalak, T., Wongkrajang, Y., Temsiririrkkul, R., Punsrirat, J., et al. (2010). Toxicity Evaluation of Sappan wood Extract in Rats. *J. Med. Assoc. Thai.* 93 Suppl 7 (12), S50–S57.

Siti, H. N., Kamisah, Y., and Kamsiah, J. (2015). The Role of Oxidative Stress, Antioxidants and Vascular Inflammation in Cardiovascular Disease (A Review). *Vascul Pharmacol.* 71, 40–56. doi:10.1016/j.vph.2015.03.005

Suh, S. J., Jin, U. H., Kim, S. H., Chang, H. W., Son, J. K., Lee, S. H., et al. (2006). Ochnaflavone Inhibits TNF-Alpha-Induced Human VSMC Proliferation via Regulation of Cell Cycle, ERK1/2, and MMP-9. *J. Cel. Biochem.* 99 (5), 1298–1307. doi:10.1002/jcb.20912

Sulistiyorini, I., Safitri, R., Lesmana, R., and Syamsunarno, M. R. A. A. (2020). The Viability Test of Sappan wood (*Caesalpinia Sappan* L.) Ethanol Extract in the H9C2 Cell Line. *Int. J. App Pharm.* 12, 76–78. doi:10.22159/ijap.2020.v12s3.39479

Sun, H.-J., Wu, Z.-Y., Nie, X.-W., and Bian, J.-S. (2020). Role of Endothelial Dysfunction in Cardiovascular Diseases: The Link between Inflammation and Hydrogen Sulfide. *Front. Pharmacol.* 10, 1–15. doi:10.3389/fphar.2019.01568

Suwan, T., Wanachantararak, P., Khongkhunthian, S., and Okonogi, S. (2018). Antioxidant Activity and Potential of *Caesalpinia Sappan* Aqueous Extract on Synthesis of Silver Nanoparticles. *Drug Discov. Ther.* 12 (5), 259–266. doi:10.5582/ddt.2018.01059

Tewtrakul, S., Tungcharoen, P., Sudsai, T., Karalai, C., Ponglimanont, C., and Yodsaoue, O. (2015). Antiinflammatory and Wound Healing Effects of *Caesalpinia Sappan* L. *Phytother. Res.* 29 (6), 850–856. doi:10.1002/ptr.5321

Tinker, A., Aziz, Q., Li, Y., and Specterman, M. (2018). ATP-sensitive Potassium Channels and Their Physiological and Pathophysiological Roles. *Compr. Physiol.* 8 (4), 1463–1511. doi:10.1002/cphy.c170048

Tong, X. Z., Zhu, H., Shi, Y., Xu, H. T., Wang, B., and Zhao, J. H. (2013). An LC/MS/MS Method for Simultaneous Quantitation of Two Homoisoflavones: Protosappanin B and Brazilin with Hypoglycemic Activity in Rat Plasma and its Application to a Comparative Pharmacokinetic Study in normal and Streptozotocin-Treated Rats. *J. Ethnopharmacol.* 148 (2), 682–690. doi:10.1016/j.jep.2013.05.029

Tu, W., Wang, H., Li, S., Liu, Q., and Sha, H. (2019). The Anti-inflammatory and Anti-oxidant Mechanisms of the keap1/Nrf2/ARE Signaling Pathway in Chronic Diseases. *Aging Dis.* 10 (3), 637–651. doi:10.14336/AD.2018.0513

Uddin, G. M., Kim, C. Y., Chung, D., Kim, K. A., and Jung, S. H. (2015). One-step Isolation of Sappanol and Brazilin from *Caesalpinia Sappan* and Their Effects on Oxidative Stress-Induced Retinal Death. *BMB Rep.* 48 (5), 289–294. doi:10.5483/BMBRep.2015.48.5.189

Voskoboinik, I., Whisstock, J. C., and Trapani, J. A. (2015). Perforin and Granzymes: Function, Dysfunction and Human Pathology. *Nat. Rev. Immunol.* 15 (6), 388–400. doi:10.1038/nri3839

Wan, Y. J., Xu, L., Song, W. T., Liu, Y. Q., Wang, L. C., Zhao, M. B., et al. (2019). The Ethanolic Extract of *Caesalpinia Sappan* Heartwood Inhibits Cerebral Ischemia/reperfusion Injury in a Rat Model through a Multi-Targeted Pharmacological Mechanism. *Front. Pharmacol.* 10, 29–15. doi:10.3389/fphar.2019.00029

Wang, D. S., Nie, W., Jiang, T. T., Ding, L. F., Song, L. D., Wu, X. D., et al. (2020a). Caesalpanins A-C, Three Dimeric Cassane Diterpenoids from the Seeds of Caesalpinia Sappan L. *Chem. Biodivers.* 17 (5), e2000103. doi:10.1002/cbdv.202000103

Wang, M., Chen, Z., Yang, L., and Ding, L. (2021). Sappanone A Protects against Inflammation, Oxidative Stress and Apoptosis in Cerebral Ischemia-Reperfusion Injury by Alleviating Endoplasmic Reticulum Stress. *Inflammation* 44 (3), 934–945. doi:10.1007/s10753-020-01388-6

Wang, M., Tan, J., Chen, J., Xie, T., Lin, L. M., Zhong, L. L., et al. (2020b). Three New Ester Glycosides with Cytotoxic Activity from the Seeds of *Caesalpinia Sappan*. *Nat. Prod. Res.* 9, 1–8. doi:10.1080/14786419.2020.1721488

Wang, Z., Sun, J. B., Qu, W., Guan, F. Q., Li, L. Z., and Liang, J. Y. (2014). Caesappin A and B, Two Novel Protosappanins from *Caesalpinia Sappan* L. *Fitoterapia* 92, 280–284. doi:10.1016/j.fitote.2013.12.004

Warriers, P. K., Nambiar, V. P. K., Ramankutty, C., and VV, P. (1993). *Indian Medicinal Plants, A Compendium of 500 Species*. Madras: Orient Longman Ltd.

WHO (2017). Cardiovascular Diseases (CVDs)-Key Facts. Available at: https://www.who.int/news-room/fact-sheets/detail/cardiovascular-diseases-(cvds (Accessed MarchNovembe 18, 2020).

Wu, J., Hou, J. B., Zhang, M. M., Zou, Y. P., and Yu, B. (2008). Protosappanin A, an Immunosuppressive Constituent from a Chinese Herb, Prolongs Graft Survival and Attenuates Acute Rejection in Rat Heart Allografts. *Transpl. Proc.* 40 (10), 3719–3722. doi:10.1016/j.transproceed.2008.06.097

Wu, J., Zhang, M., Jia, H., Huang, X., Zhang, Q., Hou, J., et al. (2010). Protosappanin A Induces Immunosuppression of Rats Heart Transplantation Targeting T Cells in Grafts via NF-kappaB Pathway. *Naunyn Schmiedebergs Arch. Pharmacol.* 381 (1), 83–92. doi:10.1007/s00210-009-0461-5

Xie, Y. W., Ming, D. S., Xu, H. X., Dong, H., and But, P. P. (2000). Vasorelaxing Effects of *Caesalpinia Sappan* Involvement of Endogenous Nitric Oxide. *Life Sci.* 67 (15), 1913–1918. doi:10.1016/S0024-3205(00)00772-4

Yan, Y., Chen, Y. C., Lin, Y. H., Guo, J., Niu, Z. R., Li, L., et al. (2015). Brazilin Isolated from the Heartwood of *Caesalpinia Sappan* L Induces Endothelium-dependent and -independent Relaxation of Rat Aortic Rings. *Acta Pharmacol. Sin.* 36 (11), 1318–1326. doi:10.1038/aps.2015.113

Yan-yan, J., Yan, L., Ying, S., Jinyi, Z., Fang, D., Yuan, S., et al. (2014). A Simple High-Performance Liquid Chromatographic Method for the Determination of Brazilin and its Application to a Pharmacokinetic Study in Rats. *J. Ethnopharmacol.* 151 (1), 108–113. doi:10.1016/j.jep.2013.08.054

Yodsaoue, O., Cheenpracha, S., Karalai, C., Ponglimanont, C., Chantrapromma, S., Fun, H. K., et al. (2008). Phanginin A-K, Diterpenoids from the Seeds of *Caesalpinia Sappan* Linn. *Phytochemistry* 69 (5), 1242–1249. doi:10.1016/j.phytochem.2007.11.013

Younis, N. S., Abduldaium, M. S., and Mohamed, M. E. (2020). Protective Effect of Geraniol on Oxidative, Inflammatory and Apoptotic Alterations in Isoproterenol-Induced Cardiotoxicity: Role of the Keap1/Nrf2/HO-1 and PI3K/Akt/mTOR Pathways. *Antioxidants (Basel)* 9 (10), 1–17. doi:10.3390/antiox9100977

Yu, B., Hou, J. B., and Lu, H. (2004). Effect of Different Extracts of *Caesalpinia Sappan* L on T Lymphocyte Subsets and Myocardial Protectively Function after Rat Heart Transplantation. *Chin. J. Endemiol.* 23, 539. doi:10.1016/j.healun.2003.11.366

Yuan, Z. Y., Lei, F., Chai, Y. S., Wu, H., Zhao, S., Wang, Y. G., et al. (2016). Reproductive Toxicity of Brazilein in ICR Mice. *Chin. J. Nat. Med.* 14 (6), 441–448. doi:10.1016/S1875-5364(16)30041-3

Zeng, K. W., Yu, Q., Song, F. J., Liao, L. X., Zhao, M. B., Dong, X., et al. (2015). Deoxysappanone B, a Homoisoflavone from the Chinese Medicinal Plant Caesalpinia Sappan L., Protects Neurons from Microglia-Mediated Inflammatory Injuries via Inhibition of IκB Kinase (IKK)-NF-κB and P38/ERK MAPK Pathways. *Eur. J. Pharmacol.* 748, 18–29. doi:10.1016/j.ejphar.2014.12.013

Zhang, J., Wang, X., Vikash, V., Ye, Q., Wu, D., Liu, Y., et al. (2016). ROS and ROS-Mediated Cellular Signaling. *Oxid. Med. Cel. Longev.* 2016, 4350965. doi:10.1155/2016/4350965

Zhang, M., Li, F., Wang, X., Gong, J., Xian, Y., Wang, G., et al. (2020). MiR-145 Alleviates Hcy-Induced VSMC Proliferation, Migration, and Phenotypic

Switch through Repression of the PI3K/Akt/mTOR Pathway. *Histochem. Cel. Biol.* 153 (5), 357–366. doi:10.1007/s00418-020-01847-z

Zhao, J., Zhu, A., Sun, Y., Zhang, W., Zhang, T., Gao, Y., et al. (2020). Beneficial Effects of Sappanone A on Lifespan and Thermotolerance in *Caenorhabditis elegans*. *Eur. J. Pharmacol.* 888 (38), 173558. doi:10.1016/j.ejphar.2020.173558

Zhao, M. B., Li, J., Shi, S. P., Cai, C. Q., Tu, P. F., Tang, L., et al. (2014). Two New Phenolic Compounds from the Heartwood of *Caesalpinia Sappan* L. *Molecules* 19 (1), 1–8. doi:10.3390/molecules19010001

Zhao, Y. N., Pan, Y., Tao, J. L., Xing, D. M., and Du, L. J. (2006). Study on Cardioactive Effects of Brazilein. *Pharmacology* 76 (2), 76–83. doi:10.1159/000089721

Zheng, J. X., Zhou, Y. B., and Liu, Y. Z. (2008). [Effect of Ethyl Acetate Extract of Sappan wood on Expression of Myocardial GrB mRNA in Rat Model of Allogeneic Ectopic Cardiac Transplantation]. *Zhongguo Zhong Xi Yi Jie He Za Zhi* 28 (6), 537–540.

Zheng, J., Zhang, S., Chen, H., Cai, X., Zhang, C., Li, S., et al. (2020). Protosappanin-A and Oleanolic Acid Protect Injured Podocytes from Apoptosis through Inhibition of AKT-mTOR Signaling. *Cell Biol. Int.* 44 (1), 189–199. doi:10.1002/cbin.11218

Zhou, Y. B., Yao, F. Z., and Han, J. R. (2003). [Effect of Sappan wood on Perforin mRNA Expression in Myocardium of Rats after Allogeneic Cardiac Transplantation]. *Zhongguo Zhong Xi Yi Jie He Za Zhi* 23 (5), 370–372.

Zhu, N. L., Sun, Z. H., Hu, M. G., Wu, T. Y., Yuan, J. Q., Wu, H. F., et al. (2017). New Cassane Diterpenoids from *Caesalpinia Sappan* and Their Antiplasmodial Activity. *Molecules* 22 (10), 1–7. doi:10.3390/molecules22101751

Conflict of Interest: The authors declare that the research was conducted in the absence of any commercial or financial relationships that could be construed as a potential conflict of interest.

Publisher's Note: All claims expressed in this article are solely those of the authors and do not necessarily represent those of their affiliated organizations, or those of the publisher, the editors and the reviewers. Any product that may be evaluated in this article, or claim that may be made by its manufacturer, is not guaranteed or endorsed by the publisher.

frontiers in Pharmacology

ORIGINAL RESEARCH
published: 14 October 2021
doi: 10.3389/fphar.2021.741623

Parkia speciosa Hassk. Empty Pod Extract Alleviates Angiotensin II-Induced Cardiomyocyte Hypertrophy in H9c2 Cells by Modulating the Ang II/ROS/NO Axis and MAPK Pathway

Hawa Nordin Siti[1,2], *Juriyati Jalil*[3], *Ahmad Yusof Asmadi*[4] *and Yusof Kamisah*[1,5]*

[1]Department of Pharmacology, Faculty of Medicine, Universiti Kebangsaan Malaysia, Kuala Lumpur, Malaysia, [2]Unit of Pharmacology, Department of Basic Medical Sciences, Faculty of Medicine, Universiti Sultan Zainal Abidin, Kuala Terengganu, Malaysia, [3]Drug and Herbal Research Centre, Faculty of Pharmacy, Universiti Kebangsaan Malaysia, Kuala Lumpur, Malaysia, [4]Unit of Pharmacology, Faculty of Medicine and Defense Health, Universiti Pertahanan Nasional Malaysia, Kuala Lumpur, Malaysia, [5]Cardiovacular Health Research Group, Faculty of Medicine, Universiti Kebangsaan Malaysia, Kuala Lumpur, Malaysia

OPEN ACCESS

Edited by:
Uraiwan Panich,
Mahidol University, Thailand

Reviewed by:
Raquel Bridi,
Pontificia Universidad Católica de Chile, Chile
Lei Chen,
Guangdong Ocean University, China

***Correspondence:**
Yusof Kamisah
kamisah_y@yahoo.com

Specialty section:
This article was submitted to Ethnopharmacology, a section of the journal Frontiers in Pharmacology

Received: 15 July 2021
Accepted: 28 September 2021
Published: 14 October 2021

Citation:
Siti HN, Jalil J, Asmadi AY and Kamisah Y (2021) Parkia speciosa Hassk. Empty Pod Extract Alleviates Angiotensin II-Induced Cardiomyocyte Hypertrophy in H9c2 Cells by Modulating the Ang II/ROS/NO Axis and MAPK Pathway. Front. Pharmacol. 12:741623. doi: 10.3389/fphar.2021.741623

Cardiac hypertrophy is characteristic of heart failure in patients who have experienced cardiac remodeling. Many medicinal plants, including *Parkia speciosa* Hassk., have documented cardioprotective effects against such pathologies. This study investigated the activity of *P. speciosa* empty pod extract against cardiomyocyte hypertrophy in H9c2 cardiomyocytes exposed to angiotensin II (Ang II). In particular, its role in modulating the Ang II/reactive oxygen species/nitric oxide (Ang II/ROS/NO) axis and mitogen-activated protein kinase (MAPK) pathway was examined. Treatment with the extract (12.5, 25, and 50 µg/ml) prevented Ang II-induced increases in cell size, NADPH oxidase activity, B-type natriuretic peptide levels, and reactive oxygen species and reductions in superoxide dismutase activity. These were comparable to the effects of the valsartan positive control. However, the extract did not significantly ameliorate the effects of Ang II on inducible nitric oxide synthase activity and nitric oxide levels, while valsartan did confer such protection. Although the extract decreased the levels of phosphorylated extracellular signal-related kinase, p38, and c-Jun N-terminal kinase, valsartan only decreased phosphorylated c-Jun N-terminal kinase expression. Phytochemical screening identified the flavonoids rutin (**1**) and quercetin (**2**) in the extract. These findings suggest that *P. speciosa* empty pod extract protects against Ang II-induced cardiomyocyte hypertrophy, possibly by modulating the Ang II/ROS/NO axis and MAPK signaling pathway via a mechanism distinct from valsartan.

Keywords: *Parkia speciosa*, angiotensin II, NADPH oxidase, iNOS, ERK, p38, JNK

INTRODUCTION

Cardiac hypertrophy initially develops as an adaptive response to compensate for reduced cardiac function (Bernardo and McMullen, 2016). Unfortunately, the sustained effects of pathological stimuli promote pathophysiological changes that lead to cardiac remodeling and, ultimately, heart failure (Wang et al., 2016). Angiotensin II (Ang II), a potent stimulus of cardiac myocyte growth factors, has been found to be elevated in cardiac failure (Zucker et al., 2015). Ang II can be used to mimic pressure-overload-induced cardiac hypertrophy (Ying et al., 2014) and has been widely employed as a hypertrophic stimulus in various *in vitro* cardiac disease models (Ding et al., 2019).

Exposure to Ang II stimulates the development of cardiac hypertrophy by activating G-protein-coupled receptors, which, in turn, activate several cascades, including the Ang II/reactive oxygen species/nitric oxide (Ang II/ROS/NO) axis as well as signaling kinases and phosphatases (Takano et al., 2003). Substantial evidence has linked Ang II-stimulated pathways to the activation of NADPH oxidase (NOX), which is a significant source of ROS in cardiovascular cells (Nguyen Dinh Cat et al., 2013). ROS have been implicated in the activation of mitogen-activated protein kinase (MAPK) and nuclear factor kappa B (NF-κB) pathways in Ang II-induced cardiac hypertrophy (Chen et al., 2020; Zhu et al., 2020). MAPK has three subfamilies—extracellular signal-related kinase (ERK1/2), c-Jun N-terminal kinase (JNK), and p38 kinase (p38)—that have been reported to play a role in cardiac hypertrophy (Zhang et al., 2003; Muslin, 2008; Cheng et al., 2017). Ang II also causes cardiac inflammation by promoting inducible nitric oxide synthase (iNOS) activity (Huang et al., 2017). These overlapping pathways eventually lead to cardiac remodeling and hypertrophy.

A potential therapeutic target for halting the progression of cardiac failure involves the prevention of pathological cardiac hypertrophy, for which numerous studies have attempted to identify novel therapies. While no drugs directly or specifically targeting pathological cardiac hypertrophy have been identified (Tran et al., 2016), neurohormonal blockers have been found to reduce cardiac hypertrophy indirectly. Ethnopharmacology is a promising screening tool in drug discovery, and many medicinal plants, including *Eriobotrya japonica* (Thunb.) Lindl (Chiang et al., 2018) and *Nelumbo nucifera* Gaertn. (Cho et al., 2019), have been shown to display cardioprotective activity against Ang II-induced cardiomyocyte hypertrophy.

Parkia speciosa Hassk., a leguminous plant in the family Fabaceae, grows indigenously in Southeast Asia and has traditionally been used to manage hypertension (Azliza et al., 2012) and heart problems (Yullia, 2008). The plant's empty pods have been reported to display various pharmacological activities, including anti-inflammatory (Mustafa et al., 2018; Gui et al., 2019a), antioxidant (Gui et al., 2019b), and α-glucosidase-inhibiting (Saleh et al., 2021) properties. Extracts from its pods contain a higher antioxidant capacity than its seeds (Kamisah et al., 2013), likely associated with the pod's flavonoid and phenolic components, including gallic acid, quercetin, gossypetin, and catechin (Ko et al., 2014; Saleh et al., 2021). Experiments in hypertensive rats support the pods' hypotensive and cardioprotective properties (Kamisah et al., 2017). However, their effects on cardiomyocyte hypertrophy have yet to be investigated. As plant extracts with high flavonoid content have been shown to protect against cardiomyocyte hypertrophy (Sun et al., 2018; Cho et al., 2019), this study aimed to investigate the effects of *P. speciosa* empty pod extract on the Ang II/ROS/NO axis and MAPK signaling pathway in Ang II-treated cardiomyocytes.

MATERIALS AND METHODS

Materials

P. speciosa pods (**Figure 1**) were purchased from a local trader at Slim River, Perak, Malaysia (3°49′31.0″N 101°29′12.1″E) in January 2018. A voucher specimen (UKMB40383) was deposited at the Universiti Kebangsaan Malaysia Herbarium. H9c2 cardiomyocytes were obtained commercially (American Type Culture Collection, Rockville, MD, United States). All chemicals were purchased from Sigma-Aldrich (St. Louis, MO, United States), and all antibodies for Western blotting were purchased from Cell Signaling Technology (Danvers, MA, United States) unless otherwise noted.

Empty Pod Extraction

The pods were cleaned, deseeded, and dried at room temperature. The dried, empty pods were ground and extracted in 95% ethanol in a 100 g:1 L ratio at room temperature for 9 days (Ko et al., 2014), with the ethanol changed every 3 days to improve yield. The extract was then filtered through cotton wool, and the filtrate was concentrated with a rotary vacuum evaporator (Buchi Rotavapor R-200 System, Marshall Scientific, Hampton, NH, United States). After freeze-drying (Labconco, Kansas City, MO, United States) for 5 days, the powder was stored at 4°C.

Phytochemical Screening

Phytochemical screening was conducted using high-performance liquid chromatography (HPLC) following the method of Tuszyńska (2014) with some modifications. Briefly, *P. speciosa* extract powder was dissolved in 100% aqueous methanol (10 mg/ml) before filtering through a nylon membrane (0.45 µm) (#PP013045; Membrane Solutions, Auburn, WA, United States). Since hydrolyzed glycosides are not applicable for *in vitro* experiments, the extract was not subjected to acid hydrolysis. HPLC was performed on a C_{18} column (150 × 4.6 mm, 5 µm; Phenomenex, Torrance, CA) using a Waters Series 600 (Waters, Milford, MA) fitted with a photodiode array detector and an autosampler with an injection volume of 20 µl. The samples were isocratically eluted using 0.2% orthophosphoric acid in methanol/water (60/40) at 0.75 ml/min with detection at 370 nm. This procedure was repeated on three separate days (interday) with at least three replicates/day (intraday) to determine precision.

Peaks in the extract samples were compared to catechin (K4512), rutin (R5143), quercetin (Q4951), kaempferol (K0133), ellagic acid (E2250), gallic acid (27,645), and caffeic

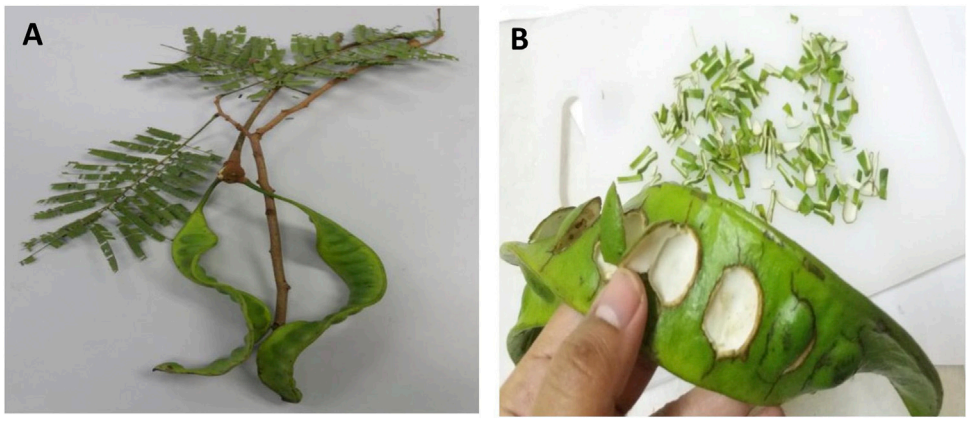

FIGURE 1 | (A) *Parkia speciosa* pods and **(B)** its slived deseeded pod.

acid (C0625) standards. The area under the curve (AUC) was calculated for five concentrations (62.5–1,000 μg/ml) of each standard run in triplicate and was used to prepare calibration curves. Fitted equations for the calibration curves were used to calculate the concentration of the compounds in *P. speciosa* extract.

H9c2 Cell Culture

H9c2 cells were cultured in Dulbecco's Modified Eagle Medium (DMEM; Gibco BRL Life Technologies, Grand Island, NY, United States) supplemented with 10% fetal bovine serum (FBS), 100 U/ml penicillin G, and 100 μg/ml streptomycin at 37°C in a humidified atmosphere containing 5% CO_2. The medium was changed every 2 d. The cells were grown to 60–70% confluency and serum-starved for 24 h prior to the experiment (Yan et al., 2013). Cells passaged 5–7 times and grown to a density of 1.6×10^4 cells/ml were used for the experiments.

Cytotoxicity Study

Cells were seeded in a 96-well plate and incubated with various concentrations of *P. speciosa* extract (3.125–400 μg/ml) for 24 h. Cell viability was assayed using 3-(4,5-dimethylthiazol-2-yl)-5-(3-carboxymethoxyphenyl)-2-(4-sulfophenyl)-2H-tetrazolium (MTS; Cat No: 197010, Abcam, Cambridge, United Kingdom) with detection at 490 nm. Dimethyl sulfoxide (DMSO) (<0.1%) was used as the vehicle for *P. speciosa* extract. A minimum of three biological replicates was performed in triplicate ($n = 3$).

Concentration-Response Study of *P. speciosa* Extract on H9c2 Cell Size

Cells were treated concurrently with Ang II (600 nM) (Siti et al., 2021) and various concentrations of *P. speciosa* extract (3.125–100 μg/ml) for 24 h in eight-well chamber slides. Cell size was measured using immunofluorescence staining. The best three extract concentrations for protecting against Ang II-induced cardiomyocyte hypertrophy were selected for further study. At least three biological replicates were performed in triplicate ($n = 3$).

Experimental Groups

H9c2 cells were randomly assigned to seven groups: 1) control (vehicle), 2) 50 μg/ml *P. speciosa* extract, 3) Ang II (600 nM; Siti et al., 2021), 4) Ang II and 12.5 μg/ml extract, 5) Ang II and 25 μg/ml extract, 6) Ang II and 50 μg/ml extract, and 7) Ang II and 20 μM valsartan (Al-Mazroua et al., 2013). Valsartan served as the positive control. Cells were treated concurrently with the extract and Ang II for 24 h.

Cell Size Quantification

Cell size was measured following the method of Jeong et al. (2015) with slight modifications described by Siti et al. (2021). Cells were stained with a primary antibody against α-actinin (1: 200 dilution; ab9465, Abcam, Cambridge, MA, United States) followed by an Alexa Fluor 488-conjugated anti-mouse secondary antibody (1:200 dilution; A-11059, Invitrogen, Waltham, MA, United States) and visualized via fluorescence microscopy (Olympus Optical, Tokyo, Japan). A blinded assessor quantified the cardiomyocytes' surface areas (>60 cells) using ImageJ software (U. S. National Institutes of Health, Bethesda, MD, United States) and compared them to control cells. A minimum of three biological replicates was performed in triplicate ($n = 3$).

Cellular B-Type Natriuretic Peptide and iNOS Levels

The cellular levels of B-type natriuretic peptide (BNP) and iNOS were estimated from cell lysates using commercial kits (Elabscience, Houston, TX, United States). Briefly, the biotinylated detection antibody and samples were incubated in micro-ELISA wells precoated with BNP or rat NOS2/iNOS antibodies, excess conjugates were removed, and an avidin-horseradish peroxidase (HRP) conjugate was added to develop a blue color. Upon addition of a stop solution, a yellow color change occurred, which was measured at 450 nm. BNP and

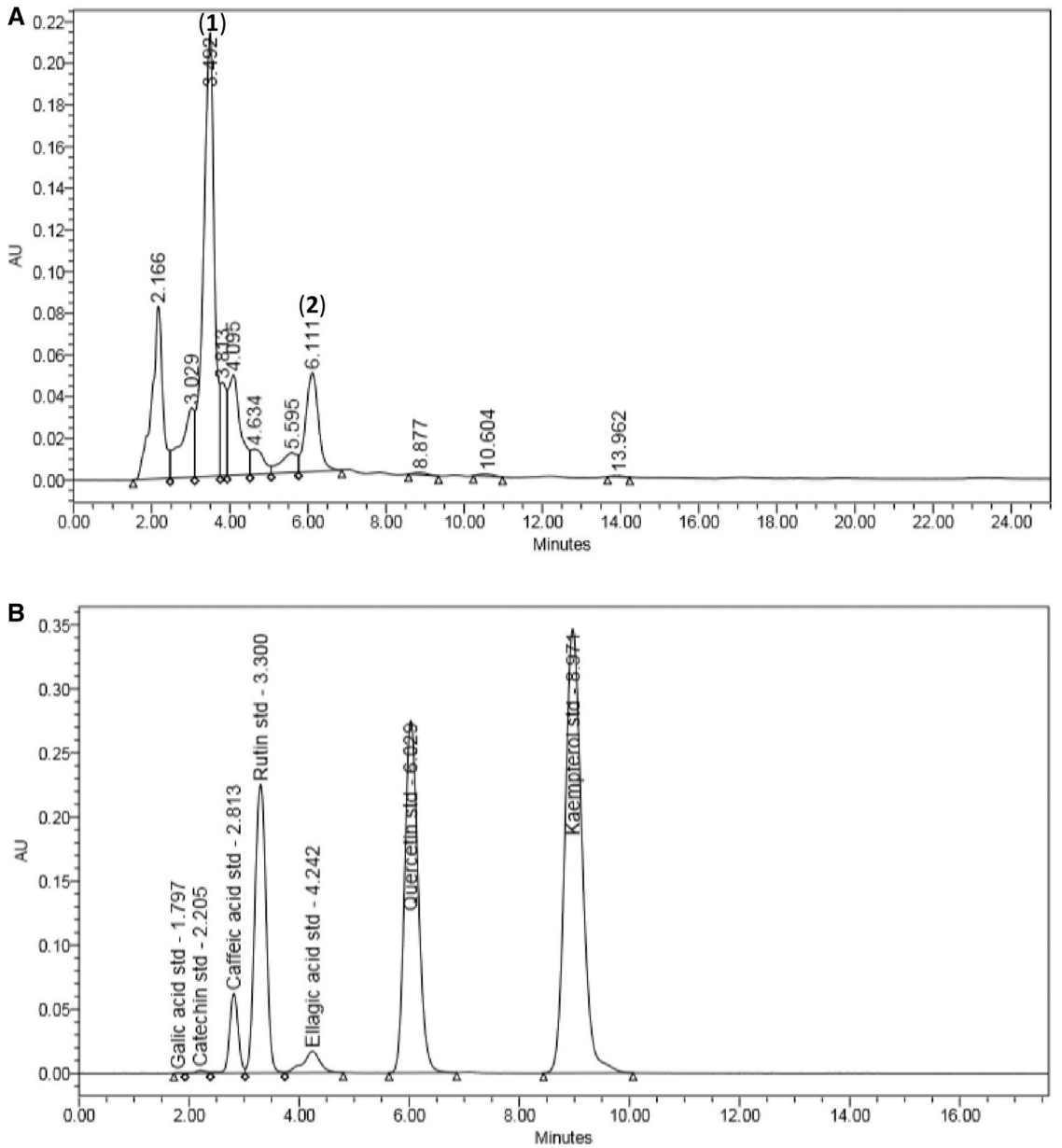

FIGURE 2 | Chromatographic analysis of **(A)** *Parkia speciosa* empty pod crude extract with detected rutin (**1**) and quercetin (**2**), and **(B)** the standard known compounds.

iNOS levels were estimated against standard curves. A minimum of three biological replicates was performed in triplicate (n = 3).

Cellular Nitrite and Intracellular ROS Detection

Nitrite, a stable metabolite of NO, was measured following the method described by Siti et al. (2019). Cardiomyocytes were seeded in 96-well plates. Sample cell lysate (50 µl) was reacted with an equal volume of modified Griess reagent for 15 min at room temperature in the dark. The absorbance was measured at 540 nm (EnSpire® Multimode Plate Reader, PerkinElmer, Inc., MA, United States) and compared to a sodium nitrite standard curve to determine nitrite concentrations.

Global levels of ROS, including peroxynitrite and superoxide, were assessed in living cells using a commercial kit (ROS-ID® Total ROS/Superoxide Detection Kit, ENZ-51010, Enzo, NY, United States) according to the manufacturer's protocol. Fluorescence signals were measured at 488 nm using a microplate reader (EnSpire® Multimode Plate Reader, PerkinElmer, Inc., MA, United States).

At least three biological replicates were performed in triplicate (n = 3) for all experiments.

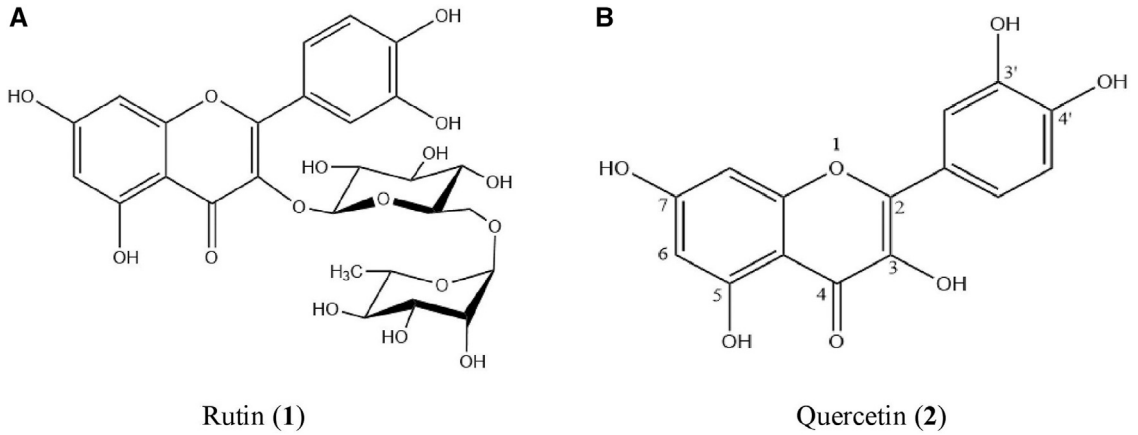

FIGURE 3 | The structure of **(A)** rutin (**1**) and **(B)** quercetin (**2**).

TABLE 1 | Retention time (t_R) of quercetin and rutin in 10 mg *Parkia speciosa* crude extract compared to standard compounds.

	Retention time, t_R (min)	
Sample	Quercetin	Rutin
Standard	6.168 ± 0.070	3.348 ± 0.025
P. speciosa extract	6.461 ± 0.171	3.551 ± 0.064

Values reported as mean ± SEM (n = 3). Each sample was measured at least three times on three different days.

NOX and Superoxide Dismutase Activities

NOX activity was measured according to the method described by Mustapha et al. (2010). Briefly, cell lysate (50 µg protein/sample), cytochrome *c* (250 µg/L), and NADPH (100 µM) were incubated at 37°C for 2 h with or without diphenyleneiodonium (DPI, 100 µM). The absorbance of the mixture was quantified at 550 nm. NOX activity was calculated using an extinction coefficient of 21 $mMcm^{-1}$.

Superoxide dismutase (SOD) activity (U/mg of protein) was measured according to the procedure of Beyer and Fridovich (1987). Sample cell lysate (20 µl) and riboflavin (10 µl, 50 µM) were added into an assay mixture containing 27 ml of phosphate buffer (pH 7.8, 50 mM), EDTA (50 µM), 1.5 ml of L-methionine (20 mM), and 1 ml of nitroblue tetrazolium (1.5 mM). The mixture was illuminated for 7 min in an aluminum foil-coated box equipped with a 40 W fluorescent bulb, and absorbance was measured at 550 nm.

At least three biological replicates were performed in triplicate (n = 3) for all experiments.

Western Blot Analysis

Protein expression was measured by Western blot as previously described (Siti et al., 2021). Anti-phospho-ERK1/2 rabbit polyclonal (1:1,000) (#4377), anti-phospho-JNK1/2 rabbit monoclonal (1:1,000) (#4668), and anti-phospho-p38 mouse monoclonal (1:500) (sc-166182; Santa Cruz Biotechnology, Dallas, TX, United States) were the primary antibodies used in this study. β-Actin mouse monoclonal antibodies (1:500) (sc-47778; Santa Cruz Biotechnology, Dallas, TX, United States) served as the loading control. HRP-conjugated IgG anti-mouse (1:2000) (sc-516102; Santa Cruz Biotechnology, Dallas, TX, United States) was used as the secondary antibody. Blots were visualized on a gel doc system and analyzed with ImageJ software (U. S. National Institutes of Health, Bethesda, MD, United States). A minimum of three biological replicates was performed in triplicate (n = 3).

Statistical Analysis

All data are reported as mean ± standard error of the mean (SEM) from a minimum of three biological replicates performed in triplicate. The Shapiro-Wilk test was used to test for normality. Results were analyzed using one-way analysis of variance (ANOVA) followed by Tukey's post hoc test in SPSS version 24.0 software (IBM Corp., Armonk, NY, United States), with $p < 0.05$ considered significant.

RESULTS

Phytochemical Screening of the Extract

There were 11 peaks detected in the sample extract chromatogram (**Figure 2A**). Two peaks were identified as rutin (**1**) and quercetin (**2**) (**Figure 3**) when compared against the peaks of the standards (**Figure 2B**). The remaining compounds could not be unequivocally identified owing to peak shape (blunted or multiple peaks). The retention time (t_R) for rutin (1) and quercetin (2) in the extract resembled that of the standards (**Table 1**). Based on the rutin and quercetin calibration curves (**Figure 4**), the *P. speciosa* empty pod crude ethanolic extract contained 15.5 µg rutin/mg extract (**1**) and 0.11 µg quercetin/mg extract (**2**) (**Table 2**).

Extract Cytotoxicity

Treatment with 0.1% DMSO alone had no effect on cell viability as compared to the control (data not shown), indicating that its use as a vehicle for *P. speciosa* extract did not contribute to cytotoxicity. The median inhibitory concentration (IC_{50}) of the

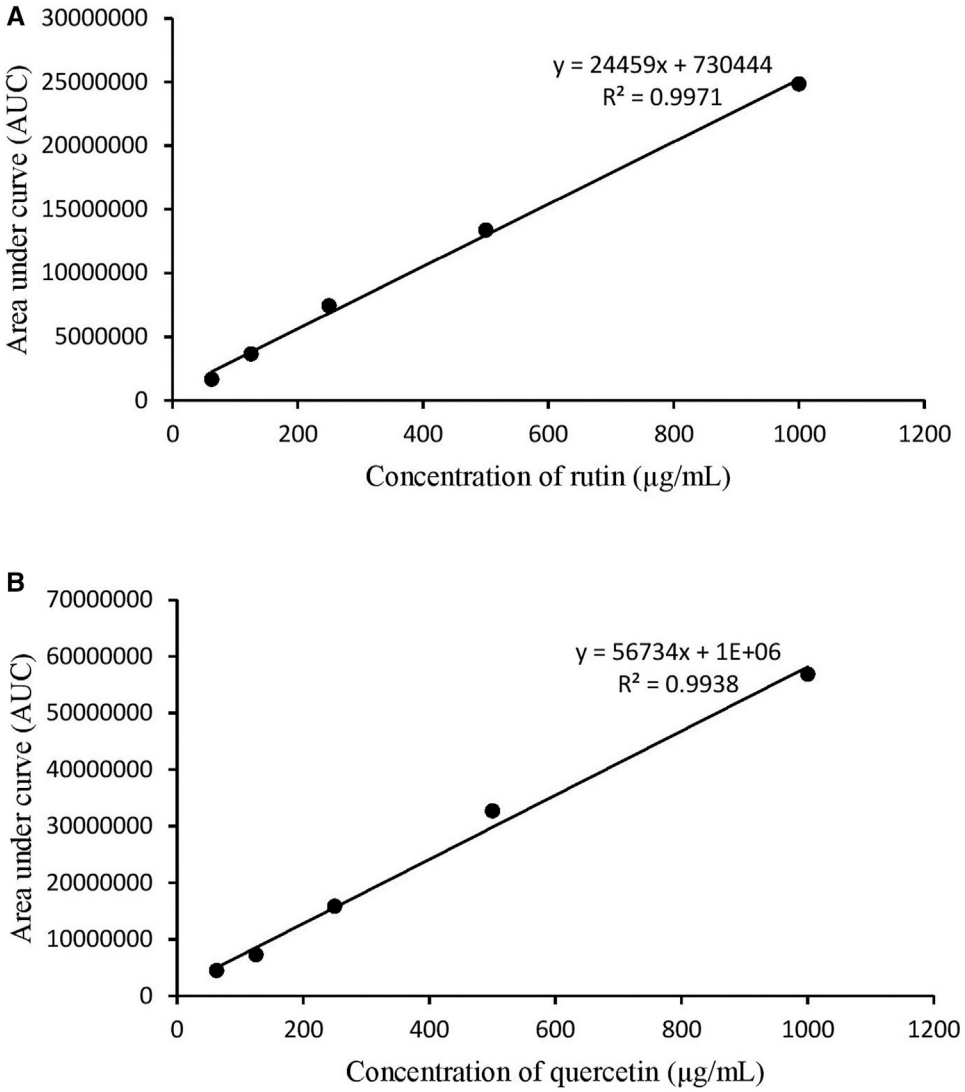

FIGURE 4 | Calibration curves for **(A)** rutin and **(B)** quercetin.

TABLE 2 | Concentration of quercetin and rutin in 10 mg *Parkia speciosa* crude extract.

	Area under the curve	Concentration (μg/ml)	Percentage (%)
Rutin	4,603,554 ± 250,,072	158.35 ± 7.02	1.58
Quercetin	1,168,863 ± 86,994	20.60 ± 1.53	0.21

Values reported as mean ± SEM (n = 3). Each sample was measured at least three times on three different days.

extract was approximately 108.35 μg/ml (**Figure 5**). Subsequent experiments used sub-IC_{50} extract concentrations.

Optimizing Extract Concentration for Antihypertrophic Activity

Ang II-induced cardiomyocyte hypertrophy was significantly alleviated with 6.25, 12.5, 25, and 50 μg/ml extract (**Figure 6**). Cell size was significantly reduced at 100 μg/ml extract compared to both the control and Ang II treatments ($p < 0.05$). Based on these findings, 12.5, 25, and 50 μg/ml extract were used in the subsequent experiments.

Cell Size and BNP Levels

Ang II-treated cells showed a significant increase in cell size (1.52 ± 0.04 times) and cellular BNP levels (50.49 ± 1.16 ng/mg

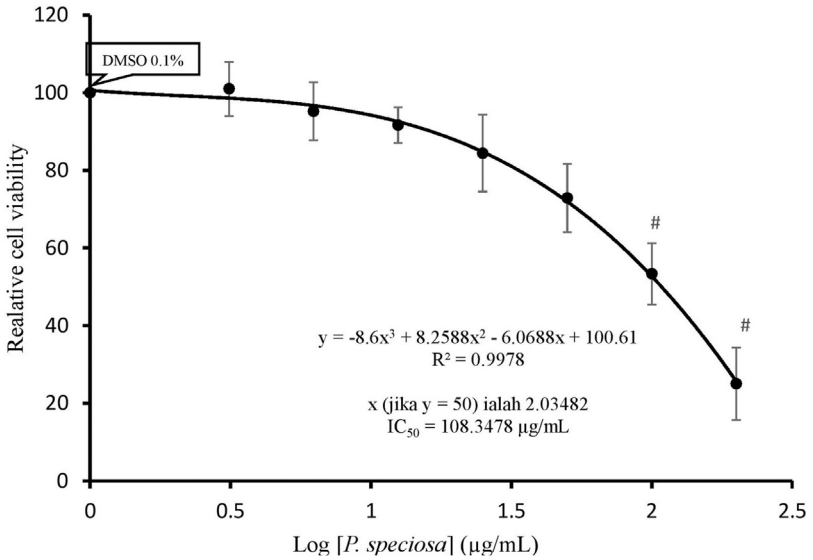

FIGURE 5 | Cell viability of H9c2 cells after 24 h exposure to *Parkia speciosa* empty pod extract at increasing concentrations. *$p < 0.05$ vs. control. Results are presented as the mean ± SEM ($n = 3$).

protein) compared to the control (27.29 ± 2.08 ng/mg protein) (**Figure 7**). Treatment with valsartan or the selected extract concentrations significantly reduced Ang II-induced changes in cell size and BNP levels ($p < 0.05$). There were no significant differences in these effects across the three extract concentrations or valsartan treatments. Treatment with 50 µg/ml extract alone did not significantly affect cell size or BNP levels.

Intracellular ROS Levels and NOX and SOD Activities

While Ang II significantly increased the intracellular ROS levels and NOX activity and decreased the SOD activity in H9c2 cells compared to the control (**Figures 8A–C**), co-treatment with valsartan or the selected extract concentrations prevented these effects. There were no significant differences in intracellular ROS levels across the three extract concentrations. SOD activity was rescued similarly across all treatments. Treatment with 50 µg/ml extract alone did not significantly affect these parameters.

Cellular iNOS and Nitrite Levels

Ang II significantly increased H9c2 cellular iNOS levels (0.016 ± 0.002 pg/mg protein, $p < 0.05$) compared to the control (0.008 ± 0.001 pg/mg protein) (**Figure 9A**). While co-treatment with *P. speciosa* empty pod extract did not prevent this change, iNOS levels were rescued with valsartan ($p < 0.05$). Exposure to Ang II significantly reduced H9c2 cellular nitrite levels (18.96 ± 3.49 mM/mg protein, $p < 0.05$) compared to the control (31.79 ± 4.29 mM/mg protein) (**Figure 9B**). Neither valsartan nor the selected extract concentrations significantly prevented this change ($p > 0.05$). Treatment with 50 µg/ml extract alone did not significantly affect these parameters.

MAPK Protein Expression

After 24 h, Ang II-treated H9c2 cells expressed elevated levels of phosphorylated ERK1/2, p38, and JNK ($p < 0.05$) (**Figure 10**). Co-treatment with all three selected extract concentrations prevented these elevated levels to a similar extent, while valsartan only rescued *p*-JNK expression. Treatment with 50 µg/ml extract alone did not significantly affect MAPK protein expression.

DISCUSSION

Exposure to Ang II induced an ROS/NO axis imbalance, apparent in augmented intracellular superoxide/ROS ($O_2^{-\bullet}$/ROS) levels, increased NOX and iNOS activities, and decreased SOD activity. This imbalance led to cardiomyocyte hypertrophy, which manifested in increased cell size and elevated BNP levels, indicative of ventricular dysfunction. Ang II is reported to promote cardiac hypertrophy by stimulating growth factors (Ding et al., 2019). The findings of this study confirm previous reports regarding the involvement of oxidative stress in the development of Ang II-induced cardiomyocyte hypertrophy (Guan et al., 2017; Hong et al., 2019). Binding of Ang II to the Ang II type 1 receptor (AT_1R) enhances the activation of NOX (Masi et al., 2019), which is a substantial producer of ROS, including $O_2^{-\bullet}$ (Wen et al., 2019). The elevated levels of $O_2^{-\bullet}$ detected in the H9c2 cells depleted the antioxidant SOD, which functions as a first line of defense against cardiomyocyte hypertrophy by converting the radical anion into water and hydrogen peroxide (Campos-Shimada et al., 2020).

The detrimental effects of Ang II on the ROS/NO axis were prevented by co-treating with *P. speciosa* empty pod extract.

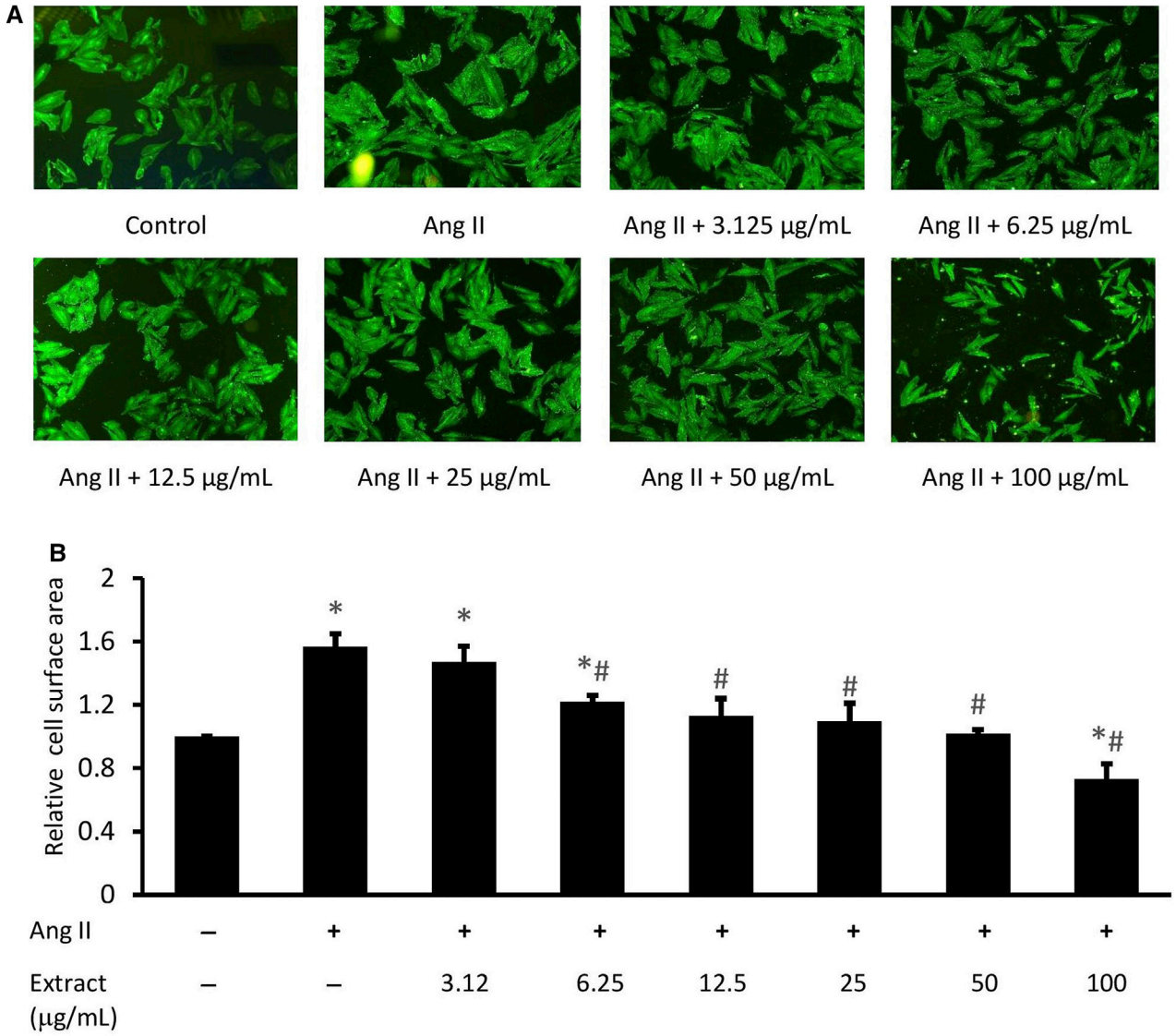

FIGURE 6 | Effect of various concentrations of *Parkia speciosa* empty pod extract on cell size in H9c2 cells exposed to Ang II (600 nM) for 24 h. **(A)** Representative immunofluorescent image (magnification × 100) and **(B)** quantitative analysis of immunofluorescent cells. *$p < 0.05$ vs. control (no treatment) group. #$p < 0.05$ vs. Ang II group. Bars represent the mean ± SEM ($n = 3$).

Notably, the cardioprotective effects of the extract were not concentration-dependent. These findings highlight the extract's antioxidant properties, in agreement with previous work (Kamisah et al., 2017; Gui et al., 2019b). The empty pod extract was employed in this study as it is reported to contain a higher antioxidant capacity than the seed extract (Kamisah et al., 2013; Zaini and Mustaffa 2017). The cardioprotective effects of the extract are likely associated with its flavonoid content, with rutin (**1**) and quercetin (**2**) identified among its primary metabolites in this work. Studies have reported the presence of other flavonoids (Ko et al., 2014; Ghasemzadeh et al., 2018) not detected in this work, likely due to differences in chromatographic analysis. HPLC analysis in this study was unable to identify the remaining contents in the extract unambiguously, which may have included other flavonoids and phenolic acids. As these other metabolites could play a role in the cardioprotective effects of *P. speciosa* extract, additional studies should focus on their identification. The purpose of identifying the metabolites in this study was to aid in understanding how the extract could provide its cardioprotective effects. To determine the specific mechanisms by which the extract prevents cardiomyocyte hypertrophy, studies should investigate the activity of the individual extract components. For example, previous work using commercial quercetin and rutin demonstrated their antioxidant and antihypertrophic activities in Ang II-treated cardiomyocytes (Siti et al., 2021). Flavonoids, such as quercetin and rutin, can exert their antioxidant effects by binding SOD and increasing its

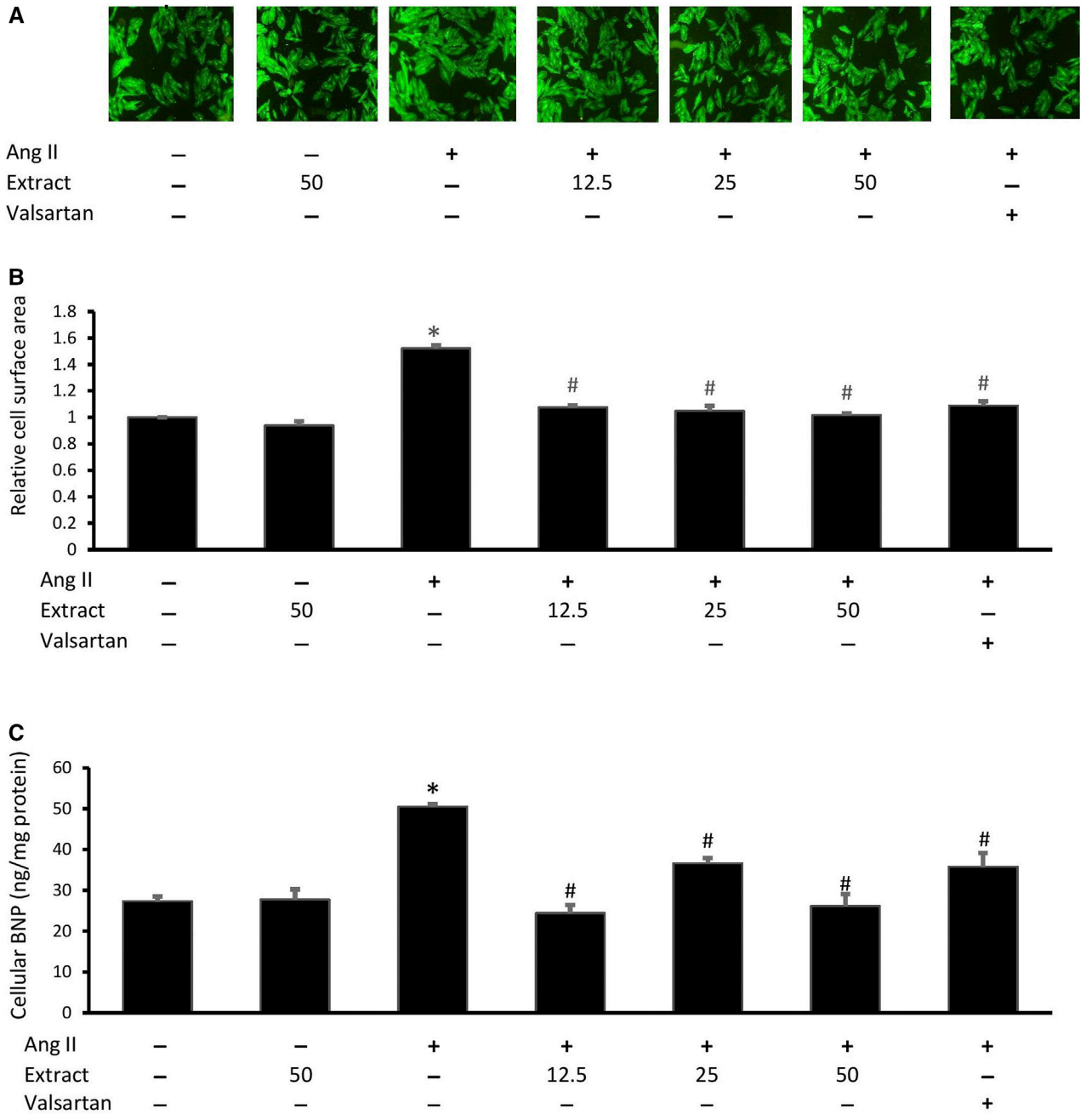

FIGURE 7 | Effect of *Parkia speciosa* empty pod extract (μg/ml) or valsartan (20 μM, positive control) co-incubation on Ang II (600 nM)-induced H9c2 cell hypertrophy seen in **(A)** representative immunofluorescent-stained cells (magnification × 100), **(B)** cell surface area, and **(C)** B-type natriuretic peptide (BNP) after 24 h *$p < 0.05$ vs. control (no treatment) group. #$p < 0.05$ vs. Ang II group. Results are presented as the mean ± SEM ($n = 3$).

activity (Cos et al., 1998; Zhuang et al., 2016). Metabolites in the extract may also directly prevent the prooxidant effects of Ang II itself.

Another source of cellular ROS is iNOS, which is upregulated in response to increased microenvironmental inflammation (Cinelli et al., 2020). Ang II was found to activate iNOS activity in this work, consistent with previous findings (Restini et al., 2017). Ang II promotes inflammation via activation of the NF-κB signaling pathway and the release of tumor necrosis factor-α (TNFα) and interleukin 6 (Huang et al., 2017). However, this study found that despite increasing iNOS activity, exposure to Ang II decreased NO levels. NO can react with $O_2^{-\bullet}$ to generate peroxynitrite radicals (Radi, 2018), reducing its own level. Co-treatment with the extract did not prevent the harmful effects of Ang II on iNOS activity or NO levels. However, ethyl acetate fractions of the extract have been

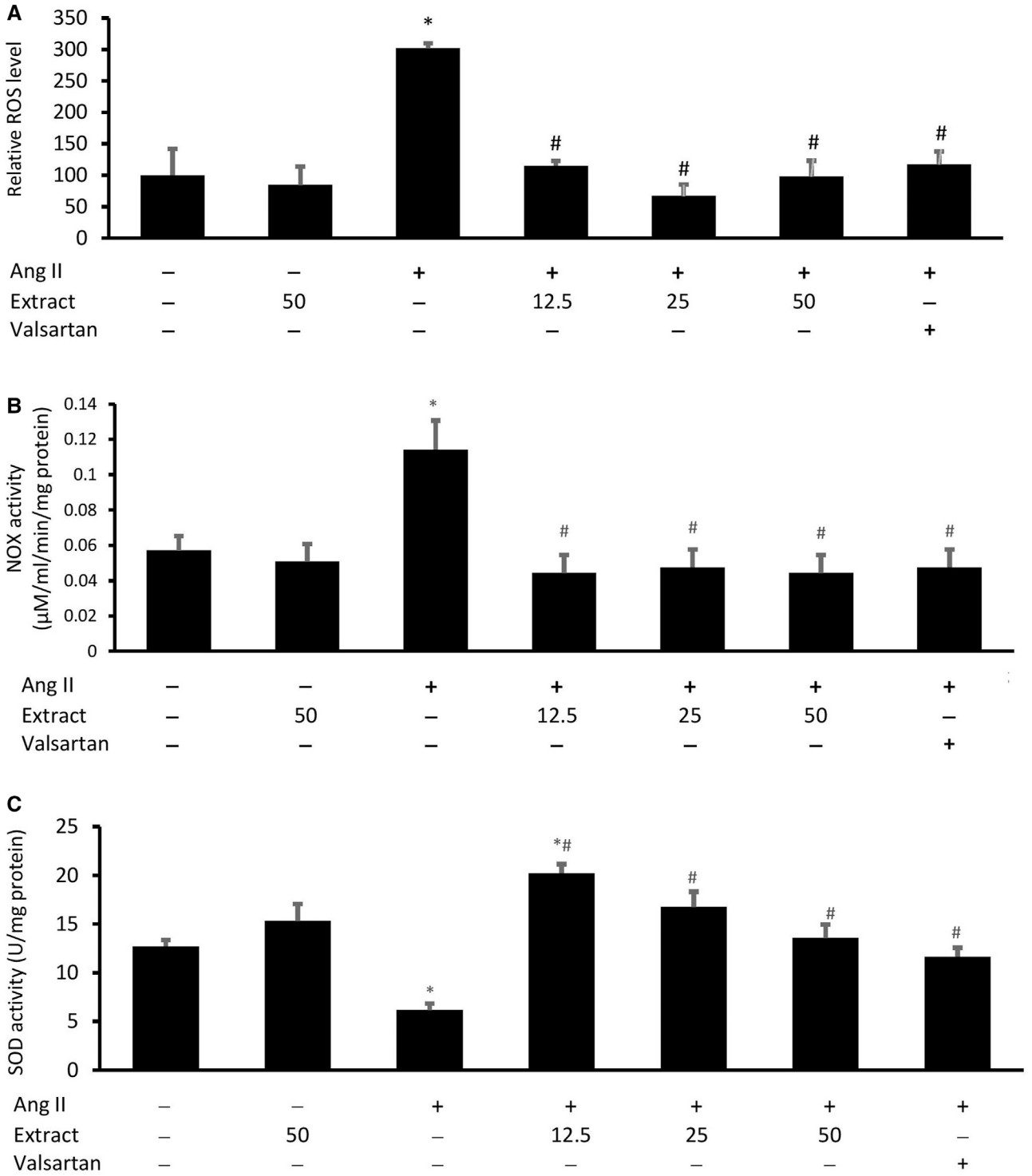

FIGURE 8 | (A) Cellular reactive oxygen species (ROS) level, **(B)** NADPH oxidase (NOX) activities, and **(C)** superoxide dismutase (SOD) activities in cells co-treated with Ang II (600 nM) and three concentrations of *Parkia speciosa* extract (μg/ml) or valsartan (20 μM, positive control) for 24 h *$p < 0.05$ vs. control (no treatment) group. #$p < 0.05$ vs. Ang II group. Bars represent means ± SEM ($n = 3$).

reported to reduce both parameters in cardiomyocytes and human umbilical vein endothelial cells exposed to TNFα (Mustafa et al., 2018; Gui JS. et al., 2019). The discrepancy between these findings could stem from differences in the models and the type of fraction used. Rutin (50 μM) and quercetin (331 μM) have been reported to reverse the effects

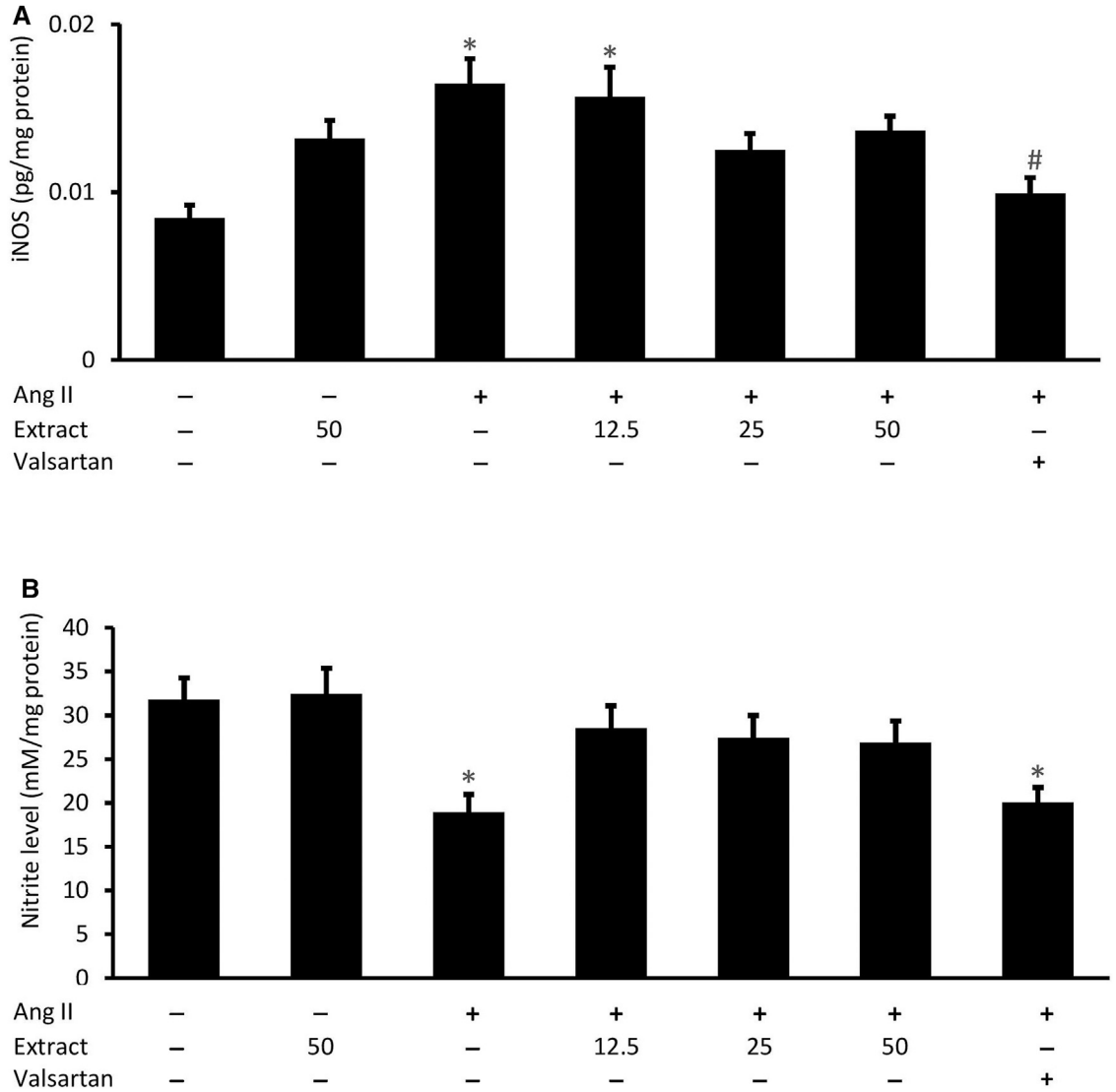

FIGURE 9 | Cellular **(A)** inducible nitric oxide synthase (iNOS) activity and **(B)** nitrite level in groups co-treated with Ang II (600 nM) and three concentrations of *Parkia speciosa* empty pod extract or valsartan (20 μM, positive control) for 24 h *$p < 0.05$ vs. control (no treatment) group. #$p < 0.05$ vs. Ang II cells. Bars represent means ± SEM ($n = 3$).

of Ang II on iNOS activity and NO levels (Siti et al., 2021). The highest concentration of extract used in this work (50 μg/ml) contained much lower concentrations of the flavonoids [0.790 μg/ml rutin (**1**) and 0.105 μg/ml quercetin (**2**)], possibly rationalizing the poor protection.

Valsartan was used as the positive control in this work due to its ability to reduce cardiomyocyte hypertrophy and BNP levels (Xu et al., 2015; Wu et al., 2017), as well as its use in the clinical management of heart failure (Vaduganathan et al., 2020). The antioxidant activity of valsartan has manifested in suppressed ROS levels (Chen et al., 2014; Tian et al., 2018). Valsartan displayed similar protective effects against Ang II-induced cardiomyocyte hypertrophy and oxidative stress in this study. It acts as an AT_1R blocker to prevent Ang II receptor activation and downstream pathological events. Valsartan demonstrated better anti-inflammatory properties than the extract in suppressing the negative effects of Ang II. Previous work reported similar beneficial effects of valsartan on iNOS expression (Mohammed et al., 2015).

Ang II treatment was found to increase the levels of phosphorylated ERK1/2, JNK1/2, and p38, consistent with previous studies (Sriramula and Francis, 2015; Yokota and Wang, 2016; Lu et al., 2020). Exposure to Ang II triggers signal transduction, which activates the MAPK cascade via phosphorylation of ERK1/2, JNK, and p38 prior to nuclear translocation. This leads to the activation of numerous transcription factors (Zhang et al., 2003), some of which regulate the expression of hypertrophic gene products, such as BNP (Nayer et al., 2014).

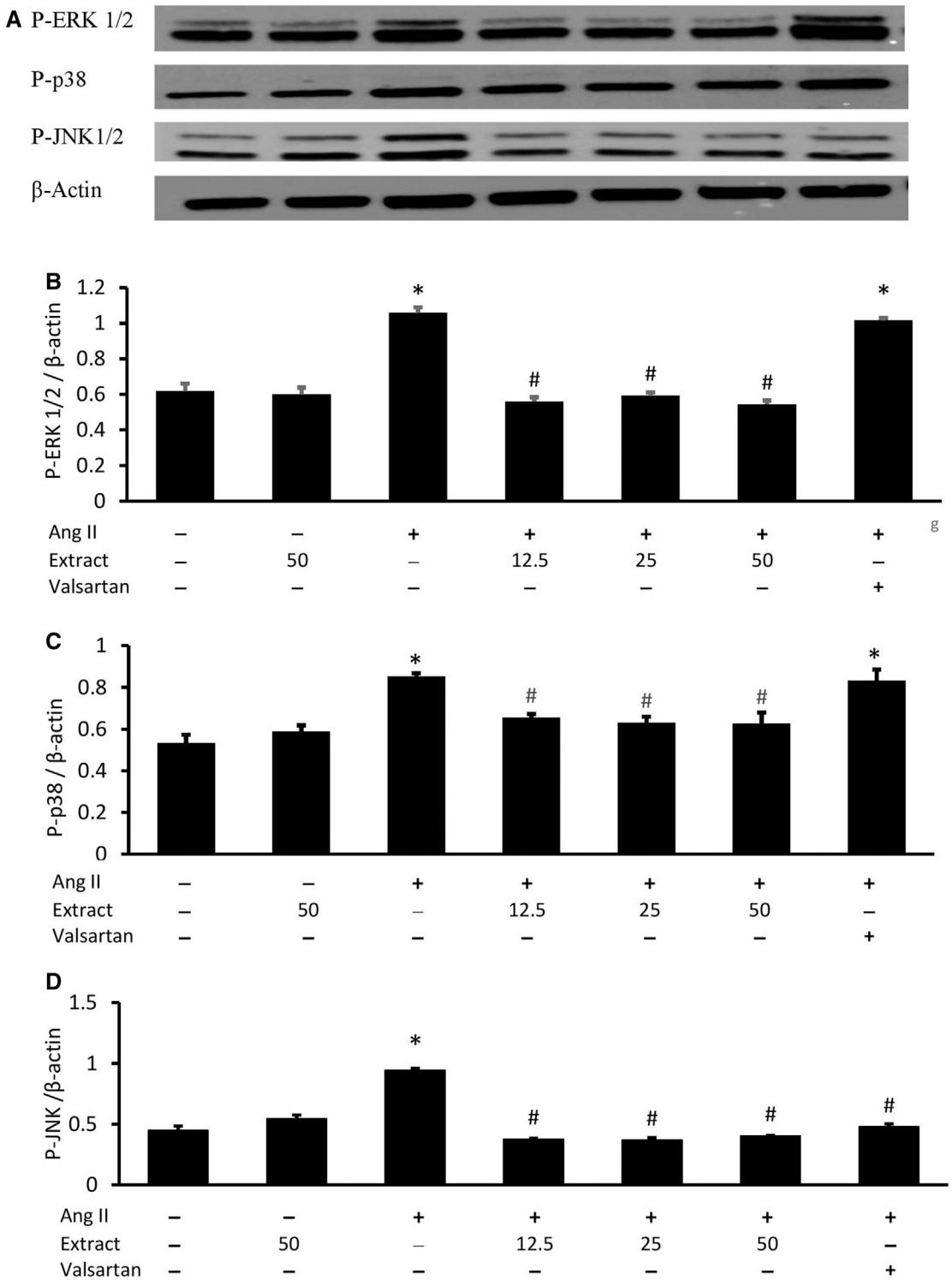

FIGURE 10 | Effects of *Parkia speciosa* empty pod extract and valsartan (20 μM, positive control) on **(A)** representative immunoblots via Western blot analysis, quantitative analysis of phosphorylated **(B)** extracellular signal-related kinases (P-ERK1/2), **(C)** p38 kinase (P-p38), and **(D)** c-Jun N-terminal kinases (P-JNK) protein expressions in H9c2 cells that were exposed to Ang II (600 nM) for 24 h *$p < 0.05$ vs. control (no treatment) group. #$p < 0.05$ vs. Ang II cells. Bars represent means ± SEM ($n = 3$).

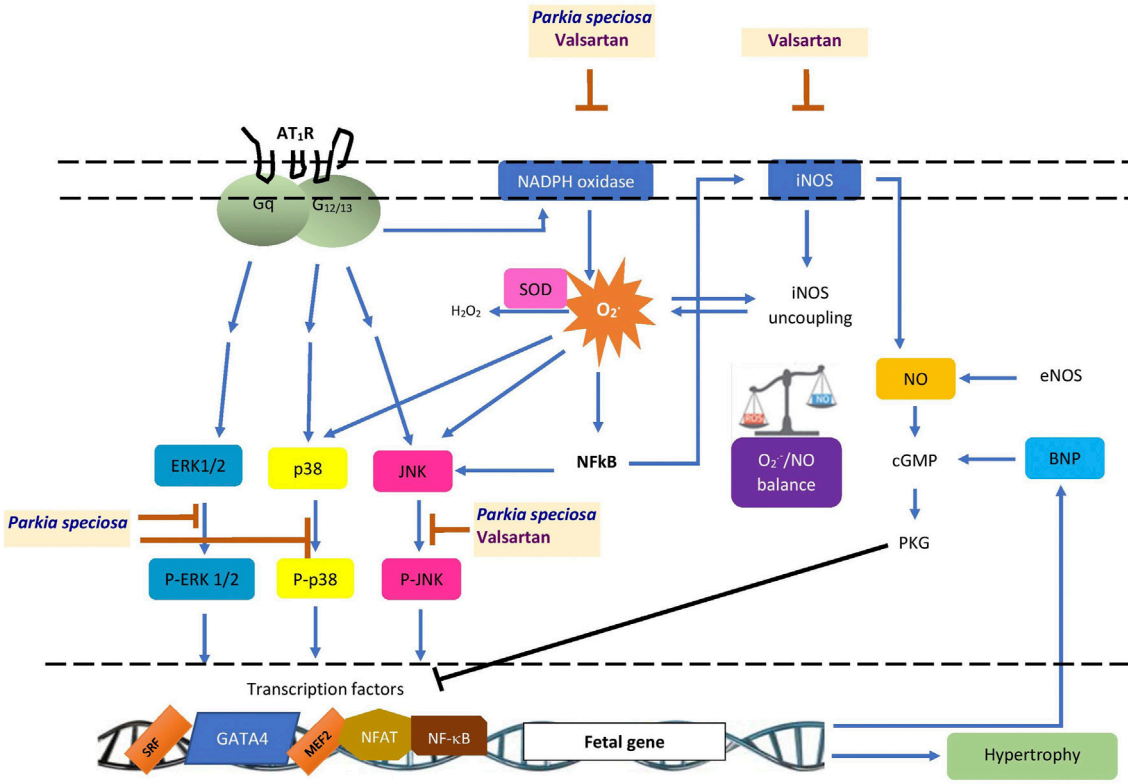

FIGURE 11 | Schematic summary of the possible site of cardioprotective effects of *Parkia speciosa* empty pod extract. AT_1R, angiotensin II type 1 receptor; BNP, B-type natriuretic peptide; cGMP, cyclic guanosine monophosphate; eNOS, endothelial nitric oxide synthase; ERK1/2, extracellular signal-related kinase; iNOS, inducible nitric oxide synthase; JNK, c-Jun N-terminal kinase; MEF2, myocyte enhancer factor-2; NFAT, nuclear factor of activated T-cells; NF-κB, nuclear factor kappa B; NO, nitric oxide; PKG, protein kinase G; p38, p38 kinase; P-ERK1/2, phosphorylated extracellular signal-related kinase (ERK1/2), P-JNK, phosphorylated c-Jun N-terminal kinase; P-p38, phosphorylated p38 kinase; SOD, superoxide dismutase; SRF, serum response factor; ⊥, inhibition.

Treatment with *P. speciosa* extract reduced the expression of P-ERK, P-p38, and P-JNK, suggesting that its antihypertrophic activity may function via modulation of the MAPK signaling pathway. The extract may prevent Ang II from binding AT_1R, suppressing downstream events leading to hypertrophy, although this requires further investigation. Quercetin (**2**) has been shown to block activation of the MAPK signaling pathway. As rutin (**1**) lacks this property (Siti et al., 2021), the inhibitory effects of the extract on the MAPK signaling pathway are most likely due to quercetin and/or other unidentified phytochemical contents. Nevertheless, both rutin and quercetin have been reported to ameliorate cardiac hypertrophy via multiple routes, including apoptosis, autophagy, and prohypertrophic pathways (Siti et al., 2020a; Siti et al., 2020b). Therefore, rutin may confer protection via mechanisms other than inhibition of MAPK signaling.

Apart from reducing P-JNK levels, valsartan had no effect on MAPK signaling. Similar effects have been reported for losartan, another AT_1R blocker, in a study on myocardial hypertrophy in hypertensive rats (Izumi et al., 2000). Valsartan has been shown to mitigate the Ang II-induced activation of p38, ERK1/2, and JNK in HL-1 cardiomyocytes (Liu et al., 2015). These contradictory findings could derive from differences in the types of cells or models used. The findings in this work suggest that the cardioprotective effect of valsartan on cardiomyocyte hypertrophy occurs via modulation of the Ang II/ROS/NO axis rather than regulation of the MAPK pathway.

Few studies apart from this one have investigated the cardioprotective potential of *P. speciosa* extract. This study demonstrated the protective effects of *P. speciosa* empty pod extract against Ang II-induced cardiomyocyte hypertrophy in H9c2 cells (**Figure 11**), and may support the traditional use of the plant in ameliorating cardiac problems. The antihypertrophic properties of the extract were investigated by cotreating cardiomyocytes with extract and Ang II. While this study presents promising findings, the antihypertrophic effects of the extract should be investigated as a post-treatment in future investigations. Results from this work suggest that the extract could be used as a supplement to ameliorate cardiac remodeling, although further studies are required before clinical use. Future research should also explore other possible mechanisms of action, such as the extract's effects on calcium regulatory proteins or other pathways, including the specificity protein-1/GATA binding protein-4 (Sp1/GATA4) or

phosphatidylinositol 3-kinase/protein kinase B/glycogen synthase kinase-3β (PI3K/Akt/GSK-3β) signaling pathways in hypertrophied cardiomyocytes.

CONCLUSION

P. speciosa empty pod extract afforded protection against Ang II-induced cardiomyocyte hypertrophy by mitigating oxidative stress and modulating the MAPK signaling pathway. These effects may be attributed to its rich rutin (**1**) and quercetin (**2**) content. Notably, the protective effects of the extract appear to occur via mechanisms distinct from valsartan.

DATA AVAILABILITY STATEMENT

The raw data supporting the conclusions of this article will be made available by the authors, without undue reservation.

AUTHOR CONTRIBUTIONS

HS performed the experiments, as well as wrote the article. JJ supervised the extraction and phytochemical screening. AA and YK supervised the study. All authors designed the study, revised the article and approved its submission.

FUNDING

This study received a funding from the Faculty of Medicine, Universiti Kebangsaan Malaysia (FF-2019-021).

ACKNOWLEDGMENTS

The authors would like to acknowledge technical assistance given by En Fadhlullah Zuhair Japar Sidik and Puan Juliana Abdul Hamid.

REFERENCES

Al-Mazroua, H. A., Al-Rasheed, N. M., and Korashy, H. M. (2013). Downregulation of the Cardiotrophin-1 Gene Expression by Valsartan and Spironolactone in Hypertrophied Heart Rats *In Vivo* and Rat Cardiomyocyte H9c2 Cell Line *In Vitro*: A Novel Mechanism of Cardioprotection. *J. Cardiovasc. Pharmacol.* 61 (4), 337–344. doi:10.1097/FJC.0b013e318283a565

Azliza, M. A., Ong, H. C., Vikineswary, S., Noorlidah, A., and Haron, N. W. (2012). Ethno-medicinal Resources Used by the Temuan in Ulu Kuang Village. *Stud. Ethno-Medicine* 6 (1), 17–22. doi:10.1080/09735070.2012.11886415

Bernardo, B. C., and McMullen, J. R. (2016). Molecular Aspects of Exercise-Induced Cardiac Remodeling. *Cardiol. Clin.* 34 (4), 515–530. doi:10.1016/j.ccl.2016.06.002

Beyer, W. F., and Fridovich, I. (1987). Assaying for Superoxide Dismutase Activity: Some Large Consequences of Minor Changes in Conditions. *Anal. Biochem.* 161 (2), 559–566. doi:10.1016/0003-2697(87)90489-1

Campos-Shimada, L. B., Hideo Gilglioni, E., Fernandes Garcia, R., Rizato Martins-Maciel, E., Luiza Ishii-Iwamoto, E., and Luzia Salgueiro-Pagadigorria, C. (2020). Superoxide Dismutase: a Review and a Modified Protocol for Activities Measurements in Rat Livers. *Arch. Physiol. Biochem.* 126 (4), 292–299. doi:10.1080/13813455.2018.1520891

Chen, G., Pan, S. Q., Shen, C., Pan, S. F., Zhang, X. M., and He, Q. Y. (2014). Puerarin Inhibits Angiotensin II-Induced Cardiac Hypertrophy via the Redox-Sensitive ERK1/2, P38 and NF-Kb Pathways. *Acta Pharmacol. Sin.* 35 (4), 463–475. doi:10.1038/aps.2013.185

Chen, Y., Ge, Z., Huang, S., Zhou, L., Zhai, C., Chen, Y., et al. (2020). Delphinidin Attenuates Pathological Cardiac Hypertrophy via the AMPK/NOX/MAPK Signaling Pathway. *Aging (Albany NY)* 12 (6), 5362–5383. doi:10.18632/aging.102956

Cheng, C. I., Lee, Y. H., Chen, P. H., Lin, Y. C., Chou, M. H., and Kao, Y. H. (2017). Cobalt Chloride Induces RhoA/ROCK Activation and Remodeling Effect in H9c2 Cardiomyoblasts: Involvement of PI3K/Akt and MAPK Pathways. *Cell Signal* 36, 25–33. doi:10.1016/j.cellsig.2017.04.013

Chiang, J. T., Badrealam, K. F., Shibu, M. A., Kuo, C. H., Huang, C. Y., Chen, B. C., et al. (2018). *Eriobotrya Japonica* Ameliorates Cardiac Hypertrophy in H9c2 Cardiomyoblast and in Spontaneously Hypertensive Rats. *Environ. Toxicol.* 33 (11), 1113–1122. doi:10.1002/tox.22589

Cho, S., Cho, H. W., Woo, K. W., Jeong, J., Lim, J., Park, S., et al. (2019). *Nelumbo nucifera* Receptaculum Extract Suppresses Angiotensin II-Induced Cardiomyocyte Hypertrophy. *Molecules* 24 (9), 1647. doi:10.3390/molecules24091647

Cinelli, M. A., Do, H. T., Miley, G. P., and Silverman, R. B. (2020). Inducible Nitric Oxide Synthase: Regulation, Structure, and Inhibition. *Med. Res. Rev.* 40 (1), 158–189. doi:10.1002/med.21599

Cos, P., Ying, L., Calomme, M., Hu, J. P., Cimanga, K., Van Poel, B., et al. (1998). Structure-activity Relationship and Classification of Flavonoids as Inhibitors of Xanthine Oxidase and Superoxide Scavengers. *J. Nat. Prod.* 61 (1), 71–76. doi:10.1021/np970237h

Ding, J., Tang, Q., Luo, B., Zhang, L., Lin, L., Han, L., et al. (2019). Klotho Inhibits Angiotensin II-Induced Cardiac Hypertrophy, Fibrosis, and Dysfunction in Mice through Suppression of Transforming Growth Factor-B1 Signaling Pathway. *Eur. J. Pharmacol.* 859, 172549. doi:10.1016/j.ejphar.2019.172549

Ghasemzadeh, A., Jaafar, H. Z. E., Bukhori, M. F. M., Rahmat, M. H., and Rahmat, A. (2018). Assessment and Comparison of Phytochemical Constituents and Biological Activities of Bitter Bean (Parkia Speciosa Hassk.) Collected from Different Locations in Malaysia. *Chem. Cent. J.* 12 (1), 12. doi:10.1186/s13065-018-0377-6

Guan, X. H., Hong, X., Zhao, N., Liu, X. H., Xiao, Y. F., Chen, T. T., et al. (2017). CD38 Promotes Angiotensin II-Induced Cardiac Hypertrophy. *J. Cel. Mol. Med.* 21 (8), 1492–1502. doi:10.1111/jcmm.13076

Gui, J. S., Jalil, J., Jubri, Z., and Kamisah, Y. (2019a). Parkia Speciosa Empty Pod Extract Exerts Anti-inflammatory Properties by Modulating NFκB and MAPK Pathways in Cardiomyocytes Exposed to Tumor Necrosis Factor-α. *Cytotechnology* 71, 79–89. doi:10.1007/s10616-018-0267-8

Gui, J. S., Mustafa, N., Jalil, J., Jubri, Z., and Kamisah, Y. (2019b). Modulation of NOX4 and MAPK Signalling Pathways by *Parkia Speciosa* Empty Pods in H9c2 Cardiomyocytes Exposed to H_2O_2. *Indian J. Pharm. Sci.* 81, 1029–1035. doi:10.36468/pharmaceutical-sciences.600

Hong, E. Y., Kim, T. Y., Hong, G. U., Kang, H., Lee, J. Y., Park, J. Y., et al. (2019). Inhibitory Effects of Roseoside and Icariside E4 Isolated from a Natural Product Mixture (No-Ap) on the Expression of Angiotensin Ii Receptor 1 and Oxidative Stress in Angiotensin II-Stimulated H9C2 Cells. *Molecules* 24 (3), 414. doi:10.3390/molecules24030414

Huang, X., Wang, Y., Zhang, Z., Wang, Y., Chen, X., Wang, Y., et al. (2017). Ophiopogonin D and EETs Ameliorate Ang II-Induced Inflammatory Responses via Activating PPARα in HUVECs. *Biochem. Biophys. Res. Commun.* 490 (2), 123–133. doi:10.1016/j.bbrc.2017.06.007

Izumi, Y., Kim, S., Zhan, Y., Namba, M., Yasumoto, H., and Iwao, H. (2000). Important Role of Angiotensin II-Mediated C-Jun NH(2)-terminal Kinase Activation in Cardiac Hypertrophy in Hypertensive Rats. *Hypertension* 36 (4), 511–516. doi:10.1161/01.hyp.36.4.511

Jeong, M. H., Kim, S. J., Kang, H., Park, K. W., Park, W. J., Yang, S. Y., et al. (2015). Cucurbitacin I Attenuates Cardiomyocyte Hypertrophy via Inhibition of Connective Tissue Growth Factor (CCN2) and TGF-β/Smads Signalings. *PLoS One* 10, e0136236. doi:10.1371/journal.pone.0136236

Kamisah, Y., Othman, F., Qodriyah, H. M., and Jaarin, K. (2013). Parkia Speciosa Hassk.: A Potential Phytomedicine. *Evid. Based Complement. Alternat Med.* 2013, 709028. doi:10.1155/2013/709028

Kamisah, Y., Zuhair, J. S. F., Juliana, A. H., and Jaarin, K. (2017). *Parkia Speciosa* Empty Pod Prevents Hypertension and Cardiac Damage in Rats Given N(G)-nitro-L-arginine Methyl Ester. *Biomed. Pharmacother.* 96, 291–298. doi:10.1016/j.biopha.2017.09.095

Ko, H.-J., Ang, L.-H., and Ng, L.-T. (2014). Antioxidant Activities and Polyphenolic Constituents of Bitter BeanParkia Speciosa. *Int. J. Food Properties* 17 (9), 1977–1986. doi:10.1080/10942912.2013.775152

Liu, L., Geng, J., Zhao, H., Yun, F., Wang, X., Yan, S., et al. (2015). Valsartan Reduced Atrial Fibrillation Susceptibility by Inhibiting Atrial Parasympathetic Remodeling through MAPKs/Neurturin Pathway. *Cell. Physiol. Biochem.* 36 (5), 2039–2050. doi:10.1159/000430171

Lu, Y., Sun, X., Peng, L., Jiang, W., Li, W., Yuan, H., et al. (2020). Angiotensin II-Induced Vascular Remodeling and Hypertension Involves Cathepsin L/V-MEK/ERK Mediated Mechanism. *Int. J. Cardiol.* 298, 98–106. doi:10.1016/j.ijcard.2019.09.070

Masi, S., Uliana, M., and Virdis, A. (2019). Angiotensin II and Vascular Damage in Hypertension: Role of Oxidative Stress and Sympathetic Activation. *Vascul Pharmacol.* 115, 13–17. doi:10.1016/j.vph.2019.01.004

Mohammed, H. E., Askar, M. E., Ali, S. I., and Fathy, O. M. (2015). Effect of Rennin Inhibitors and Sngiotensin II Receptor Antagonists on Left Ventricular Hypertrophy in Renovascular Hypertensive Rats. *Int. J. Pharm. Pharm. Sci.* 7 (9), 292–298.

Muslin, A. J. (2008). MAPK Signalling in Cardiovascular Health and Disease: Molecular Mechanisms and Therapeutic Targets. *Clin. Sci. (Lond)* 115 (7), 203–218. doi:10.1042/CS20070430

Mustafa, N. H., Ugusman, A., Jalil, J., and Kamisah, Y. (2018). Anti-inflammatory Property of *Parkia Speciosa* Empty Pod Extract in Human Umbilical Vein Endothelial Cells. *J. App Pharm. Sci.* 8, 152–158. doi:10.7324/JAPS.2018.8123

Mustapha, N. M., Tarr, J. M., Kohner, E. M., and Chibber, R. (2010). NADPH Oxidase versus Mitochondria-Derived ROS in Glucose-Induced Apoptosis of Pericytes in Early Diabetic Retinopathy. *J. Ophthalmol.* 2010, 746978. doi:10.1155/2010/746978

Nayer, J., Aggarwal, P., and Galwankar, S. (2014). Utility of point-of-care Testing of Natriuretic Peptides (Brain Natriuretic Peptide and N-Terminal Pro-brain Natriuretic Peptide) in the Emergency Department. *Int. J. Crit. Illn. Inj. Sci.* 4 (3), 209–215. doi:10.4103/2229-5151.141406

Nguyen Dinh Cat, A., Montezano, A. C., Burger, D., and Touyz, R. M. (2013). Angiotensin II, NADPH Oxidase, and Redox Signaling in the Vasculature. *Antioxid. Redox Signal.* 19 (10), 1110–1120. doi:10.1089/ars.2012.4641

Radi, R. (2018). Oxygen Radicals, Nitric Oxide, and Peroxynitrite: Redox Pathways in Molecular Medicine. *Proc. Natl. Acad. Sci. U S A.* 115, 5839–5848. doi:10.1073/pnas.1804932115

Restini, C. B. A., Garcia, A. F. E., Natalin, H. M., Natalin, G. M., and Rizzi, E. (2017). "Signaling Pathways of Cardiac Remodeling Related to Angiotensin II," in *Renin-Angiotensin System: Past, Present and Future*. Editor A. N. Tolekova. Rijeka, Croatia IntechOpen, 51–68. doi:10.5772/66076

Saleh, M. S. M., Jalil, J., Mustafa, N. H., Ramli, F. F., Asmadi, A. Y., and Kamisah, Y. (2021). UPLC-MS-Based Metabolomics Profiling for α-Glucosidase Inhibiting Property of Parkia Speciosa Pods. *Life* 11 (2), 78. doi:10.3390/life11020078

Siti, H. N., Jalil, J., Asmadi, A. Y., and Kamisah, Y. (2021). Rutin Modulates MAPK Pathway Differently from Quercetin in Angiotensin II-Induced H9c2 Cardiomyocyte Hypertrophy. *Int. J. Mol. Sci.* 22 (10), 5063. doi:10.3390/ijms22105063

Siti, H. N., Kamisah, Y., Mohamed, S., and Jaarin, K. (2019). Effects of Citrus Leaf Extract on Aortic Vascular Reactivity in Hypertensive Rats Fed Repeatedly Heated Vegetable Oil. *Appl. Physiol. Nutr. Metab.* 44 (4), 373–380. doi:10.1139/apnm-2018-0175

Siti, H. N., Jalil, J., Asmadi, A. Y., and Kamisah, Y. (2020b). Effects of Quercetin on Cardiac Function in Pressure Overload and Postischemic Cardiac Injury in Rodents: a Systematic Review and Meta-Analysis. *Cardiovasc. Drugs Ther* doi:10.1007/s10557-020-07100-y

Siti, H. N., Jalil, J., Asmadi, A. Y., and Kamisah, Y. (2020a). Roles of Rutin in Cardiac Remodeling. *J. Funct. Foods* 64, 103606. doi:10.1016/j.jff.2019.103606

Sriramula, S., and Francis, J. (2015). Tumor Necrosis Factor - Alpha Is Essential for Angiotensin II-Induced Ventricular Remodeling: Role for Oxidative Stress. *PLoS One* 10 (9), e0138372. doi:10.1371/journal.pone.0138372

Sun, S., Li, T., Jin, L., Piao, Z. H., Liu, B., Ryu, Y., et al. (2018). *Dendropanax Morbifera* Prevents Cardiomyocyte Hypertrophy by Inhibiting the Sp1/GATA4 Pathway. *Am. J. Chin. Med.* 46 (5), 1021–1044. doi:10.1142/S0192415X18500532

Takano, H., Zou, Y., Hasegawa, H., Akazawa, H., Nagai, T., and Komuro, I. (2003). Oxidative Stress-Induced Signal Transduction Pathways in Cardiac Myocytes: Involvement of ROS in Heart Diseases. *Antioxid. Redox Signal.* 5 (6), 789–794. doi:10.1089/152308603770380098

Tian, H., Yu, D., Hu, Y., Zhang, P., Yang, Y., Hu, Q., et al. (2018). Angiotensin II Upregulates Cyclophilin A by Enhancing ROS Production in Rat Cardiomyocytes. *Mol. Med. Rep.* 18 (5), 4349–4355. doi:10.3892/mmr.2018.9448

Tran, H. A., Lin, F., and Greenberg, B. H. (2016). Potential New Drug Treatments for Congestive Heart Failure. *Expert Opin. Investig. Drugs* 25 (7), 811–826. doi:10.1080/13543784.2016.1181749

Tuszyńska, M. (2014). Validation of the Analytical Method for the Determination of Flavonoids in Broccoli. *J. Hortic. Res.* 22 (1), 131–140. doi:10.2478/johr-2014-0016

Vaduganathan, M., Claggett, B. L., Desai, A. S., Anker, S. D., Perrone, S. V., Janssens, S., et al. (2020). Prior Heart Failure Hospitalization, Clinical Outcomes, and Response to Sacubitril/valsartan Compared with Valsartan in HFpEF. *J. Am. Coll. Cardiol.* 75 (3), 245–254. doi:10.1016/j.jacc.2019.11.003

Wang, K., Long, B., Liu, F., Wang, J. X., Liu, C. Y., Zhao, B., et al. (2016). A Circular RNA Protects the Heart from Pathological Hypertrophy and Heart Failure by Targeting miR-223. *Eur. Heart J.* 37 (33), 2602–2611. doi:10.1093/eurheartj/ehv713

Wen, Y., Liu, R., Lin, N., Luo, H., Tang, J., Huang, Q., et al. (2019). NADPH Oxidase Hyperactivity Contributes to Cardiac Dysfunction and Apoptosis in Rats with Severe Experimental Pancreatitis through ROS-Mediated MAPK Signaling Pathway. *Oxid. Med. Cel. Longev.* 2019, 4578175. doi:10.1155/2019/4578175

Xu, W. P., Yao, T. Q., Jiang, Y. B., Zhang, M. Z., Wang, Y. P., Yu, Y., et al. (2015). Effect of the Angiotensin II Receptor Blocker Valsartan on Cardiac Hypertrophy and Myocardial Histone Deacetylase Expression in Rats with Aortic Constriction. *Exp. Ther. Med.* 9 (6), 2225–2228. doi:10.3892/etm.2015.2374

Yan, L., Zhang, J. D., Wang, B., Lv, Y. J., Jiang, H., Liu, G. L., et al. (2013). Quercetin Inhibits Left Ventricular Hypertrophy in Spontaneously Hypertensive Rats and Inhibits Angiotensin II-Induced H9C2 Cells Hypertrophy by Enhancing PPAR-γ Expression and Suppressing AP-1 Activity. *PLoS One* 8 (9), e72548. doi:10.1371/journal.pone.0072548

Ying, H., Xu, M. C., Tan, J. H., Shen, J. H., Wang, H., and Zhang, D. F. (2014). Pressure Overload-Induced Cardiac Hypertrophy Response Requires Janus Kinase 2-histone Deacetylase 2 Signaling. *Int. J. Mol. Sci.* 15 (11), 20240–20253. doi:10.3390/ijms151120240

Yokota, T., and Wang, Y. (2016). p38 MAP Kinases in the Heart. *Gene* 575 (2 Pt 2), 369–376. doi:10.1016/j.gene.2015.09.030

Yullia, T. (2008). "Prakata," in *Variasi Masakan Petai & Jengkol, Tim Dapur DeMedia (Jakarta Selatan, DeMedia Pustaka)*. Jakarta Selatan and DeMedia, 2.

Zaini, N., and Mustaffa, F. (2017). Review: Parkia Speciosa as Valuable, Miracle of Nature. *Ajmah* 2 (3), 1–9. doi:10.9734/AJMAH/2017/30997

Zhang, W., Elimban, V., Nijjar, M. S., Gupta, S. K., and Dhalla, N. S. (2003). Role of Mitogen-Activated Protein Kinase in Cardiac Hypertrophy and Heart Failure. *Exp. Clin. Cardiol.* 8 (4), 173–183.

Zhu, W., Wu, R. D., Lv, Y. G., Liu, Y. M., Huang, H., and Xu, J. Q. (2020). BRD4 Blockage Alleviates Pathological Cardiac Hypertrophy through the Suppression of Fibrosis and Inflammation via Reducing ROS Generation. *Biomed. Pharmacother.* 121, 109368. doi:10.1016/j.biopha.2019.109368

Zhuang, X., Zhao, B., Liu, S., Song, F., Cui, F., Liu, Z., et al. (2016). Noncovalent Interactions between Superoxide Dismutase and Flavonoids Studied by Native Mass Spectrometry Combined with Molecular Simulations. *Anal. Chem.* 88 (23), 11720–11726. doi:10.1021/acs.analchem.6b03359

Zucker, I. H., Schultz, H. D., Patel, K. P., and Wang, H. (2015). Modulation of Angiotensin II Signaling Following Exercise Training in Heart Failure. *Am. J. Physiol. Heart Circ. Physiol.* 308 (8), H781–H791. doi:10.1152/ajpheart.00026.2015

Conflict of Interest: The authors declare that the research was conducted in the absence of any commercial or financial relationships that could be construed as a potential conflict of interest.

Publisher's Note: All claims expressed in this article are solely those of the authors and do not necessarily represent those of their affiliated organizations, or those of the publisher, the editors and the reviewers. Any product that may be evaluated in this article, or claim that may be made by its manufacturer, is not guaranteed or endorsed by the publisher.

GLOSSARY

Ang II angiotensin II

ANOVA one-way analysis of variance

AT_1R Ang II type 1 receptor

AUC area under the curve

BNP B-type natriuretic peptide

cGMP cyclic guanosine monophosphate

DMEM Dulbecco's Modified Eagle Medium

DMSO dimethyl sulfoxide

DPI diphenyleneiodonium

EDTA ethylenediaminetetraacetic acid

ELISA enzyme-linked immunosorbent assay

eNOS endothelial nitric oxide synthase

ERK1/2 extracellular signal-related kinase

FBS fetal bovine serum

HPLC high-performance liquid chromatography

HRP horseradish peroxidase

IC_{50} median inhibitory concentration

iNOS inducible nitric oxide synthase

JNK c-Jun N-terminal kinase

MAPK mitogen-activated protein kinase

MEF2 myocyte enhancer factor-2

MTS 3-(4,5-dimethylthiazol-2-yl)-5-(3-carboxymethoxyphenyl)-2-(4-sulfophenyl)-2H-tetrazolium

NADPH nicotinamide adenine dinucleotide phosphate

NF-κB nuclear factor kappa-B

NO nitric oxide

NOX NADPH oxidase

NFAT nuclear factor of activated T-cells

NOS2 nitric oxide synthase 2

$O_2^{-\bullet}$ superoxide anion

P-ERK1/2 phosphorylated ERK1/2

p38 p38 kinase

PI3K/Akt/GSK-3β phosphatidylinositol 3-kinase/protein kinase B/glycogen synthase kinase-3β

P-p38 phosphorylated p38

P-JNK phosphorylated JNK

PKG protein kinase G

ROS reactive oxygen species

SEM standard error of the mean

SOD superoxide dismutase

Sp1/GATA4 specificity protein-1/GATA binding protein-4

SPSS Statistical Product and Service Solutions

SRF serum response factor

TNFα tumor necrosis factor-α

t_R retention time

frontiers in Pharmacology

STUDY PROTOCOL
published: 18 October 2021
doi: 10.3389/fphar.2021.764669

BuqiTongluo Granule for Ischemic Stroke, Stable Angina Pectoris, Diabetic Peripheral Neuropathy with Qi Deficiency and Blood Stasis Syndrome: Rationale and Novel Basket Design

Weidi Liu[1,2†], Li Zhou[1], Luda Feng[1†], Dandan Zhang[1,2], Chi Zhang[1†] and Ying Gao[1,2*†] behalf of the BOSS Group*

[1]Dongzhimen Hospital, Beijing University of Chinese Medicine, Beijing, China, [2]Institute for Brain Disorders, Beijing University of Chinese Medicine, Beijing, China

Background: BuqiTongluo (BQTL) granules are herbal phenotypic drugs for Qi deficiency and blood stasis (QDBS) syndrome. Its discovery relied primarily on knowledge of observable phenotypic changes associated with diseases. Although BQTL granules have been widely advocated by Chinese Medicine (CM) practitioners, its use lacks empirical support.

Aim of the study: In this basket trial, the efficacy of BQTL granules in multiple diseases that have the QDBS syndrome in common will be compared with placebo.

Materials and Methods: The BuqiTongluo granule for Qi deficiency and blood stasis syndrome (BOSS) study is a basket herbal trial (ClinicalTrials.gov, NCT04408261). It will be a double-blinded, randomized, placebo-controlled, parallel, multicenter, clinical trial. In total, 432 patients (1:1:1 ischemic stroke, stable angina pectoris, and diabetic peripheral neuropathy), who meet the operationalized diagnostic criteria for QDBS syndrome, have been recruited and randomized in a ratio of 1:1 to receive 6 weeks' treatment with BQTL granules or placebo. The primary outcome is the change in the QDBS syndrome score at week 6 from baseline. Secondary outcomes include objective outcome measures for the three diseases and adverse events. Omics will help to understand these responses by molecular events.

OPEN ACCESS

Edited by:
Yue Liu,
Xiyuan Hospital, China

Reviewed by:
Zehuai Wen,
Guangdong Provincial Hospital of Chinese Medicine, China
Linda LD Zhong,
Hong Kong Baptist University, Hong Kong, SAR China

***Correspondence:**
Chi Zhang
saga618@126.com
Ying Gao
gaoying973@163.com

†ORCID ID:
Weidi Liu
orcid.org/0000-0002-0081-2530
Luda Feng
orcid.org/0000-0002-7259-4421
Chi Zhang
orcid.org/0000-0001-5427-2966
Ying Gao
orcid.org/0000-0001-6972-3846

Specialty section:
This article was submitted to Ethnopharmacology, a section of the journal Frontiers in Pharmacology

Received: *25 August 2021*
Accepted: *30 September 2021*
Published: *18 October 2021*

Citation:
Liu W, Zhou L, Feng L, Zhang D, Zhang C and Gao Y (2021) BuqiTongluo Granule for Ischemic Stroke, Stable Angina Pectoris, Diabetic Peripheral Neuropathy with Qi Deficiency and Blood Stasis Syndrome: Rationale and Novel Basket Design. Front. Pharmacol. 12:764669. doi: 10.3389/fphar.2021.764669

Abbreviations: ALT, alanine aminotransferase; AR, Alisma plantago-aquatica subsp. orientale (Sam.) Sam.; AS, Angelica sinensis (Oliv.) Diels; AST, aspartate aminotransferase; BI, barthel index; BQTL, BuqiTongluo; CI, confidence interval; CIMS, clinical information management suite; CM, Chinese medicine; CIDP, chronic inflammatory demyelinating polyneuropathy; CRC, clinical research coordinator; DSMB, data and safety monitoring board; HPS, hedysarum polybotrys polysaccharide; GCP, good clinical practice; GMP, good manufacturing practice; LC, Ligusticum chuanxiong Hort.; NIHSS, national institutes of health stroke scale; NMPA, national medical products administration; NYHA, New York Heart Association; PNS, panax notoginseng saponins; QDBS, Qi deficiency and blood stasis; RCT, randomized controlled trial; SAQ, Seattle Angina Questionnaire; SAS, strategic applications software; SF-36, 36-item short form survey; VAS, visual analog scale.

Conclusion: QDBS syndrome is a common phenotypic marker that was hypothesized to predict whether patients with multiple diseases would respond to this targeted therapy. No previous basket trial has assessed the potential efficacy of an herbal intervention for multiple diseases. The unique promise of the trial is its ability to exploit a disease phenotype to discover novel treatments for three diseases for which the root cause is unknown, complex, or multifactorial, and for which scientific understanding is insufficient to provide valid molecular targets.

Keywords: basket design, BuqiTongluo granule, efficacy, herbal medicine, randomized controlled trial

INTRODUCTION

Implementation of innovative design strategies in the development of efficacious and safe herbal medicines is of major interest to patients, the pharmaceutical industry, and regulators. In China, the National Medical Products Administration (NMPA) has supported various joint efforts to develop new methodologies for increasing the efficiency of clinical trials in complicated diseases. These design strategies include integrated herbal medicine protocol designs, as well as another closely related emerging concept, the basket trial design (Yuan, 2021). The term "basket trial" refers to a design developed to enroll individuals with multiple diseases and one (or a combination of) drug targets in cohorts within a trial (Cunanan et al., 2017). Basket designs have been applied positively in oncology trials dealing with multiple types of cancer (Park et al., 2020).

In Chinese Medicine (CM) theory, multiple diseases in different people may be treated in the same manner (Zhai et al., 2020). Under this treatment principle, the same strategy is used to treat patients with multiple diseases who have the same syndrome (Zheng) (Jiang et al., 2014). Such syndromes provide a massive amount of information in terms of herbal products and the clinical symptoms for which they are used therapeutically, which are the observable disease phenotypes that are crucial for clinical diagnosis and treatment (Miao et al., 2012). The change in the syndrome reflects either remission or progression of the disease.

We have adopted the concept of innovative basket trial design beyond the field of cancer research and have now developed a Phase II herbal trial protocol for treatment of patients with ischemic stroke, stable angina pectoris, and diabetic peripheral neuropathy, who share the same syndrome target [Qi deficiency and blood stasis (QDBS) syndrome] for herbal therapy. QDBS syndrome is one of the basic CM syndromes that is most strongly related to various diseases, including vascular, cardiovascular, and cerebrovascular diseases, and guides the use of herbal medicine (Zhai et al., 2020). It is a common and core pathogenesis of multiple diseases (Li et al., 2007), with a cluster of symptoms, including fatigue, shortness of breath, reticence to speak, spontaneous sweating, pale or dark complexion, local stabbing pain, pale purple tongue, or pale dark tongue. QDBS syndrome is thought to be the basic pathogenesis of ischemic stroke (Fan et al., 2014), coronary artery disease (Hui et al., 2010), and diabetic peripheral neuropathy (Miao et al., 2003) according to CM. Previous studies have demonstrated that changes in the phenotype of QDBS syndrome in patients with ischemic stroke, coronary artery disease, and diabetic peripheral neuropathy were associated with improvement in both symptoms and clinical outcomes of these three diseases (Zhou and Wang, 2014). Herbal medicine adopts a broad pharmacological approach to treat complicated diseases, by deploying a combination of herbal medicines with different treatment effects.

BuqiTongluo (BQTL) granule is a typical herbal formulae created by Yong-yan Wang, a famous Chinese medical scientist, to tonify Qi and promote blood circulation (Xie, 2020). The herbal formulae originates from Yi Lin Gai Cuo (Correcting the Errors in the Forest of Medicine) (Wang, 2007). It is composed of eight herbs, including Hedysarum polybotrys Hand.-Mazz (Hongqi), Panax notoginseng (Burkill) F.H.Chen (Sanqi), Alisma plantago-aquatica subsp. orientale (Sam.) Sam (Zexie), Angelica sinensis (Oliv.) Diels (Danggui), Ligusticum chuanxiong Hort (Chuanxiong), Periostracum Cicadae (Chantui), Curcuma aromatica Salisb (Yujin), Neolitsea cassia (L.), Kosterm (Guizhi). Now CM physicians often apply BQTL herbal formulae to treat nerve damage, cardiovascular and cerebrovascular diseases in clinical practice.

Among the herbs cited above, Hedysarum polybotrys Hand.-Mazz. contributes to regulating Qi. According to the Chinese medicine compatibility theory of "sovereign, ministerial, adjuvant and messenger", the Hedysarum polybotrys Hand.-Mazz is sovereign herb in the BQTL, and it also showed pharmacological activity in well designed experiments. Hedysarum polybotrys polysaccharide (HPS) has significant protective effect against heart and brain hypoxia (Dong et al., 2013). It can protect the endomembrane barrier (Wang et al., 2013), promote peripheral nerve regeneration and improve the recovery of nerve function (Wei et al., 2009), and enhance nerve amplification effect by encouraging proximal axons to grow more lateral buds and effectively improve peripheral nerve (Wang et al., 2013). Panax notoginseng saponins (PNS) is isolated from the roots and rhizomes of Panax notoginseng (Burkill) F.H.Chen, a highly valued Chinese materia medica with the efficacy of promoting blood circulation and removing blood stasis. PNS has been shown to exert strong anti-inflammatory effects against atherosclerosis-related cardiac-cerebral vascular disease (Wan et al., 2009). A new study also suggested that PNS exerted long-term neuroprotective effects that assisted in stroke recovery (Zhou et al., 2021). PNS

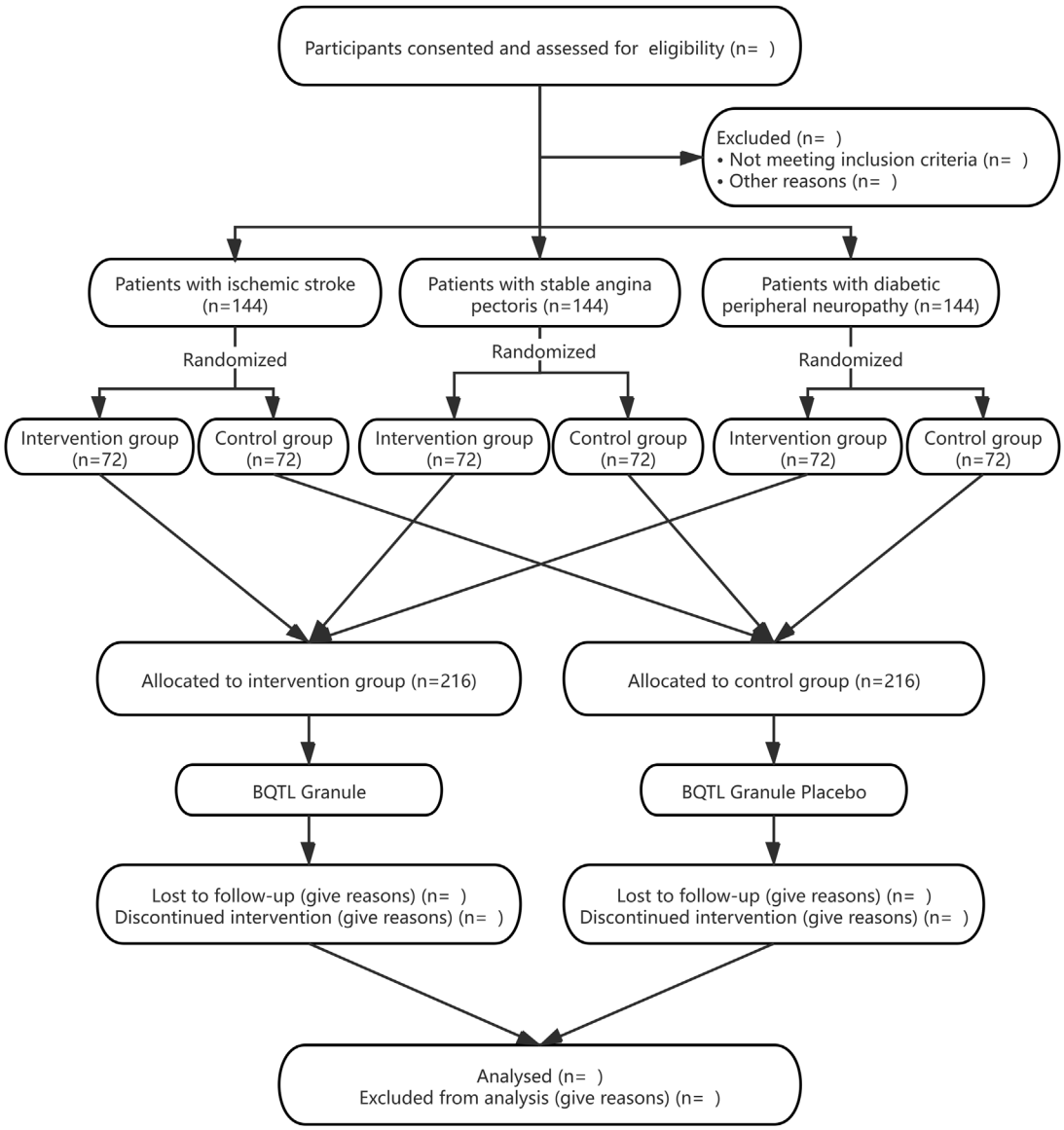

FIGURE 1 | The flowchart of participants disposition throughout the study.

ameliorates diabetic peripheral neuropathy by attenuating electrophysiological, circulatory and morphological alterations (Hao et al., 2017).

Taken together, BQTL herbal formulae has been widely used to treat multiple diseases involving the QDBS syndrome. However, no large, randomized trial has studied the effect of BQTL granules on QDBS syndrome. The aims of this basket randomized controlled trial (RCT) are firstly to optimize parameters and examine the feasibility of a subsequent phase III RCT through preliminary evidence on the clinical efficacy and safety of BQTL granules on three diseases (ischemic stroke, stable angina pectoris, and diabetic peripheral neuropathy) involving QDBS syndrome, as compared with placebo. Secondly, it aims to elucidate the mechanism by which BQTL granules exert an effect on QDBS syndrome.

MATERIALS AND METHODS

Study Design

The BuqiTongluo granule for Qi deficiency and blood stasis syndrome (BOSS) study is a basket herbal trial studying the effect of BQTL granules across multiple cohorts of three diseases (ClinicalTrials.gov, NCT04408261). The BOSS protocol includes three multicenter randomized, double-blinded, placebo-controlled sub trials that will study BQTL granules in three independent patient populations: ischemic stroke (sub trial I), stable angina pectoris (sub trial II), and diabetic peripheral neuropathy (sub trial III). This study is currently open at 14 sites across China. In each sub trial, patients will be randomly divided into an intervention group (BQTL granule) and placebo group (placebo) using an 1:1 allocation ratio, adhering to the

TABLE 1 | The schedule of enrolment, interventions, and assessments in the BOSS trial.

	STUDY PERIOD							
	Enrolment	Allocation	Post-allocation					Close-out
TIMEPOINT	*D-3*	*D0*	*D1*	*D14±2*	*D28±2*	*D42±3*	*D56±4*[11]	*D90±7*[12]
ENROLMENT:								
Eligibility screen[1]	X							
Informed consent	X							
Demographics data	X							
Basic medical history	X							
Physical examination	X					X		
Internal medical assessment (vital signs)[2]	X		X	X	X	X	X	X
Laboratory examination[3]	X					X		
12 lead ECG	X					X		
Allocation		X						
INTERVENTIONS:								
Bugitongluo Granule			←	—	→			
Bugitongluo Granule Placebo			←	—	→			
ASSESSMENTS:								
Evaluation Scale of Qi Deficiency and Blood Stasis Syndrome[4]			X	X	X	X	X	
NIHSS[5]	X		X	X	X	X		
SAQ[6]			X		X		X	X
TCSS[7]			X	X	X	X	X	X
VAS[4]			X	X	X	X	X	
mRS[5]			X			X		X
BI[6]			X			X		X
SF-36 Quality of Life Scale[4]			X			X		X
Adverse events assessment			*Record at any time*					
Concomitant medication[8]	X		X	X	X	X	X	X
OTHERS:								
Serum specimen collection[9]			X			X		
Tongue and facial images collection[10]			X	X	X	X	X	

Note.

[a]*Eligibility screen: Including inclusion and exclusion criteria, HbA1c, pregnancy test. Only patients with diabetic peripheral neuropathy will be tested for HbA1c, and only fertile women will be tested for blood pregnancy test within 24 h before the first medication.*

[b]*Vital signs: Including temperature, respiration, pulse and blood pressure.*

[c]*Laboratory examination: Including Routine Blood Examination (RBC, WBC, HGB, PLT, NEU, NE%) , Routine Urine Examination (GLU, LEU, PRO, KET, BLD, SG, pH) , Routine Stool Examination (RBC, WBC, fecal occult blood) , Blood Lipid Examination (TC, TG, LDL, HDL) , FBS, Electrolyte Examination (Na, K, Cl, Ca, P) , Liver Function (ALT, AST, GGT, ALP, TBIL) ,*

Renal Function (BUN, Cr) , Coagulation Function (PT, APTT, TT, FIB, INR). Patients with diabetic peripheral neuropathy will also be tested for Urine Microalbumin and Urine NAG. During the trial, the investigator can decide whether to increase the safety indicator test items and times according to patients' condition.

[d]Evaluation Scale of Qi Deficiency and Blood Stasis Syndrome, VAS and SF-36 Quality of Life Scale are applicable to all subjects.

[e]NIHSS, mRS and BI evaluation are only applicable to subjects with convalescence of ischemic stroke.

[f]SAQ evaluation is only applicable to subjects with stable angina pectoris of coronary artery disease.

[g]TCSS evaluation is only applicable to subjects with diabetic peripheral neuropathy.

[h]Concomitant medication: During the screening period and the whole process of the trial, antihypertensive agents are allowed to be used for blood pressure control. The concomitant medication will be recorded from 3 months before enrollment to the end of the trial.

[i]Serum specimen collection: The blood samples of 1/3 subjects (ie., the subjects with tongue and facial images collection) will be collected. The collection, processing and storage of blood samples will be carried out according to the "SOP for collection and management of clinical serum samples."

[j]Tongue and facial images collection: All the subjects will use the mobile phone APP for tongue and facial images collection. And 1/3 subjects will use the TCM Tongue and Facial Imaging and Analysis Instrument for tongue and facial images collection.

[k]About D56: It refers to the 14th day after drug withdrawal.

[l]About D90: It refers to the 90th day after onset for subjects with convalescence of ischemic stroke, and refers to the 90th day after medication for subjects with stable angina pectoris of coronary artery disease and diabetic peripheral neuropathy.

Standard Protocol Items: Recommendations for Interventional Trials (SPIRIT) statement (Chan et al., 2013). The study period includes 6 weeks of medication and 90 days of follow-up. The study procedure is summarized in the CONSORT diagram (**Figure 1**), and the schedule of enrolment, interventions, and assessments is summarized in **Table1**. The trial will be performed in accordance with the Declaration of Helsinki and Good Clinical Practice Guidelines. Informed consent will be obtained from all participants.

Participants

For inclusion, all participants will have a diagnosis of QDBS syndrome and should be aged from 35 to 80 years. QDBS syndrome follows the Guideline for clinical research of new Chinese medicine (The State Drug Administration, 2002).

For the ischemic stroke trial (sub Trial I), patients will be diagnosed with ischemic stroke (Sacco et al., 2013), with an interval from onset to recruitment of 14–30 days, and will have a National Institutes of Health Stroke Scale (NIHSS) score ≥4 and ≤22 (Kasner, 2006). Patients will be excluded from sub Trial I if they have a confirmed secondary stroke caused by tumors, brain trauma, or hematological diseases by clinical examination. Patients with other conditions that lead to motor dysfunction (e.g., lameness, osteoarthrosis, rheumatoid arthritis, gouty arthritis), which render a neurological function examination unlikely, will also be excluded.

In the stable angina pectoris trial (sub Trial II), patients will be included if they are diagnosed with stable angina pectoris and have a Canadian Cardiovascular Society classification of Angina Pectoris class I–III (Knuuti et al., 2020). Patients will be excluded from this trial if they have had acute coronary syndrome or unstable angina pectoris in the previous 3 months, or have other heart diseases (e.g., cardiomyopathy, pericardial disease) such as severe cardiopulmonary insufficiency (congestive heart failure NYHA class IV, severe abnormal pulmonary function), or severe arrhythmias (e.g., rapid atrial fibrillation, atrial flutter, paroxysmal ventricular tachycardia).

In the diabetic peripheral neuropathy trial (sub Trial III), patients with a diagnosis of diabetic peripheral neuropathy will be included (Executive summary, 2014). Patients will be excluded if they have HbA1c >10% during the screening period, have had acute, critical diabetes mellitus conditions in the previous 3 months (e.g., hyperglycemia and hypertonic syndrome, diabetic lactic acidosis, diabetic ketoacidosis), or have severe heart disease, brain disease, or kidney disease. Moreover, patients with spinal cord injury, cervical or lumbar vertebral disease (nerve root compression, spinal stenosis, cervical or lumbar vertebra degenerative disease), or sequelae of cerebrovascular disease, neuromuscular junction, or muscular disease; or neuropathies caused by other diseases (e.g., Guillain-Barré syndrome, chronic inflammatory demyelinating polyneuropathy (CIDP), Vitamin B deficiency, hypothyroidism, alcoholism, or severe arteriovenous vasculopathy such as venous embolism, lymphangitis) will be excluded.

Additionally, patients with uncontrolled hypertension (systolic blood pressure ≥160 mmHg or diastolic blood pressure ≥100 mmHg), or renal or hepatic insufficiency (hepatic insufficiency defined as an alanine aminotransferase (ALT) or aspartate aminotransferase (AST) value that is 1.5 times the upper limit of normal; renal insufficiency defined as a serum creatinine concentration value that is above the upper limit of normal) will be excluded from all trials. Patients with other conditions or mental disorders that, according to the judgment of investigators, would restrict evaluation of mental function or render outcomes or follow-up unlikely to be assessable will also be excluded. Furthermore, pregnant or lactating women, or women who are planning a pregnancy within the next few years, patients who are allergic to the study drug or have a severely allergic constitution, those with a yellow, thick, slimy tongue coating, and those who have participated in other drug or device clinical trials in the past 3 months will also be excluded from all trials.

Sample Size

For a main phase II trial assessing natural drugs, according to the NMPA recommendation (No. 28, 2007 and No. 109, 2018) and data from our pilot study, the sample size should not be less than 60 per treatment arm for each disease to estimate the parameter. We enrolled 432 participants to allow for dropouts.

Recruitment

A total of 432 patients who fulfill the screening criteria will be recruited at 14 Good Clinical Practice (GCP)-approved hospitals in China. Local advertisements will be used for recruitment. A contract research organization will help to monitor the on-schedule recruitment progress and take measures in a timely manner. Investigators will provide research information, such as

TABLE 2 | Standard formulation of BuqiTongluo Granule.

Pinyin name	Scientific name	Proportion (g)
Hongqi	Hedysarum polybotrys Hand.-Mazz	500
Sanqi	Panax notoginseng (Burkill) F.H.Chen	100
Zexie	Alisma plantago-aquatica subsp. orientale (Sam.) Sam	333
Danggui	Angelica sinensis (Oliv.) Diels	333
Chuanxiong	Ligusticum chuanxiong Hort	200
Chantui	Periostracum Cicadae	100
Yujin	Curcuma aromatica Salisb	200
Guizhi	Neolitsea cassia (L.) Kosterm	100

the purpose, the procedures, the potential risks and benefits of participants through standardized interviews before their participation. Written informed consent will then be obtained from all participants.

Randomization, Allocation Concealment, and Blinding

All eligible patients who consent to participation will be randomized into either the BQTL granule group or the placebo group in an 1:1 ratio. A random sequence table will be generated by using Strategic Applications Software (SAS, version 9.4, SAS Institute, Inc., Cary, NC, United States), and randomization will be conducted using a central web-based interactive randomization service system (CIMS, Chengdu, China) with permuted blocks. The system automatically randomizes patients and generates the randomization code and drug code corresponding to the assigned treatment. The system will not release the randomization code until the patient has been recruited into the trial to ensure allocation concealment. Randomization will be conducted without any influence from research clinicians. All participants, physicians, nurses, data managers, statisticians, and other staff will be blinded to the treatment allocations until the trial is completed. In case of emergency, the principal investigator of each center, who has the only authority to view the blind codes, can log into the central randomization system for emergency unblinding. To ensure the implementation of blinding, the placebo will be identical to the BQTL granule in physical appearance, sensory perception, packaging, and labeling, and will have no pharmaceutical activity.

Drug Administration

The BQTL granules contained Hedysarum polybotrys Hand.-Mazz (Hongqi), Panax notoginseng (Burkill) F.H.Chen (Sanqi), Alisma plantago-aquatica subsp. orientale (Sam.) Sam (Zexie), Angelica sinensis (Oliv.) Diels (Danggui), Ligusticum chuanxiong Hort (Chuanxiong), Periostracum Cicadae (Chantui), Curcuma aromatica Salisb (Yujin), and Neolitsea cassia (L.), Kosterm (Guizhi). The criteria for the quality of these ingredients were in accordance with the 2015 Chinese pharmacopoeia. Eligible patients will receive BQTL granules or placebo (10 g) (**Table 2**) dissolved in boiled water, administered orally three times a day for 6 weeks (one sachet per time). The study drug will be prepared by Shaanxi Buchang Pharmaceuticals Co., Ltd., China. The quality control of the production process strictly adhered to the good manufacturing practice (GMP) of national drug production.

Interventions

Eligible patients will be randomized in equal proportions between the BQTL granule groups and placebo groups, receiving either BQTL granules or placebo. The granules will be dispensed through the clinical trial pharmacies of the 14 hospitals, complying with the standard of pharmacy practice. Two fully registered CM practitioners will be responsible for clinical diagnosis and prescription. During the trial, it will be forbidden to use acupuncture, CM decoctions (compound granules), Chinese medicine injections, Chinese patent medicines (including external use), and external washing with traditional Chinese medicine and health products with a composition or efficacy similar to the study drug. Participants will be allowed to accept standard rehabilitation treatment and use necessary drugs that do not affect the evaluation of study parameters for concomitant diseases. The use of drugs should be standardized according to the guidelines, and the name, dosage, times, and time of use must be recorded for analysis and report.

Primary Outcomes

The primary outcome of the study is improvement in QDBS syndrome, defined as a change in the national approved QDBS syndrome evaluation scale from before to after the 6-week treatment. The QDBS syndrome evaluation scale (Wang et al., 2015) was chosen because of its practical use in the evaluation of the QDBS syndrome. The scale is a 21-item clinician-rated scale with anchored item descriptions. It lists 21 clinical symptoms and physical signs related to the QDBS syndrome. The scale ranges from 0 to 51 with 51 indicating the worst score possible. The higher the score, the more severe the degree of the syndrome. The scale has been developed, validated, and applied in the Department of Neurology, Cardiology, Endocrinology, and multiple investigators have used this method to assess patients with QDBS syndrome. This scale has excellent inter-rater reliability and internal consistency. It is NMPA's recommended outcome measure in Guideline for clinical research of new Chinese medicine drugs with syndrome.

Secondary Outcomes

For sub Trial I, secondary outcomes will be the following: Neurological impairment will be evaluated using the NIHSS (Time Frame: baseline, and on days 14, 28, and 42 during

treatment). Self-rating symptoms will be evaluated using a visual analog scale (VAS) (Bijur et al., 2001). This will include VAS scores for limb numbness, swelling of hands or feet, and spontaneous sweating (hemilateral sweating) (Time Frame: baseline, and on days 14, 28, and 42 during treatment, as well as at day 14 after treatment). Continuous changes in the Modified Rankin Scale score (Uyttenboogaart et al., 2005) (Time Frame: baseline, at day 42 during treatment, and at day 90 after onset) will also be recorded. Activities of daily living will be measured using the Barthel Index (BI) score (Uyttenboogaart et al., 2005) (Time Frame: baseline, at day 42 during treatment, and at day 90 after onset).

For sub Trial II, secondary outcomes will include the following: Changes in the Seattle Angina Questionnaire (SAQ) score (Time Frame: baseline, at day 28 during treatment, at day 14 after treatment, and at day 90 after recruitment). Self-rating symptoms will be evaluated using a VAS for chest tightness, chest pain, palpitation, fatigue, and spontaneous sweating (Time Frame: baseline, and on days 14, 28, and 42 during treatment, as well as at day 14 after treatment).

In sub Trial III, the secondary outcomes will be as follows: Changes in the Toronto Clinical Scoring System (Bril and Perkins, 2002) (Time Frame: baseline, and on days 14, 28, and 42 during treatment, day 14 after treatment, as well as day 90 after recruitment). Self-rating symptoms will be evaluated using a VAS for local pain, limb numbness, and paresthesia (e.g., burning sensation, formication, electrical sensation) (Time Frame: baseline, and on days 14, 28, and 42 during treatment, as well as at day 14 after treatment).

For all sub trials, quality of life will be measured as a secondary outcome, using the 36-Item Short Form Survey (SF-36) (Time Frame: Baseline, at day 42 during treatment, and at day 90 after onset/recruitment). Blood, urine, and feces samples will be collected at baseline and day 42 for metabolomics, proteomics, microbiota, and flow-cytometry studies.

Safety Outcomes

The safety outcomes will include any adverse events and clinically meaningful changes in vital signs or laboratory parameters during the trial. Participants will be asked to report any abnormal reactions occurring during the trial to the investigators. At week 6, participants will undergo liver function and renal function tests to monitor hepatotoxicity and nephrotoxicity.

Adverse Events Management

All details of related and unexpected adverse events, including time of occurrence, degree and duration, suspected causes, and effective measures and outcomes will be recorded. The investigators will immediately take appropriate treatment measures for the participants, report and follow-up, and assess the relatedness of the event to the study drug from a clinical point of view. Any adverse event will be treated suitably and recorded accurately and completely. The causality between adverse events and intervention will be assessed by a causality assessment tool, the World Health Organization-Uppsala Monitoring Centre (WHO-UMC) case causality assessment, to evaluate the likelihood that an adverse event is associated with the intervention. The causality assessment will be accomplished by a combined assessment taking into account the clinical-pharmacological aspects of the case history and the quality of the documentation of the observation with a table of predefined statements and classifies events as the following categorization: certain, probable/likely, possible, unlikely, and two sub-categories: conditional/unclassified (when information pending), and unassessable/unclassifiable (when sufficient information is not available).

Data Collection and Management

Data will be collected at baseline, at 14, 28, 42, and 56 days post-allocation, and at the 90 days follow-up. To promote data quality, each site's investigator will be trained centrally regarding the study requirements, including standardized evaluation of scales involved in the trial, operation of the CM tongue and facial imaging and analysis instrument, requirements for serum specimen collection, and on eliciting information from participants in a uniform and reproducible manner.

An electronic data capture system will be used in this study. The investigator/clinical research coordinator (CRC) will input the original data into the electronic data capture system accurately, in a timely, complete, and standard manner. After data entry, data may not be changed at will. If data entries need to be modified, the investigator/CRC will need to record the reason for modification according to the system prompt. All the operations in the system are traceable.

The data manager will develop a detailed data verification plan according to the protocol and case report form, including logic verification, scope verification, time window verification, consistency verification, and compliance verification. The efficiency indicators and key safety indicators should be fully verified to ensure the accuracy and integrity of the data. Data verification should be carried out in the case of an unknown test group, and the generated data query content should avoid deviation or induced questions.

After all the data are inputted and queried, a blind review meeting will be held to determine the data set division. After reaching a consensus on all data questions, the sponsor, principal investigator, data manager, and statistician will jointly sign the approval document for locking the database. After obtaining approval, the data manager will execute the database locking operation and remove the system operation authority of the relevant personnel. The study documents will be retained in a secure location for at least 5 years after trial completion.

Quality Control and Data Monitoring

The trial is managed by the Dongzhimen Hospital, Beijing University of Chinese Medicine. The protocol compliance, safety, and the trial data will be supervised by the Data and Safety Monitoring Board (DSMB), an independent group of experts that advises funding agencies and study investigators. DSMB members include experts from different fields (Western Medical Sciences, Chinese Medicine, Clinical Epidemiology, and Statistics). An auditing will be conducted twice a month during the enrollment period and every month during the follow-up period, and the process will be independent from investigators.

Statistical Methods

Statistical analysis will be performed using Statistical Analysis System version 9.4 (SAS Institute Inc., Cary, North Carolina, United States) statistical software packages. Outcome measurements will be analyzed using full analysis sets and per protocol sets according to intention-to-treat (ITT) analysis. Safety analysis will be performed in a safety set, which is defined as a subset of subjects who received at least one treatment and had actual safety indicators record data. The statistical analysis will include baseline characteristics of participants, compliance and concomitant medication, efficacy analysis and safety analysis. For continuous data, we will describe the results using the mean (standard deviation, SD), maximum, minimum, median and non-parametric test median (quartile deviation, QD). Categorical data will be described as absolute values and proportions. For continuous outcomes, paired *t*-test or Wilcoxon signed-rank test will be used to analyze significant differences between baseline and each time point. The Wilcoxon rank-sum test will be employed for comparisons between treatment groups. Chi-squared test will be used for categorical data and Wilcoxon rank-sum test will be used for ranked data. Analysis of covariance (ANCOVA) will be used to control potential confounding variables.

We will use a two-sided 5% significance level and 85% power. Baseline characteristics in each group will be analyzed using descriptive statistics. Compliance analysis will be based on full analysis sets, and analysis of concomitant medications will be based on safety sets. Regarding the primary outcome variable, between-group comparisons of the change in syndrome score will be analyzed between pre- and post-treatment using paired t-test or Wilcoxon signed-rank test. As to the secondary outcomes, comparisons of the changes in NIHSS score in sub Trial I, the Seattle Angina Questionnaire score in sub Trial II, and the Toronto Clinical Scoring System in sub Trial III, will be analyzed using paired t-test or Wilcoxon signed-rank test between baseline and each time point. The Wilcoxon rank-sum test will be employed for comparisons between treatment groups. Any factors impacting efficacy, such as age and sex, should be taken into account as covariate. Safety will be analyzed in terms of all the adverse events occurred during the trial, and the incidence will be compared between groups using the chi-squared test or Fisher's exact probability method.

Last observation carry forward (LOCF) approach will be used to impute missing data of primary outcome according to intention-to-treat analysis. A sensitivity analysis will be conducted to determine the robustness of the results under the missing at random assumption, to evaluate the role of lost to follow-up (i.e., participants who did not follow-up to V4), by using the LOCF method. And a p value of less than 0.05 will be considered statistically significant.

DISCUSSION

The BOSS trial is the first study that implements basket design in the context of herbal medicine (Yuan, 2021). Before BOSS, basket design is conceptual phase in this field. Basket trials have been developed as an efficient way to screen for experimental therapeutics across multiple patient populations in the early phase of drug development. Rather than being viewed as opposing alternatives in herbal drug development, the basket trial design (different diseases treated with the same therapy) and conventional RCT design (one disease treated with one therapy) should be seen as complementary methodologies that can increase the odds of developing herbal drugs with promising phenotypic predictors. To our knowledge, the basket trial approach has not been fruitfully applied to evaluate the efficacy of herbal medicine for CM syndromes in patients with different diseases. BQTL granules are the first new CM drug approved for application in Phase II trials by the NMPA. A positive outcome of the BOSS trial would set the stage for future investigations using the basket trial design to increase the feasibility of herbal medicine for individuals with specific CM syndromes.

We present this protocol and a detailed statistical analysis plan prior to the analyses of any data in the BOSS trial. Recruitment for the study started on July 22, 2020, and the trial is expected to be completed in December 2022. The strengths of our trial include the high methodological standards of a double-blind, placebo-controlled, randomized clinical trial, and high external validity, with 14 sites, which will ensure robust results and reduces the influence of confounding covariates. We will report patient-centered outcomes and disease-related objective assessments of severity, measured using VASs. The trial will be monitored according to GCP standards. The proposed study may provide direct and convincing evidence to support BQTL granules as a treatment for improving QDBS syndrome, which could then be introduced into clinical settings. It will support symptomatic treatment of QDBS syndrome with BQTL granules, and holds potential to make a meaningful difference to patients. The unique promise of the BOSS trial is its ability to exploit a disease phenotype to discover novel treatments for three diseases for which the root cause is unknown, complex, or multifactorial, and for which scientific understanding is insufficient to provide valid molecular targets.

ETHICS STATEMENT

The studies involving human participants were reviewed and approved by the Dongzhimen Hospital, Beijing University of Chinese Medicine (No. DZMEC-JG-2019–161). The patients/participants provided their written informed consent to participate in this study.

AUTHOR CONTRIBUTIONS

WL drafted the manuscript. CZ and YG revised the manuscript for important intellectual content. YG, LZ, and CZ proposed the conception of the study. WL, LZ, LF, DZ, CZ, and YG designed the study and oversaw all the scientific aspects regarding its

implementation. All co-authors read and approved the final manuscript.

FUNDING

This research was financially supported by the Beijing University of Chinese Medicine Project (2020-tsxk-001), the Chinese Medicine Inheritance and Innovation Talent Project-Leading Talent Support Program of National Traditional Chinese Medicine (2018, 12), the Dongzhimen Hospital Project (2020TSRC-002).

ACKNOWLEDGMENTS

The authors acknowledge contributions from the BOSS team members all over China.

SUPPLEMENTARY MATERIAL

The Supplementary Material for this article can be found online at: https://www.frontiersin.org/articles/10.3389/fphar.2021.764669/full#supplementary-material

REFERENCES

Bijur, P. E., Silver, W., and Gallagher, E. J. (2001). Reliability of the Visual Analog Scale for Measurement of Acute Pain. *Acad. Emerg. Med.* 8, 1153–1157. doi:10.1111/j.1553-2712.2001.tb01132.x

Bril, V., and Perkins, B. A. (2002). Validation of the Toronto Clinical Scoring System for Diabetic Polyneuropathy. *Diabetes Care* 25 (11), 2048–2052. doi:10.2337/diacare.25.11.2048

Chan, A. W., Tetzlaff, J. M., Gøtzsche, P. C., Altman, D. G., Mann, H., Berlin, J. A., et al. (2013). SPIRIT 2013 Explanation and Elaboration: Guidance for Protocols of Clinical Trials. *BMJ* 346 (jan08 15), e7586. doi:10.1136/bmj.e7586

Cunanan, K. M., Iasonos, A., Shen, R., Begg, C. B., and Gönen, M. (2017). An Efficient Basket Trial Design. *Stat. Med.* 36 (10), 1568–1579. doi:10.1002/sim.7227

Dong, Y., Tang, D., Zhang, N., Li, Y., Zhang, C., Li, L., et al. (2013). Phytochemicals and Biological Studies of Plants in Genus Hedysarum. *Chem. Cent. J.* 7 (1), 124. doi:10.1186/1752-153x-7-124

Executive summary (2014). Standards of Medical Care in Diabetes--2014. *Diabetes Care* 37 (Suppl. 1), S5–S13. doi:10.2337/dc14-S005

Fan, L., Zhang, F., and Sun, X. (2014). Study Progress on Stroke with Syndrome of Qi Deficiency and Blood Stasis. *World Chin. Med.* 9 (02), 257–260. doi:10.3969/j.issn.1673-7202.2014.02.036

Hao, G. M., Liu, Y. G., Wu, Y., Xing, W., Guo, S. Z., Wang, Y., et al. (2017). The Protective Effect of the Active Components of ERPC on Diabetic Peripheral Neuropathy in Rats. *J. Ethnopharmacol* 202 (Complete), 162–171. doi:10.1016/j.jep.2017.03.015

Jiang, M., Zhang, C., Zheng, G., Guo, H., Li, L., Yang, J., et al. (2014). Traditional Chinese Medicine Zheng in the Era of Evidence-Based Medicine: A Literature Analysis. *Evidence-Based Complementary Alternative Medicine* 2012, 9. doi:10.1155/2012/409568

Kasner, S. E. (2006). Clinical Interpretation and Use of Stroke Scales. *Lancet Neurol.* 5 (7), 603–612. doi:10.1016/s1474-4422(06)70495-1

Knuuti, J., Wijns, W., Saraste, A., Capodanno, D., Barbato, E., Funck-Brentano, C., et al. (2020). 2019 ESC Guidelines for the Diagnosis and Management of Chronic Coronary Syndromes. *Eur. Heart J.* 41 (3), 407–477. doi:10.1093/eurheartj/ehz425

Li, L., Wang, J., Ren, J., Xiang, J., Tang, Y., Liu, J., et al. (2007). Metabonomics Analysis of the Urine of Rats with Qi Deficiency and Blood Stasis Syndrome Based on NMR Techniques. *Chin. Sci. Bull.* 52 (22), 3068–3073. doi:10.1007/s11434-007-0389-4

Miao, G. Z., Liang, X. Z., and Wang, Y. H. (2003). Clinical Observation on Treatment of Diabetic Peripheral Neuropathy with Qi-Supplementing and Blood-Activating Therapy. *Zhongguo Zhong Xi Yi Jie He Za Zhi* 23 (11), 826–828.

Miao, J., Cheng, L., Chi, Z., Jing, Y., Yong, T., Lu, A., et al. (2012). Syndrome Differentiation in Modern Research of Traditional Chinese Medicine. *J. Ethnopharmacology* 140 (3), 634–642. doi:10.1016/j.jep.2012.01.033

Park, J. J. H., Hsu, G., Siden, E. G., Thorlund, K., and Mills, E. J. (2020). An Overview of Precision Oncology Basket and Umbrella Trials for Clinicians. *CA Cancer J. Clin.* 70, 125–137. doi:10.3322/caac.21600

Sacco, R. L., Kasner, S. E., Broderick, J. P., Caplan, L. R., Connors, J. J., Culebras, A., et al. (2013). An Updated Definition of Stroke for the 21st century: a Statement for Healthcare Professionals from the American Heart Association/American Stroke Association. *Stroke* 44 (7), 2064–2089. doi:10.1161/STR.0b013e318296aeca

The State Drug Administration (2002). *Guideline for Clinical Research of New Chinese Medicine*. Beijing: China Medical Science Press.

Uyttenboogaart, M., Stewart, R. E., Vroomen, P. C., De Keyser, J., and Luijckx, G. J. (2005). Optimizing Cutoff Scores for the Barthel Index and the Modified Rankin Scale for Defining Outcome in Acute Stroke Trials. *Stroke* 36 (9), 1984–1987. doi:10.1161/01.STR.0000177872.87960.61

Wan, J. B., Lee, S. M., Wang, J. D., Wang, N., He, C. W., Wang, Y. T., et al. (2009). Panax Notoginseng Reduces Atherosclerotic Lesions in ApoE-Deficient Mice and Inhibits TNF-Alpha-Induced Endothelial Adhesion Molecule Expression and Monocyte Adhesion. *J. Agric. Food Chem.* 57 (15), 6692–6697. doi:10.1021/jf900529w

Wang, Q.-r. (2007). in *Yi Lin Gai Cuo (Correcting the Errors in the Forest of Medicine) (Chinese and English Edition*. Editors H. O. S. B. Yuhsin Chung and T. B. Flaws. 1 ed. (Boulder, Colorado: Blue Poppy Press).

Wang, S., Liu, Q., Guo, S., Zhou, L., and Gao, Y. (2015). Item Selection Analysis of Qi Deficiency and Blood Stasis Syndrome Evaluation Scale. *Jilin J. Traditional Chin. Med.* 35 (07), 656–660. doi:10.13463/j.cnki.jlzyy.2015.07.003

Wang, Z., Zhang, P., Kou, Y., Yin, X., Han, N., and Jiang, B. (2013). Hedysari Extract Improves Regeneration after Peripheral Nerve Injury by Enhancing the Amplification Effect. *PLoS One* 8 (7), e67921. doi:10.1371/journal.pone.0067921

Wei, S. Y., Zhang, P. X., Han, N., Dang, Y., Zhang, H. B., Zhang, D. Y., et al. (2009). Effects of Hedysari Polysaccharides on Regeneration and Function Recovery Following Peripheral Nerve Injury in Rats. *Am. J. Chin. Med.* 37 (1), 57–67. doi:10.1142/S0192415X09006618

Xie, P. M. J. R. X. L. Y. (2020). Wang Yongyan's Experience in Treating Stroke: Case Series of Chinese Medicine Tonify Qi and Promote Blood Circulation. *J. Beijing Univ. Traditional Chin. Medicine(Clinical Medicine)* 27 (3), 4.

Yuan, B. (2021). Towards a Clinical Efficacy Evaluation System Adapted for Personalized Medicine. *Pharmgenomics Pers Med.* 14, 487–496. doi:10.2147/pgpm.S304420

Zhai, X., Wang, X., Wang, L., Xiu, L., Wang, W., and Pang, X. (2020). Treating Different Diseases With the Same Method-A Traditional Chinese Medicine Concept Analyzed for its Biological Basis. *Front. Pharmacol.* 11, 946. doi:10.3389/fphar.2020.00946

Zhang, H., Wang, W. R., Lin, R., Zhang, J. Y., Ji, Q. L., Lin, Q. Q., et al. (2010). Buyang Huanwu Decoction Ameliorates Coronary Heart Disease with Qi Deficiency and Blood Stasis Syndrome by Reducing CRP and CD40 in Rats. *J. Ethnopharmacol* 130 (1), 98–102. doi:10.1016/j.jep.2010.04.017

Zhou, D., Cen, K., Liu, W., Liu, F., Liu, R., Sun, Y., et al. (2021). Xuesaitong Exerts Long-Term Neuroprotection for Stroke Recovery by Inhibiting the ROCKII Pathway, *In Vitro* and *In Vivo*. *J. Ethnopharmacol* 272 (3), 113943. doi:10.1016/j.jep.2021.113943

Zhou, W., and Wang, Y. (2014). A Network-Based Analysis of the Types of Coronary Artery Disease from Traditional Chinese Medicine Perspective: Potential for Therapeutics and Drug Discovery. *J. Ethnopharmacol* 151 (1), 66–77. doi:10.1016/j.jep.2013.11.007

Conflict of Interest: The authors declare that the research was conducted in the absence of any commercial or financial relationships that could be construed as a potential conflict of interest.

Publisher's Note: All claims expressed in this article are solely those of the authors and do not necessarily represent those of their affiliated organizations, or those of the publisher, the editors and the reviewers. Any product that may be evaluated in this article, or claim that may be made by its manufacturer, is not guaranteed or endorsed by the publisher.

frontiers in Pharmacology

ORIGINAL RESEARCH
published: 18 November 2021
doi: 10.3389/fphar.2021.730525

Danlou Tablet Activates Autophagy of Vascular Adventitial Fibroblasts Through PI3K/Akt/mTOR to Protect Cells From Damage Caused by Atherosclerosis

*Li Wang[1†], Tong Wu[2†], Chunying Si[1], He Wang[1], Ke Yue[3], Shasha Shang[1], Xiaohui Li[1], Yushan Chen[1] and Huaimin Guan[1]**

[1]Department of Cardiovascular Medicine, The First Affiliated Hospital of Henan University of Chinese Medicine, Zhengzhou, China, [2]Department of Cardiovascular Medicine, The First Affiliated Hospital of Guangzhou University of Chinese Medicine, Guangzhou, China, [3]The First Clinical Medical College, Henan University of Chinese Medicine, Zhengzhou, China

OPEN ACCESS

Edited by:
Mas Rizky A. A Syamsunarno, Padjadjaran University, Indonesia

Reviewed by:
Gao Zhu Ye, China Academy of Chinese Medical Sciences, China
Chongming Wu, Chinese Academy of Medical Sciences and Peking Union Medical College, China

***Correspondence:**
Huaimin Guan
guanhuaimin2021@163.com

†These authors have contributed equally to this work and share first authorship

Specialty section:
This article was submitted to Ethnopharmacology, a section of the journal Frontiers in Pharmacology

Received: *25 June 2021*
Accepted: *11 October 2021*
Published: *18 November 2021*

Citation:
Wang L, Wu T, Si C, Wang H, Yue K, Shang S, Li X, Chen Y and Guan H (2021) Danlou Tablet Activates Autophagy of Vascular Adventitial Fibroblasts Through PI3K/Akt/mTOR to Protect Cells From Damage Caused by Atherosclerosis. Front. Pharmacol. 12:730525. doi: 10.3389/fphar.2021.730525

Danlou tablet (DLT), a commercial Chinese patent medicine, has been widely used to treat cardiovascular diseases for many years. Atherosclerosis (AS) is the leading cause of cardiovascular disease. Increasing evidence indicates that autophagy plays a vital role in the development of AS. Here we investigated whether DLT could activate autophagy to improve AS and further clarified its underlying mechanisms. In an ApoE$^{-/-}$ mice model, the results of Oil red O, Masson's trichrome, and H&E staining techniques showed that DLT significantly inhibited lipid accumulation and fibrosis formation in atherosclerotic plaque tissue. DLT also inhibited serum triglyceride, cholesterol, and low-density lipoprotein levels and suppressed serum levels of inflammatory factors interleukin-6 and tumor necrosis factor-α in ApoE$^{-/-}$ mice. Moreover, DLT suppressed proliferation, migration, and invasion of human vascular adventitial fibroblasts (HVAFs) by inhibiting the PI3K/Akt/mTOR pathway. In addition, western blot analysis showed that Danlou tablet treatment decreased the expression of p62 and increased Beclin 1 and LC3 I -to-LC3 II ratios in HVAFs. The role of autophagy in treating atherosclerosis by DLT is confirmed by 3-methyladenine (autophagy inhibitor) and rapamycin (autophagy activator) in HVAFs. In summary, DLT activated PI3K/Akt/mTOR-mediated autophagy of vascular adventitial fibroblasts to protect cells from damage caused by atherosclerosis.

Keywords: atherosclerosis, danlou tablet, autophagy, PI3K/AKT/mTOR, Chinese patent medicine

INTRODUCTION

Atherosclerosis (AS), characterized by the accumulation of lipids and inflammatory cells in arterial walls, is a common pathological basis for many cardiovascular diseases (CVDs) (Falk, 2006). Although hypolipidemic agents, interventional therapy, and other conventional treatments have been used to treat this condition, atherosclerosis and its associated CVDs remain the leading cause of

Abbreviations: AS, atherosclerosis; HVAFs, human vascular adventitial fibroblasts; LDL, low-density lipoprotein; TC, total cholesterol; TG, triglyceride; DLT, danlou tablet; RST, rosuvastatin; ICAM-1, intercellular adhesion molecule-1; VCAM-1, vascular cell adhesion molecules-1.

death worldwide (Wu et al., 2020). Therefore, it is necessary to develop novel treatment strategies for AS.

Abnormal lipid metabolism usually occurs in the initial stages of AS (Schaftenaar et al., 2016), especially concerning oxidized low-density lipoproteins (Ox-LDL), leading to the accumulation of foam cells and the formation of lipid plaques on blood vessel walls; this leads to luminal stenosis and alterations in the structure of blood vessel walls (Ference, 2018; Pirillo et al., 2018). At present, studies on the mechanism of AS mainly focus on the inflammatory response (Tedgui and Mallat, 2006; Fatkhullina et al., 2016; Zhu et al., 2018), oxidative stress (Khosravi et al., 2019), and autophagy (Grootaert et al., 2018; Tang et al., 2018). Inflammatory factors IL-6 and TNF-α play an essential role in all the stages of atherosclerosis, including plaque formation, progression, and rupture. Therefore, anti-inflammatory therapy can be a part of anti-atherosclerosis treatment (Poznyak et al., 2021). Autophagy is a biological process in which macromolecular substances and organelles in the cytoplasm are degraded in autolysosomes, meeting the metabolic needs of cells and renewing some organelles (Jenzer and Legouis, 2017; Ravanan et al., 2017). Previous studies have shown that autophagy might be a potential therapeutic strategy against AS. mTOR pathway plays a vital role in autophagy (Wang and Zhang, 2019). PI3K/Akt and MAPK signaling pathways activate mTOR pathways to inhibit autophagy, while AMPK and P53 signaling pathways suppress the activation of mTOR pathways to promote autophagy (Kim et al., 2017; Ba et al., 2019). It has been clinically verified that mTOR inhibitors, such as rapamycin, can efficiently inhibit the growth of atherosclerotic plaques (Martinet et al., 2014; Zhai et al., 2014).

Danlou tablet (DLT), a commercial Chinese patent medicine, has been approved by the China Food and Drug Administration (No. Z20050244) and is composed of 10 herbs, including *Trichosanthes kirilowii* Maxim. (Cucurbitaceae; Trichosanthis pericarpium), *Allium macrostemon* Bunge (*Amaryllidaceae*; Allii macrostemonis bulbus), *Pueraria montana* var. lobata (Willd.) Maesen and S.M.Almeida ex Sanjappa & Predeep (Fabaceae; Puerariae lobatae radix), Conioselinum anthriscoides "Chuanxiong" (Apiaceae; Chuanxiong rhizoma), Salvia miltiorrhiza Bunge (Lamiaceae; *Salviae miltiorrhizae* radix et rhizoma], *Paeonia lactiflora* Pall. (Paeoniaceae; Paeoniae radix rubra), Alisma plantago-aquatica subsp. orientale (Sam.) Sam. (Alismataceae; Alismatis rhizome), *Astragalus* mongholicus Bunge (Fabaceae; *Astragali radix*), *Davallia trichomanoides* Blume (Polypodiaceae) and *Curcuma aromatica* Salisb. (Zingiberaceae; Curcumae radix) (Gao et al., 2020). Studies have shown that DLT effectively alleviates the symptoms of angina pectoris, reduces the total cholesterol (TC) and low-density lipoprotein (LDL), mitigates inflammation, improves heart function, and reduces the incidence of cardiovascular events (Mao et al., 2016; Chen et al., 2017). Some clinical studies have shown that DLT combined with rosuvastatin dramatically reduces blood lipid levels and suppresses the formation of AS plaques in the carotid artery (Cao et al., 2015b; Liu et al., 2019). A study confirmed the role of DLT in regulating the expression of PI3K and Akt protein in an animal model of AS (Cao et al., 2015a). However, further research is still required to determine whether DLT can regulate PI3K/Akt/mTOR-mediated autophagy to alleviate AS.

This study aimed to explore the role of DLT in the development of AS and clarified its regulatory mechanisms *in vitro* and *in vivo* to provide a theoretical and practical basis for the therapeutic efficacy of DLT for AS.

METHODS

Drug Preparation

DLT was manufactured by Jilin Connell Pharmaceutical Co. Ltd., China, following the Chinese Pharmacopoeia 2015 (Commission of Chinese Pharmacopoeia, 2015). Conioselinum anthriscoides "Chuanxiong" (52 g), *Curcuma aromatica* Salisb (52 g) and Alisma plantago-aquatica subsp. orientale (Sam.) Sam. (138 g) are ground into fine powders, then sieved and mixed. *Paeonia lactiflora* Pall (52 g), *Trichosanthes kirilowii* Maxim (86 g), and Allium macrostemon Bunge (40 g) are extracted twice by heat reflux with 70% ethanol for 1.5 h. The ethanol extract is collected and filtered, then condensed in vacuo to a final relative density of 1.25 and 1.30 (65°C). Pueraria *montana* var. lobata (Willd.) Maesen and S.M. Almeida ex Sanjappa and Predeep (138 g) and Salvia miltiorrhiza Bunge (138 g) (individually packed) are extracted three times with ethanol by heat reflux for 1 h. Extracts are collected and filtered, then condensed in vacuo to final relative densities between 1.25 and 1.30 (65°C). *Astragalus* mongholicus Bunge (114 g), *Davallia* trichomanoides Blume (26 g), and the extracted residue from Salvia miltiorrhiza Bunge are extracted twice with water for 1.5 h. Extracts are collected and filtered, then condensed in vacuo to final relative densities between 1.25 and 1.30 (65°C). The condensed extracts are mixed with the fine powder, desiccated in vacuo, ground, and pelletised. The mixture is made into 1,000 tablets (0.3 g per tablet) and film-coated. DLT-containing serum was added to the medium for the treatment of cells in culture. DLT-containing serum was prepared as follows: Twenty healthy male SD rats (Guangdong Medical Laboratory Animal Center) were randomly divided into two groups: Rats in the DLT group were administered the drug, 1,400 mg/kg/d. Normal saline was administered to rats in the blank-controlled group. Volumes administered were the same for both groups of animals. Drug or saline was given by gavage for 7 days. Rats were sacrificed 2 h after the last oral administration. Blood samples were collected from the abdominal aorta, centrifuged at 4°C, 3,000 rpm for 20 min. Supernatants were filtered, sterilized, and stored at −80°C for later use.

Animal Model

Six-week-old male C57BL/6 mice and $ApoE^{-/-}$ mice were purchased from Guangdong Medical Laboratory Animal Center. DLT was purchased from Jilin Cornell Pharmaceutical Co., LTD (Jilin, China). The mice were housed in plastic cages and fed with food and water at an ambient temperature of 23 ± 2°C. All of the mice were divided into six groups (n = 8) randomly after a week: (1) normal control group (NC), (2) atherosclerosis model group (AS model), (3) atherosclerosis model group with low-Danlou tablet (AS model + Low-DLT), (4) atherosclerosis model group with medium-Danlou tablet (AS model + Med-DLT), (5) atherosclerosis model group with high-Danlou tablet (AS model + High-DLT), and (6) atherosclerosis model group with rosuvastatin calcium tablet (AS model + RST). C57BL/6 mice were used as a normal group and fed with a normal

diet. ApoE$^{-/-}$ mice were used to establish an atherosclerosis model, fed with a high-fat diet and different doses of drug: Low-DLT (700 mg/kg/d); Med-DLT (1,400 mg/kg/d); High-DLT (2,800 mg/kg/d); rosuvastatin calcium tablet (10 mg/kg/d), via intragastric gavage, for 10 weeks. DLT powder was suspended and diluted with physiological saline and then administered to mice. After the last drug administration, the mice were euthanized by inhaling an overdose of ether; then, blood and aortic sinus samples were collected for testing. All the animal procedures were approved by the Ethics Committee of The First Affiliated Hospital of Henan University of Chinese Medicine (YFYDW2019-041).

Histological Examination

The mice were euthanized, and the sections of aortic sinuses were harvested. The tissues were immediately fixed in 4% paraformaldehyde. Paraffin-embedded tissues were sectioned (4 μm in thickness), placed on poly-l-lysine-coated slides, and incubated for 1.5 h at 60°C. Conventional hematoxylin and eosin staining was performed (H&E), and the degree of inflammation was graded. The fibrosis level was evaluated by Masson staining of collagen accumulation according to the manufacturer's protocol (Solarbio, China). Oil red O staining was performed using the lipid staining kit (Oil Red O) according to the manufacturer's instructions. The stained sections were observed under a light microscope (Nikon, Ci-E).

ELISA

Serum was harvested from the peripheral blood of the mice. The HDL level was assessed using ELISA kit (Elabscience, E-EL-M1402c) following the manufacturer's instructions. The TC and LDL levels were assessed using the total cholesterol colorimetric test kit (Elabscience, E-BC-K109-M; NJJCBIO A113-1-1). The TG level was assessed by the triglyceride test kit (NJJCBIO, A110-1-1), according to the manufacturer's instructions. A commercially available ELISA kit was used to measure the serum levels of inflammatory markers: IL-6 (MEIMIAN, MM-0163M1) and TNF-α (MEIMIAN, MM-0132M2).

Cell Culture

Human vascular adventitial fibroblasts (HVAFs) were obtained from WUHAN PROCELL LIFE SCI&TECH CO., LTD. HVAFs were inoculated into a Petri dish pre-coated with polylysine and incubated at 37°C under 5% CO_2. The culture medium was changed 48 h later for the first time and then every 3 days. The cells were then overgrown for use. OX-LDL was used to induce an atherosclerotic cell model.

Cell Viability Assays

Cell proliferation was determined by the cell counting kit 8 assay (CCK8, Dojindo) and EdU staining assay (RIBOBIO, Cat. No. C10327) following the manufacturer's protocol. Different groups of cells were treated as indicated in the figure legend for 3 days. At different time intervals (0, 1, 2, and 3 days) after plating, CCK-8 and EdU solutions were added to each well. CCK-8 assay was measured at 450 nm using a microplate reader (SpectraMax M3, Molecular Devices). The cells in the EdU assay were fixed in 4% paraformaldehyde overnight at room temperature and photographed under an inverted fluorescence microscope (Leica, Germany).

Wound Healing Assays

After being seeded in 6-well plates at a confluence of about 80–90% after 24 h of incubation, the cells were wounded using a 200-μL pipette tip to scratch the monolayer of the subconfluent cell. Then, the cells underwent different drug treatments for 24 h. For the next 48 h, the cells were cultured in a serum-free medium and allowed to migrate. The images of cell migration were captured using an inverted microscope. The migration speed was calculated by dividing the length of the gap by the wound areas in the captured images.

Transwell Assays

Millicell chambers with polycarbonate microporous membranes and artificial matrigel were used. The cells were digested, collected, and washed with phosphate buffered saline (PBS) once and suspended with a serum-free medium to adjust the concentration to 2×10^5/ml; 800 μL of 10% serum medium was added to the bottom chamber, and then 100–150 μL of cell suspension was added to the upper chamber. The culture continued for 12 h in the incubator. The chamber was retrieved and fixed with methanol for 30 min at room temperature. Next, the chambers were moved to a well with 800 μL of crystal violet solution to be stained at room temperature for 15 min. The cells on the membrane surface at the bottom of the upper chamber were carefully wiped off using a wet cotton swab. Then the membrane was carefully removed with forceps and dried upward. The membrane was transferred to a slide and sealed with neutral resin, and photographs were taken under an inverted fluorescence microscope. Nine random fields were selected and counted.

Immunofluorescence Microscopy Analysis

The cell slides were fixed with 4% paraformaldehyde solution at room temperature. After 15 min, the cells were washed with PBS three times and permeabilized by immersion in 0.3% Triton X-100 in PBS for 10 min. Then the slides were blocked with 2% bovine serum albumin (BSA) in PBS for 1 h at room temperature and incubated with the primary antibodies Vimentin (ab8978, 1:500, Abcam) and LC3B (ab229327, 1:200, Abcam) at 4°C overnight. Afterward, the slides were stained with fluorescently-labeled secondary antibody for 1 h at room temperature and mounted by VECTASHIED solution (vector) with DAPI. The images were taken under a confocal fluorescence microscope (Olympus, Japan) and analyzed by NIS elements imaging software.

Western Blot

The total protein extraction was performed with RIPA lysis buffer (mixed with phosphatase and protease inhibitor), and protein quantification was carried out with a BCA kit. The samples were separated on 4–20% SDS-PAGE gel and then transferred to a nitrocellulose membrane. After blocking by 5% skimmed milk for 1 h, the membrane was incubated overnight at 4°C with specific antibodies: p-mTOR (#5536, 1:1,000, CST), mTOR (#2983, 1:1,000, CST), AKT (#4691, 1:1,000, CST), p-AKT (#4060, 1:1,000, CST) p-S6 (#2215, 1:1,000, CST), LC3A/B (#12741, 1:1,000, CST), P62

(#5114, 1:1,000, CST), Beclin-1 (ab210498, 1:1,000, Abcam), ICAM-1 (ab53013, 1:1,000, Abcam), VCAM-1 (ab115135, 1:1,000, Abcam), and GAPDH (ab8245, 1:5,000, Abcam). After being washed with TBST buffer three times, the membrane was further incubated with the secondary antibody for 1 h, washed three times with TBST buffer, and then exposed in ECL developer in Image lab.

Transmission Electron Microscope Analysis

The samples were dropped on a carbon support membrane copper mesh for 3–5 min, and then a filter paper was used to absorb excess liquid. Then, 2% phosphotungstate was dropped on the carbon support membrane copper mesh for 2–3 min and air-dried at room temperature. The images were observed under a transmission electron microscope (HT7700 HITACHI) and captured for analysis.

Statistical Analysis

GraphPad Prism software was used to perform statistical analyses. The experimental data were expressed as the mean ± SD, analyzed by one-way ANOVA, followed by Student's t-tests. Differences with $p < 0.05$ were considered statistically significant ($^{*}p < 0.05$, $^{**}p < 0.01$, and $^{***}p < 0.001$).

RESULTS

Danlou Tablet Relieves Pathological Lesion of AS in ApoE$^{-/-}$ Mice Model

To detect the influence of the medical tablet on AS *in vivo*, we first established an AS mouse model using the ApoE$^{-/-}$ mice by a high-fat diet, and significant AS plaque was observed as previously described (Emini Veseli et al., 2017). To further elucidate the therapeutic effect of Danlou tablet, different doses of Danlou tablet and rosuvastatin calcium tablet were administrated, and AS plaque tissues were harvested from the mice, followed by the assessment for the degree of the lesion. Histological examinations demonstrated thicker plaque in ApoE$^{-/-}$ mice than the control mice. While Danlou tablets significantly reduced the degree of pathological lesions in a dose-dependent manner based on H&E staining (**Figure 1A**), they exhibited efficacy comparable to traditional rosuvastatin calcium tablets. In addition, lipid accumulation and fibrosis formation were alleviated in the Danlou tablet-treated ApoE$^{-/-}$ mice according to the Oil Red O and Masson trichrome staining, red lipid droplets accumulated mostly at the edge of AS lesions (**Figures 1B,C**).

In order to investigate the biochemical basis that leads to the pathological results, we collected serum samples from the mice to determine the blood total cholesterol (TC), triglyceride (TG), high-density lipoprotein (HDL), and low-density lipoprotein (LDL) levels and inflammatory factors, like IL-6 and TNF-α. Interestingly, Danlou tablets significantly reduced TC (**Figure 2A**), TG (**Figure 2B**), and LDL (**Figure 2C**) levels but did not alter the HDL (**Figure 2D**) levels in ApoE$^{-/-}$ mice. Of note, two inflammatory factors, IL-6 (**Figure 2E**) and TNF-α (**Figure 2F**), were strongly decreased by high-dose treatment of Danlou tablets. Collectively, these data underline the capacity of Danlou tablets to alleviate AS *in vivo*.

DLT Inhibits the Ox-LDL Effects in HVAF Cells

LDL could accumulate in fibroblasts at the edge of some AS lesions, which might be an early indication of atherosclerosis (Lees et al., 2001). We used a human vascular adventitial fibroblasts (HVAFs) cell line to identify the mechanism of Danlou tablets (DLT) in alleviating AS. We confirmed the high expression of vimentin, a well-known marker of HVAFs, by immunofluorescence cytometry (**Figure 3A**). Next, an AS cell model was established by adding ox-LDL to the HVAFs culture medium. Therefore, the effect of DLT was evaluated *in vitro* by this AS cell model. As indicated in **Figure 3B**, DLT-containing serum notably reduced the growth of HVAFs, which were significantly stimulated by ox-LDL through the CCK8 experiment. The anti-proliferation ability of DLT was also similar to rosuvastatin (RST), consistent with the EDU staining assay (**Figure 3D**). The cell wound healing assay and transwell assay illustrated that DLT significantly down-regulated cell migration and invasion ability compared to RST treatment (**Figures 3C,E**). After activation, HVAFs can secrete a large amount of intercellular adhesion molecule-1 (ICAM-1), vascular cell adhesion molecules (VCAM-1) (Liu et al., 2010), chemokines, and inflammatory factors to accelerate the chemotaxis of monocytes and lymphocytes and mediate the inflammatory response. Therefore, we used western blotting to detect the ICAM-1 and VCAM-1 expression after ox-LDL treatment, and the results were consistent with the phenotype of HVAFs (**Figure 4E**). In short, these data suggest that DLT might slow down the formation of AS by suppressing the activity of HVAFs.

DLT Activates Autophagy in HVAFs

It is well established that vascular endothelial cells undergo autophagy to protect their structures from inflammation and oxidative stress when stimulated by ox-LDL in AS. Here, we speculated that the reduced activity of HVAFs might result from the alteration of autophagy. To directly determine the degree of autophagy in HVAFs, we detected the LC3B level by immunofluorescence cytometry. As shown in **Figure 4A**, DLT increased the expression of LC3B, indicating a high rate of autophagy. Moreover, we also observed the extensive formation of phagosomes under the transmission electron microscope (**Figure 4B**). Consistent with this finding, increased expression of Beclin1 and LC3 I-to-LC3 II ratio further supported our hypothesis (**Figure 4D**). In addition, the increased expression of p62 in the autophagosome degradation stage is usually regarded as a sign of inhibited autophagy activity. We also showed *via* Western blot that DLT reduced the expression of p62 (**Figure 4D**). Altogether, we concluded that DLT activates autophagy to protect HVAFs from damage caused by AS.

DLT Activates Autophagy Through PI3K/Akt/mTOR Pathway

To explain our findings, we analyzed the signal molecular mechanisms involved in autophagy as previous studies have demonstrated that the mTOR pathway is a key link of the autophagy process. PI3K/Akt and MAPK signaling pathways induce the activation of mTOR to inhibit autophagy. For instance, the activated PI3K-I generates PIP3 in cells,

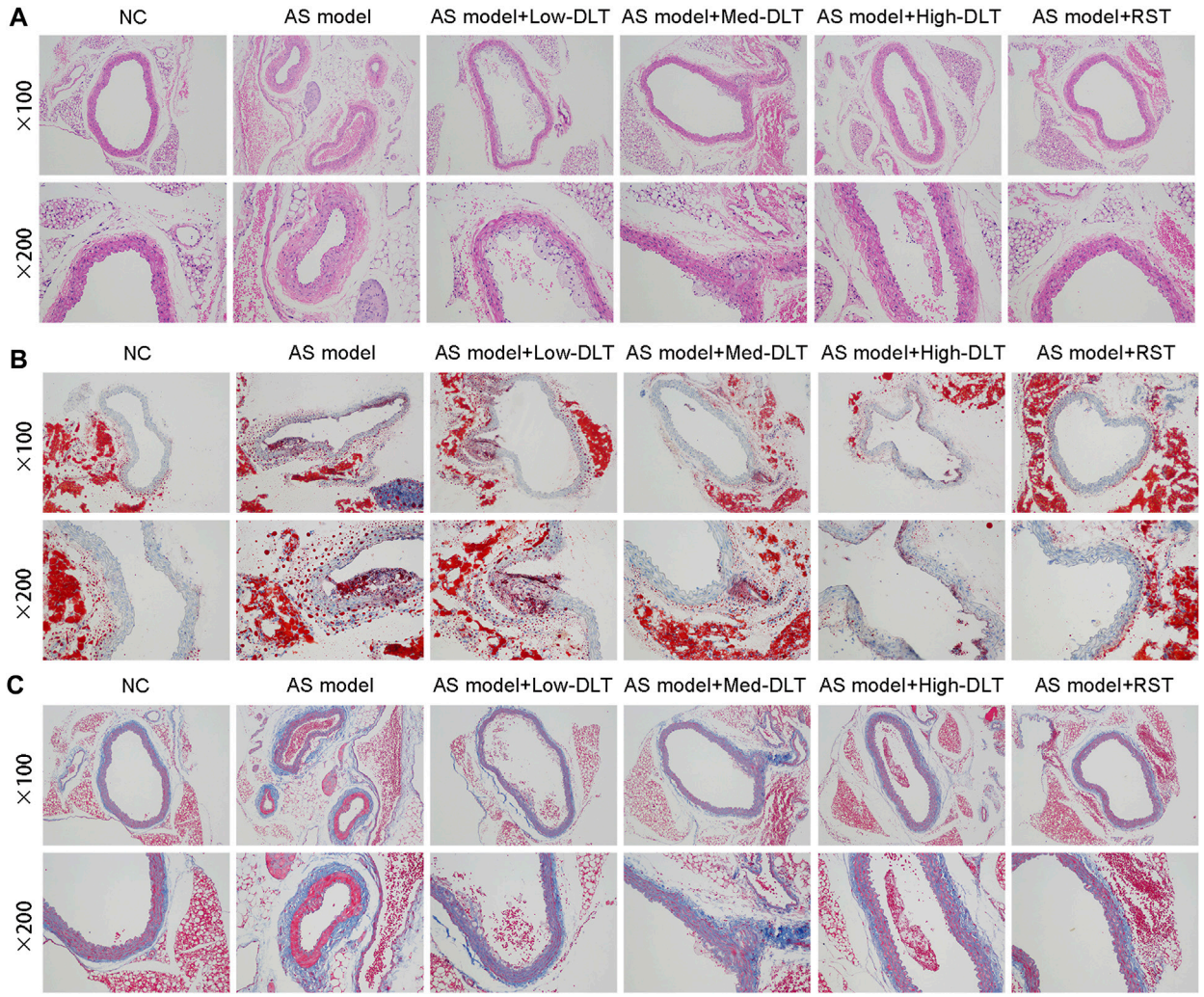

FIGURE 1 | Danlou tablets relieve the pathological lesion of AS in the ApoE$^{-/-}$ mice model. **(A)** Representative photomicrographs of hematoxylin eosin-stained aortic sinuses. **(B)** Representative photomicrographs of Oil red O-stained aortic sinuses. **(C)** Masson trichrome staining to show the fibrosis in different groups.

activating Akt with the assistance of PDK1, inhibiting the TSC1/2 complex and activating mTORC1 (Dieterle et al., 2014). Ribosomal protein S6 is a downstream target of mTOR. Levels of phospho-S6 are a frequently used marker of activation of the mTOR pathway. Phosphorylation of S6 exerts an inhibitory effect on autophagic proteolysis (Hay and Sonenberg, 2004; Lu et al., 2019). To exploit the contribution of mTOR pathways to the alteration of autophagy in HVAFs, we analyzed the indicated signaling pathways by western blotting. As the level of phosphorylated mTOR, Akt, and S6 were notably decreased by the administration of DLT (**Figure 4C**), these findings indicate that DLT activated autophagy partly through inhibiting the mTOR via the PI3K/Akt pathway.

mTOR Pathway Agonist Reverses the Effect of DLT

To verify the influence of DLT on the mTOR signaling pathway, we further performed 3-MA, an mTOR pathway agonist (Wu et al., 2013), to study whether activated autophagy could be reversed. As expected, the decreased proliferation of HVAFs was distinctly restored by 3-MA (**Figures 5A,B**). Of note, the efficiency of DLT in the cells was comparable to Rapa, a conventional antagonist of the mTOR signaling pathway (Cai et al., 2018). The results presented in **Figures 5C,D** also indicated that 3-MA increased the motility of HVAFs. The raised expression of ICAM-1 and VCAM-1 via western blotting (**Figure 6E**) further manifested the recuperative activity of HVAFs.

3-methyladenine (3-MA) is a widely used inhibitor of autophagy due to its inhibitory effect on PI3K and suppression of the conversion of LC3-I to LC3-II (Zhang et al., 2020). Here we observed reduced autophagy by the lower expression of LC3B by immunofluorescence cytometry (**Figure 6A**) and decreased formation of phagosomes under the transmission electron microscope in the 3-MA group (**Figure 6B**). The lower expression of Beclin1 and LC3 I -to-LC3 II ratio by western blotting were consistent with the phenotype. In addition, we also demonstrated increased expression of P62 via

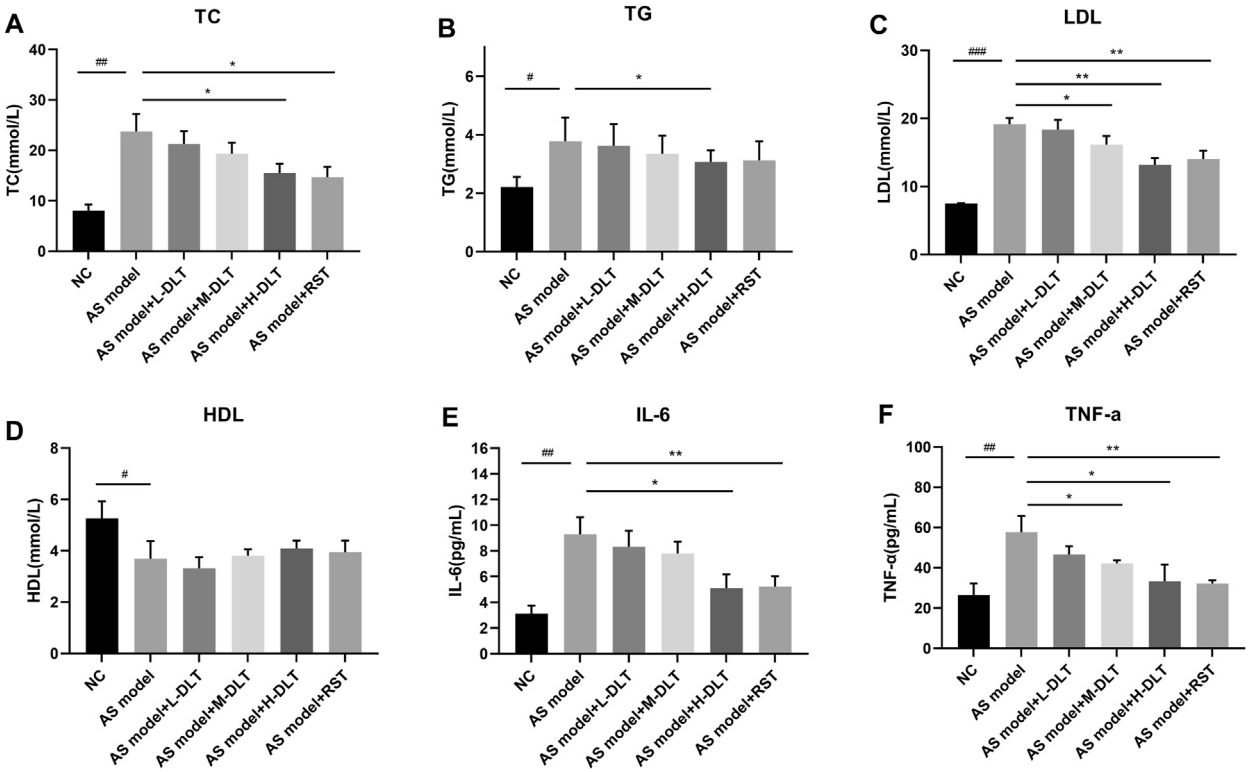

FIGURE 2 | The AS-related cytokines detection in a Danlou tablet-treated ApoE$^{-/-}$ mice model. **(A–D)** Lipid levels were detected by ELISA and biochemical test, including LDL, HDL, TC, TG. **(E, F)** ELISA kits were used to check the immune factors (IL-6 and TNF-α) in different groups (#$p < 0.05$, ##$p < 0.01$, ###$p < 0.001$ AS model group vs. normal control group; *$p < 0.05$, **$p < 0.01$, ***$p < 0.001$ drug treatment group vs. AS model group, $n = 8$, tested by one-way ANOVA).

western blotting (**Figure 6D**). Data from western blotting also confirmed that 3-MA reversed the activated autophagy by DLT by stimulating the mTOR via the PI3K/Akt pathway (**Figure 6C**). Treatment with DLT decreased p-mTOR protein levels, increased conversion of LC3-I to LC3-II, and activated autophagy compared with the ox-LDL group, but the effect could be reversed by 3-MA (**Figures 6 B–D**). In conclusion, the therapeutic effect of DLT could be reversed by inhibiting autophagy through the mTOR pathway agonist, indicating the pivotal role of the PI3K/Akt/mTOR pathway in this process.

DISCUSSION

Atherosclerosis, a complex and common condition involving chronic inflammation and vascular remodeling processes, is the pathological basis of many cardiovascular diseases (Peng et al., 2016). Apolipoprotein E (ApoE) is a protein involved in the transformation and metabolism of lipoproteins. Lack of ApoE might result in the accumulation of cholesterol in the circulating blood, leading to the formation of atherosclerotic lesions (Wang et al., 2017). The pathological characteristics of ApoE$^{-/-}$ mice with atherosclerosis are very similar to those of humans with atherosclerosis. Moreover, compared with the ApoE$^{-/-}$ mice with normal diets, there were significantly increased atherosclerotic plaques, inflammatory cells, deposits of neutral lipid droplets, and decreased matrix fiber components in the fiber caps in ApoE$^{-/-}$ mice fed a high-fat diet (Zhou et al., 2009). Therefore, the high-fat diet-fed ApoE$^{-/-}$ mouse model is ideal for studying atherosclerosis. Therefore, a high-fat diet-fed ApoE$^{-/-}$ mouse model was used in our study to explore the effect and underlying mechanism of DLT on atherosclerosis.

Danlou tablet, a traditional Chinese medicine, consists of 10 herbs and has been approved to treat ischemic heart disease for a long time (Mao et al., 2016; Ding et al., 2019). The Danlou tablet has been demonstrated to alleviate phlegm and stasis mutual obstruction syndrome, reduce serum inflammatory factor levels, and improve the quality of life in patients with unstable angina pectoris (Wang et al., 2016). Current research data indicate that Danlou tablet inhibits atherosclerosis *via* various mechanisms, including the inhibition of Angptl4 protein level through the HIF-1α-Angptl4 mRNA signaling pathway (Tang et al., 2020), inhibition of the NF-κB-mediated inflammatory response (Gao et al., 2020), and prevention of PPARα/ABCA1-regulated lipid deposition (Hao et al., 2019). In our research, Danlou tablets significantly relieved the pathological process of atherosclerosis in ApoE$^{-/-}$ mice, including decreased lipid accumulation, fibrosis formation, and inflammation responses. Interestingly, the capability of Danlou tablets is even comparable to rosuvastatin.

Autophagy is a biological process in which cells degrade damaged proteins and disordered organelles *via* autolysosomes. It plays an

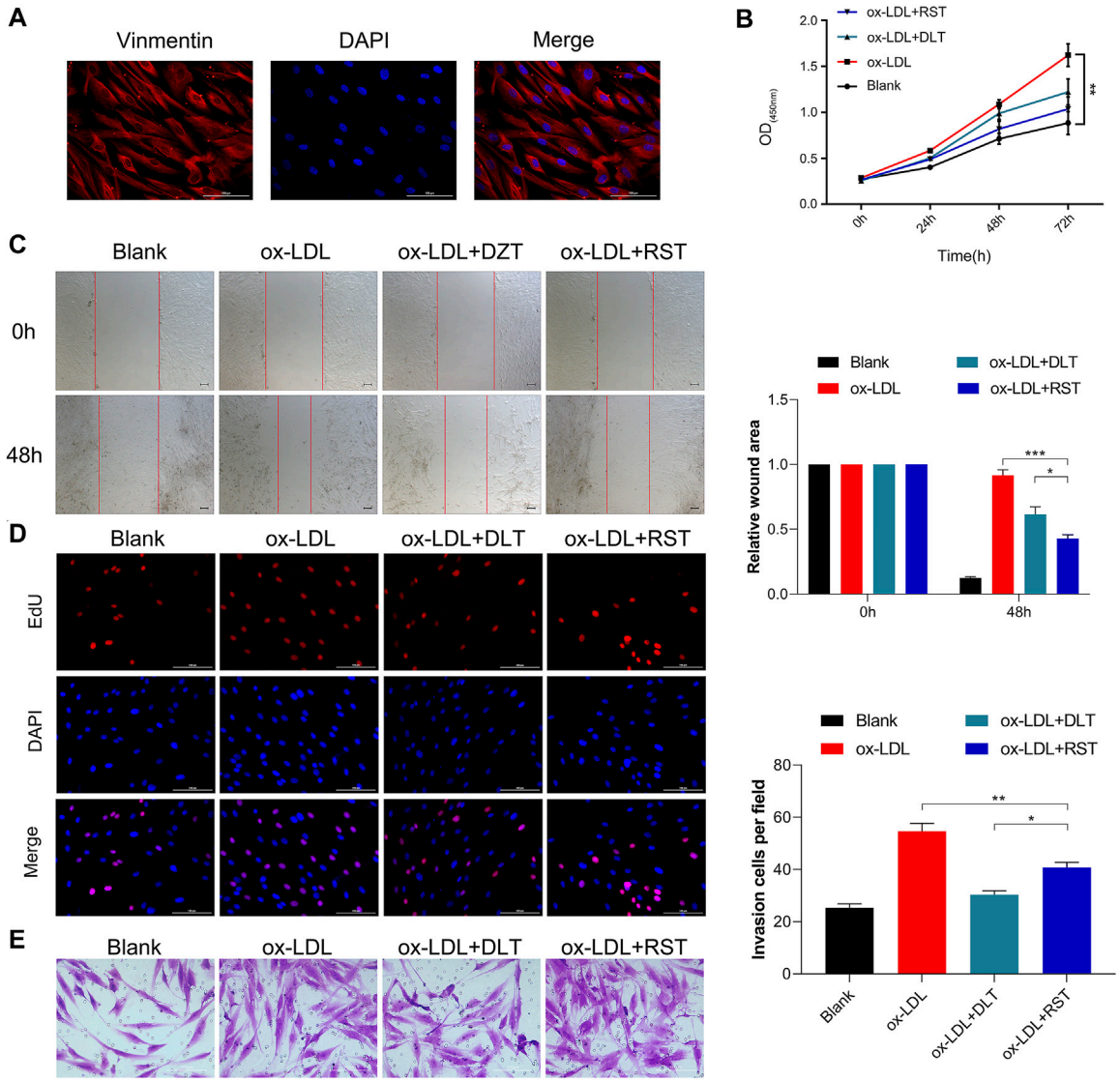

FIGURE 3 | DLT inhibits the ox-LDL effects in the HVAF line. **(A)** Vimentin staining was used to identify the human vascular adventitial fibroblasts (HVAFs). **(B, D)** Cell proliferation was evaluated by CCK8 and EDU staining. **(C, E)** Wound healing and transwell assay showed the migration ability in the ox-LDL-induced model and DLT treatment group (*$p < 0.05$, **$p < 0.01$, ***$p < 0.001$).

essential role in maintaining cell homeostasis (Jenzer and Legouis, 2017; Ravanan et al., 2017). Growing evidence shows that impaired autophagy is responsible for atherosclerotic plaque development, disordered lipid metabolism, and vascular endothelial cell dysfunction (Peng et al., 2016). Inflammation is responsible for development of atherosclerosis (Li et al., 2017). Recently, a pivotal regulatory role has been confirmed in the ATG16L1 (autophagy-related 16-like 1)-deficient mice for autophagy in generating proinflammatory cytokines, including IL-1β and IL-18 (Saitoh et al., 2008). This evidence suggests that autophagy plays a crucial role in the regulation of inflammatory responses. Dysfunctional autophagy significantly activates the inflammatory response, promoting atherosclerosis (Razani et al., 2012). In our study, DLT significantly reduced inflammatory factor IL-6 and TNF-α levels in AS model, activated autophagy of vascular adventitial fibroblasts, which may be part of its anti-atherosclerosis mechanism. Moreover, a growing body of evidence demonstrates that mTOR inhibitors, such as rapamycin, possess obvious anti-atherosclerotic effects and should be considered supplementary therapy for atherosclerosis. Therefore, autophagy-mediated inflammatory responses might be a potential therapeutic strategy against atherosclerosis, opening up new horizons for the treatment of atherosclerosis.

In the human vascular adventitial fibroblasts cell model, we discovered that Danlou tablets prominently suppressed cell proliferation and mobility. Furthermore, Danlou tablets activated the autophagy process by regulating the PI3K/Akt/mTOR pathway to intervene in the activity of HVAFs. As was expected, the autophagy inhibitor 3-MA significantly suppressed the effect of Danlou tablets on

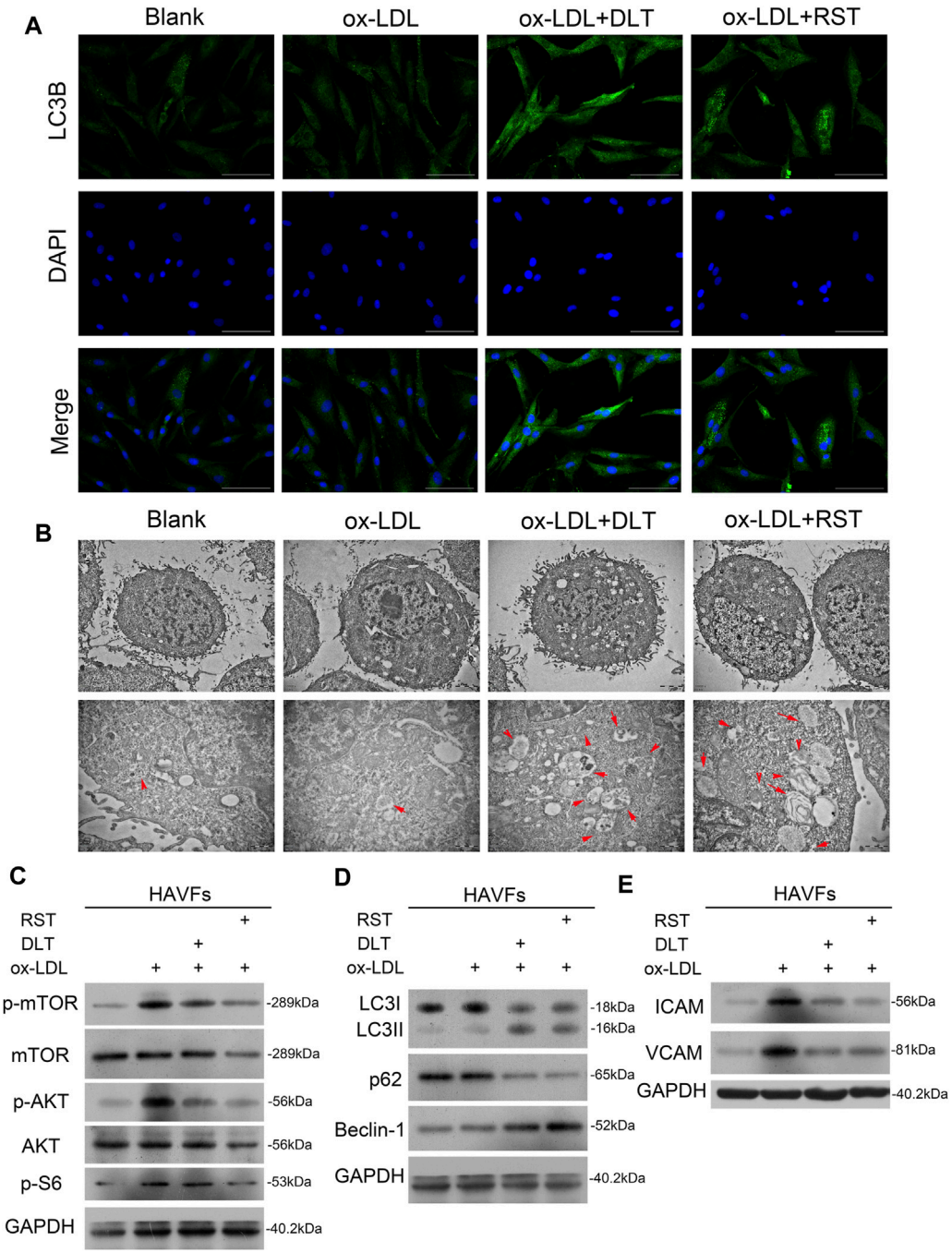

FIGURE 4 | DLT activates the autophagy pathway in HVAFs through the PI3K/Akt-mTOR pathway. **(A)** Immunofluorescence staining of LC3 to show the activation of autophagy in the DLT treatment group. **(B)** Transmission electron microscopy analysis to show the autophagosome in the DLT treatment group (red arrow). **(C)** Western blot showed DLT treatment reversed the ox-LDL-induced activation of the PI3K/Akt-mTOR pathway. **(D)** The autophagy marker expression was detected by western blotting and increased in the DLT treatment model. **(E)** The HVAFs activation markers ICAM-1 and VCAM-1 were checked in the DLT-treated and ox-LDL model.

atherosclerosis, while rapamycin, an autophagy activator, significantly enhanced the effect of Danlou tablets on atherosclerosis. This evidence suggests that Danlou tablets can activate PI3K/Akt/mTOR-mediated autophagy to improve atherosclerosis.

In-vitro experiment with medicated serum of traditional Chinese medicine has been applied to diseases research (Shi et al., 2016; Deng et al., 2021). In order to find the appropriate serum concentration to evaluate drug effect, the animal is usually gavaged with the equivalent of 1–10 times the clinical dose for several days, and then the medicated serums are collected 0.5–2 h after the last dose. Finally, the serums are diluted with different concentration for preliminary

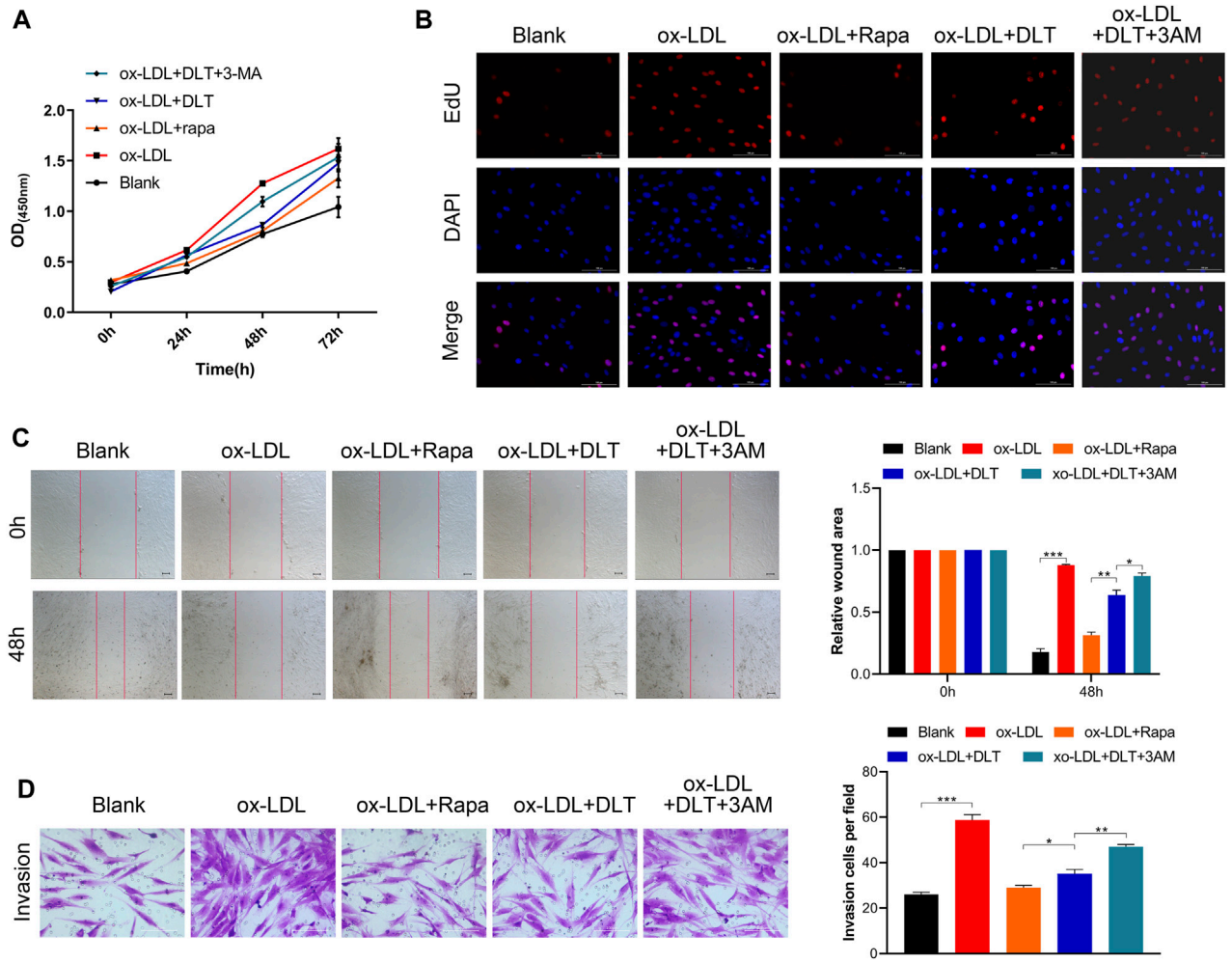

FIGURE 5 | mTOR pathway agonist reverses the effect of DLT. **(A, B)** CCK8 and EDU assay were used to evaluate the proliferation of DLT and mTOR pathway agonist effects in the AS model. **(C, D)** The wound healing and transwell showed that the mTOR pathway agonist could increase the DLT-induced migration in the AS cell model (*$p < 0.05$, **$p < 0.01$, ***$p < 0.001$).

experiments to determine the concentration for *in vitro* experiments (Ma et al., 2017). The human dosage of DLT is 4.5 g per day (75 mg/kg/d for a 60 kg person) according to drug instructions. A guide for human and animal dose conversion indicates that drug consumption for rat is 6.2 times that for humans (Nair and Jacob, 2016). In our experiment, DLT (1,400 mg/kg/day) with 3 times the effective dosage for human body was given to rats by intragastric administration to prepare medicated serums. Then, DLT-containing serums at concentrations of 2.5, 5, 10, and 20% were used for preliminary *in vitro* experiments respectively. The results showed that the DLT-containing serum at the concentration of 10% exerted the most obvious activation effect on autophagy. Therefore, according to the results of the preliminary experiment, the DLT-containing serum at the concentration of 10% was used for *in vitro* experiments.

We have discovered part of the mechanism of DLT in the treatment of atherosclerosis through *in vivo* and *in vitro* experiment, but there are still several problems to be solved. First, only the effect of DLT on vascular adventitia fibroblasts was studied in our experiments, and its effects on vascular endothelial cells, smooth muscle cells, and immune cells remain to be further studied. Second, DLT is a mixture of multiple compounds, so it is difficult to study its core active ingredients. A total of 33 representative components in 20 batches of DLT were simultaneously quantified by ultra-high performance liquid chromatography (UHPLC), and therefore proved the stability of DLT pharmaceutical ingredient (Lin et al., 2020). The study also shows that Danshensu and Lithospermate B are the most important quantitative markers for DLT quality control, and are probably the core chemical substance basis for its pharmacological effects, which is worthy of further research. Finally, the interaction between molecular substances in other signaling pathways should be fully considered; DLT may also exert its anti-atherosclerotic effect through other mechanisms. In the future, network

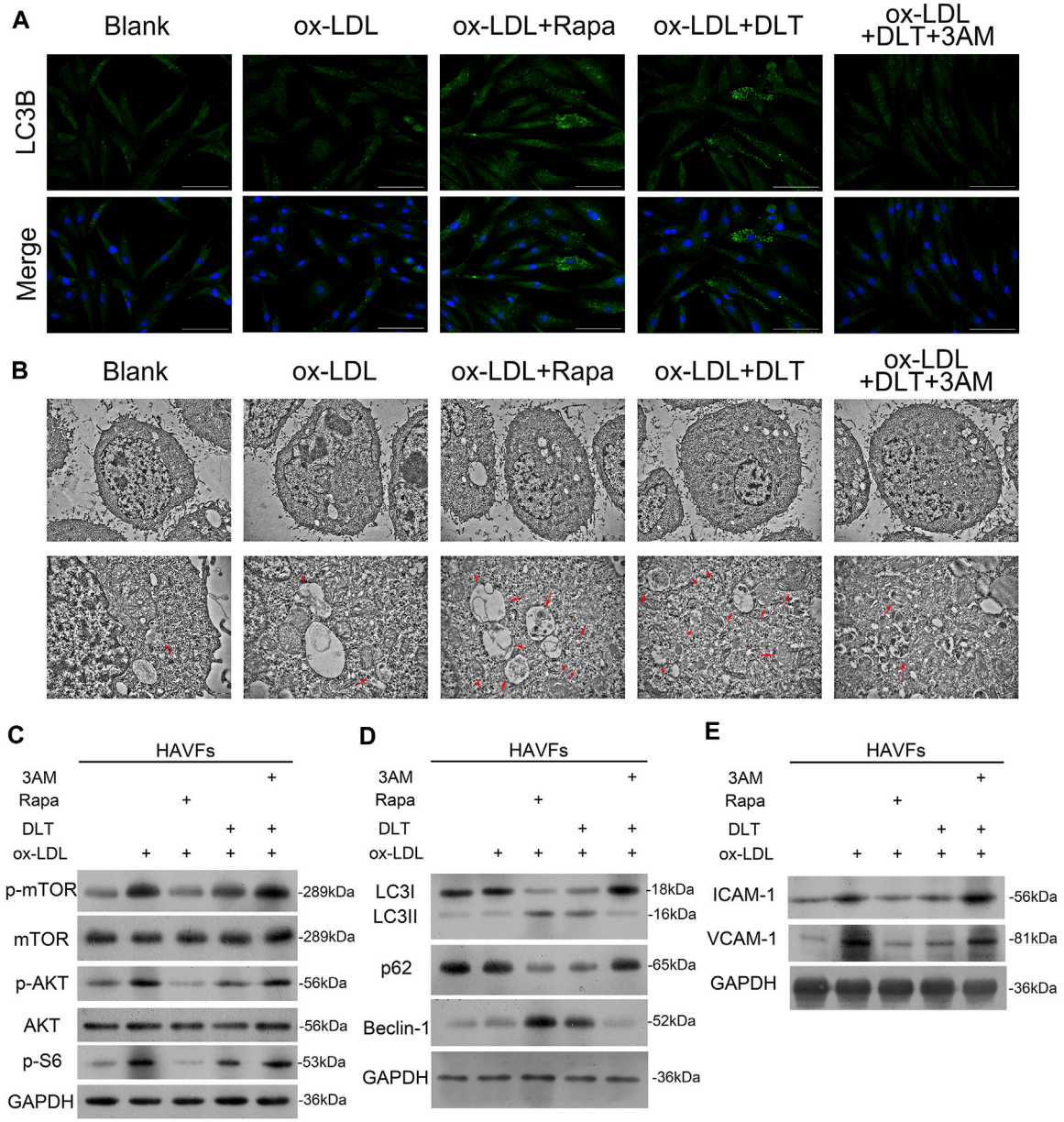

FIGURE 6 | mTOR pathway agonist decreases autophagy by DLT in the AS model. **(A, B)** Immunofluorescence staining of LC3 and transmission electron microscopy analysis to show the activation of autophagy in the DLT treatment group and inhibition by the mTOR agonist. **(C)** Western blot showed the activation of the PI3K/Akt-mTOR pathway by the mTOR agonist. **(D)** The autophagy marker expression was detected by western blotting and reduced in the DLT-mTOR agonist double treatment group. **(E)** The HVAFs activation markers ICAM-1 and VCAM-1 were checked in the DLT-mTOR agonist double treatment group.

pharmacology can be used to predict the target of DLT's anti-atherosclerotic effect and evaluate its other potential pharmacological effects.

CONCLUSION

In conclusion, we demonstrated that Danlou tablets provoke the autophagy of vascular adventitial fibroblasts by regulating the PI3K/Akt/mTOR pathway to protect cells from damage caused by atherosclerosis. Thus, Danlou tablets should be regarded as a new candidate for atherosclerosis treatment.

DATA AVAILABILITY STATEMENT

The raw data supporting the conclusion of this article will be made available by the authors, without undue reservation.

ETHICS STATEMENT

The animal study was reviewed and approved by The Ethics Committee of the First Affiliated Hospital of Henan University of Chinese Medicine.

AUTHOR CONTRIBUTIONS

LW and YC and HG contributed to conception and design of the study and obtained funding. The experiments were performed by LW, TW, and KY. CS and HW directed the experiments and organized the database. SS performed the statistical analysis. LW and TW wrote the first draft of the manuscript. XL wrote sections of the manuscript. All authors contributed to manuscript revision, read, and approved the submitted version.

FUNDING

This study was supported by the National Natural Science Foundation of China (81803940); Science and Technology Planning Project of Henan Province of China (182102311162). Chinese Medicine Scientific Research Project of Henan Province of China (2019JDZX 2010).

REFERENCES

Ba, L., Gao, J., Chen, Y., Qi, H., Dong, C., Pan, H., et al. (2019). Allicin Attenuates Pathological Cardiac Hypertrophy by Inhibiting Autophagy via Activation of PI3K/Akt/mTOR and MAPK/ERK/mTOR Signaling Pathways. *Phytomedicine* 58, 152765. doi:10.1016/j.phymed.2018.11.025

Cai, Z., He, Y., and Chen, Y. (2018). Role of Mammalian Target of Rapamycin in Atherosclerosis. *Curr. Mol. Med.* 18 (4), 216–232. doi:10.2174/1566524018666180926163917

Cao, S., Han, Q. Q., Liu, Z. Y., Zhang, F. F., and Zhou, Y. F. (2015a). Study on Anti-atherosclerotic Arterial of Danlou Tablet in Regulating PI3K/Akt Pathway. *China J. Traditional Chin. Med. Pharm.* 30 (06), 2223–2225.

Cao, S., Wang, F., Liu, Z. Y., Qiang, F. U., Guan, H. M., and Shen, X. J. (2015b). Clinical Study on Danlou Tablets in Anti-atherosclerosis. *Chin. J. Exp. Traditional Med. Formulae* 2015, 156–159. doi:10.13422/j.cnki.syfjx.2015130156

Chen, F., Sun, J., Chun-Ying, S. I., Gao, A. S., Sun, X. P., and Zhu, Z. Y. (2017). Analysis of the Therapeutic Effect of Dan Lou Tablet on the Degenerative Aortic Calcification in Elderly Patients. *Prog. Mod. Biomed.* 2017 (14), 2666–2670.

Commission of Chinese Pharmacopoeia (2015). *Chinese Pharmacopoeia*. Beijing: China Medical Science and Technology Press.

Deng, D., Qu, Y., Sun, L., Jia, L., Bu, J., Ye, M., et al. (2021). Fuyuan Xingnao Decoction Promotes Angiogenesis through the Rab1/AT1R Pathway in Diabetes Mellitus Complicated with Cerebral Infarction. *Front. Pharmacol.* 12, 616165. doi:10.3389/fphar.2021.616165

Dieterle, A. M., Böhler, P., Keppeler, H., Alers, S., Berleth, N., and Drießen, S. (2014). PDK1 Controls Upstream PI3K Expression and PIP3 Generation. *Oncogene* 33 (23), 3043–3053. doi:10.1038/onc.2013.266

Ding, M., Ma, W., Wang, X., Chen, S., Zou, S., Wei, J., et al. (2019). A Network Pharmacology Integrated Pharmacokinetics Strategy for Uncovering Pharmacological Mechanism of Compounds Absorbed into the Blood of Dan-Lou Tablet on Coronary Heart Disease. *J. Ethnopharmacol* 242, 112055. doi:10.1016/j.jep.2019.112055

Emini Veseli, B., Perrotta, P., De Meyer, G. R. A., Roth, L., Van der Donckt, C., Martinet, W., et al. (2017). Animal Models of Atherosclerosis. *Eur. J. Pharmacol.* 816, 3–13. doi:10.1016/j.ejphar.2017.05.010

Falk, E. (2006). Pathogenesis of Atherosclerosis. *J. Am. Coll. Cardiol.* 47 (8), C7–C12. doi:10.1016/j.jacc.2005.09.068

Fatkhullina, A. R., Peshkova, I. O., and Koltsova, E. K. (2016). The Role of Cytokines in the Development of Atherosclerosis. *Biochemistry-Mosc* 81 (11), 1358–1370. doi:10.1134/s0006297916110134

Ference, B. A. (2018). Causal Effect of Lipids and Lipoproteins on Atherosclerosis: Lessons from Genomic Studies. *Cardiol. Clin.* 36 (2), 203–211. doi:10.1016/j.ccl.2017.12.001

Gao, S., Xue, X., Yin, J., Gao, L., Li, Z., Li, L., et al. (2020). Danlou Tablet Inhibits the Inflammatory Reaction of High-Fat Diet-Induced Atherosclerosis in ApoE Knockout Mice with Myocardial Ischemia via the NF-Kb Signaling Pathway. *J. Ethnopharmacol* 263, 113158. doi:10.1016/j.jep.2020.113158

Grootaert, M. O. J., Roth, L., Schrijvers, D. M., De Meyer, G. R. Y., and Martinet, W. (2018). Defective Autophagy in Atherosclerosis: To Die or to Senesce. *Oxidative Med. Cell Longevity.* 2018, 1–12. doi:10.1155/2018/7687083

Hao, D., Danbin, W., Maojuan, G., Chun, S., Bin, L., Lin, Y., et al. (2019). Ethanol Extracts of Danlou Tablet Attenuate Atherosclerosis via Inhibiting Inflammation and Promoting Lipid Effluent. *Pharmacol. Res.* 146, 104306. doi:10.1016/j.phrs.2019.104306

Hay, N., and Sonenberg, N. (2004). Upstream and Downstream of mTOR. *Genes Develop.* 18 (16), 1926–1945. doi:10.1101/gad.1212704

Jenzer, C., and Legouis, R. (2017). Multiple Functions of Autophagy during Development. *Med. Sci. (Paris)* 33 (3), 238–245. doi:10.1051/medsci/20173303009

Khosravi, M., Poursaleh, A., Ghasempour, G., Farhad, S., and Najafi, M. (2019). The Effects of Oxidative Stress on the Development of Atherosclerosis. *Biol. Chem.* 400 (6), 711–732. doi:10.1515/hsz-2018-0397

Kim, K. Y., Park, K. I., Kim, S. H., Yu, S. N., Park, S. G., Kim, Y. W., et al. (2017). Inhibition of Autophagy Promotes Salinomycin-Induced Apoptosis via Reactive Oxygen Species-Mediated PI3K/AKT/mTOR and ERK/p38 MAPK-dependent Signaling in Human Prostate Cancer Cells. *Int. J. Mol. Sci.* 18 (5). doi:10.3390/ijms18051088

Lees, A. M., Veys, J. A., and Lees, R. S. (2001). Reversible and Irreversible Non-internalized LDL and Methyl LDL Accumulation by Human Fibroblasts. *Atherosclerosis* 157 (1), 65–74. doi:10.1016/s0021-9150(00)00707-3

Li, B., Li, W., Li, X., and Zhou, H. (2017). Inflammation: A Novel Therapeutic Target/Direction in Atherosclerosis. *Curr. Pharm. Des.* 23 (8), 1216–1227. doi:10.2174/1381612822666161230142931

Lin, P., Wang, Q., Liu, Y., Qin, Z., Gao, H., Ye, M., et al. (2020). Characterization of Chemical Profile and Quantification of Representative Components of DanLou Tablet, a Traditional Chinese Medicine Prescription, by UHPLC-Q/TOF-MS Combined with UHPLC-TQ-MS. *J. Pharm. Biomed. Anal.* 180, 113070. doi:10.1016/j.jpba.2019.113070

Liu, P., Zhang, C., Zhao, Y. X., Feng, J. B., Liu, C. X., Chen, W. Q., et al. (2010). Gax Gene Transfer Inhibits Vascular Remodeling Induced by Adventitial Inflammation in Rabbits. *Atherosclerosis* 212 (2), 398–405. doi:10.1016/j.atherosclerosis.2010.06.001

Liu, Y., Liu, C., and University, S. T. (2019). Research Progress about the Pharmacologic Actions and Clinical Application of Compound Danlou Tablets. *Heb Med. J.* 2019 (18), 2861–2865.

Lu, T., Zhu, Z., Wu, J., She, H., Han, R., Xu, H., et al. (2019). DRAM1 Regulates Autophagy and Cell Proliferation via Inhibition of the Phosphoinositide 3-Kinase-Akt-mTOR-Ribosomal Protein S6 Pathway. *Cell Commun. Signaling* 17. doi:10.1186/s12964-019-0341-7

Ma, F. X., Xue, P. F., Wang, Y. Y., Wang, Y. N., and Xue, S. Y. (2017). Research Progress of Serum Pharmacochemistry of Traditional Chinese Medicine. *Zhongguo Zhong Yao Za Zhi* 42 (7), 1265–1270. doi:10.19540/j.cnki.cjcmm.20170224.010

Mao, S., Wang, L., Ouyang, W., Zhou, Y., Qi, J., Guo, L., et al. (2016). Traditional Chinese Medicine, Danlou Tablets Alleviate Adverse Left Ventricular Remodeling after Myocardial Infarction: Results of a Double-Blind, Randomized, Placebo-Controlled, Pilot Study. *BMC Complement. Altern. Med.* 16 (1), 447. doi:10.1186/s12906-016-1406-4

Martinet, W., De Loof, H., and De Meyer, G. R. Y. (2014). mTOR Inhibition: a Promising Strategy for Stabilization of Atherosclerotic Plaques. *Atherosclerosis* 233 (2), 601–607. doi:10.1016/j.atherosclerosis.2014.01.040

Nair, A. B., and Jacob, S. (2016). A Simple Practice Guide for Dose Conversion between Animals and Human. *J. Basic Clin. Pharm.* 7 (2), 27–31. doi:10.4103/0976-0105.177703

Peng, J., Yang, Q., Li, A. F., Li, R. Q., Wang, Z., Liu, L. S., et al. (2016). Tet Methylcytosine Dioxygenase 2 Inhibits Atherosclerosis via Upregulation of Autophagy in ApoE-/- Mice. *Oncotarget* 7 (47), 76423–76436. doi:10.18632/oncotarget.13121

Pirillo, A., Bonacina, F., Norata, G. D., and Catapano, A. L. (2018). The Interplay of Lipids, Lipoproteins, and Immunity in Atherosclerosis. *Curr. Atheroscler. Rep.* 20 (3), 12. doi:10.1007/s11883-018-0715-0

Poznyak, A. V., Bharadwaj, D., Prasad, G., Grechko, A. V., Sazonova, M. A., and Orekhov, A. N. (2021). Anti-Inflammatory Therapy for Atherosclerosis: Focusing on Cytokines. *Int. J. Mol. Sci.* 22 (13). doi:10.3390/ijms22137061

Ravanan, P., Srikumar, I. F., and Talwar, P. (2017). Autophagy: The Spotlight for Cellular Stress Responses. *Life Sci.* 188, 53–67. doi:10.1016/j.lfs.2017.08.029

Razani, B., Feng, C., Coleman, T., Emanuel, R., Wen, H., Hwang, S., et al. (2012). Autophagy Links Inflammasomes to Atherosclerotic Progression. *Cell Metab* 15 (4), 534–544. doi:10.1016/j.cmet.2012.02.011

Saitoh, T., Fujita, N., Jang, M. H., Uematsu, S., Yang, B. G., Satoh, T., et al. (2008). Loss of the Autophagy Protein Atg16L1 Enhances Endotoxin-Induced IL-1beta Production. *Nature* 456 (7219), 264–268. doi:10.1038/nature07383

Schaftenaar, F., Frodermann, V., Kuiper, J., and Lutgens, E. (2016). Atherosclerosis: the Interplay between Lipids and Immune Cells. *Curr. Opin. Lipidol.* 27 (3), 209–215. doi:10.1097/mol.0000000000000302

Shi, L., Zhao, F., Zhu, F., Liang, Y., Yang, F., Zhang, G., et al. (2016). Traditional Chinese Medicine Formula "Xiaofeng Granules" Suppressed Gouty Arthritis Animal Models and Inhibited the Proteoglycan Degradation on Chondrocytes Induced by Monosodium Urate. *J. Ethnopharmacol* 191, 254–263. doi:10.1016/j.jep.2016.06.008

Tang, J. J., Li, G. X., Liu, Z. G., Yi, R., Yu, D., Zhang, Y. B., et al. (2020). Danlou Tablet () Improves Chronic Intermittent Hypoxia-Induced Dyslipidemia and Arteriosclerosis by HIF-1 α-Angptl4 mRNA Signaling Pathway. *Chin. J. Integr. Med.* 82. doi:10.1007/s11655-020-3255-8

Tang, Y., Wu, H., Shao, B., Wang, Y., Liu, C., and Guo, M. (2018). Celosins Inhibit Atherosclerosis in ApoE(-/-) Mice and Promote Autophagy Flow. *J. Ethnopharmacol* 215, 74–82. doi:10.1016/j.jep.2017.12.031

Tedgui, A., and Mallat, Z. (2006). Cytokines in Atherosclerosis: Pathogenic and Regulatory Pathways. *Physiol. Rev.* 86 (2), 515–581. doi:10.1152/physrev.00024.2005

Wang, L., Zhao, X., Mao, S., Liu, S., Guo, X., Guo, L., et al. (2016). Efficacy of Danlou Tablet in Patients with Non-ST Elevation Acute Coronary Syndrome Undergoing Percutaneous Coronary Intervention: Results from a Multicentre, Placebo-Controlled, Randomized Trial. *Evid. Based Complement. Alternat Med.* 2016, 7960503. doi:10.1155/2016/7960503

Wang, Y. S., Hsi, E., Cheng, H. Y., Hsu, S. H., Liao, Y. C., and Juo, S. H. (2017). Let-7g Suppresses Both Canonical and Non-canonical NF-Kb Pathways in Macrophages Leading to Anti-atherosclerosis. *Oncotarget* 8 (60), 101026–101041. doi:10.18632/oncotarget.18197

Wang, Y., and Zhang, H. (2019). Regulation of Autophagy by mTOR Signaling Pathway. *Adv. Exp. Med. Biol.* 1206, 67–83. doi:10.1007/978-981-15-0602-4_3

Wu, M., Yang, S., Wang, S., Cao, Y., Zhao, R., Li, X., et al. (2020). Effect of Berberine on Atherosclerosis and Gut Microbiota Modulation and Their Correlation in High-Fat Diet-Fed ApoE-/- Mice. *Front. Pharmacol.* 11, 223. doi:10.3389/fphar.2020.00223

Wu, Y., Wang, X., Guo, H., Zhang, B., Zhang, X. B., Shi, Z. J., et al. (2013). Synthesis and Screening of 3-MA Derivatives for Autophagy Inhibitors. *Autophagy* 9 (4), 595–603. doi:10.4161/auto.23641

Zhai, C., Cheng, J., Mujahid, H., Wang, H., Kong, J., Yin, Y., et al. (2014). Selective Inhibition of PI3K/Akt/mTOR Signaling Pathway Regulates Autophagy of Macrophage and Vulnerability of Atherosclerotic Plaque. *PLoS One* 9 (3), e90563. doi:10.1371/journal.pone.0090563

Zhang, P., Li, Y., Fu, Y., Huang, L., Liu, B., Zhang, L., et al. (2020). Inhibition of Autophagy Signaling via 3-methyladenine Rescued Nicotine-Mediated Cardiac Pathological Effects and Heart Dysfunctions. *Int. J. Biol. Sci.* 16 (8), 1349–1362. doi:10.7150/ijbs.41275

Zhou, J., Li, Z., and Zeng, Q. (2009). Molecular and Pathological Characteristics of AS Plaque Formation Induced by High-Fat Diet of LDLR and the APOE Gene Knock-Out Mice. *China J. Mod. Med.* 19 (10), 1460–1464.

Zhu, Y., Xian, X., Wang, Z., Bi, Y., Chen, Q., Han, X., et al. (2018). Research Progress on the Relationship between Atherosclerosis and Inflammation. *Biomolecules* 8 (3), 80. doi:10.3390/biom8030080

Conflict of Interest: The authors declare that the research was conducted in the absence of any commercial or financial relationships that could be construed as a potential conflict of interest.

frontiers in Pharmacology

ORIGINAL RESEARCH
published: 24 November 2021
doi: 10.3389/fphar.2021.773834

Ferruginol Restores SIRT1-PGC-1α-Mediated Mitochondrial Biogenesis and Fatty Acid Oxidation for the Treatment of DOX-Induced Cardiotoxicity

Weili Li[1†], Jing Cao[2†], Xiaoping Wang[2], Yawen Zhang[2], Qianbin Sun[1], Yanyan Jiang[1], Junkai Yao[2], Chun Li[3], Yong Wang[2,1] and Wei Wang[2,4,5]**

[1]School of Life Science, Beijing University of Chinese Medicine, Beijing, China, [2]School of Traditional Chinese Medicine, Beijing University of Chinese Medicine, Beijing, China, [3]Modern Research Center for Traditional Chinese Medicine, Beijing University of Chinese Medicine, Beijing, China, [4]Beijing Key Laboratory of TCM Syndrome and Formula, Beijing, China, [5]Key Laboratory of TCM Syndrome and Formula (Beijing University of Chinese Medicine), Ministry of Education, Beijing, China

OPEN ACCESS

Edited by:
Konrad Urbanek,
Magna GrÃ¦cia University of Catanzaro, Italy

Reviewed by:
Giuseppina Milano,
Centre Hospitalier Universitaire Vaudois (CHUV), Switzerland
Arun Samidurai,
Virginia Commonwealth University, United States

***Correspondence:**
Yong Wang
wangyong@bucm.edu.cn
Wei Wang
wangwei26960@126.com

†These authors have contributed equally to this work

Specialty section:
This article was submitted to Cardiovascular and Smooth Muscle Pharmacology, a section of the journal Frontiers in Pharmacology

Received: 23 September 2021
Accepted: 21 October 2021
Published: 24 November 2021

Citation:
Li W, Cao J, Wang X, Zhang Y, Sun Q, Jiang Y, Yao J, Li C, Wang Y and Wang W (2021) Ferruginol Restores SIRT1-PGC-1α-Mediated Mitochondrial Biogenesis and Fatty Acid Oxidation for the Treatment of DOX-Induced Cardiotoxicity. Front. Pharmacol. 12:773834. doi: 10.3389/fphar.2021.773834

Background: Doxorubicin (DOX), a broad-spectrum chemotherapy drug, has life-threatening cardiotoxicity. Therefore, searching cardioprotective drugs for DOX-induced cardiotoxicity (DIC) is urgently needed.

Objectives: This study aimed to explore cardioprotective effect and specific mechanism by which Ferruginol (FGL) attenuated DIC *in vivo* and *in vitro*.

Methods: We evaluated the cardioprotection of FGL and performed high-throughput RNA-Seq on a DIC mouse. Whereafter, multiple methods, including western blot, RT-qPCR, a transmission electron microscope, CO-IP, immunofluorescence, and other staining methods, and antagonist of SIRT1 and PGC-1α were utilized to confirm the cardioprotection and molecular mechanism of FGL.

Results: FGL-exerted cardioprotection manifested as enhanced cardiac function and reduced structural damage and apoptosis. The transcriptome and other results revealed that FGL facilitated PGC-1α-mediated mitochondrial biogenesis and fatty acid oxidation (MB and FAO) by increasing the expression of PGC-1α and concurrently promoting the expression of SIRT1-enhancing deacetylase SIRT1 deacetylating and activating PGC-1α.

Conclusions: These results documented that FGL exerted cardioprotective effects restoring MB&FAO via the SIRT1–PGC-1α axis.

Keywords: ferruginol, mitochondrial biogenesis, fatty acid oxidation, SIRT1, PGC-1α, doxorubicin

INTRODUCTION

The anthracycline antibiotic doxorubicin (DOX) is widely used as an effective chemotherapeutic drug for a wide range of cancers (Carter, 1975; Carvalho et al., 2009). However, the dose-dependent cardiotoxicity of DOX severely limits its clinical application. The cardiotoxicity experienced with DOX can range from asymptomatic reductions in the left ventricular ejection fraction to cardiomyopathy, badly myocardial infarction, and congestive heart failure (Shakir and Rasul,

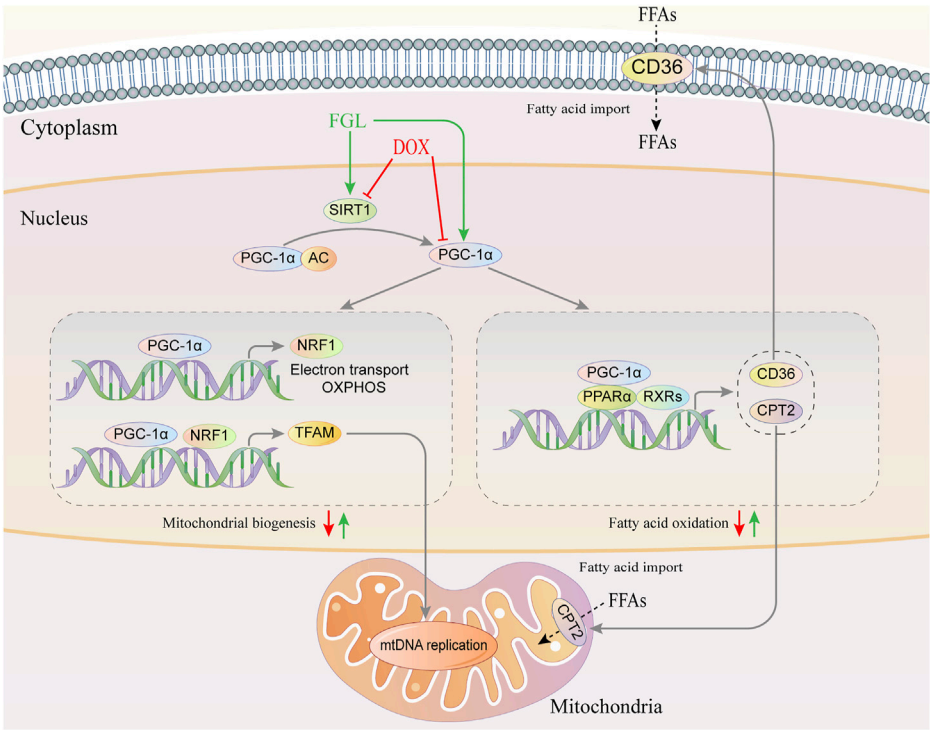

GRAPHICAL ABSTRACT | Graphical abstract of the pathogenic mechanism of DOX and the cardioprotective mechanism of FGL.

2009; Bernstein and Burridge, 2014). Dexrazoxane is the only cardioprotectant currently approved by the United States Food and Drug Administration for combining with DOX in cancer therapy (Schuchter et al., 2002; Kane et al., 2008). Unfortunately, dexrazoxane is criticized for inducing secondary malignancies and aggravating myelosuppression and has been prohibited in children by the European Medicines Agency in 2011 (Tebbi et al., 2007; European Medicines Agency, 2011). Therefore, a new cardioprotectant for DOX-induced cardiotoxicity (DIC) is urgently needed.

Over the past decades, extensive studies sought to elucidate the mechanistic underpinnings that reveal the pathological occurrence and development of DIC and provide research links for its treatment (Sokolove, 1994; Arola et al., 2000; Minotti et al., 2004). Impressively, abnormalities in mitochondrial functions including defects in the respiratory chain/oxidative phosphorylation (OXPHOS) system, reduction of fatty acid oxidation, mitochondrial DNA damage, and modulation of mitochondrial sirtuin activity have become primary causative factors of DIC (Zhou et al., 2001a; Zhou et al., 2001b; Tokarska-Schlattner et al., 2002). Thus, there is a high level of interest in developing therapeutic strategies aiming at modulating the regulatory pathways that control mitochondrial function.

PGC-1α, as a member of the peroxisome proliferator-activated receptor gamma coactivator-1 (PGC-1) family, plays a major role in transducing and integrating physiological signals governing metabolism, differentiation, and cell growth to the transcriptional machinery controlling mitochondrial biogenesis and function through direct interaction and coactivation with PPARs, ERRs, and NRFs (Rowe et al., 2010; Scarpulla et al., 2012). To date, more reports have verified that PGC-1α is directly deacetylated and reactivated in nuclei by the NAD+-dependent deacetylase SIRT1 in response to changes in energy depletion, thus influencing multiple bioprocesses mediated by PGC-1α (Lagouge et al., 2006; Gerhart-Hines et al., 2007; Jeninga et al., 2010). Therefore, we believe that DOX causes myocardial energy deficiency and alteration of the SIRT1-PGC-1α regulatory signal, which may be major pathogenic mechanisms of DIC, and also a potential druggable pathway to coordinate mitochondria-related bioprocesses for DIC treatment.

Ferruginol, a natural polyphenol and terpenoid isolated from Salvia plants, has demonstrated a variety of pharmacological potentials including antioxidant, antitumor, gastroprotective, and neuroprotective activity (Rodríguez et al., 2006; Bispo de Jesus et al., 2008; Saijo et al., 2015; Zolezzi et al., 2018). However, there were very little evidences for cardioprotective activity of FGL. Our study for the first time demonstrated strong protective effect of FGL on DIC mouse heart and H9C2 cells. Thus, we hypothesized that FGL alleviated DIC by SIRT1–PGC-1α-mediated myocardial MB&FAO, and above, the pharmacological effects and mechanisms of FGL were verified *in vivo* and *in vitro*.

METHODS

Materials

All reagents and materials used in this research are documented in the **Supplementary Material**.

Construction of DIC Mouse Model and Pharmacological Treatments

Male C57BL/6 mice (20 ± 2 g, 8–10 weeks old) were purchased from Beijing SPF Biotechnology (Beijing, China). All procedures were performed following the guidelines of the Institutional Animal Care and Use Committee and approved by the Beijing University of Chinese Medicine Animal Care Committee. The animals were housed in a 12:12-h light–dark cycle and temperature-controlled (22°C) environment and fed with standard rodent chow and tap water. A DIC model was generated as described previously (Wang et al., 2019; Wang et al., 2020). After a week of adjustable feeding, mice randomly assigned in the model, FGL, and ENA groups were injected by tail vein with DOX following a dose of 5 mg/kg once weekly for 4 weeks. Meanwhile, mice in the control group were treated with saline solution (0.9% NaCl) instead. Then, FGL at 20 mg/kg and ENA at 15 mg/kg were administered intragastrically and daily for 4 weeks at 1 week after last injection of DOX, respectively. The control and model groups also received the same volume of ultrapure water. ENA has been repeatedly reported to protect against DIC in clinical and preclinical studies (Hullin et al., 2018); thus, we applied ENA as a positive control for animal experiments.

RNA Sequencing and Analysis

Samples were prepared according to the protocol of the manufacturer and then underwent RNA extraction, reverse transcription, and DNA amplification, followed by sequencing on an Illumina HiSeq. We identified differentially expressed genes (DEGs) based on the following criteria: $p < 0.05$ and absolute value of log2fold-change>0. Biological and pathway analysis of DEGs was explored by GO term enrichment analysis and KEGG pathway enrichment analysis, respectively. Protein–protein interaction (PPI) network analysis of DEGs was acquired from the Search Tool for the Retrieval of Interacting Genes (STRING) database (version 11.0; https://www.string-db.org/).

Echocardiographic Assessment of Cardiac Functions

After 4 weeks' administration, the mice were immobilized and anesthetized with isoflurane gas for echocardiography. The transthoracic echocardiography was performed in M-mode with the VEVO 2100 echocardiography system (Visual Sonics, Toronto, ON, Canada) by the same operator on all mice. Left ventricular end-systolic volume (LVESV), left ventricular end-diastolic volume (LVEDV), left ventricular end-diastolic dimension (LVEDD), and left ventricular end-systolic dimension (LVESD) were measured using computer algorithms for at least three uninterrupted cardiac cycles. The calculated EF and FS values of the mice treated by DOX were uniformly decreased compared to those in the control group.

Histological Examination

Cardiac tissue samples were immersed in 4% paraformaldehyde and then embedded in paraffin and cut into 4-μm serial sections. The sections were stained with hematoxylin–eosin (H&E) and Masson trichromatic solution and were then observed under an optical microscope at ×400 magnification.

Assessment of Serum Biomarkers

Blood samples were obtained from abdominal aorta, and the sera were isolated to measure tissue injury markers, lactate dehydrogenase (LDH), and creatine kinase isoenzymes (CK-MB) with standard diagnostic kits (Nanjing Jiancheng Bioengineering Institute, Jiangsu, China).

Cell Culture and Pharmacological Treatments

H9C2, HepG2, and MCF-7 cells were grown in DMEM with 10% fetal bovine serum supplement and incubated in humidified air (5% CO_2) at 37°C. H9C2, HepG2, and MCF-7 cells were grown on 96-well plates at a density of 4 × 104 cells/ml for 24 h and then divided into the control, DOX, and 0.1–50 μM FGL groups. Next, FGL groups were pretreated with FGL, followed by cotreating with 1 μM DOX as previously confirmed (Wang et al., 2020) and FGL (0.1–50 μM) in FGL groups while merely with 1 μM DOX in the DOX group for 24 h. Subsequently, cell viability was detected using 10% CCK-8 (Dojindo, Kumamoto, Japan). H9C2 cells were divided into five groups as follows: control group, DOX group, DOX + FGL, DOX + FGL + Selisistat, and DOX + FGL + SR-18292. Selisistat is an inhibitor of SIRT1, inhibiting the deacetylation activity of SIRT1. SR-18292 is an inhibitor of PGC-1α, promoting the acetylation of PGC-1α and inhibiting its activity as a transcriptional coactivator. Amounts of 1 μM DOX, 0.1 μM FGL, 20 μM Selisistat, and 20 μM SR-18292 were applied, respectively.

Detection of Apoptosis

The apoptosis of cardiac tissue was determined by terminal deoxynucleotidyl transferase-mediated nick end labeling (TUNEL) according to the instructions of the manufacturer and then staining with DAPI to label the nuclei. In addition, H9C2 cells were incubated with 2 mg/ml Hoechst 33,342 for 30 min at 37°C in the dark for detecting the apoptosis of H9C2 cells. Finally, a fluorescence microscope was used to visualize apoptotic cells.

Transmission Electron Microscopy

The process was performed as described previously (Wang et al., 2019). Images were acquired under an electron microscope (Leica, Buffalo Grove, IL, United States). Mitochondria were counted randomly based on six images from various fields of view (×2,500 magnification).

Mitochondrial Membrane Potential

Changes of mitochondrial membrane potential ($\Delta\Psi m$) were detected using the fluorescent probe JC-1 (Beijing Solaibao Technology Co., Ltd., Beijing, China) according to the user manual. JC-1 is a cationic dye that accumulates in the mitochondria in a potential-sensitive manner. At high $\Delta\Psi m$, JC-1 accumulates in the mitochondria forming J-aggregates and emitting red fluorescence; at low $\Delta\Psi m$, the J-monomers generate

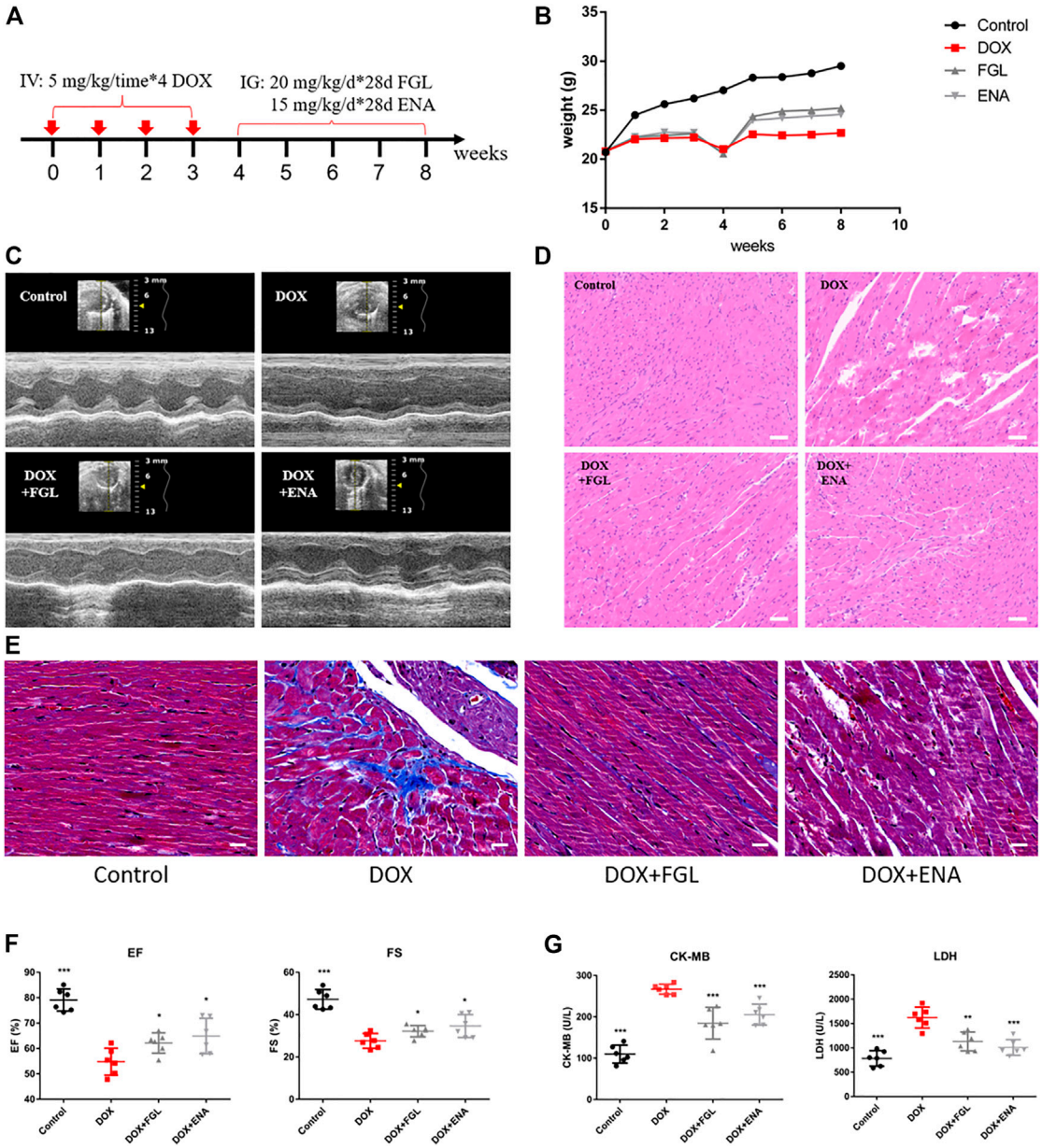

FIGURE 1 | FGL relieved DOX-induced cardiac structural and functional lesion. **(A)** A schematic diagram of animal model generation and drug administration. **(B)** Body weight changes in various groups (n = 10). **(C)** Representative images of echocardiograms. **(D)** Representative images of morphological and structural changes in the myocardium. Scale bar: 50 μm. **(E)** Myocardial fibrosis detection by Masson staining. **(F)** The effects of FGL and ENA on DOX-induced cardiac EF and FS (n = 6). **(G)** The effects of FGL and ENA on cardiac serum CK-MB and LDH (n = 6). $^{*}p < 0.05$, $^{**}p < 0.01$, $^{***}p < 0.001$ vs DOX group.

green fluorescence. After pharmacological treatments, the cells were incubated with 1×JC-1 working solution for 30 min and washed twice with JC-1 dye buffer. Finally, the images were monitored under a fluorescence microscope. ΔΨm was evaluated and calculated by the ratio of red/green fluorescence intensities.

ROS Detection

DCFH-DA staining was performed for the detection of ROS in H9C2 cells. Pretreated H9C2 cells were cultured with 10 μM DCFH-DA for 30 min at 37°C in the dark. Then DAPI was used to stain the nuclei. The images were acquired using a laser scanning confocal microscope at ×100 magnification.

Adenosine Triphosphate Content

ATP levels in H9C2 cells were detected by using an ATP assay kit (Beyotime Biotechnology, Shanghai, China). Briefly, H9C2 cells were lysed and centrifuged, and the supernatant was collected for the determination of ATP and total protein content. The content of ATP was normalized to the cellular protein concentration.

Real-Time Quantitative PCR for RNA Expression Analysis

The process was performed as described previously (Wang et al., 2019). The primers used in this study are shown in Supplementary Material.

Immunofluorescence Staining

H9C2 cells were fixed with 4% formaldehyde, washed twice with PBS, and then permeabilized with 0.3% Triton X-100. After being blocked with 5% bovine serum albumin, cells were incubated with primary antibodies against SIRT1 and PGC-1α, and then with the corresponding secondary antibodies. The nuclei were counterstained with DAPI. Images were captured by a laser scanning confocal microscope at 1,000× magnification.

Co-Immunoprecipitation Assay

Co-IP was executed according to the indicated procedures of the manufacturer (Cell Signaling Technology, United States). H9C2 cells were lysed in a lysis buffer. Equivalent proteins from each sample were combined with anti-PGC-1α antibody or control IgG antibody overnight at 4°C. Later, the resulting immunocomplex was precipitated employing Protein G magnetic beads, followed by washing five times. Thereafter, precipitates mixed in the SDS buffer solution were analyzed by western blot with either anti-acetylated lysine antibody to determine the extent of PGC-1α acetylation or PGC-1α antibody to determine the total amount of PGC-1α.

Western Blotting Analysis

To detect protein expression, western blotting was carried out as previously described (Wang et al., 2019; Wang et al., 2020). The antibodies used in the study are shown in Supplementary Material.

Statistical Analysis

Statistical analysis was performed using the GraphPad software 6. Numerical results are displayed as mean ± s.d. Statistical significance was evaluated by applying two-tailed unpaired Student's t-test. Alternatively, comparisons of more than two groups were performed by one-way analysis of variance (ANOVA) with Bonferroni *post hoc* tests for multiple groups to calculate the differences. A p-value of <0.05 was considered as statistically significant.

RESULTS

Ferruginol Relieved Doxorubicin-Induced Cardiac Structural and Functional Lesion

The design of animal experiments, including the generation of a DIC model and subsequent pharmacological treatment, is shown in **Figure 1A**. The body weight of mice was recorded throughout the animal experiment (**Figure 1B**). Comparison with the control group indicated an evident decline in the body weight in the DOX-treated group. Meanwhile, the body weight of mice in the FGL and ENA groups was significantly increased during weeks 5–8 compared with that in the model group. The mice underwent echocardiography to evaluate cardiac function after 4 weeks of pharmacological intervention. FGL alleviated the decrease in EF and FS values caused by DOX (**Figures 1C,F**). Consistently, H&E and Masson staining of heart sections showed that DOX induced myofibrillar loss, disordered arrangement, enlarged intercellular structures, and plasma-dissolved cardiomyocytes and myocardial fibrosis, which could be attenuated by FGL (**Figures 1D,E**). Additionally, increased serum content of LDH and CK-MB, markers of myocardial damage, was observed in the DOX group, while FGL treatment partially reversed these changes (**Figure 1G**).

Doxorubicin-Induced Deficiency of Mitochondrial Biogenesis and Fatty Acid Oxidation Mediated by Proliferator-Activated Receptor Gamma Coactivator-1 Were Significantly Improved by Ferruginol

To further explore the pathogenic mechanism of DOX and underlying molecular mechanisms of FGL on cardiac protection, we performed high-throughput RNA-Seq to investigate DEGs in the control, DOX, and DOX + FGL groups of mice. **Figure 2A** showed distinct hierarchical clustering of the genes and groups. Gene ontology and KEGG analysis between the control and DOX groups revealed that genes related to mitochondria/metabolism, fatty acid oxidation, PPAR signal pathway, etc. were significantly enriched (**Figures 2B,C**). Then we presented eight DEGs involved in mitochondrial metabolism, biogenesis, and PPAR signaling pathways between the control and DOX groups in the form of heatmap (**Figure 2D**). Protein–protein interaction (PPI) network analysis (version 11.0; https://www.string-db.org/) indicated that a cluster containing eight nodes (Sirt1, Ppargc1a, Ppara, Nrf1, Tfam, Cd36, Lpl, and Cpt2) possessed a strong connection (**Figure 2E**).

To validate the results of RNA-Seq and quantify the expression of these key genes, we assessed eight DEGs involved in mitochondrial biogenesis and the PPAR signaling pathway by quantitative RT-PCR on three to five heart samples. The results of the RT-qPCR analysis were in good agreement with the RNA-Seq data that DOX resulted in the downregulation of eight genes compared with the control group, while FGL significantly increased the RNA levels of all genes except Ppara compared with the DOX group (**Figure 2F**).

Ferruginol Inhibited Doxorubicin-Induced Apoptosis and Oxidative Injury via SIRT1 and Proliferator-Activated Receptor Gamma Coactivator-1 *In Vivo* and *In Vitro*

DOX-induced apoptosis has long been considered to be one of the leading causes of cardiac function decline. Therefore, we evaluated the apoptosis of cardiomyocytes *in vivo* and *in vitro*. As shown in **Figure 3C**, the minimum concentration of FGL that enhanced cell viability was 0.1 μM. TUNEL staining of mouse

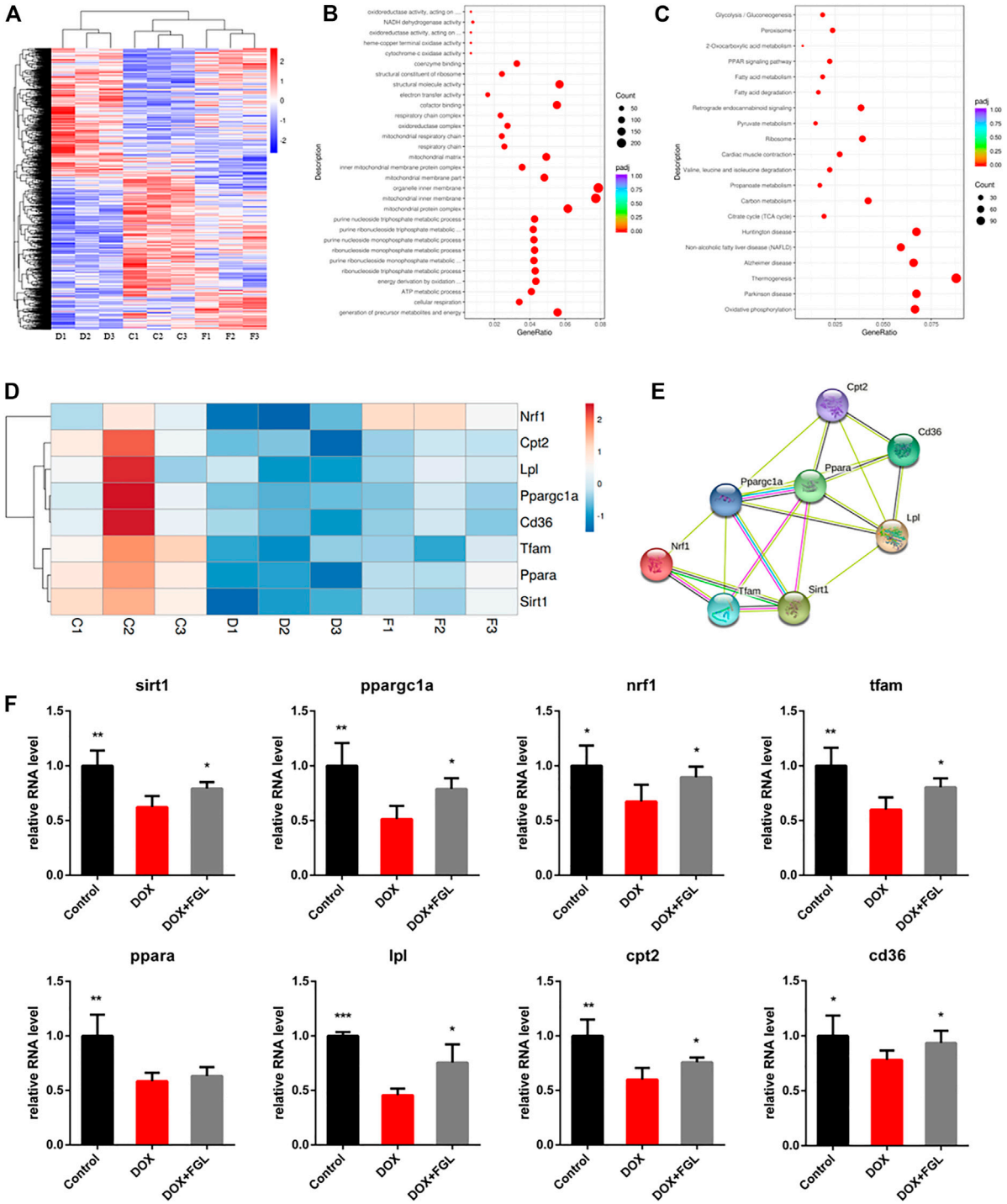

FIGURE 2 | The results of mRNA sequencing and analysis. **(A)** Hierarchical clustering of proteins and samples. **(B, C)** GO and KEGG enrichment analysis between the control and DOX groups. **(D, E)** Representative gene heatmap and PPI diagram associated with MB&FAO. **(F)** Quantitative analysis of representative mRNA associated with MB&FAO by RT-qPCR. (n = 3–5). *$p < 0.05$, **$p < 0.01$, ***$p < 0.001$ vs DOX group.

heart slices and Hoechst staining of H9C2 cells showed that FGL alleviated DOX-induced apoptosis (**Figures 3A,B,D,E**). Moreover, mitochondrial membrane potential reduction is a hallmark event of early apoptosis. The results showed that DOX caused the notable drop of the mitochondrial membrane potential, which could be alleviated by FGL. Compared with the FGL-treatment group, selisistat and SR-18292 reduced the mitochondrial membrane potential (**Figures 3F,G**). We also

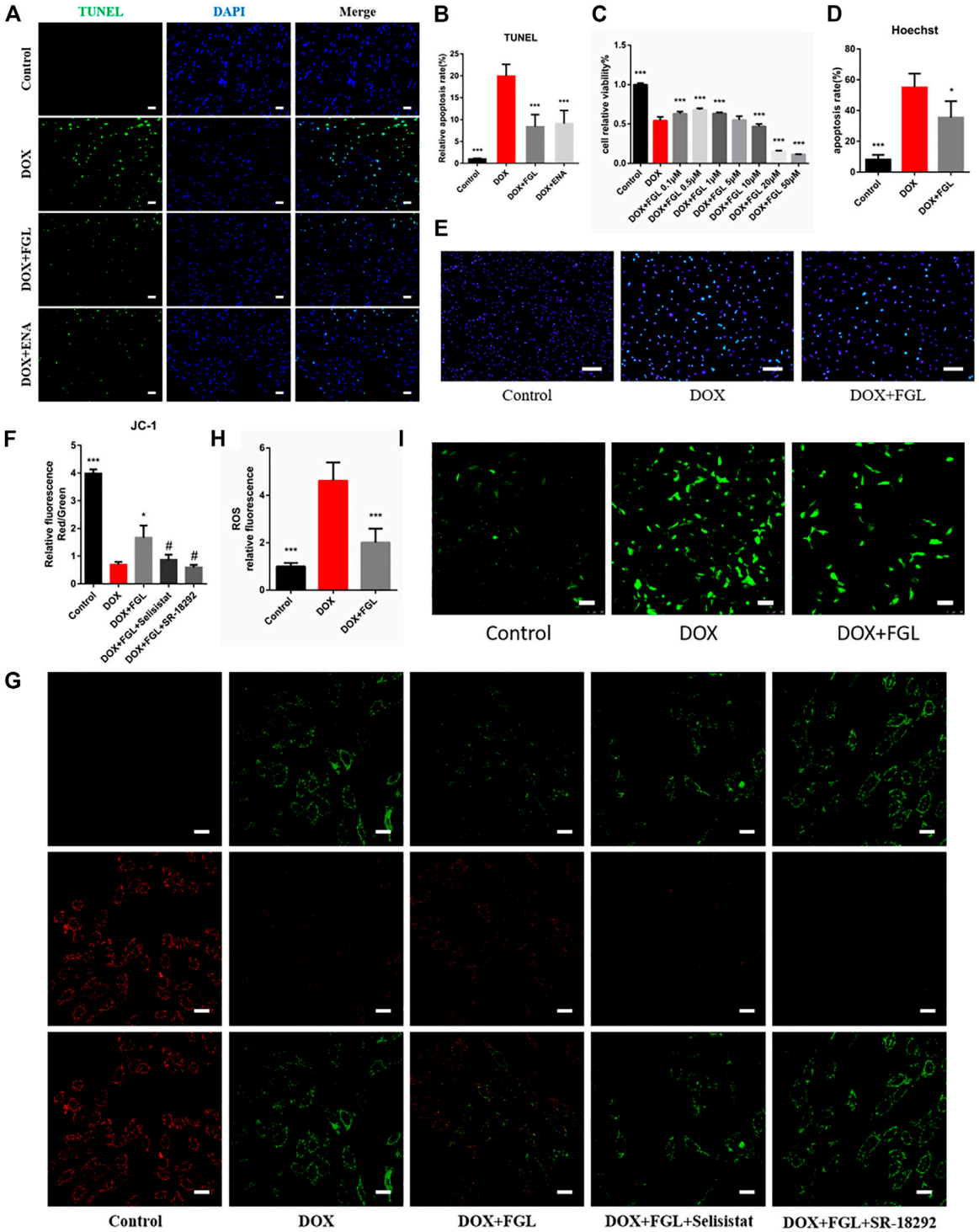

FIGURE 3 | FGL inhibited DOX-induced apoptosis and oxidative injury *in vivo* and *in vitro*. **(A, B)** Representative images and quantitative analysis of apoptosis by TUNEL in the mouse myocardium (n = 6). Scale bar: 20 μm. **(C)** Effective concentration of FGL in H9C2 cells (n = 6). **(D, E)** Representative images and quantitative analysis of apoptosis by Hoechst staining in H9C2 cells (n = 5). Scale bar: 100 μm. **(F, G)** Representative images and quantitative analysis of mitochondrial membrane potential measured by JC-1 staining in H9C2 cells (n = 3). Scale bar: 25 μm. **(H, I)** Representative images and quantitative analysis of ROS by DCFH-DA staining in H9C2 cells (n = 6). Scale bar: 100 μm $^{*}p < 0.05$, $^{***}p < 0.001$ vs DOX group. $\#p < 0.05$ vs. (DOX + FGL) group.

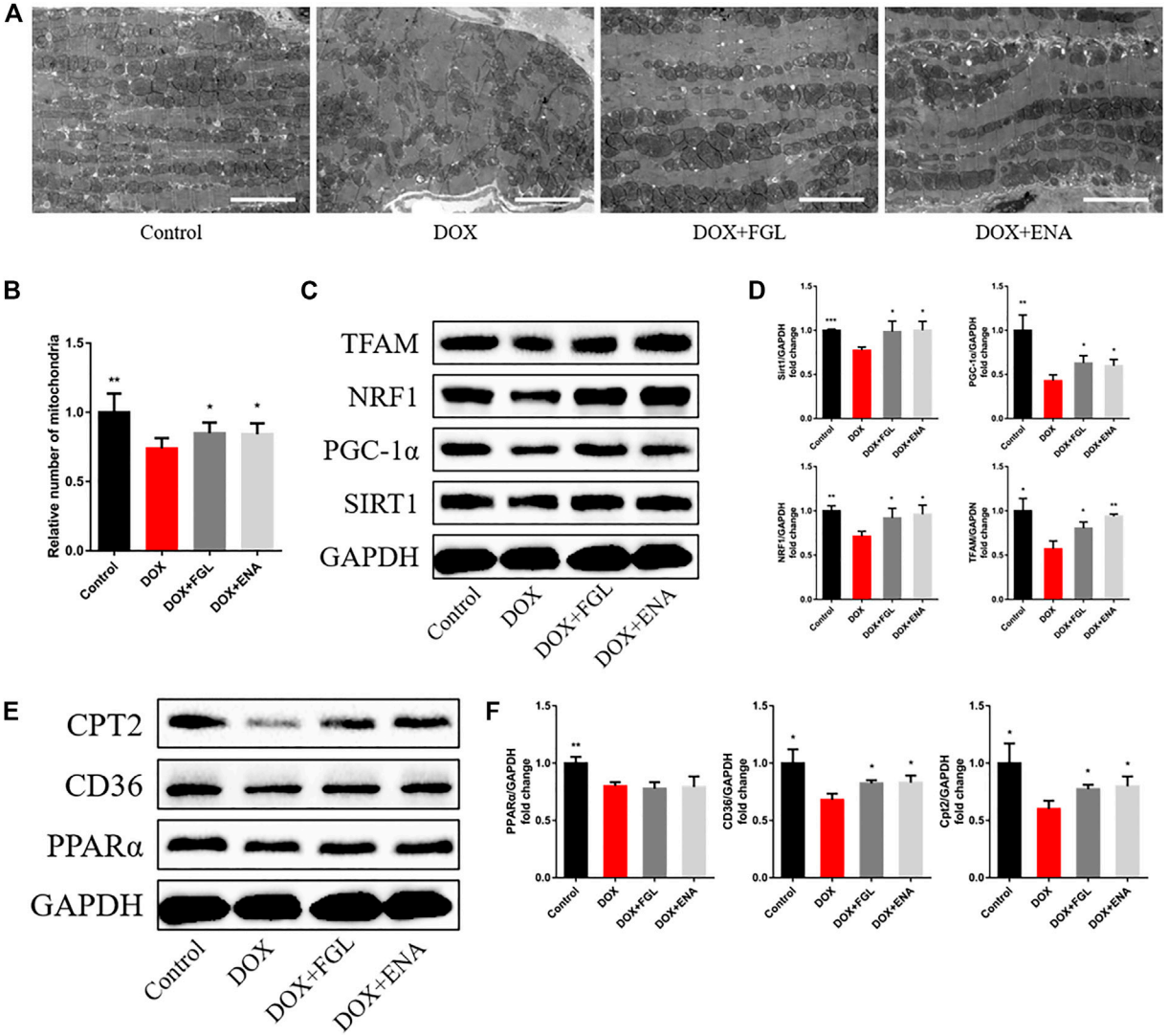

FIGURE 4 | FGL promoted mitochondrial biogenesis and fatty acid oxidization *in vivo*. **(A, B)** Representative images and quantitative analysis of electron micrographs of the heart (n = 6). Scale bar: 5.0 μm. **(C–F)** Expression levels of mitochondrial biogenesis and fatty acid oxidization-associated proteins were quantified and shown as relative protein expression levels after normalization to GAPDH (n = 3–5). $^{*}p < 0.05$, $^{**}p < 0.01$, $^{***}p < 0.001$ vs DOX group.

found that DOX caused a large amount of ROS production, while FGL significantly reduced ROS production. These results suggested that FGL alleviated apoptosis and ROS production by associating with SIRT1 and PGC-1α.

Ferruginol Promoted Mitochondrial Biogenesis and Fatty Acid Oxidization *In Vivo*

We then hypothesized that FGL exerted cardioprotection by improving mitochondrial biogenesis and fatty acid oxidization. In DIC mice, we found that DOX led to loose arrangement of mitochondria and a large reduction in the number of mitochondria via TEM, while FGL relieved the above adverse changes (**Figures 4A,B**). Moreover, coinciding with the results of RNA-seq, the expressions of mitochondrial biogenesis and fatty acid oxidization markers were decreased in the DOX group compared to those in the control group, and these changes were relieved by FGL (**Figures 4C–F**). However, DOX-induced reduction in the protein levels of PPARα was not mitigated by FGL. PGC-1α acts as a transcriptional coactivator to promote the transcriptional regulation of PPARα to downstream proteins (CD36, CPT2, LPL, etc.). We concluded that FGL merely upregulated the expression of PGC1-α without improving the expression of PPARα and thus activated the transcriptional activity of PPARα to promote the expression of downstream genes. In addition, the expression of SIRT1, a deacetylase, was also significantly enhanced by FGL treatment. Combined with reported research that SIRT1 deacetylated PGC-1α and activated its transcriptional activity, we proposed that FGL

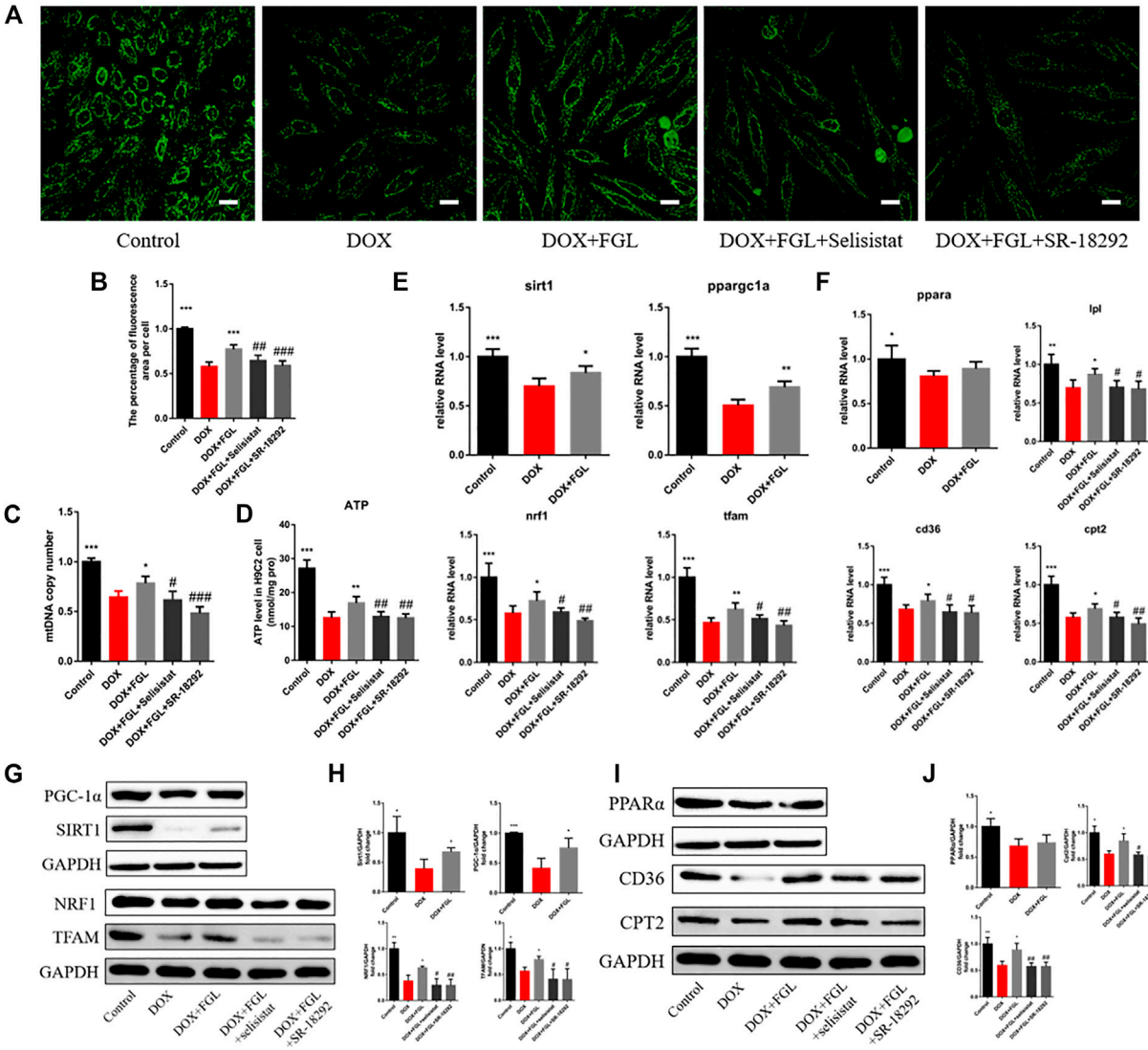

FIGURE 5 | FGL promoted mitochondrial biogenesis and fatty acid oxidization *in vitro*. **(A, B)** Representative images and quantitative analysis of the number of mitochondria by mitotracker staining in H9C2 cells (n = 6). Scale bar: 25 μm. **(C)** The assessment of the mtDNA copy number in H9C2 cells by RT-qPCR (n = 4). **(D)** The content of ATP in H9C2 cells (n = 5). **(E, F)** The expression level of mitochondrial biogenesis and fatty acid oxidization-associated mRNA in H9C2 cells quantified and shown as relative RNA levels after normalization to GAPDH (n = 5). **(G–J)** The expression level of mitochondrial biogenesis and fatty acid oxidization-associated proteins in H9C2 cells quantified and shown as relative protein expression levels after normalization to GAPDH (n = 3–5). *$p < 0.05$, **$p < 0.01$, ***$p < 0.001$ vs DOX group. #$p < 0.05$, ##$p < 0.01$, ###$p < 0.001$ vs. (DOX + FGL) group.

may promote downstream MB&FAO through the SIRT1–PGC-1α axis.

Ferruginol Facilitated Mitochondrial Biogenesis and Fatty Acid Oxidization via SIRT1-Proliferator-Activated Receptor Gamma Coactivator-1 Axis *In Vitro*

To further confirm whether FGL facilitated MB&FAO through the SIRT1–PGC-1α pathway, we cotreated FGL with selisistat and SR-18292 *in vitro*, respectively. First, we found that DOX resulted in a decrease in the number of mitochondria per unit area *in vitro* consistent with the results of electron microscopy *in vivo*, mtDNA copy number, and ATP content *in vitro*. Contrariwise, FGL contributed to a marked increase in these aspects compared to the DOX group, which were significantly reversed by selisistat and SR-18292 (**Figures 5A–D**). Impressively, we found that FGL inhibited the downregulation of MB&FAO marker except PPARα induced by DOX; however, both selisistat and SR-18292 significantly reversed the effects of FGL on the downstream mitochondrial biogenesis marker (Nrf1 and TFAM) and the fatty acid oxidation marker (CD36, CPT2, and LPL) (**Figures 5E–J**). These collective data documented that FGL coordinated MB&FAO through SIRT1 and PGC-1α.

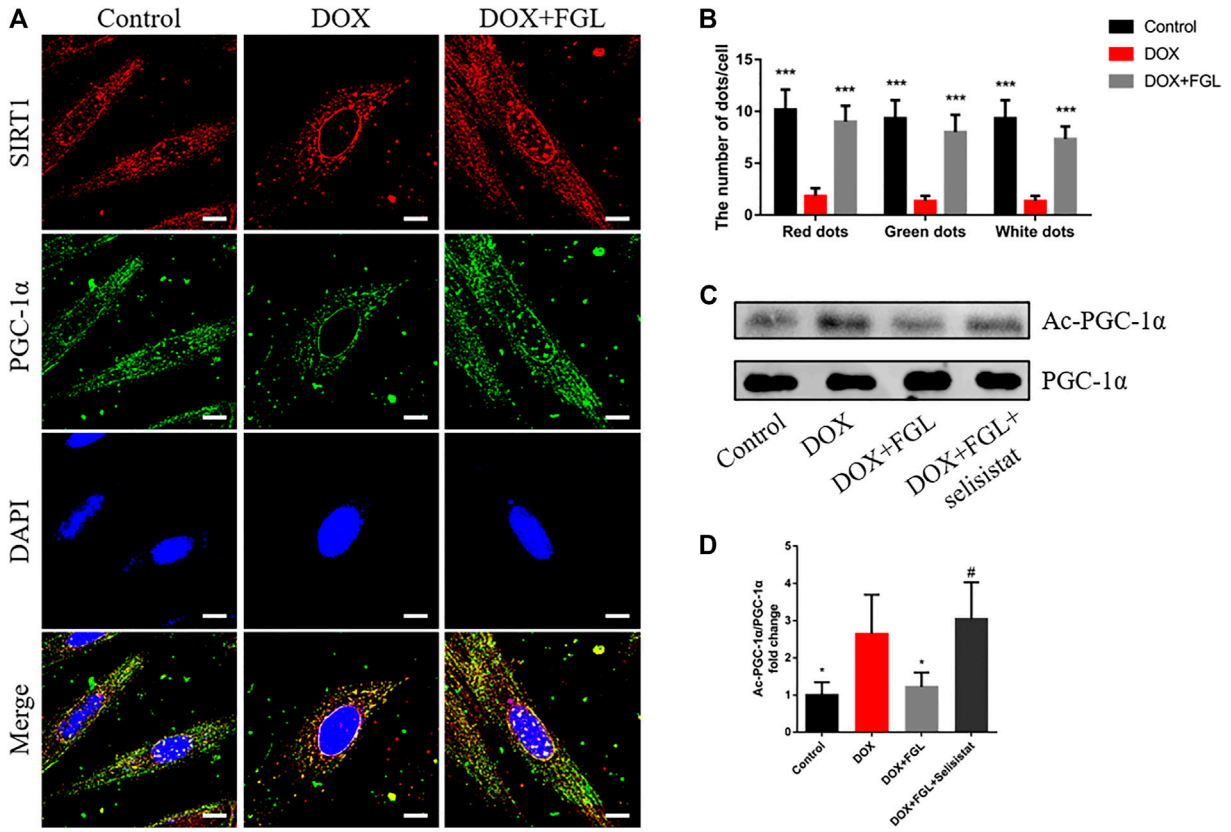

FIGURE 6 | FGL promoted the deacetylation of SIRT1 to PGC-1α *in vitro*. **(A, B)** Representative images and quantitative analysis of SIRT1 and PGC-1α and their colocalization in the nucleus (n = 6). Scale bar: 10 μm. **(C, D)** Representative bands and the ratio of acetylated PGC-1α to total PGC-1α detected by CO-IP of PGC-1α and acetylated lysine (n = 4). *$p < 0.05$, **$p < 0.01$, ***$p < 0.001$ vs DOX group. #$p < 0.05$ vs. (DOX + FGL) group.

However, its specific molecular mechanism between SIRT1 and PGC-1α still needs to be further confirmed.

Ferruginol Promoted the Deacetylation of Proliferator-Activated Receptor Gamma Coactivator-1 by SIRT1

In order to confirm the specific interaction between SIRT1 and PGC-1α and whether FGL could interfere with this interaction, the binding of SIRT1 and PGC-1α and the acetylation level of PGC-1α were detected by immunocoprecipitation and immunofluorescence. As shown in **Figure 6A**, SIRT1 and PGC-1α were distributed in both the cytoplasm and the nucleus, and both of them showed obvious fluorescent spots in the nucleus. Compared with the control group, in the nucleus, DOX resulted in a significant reduction of SIRT1 (red) and PGC-1α (green) and a decrease in colocalization (white). Compared with the DOX group, FGL increased the number of SIRT1 and PGC-1α fluorescence spots and colocalization of both (**Figures 6A,B**). These results revealed that DOX treatment reduced the expression and binding of SIRT1 and PGC-1α in the nucleus, while FGL promoted the expression and binding of SIRT1 and PGC-1α in the nucleus. The results of CO-IP showed that FGL inhibited the increased acetylation of PGC-1α induced by DOX (**Figures 6C,D**), while selisistat increased the acetylation of PGC-1α. Collectively, we concluded that FGL inhibited the acetylation of PGC-1α by promoting the expression of SIRT1 and, concurrently, increased the expression of PGC-1α to facilitate PGC-1α-mediated MB&FAO.

Ferruginol Did Not Interfere With Antitumor Effect of Doxorubicin

According to current research on DIC, identification of cardioprotective agents without interfering with the anticancer effect of DOX has been of interest to oncologists and cardiologists. Thus, in addition to confirming the protective effect of FGL on cardiomyocytes, we evaluated whether FGL interferes with the anticancer effect of DOX on the human breast carcinoma cell line MCF-7 and human hepatocellular carcinoma cell line HepG2. As shown in **Figure 7**, FGL within 0.1–1 μM did not affect the inhibition of cancer cell viability by DOX (**Figures 7A,B**).

DISCUSSION

Doxorubicin is a first-line anthracycline quinone and effective anticancer drug extensively used for the treatment of solid and

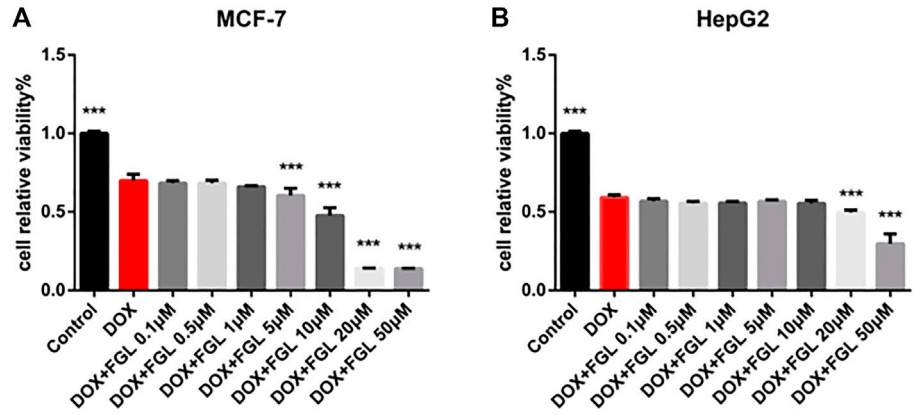

FIGURE 7 | FGL did not interfere with the antitumor effect of DOX. **(A, B)** The influence of FGL on the anticancer effect of DOX on MCF-7 and HepG2 cells was determined by CCK-8 assay (n = 6). ***$p < 0.001$ vs DOX group.

hematologic malignancies (Carter, 1975; Carvalho et al., 2009). However, its clinical use is evidently impeded by life-threatening cardiotoxicity that eventually causes dilated cardiomyopathy and heart failure (McGowan et al., 2017; Mancilla et al., 2019). To date, dexrazoxane is the only FDA-approved cardioprotectant for the prevention of DIC (Schuchter et al., 2002; Kane et al., 2008). However, its use in children was contraindicated by the European Medicines Agency in 2011 (Tebbi et al., 2007; European Medicines Agency, 2011) because of concerns of growing incidence of infection, myelosuppression, second primary malignancies, tumor-killing capacity reduction, and its unestablished efficacy in children. Accordingly, developing new, safe, and effective cardioprotectant to minimize DOX-induced cardiotoxicity is of great significance. For the first time, our study discovered the impressively cardioprotective effect and comprehensively documented the mechanism of FGL against DIC.

Mitochondrial damage events including deficiency of mitochondrial biogenesis and OXPHOS system, reduction of fatty acid oxidation, and ATP production and DNA damage were identified as the leading cause of DIC by most studies (Zhang et al., 2012; Carvalho et al., 2014; Osataphan et al., 2020). The deterioration of the mitochondrial function resulting from DOX eventually drives apoptosis, necrotic cell death, etc., which is fatal to energy-hungry heart with negligible regeneration and leads to subsequent life-threatening left ventricular dysfunction, cardiomyopathy, and heart failure (Felker et al., 2000; Cardinale et al., 2015). Consistently, GO and KEGG analysis of our transcriptome results displayed that DOX-induced DEGs were significantly enriched in mitochondria-associated bioprocesses and signaling pathways compared with the control group. These findings positively suggest that mitochondrial protection strategies should be proposed as potential solutions. Enlighteningly, our study found that FGL well alleviated DOX-induced cardiac structural and functional damage and deficiency of MB&FAO, which suggested that FGL targeted MB&FAO to protect against DIC.

PGC-1α is a transcriptional coactivator that modulates MB and FAO. In particular, PGC-1α dramatically induces the gene expression of NRF1 and physically interacts with Nrf1 and coactivates its transcriptional activity on TFAM, a key transcriptional activator that translocates to mitochondria and activates mitochondrial DNA replication and transcription (Lin et al., 2005). From another aspect, PGC-1 binds to and coactivates PPARα, thereby inducing numerous genes crucial for fatty acid metabolism, including CD36, CPT2, and lipidolysis LPL (Burkart et al., 2007; Pawlak et al., 2015). Both reported studies and our results demonstrated that DOX undermined the PGC-1α signaling pathway resulting in dysfunctional mitochondrial biogenesis, thus triggering a cardiac injury (Guo et al., 2014; Du et al., 2019). Thus, PGC-1α is promising to be a target for the treatment of DIC. So far, accumulating studies reported that PGC-1α is significantly regulated posttranslationally by phosphorylation, acetylation, and methylation (Puigserver et al., 2001; Rodgers et al., 2005; Li et al., 2007), among which deacetylation and reactivation of PGC-1α mediated by NAD+-dependent SIRT1 deacetylase have gradually attracted the attention of cardiologists.

Based on the analysis of transcriptome results, experimental verification, and literature review, we hypothesized that FGL protected against DIC by promoting MB&FAO through the SIRT1–PGC-1α axis. The results demonstrated that FGL increased the number of mitochondria, the mtDNA copy number, the mitochondrial membrane potential, the ATP production, and the mRNA and protein expression of MB&FAO markers, while selisistat and SR-18292 significantly reversed these changes. More specifically, FGL promoted the binding of SIRT1 and PGC-1α and deacetylation of PGC-1α, while selisistat inhibited the deacetylation activity of SIRT1 and strikingly enhanced the acetylation level of PGC-1α. In addition, we found that FGL promoted the expression of SIRT1 and enhanced the deacetylation and transcriptional coactivator activity of PGC-1α without affecting the expression of PPARα.

This indicated that FGL promotes the expression of downstream genes of PPARα through the SIRT1–PGC-1α axis instead of PPARα.

In conclusion, our study innovatively found the cardioprotective effect of FGL without interfering with the antitumor effect of DOX and documented the molecular underpinning that FGL increased the deacetylation of PGC-1α by deacetylase SIRT1 through promoting the expression of SIRT1, and concurrently increased the expression of PGC-1α, to facilitate PGC-1α-mediated MB and FAO.

DATA AVAILABILITY STATEMENT

The datasets presented in this study can be found in online repositories. The names of the repository/repositories and accession number(s) can be found below: https://www.ncbi.nlm.nih.gov/sra; PRJNA765675.

ETHICS STATEMENT

The animal study was reviewed and approved by the Beijing University of Chinese Medicine Animal Care Committee. Written informed consent was obtained from the owners for the participation of their animals in this study.

AUTHOR CONTRIBUTIONS

WL and JC performed the research, analyzed the data, and wrote the manuscript. XW revised the manuscript. YZ, QS, JY, and YJ contributed to the collection of heart and blood and partial animal experiments. YZ contributed to echocardiography and analyzed the data. XW and CL contributed to the design of the study. All authors read and approved the final version of the manuscript.

FUNDING

This work was supported by the National Natural Science Foundation of China (grant numbers 82174364, 81822049, 81673712, 8193000257, and 81673802), Major New Drug Creation of Ministry of Science and Technology (grant number 2019ZX09201004–001-011), the Fundamental Research Funds for the Central Universities (Distinguished project), and Excellent Young Scientist Foundation of BUCM (BUCM-2019-JCRC005).

SUPPLEMENTARY MATERIAL

The Supplementary Material for this article can be found online at: https://www.frontiersin.org/articles/10.3389/fphar.2021.773834/full#supplementary-material

REFERENCES

Arola, O. J., Saraste, A., Pulkki, K., Kallajoki, M., Parvinen, M., and Voipio-Pulkki, L. M. (2000). Acute Doxorubicin Cardiotoxicity Involves Cardiomyocyte Apoptosis. *Cancer Res.* 60, 1789–1792.

Bernstein, D., and Burridge, P. (2014). Patient-Specific Pluripotent Stem Cells in Doxorubicin Cardiotoxicity: A New Window into Personalized Medicine. *Prog. Pediatr. Cardiol.* 37 (1-2), 23–27. doi:10.1016/j.ppedcard.2014.10.006

Bispo de Jesus, M., Zambuzzi, W. F., Ruela de Sousa, R. R., Areche, C., Santos de Souza, A. C., Aoyama, H., et al. (2008). Ferruginol Suppresses Survival Signaling Pathways in Androgen-independent Human Prostate Cancer Cells. *Biochimie* 90 (6), 843–854. doi:10.1016/j.biochi.2008.01.011

Burkart, E. M., Sambandam, N., Han, X., Gross, R. W., Courtois, M., Gierasch, C. M., et al. (2007). Nuclear Receptors PPARbeta/delta and PPARalpha Direct Distinct Metabolic Regulatory Programs in the Mouse Heart. *J. Clin. Invest.* 117, 3930–3939. doi:10.1172/JCI32578

Cardinale, D., Colombo, A., Bacchiani, G., Tedeschi, I., Meroni, C. A., Veglia, F., et al. (2015). Early Detection of Anthracycline Cardiotoxicity and Improvement with Heart Failure Therapy. *Circulation* 131 (22), 1981–1988. doi:10.1161/CIRCULATIONAHA.114.013777

Carter, S. K. (1975). Adriamycin-a Review. *J. Natl. Cancer Inst.* 55 (6), 1265–1274. doi:10.1093/jnci/55.6.1265

Carvalho, C., Santos, R. X., Cardoso, S., Correia, S., Oliveira, P. J., Santos, M. S., et al. (2009). Doxorubicin: the Good, the Bad and the Ugly Effect. *Curr. Med. Chem.* 16 (25), 3267–3285. doi:10.2174/092986709788803312

Carvalho, F. S., Burgeiro, A., Garcia, R., Moreno, A. J., Carvalho, R. A., and Oliveira, P. J. (2014). Doxorubicin-induced Cardiotoxicity: from Bioenergetic Failure and Cell Death to Cardiomyopathy. *Med. Res. Rev.* 34 (1), 106–135. doi:10.1002/med.21280

Du, J., Hang, P., Pan, Y., Feng, B., Zheng, Y., Chen, T., et al. (2019). Inhibition of miR-23a Attenuates Doxorubicin-Induced Mitochondria-dependent Cardiomyocyte Apoptosis by Targeting the PGC-1α/Drp1 Pathway. *Toxicol. Appl. Pharmacol.* 369, 73–81. doi:10.1016/j.taap.2019.02.016

European Medicines Agency (2011). *Dexrazoxane*. United States: U.S. National Library of Medicine. Available at: https://www.ema.europa.eu/en/medicines/human/referrals/dexrazoxane.

Felker, G. M., Thompson, R. E., Hare, J. M., Hruban, R. H., Clemetson, D. E., Howard, D. L., et al. (2000). Underlying Causes and Long-Term Survival in Patients with Initially Unexplained Cardiomyopathy. *N. Engl. J. Med.* 342 (15), 1077–1084. doi:10.1056/NEJM200004133421502

Gerhart-Hines, Z., Rodgers, J. T., Bare, O., Lerin, C., Kim, S. H., Mostoslavsky, R., et al. (2007). Metabolic Control of Muscle Mitochondrial Function and Fatty Acid Oxidation through SIRT1/PGC-1alpha. *EMBO J.* 26 (7), 1913–1923. doi:10.1038/sj.emboj.7601633

Guo, J., Guo, Q., Fang, H., Lei, L., Zhang, T., Zhao, J., et al. (2014). Cardioprotection against Doxorubicin by Metallothionein Is Associated with Preservation of Mitochondrial Biogenesis Involving PGC-1α Pathway. *Eur. J. Pharmacol.* 737, 117–124. doi:10.1016/j.ejphar.2014.05.017

Hullin, R., Métrich, M., Sarre, A., Basquin, D., Maillard, M., Regamey, J., et al. (2018). Diverging Effects of Enalapril or Eplerenone in Primary Prevention against Doxorubicin-Induced Cardiotoxicity. *Cardiovasc. Res.* 114 (2), 272–281. doi:10.1093/cvr/cvx162

Jeninga, E. H., Schoonjans, K., and Auwerx, J. (2010). Reversible Acetylation of PGC-1: Connecting Energy Sensors and Effectors to Guarantee Metabolic Flexibility. *Oncogene* 29 (33), 4617–4624. doi:10.1038/onc.2010.206

Kane, R. C., McGuinn, W. D., Jr, Dagher, R., Justice, R., and Pazdur, R. (2008). Dexrazoxane (Totect): FDA Review and Approval for the Treatment of Accidental Extravasation Following Intravenous Anthracycline Chemotherapy. *Oncologist* 13 (4), 445–450. doi:10.1634/theoncologist.2007-0247

Lagouge, M., Argmann, C., Gerhart-Hines, Z., Meziane, H., Lerin, C., Daussin, F., et al. (2006). Resveratrol Improves Mitochondrial Function and Protects against Metabolic Disease by Activating SIRT1 and PGC-1alpha. *Cell* 127 (6), 1109–1122. doi:10.1016/j.cell.2006.11.013

Li, X., Monks, B., Ge, Q., and Birnbaum, M. J. (2007). Akt/PKB Regulates Hepatic Metabolism by Directly Inhibiting PGC-1alpha Transcription Coactivator. *Nature* 447, 1012–1016. doi:10.1038/nature05861

Lin, J., Handschin, C., and Spiegelman, B. M. (2005). Metabolic Control through the PGC-1 Family of Transcription Coactivators. *Cell Metab* 1 (6), 361–370. doi:10.1016/j.cmet.2005.05.004

Mancilla, T. R., Iskra, B., and Aune, G. J. (2019). Doxorubicin-Induced Cardiomyopathy in Children. *Compr. Physiol.* 9 (3), 905–931. doi:10.1002/cphy.c180017

McGowan, J. V., Chung, R., Maulik, A., Piotrowska, I., Walker, J. M., and Yellon, D. M. (2017). Anthracycline Chemotherapy and Cardiotoxicity. *Cardiovasc. Drugs Ther.* 31 (1), 63–75. doi:10.1007/s10557-016-6711-0

Minotti, G., Menna, P., Salvatorelli, E., Cairo, G., and Gianni, L. (2004). Anthracyclines: Molecular Advances and Pharmacologic Developments in Antitumor Activity and Cardiotoxicity. *Pharmacol. Rev.* 56 (2), 185–229. doi:10.1124/pr.56.2.6

Osataphan, N., Phrommintikul, A., Chattipakorn, S. C., and Chattipakorn, N. (2020). Effects of Doxorubicin-Induced Cardiotoxicity on Cardiac Mitochondrial Dynamics and Mitochondrial Function: Insights for Future Interventions. *J. Cel Mol Med* 24 (12), 6534–6557. doi:10.1111/jcmm.15305

Pawlak, M., Lefebvre, P., and Staels, B. (2015). Molecular Mechanism of PPARα Action and its Impact on Lipid Metabolism, Inflammation and Fibrosis in Non-alcoholic Fatty Liver Disease. *J. Hepatol.* 62 (3), 720–733. doi:10.1016/j.jhep.2014.10.039

Puigserver, P., Rhee, J., Lin, J., Wu, Z., Yoon, J. C., Zhang, C. Y., et al. (2001). Cytokine Stimulation of Energy Expenditure through P38 MAP Kinase Activation of PPARgamma Coactivator-1. *Mol. Cel* 8, 971–982. doi:10.1016/s1097-2765(01)00390-2

Rodgers, J. T., Lerin, C., Haas, W., Gygi, S. P., Spiegelman, B. M., and Puigserver, P. (2005). Nutrient Control of Glucose Homeostasis through a Complex of PGC-1alpha and SIRT1. *Nature* 434 (7029), 113–118. doi:10.1038/nature03354

Rodríguez, J. A., Theoduloz, C., Yáñez, T., Becerra, J., and Schmeda-Hirschmann, G. (2006). Gastroprotective and Ulcer Healing Effect of Ferruginol in Mice and Rats: Assessment of its Mechanism of Action Using *In Vitro* Models. *Life Sci.* 78 (21), 2503–2509. doi:10.1016/j.lfs.2005.10.018

Rowe, G. C., Jiang, A., and Arany, Z. (2010). PGC-1 Coactivators in Cardiac Development and Disease. *Circ. Res.* 107 (7), 825–838. doi:10.1161/CIRCRESAHA.110.223818

Saijo, H., Kofujita, H., Takahashi, K., and Ashitani, T. (2015). Antioxidant Activity and Mechanism of the Abietane-type Diterpene Ferruginol. *Nat. Prod. Res.* 29 (18), 1739–1743. doi:10.1080/14786419.2014.997233

Scarpulla, R. C., Vega, R. B., and Kelly, D. P. (2012). Transcriptional Integration of Mitochondrial Biogenesis. *Trends Endocrinol. Metab.* 23 (9), 459–466. doi:10.1016/j.tem.2012.06.006

Schuchter, L. M., Hensley, M. L., Meropol, N. J., and Winer, E. P. (2002). 2002 Update of Recommendations for the Use of Chemotherapy and Radiotherapy Protectants: Clinical Practice Guidelines of the American Society of Clinical Oncology. *J. Clin. Oncol.* 20, 2895–2903. doi:10.1200/JCO.2002.04.178

Shakir, D. K., and Rasul, K. I. (2009). Chemotherapy Induced Cardiomyopathy: Pathogenesis, Monitoring and Management. *J. Clin. Med. Res.* 1 (1), 8–12. doi:10.4021/jocmr2009.02.1225

Sokolove, P. M. (1994). Interactions of Adriamycin Aglycones with Mitochondria May Mediate Adriamycin Cardiotoxicity. *Int. J. Biochem.* 26, 1341–1350. doi:10.1016/0020-711x(94)90176-7

Tebbi, C. K., London, W. B., Friedman, D., Villaluna, D., De Alarcon, P. A., Constine, L. S., et al. (2007). Dexrazoxane-associated Risk for Acute Myeloid Leukemia/myelodysplastic Syndrome and Other Secondary Malignancies in Pediatric Hodgkin's Disease. *J. Clin. Oncol.* 25, 493–500. doi:10.1200/JCO.2005.02.3879

Tokarska-Schlattner, M., Wallimann, T., and Schlattner, U. (2002). Multiple Interference of Anthracyclines with Mitochondrial Creatine Kinases: Preferential Damage of the Cardiac Isoenzyme and its Implications for Drug Cardiotoxicity. *Mol. Pharmacol.* 61, 516–523. doi:10.1124/mol.61.3.516

Wang, X., Li, C., Wang, Q., Li, W., Guo, D., Zhang, X., et al. (2019). Tanshinone IIA Restores Dynamic Balance of Autophagosome/Autolysosome in Doxorubicin-Induced Cardiotoxicity via Targeting Beclin1/LAMP1. *Cancers (Basel)* 11 (7), 910. doi:10.3390/cancers11070910

Wang, X., Wang, Q., Li, W., Zhang, Q., Jiang, Y., Guo, D., et al. (2020). TFEB-NF-κB Inflammatory Signaling axis: a Novel Therapeutic Pathway of Dihydrotanshinone I in Doxorubicin-Induced Cardiotoxicity. *J. Exp. Clin. Cancer Res.* 39 (1), 93. doi:10.1186/s13046-020-01595-x

Zhang, S., Liu, X., Bawa-Khalfe, T., Lu, L. S., Lyu, Y. L., Liu, L. F., et al. (2012). Identification of the Molecular Basis of Doxorubicin-Induced Cardiotoxicity. *Nat. Med.* 18 (11), 1639–1642. doi:10.1038/nm.2919

Zhou, S., Heller, L. J., and Wallace, K. B. (2001a). Interference with Calcium-dependent Mitochondrial Bioenergetics in Cardiac Myocytes Isolated from Doxorubicin-Treated Rats. *Toxicol. Appl. Pharmacol.* 175, 60–67. doi:10.1006/taap.2001.9230

Zhou, S., Starkov, A., Froberg, M. K., Leino, R. L., and Wallace, K. B. (2001b). Cumulative and Irreversible Cardiac Mitochondrial Dysfunction Induced by Doxorubicin. *Cancer Res.* 61, 771–777.

Zolezzi, J. M., Lindsay, C. B., Serrano, F. G., Ureta, R. C., Theoduloz, C., Schmeda-Hirschmann, G., et al. (2018). Neuroprotective Effects of Ferruginol, Jatrophone, and Junicedric Acid against Amyloid-β Injury in Hippocampal Neurons. *J. Alzheimers Dis.* 63 (2), 705–723. doi:10.3233/JAD-170701

Conflict of Interest: The authors declare that the research was conducted in the absence of any commercial or financial relationships that could be construed as a potential conflict of interest.

Publisher's Note: All claims expressed in this article are solely those of the authors and do not necessarily represent those of their affiliated organizations, or those of the publisher, the editors and the reviewers. Any product that may be evaluated in this article, or claim that may be made by its manufacturer, is not guaranteed or endorsed by the publisher.

frontiers in Pharmacology

ORIGINAL RESEARCH
published: 03 December 2021
doi: 10.3389/fphar.2021.742562

Centella asiatica (L.) Urb. Prevents Hypertension and Protects the Heart in Chronic Nitric Oxide Deficiency Rat Model

Mohd Khairulanwar Bunaim[1,2], *Yusof Kamisah*[1], *Mohd Noor Mohd Mustazil*[1], *Japar Sidik Fadhlullah Zuhair*[1], *Abdul Hamid Juliana*[1] *and Norliza Muhammad*[1]*

[1]*Department of Pharmacology, Faculty of Medicine, Universiti Kebangsaan Malaysia, Kuala Lumpur, Malaysia,* [2]*Department of Biomedical Sciences and Therapeutics, Faculty of Medicine and Health Sciences, Universiti Malaysia Sabah, Kota Kinabalu, Malaysia*

Background: Hypertension is a major risk factor for cardiovascular disease (CVD), which is the number one cause of global mortality. The potential use of natural products to alleviate high blood pressure has been demonstrated to exert a cardioprotective effect. *Centella asiatica (L.)* Urb. belongs to the plant family Apiaceae (Umbelliferae). It contains a high amount of triterpenoid and flavonoid that have antioxidant properties and are involved in the renin-angiotensin-aldosterone system which is an important hormonal system for blood pressure regulation.

Objective: This study aimed to investigate the effects of *C. asiatica* ethanolic extract on blood pressure and heart in a hypertensive rat model, which was induced using oral N(G)-nitro-L-arginine methyl ester (L-NAME).

Methods: Male Sprague-Dawley rats were divided into five groups and were given different treatments for 8 weeks. Group 1 only received deionized water. Groups 2, 4, and 5 were given L-NAME (40 mg/kg, orally). Groups 4 and 5 concurrently received *C. asiatica* extract (500 mg/kg, orally) and captopril (5 mg/kg, orally), respectively. Group 3 only received *C. asiatica* extract (500 mg/kg body weight, orally). Systolic blood pressure (SBP) was measured at weeks 0, 4, and 8, while serum nitric oxide (NO) was measured at weeks 0 and 8. At necropsy, cardiac and aortic malondialdehyde (MDA) contents, cardiac angiotensin-converting enzyme (ACE) activity, and serum level of brain natriuretic peptide (BNP) were measured.

Results: After 8 weeks, the administrations of *C. asiatica* extract and captopril showed significant ($p < 0.05$) effects on preventing the elevation of SBP, reducing the serum nitric oxide level, as well as increasing the cardiac and aortic MDA content, cardiac ACE activity, and serum brain natriuretic peptide level.

Conclusion: *C. asiatica* extract can prevent the development of hypertension and cardiac damage induced by L-NAME, and these effects were comparable to captopril.

Keywords: *Centella asiatica*, cardiac damage, hypertension, nitro-l-arginine methyl ester, nitric oxide

OPEN ACCESS

Edited by:
Li-Tung Huang, Kaohsiung Chang Gung Memorial Hospital, Taiwan

Reviewed by:
Seyed Zachariah Moradi, Kermanshah University of Medical Sciences, Iran
Songül Karakaya, Atatürk University, Turkey

***Correspondence:**
Norliza Muhammad
norliza_ssp@ppukm.ukm.edu.my

Specialty section:
This article was submitted to Ethnopharmacology, a section of the journal Frontiers in Pharmacology

Received: *16 July 2021*
Accepted: *03 November 2021*
Published: *03 December 2021*

Citation:
Bunaim MK, Kamisah Y, Mohd Mustazil MN, Fadhlullah Zuhair JS, Juliana AH and Muhammad N (2021) Centella asiatica (L.) *Urb. Prevents Hypertension and Protects the Heart in Chronic Nitric Oxide Deficiency Rat Model. Front. Pharmacol. 12:742562. doi: 10.3389/fphar.2021.742562*

INTRODUCTION

Cardiovascular disease (CVD) remains the number one cause of global mortality with hypertension contributes to the major risk factor (World Health Organization, 2017). Hypertension promotes mechanical stress that induces cardiomyocyte hypertrophy, apoptosis, and remodeling. Subsequently, the heart can change its size, shape, structure, and function with a consequent cardiac dysfunction (Nadruz, 2015). There is growing evidence showing that the development of hypertension and cardiac damage is associated with elevation of oxidative stress status, suppression of nitric oxide (NO) synthesis in the vasculature, and overactivation of the renin-angiotensin-aldosterone system (RAAS) (Schulz et al., 2011; Münzel et al., 2017; Bakogiannis et al., 2019; Wunpathe et al., 2020).

Elevation of oxidative stress is largely attributable to excessive production of reactive oxygen species (ROS) such as superoxide, hydrogen peroxide, and hydroxyl radicals, which are toxic byproducts of human aerobic metabolism (Sedeek et al., 2009). Importantly, an increase in oxidative stress profile induces endothelial dysfunction, inflammatory processes, and vascular smooth muscle tone (Touyz and Briones, 2011). Meanwhile, NO that is produced in endothelial tissues, activates soluble guanylate cyclase to produce 3′,5′-cyclase guanosine monophosphate (cGMP), which has an important role in vasodilatory processes, inhibition of platelet adhesion, and smooth muscle proliferation (Zhou et al., 2004). This vasodilatory action reduces vascular resistance and blood circulatory pressure, which eventually contributes to a lower risk of hypertension. As expected, vascular NO deficiency is a major finding in dysfunctional endothelium and arterial hypertension (Lüscher and Vanhoutte, 1986; Panza et al., 1990). RAAS is an important neurohormonal system that involves the regulation of blood pressure and tissue perfusion. Angiotensin-converting enzyme (ACE) is one of the RAAS components and it converts angiotensin I (AT-I) into angiotensin II (AT-II). If this hormonal system is overactivated, AT-II will be released excessively and chronically, leading to vasoconstriction, aldosterone secretion, activation of the sympathetic nervous system, anti-natriuretic mechanism, and hypertension. Besides that, AT-II can be produced locally in the heart, primarily induced by an increase in cardiac wall stress. The binding of AT-II to angiotensin II type I receptor (AT1R) stimulates the formation of heart collagen by fibroblast cells, which subsequently increases the risk for cardiac hypertrophy, fibrosis, and cardiomyocyte apoptosis (Singh et al., 2008; Dai et al., 2011; Jia et al., 2012). For instance, AT-II infusion for 2 weeks induced cardiac hypertrophy and elevated oxidative stress markers in rat cardiac tissue (Kakishita et al., 2003).

Despite a variety of anti-hypertensive agents such as ACE inhibitors, angiotensin II receptor blockers (ARB), β-adrenergic receptor blocker, and calcium channel antagonists are being used in the treatment of hypertension and cardiac hypertrophy, the progression of myocardial injury and subsequent cardiac dysfunction remains a major problem in chronic hypertensive subjects (Eirin et al., 2014). There has been considerable interest in the potential use of natural products to alleviate blood pressure, which has been demonstrated to exert a cardioprotective effect. One of them is *Centella asiatica (L.)* Urb., which is also known as Indian pennywort, abundantly found in tropical countries including China, India, and the South-East Asian countries (Brinkhaus et al., 2000). Apart from fever and wound healing, this medicinal plant was used traditionally to treat stomach upset, leprosy, bladder inactivity, and urinary tract infection (Brinkhaus et al., 2000). Triterpenoid compounds such as asiatic acid, madecassic acid, asiaticoside, and madecassoside are the major biologically active compounds in *C. asiatica* (James and Dubery, 2009). Other compounds isolated from this plant are flavonoids, brahmoside, brahminoside, glycosides isothankuniside, and thankuniside (Azerad, 2016). In modern medicine, *C. asiatica* has been reported to have high antioxidant property due to its abundant triterpenoid and flavonoid contents (Pittella et al., 2009). The herb and its bioactive compounds may have a role in therapeutic application in diseases associated with oxidative stress, such as hypertension and cardiac failure. Studies using triterpenoid- and flavonoid-rich chloroform fractions of *C. asiatica* in a hypertensive rat model showed the effectiveness of the extract in reducing the acute rise in blood pressure with a single dose (Harwoko and Nugroho, 2014; Nansy et al., 2015). In addition, asiatic acid, one of the main triterpenoid compounds in *C. asiatica*, was reported to prevent RAAS activation in metabolic syndrome rats (Maneesai et al., 2016a). Furthermore, flavonoid-rich fruits such as apple and kiwi inhibited ACE activity in some *in vitro* studies (24, 25), suggesting similar potential cardiovascular benefits offered by *C. asiatica*.

Although previous *in vivo* studies have reported the anti-hypertensive effect of *C. asiatica* (Harwoko and Nugroho, 2014; Nansy et al., 2015), those studies were carried out either in a single dosage of *C. asiatica* extract or by bioactive compounds isolated from the plant. To date, there has been no studies that investigate the effects of *C. asiatica* extract on chronic hypertension and cardiac damage. Therefore, to bridge the research gap, this study was conducted to explore the blood pressure-lowering and cardioprotective effects of *C. asiatica* in chronic hypertensive rats. N(G)-nitro-L-arginine methyl (L-NAME) was administered to induce systemic hypertension and cardiac damage in rats.

MATERIALS AND METHODS

Drugs, Chemicals and Kits

L-NAME and other chemicals were obtained from Sigma-Aldrich (St. Louis, MO, United States) unless stated otherwise. Captopril tablet was purchased from Y.S.P Industries (Selangor, Malaysia). The kits for cardiac ACE activity and serum brain natriuretic peptide (BNP) level measurements were purchased from Elabscience (Wuhan, China).

Plant Material and Extraction

The fresh leaves of *C. asiatica* were collected in February 2020 from Kepala Batas, Pulau Pinang, Malaysia. The specimen was identified by a botanist in Universiti Kebangsaan Malaysia Herbarium and a voucher specimen of the plant (UKMB 40434) was deposited at that institute. The cold extraction

method was employed using the maceration technique. A 1 kg of the dried leaves was soaked in 4 L of 80% ethanol and agitated on a shaker at 16 rpm for 24 h. The extracts were filtered and the residual sample was soaked again two more times using fresh ethanol, making a total of 12 L. The combined extracts were concentrated and freed of solvent using a rotary evaporator, then dried in a freeze-dryer. The yield percentage of the ethanolic extract was 16.6%.

Animals

Two-month-old male Sprague-Dawley rats (200–250 g) were obtained from Laboratory Animal Resources Unit, Universiti Kebangsaan Malaysia. They were maintained at room temperature (27 ± 2°C) with natural light at the Laboratory Animal Center, Department of Pharmacology, Universiti Kebangsaan Malaysia. All procedures were complied with the standards for the care and use of experimental animals and were approved by the Animal Ethics of Universiti Kebangsaan Malaysia (FAR/PP/2019/NORLIZA/30-OCT./1048-OCT.2019-AUG.-2020). Rats were fed with a commercial diet (Gold Coin Feed-mills (M) Sdn Bhd, Selangor, Malaysia) and tap water *ad libitum*.

Experimental Protocol

Thirty rats were randomly divided into five groups (n = six rats/group). At a baseline, rat blood was taken via cardiac puncture after being given ketamine (0.1 ml/100 g body weight) and xylazine (0.01 ml/100 g body weight) via intraperitoneal injection as anesthesia. Groups 2, 4, and 5 were given L-NAME (40 mg/kg body weight, orally) for 8 weeks. Groups 4 and 5 concurrently received *C. asiatica* extract (500 mg/kg body weight, orally) and captopril (5 mg/kg, orally), respectively. Groups 1 and 3 only received deionized water and *C. asiatica* extract (500 mg/kg, orally body weight) respectively. The dose of the extract was selected based on a pilot study (**Supplementary Material**). All treatments were given every day for 8 weeks via oral gavage. Body weight was measured at the baseline and after the study ended. After 8 weeks of study, blood was taken via cardiac puncture, and all animals were sacrificed. Heart and aortic tissues were harvested after completing the study for biochemical analysis.

Indirect Measurement of Blood Pressure in Conscious Rats

Animal systolic blood pressure (SBP) was measured at baseline, fourth week and eighth week of study using non-invasive tail-cuff plethysmography (Kent Scientific Cooperation, Torrington, US). In brief, conscious rats were placed in a restrainer and allowed to be calm before SBP measurement. The rat tail was placed inside the tail-cuff, and the cuff was automatically inflated and released. For each rat, five stable SBP readings were chosen and averaged from each cycle.

Biochemical Analysis

Serum nitric oxide (NO) level was measured using Griess reagent against sodium nitrite standard curve. It was expressed as the percentage difference between weeks 0 and 8. Cardiac and aortic malondialdehyde (MDA) contents were measured as thiobarbituric acid reactive substance (TBARS) according to the method of Ledwozyw et al. (1986). Malondialdehyde tetraethyl acetal was used as the standard and the TBARS content was expressed as MDA per protein (μmol/mg). The protein content was determined based on the method described by Bradford (1976). Cardiac ACE activity and serum BNP level were determined using a commercial kit (Elabscience, Wuhan, China) based on the sandwich enzyme immunoassay principle.

Statistical Analysis

All results were expressed as mean ± standard error of the mean (SEM). The data were analyzed for normality test using the Shapiro-Wilk test. Analysis of variance (ANOVA) with Bonferroni posthoc test was used for the SBP parameter. The differences between the groups for body weight, NO, MDA, BNP, and ACE parameters were compared using one-way ANOVA with Tukey's Honestly Significant Differences posthoc test. Statistical significance was defined as $p < 0.05$. Statistical analyses were conducted using the Statistical Product for Social Science 23 software (SPSS Inc., Chicago, IL).

RESULTS

Body Weight

There was no significant difference ($p > 0.05$) in body weight among the rat groups at the baseline (**Figure 1**). After 8 weeks of treatment, there was a significant increase ($p < 0.05$) in body weight seen in all groups compared to the baseline. However, group 2 (366.17 ± 5.04 g) demonstrated a significantly lower ($p < 0.05$) body weight when compared to the control group (391.17 ± 2.09 g).

Systolic Blood Pressure

SBP was significantly elevated ($p < 0.05$) in group 2 (148.50 ± 0.64 mmHg) with chronic L-NAME exposure when compared with the control group (group 1) after 8 weeks (127.22 ± 0.99 mmHg) (**Figure 2**). The increase in SBP induced by L-NAME was attenuated in groups 4 and 5 given *C. asiatica* (131.78 ± 1.60 mmHg) and captopril (130.72 ± 0.83 mmHg), respectively. No significant difference ($p > 0.05$) was noted between these two groups. *C. asiatica* had no effect ($p > 0.05$) on SBP in *C. asiatica* control rats of group 3 (127.83 ± 1.46 mmHg).

Serum Nitric Oxide Level

A significant ($p < 0.05$) reduction in serum NO was seen in the group 2 (−18.68 ± 1.81% mmHg) after 8 weeks compared to the control of group 1 (−1.94 ± 1.54% mmHg) (**Figure 3**). Concurrent treatment of L-NAME administered in groups 4 and 5 with *C. asiatica* (−6.65 ± 0.92% mmHg) and captopril (−7.33 ± 0.69% mmHg), respectively had significantly ($p < 0.05$) prevented the NO reduction induced by L-NAME.

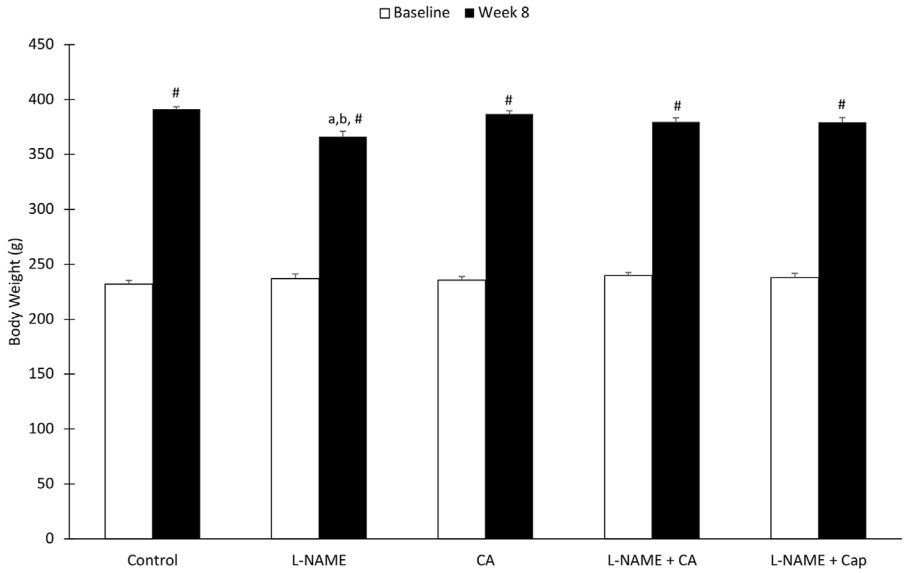

FIGURE 1 | Rat body weight before and after administration of L-NAME (40 mg/kg orally) and *C. asiatica* extract (500 mg/kg orally) or captopril (5 mg/kg orally) during the 8-weeks of study. The values represent mean ± SEM (n = 6). [#]versus baseline ($p < 0.05$), [a]versus control ($p < 0.05$), [b]versus *C. asiatica* ($p < 0.05$).

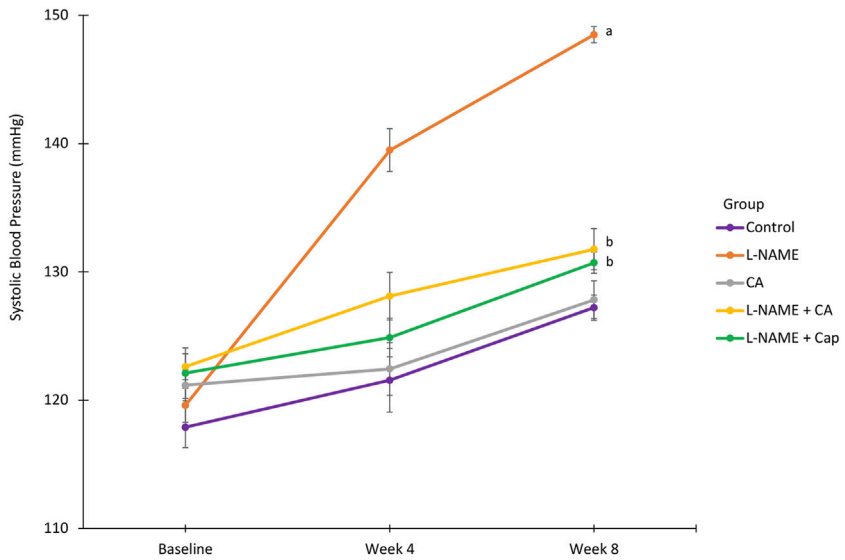

FIGURE 2 | Systolic blood pressure in rats treated with concurrent L-NAME (40 mg/kg orally) and *C. asiatica* (500 mg/kg orally) or captopril (5 mg/kg orally). Line graph represent mean ± SEM (n = 6). [a]versus control ($p < 0.05$), [b]versus L-NAME ($p < 0.05$).

Cardiac Angiotensin-Converting Enzyme Activity

The ACE activity in the heart was significantly ($p < 0.05$) elevated in the group 2 (7.26 ± 0.25 μg/mg) as compared to the control of group 1 (4.11 ± 0.23 μg/mg). The elevation was inhibited by the concurrent treatment of *C. asiatica* (4.90 ± 0.47 μg/mg) and captopril (3.58 ± 0.30 μg/mg) in groups 4 and 5, respectively (**Figure 4**). No significant ($p > 0.05$) difference in cardiac ACE activity was observed among groups 1, 2, and 5.

Cardiac and Aortic Thiobarbituric Acid Reactive Substance Content

L-NAME administration in group 2 for 8 weeks significantly ($p < 0.05$) increased cardiac and aortic TBARS content when

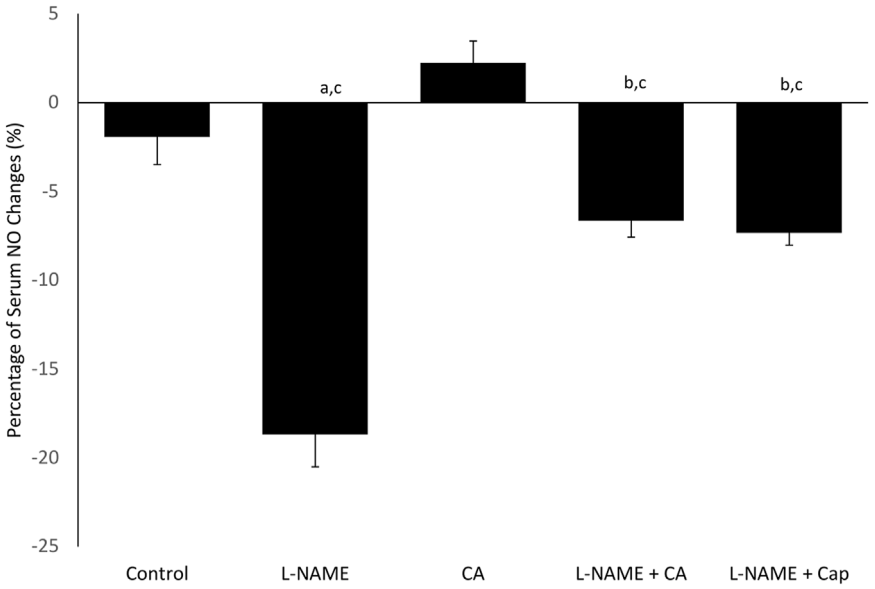

FIGURE 3 | Percentage of plasma nitric oxide (NO) change in rats given *C. asiatica* extract (500 mg/kg orally) and captopril (5 mg/kg orally) together with L-NAME (40 mg/kg orally) for 8 weeks. Bars represent mean ± SEM (n = 6). [a]versus control ($p < 0.05$), [b]versus L-NAME ($p < 0.05$), [c]versus *C. asiatica* ($p < 0.05$).

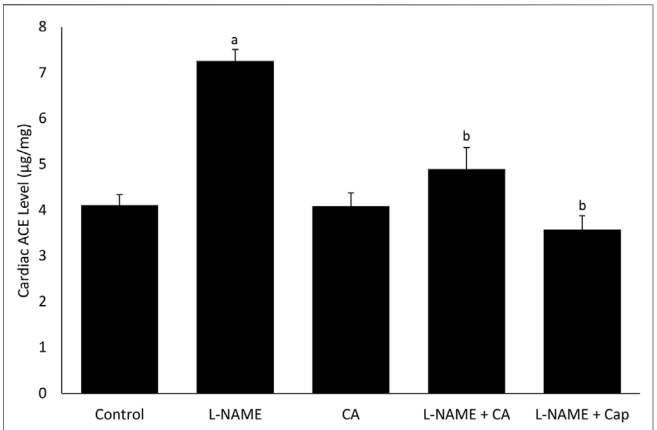

FIGURE 4 | Cardiac angiotensin-converting enzyme (ACE) activity in rats treated with *C. asiatica* extract (500 mg/kg orally) or captopril (5 mg/kg orally) together with L-NAME (40 mg/kg orally) for 8 weeks. Bars represent mean ± SEM (n = 6). [a]versus control ($p < 0.05$), [b]versus L-NAME ($p < 0.05$).

compared to the control group (group 1) (**Figures 5A,B**). Treatments with *C. asiatica* and captopril in groups 4 and 5, respectively had similarly prevented the elevation of TBARS content induced by L-NAME in both heart and aorta.

Serum Brain Natriuretic Peptide Level

Serum BNP level was significantly ($p < 0.05$) higher in group 2 (652.42 ± 20.79 pg/ml) receiving L-NAME for 8 weeks than the control group 1 (373.56 ± 30.59 pg/ml) (**Figure 6**). Treatments with *C. asiatica* (398.88 ± 28.17 pg/ml) and captopril (353.27 ± 21.18 pg/ml) in groups 4 and 5, respectively had similarly prevented the rise in the serum BNP level.

DISCUSSIONS

The present study exhibited the effects of ethanolic extract of *Centella asiatica (L.)* Urb. on the cardiovascular system in L-NAME-induced hypertensive rats as summarized in **Table 1**. Ethanol extraction was chosen because it was proven to produce a high yield of flavonoid (Andarwulan et al., 2010; Nansy et al., 2015) and triterpenoids such as asiatic acid, asiaticoside, madecassic acid, and madecacosside (Hashim et al., 2011). Nansy et al. (2015) and Harwoko and Nugroho (2014) showed that triterpenoid and flavonoid-rich fractions isolated from ethanolic extract of *C. asiatica* and administered at bolus dose, respectively, reduced blood pressure in phenylephrine-induced hypertensive rats. Asiatic acid, another bioactive compound in *C. asiatica*, had been shown to exert significant anti-hypertensive effect in numerous types of hypertensive rat model (Bunbupha et al., 2014; Maneesai et al., 2016a; Maneesai et al., 2017). The ethanolic extract was also reported to possess cardioprotective benefit in myocardial infarction (Pragada et al., 2004) in addition to its high antioxidant activities (Muchtaromah et al., 2016). Nevertheless, we could not find any literature on the cardioprotective ability of *C. asiatica* extracted using other methods.

In the current study, we used L-NAME to induce chronic hypertension in our rats. It appeared that this compound had a detrimental effect on the rat's growth as evidence by the reduction in body weight. Chronic L-NAME administration was shown to attenuate weight gain in normal and high-fat diet-fed rats, possibly due to decreased food intake in the L-NAME group (Tsuchiya et al., 2007). Nonetheless, concomitant treatment with *C. asiatica* reversed the effect in the present study. This herbal extract was capable of overcoming this noxious effect on weight gain, conceivably due to its high flavonoid content, which

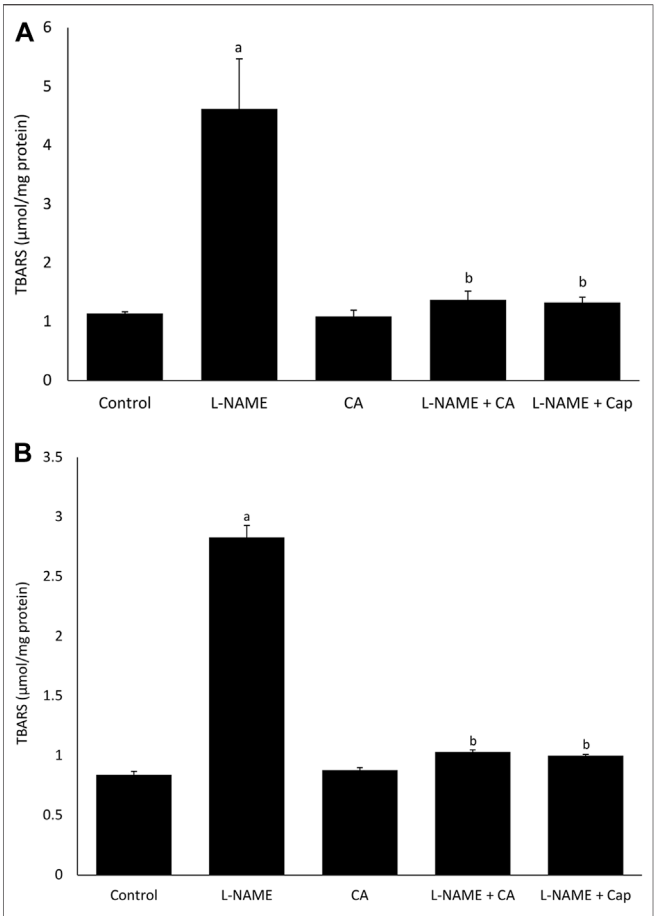

FIGURE 5 | The effects of *C. asiatica* (500 mg/kg orally) and captopril (5 mg/kg orally) on **(A)** aortic and **(B)** cardiac TBARS content in L-NAME-administered rats (40 mg/kg orally) after 8 weeks. Bars represent mean ± SEM (n = 6). [a]versus control ($p < 0.05$), [b]versus L-NAME ($p < 0.05$).

contributed to lower energy consumption and a more efficient digestive system (Ke et al., 2015). The safety of *C. asiatica* consumption was proven in an acute toxicity testing, in which *C. asiatica* extract at the maximum dose of 2000 mg/kg body weight showed no toxic signs and mortality in rats. In a subacute toxicity testing, there was no significant alteration in body weight, general health, and food intake in rats after receiving *C. asiatica* extract ranged from 10 to 1,000 mg/kg/day for 90 days in comparison to the control group (Kumari et al., 2016).

The paradigm of using L-NAME to establish experimental hypertension has become a widely accepted method for testing anti-hypertensive drugs. Our observation that chronic eNOS inhibition is responsible for the development of hypertension, which is also supported by other studies (Sung et al., 2013; Bunbupha et al., 2014). L-NAME is a potent inhibitor of eNOS that depreciates NO synthesis in cells. In blood vessels, it diminishes vascular relaxation due to a reduction in the availability of NO, a potent vasodilator. As expected, group 2 administered with L-NAME alone demonstrated a greater reduction in NO at the end of the study. This led to an increase in blood pressure, as similarly reported by Aluko et al. (2019) and Berkban et al. (2015). However, concomitant treatment of *C. asiatica* for 8 weeks managed to restore the serum NO level and eventually prevented the elevation of blood pressure, despite the chronic L-NAME exposure (**Figure 7**). NO promotes vasodilation via induction of soluble guanylate cyclase and increases cyclic guanosine monophosphate (cGMP) in smooth muscle cells (Capettini et al., 2010; Förstermann and Sessa, 2012). Previous evidence suggested that a high content of asiatic acid in *C. asiatica* might contribute to the normalization of serum NO level and blood pressure, as reported in a range of different experimental models of hypertension including metabolic syndrome, renovascular, and L-NAME-induced hypertension (Bunbupha et al., 2014; Maneesai et al., 2016a; Maneesai et al., 2017). Asiatic acid also upregulated eNOS protein expression and ameliorated systemic vasodilation in these studies, further explaining the anti-hypertensive effects of *C. asiatica* on chronic NO deficiency induced by L-NAME.

Excessive lipid peroxidation alarms a weak antioxidant defense and subsequent oxidative damage that increases the oxidative status, resulting from overproduction of ROS (Yu,

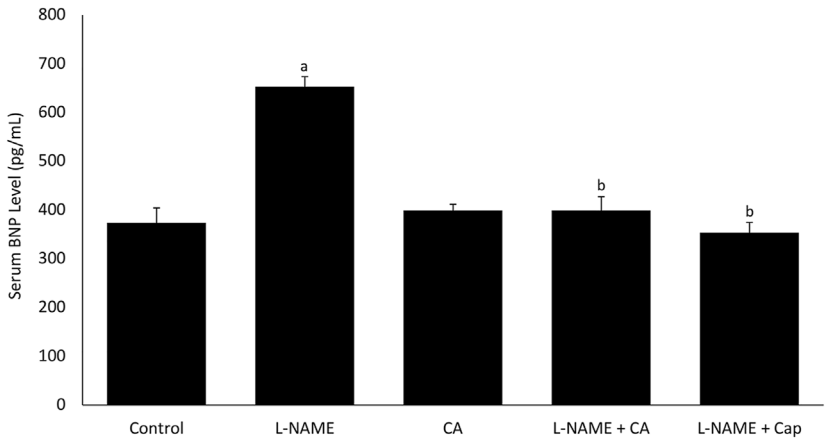

FIGURE 6 | Serum B-natriuretic peptide (BNP) level in rats co-treated with L-NAME (40 mg/kg orally) and *C. asiatica* extract (500 mg/kg orally) or captopril (5 mg/kg orally) for 8 weeks. Bars represent mean ± SEM (n = 6). [a]versus control ($p < 0.05$), [b]versus L-NAME ($p < 0.05$).

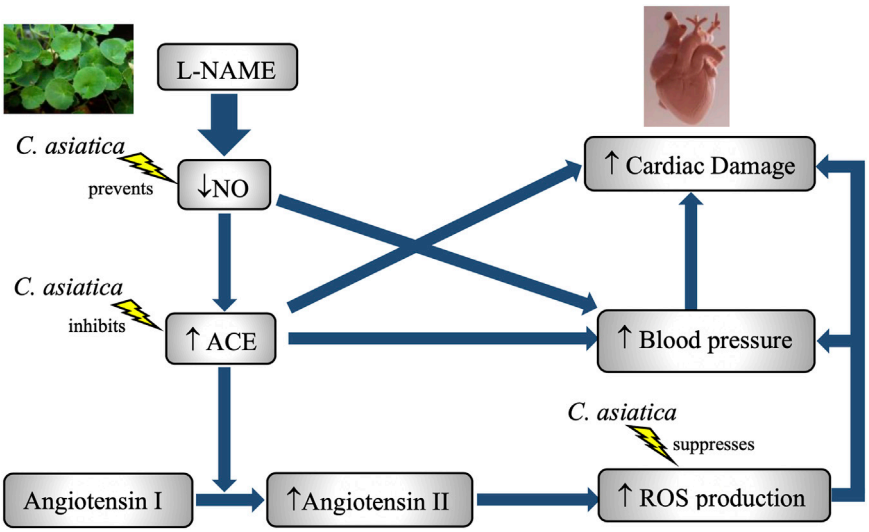

FIGURE 7 | A schematic diagram on the role of NO deficiency in L-NAME-induced hypertension and cardiotoxicity in rats. Treatment with *C. asiatica* extract exhibited anti-hypertensive and cardioprotective effects via the enhancement of NO bioavailability, the suppression of RAAS and amelioration of oxidative stress status in L-NAME-treated group.

TABLE 1 | Summary of result from measured parameters. The values represent mean ± SEM (n = 6).

	Control	L-NAME	*C. asiatica*	L-NAME + *C. asiatica*	L-NAME + captopril
Baseline Body Weight (g)	232.00 ± 3.34	237.00 ± 4.16	235.50 ± 3.36	239.83 ± 2.66	237.67 ± 4.12
Final Body Weight (g)	391.17 ± 2.09	366.17 ± 5.04[a,b]	386.67 ± 2.95	379.67 ± 3.65	379.33 ± 4.39
Baseline Systolic Blood Pressure (mmHg)	117.89 ± 1.58	119.61 ± 1.33	121.17 ± 1.22	122.61 ± 1.01	121.11 ± 1.97
Final Systolic Blood Pressure (mmHg)	127.22 ± 0.99	148.50 ± 0.64[a]	127.83 ± 1.46	131.78 ± 1.60[c]	130.72 ± 0.83[c]
Serum NO Change (%)	-1.94 ± 1.54	-18.68 ± 1.81[a,b]	2.24 ± 1.23	-6.65 ± 0.92[b,c]	-7.33 ± 0.69[b,c]
Cardiac ACE (μg/mg)	4.11 ± 0.23	7.26 ± 0.25[a]	4.09 ± 0.29	4.90 ± 0.47[c]	3.58 ± 0.30[c]
Aortic TBARS (μmol/mg protein)	1.14 ± 0.03	4.62 ± 0.85[a]	1.09 ± 0.11	1.37 ± 0.15[c]	1.33 ± 0.09[c]
Cardiac TBARS (μmol/mg protein)	0.84 ± 0.03	2.83 ± 0.10[a]	0.88 ± 0.02	1.03 ± 0.02[c]	1.00 ± 0.01[c]
Serum BNP (pg/ml)	373.56 ± 30.59	652.42 ± 20.79[a]	399.06 ± 12.41	398.88 ± 28.17[c]	353.27 ± 21.18[c]

[a]*versus control ($p < 0.05$).*
[b]*versus L-NAME ($p < 0.05$).*
[c]*versus C. asiatica ($p < 0.05$).*

1994). Oxidative stress is a pro-hypertensive factor that aggravates endothelial dysfunction and enhances vasoconstriction, which together contributes to increasing systemic vascular resistance that results in BP elevation (Sorriento et al., 2018). MDA is a product of the reaction between lipid bilayer of membrane plasma with ROS (Samhan-Arias et al., 2011), which can react with thiobarbituric acid to produce TBARS. In the L-NAME-induced hypertensive rat, increased TBARS level in the aorta indicated a worsening oxidative stress profile, which was observed similarly in other studies (Rajeshwari et al., 2014; Kamisah et al., 2017). Endogenous NO suppresses vascular $p47^{phox}$ protein expression and superoxide production, which contribute to the source of vascular oxidative stress that initiates vascular inflammation and dysfunction (Harrison et al., 2010). Reduced bioavailability of NO may underlie the development of oxidative stress-related hypertension in the present study. Besides, a chronic NO inhibition promotes a higher expression of NADPH-dependent oxidase in aortic smooth muscle cells and a subsequent exacerbation in vascular superoxide (O_2^-) formation via excessive production of AT-II (Touyz and Schiffrin, 1999; Giani et al., 2014).

The augmented generation of ROS by L-NAME was overcome by *C. asiatica* in this study based on the low content of TBARS in aortic tissue, which was comparable to that of the control group. Our finding is in line with previous literature that demonstrates the antioxidant property of *C. asiatica* extract (Pittella et al., 2009; Kumari et al., 2016). The astounding ROS scavenging ability of this herb is also apparent in various models of organ injury (Wei et al., 2013; Pakdeechote et al., 2014). In a study by Bunbupha et al. (2014), asiatic acid was demonstrated to inhibit the overproduction of O_2^- in aortic tissue and plasma MDA via downregulation of $p47^{phox}$ expression, which subsequently restored the vascular function and improved the

hemodynamic parameters. A similar finding was also reported by Maneesai et al. (2016a) showing that anti-hypertensive effects of asiatic acid in the metabolic syndrome model were contributed by its antioxidant and anti-inflammatory properties. Besides, protection against oxidative damage in cells is mainly depending on the scavenging enzymes, which break down free radicals including superoxide and hydroxyl, and subsequently improve the oxidative stress status (Robaczewska et al., 2016; Ahmadinejad et al., 2017). *C. asiatica* extract can ward off the free radical excess via enhancement of free radical scavenging enzymes including catalase, superoxide dismutase (SOD), glutathione peroxidase (GPx), and glutathione-S-transferase (GST), which attenuate the superoxide production, ameliorate the vascular oxidative stress, and reverse the free radical-induced cellular damage (Tabassum et al., 2013). NO can react with O_2^- to produce peroxynitrite ($ONOO^-$), thus mitigate the biological effect of O_2^- (Pryor and Squadrito, 1995). Our current work showed an inverse relationship between NO and ROS level in *C. asiatica*-treated group, suggesting that this herbal extract reduced the ROS level via upregulation of NO bioavailability.

BNP is a biomarker that plays an important role in natriuresis, vasodilatation, RAAS inhibition, and the sympathetic nervous system (Weber and Hamm, 2006). It is released by injured cardiac tissue due to increased mechanical stretch, hypoxia, and tissue ischemia (D'Souza and Baxter, 2003; Kinnunen et al., 1993; Tóth et al., 1994). Its level correlates with mass increase and tissue damage in the cardiac ventricle (Conen et al., 2006). In the current study, administration of L-NAME increased the availability of BNP in plasma indicating that this compound could feasibly induce cardiac injury. Our observation is consistent with other studies which showed that there was an increase in other cardiac biomarkers such as troponin T and creatinine kinase-MB (CKMB) after 4 weeks of L-NAME administration (Adamcova et al., 2013; Aldubayan et al., 2020). These findings suggested the detrimental effects of L-NAME on cardiac tissue. More evidence was observed in our study, in which the deficient state of NO was associated with cardiac damage induced by L-NAME. Significant works had been done to show the role of NO in influencing cardiac performance. Early observation exhibited that NO enhanced Frank-Starling response and cardiac distensibility (Grocott-Mason et al., 1994). A later study by Casadei and Sears (2003) generated similar findings with intracardiac NO improved diastolic relaxation and cardiac stiffness. In addition, a downregulation of eNOS activity followed by reduced bioavailability of NO was reported to deteriorate the ventricular hypertrophy and dysfunction in chronic L-NAME exposure in rats (Kumar et al., 2014; Jin et al., 2017). In a more detailed framework, an interaction between eNOS and cardiac ACE activities was reported via a feedback regulation (Wiemer et al., 1997; Takemoto et al., 1997), which contributed to the pathophysiology of L-NAME-induced cardiac damage. Silambarasan et al. (2014) reported that increased myocardial dysfunction, cardiac hypertrophy, and fibrosis were positively correlated to the oxidative markers and ACE activity in nitric oxide inhibited rats. AT-II is produced during the early stage of heart failure via cardiac ACE action to compensate for the reduced cardiac function during the chronic deficient state of nitric oxide. However, as the disease progresses, RAAS is excessively activated. This results in increased cardiac preload and afterload, promotes cardiac hypertrophy, fibrosis, and cardiomyocyte apoptosis (Singh et al., 2008; Dai et al., 2011; Jia et al., 2012), and subsequently worsens the heart function (Jackson et al., 2000). In addition, cardiac AT-II also enhances the mitochondrial ROS generation in cardiomyocytes including the excessive production of NADPH (De Giusti et al., 2009; De Giusti et al., 2013). The elevation of oxidative stress seems to augment the progression of heart remodeling and the subsequent cardiac damage (Rababa'h et al., 2018).

Systemic administration of *C. asiatica* extract inhibited an increase in serum BNP level induced by L-NAME in our study. Possible explanations for the beneficial effects of *C. asiatica* could be the enhancement of NO bioavailability, reduction of cardiac ACE activity, and improvement of oxidative stress status. Pragada et al. (2004) reported that *C. asiatica* extract possessed a cardio-protective effect that was attributable to its high content of triterpenoid. Asiatic acid was demonstrated to prevent cardiac and aorta remodeling including left ventricular hypertrophy, myocardial fibrosis, collagen deposition, and aortic wall thickening in a chronic NO deficiency state, as reported by Bunbupha et al. (2015). Another triterpenoid compound, asiaticoside was reported to have anti-hypertensive and cardioprotective effects in pulmonary hypertension and right ventricular hypertrophy rat model via induction of PI3K/Akt/eNOS signaling pathway (Wang et al., 2018). Based on the previous literature, we speculate that the triterpenoid in *C. asiatica* upregulated eNOS activity and increased NO content in L-NAME treated rats, and these mechanisms might play a beneficial role in the amelioration of cardiac damage.

C. asiatica also inhibited the increase in cardiac ACE activity induced by L-NAME. Reports from the previous studies noted that asiatic acid managed to attenuate excessive RAAS activation in several models of hypertensive rats (Maneesai et al., 2016a; Maneesai et al., 2017). Some studies showed that flavonoid compounds isolated from kiwi and apple peel inhibited ACE activities *in vitro* (Balasuriya and Rupasinghe, 2012; Hettihewa et al., 2018). These findings may suggest the role of flavonoids in *C. asiatica* might be responsible for the suppression of RAAS activation. In addition, the high antioxidant property of *C. asiatica* showed a significant role in reducing oxidative stress in cardiomyocytes (Zainol et al., 2003; Pittella et al., 2009; Kumari et al., 2016). Ventricular hypertrophy and myocardial damage are among the complications of hypertension. In the presence of pressure overload due to systemic hypertension, the left ventricular wall thickens to minimize the wall stress (Drazner, 2011). Dysregulation of protein synthesis/processing within the endoplasmic reticulum during the hypertrophic response may be linked to the cardiomyocyte apoptosis process (González et al., 2018). Hence, the present study suggested that the protective effect of *C. asiatica* against hypertension was significant in the reduction in cardiac tissue damage in L-NAME treated group.

Our study also demonstrated the effects of captopril on SBP, serum NO, oxidative stress profile as well as a cardiac marker, and ACE activities. Captopril is one of anti-hypertensive drugs that belong to the ACE inhibitor group. This drug was chosen as a positive control since ACE inhibitors are the first line of treatment in

hypertension and cardiac failure (Kementerian Kesihatan Malaysia, 2019) and it also possesses antioxidant activity (Bartosz et al., 1997; Benzie and Tomlinson, 1998). In the current study, captopril prevented a reduction in serum NO level, as well as an increase in SBP, cardiac and aortic TBARS content, serum BNP level, and cardiac ACE activities in the L-NAME-induced hypertensive rat model. The effects of captopril were comparable to that of *C. asiatica*. The results were supported by other studies showing that daily administration of captopril (5 mg/kg) could reduce hypertension and cardiac remodeling in rats with long-term exposure to L-NAME via inhibition on ACE (Maneesai et al., 2016b; Bunbupha et al., 2019). The mechanism of L-NAME leads to raising the blood pressure by inhibiting the eNOS activity, thus diminishes NO production. Hence, a drug like sodium nitroprusside that promotes NO release could be a more suitable choice as the positive control. However, it must be administered parenterally, making its daily administration a difficult routine (Hottinger et al., 2014).

We acknowledged other limitations in the current study. We only used a single dose of ethanolic extract of *C. asiatica*, guided from the results of our pilot study using three different doses; 300, 500 and 1,000 mg/kg (**Supplementary Material**). At the dose of 300 mg/kg, *C. asiatica* was reported to have high anti-oxidant properties (Muchtaromah et al., 2016) and at the dose of 500 mg/kg, this extract possessed significant diuretic property (Roopesh et al., 2011) which had the potential as an anti-hypertensive agent. Meanwhile, *C. asiatica* at the dose of 1,000 mg/kg exhibited a significant reduction in the ischemic area of cardiac tissues in rat model with post-myocardial infarction event (Pragada et al., 2004). Our pilot study showed that 500 and 1,000 mg/kg of ethanolic extract of *C. asiatica* significantly prevented the systolic blood pressure in L-NAME-induced hypertensive rats after 3 weeks of treatment and the lower dose was chosen for our main study. The rationale of using only a single dose of the extract is to minimize the number of animals needed in animal experimentation to comply with 3Rs (refinement, reduction and replacement) for best practice using animals. Future studies should be considered to establish a detailed dose-response relationship and to investigate different routes/timing of administration of the extract. Another limitation in this study is the assessment of vascular responsiveness, serial echocardiography, and histomorphology for cardiac and aortic tissues were not performed. The vascular reactivity test and serial echocardiography demonstrate the vascular and cardiac function changes. In contrast, a histomorphology test is a useful tool for assessing tissue remodeling development in hypertension and cardiac failure. Hence, additional studies are required to obtain these results. Nevertheless, this is the first study that investigated the role of *C. asiatica* in preventing hypertension and cardiac remodeling in the chronic NO deficient state. The present findings proposed that the amelioration of oxidative status and RAAS activity are the most likely mechanisms contributing to these protective effects. Given the protective potentials of this herbal plant, *C. asiatica* is highly advocated as a promising preventive approach in hypertension and its cardiac complication. Further studies are recommended to investigate the effect of *C. asiatica* in other hypertensive rat models or more severe stages of hypertension.

DATA AVAILABILITY STATEMENT

The datasets presented in this study can be found in online repositories. The names of the repository/repositories and accession number(s) can be found in the article/**Supplementary Material**.

ETHICS STATEMENT

The animal study was reviewed and approved by Universiti Kebangsaan Malaysia Animal Ethic Committee (UKMAEC), Universiti Kebangsaan Malaysia.

AUTHOR CONTRIBUTIONS

MB designed all the experiments. MB and MM performed all experiments under the supervision of NM. MB collected and analyzed data and wrote the manuscript. MM, JSFZ and AHJ contributed to data collection. YK and NM revised the first copy of the manuscript and which was approved by all authors. NM supervised the work from designing to finalizing the manuscript for journal submission.

FUNDING

The authors would like to acknowledge the financial funding provided by the Faculty of Medicine, Universiti Kebangsaan Malaysia (Grant no. FF-2020-015).

SUPPLEMENTARY MATERIAL

The Supplementary Material for this article can be found online at: https://www.frontiersin.org/articles/10.3389/fphar.2021.742562/full#supplementary-material

REFERENCES

Adamcova, M., Ruzickova, S., and Simko, F. (2013). Multiplexed Immunoassays for Simultaneous Quantification of Cardiovascular Biomarkers in the Model of H(G)-nitro-L-arginine Methylester (L-NAME) Hypertensive Rat. *J. Physiol. Pharmacol.* 64 (2), 211–217.

Ahmadinejad, F., Geir Møller, S., Hashemzadeh-Chaleshtori, M., Bidkhori, G., and Jami, M. S. (2017). Molecular Mechanisms behind Free Radical Scavengers Function against Oxidative Stress. *Antioxidants (Basel)* 6 (3), 51. doi:10.3390/antiox6030051

Aldubayan, M. A., Ahmed, A. S., Emara, A. M., Ahmed, A. A., and Elgharabawy, R. M. (2020). Sinapic Acid Attenuates Cardiovascular Disorders in Rats by Modulating Reactive Oxygen Species and Angiotensin Receptor Expression. *Oxid Med. Cel Longev* 2020, 1436858. doi:10.1155/2020/1436858

Aluko, E. O., Adejumobi, O. A., and Fasanmade, A. A. (2019). Peristrophe Roxburghiana Leaf Extracts Exhibited Anti-hypertensive and Anti-lipidemic

Properties in L-NAME Hypertensive Rats. *Life Sci.* 234, 116753. doi:10.1016/j.lfs.2019.116753

Andarwulan, N., Batari, R., Sandrasari, D. A., Bolling, B., and Wijaya, H. (2010). Flavonoid Content and Antioxidant Activity of Vegetables from Indonesia. *Food Chem.* 121 (4), 1231–1235. doi:10.1016/j.foodchem.2010.01.033

Azerad, R. (2016). Chemical Structures, Production and Enzymatic Transformations of Sapogenins and Saponins from *Centella asiatica* (L.) Urban. *Fitoterapia* 114, 168–187. doi:10.1016/j.fitote.2016.07.011

Bakogiannis, C., Theofilogiannakos, E., Papadopoulos, C., Lazaridis, C., Bikakis, I., Tzikas, S., et al. (2019). A Translational Approach to the Renin-Angiotensin-Aldosterone System in Heart Failure. *Ann. Res. Hospitals* 3, 1–11. doi:10.21037/arh.2019.05.01

Balasuriya, N., and Rupasinghe, H. P. (2012). Antihypertensive Properties of Flavonoid-Rich Apple Peel Extract. *Food Chem.* 135 (4), 2320–2325. doi:10.1016/j.foodchem.2012.07.023

Bartosz, M., Kedziora, J., and Bartosz, G. (1997). Antioxidant and Prooxidant Properties of Captopril and Enalapril. *Free Radic. Biol. Med.* 23 (5), 729–735. doi:10.1016/s0891-5849(97)00014-2

Benzie, I. F., and Tomlinson, B. (1998). Antioxidant Power of Angiotensin-Converting Enzyme Inhibitors *In Vitro*. *Br. J. Clin. Pharmacol.* 45 (2), 168–169. doi:10.1046/j.1365-2125.1998.00664.x

Berkban, T., Boonprom, P., Bunbupha, S., Welbat, J. U., Kukongviriyapan, U., Kukongviriyapan, V., et al. (2015). Ellagic Acid Prevents L-NAME-Induced Hypertension via Restoration of eNOS and P47phox Expression in Rats. *Nutrients* 7 (7), 5265–5280. doi:10.3390/nu7075222

Bradford, M. M. (1976). A Rapid and Sensitive Method for the Quantitation of Microgram Quantities of Protein Utilizing the Principle of Protein-Dye Binding. *Anal. Biochem.* 72 (1), 248–254. doi:10.1006/abio.1976.9999

Brinkhaus, B., Lindner, M., Schuppan, D., and Hahn, E. G. (2000). Chemical, Pharmacological and Clinical Profile of the East Asian Medical Plant *Centella asiatica*. *Phytomedicine* 7 (5), 427–448. doi:10.1016/s0944-7113(00)80065-3

Bunbupha, S., Pakdeechote, P., Kukongviriyapan, U., Prachaney, P., and Kukongviriyapan, V. (2014). Asiatic Acid Reduces Blood Pressure by Enhancing Nitric Oxide Bioavailability with Modulation of eNOS and P47phox Expression in L-NAME-Induced Hypertensive Rats. *Phytother Res.* 28 (10), 1506–1512. doi:10.1002/ptr.5156

Bunbupha, S., Pakdeechote, P., Maneesai, P., Prachaney, P., and Boonprom, P. (2019). Carthamus Tinctorius L. Extract Attenuates Cardiac Remodeling in L-NAME-Induced Hypertensive Rats by Inhibiting the NADPH Oxidase-Mediated TGF-B1 and MMP-9 Pathway. *Ann. Anat.* 222, 120–128. doi:10.1016/j.aanat.2018.12.006

Bunbupha, S., Prachaney, P., Kukongviriyapan, U., Kukongviriyapan, V., Welbat, J. U., and Pakdeechote, P. (2015). Asiatic Acid Alleviates Cardiovascular Remodelling in Rats with L-NAME-Induced Hypertension. *Clin. Exp. Pharmacol. Physiol.* 42 (11), 1189–1197. doi:10.1111/1440-1681.12472

Capettini, L. S., Cortes, S. F., and Lemos, V. S. (2010). Relative Contribution of eNOS and nNOS to Endothelium-dependent Vasodilation in the Mouse Aorta. *Eur. J. Pharmacol.* 643 (2), 260–266. doi:10.1016/j.ejphar.2010.06.066

Casadei, B., and Sears, C. E. (2003). Nitric-oxide-mediated Regulation of Cardiac Contractility and Stretch Responses. *Prog. Biophys. Mol. Biol.* 82 (1-3), 67–80. doi:10.1016/s0079-6107(03)00006-3

Conen, D., Zeller, A., Pfisterer, M., and Martina, B. (2006). Usefulness of B-type Natriuretic Peptide and C-Reactive Protein in Predicting the Presence or Absence of Left Ventricular Hypertrophy in Patients with Systemic Hypertension. *Am. J. Cardiol.* 97 (2), 249–252. doi:10.1016/j.amjcard.2005.08.028

D'Souza, S. P., and Baxter, G. F., (2003). B Type Natriuretic Peptide: a Good Omen in Myocardial Ischaemia. *Heart* 89 (7), 707–709. doi:10.1136/heart.89.7.707

Dai, D. F., Johnson, S. C., Villarin, J. J., Chin, M. T., Nieves-Cintrón, M., Chen, T., et al. (2011). Mitochondrial Oxidative Stress Mediates Angiotensin II-Induced Cardiac Hypertrophy and Galphaq Overexpression-Induced Heart Failure. *Circ. Res.* 108 (7), 837–846. doi:10.1161/CIRCRESAHA.110.232306

De Giusti, V. C., Caldiz, C. I., Ennis, I. L., Pérez, N. G., Cingolani, H. E., and Aiello, E. A. (2013). Mitochondrial Reactive Oxygen Species (ROS) as Signaling Molecules of Intracellular Pathways Triggered by the Cardiac Renin-Angiotensin II-Aldosterone System (RAAS). *Front. Physiol.* 4 (126), 126. doi:10.3389/fphys.2013.00126

De Giusti, V. C., Garciarena, C. D., and Aiello, E. A. (2009). Role of Reactive Oxygen Species (ROS) in Angiotensin II-Induced Stimulation of the Cardiac Na+/HCO3- Cotransport. *J. Mol. Cel Cardiol* 47 (5), 716–722. doi:10.1016/j.yjmcc.2009.07.023

Drazner, M. H. (2011). The Progression of Hypertensive Heart Disease. *Circulation* 123 (3), 327–334. doi:10.1161/CIRCULATIONAHA.108.845792

Eirin, A., Lerman, A., and Lerman, L. O. (2014). Mitochondrial Injury and Dysfunction in Hypertension-Induced Cardiac Damage. *Eur. Heart J.* 35 (46), 3258–3266. doi:10.1093/eurheartj/ehu436

Förstermann, U., and Sessa, W. C. (2012). Nitric Oxide Synthases: Regulation and Function. *Eur. Heart J.* 33 (7), 829–837d. doi:10.1093/eurheartj/ehr304

Giani, J. F., Janjulia, T., Kamat, N., Seth, D. M., Blackwell, W. L., Shah, K. H., et al. (2014). Renal Angiotensin-Converting Enzyme Is Essential for the Hypertension Induced by Nitric Oxide Synthesis Inhibition. *J. Am. Soc. Nephrol.* 25 (12), 2752–2763. doi:10.1681/ASN.2013091030

González, A., Ravassa, S., López, B., Moreno, M. U., Beaumont, J., San José, G., et al. (2018). Myocardial Remodeling in Hypertension. *Hypertension* 72 (3), 549–558. doi:10.1161/HYPERTENSIONAHA.118.11125

Grocott-Mason, R., Fort, S., Lewis, M. J., and Shah, A. M. (1994). Myocardial Relaxant Effect of Exogenous Nitric Oxide in Isolated Ejecting Hearts. *Am. J. Physiol.* 266 (5 Pt 2), H1699–H1705. doi:10.1152/ajpheart.1994.266.5.H1699

Harrison, C. B., Drummond, G. R., Sobey, C. G., and Selemidis, S. (2010). Evidence that Nitric Oxide Inhibits Vascular Inflammation and Superoxide Production via a P47phox-dependent Mechanism in Mice. *Clin. Exp. Pharmacol. Physiol.* 37 (4), 429–434. doi:10.1111/j.1440-1681.2009.05317.x

Harwoko, P. S., and Nugroho, A. E. (2014). Triterpenoid-rich Fraction of centella Asiatica Leaves and *In Vivo* Antihypertensive Activity. *Int. Food Res. J.* 21 (1), 149–154.

Hashim, P., Sidek, H., Helan, M. H., Sabery, A., Palanisamy, U. D., and Ilham, M. (2011). Triterpene Composition and Bioactivities of *Centella asiatica*. *Molecules* 16 (2), 1310–1322. doi:10.3390/molecules16021310

Hettihewa, S. K., Hemar, Y., and Rupasinghe, H. P. V. (2018). Flavonoid-Rich Extract of Actinidia Macrosperma (A Wild Kiwifruit) Inhibits Angiotensin-Converting Enzyme *In Vitro*. *Foods* 7 (146), 1–8. doi:10.3390/foods7090146

Hottinger, D. G., Beebe, D. S., Kozhimannil, T., Prielipp, R. C., and Belani, K. G. (2014). Sodium Nitroprusside in 2014: A Clinical Concepts Review. *J. Anaesthesiol Clin. Pharmacol.* 30 (4), 462–471. doi:10.4103/0970-9185.142799

Jackson, G., Gibbs, C. R., Davies, M. K., and Lip, G. Y. (2000). ABC of Heart Failure. Pathophysiology. *BMJ* 320 (7228), 167–170. doi:10.1136/bmj.320.7228.167

James, J. T., and Dubery, I. A. (2009). Pentacyclic Triterpenoids from the Medicinal Herb, *Centella asiatica* (L.) Urban. *Molecules* 14 (10), 3922–3941. doi:10.3390/molecules14103922

Jia, N., Dong, P., Ye, Y., Qian, C., and Dai, Q. (2012). Allopurinol Attenuates Oxidative Stress and Cardiac Fibrosis in Angiotensin II-Induced Cardiac Diastolic Dysfunction. *Cardiovasc. Ther.* 30 (2), 117–123. doi:10.1111/j.1755-5922.2010.00243.x

Jin, S., Teng, X., Xiao, L., Xue, H., Guo, Q., Duan, X., et al. (2017). Hydrogen Sulfide Ameliorated L-NAME-Induced Hypertensive Heart Disease by the Akt/eNOS/NO Pathway. *Exp. Biol. Med. (Maywood)* 242 (18), 1831–1841. doi:10.1177/1535370217732325

Kakishita, M., Nakamura, K., Asanuma, M., Morita, H., Saito, H., Kusano, K., et al. (2003). Direct Evidence for Increased Hydroxyl Radicals in Angiotensin II-Induced Cardiac Hypertrophy through Angiotensin II Type 1a Receptor. *J. Cardiovasc. Pharmacol.* 42 (Suppl. 1), S67–S70. doi:10.1097/00005344-200312001-00015

Kamisah, Y., Zuhair, J. S. F., Juliana, A. H., and Jaarin, K. (2017). Parkia Speciosa Empty Pod Prevents Hypertension and Cardiac Damage in Rats Given N(G)-nitro-l-arginine Methyl Ester. *Biomed. Pharmacother.* 96, 291–298. doi:10.1016/j.biopha.2017.09.095

Ke, J. Y., Kliewer, K. L., Hamad, E. M., Cole, R. M., Powell, K. A., Andridge, R. R., et al. (2015). The Flavonoid, Naringenin, Decreases Adipose Tissue Mass and Attenuates Ovariectomy-Associated Metabolic Disturbances in Mice. *Nutr. Metab. (Lond)* 12 (1), 1. doi:10.1186/1743-7075-12-1

Kementerian Kesihatan Malaysia (2018). *Clinical Practise Guidelines Management of Hypertension*. 5th Edn, 30. Available at http://www.acadmed.org.my/index.cfm?&menuid=67 (Accessed November 11, 2021).

Kementerian Kesihatan Malaysia (2019). *Clinical Practise Guidelines on Management of Heart Failure*. 4th EdnAvailable at https://www.malaysianheart.org/?p=cpg (Accessed November 11, 2021).

Kinnunen, P., Vuolteenaho, O., and Ruskoaho, H. (1993). Mechanisms of Atrial and Brain Natriuretic Peptide Release from Rat Ventricular Myocardium: Effect of Stretching. *Endocrinology* 132 (5), 1961–1970. doi:10.1210/endo.132.5.8477647

Kumar, S., Prahalathan, P., and Raja, B. (2014). Vanillic Acid: a Potential Inhibitor of Cardiac and Aortic wall Remodeling in L-NAME Induced Hypertension through Upregulation of Endothelial Nitric Oxide Synthase. *Environ. Toxicol. Pharmacol.* 38 (2), 643–652. doi:10.1016/j.etap.2014.07.011

Kumari, S., Deori, M., Elancheran, R., Kotoky, J., and Devi, R. (2016). *In Vitro* and *In Vivo* Antioxidant, Anti-hyperlipidemic Properties and Chemical Characterization of *Centella asiatica* (L.) Extract. *Front. Pharmacol.* 7 (400), 400–412. doi:10.3389/fphar.2016.00400

Ledwozyw, A., Michalak, J., Stepień, A., and Kadziołka, A. (1986). The Relationship between Plasma Triglycerides, Cholesterol, Total Lipids and Lipid Peroxidation Products during Human Atherosclerosis. *Clin. Chim. Acta* 155 (3), 275–283. doi:10.1016/0009-8981(86)90247-0

Lüscher, T. F., and Vanhoutte, P. M. (1986). Endothelium-dependent Contractions to Acetylcholine in the Aorta of the Spontaneously Hypertensive Rat. *Hypertension* 8 (4), 344–348. doi:10.1161/01.hyp.8.4.344

Maneesai, P., Bunbupha, S., Kukongviriyapan, U., Prachaney, P., Tangsucharit, P., Kukongviriyapan, V., et al. (2016). Asiatic Acid Attenuates Renin-Angiotensin System Activation and Improves Vascular Function in High-Carbohydrate, High-Fat Diet Fed Rats. *BMC Complement. Altern. Med.* 16 (123), 123. doi:10.1186/s12906-016-1100-6

Maneesai, P., Bunbupha, S., Kukongviriyapan, U., Senggunprai, L., Kukongviriyapan, V., Prachaney, P., et al. (2017). Effect of Asiatic Acid on the Ang II-At1r-NADPH Oxidase-NF-Kb Pathway in Renovascular Hypertensive Rats. *Naunyn Schmiedebergs Arch. Pharmacol.* 390 (10), 1073–1083. doi:10.1007/s00210-017-1408-x

Maneesai, P., Prasarttong, P., Bunbupha, S., Kukongviriyapan, U., Kukongviriyapan, V., Tangsucharit, P., et al. (2016). Synergistic Antihypertensive Effect of Carthamus tinctorius L. Extract and Captopril in L-NAME-Induced Hypertensive Rats via Restoration of eNOS and AT_1R Expression. *Nutrients* 8 (3), 122. doi:10.3390/nu8030122

Muchtaromah, B., Ahmad, M., Suyono, S., Romaidi, R., Bahri, S., and Kumalasari, H. P. (2016). Dosage and Administration Length of *Centella asiatica* (L.) Urban Decrease the Level of Sod and Mda and Improve Brain Histological Condition of Rats. *Jurnal Teknologi (Sciences Engineering)* 78 (5), 57–61. doi:10.11113/jt.v78.8238

Münzel, T., Camici, G. G., Maack, C., Bonetti, N. R., Fuster, V., and Kovacic, J. C. (2017). Impact of Oxidative Stress on the Heart and Vasculature: Part 2 of a 3-Part Series. *J. Am. Coll. Cardiol.* 70 (2), 212–229. doi:10.1016/j.jacc.2017.05.035

Nadruz, W. (2015). Myocardial Remodeling in Hypertension. *J. Hum. Hypertens.* 29 (1), 1–6. doi:10.1038/jhh.2014.36

Nansy, E., Pramono, S., and Nugroho, A. (2015). Total Flavonoid Content and *In Vivo* Hypotensive Effect of Chloroform Insoluble Fraction of *Centella asiatica* Leaf Extract. *Int. Food Res. J.* 22 (5), 2119.

Pakdeechote, P., Bunbupha, S., Kukongviriyapan, U., Prachaney, P., Khrisanapant, W., and Kukongviriyapan, V. (2014). Asiatic Acid Alleviates Hemodynamic and Metabolic Alterations via Restoring eNOS/iNOS Expression, Oxidative Stress, and Inflammation in Diet-Induced Metabolic Syndrome Rats. *Nutrients* 6 (1), 355–370. doi:10.3390/nu6010355

Panza, J. A., Quyyumi, A. A., Brush, J. E., Jr., and Epstein, S. E. (1990). Abnormal Endothelium-dependent Vascular Relaxation in Patients with Essential Hypertension. *N. Engl. J. Med.* 323 (1), 22–27. doi:10.1056/NEJM199007053230105

Pittella, F., Dutra, R. C., Junior, D. D., Lopes, M. T., and Barbosa, N. R. (2009). Antioxidant and Cytotoxic Activities of *Centella asiatica* (L) Urb. *Int. J. Mol. Sci.* 10 (9), 3713–3721. doi:10.3390/ijms10093713

Pragada, R. R., Veeravalli, K. K., Chowdary, K. P., and Routhu, K. V. (2004). Cardioprotective Activity of Hydrocotyle Asiatica L. In Ischemia-Reperfusion Induced Myocardial Infarction in Rats. *J. Ethnopharmacol* 93 (1), 105–108. doi:10.1016/j.jep.2004.03.025

Pryor, W. A., and Squadrito, G. L. (1995). The Chemistry of Peroxynitrite: a Product from the Reaction of Nitric Oxide with Superoxide. *Am. J. Physiol.* 268 (5 Pt 1), L699–L722. doi:10.1152/ajplung.1995.268.5.L699

Rababa'h, A. M., Guillory, A. N., Mustafa, R., and Hijjawi, T. (2018). Oxidative Stress and Cardiac Remodeling: An Updated Edge. *Curr. Cardiol. Rev.* 14 (1), 53–59. doi:10.2174/1573403X14666180111145207

Rajeshwari, T., Raja, B., Manivannan, J., and Silambarasan, T. (2014). Valproic Acid Attenuates Blood Pressure, Vascular Remodeling and Modulates ET-1 Expression in L-NAME Induced Hypertensive Rats. *Biomed. Prev. Nutr.* 4 (2), 195–202. doi:10.1016/j.bionut.2013.09.002

Robaczewska, J., Kedziora-Kornatowska, K., Kozakiewicz, M., Zary-Sikorska, E., Pawluk, H., Pawliszak, W., et al. (2016). Role of Glutathione Metabolism and Glutathione-Related Antioxidant Defense Systems in Hypertension. *J. Physiol. Pharmacol.* 67 (3), 331–337.

Roopesh, C., Salomi, K. R., Nagarjuna, S., and Reddy, Y. P. (2011). Diuretic Activity of Methanolic and Ethanolic Extracts of *Centella asiatica* Leaves in Rats. *Int. Res. J. Pharm.* 2 (11), 163–165.

Samhan-Arias, A. K., Tyurina, Y. Y., and Kagan, V. E. (2011). Lipid Antioxidants: Free Radical Scavenging versus Regulation of Enzymatic Lipid Peroxidation. *J. Clin. Biochem. Nutr.* 48 (1), 91–95. doi:10.3164/jcbn.11-009FR

Schulz, E., Gori, T., and Münzel, T. (2011). Oxidative Stress and Endothelial Dysfunction in Hypertension. *Hypertens. Res.* 34 (6), 665–673. doi:10.1038/hr.2011.39

Sedeek, M., Hébert, R. L., Kennedy, C. R., Burns, K. D., and Touyz, R. M. (2009). Molecular Mechanisms of Hypertension: Role of Nox Family NADPH Oxidases. *Curr. Opin. Nephrol. Hypertens.* 18 (2), 122–127. doi:10.1097/MNH.0b013e32832923c3

Silambarasan, T., Manivannan, J., Krishna Priya, M., Suganya, N., Chatterjee, S., and Raja, B. (2014). Sinapic Acid Prevents Hypertension and Cardiovascular Remodeling in Pharmacological Model of Nitric Oxide Inhibited Rats. *PloS one* 9 (12), e115682. doi:10.1371/journal.pone.0115682

Singh, V. P., Le, B., Khode, R., Baker, K. M., and Kumar, R. (2008). Intracellular Angiotensin II Production in Diabetic Rats Is Correlated with Cardiomyocyte Apoptosis, Oxidative Stress, and Cardiac Fibrosis. *Diabetes* 57 (12), 3297–3306. doi:10.2337/db08-0805

Sorriento, D., De Luca, N., Trimarco, B., and Iaccarino, G. (2018). The Antioxidant Therapy: New Insights in the Treatment of Hypertension. *Front. Physiol.* 9, 258. doi:10.3389/fphys.2018.00258

Sung, J. H., Jo, Y. S., Kim, S. J., Ryu, J. S., Kim, M. C., Ko, H. J., et al. (2013). Effect of Lutein on L-NAME-Induced Hypertensive Rats. *Korean J. Physiol. Pharmacol.* 17 (4), 339–345. doi:10.4196/kjpp.2013.17.4.339

Tabassum, R., Vaibhav, K., Shrivastava, P., Khan, A., Ejaz Ahmed, M., Javed, H., et al. (2013). *Centella asiatica* Attenuates the Neurobehavioral, Neurochemical and Histological Changes in Transient Focal Middle Cerebral Artery Occlusion Rats. *Neurol. Sci.* 34 (6), 925–933. doi:10.1007/s10072-012-1163-1

Takemoto, M., Egashira, K., Usui, M., Numaguchi, K., Tomita, H., Tsutsui, H., et al. (1997). Important Role of Tissue Angiotensin-Converting Enzyme Activity in the Pathogenesis of Coronary Vascular and Myocardial Structural Changes Induced by Long-Term Blockade of Nitric Oxide Synthesis in Rats. *J. Clin. Invest.* 99 (2), 278–287. doi:10.1172/JCI119156

Tóth, M., Vuorinen, K. H., Vuolteenaho, O., Hassinen, I. E., Uusimaa, P. A., Leppäluoto, J., et al. (1994). Hypoxia Stimulates Release of ANP and BNP from Perfused Rat Ventricular Myocardium. *Am. J. Physiol.* 266 (4 Pt 2), H1572–H1580. doi:10.1152/ajpheart.1994.266.4.H1572

Touyz, R. M., and Briones, A. M. (2011). Reactive Oxygen Species and Vascular Biology: Implications in Human Hypertension. *Hypertens. Res.* 34 (1), 5–14. doi:10.1038/hr.2010.201

Touyz, R. M., and Schiffrin, E. L. (1999). Ang II-Stimulated Superoxide Production Is Mediated via Phospholipase D in Human Vascular Smooth Muscle Cells. *Hypertension* 34 (4 Pt 2), 976–982. doi:10.1161/01.hyp.34.4.976

Tsuchiya, K., Sakai, H., Suzuki, N., Iwashima, F., Yoshimoto, T., Shichiri, M., et al. (2007). Chronic Blockade of Nitric Oxide Synthesis Reduces Adiposity and Improves Insulin Resistance in High Fat-Induced Obese Mice. *Endocrinology* 148 (10), 4548–4556. doi:10.1210/en.2006-1371

Wang, X., Cai, X., Wang, W., Jin, Y., Chen, M., Huang, X., et al. (2018). Effect of Asiaticoside on Endothelial Cells in Hypoxia-induced P-ulmonary H-ypertension. *Mol. Med. Rep.* 17 (2), 2893–2900. doi:10.3892/mmr.2017.8254

Weber, M., and Hamm, C. (2006). Role of B-type Natriuretic Peptide (BNP) and NT-proBNP in Clinical Routine. *Heart* 92 (6), 843–849. doi:10.1136/hrt.2005.071233

Wei, J., Huang, Q., Huang, R., Chen, Y., Lv, S., Wei, L., et al. (2013). Asiatic Acid from Potentilla Chinensis Attenuate Ethanol-Induced Hepatic Injury via Suppression of Oxidative Stress and Kupffer Cell Activation. *Biol. Pharm. Bull.* 36 (12), 1980–1989. doi:10.1248/bpb.b13-00634

Wiemer, G., Linz, W., Hatrik, S., Schölkens, B. A., and Malinski, T. (1997). Angiotensin-converting Enzyme Inhibition Alters Nitric Oxide and Superoxide Release in Normotensive and Hypertensive Rats. *Hypertension*. 1979 30 (5), 1183–1190. doi:10.1161/01.hyp.30.5.1183

World Health Organization (2017). Cardiovascular Diseases (CVDs). Available at https://www.who.int/en/news-room/fact-sheets/detail/cardiovascular-diseases-(cvds) (Accessed November 11, 2021).

Wunpathe, C., Maneesai, P., Rattanakanokchai, S., Bunbupha, S., Kukongviriyapan, U., Tong-Un, T., et al. (2020). Tangeretin Mitigates L-NAME-Induced Ventricular Dysfunction and Remodeling through the AT1R/pERK1/2/pJNK Signaling Pathway in Rats. *Food Funct.* 11 (2), 1322–1333. doi:10.1039/c9fo02365h

Yu, B. P. (1994). Cellular Defenses against Damage from Reactive Oxygen Species. *Physiol. Rev.* 74 (1), 139–162. doi:10.1152/physrev.1994.74.1.139

Zainol, M. K., Abd-Hamid, A., Yusof, S., and Muse, R. (2003). Antioxidative Activity and Total Phenolic Compounds of Leaf, Root and Petiole of Four Accessions of *Centella asiatica* (L.) Urban. *Food Chem.* 81 (4), 575–581. doi:10.1016/s0308-8146(02)00498-3

Zhou, M. S., Schulman, I. H., and Raij, L. (2004). Nitric Oxide, Angiotensin II, and Hypertension. *Semin. Nephrol.* 24 (4), 366–378. doi:10.1016/j.semnephrol.2004.04.008

Conflict of Interest: The authors declare that the research was conducted in the absence of any commercial or financial relationships that could be construed as a potential conflict of interest.

Publisher's Note: All claims expressed in this article are solely those of the authors and do not necessarily represent those of their affiliated organizations, or those of the publisher, the editors and the reviewers. Any product that may be evaluated in this article, or claim that may be made by its manufacturer, is not guaranteed or endorsed by the publisher.

frontiers in Pharmacology

MINI REVIEW
published: 15 December 2021
doi: 10.3389/fphar.2021.758929

Anti-Inflammatory Effects of Thymoquinone in Atherosclerosis: A Mini Review

Xin-Fang Leong[1]*, *Ker Woon Choy*[2]* and *Aspalilah Alias*[3]

[1]Department of Craniofacial Diagnostics and Biosciences, Faculty of Dentistry, Universiti Kebangsaan Malaysia, Kuala Lumpur, Malaysia, [2]Department of Anatomy, Faculty of Medicine, Universiti Teknologi MARA, Selangor, Malaysia, [3]Department of Basic Sciences and Oral Biology, Faculty of Dentistry, Universiti Sains Islam Malaysia, Kuala Lumpur, Malaysia

Atherosclerosis poses serious health problems and increases the risk of various cardiovascular diseases, including myocardial infarction, heart failure, ischemic stroke, and peripheral arterial disease. Atherosclerosis patients require long-term medications to prevent complications, some of which are costly and may result in unwanted adverse reactions. Natural products have emerged as potential sources of bioactive compounds that provide health benefits in cardiovascular diseases. Increased inflammation and vascular remodeling have been associated with atherosclerosis pathogenesis. The molecules involved in signaling pathways are considered valuable targets for new treatment approaches. Therefore, this review aimed to summarize the available evidence of the anti-inflammatory effects of thymoquinone, the major active compound isolated from *Nigella sativa* L., *via* inflammatory signaling pathways in atherosclerosis. Specifically, nuclear factor-κB and mitogen-activated protein kinase signaling pathways were considered. Furthermore, the potential toxic effects elicited by thymoquinone were addressed. These findings suggest a potential role of thymoquinone in managing atherosclerosis, and further studies are required to ascertain its effectiveness and safety profile.

Keywords: atherosclerosis, inflammation, thymoquinone, nuclear factor-kappa B, mitogen-activated protein kinase

OPEN ACCESS

Edited by:
Yusof Kamisah, Universiti Kebangsaan Malaysia, Malaysia

Reviewed by:
Ajaz Ahmad, King Saud University, Saudi Arabia
Mohamed Fawzy Ramadan Hassanien, Zagazig University, Egypt
Reza Mohebbati, Mashhad University of Medical Sciences, Iran

***Correspondence:**
Xin-Fang Leong
leongxinfang@ukm.edu.my
Ker Woon Choy
choykerwoon@uitm.edu.my

Specialty section:
This article was submitted to Cardiovascular and Smooth Muscle Pharmacology, a section of the journal Frontiers in Pharmacology

Received: *16 August 2021*
Accepted: *23 November 2021*
Published: *15 December 2021*

Citation:
Leong X-F, Choy KW and Alias A (2021) Anti-Inflammatory Effects of Thymoquinone in Atherosclerosis: A Mini Review. Front. Pharmacol. 12:758929. doi: 10.3389/fphar.2021.758929

INTRODUCTION

Atherosclerosis is a major cause of cardiovascular disease (CVD) worldwide, including myocardial infarction, heart failure, ischemic stroke, and peripheral arterial disease. According to the Global Burden of Cardiovascular Diseases and Risk Factors (Roth et al., 2020), CVD prevalence has increased from 271 million to 523 million from 1990 to 2019. The CVD mortality had a relative increase of 6.5% in 2019, reaching 18.6 million deaths. It is estimated that 23.6 million people globally will die from CVDs by 2030 (WHO, 2013). The rising burden of CVDs on individuals and the healthcare system warrants research on atherosclerotic diseases and implementation of preventive measures.

There are several theories on atherosclerosis pathogenesis, including lipid theory, oxidative theory, response to injury theory, and inflammatory theory (Minelli et al., 2020). Various inflammatory cells and inflammatory mediators are responsible for fatty streak formation, progression, and rupture of atheromatous plaques (Libby, 2021). The major signaling pathways that mediate inflammation include nuclear factor-κB (NF-κB) and mitogen-activated protein kinase (MAPK). Hence, modulating these inflammatory signaling

pathways to produce anti-inflammatory actions may serve as potential therapeutic targets for atherosclerosis management.

There has been increasing interest in medicinal herbs or plants for the treatment and prevention of various diseases, including atherosclerosis. Plant-based traditional medicines have attracted considerable attention owing to their availability, cost, safety, and efficacy. The World Health Organization (WHO) reported that approximately 60–80% of the population use traditional medicines or herbal remedies for their primary health care, particularly in developing countries. It is recommended that the WHO Traditional Medicine Strategy 2014–2023 is implemented for national traditional medicine programs. This strategy aims to explore the potential use of traditional medicine for health and wellness, in addition to encouraging its safe and effective use (Zhang, 2018).

Nigella sativa L., also known as black seed or black cumin, is a plant traditionally used for medicinal purposes in the Middle East, India, Northern Africa, and Europe. *N. sativa* L. has been used to treat various ailments, including asthma, hypertension, diabetes, inflammation, cough, headache, eczema, fever, and dizziness (Salehi et al., 2021). *N. sativa* L. is a flowering plant belonging to the family Ranunculaceae. The fruit contains angular-shaped black seeds, which are regarded as the most important component in view of their beneficial health effects (Tavakkoli et al., 2017).

N. sativa L. contains various bioactive compounds, including thymoquinone (TQ), dithymoquinone, thymol, and thymohydroquinone. Among the isolated compounds, TQ was the most abundant. Hence, the extensive therapeutic benefits exerted by *N. sativa* L. may be attributed to TQ (Alagawany et al., 2021). Previous studies have shown that TQ possesses various pharmacological properties, including antioxidant (Abd-Elkareem et al., 2021), antimicrobial (Mouwakeh et al., 2018), antihypertensive (Enayatfard et al., 2018), antidiabetic (Bule et al., 2020), lipid-lowering (Majdalawieh et al., 2021), neuroprotective (Abulfadl et al., 2018), gastroprotective (Bukar et al., 2017), anticancer (Edris, 2021), and anti-inflammatory (Alkharfy et al., 2018; Ahmad et al., 2020). Given the potential health benefits of TQ, the present study aimed to examine the available evidence on its anti-inflammatory effects in atherosclerosis *via* signaling pathway modulation, and to highlight its potential toxicity.

INFLAMMATORY SIGNALING PATHWAYS

NF-κB Pathway

NF-κB pathway activation is regulated by inhibitory proteins of the κB family (IκB) kinase through IκB phosphorylation (Christian et al., 2016), which causes its degradation by the proteasome, leading to the release of NF-κB for nuclear translocation and gene transcription activation. This pathway regulates inflammatory cytokine production and inflammatory cell recruitment, which contribute to the inflammatory response.

MAPK Pathway

MAPKs consist of three members: extracellular signal-regulated kinases (ERKs), p38 MAPK, and c-Jun N-terminal kinases (JNKs). ERKs are generally activated by mitogens and differentiation signals (Sun et al., 2015), while p38 MAPK and JNK are activated by inflammatory stimuli and stress (Chan et al., 2017). MAPK activation leads to phosphorylation and activation of transcription factors, which are responsible for inflammatory response regulation (Chen et al., 2018).

ATHEROPROTECTIVE EFFECTS OF TQ *VIA* MODULATION OF SIGNALING PATHWAYS

Studies involving signaling pathways have documented that cytokine-mediated inflammation is a crucial element in atherosclerosis pathogenesis. Hence, inflammatory response regulation is a fundamental aspect in atherosclerosis prevention and treatment (Liu et al., 2017; Sun et al., 2018). The proposed atheroprotective effects of TQ *via* NF-κB and MAPK pathway modulation are shown in **Figure 1**.

Effect of TQ in NF-κB Pathway

Vascular cell adhesion molecule 1, intercellular adhesion molecule 1, chemokines interleukin 8 (IL-8), and monocyte chemoattractant protein 1 (MCP-1) are major molecules that recruit circulating mononuclear leukocytes to the arterial intima. This process is important in atherosclerosis and is mediated by NF-κB activation (Mussbacher et al., 2019). Amartey et al. (2019) reported that concurrent treatment with TQ (6.25 μg/ml) showed a tendency to reduce inflammatory response by suppressing IL-6 and IL-8 protein levels in human vascular endothelial cells (HVECs) exposed to lipopolysaccharides (LPS, 100 ng/ml) at 24 h. Furthermore, TQ downregulated the mRNA expression of important inflammation regulators vascular endothelial growth factor (VEGF) and MCP-1 in LPS-treated cells. VEGF mediates angiogenesis, whereas MCP-1 is involved in endothelial monocyte activation.

Furthermore, the expression of NOD-like receptor protein 3 (NLRP3) inflammasome and IL-1β was attenuated by TQ in HVECs exposed to LPS for 24 h. In the presence of inflammation, ten-eleven translocation 2 (TET-2) gene expression increased with concurrent administration of TQ (Amartey et al., 2019). The role of TET-2 in atherosclerosis has been elucidated by Fuster et al. (2017). Macrophages with TET-2 deficiency led to increased pro-inflammatory cytokine IL-1β secretion, which is dependent on the action of NLRP3 (Grebe et al., 2018). According to these findings, TQ plays a regulatory role in inflammation and monocyte recruitment, and modulates NLRP3 and TET-2 *in vitro*. However, no positive controls were used in this study. Media-treated cells were used as a control to differentiate the effects of LPS and TQ. Further studies on multiple cell lines and *in vivo* studies are required to confirm the anti-inflammatory effect of TQ against atherosclerosis. This study did not investigate the mechanism of action of TQ. The anti-inflammatory action of TQ could be due to NF-κB suppression in view of its regulatory role in NRLP3 and pro-inflammatory cytokines such as the IL-1 family (Liu et al., 2017).

Hyperlipidemia has been reported to accelerate lipid accumulation, atherosclerosis, and chronic inflammation in apolipoprotein E knockout ($ApoE^{-/-}$) or low-density lipoprotein

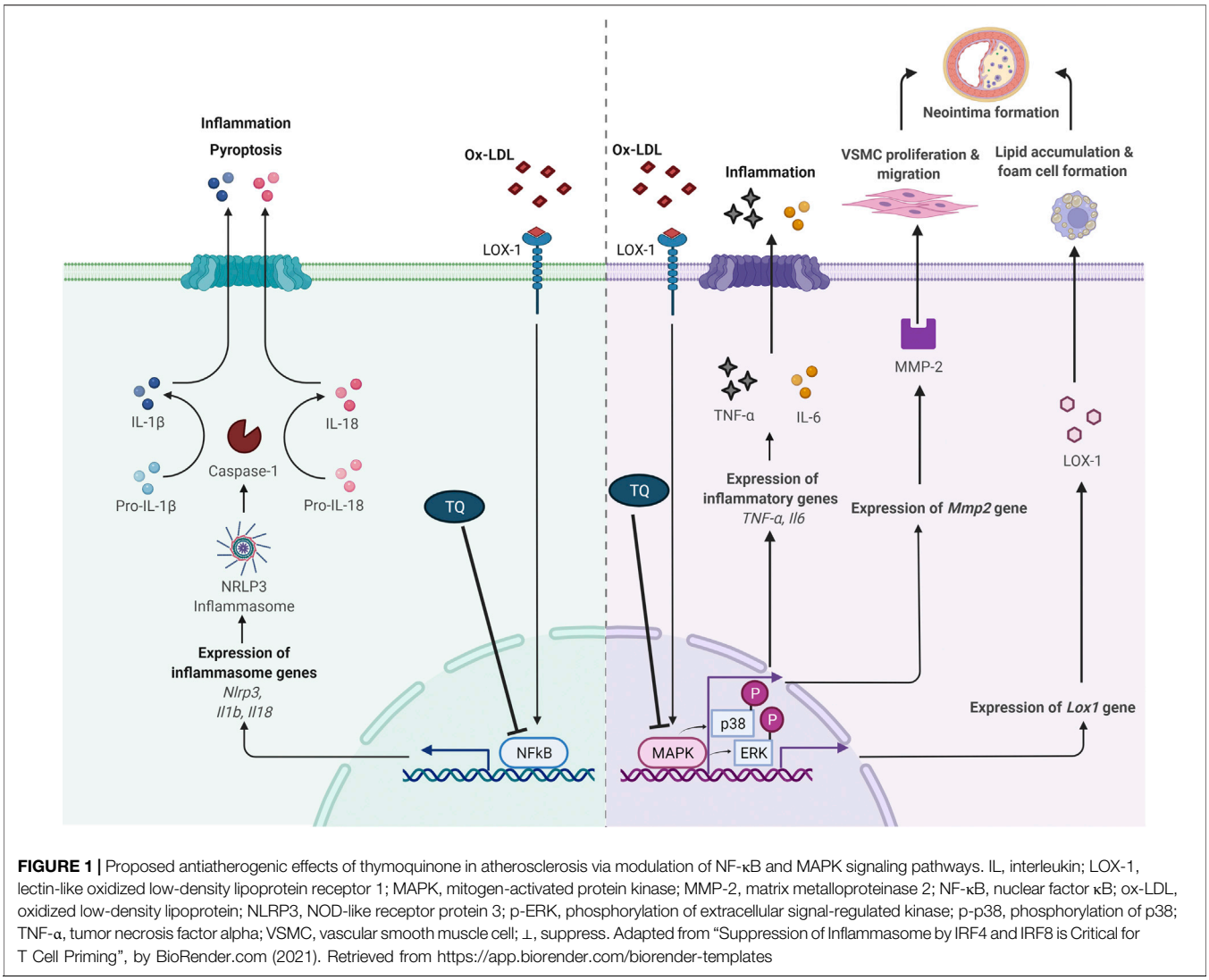

FIGURE 1 | Proposed antiatherogenic effects of thymoquinone in atherosclerosis via modulation of NF-κB and MAPK signaling pathways. IL, interleukin; LOX-1, lectin-like oxidized low-density lipoprotein receptor 1; MAPK, mitogen-activated protein kinase; MMP-2, matrix metalloproteinase 2; NF-κB, nuclear factor κB; ox-LDL, oxidized low-density lipoprotein; NLRP3, NOD-like receptor protein 3; p-ERK, phosphorylation of extracellular signal-regulated kinase; p-p38, phosphorylation of p38; TNF-α, tumor necrosis factor alpha; VSMC, vascular smooth muscle cell; ⊥, suppress. Adapted from "Suppression of Inflammasome by IRF4 and IRF8 is Critical for T Cell Priming", by BioRender.com (2021). Retrieved from https://app.biorender.com/biorender-templates

receptor-deficient (LDL-R$^{-/-}$) mice (Zhao et al., 2018). ApoE$^{-/-}$ and LDL-R$^{-/-}$ mice are two models commonly used in atherosclerosis research that require hypercholesterolemia induction. Their mechanisms of enhancing atherosclerosis development and the involved lipoproteins are different (Getz and Reardon, 2016). ApoE deficiency in macrophages may contribute to hypercholesterolemia, while the lack of LDL-R in hepatocytes is responsible for hypercholesterolemia in ApoE$^{-/-}$ and LDL-R$^{-/-}$ models. The following studies utilized normal diet-fed mice as the control group.

Xu et al. (2018) reported that concurrent treatment with TQ (oral, 25 mg/kg/day for 8 weeks) decreased serum high-sensitivity C-reactive protein levels in high-cholesterol diet-fed adult male ApoE$^{-/-}$ mice. Additionally, TQ suppressed the upregulation of tumor necrosis factor α (TNF-α) and IL-6 expression in cardiac tissues isolated from high-cholesterol diet-fed mice. Similar results were reported by Pei et al. (2020) in LDL-R$^{-/-}$ mice. Pei et al. (2020) documented that a high-cholesterol diet supplemented with TQ (oral, 50 mg/kg/day for 8 weeks) reduced TNF-α and IL-6 serum levels and gene expression in mice. Cluster of differentiation 68 markers, which are highly expressed in macrophages, were reduced following TQ administration, indicating a reduction in macrophage numbers in the cardiac tissue of high-cholesterol diet-fed LDL-R$^{-/-}$ mice. In addition, TQ administration downregulated the increased protein and gene expression of NLRP3, caspase-1, IL-1β, and IL-18 induced by a high-cholesterol diet. Decreased NF-κB protein expression was observed following concurrent high-cholesterol diet with TQ supplementation in LDL-R$^{-/-}$ mice (Pei et al., 2020). Pyroptosis, a programmed cell death mechanism mediated by NLRP3 activation, has been associated with hyperlipidemia development. NLRP3 activation stimulates caspase-1, an IL-1 converting enzyme that cleaves precursors of the inflammatory cytokines IL-1β and IL-18. Subsequently, the release of pro-inflammatory cytokines is enhanced, leading to pyroptosis (Borges et al., 2017).

Effect of TQ in MAPK Pathway

Oxidized low-density lipoprotein (ox-LDL) contributes to atherosclerosis-associated inflammation (Rhoads and Major, 2018). Ox-LDL causes endothelial dysfunction, leading to adhesion molecule expression and monocyte recruitment in the subendothelial space. Ox-LDL is taken up by macrophages *via* lectin-like ox-LDL receptor 1 (LOX-1). LOX-1 expression is upregulated by ox-LDL (Barreto et al., 2021). Additionally, ox-LDL promotes the growth and migration of smooth muscle cells, monocytes, and macrophages (Pirillo et al., 2013).

Xu et al. (2018) revealed that ApoE$^{-/-}$ mice receiving a high-cholesterol diet concurrent with TQ (oral, 25 mg/kg/day) for 8 weeks had reduced LOX-1 protein and gene expression in cardiac tissues. Lipid deposition, foam cell formation, and ERK phosphorylation (p-ERK) are regulated by protein kinases (Lin et al., 2012). Upregulated LOX-1 expression was suppressed by ERK inhibitors, suggesting that MAPK pathway activation is a crucial signaling event in LOX-1 gene regulation (Zhang et al., 2017). p-ERK was significantly reduced in ApoE$^{-/-}$ mice receiving TQ and a high-cholesterol diet than in mice without TQ supplementation (Xu et al., 2018). Therefore, TQ may regulate LOX-1 *via* the p-ERK pathway. ERK inhibition may exert potential antiatherosclerotic effects, as indicated by reduced uptake of ox-LDL and foam cell formation in hypercholesteremic TQ-supplemented ApoE$^{-/-}$ mice (Xu et al., 2018).

Pei et al. (2020) investigated the effect of TQ on hyperlipidemia-induced cardiac damage in male LDL-R$^{-/-}$mice. It was demonstrated that concurrent treatment with TQ (oral, 50 mg/kg/day) reduced total cholesterol and LDL-cholesterol levels in addition to the pro-inflammatory cytokines in mice fed a high-cholesterol diet for 8 weeks. There was a reduction in lipid accumulation and inflammatory cell infiltration in the cardiac tissue of TQ-administered mice compared to that in the non-supplemented mice. TQ decreased p38 and p-ERK levels in high-cholesterol diet-fed mice. These findings suggest that TQ suppresses high-cholesterol diet-induced inflammation and cardiac damage *via* p38 and ERK pathway inhibition.

Various pathological events are involved in vascular remodeling in response to vascular damage, including endothelial dysfunction, vascular smooth muscle cell (VSMC) proliferation and migration, arterial calcification, and extracellular matrix remodeling (Wang and Khalid, 2018; Zhang et al., 2021). Such injury-induced vascular remodeling is primarily due to excessive proliferation and migration of VSMCs and medial VSMC invasion into the intimal space, eventually leading to neointimal formation.

Zhu et al. (2019) reported that TQ (10, 12.5, 15 μmol/L) suppressed platelet-derived growth factor (PDGF, 40 ng/ml)-induced VSMC proliferation at 24 h. Furthermore, TQ decreased α-smooth muscle actin and Ki-67-positive cells, confirming the antiproliferative effect of TQ on VSMCs. Additionally, TQ (5–15 μmol/L) attenuated PDGF-stimulated VSMC migration, and TQ (15 μmol/L) blocked the activity and expression of matrix metalloproteinase 2 (MMP-2) in VSMCs at 24 h (Zhu et al., 2019). MMP-2 is involved in VSMC migration *via* extracellular matrix degradation (Xiao et al., 2018). Inhibition of p38 activation also blocked MMP-2 expression (Zhu et al., 2019). Hence, p38 might be responsible for the inhibitory effect of TQ on MMP-2 expression. TQ treatment increased the number of apoptotic VSMCs in the presence of reactive oxygen species (Zhu et al., 2019). The results showed that TQ abolished the upregulation of B-cell lymphoma 2 (Bcl-2), cleaved caspase 3, and cleaved poly (ADP-ribose) polymerase, and blocked Bcl-2-associated X protein (Bax) downregulation. It has been suggested that the pro-apoptotic effect of TQ is mediated *via* the mitochondria-dependent apoptosis pathway. Zhu et al. (2019) also documented that 8 mg/kg and 16 mg/kg TQ stopped the increase in neointimal area and neointima/media ratio, and attenuated neointimal formation in atherosclerosis at 14 days using a rat carotid artery ligation model. Therefore, the inhibitory activity of TQ on VSMC proliferation and migration may be attributed to the blockade of p38 MAPK activation.

POTENTIAL TOXICITY OF TQ

Acute and Subacute Toxicity

A single intraperitoneal (i.p.) dose of TQ was administered to BALB/c mice at doses ranging from 10 to 80 mg/kg body weight to test the oxidative effect of TQ after 24 h (**Table 1**). TQ at 40 and 80 mg/kg caused a considerable increase in malondialdehyde levels and catalase activity in the kidneys and liver (Harzallah et al., 2012). Oral acute toxicity of TQ from doses 0.5–3 g/kg was evaluated in male Swiss albino mice (Badary et al., 1998). Death occurred within the first 3 h associated with hypoactivity and respiratory problems, particularly with 2 or 3 g/kg TQ. No mortality was reported until 24 h. There was an increase of plasma activity of alanine aminotransferase, lactate dehydrogenase, creatinine phosphokinase, and increased plasma concentrations of urea and creatinine with 2 or 3 g/kg TQ. Besides, a reduction of reduced glutathione levels was reported (**Table 1**).

Al-Ali et al. (2008) showed that the LD_{50} values for TQ in albino mice were 104.7 and 870.9 mg/kg after i. p. and oral administration, respectively. Furthermore, LD_{50} values for i. p. injection and oral ingestion of TQ in Wistar rats were recorded as 57.5 and 794.3 mg/kg, respectively. Abukhader (2012) revealed that the maximum tolerated doses (MTDs) for i. p. TQ injection were 22.5 and 15 mg/kg in male and female rats, respectively, whereas the MTD for oral TQ was 250 mg/kg in both male and female rats. Thus, TQ is regarded as a reasonably safe drug, particularly when administered orally.

Acute toxicity was compared between encapsulated TQ in a nanostructured lipid carrier (TQNLC) and TQ in female BALB/c mice (Ong et al., 2016). Mice administered with 300 mg/kg TQ died within 24 h. In contrast, a mouse treated with 300 mg/kg TQNLC died after 24 h. In the subacute toxicity study (Ong et al., 2016), oral administration of 100 mg/kg TQNLC or TQ for 28 days did not cause mortality in either male or female mice.

A single injection of 25 mg/kg TQNLC was administered to the tail of female Sprague-Dawley rats (Yazan et al., 2019). The same dose was administered to the other rats at 48 h intervals. Intravenous administration of 25 mg/kg TQNLC

TABLE 1 | Toxicity profile of TQ.

Toxicity test	Dosage of TQ per kg body weight	Type of animal	Frequency/Route of administration	Observation time	Findings	References
Acute and Subacute	10, 20, 40, 80 mg/kg	BALB/c mice	Single/ Intraperitoneal	24 h	- No change in body, liver, and kidney weights - Increased tissue MDA and CAT levels at 40 or 80 mg/kg TQ	Harzallah et al. (2012)
	0.5, 1, 2, 3 g/kg	Male Swiss albino mice	Single/Oral	24 h	- LD_{50} was 2.4 g/kg - Increased plasma concentrations of urea, creatinine, ALT, LDH, CPK and reduced GSH levels in liver, kidney and heart at 2 or 3 g/kg TQ	Badary et al. (1998)
	50, 75, 100, 125, 150 mg/kg	Male and female Albino mice	Single/ Intraperitoneal	24 h	- Abdominal muscle spasms and ataxia, worsened with higher doses. - LD_{50} values 10–15 times greater than TQ dose for anti-inflammatory, antioxidant, or anticancer effects	Al-Ali et al. (2008)
	25, 50, 75, 100, 150 mg/kg	Male and female Wistar rats				
	250, 500, 1,000, 1,500, 2000 mg/kg	Male and female Albino mice	Single/Oral		- Drowsy and dyspneic over time before dying or recovering - LD_{50} values 100–150 times greater than TQ dose for beneficial effect	
	100, 500, 1,000, 1,500, 2000 mg/kg	Male and female Wistar rats				
	20, 30, and 40 mg/kg	Male and female Wistar rats	Single/ Intraperitoneal	24 h intervals for 5 days	- Loss of body weight, acute pancreatitis and elevation of serum amylase level	Abukhader (2012)
	200, 300, and 500 mg/kg		Single/Oral		Short term sign of toxicity (i.e., loss of body weight, mild abdominal distention, and dyspnea) - 500 mg/kg TQ caused two fatalities due to complication from bowel obstruction	
	TQNLC or TQ (5, 50, and 300 mg/kg)	Female BALB/c mice	Single/Oral	14 days	- No weight loss - No abnormal behavior	Ong et al. (2016)
	TQNLC or TQ (1, 10,100 mg/kg)	Male and femaleBALB/c mice	Daily/Oral	28 days	- Mild hepatotoxicity - NOAEL of TQNLC and TQ was 10 mg/kg/d for mice in both sexes	
	TQNLC (25 mg/kg)	Female Sprague-Dawley rats	Single/Intravenous	14 days	- Normal body weight, hematological, biochemical and histopathological profile - Inflammation at site of injection	Yazan et al. (2019)
	TQRFNE at 20 ml/kg (containing 44.5 mg TQ)	Male and female Sprague-Dawley rats	Single/Oral	14 days	- Normal body weight gains and hematological profile - Normal key enzymes of the liver and kidney, levels of urea and creatinine as well as liver histopathological examination	Tubesha et al. (2013)
Subchronic	30, 60, 90 mg/kg	Male Swiss albino mice	Daily/Oral	90 days	- Normal plasma concentrations of urea, creatinine, triglycerides, ALT, LDH, and CPK - Normal liver, kidneys and heart histopathological examination	Badary et al. (1998)
Teratogenic	15, 35, 50 mg/kg	Pregnant Wistar rats	Single injection on gestation day 11 or 14/Intraperitoneal	On gestation day 18	- No effects on fetus when 35 mg/kg TQ was given on day 14 of gestation - Increased serum amylase level, acute pancreatitis, organ adhesion and steatonecrosis at 35 or 50 mg/kg TQ on day 11 of gestation	AbuKhader et al. (2013)
	10, 40, 80 mg/kg	Pregnant Wistar rats	Daily for 7 days, gestation week 2 or 3/Oral	Postnatal day 14 and 21	- 40 mg/kg TQ reduced body weight of offspring while 80 mg/kg TQ led to pregnancy loss when treated at gestation week 2 - 40 or 80 mg/kg TQ caused a lower birth weight but increased body weight on postnatal days 14 and 21 when treated at gestation week 3 - 80 mg/kg TQ caused 50% reduction in the size of the litter when treated at gestation week 3	Abdollahzade Fard et al. (2021)

ALT, alanine aminotransferase; CAT, catalase; CPK, creatinine phosphokinase; GSH, reduced glutathione; LD50, median lethal dose; LDH, lactate dehydrogenase; MDA, malondialdehyde; NOAEL, no observed adverse effect level; TQ, thymoquinone; TQNLC, TQ in a nanostructured lipid carrier; TQRFNE, TQ-rich fraction nano-emulsion.

did not induce toxicity in rats during the 14-days observation period. Male and female Sprague-Dawley rats were observed for 14 days after receiving a single dose of TQ-rich fraction nano-emulsion at 20 ml/kg (Tubesha et al., 2013). The animals appeared normal and healthy throughout the study (**Table 1**).

In summary, the route of administration can influence the severity of TQ-induced toxicity. Oral administration has a better safety profile than i. p. injections. Compared to that of TQ alone, the use of TQ together with nanostructured lipid carriers or nano-emulsions has less evidence of toxicity, suggesting their potential use during TQ administration.

Subchronic Toxicity

Male Swiss albino mice were administered 30, 60, or 90 mg/kg TQ for 90 days *via* drinking water (Badary et al., 1998). No signs of toxicity were noted (**Table 1**).

Teratogenicity

Decreased maternal body weight and complete fetal resorption were reported after a single i. p. injection of 35 mg/kg or 50 mg/kg TQ to pregnant rats on day 11 of gestation (Abukhader et al., 2013). Administration of 50 mg/kg TQ on day 14 resulted in a higher incidence of fetal resorption, and viable fetuses did not show malformations (**Table 1**). Complete pregnancy loss was reported in pregnant Wistar rats administered 80 mg/kg TQ orally at the second gestational week for 7 days (Abdollahzade Fard et al., 2021). Reduced offspring body weight was recorded on postnatal days 14 and 21 by TQ (oral, 40 mg/kg). However, pregnant rats treated with TQ at gestation week 3 did not show such toxicity. In conclusion, i. p. injection of TQ between 35 mg/kg and 50 mg/kg during gestation has exhibited teratogenicity, suggesting that doses lower than 35 mg/kg could be safer to avoid fetal abnormalities or deformities. Moreover, failed pregnancy is associated with TQ administered orally at 80 mg/kg and at gestation week 2. Therefore, prenatal TQ administration should be carefully assessed.

CONCLUSION AND FUTURE PERSPECTIVES

Although *N. sativa* L. has long been used for treating diseases and enhancing general health, research into its therapeutic potential and mechanisms of action has just begun. Metabolomics is a useful technology for analyzing the chemical composition of *N. sativa* L. to allow its authentication and to ensure uniformity in bioactivity for quality control (Farag et al., 2021). Limited studies have investigated the anti-inflammatory effects of TQ in atherosclerosis. No positive controls were used in the available published studies. The comparative anti-inflammatory effects of TQ cannot be appreciated. Hence, future studies should incorporate positive controls to validate the effectiveness of TQ as an anti-inflammatory agent. Previous studies have indicated the possible involvement of the NF-κB and MAPK pathways in mediating the anti-inflammatory effects of TQ. However, its direct involvement in such signaling pathways requires exploration. Further investigation is warranted to identify the associated pathways and to determine the molecular targets that mediate the protective effects of TQ in atherosclerosis.

TQ has been shown to be toxic *in vitro* and *in vivo* studies, indicating the requirement for more in-depth research to provide a more complete toxicological profile for TQ before considering this promising natural product as a therapeutic agent for human use. The TQ dosage required to achieve optimal anti-inflammatory benefits in humans remains unknown and requires further investigation. Moreover, the protective effects of TQ have yet to be verified in clinical trials, and more safety assessments are needed to determine the potential toxicities of TQ for long-term use in humans. Therefore, more research is required to confirm its traditional use as a therapy for atherosclerosis.

AUTHOR CONTRIBUTIONS

X-FL and KC designed, wrote and revised the manuscript. AA wrote the manuscript. All authors read and approved the final version of the manuscript.

ACKNOWLEDGMENTS

The authors would like to thank Universiti Kebangsaan Malaysia, Geran Penyelidikan Khas (GPK): 600-RMC/GPK 5/3 (269/2020) from Universiti Teknologi MARA and Universiti Sains Islam Malaysia for supporting this work.

REFERENCES

Abd-Elkareem, M., Abd El-Rahman, M. A. M., Khalil, N. S. A., and Amer, A. S. (2021). Antioxidant and Cytoprotective Effects of *Nigella Sativa* L. Seeds on the Testis of Monosodium Glutamate Challenged Rats. *Sci. Rep.* 11, 13519. doi:10.1038/s41598-021-92977-4

Abdollahzade Fard, A., Saboory, E., Tahmazi, Y., Rasmi, Y., Dindarian, S., and Parsamanesh, N. (2021). Effect of Orally-Administrated Thymoquinone during Pregnancy on Litter Size, Pentylenetetrazol-Induced Seizure, and Body Weight in Rat Offspring. *Iran J. Basic Med. Sci.* 24, 30–37. doi:10.22038/ijbms.2020.47479.10930

Abukhader, M. M., Khater, S. H., and Al-Matubsi, H. Y. (2013). Acute Effects of Thymoquinone on the Pregnant Rat and Embryo-Fetal Development. *Drug Chem. Toxicol.* 36, 27–34. doi:10.3109/01480545.2011.648326

Abukhader, M. M. (2012). The Effect of Route of Administration in Thymoquinone Toxicity in Male and Female Rats. *Indian J. Pharm. Sci.* 74, 195–200. doi:10.4103/0250-474X.106060

Abulfadl, Y. S., El-Maraghy, N. N., Ahmed, A. A. E., Nofal, S., and Badary, O. A. (2018). Protective Effects of Thymoquinone on D-Galactose and Aluminum Chloride Induced Neurotoxicity in Rats: Biochemical, Histological and Behavioral Changes. *Neurol. Res.* 40, 324–333. doi:10.1080/01616412.2018.1441776

Ahmad, A., Alkharfy, K. M., Jan, B. L., Ahad, A., Ansari, M. A., Al-Jenoobi, F. I., et al. (2020). Thymoquinone Treatment Modulates the Nrf2/HO-1 Signaling

Pathway and Abrogates the Inflammatory Response in an Animal Model of Lung Fibrosis. *Exp. Lung Res.* 46, 53–63. doi:10.1080/01902148.2020.1726529

Al-Ali, A., Alkhawajah, A. A., Randhawa, M. A., and Shaikh, N. A. (2008). Oral and Intraperitoneal LD_{50} of Thymoquinone, an Active Principle of *Nigella Sativa*, in Mice and Rats. *J. Ayub. Med. Coll. Abbottabad.* 20, 25–27.

Alagawany, M., Elnesr, S. S., Farag, M. R., Abd El-Hack, M. E., Khafaga, A. F., Sharun, K., et al. (2021). ""Health-Promoting Activities of Nigella Sativa Essential Oil," in Black Cumin (Nigella Sativa)," in *Seeds: Chemistry, Technology, Functionality, and Applications. Food Bioactive Ingredients*. Editor M. Fawzy Ramadan (Cham: Springer). doi:10.1007/978-3-030-48798-0_29

Alkharfy, K. M., Ahmad, A., Jan, B. L., and Raish, M. (2018). Thymoquinone Reduces Mortality and Suppresses Early Acute Inflammatory Markers of Sepsis in a Mouse Model. *Biomed. Pharmacother.* 98, 801–805. doi:10.1016/j.biopha.2018.01.028

Amartey, J., Gapper, S., Hussein, N., Morris, K., and Withycombe, C. E. (2019). *Nigella Sativa* Extract and Thymoquinone Regulate Inflammatory Cytokine and TET-2 Expression in Endothelial Cells. *Artery Res.* 25, 157–163. doi:10.2991/artres.k.191114.002

Badary, O. A., Al-Shabanah, O. A., Nagi, M. N., Al-Bekairi, A. M., and Elmazar, M. M. A. (1998). Acute and Subchronic Toxicity of Thymoquinone in Mice. *Drug Dev. Res.* 44, 56–61. doi:10.1002/(sici)1098-2299(199806/07)44:2/3<56:aid-ddr2>3.0.co;2-9

Barreto, J., Karathanasis, S. K., Remaley, A., and Sposito, A. C. (2021). Role of LOX-1 (Lectin-like Oxidized Low-Density Lipoprotein Receptor 1) as a Cardiovascular Risk Predictor: Mechanistic Insight and Potential Clinical Use. *Arterioscler. Thromb. Vasc. Biol.* 41, 153–166. doi:10.1161/ATVBAHA.120.315421

Borges, P. V., Moret, K. H., Raghavendra, N. M., Maramaldo Costa, T. E., Monteiro, A. P., Carneiro, A. B., et al. (2017). Protective Effect of Gedunin on TLR-Mediated Inflammation by Modulation of Inflammasome Activation and Cytokine Production: Evidence of a Multitarget Compound. *Pharmacol. Res.* 115, 65–77. doi:10.1016/j.phrs.2016.09.015

Bukar, M. A., Ishaya, H. B., Dibal, N. I., and Attah, M. O. (2017). Gastroprotective Effect of *Nigella Sativa* Seed on Ethanol-Induced Gastric Ulcer in Rats. *Libyan J. Med. Sci.* 1, 63–67. doi:10.4103/LJMS.LJMS_23_17

Bule, M., Nikfar, S., Amini, M., and Abdollahi, M. (2020). The Antidiabetic Effect of Thymoquinone: A Systematic Review and Meta-Analysis of Animal Studies. *Food Res. Int.* 127, 108736. doi:10.1016/j.foodres.2019.108736

Chan, L. P., Liu, C., Chiang, F. Y., Wang, L. F., Lee, K. W., Chen, W. T., et al. (2017). IL-8 Promotes Inflammatory Mediators and Stimulates Activation of P38 MAPK/ERK-NF-κB Pathway and Reduction of JNK in HNSCC. *Oncotarget* 8, 56375–56388. doi:10.18632/oncotarget.16914

Chen, L., Deng, H., Cui, H., Fang, J., Zuo, Z., Deng, J., et al. (2018). Inflammatory Responses and Inflammation-Associated Diseases in Organs. *Oncotarget* 9, 7204–7218. doi:10.18632/oncotarget.23208

Christian, F., Smith, E. L., and Carmody, R. J. (2016). The Regulation of NF-Kb Subunits by Phosphorylation. *Cells* 5, 12. doi:10.3390/cells5010012

Edris, A. E. (2021). in *"Thymoquinone: Chemistry and Functionality," in Black Cumin (Nigella Sativa) Seeds: Chemistry, Technology, Functionality, and Applications. Food Bioactive Ingredients*. Editor M. Fawzy Ramadan (Cham: Springer). doi:10.1007/978-3-030-48798-0_8

Enayatfard, L., Mohebbati, R., Niazmand, S., Hosseini, M., and Shafei, M. N. (2018). The Standardized Extract of *Nigella Sativa* and its Major Ingredient, Thymoquinone, Ameliorates Angiotensin II-Induced Hypertension in Rats. *J. Basic Clin. Physiol. Pharmacol.* 30, 51–58. doi:10.1515/jbcpp-2018-0074

Farag, M. A., Saad, H. H., and Hegazi, N. M. (2021). "Rediscovering Nigella Seeds Bioactives Chemical Composition Using Metabolomics Technologies," in *" in Black Cumin (Nigella Sativa) Seeds: Chemistry, Technology, Functionality, and Applications. Food Bioactive Ingredients*. Editor M. Fawzy Ramadan (Cham: Springer). doi:10.1007/978-3-030-48798-0_10

Fuster, J. J., MacLauchlan, S., Zuriaga, M. A., Polackal, M. N., Ostriker, A. C., Chakraborty, R., et al. (2017). Clonal Hematopoiesis Associated with TET2 Deficiency Accelerates Atherosclerosis Development in Mice. *Science* 355, 842–847. doi:10.1126/science.aag1381

Getz, G. S., and Reardon, C. A. (2016). Do the Apoe-/- and Ldlr-/- Mice Yield the Same Insight on Atherogenesis? *Arterioscler. Thromb. Vasc. Biol.* 36, 1734–1741. doi:10.1161/ATVBAHA.116.306874

Grebe, A., Hoss, F., and Latz, E. (2018). NLRP3 Inflammasome and the IL-1 Pathway in Atherosclerosis. *Circ. Res.* 122, 1722–1740. doi:10.1161/CIRCRESAHA.118.311362

Harzallah, H. J., Rjiba, K., Maaloul, A., Abid-Essafi, S., and Mahjoub, T. (2012). Oxidative and Genotoxic Effects of Thymoquinone, Nigella Sativa Active compoundBalb/c Mice. *Afr. J. Food Sci.* 6, 529–534. doi:10.5897/AJFS12.06610.5897/ajmr11.1073

Libby, P. (2021). Inflammation in Atherosclerosis-No Longer a Theory. *Clin. Chem.* 67, 131–142. doi:10.1093/clinchem/hvaa275

Lin, C. S., Lin, F. Y., Ho, L. J., Tsai, C. S., Cheng, S. M., Wu, W. L., et al. (2012). PKCδ Signalling Regulates SR-A and CD36 Expression and Foam Cell Formation. *Cardiovasc. Res.* 95, 346–355. doi:10.1093/cvr/cvs189

Liu, T., Zhang, L., Joo, D., and Sun, S. C. (2017). NF-κB Signaling in Inflammation. *Signal. Transduct. Target. Ther.* 2, 17023. doi:10.1038/sigtrans.2017.23

Majdalawieh, A. F., Yousef, S. A., and Abu-Yosef, I. A. (2021). Thymoquinone, a Major Constituent in *Nigella Sativa* Seeds, Is a Potential Preventative and Treatment Option for Atherosclerosis. *Eur. J. Pharmacol.* 909, 174420. doi:10.1016/j.ejphar.2021.174420

Minelli, S., Minelli, P., and Montinari, M. R. (2020). Reflections on Atherosclerosis: Lesson from the Past and Future Research Directions. *J. Multidiscip. Healthc.* 13, 621–633. doi:10.2147/JMDH.S254016

Mouwakeh, A., Telbisz, Á., Spengler, G., Mohácsi-Farkas, C., and Kiskó, G. (2018). Antibacterial and Resistance Modifying Activities of Nigella Sativa Essential Oil and its Active Compounds against. *Listeria Monocytogenes* 32, 737–743. doi:10.21873/invivo.11230210.21873/invivo.11302

Mussbacher, M., Salzmann, M., Brostjan, C., Hoesel, B., Schoergenhofer, C., Datler, H., et al. (2019). Cell Type-specific Roles of NF-Kb Linking Inflammation and Thrombosis. *Front. Immunol.* 10, 85. doi:10.3389/fimmu.2019.00085

Ong, Y. S., Saiful Yazan, L., Ng, W. K., Noordin, M. M., Sapuan, S., Foo, J. B., et al. (2016). Acute and Subacute Toxicity Profiles of Thymoquinone-Loaded Nanostructured Lipid Carrier in BALB/c Mice. *Int. J. Nanomedicine* 11, 5905–5915. doi:10.2147/IJN.S114205

Pei, Z. W., Guo, Y., Zhu, H. L., Dong, M., Zhang, Q., and Wang, F. (2020). Thymoquinone Protects against Hyperlipidemia-Induced Cardiac Damage in Low-Density Lipoprotein Receptor-Deficient ($LDL\text{-}R^{-/-}$) Mice via its Anti-inflammatory and Antipyroptotic Effects. *Biomed. Res. Int.* 2020, 4878704. doi:10.1155/2020/4878704

Pirillo, A., Norata, G. D., and Catapano, A. L. (20132013). LOX-1, OxLDL, and Atherosclerosis. *Mediators Inflamm.*, 152786. doi:10.1155/2013/152786

Rhoads, J. P., and Major, A. S. (2018). How Oxidized Low-Density Lipoprotein Activates Inflammatory Responses. *Crit. Rev. Immunol.* 38, 333–342. doi:10.1615/CritRevImmunol.2018026483

Roth, G. A., Mensah, G. A., Johnson, C. O., Addolorato, G., Ammirati, E., Baddour, L. M., et al. (2020). Global burden of Cardiovascular Diseases and Risk Factors, 1990-2019: Update from the GBD 2019 Study. *J. Am. Coll. Cardiol.* 76, 2982–3021. doi:10.1016/j.jacc.2020.11.010

Salehi, B., Quispe, C., Imran, M., Ul-Haq, I., Živković, J., Abu-Reidah, I. M., et al. (2021). Sen S, Nigella Plants - Traditional Uses, Bioactive Phytoconstituents, Preclinical and Clinical Studies. *Front. Pharmacol.* 12, 625386. doi:10.3389/fphar.2021.625386

Sun, L. F., An, D. Q., Niyazi, G. L., Ma, W. H., Xu, Z. W., and Xie, Y. (2018). Effects of Tianxiangdan Granule Treatment on Atherosclerosis via NF-Kb and P38 MAPK Signaling Pathways. *Mol. Med. Rep.* 17, 1642–1650. doi:10.3892/mmr.2017.8067

Sun, Y., Liu, W. Z., Liu, T., Feng, X., Yang, N., and Zhou, H. F. (2015). Signaling Pathway of MAPK/ERK in Cell Proliferation, Differentiation, Migration, Senescence and Apoptosis. *J. Recept. Signal. Transduct. Res.* 35, 600–604. doi:10.3109/10799893.2015.1030412

Tavakkoli, A., Mahdian, V., Razavi, B. M., and Hosseinzadeh, H. (2017). Review on Clinical Trials of Black Seed (Nigella Sativa) and its Active Constituent, Thymoquinone. *J. Pharmacopuncture* 20, 179–193. doi:10.3831/KPI.2017.20.021

Tubesha, Z., Imam, M. U., Mahmud, R., and Ismail, M. (2013). Study on the Potential Toxicity of a Thymoquinone-Rich Fraction Nanoemulsion in Sprague Dawley Rats. *Molecules* 18, 7460–7472. doi:10.3390/molecules18077460

Wang, X., and Khalil, R. A. (2018). Matrix Metalloproteinases, Vascular Remodeling, and Vascular Disease. *Adv. Pharmacol.* 81, 241–330. doi:10.1016/bs.apha.2017.08.002

WHO (2013). *Global Health Observatory*. Geneva, Switzerland: World Health Organization.

Xiao, X. L., Hu, N., Zhang, X. Z., Jiang, M., Chen, C., Ma, R., et al. (2018). Niclosamide Inhibits Vascular Smooth Muscle Cell Proliferation and Migration and Attenuates Neointimal Hyperplasia in Injured Rat Carotid Arteries. *Br. J. Pharmacol.* 175, 1707–1718. doi:10.1111/bph.14182

Xu, J., Zhu, L., Liu, H., Li, M., Liu, Y., Yang, F., et al. (2018). Thymoquinone Reduces Cardiac Damage Caused by Hypercholesterolemia in Apolipoprotein E-Deficient Mice. *Lipids Health Dis.* 17, 173. doi:10.1186/s12944-018-0829-y

Yazan, L. S., Mohd Azlan, S. N., Ansar, F. H. Z., and Gopalsamy, B. (2019). Acute Toxicity Study of Intravenous Administration of Thymoquinone-Loaded Nanostructured Lipid Carrier (TQ-NLC) in Sprague Dawley Rat. *Mal. J. Med. Health Sci.* 15, 51–57.

Zhang, L., Yao, J., Yao, Y., and Boström, K. I. (2021). Contributions of the Endothelium to Vascular Calcification. *Front. Cel. Dev. Biol.* 9, 620882. doi:10.3389/fcell.2021.620882

Zhang, Q. (2018). Global Situation and WHO Strategy on Traditional Medicine. *Tradit. Med. Mod. Med.* 1, 11–13. doi:10.1142/S257590001820001X

Zhang, Z., Zhang, D., Du, B., and Chen, Z. (2017). Hyperoside Inhibits the Effects Induced by Oxidized Low-Density Lipoprotein in Vascular Smooth Muscle Cells via oxLDL-LOX-1-ERK Pathway. *Mol. Cel. Biochem.* 433, 169–176. doi:10.1007/s11010-017-3025-x

Zhao, Y., Yang, Y., Xing, R., Cui, X., Xiao, Y., Xie, L., et al. (2018). Hyperlipidemia Induces Typical Atherosclerosis Development in Ldlr and Apoe Deficient Rats. *Atherosclerosis* 271, 26–35. doi:10.1016/j.atherosclerosis.2018.02.015

Zhu, N., Xiang, Y., Zhao, X., Cai, C., Chen, H., Jiang, W., et al. (2019). Thymoquinone Suppresses Platelet-Derived Growth Factor-BB-Induced Vascular Smooth Muscle Cell Proliferation, Migration and Neointimal Formation. *J. Cel. Mol. Med.* 23, 8482–8492. doi:10.1111/jcmm.14738

Conflict of Interest: The authors declare that the research was conducted in the absence of any commercial or financial relationships that could be construed as a potential conflict of interest.

The handling editor declared a shared affiliation, though no other collaboration, with one of the authors XL.

Publisher's Note: All claims expressed in this article are solely those of the authors and do not necessarily represent those of their affiliated organizations, or those of the publisher, the editors and the reviewers. Any product that may be evaluated in this article, orclaim that may be made by its manufacturer, is not guaranteed or endorsed by the publisher.

frontiers in Pharmacology

REVIEW
published: 24 January 2022
doi: 10.3389/fphar.2021.724439

The Potency of *Moringa oleifera* Lam. as Protective Agent in Cardiac Damage and Vascular Dysfunction

Fenty Alia[1], *Mirasari Putri*[2], *Neni Anggraeni*[3] *and Mas Rizky A. A Syamsunarno*[4]*

[1]Study Program of Biomedical Engineering, School of Electrical Engineering, Telkom University, Bandung, Indonesia, [2]Department of Biochemistry, Nutrition, and Biomolecular, Faculty of Medicine, Universitas Islam Bandung, Bandung, Indonesia, [3]Medical Laboratory Technologist, Bakti Asih School of Analyst, Bandung, Indonesia, [4]Department of Biomedical Sciences, Faculty of Medicine, Universitas Padjadjaran, Jatinangor, Indonesia

Cardiac damage and vascular dysfunction due to underlying diseases, such as hypertension and cardiac thrombosis, or side effects from certain drugs may lead to critical illness conditions and even death. The phytochemical compounds in natural products are being prospected to protect the heart and vascular system from further damage. *Moringa* genus is a subtropical tree native to Asia and Africa, which includes 13 species; *Moringa oleifera* Lam. (MO) is the most cultivated for its beneficial uses. MO is also known as the "miracle tree" because it has been used traditionally as a food source and medicine to treat various diseases such as anemia, diabetes, and infectious or cardiovascular diseases. The phytochemical compounds identified in MO with functional activities associated with cardiovascular diseases are N,α-L-rhamnopyranosyl vincosamide, isoquercetin, quercetin, quercetrin, and isothiocyanate. This study aims to investigate the potency of the phytochemical compounds in MO as a protective agent to cardiac damage and vascular dysfunction in the cardiovascular disease model. This is a scoping review by studying publications from the reputed database that assessed the functional activities of MO, which contribute to the improvement of cardiac and vascular dysfunctions. Studies show that the phytochemical compounds, for example, N,α-L-rhamnopyranosyl vincosamide and quercetin, have the molecular function of antioxidant, anti-inflammation, and anti-apoptosis. These lead to improving cardiac contractility and protecting cardiac structural integrity from damage. These compounds also act as natural vasorelaxants and endothelium protective agents. Most of the studies were conducted on *in vivo* studies; therefore, further studies should be applied in a clinical setting.

Keywords: antioxidant, anti-inflammation, anti-apoptosis, cardiac damage, *Moringa oleifera*, quercetin, vascular dysfunction, N,α-L-rhamnopyranosyl vincosamide

OPEN ACCESS

Edited by:
Ashwell Rungano Ndhlala, University of Limpopo, South Africa

Reviewed by:
Muhammad Nadeem, University of Veterinary and Animal Sciences, Pakistan
Bin Zeng, South China Agricultural University, China

***Correspondence:**
Mas Rizky A. A Syamsunarno
rizky@unpad.ac.id

Specialty section:
This article was submitted to Ethnopharmacology, a section of the journal Frontiers in Pharmacology

Received: *13 June 2021*
Accepted: *14 December 2021*
Published: *24 January 2022*

Citation:
Alia F, Putri M, Anggraeni N and Syamsunarno MRAA (2022) The Potency of Moringa oleifera *Lam. as Protective Agent in Cardiac Damage and Vascular Dysfunction. Front. Pharmacol. 12:724439. doi: 10.3389/fphar.2021.724439*

1 INTRODUCTION

Hypertension, cardiac thrombosis, and certain drugs can cause critical illness due to cardiac damage and dysfunction of the vascular system, leading to death (Çakmak and Demir, 2020). Cardiac and vascular disorders are classified as cardiovascular diseases (CVDs). As the underlying number one cause of death worldwide, 32% of the global population (17.9 million people) have died of CVDs, of which 85% were due to heart attacks and strokes (World Health Organization, 2021). The most risk

factor for CVDs is overweight, defined by having body mass index (BMI) outside the normal range. On the other hand, being overweight can also cause many illnesses such as hypertension or high blood pressure that increase CVD risk (Tran et al., 2021).

Coronary heart disease is affected by the integrity and contractility of endothelial cell damage. The occurrence of endothelial dysfunction disrupts the mechanism of vascular homeostasis, resulting in blood vessels vasoconstriction, thrombosis, coagulation impairment, leukocyte adhesion, platelet activation, and oxidative stress formation that leads to inflammation. This condition triggers the accumulation of cholesterol plaque in the blood vessels known as atherosclerosis, one of the pathological processes of CVD (Favero et al., 2014; Thygesen et al., 2018).

Considering the mortality of CVD, reducing its development and progression is very important. Therefore, pharmacological treatments have been established (Mayr and Jilma, 2006; Lavie et al., 2018), as well as the study of natural products that contain various phytochemical compounds prospected to protect the heart and blood vessels from further damage (Shaito et al., 2020).

One such natural product is *Moringa oleifera* Lam. (MO). MO has been suggested as anti-apoptosis, improving cardiac contractility and protecting cardiac structural integrity from damage. In addition, MO could act as a cardioprotective by improving inflammation and oxidative stress (Aekthammarat et al., 2019; Khalil et al., 2020). This review aims to investigate the potency of the phytochemical compounds in MO as a protective agent to cardiac damage and vascular dysfunction in the CVD model.

2 *MORINGA OLEIFERA* LAM. AT GLANCE

Moringa oleifera Lam. (MO) is one of the 13 species of *Moringa* genus that belongs to *Moringaceae* family (Swati et al., 2018). It is a subtropical tree native to Asia and Africa. It is mostly confined to the Sub-Himalayas but is now being cultivated worldwide attributed to its beneficial uses. It can grow fast in high-temperature regions and lands with a low water supply (Nouman et al., 2013, Nouman et al., 2014). The leaves, bark, roots, flowers, fruit, and seeds of this soft-wood tree have been utilized for its nutritional and medicinal values (Das, 2012). Since the first international conference of MO was held in 2001, this plant has been widely examined and labeled as "miracle tree," "natural gift," or "mother's best friend" (Leone et al., 2015).

Over the last thousand years, MO has been recognized as highly beneficial for improving wellness. The leaves, flowers, seedpods, seeds, roots, bark, and gum are used as food sources, traditional treatment of various illnesses, and to improve health (Gopalakrishnan et al., 2016; Khalid Abbas et al., 2018). However, leaves and seeds have the most pharmaceutical potential and nutritional and medicinal benefits (Leone et al., 2015). The leaves are rich in protein, minerals, and antioxidant compounds. People usually consume them in the form of fresh leaves or process them into powder. The leaves are taken as vegetables, snacks, herbal tea, and spice. The leaves are used as complementary food for babies and lactating women to prevent malnutrition and anemia (Idohou-Dossou et al., 2011; Baiyeri and Akinnagbe, 2013). In terms of traditional medicine, people use MO leaves for the treatment of infectious diseases, fever, high blood pressure, high blood sugar, male impotence, and skin diseases (Baiyeri and Akinnagbe, 2013). MO leaves are used not only for human consumption but also for animal nutrition and plant fertilizer (Abd El-Hack et al., 2018). The seeds have a high protein content and have hence been used to increase protein intake. Oil, as the main component of the seeds, can be collected traditionally by boiling shelled seeds with water or by using different extraction methods. The oil is known as "Ben oil" or "Behen oil". The oil is not widely used as edible oil for cooking; it is usually utilized as non-food applications, such as skincare ingredients, biodiesel, or other oil mixtures due to its oxidative stability (Leone et al., 2016; Nadeem and Imran, 2016; Leone et al., 2018). This plant is known as a superfood based on its nutritional properties. Various research have reported that MO contains seven times more vitamin C than oranges, 10 times more vitamin A than carrots, 17 times more calcium than milk, nine times more protein than yogurt, 15 times more potassium than bananas, and 25 times more iron than spinach (Rockwood et al., 2013; Gopalakrishnan et al., 2016). MO leave can be used to treat malnutrition due to the high protein and fiber content (Khalid Abbas et al., 2018). Studies showed that the pods are fibrous, with 46.78% fiber and 20.66% protein. Although amino acids are more concentrated in flowers (~31%) compared to pods (~30%), the contents of palmitic, linolenic, linoleic, and oleic acids are comparable in flowers and immature pods (Gopalakrishnan et al., 2016). MO seed oil contains 76% PUFA that consists of linoleic, linolenic, and oleic acids (Lalas and Tsaknis, 2002). This dietary component may have remediating effects on metabolic syndrome by controlling cholesterol, reducing plasma triglycerides, and preventing CVDs (Burghardt et al., 2010).

A complete analysis of the nutrients of MO is shown in **Table 1**.

MO not only is rich in nutrients but also contains anti-nutrients like flavonoids, which act as antioxidants (Stevens et al., 2016; Tiloke et al., 2018). Phytochemical compounds from all parts of MO are mainly flavonoids, phenolic acids, tannins, saponin, alkaloids, glucosinolates, and glycosides (Valdez-Solana et al., 2015; Brilhante et al., 2017; Paikra et al., 2017; Borgonovo et al., 2020). Various compounds from different parts of MO tree, such as leaves seeds, pods, bark, flowers, root, and stem that have been investigated, are shown in **Table 2**. These bioactive compounds act synergistically in their therapeutic effects, such as reducing blood glucose levels, anticancer, antibacterial, antifungal, neuroprotective, cardioprotective, anti-inflammatory properties, and modulating the immune system (Madi et al., 2016; Tiloke et al., 2018). MO leaves are high in polyphenols and rich in simple sugars, rhamnose, and glucosinolates and isothiocyanates (El-Massry et al., 2013). Meanwhile, MO seeds contain flavonoids (El-Massry et al., 2013) and known contain components that have hepatoprotectant activity,

TABLE 1 | Nutrition composition of *Moringa oleifera* (value in 100 g of plant materials) (Olagbemide and Philip, 2014; Gopalakrishnan et al., 2016).

Principle	Fresh leaves	Dry leaves	Leaf powder	Seed	Pods
Calories (cal)	92	329	205	—	26
Protein (g)	6.7	29.4	27.1	35.97	2.5
Fat (g)	1.7	5.2	2.3	38.67	0.1
Carbohydrate (g)	12.5	41.2	38.2	8.67	3.7
Fiber (g)	0.9	12.5	19.2	2.87	4.8
Vitamins					
Vitamin B1 (mg)	0.06	2.02	2.64	0.05	0.05
Vitamin B2 (mg)	0.05	21.3	20.5	0.06	0.07
Vitamin B3 (mg)	0.8	7.6	8.2	0.2	0.2
Vitamin C (mg)	220	15.8	17.3	4.5	120
Vitamin E (mg)	448	10.8	113	751.67	-
Electrolytes					
Potassium (mg)	259	1,236	1,324	—	—
Minerals					
Calcium (mg)	440	2,185	2003	45	30
Iron (mg)	0.85	25.6	28.2	-	5.3
Magnesium (mg)	42	448	368	635	24
Copper (mg)	0.07	0.49	0.57	5.20	3.1
Sulphur (mg)	—	—	—	0.05	137

TABLE 2 | Phytochemical compounds of different parts of *Moringa oleifera* (Brilhante et al., 2017; Paikra et al., 2017; Borgonovo et al., 2020).

Plant part	Phytochemical compounds
Leaves	Quercetin, Kaempferol, 4-[(alpha-L-rhamnosyloxy)benzyl]isothiocyanate (Moringin), Niazirin, Niazirinin, Benzylglucosinolate
Seeds	Quercetin, Kaempferol, Moringin, Niazimin, Niazirin, 4-[(alpha-L-rhamnopiranosyloxy)benzyl]glucosinolate, ß-sitosterol
Pods	Moringin, ß-sitosterol
Bark	4-[(alpha-L-rhamnopiranosyloxy)benzyl]glucosinolate
Flowers	Quercetin, Isoquercetin, Kaempferol
Root	Quercetin, Kaempferol, Moringin, Moringinine, 4-[(alpha-L-rhamnopiranosyloxy)benzyl]glucosinolate
Stem	Quercetin, Kaempferol, ß-sitosterol

namely, gastrodigenin rhamnopyranoside (1-[O-(4-hydroxymethylphenyl)]-α-L-rhamno-pyranoside, GR) (Li et al., 2019; Sun et al., 2019).

3 PHARMACOKINETIC STUDIES AND TOXICITY OF *MORINGA OLEIFERA* LAM.

Pharmacokinetic studies of MO have not been carried out, especially those related to the absorption and elimination of MO. However, studies of the GR were conducted by Li et al. (2019). The pharmacokinetic studies of GR showed that the time for GR to reach a maximal concentration (Cmax) orally was 10 and 5 min intravenous. GR as much as 10 mg/kg was distributed in the tissue in the range of 5–30 min and eliminated within 3 h. The distribution of GR was mostly found in the heart, kidneys, and spleen. However, GR levels in the kidneys will decrease faster than other organs, which is about 30 min. The liver, lungs, and brain receive less GR distribution than the kidneys, heart, and spleen (Li et al., 2019).

MO both in leaves and bark did not show toxicity signs using acute, sub-acute, and chronic toxicity test (Awodele et al., 2012; Reddy et al., 2013). However, several studies have shown that the different solvents of MO extract affect the test. On the basis of the sub-acute toxicity study of MO using Swiss Albino rats, it was shown that ethanol solvent was safer than aqueous (Kasolo et al., 2012). Sub-acute toxicity of MO leaves using an aqueous extract showed signs of mild organ toxicity, as seen based on an increase in WBC, chloride, potassium, calcium ions (Cl^-, K^+, and Ca^{2+}) concentrations, an increase in the average ALP (alkaline phosphatase), ALT (alanine aminotransferase), AST (alanine aminotransferase), and total bilirubin (Kasolo et al., 2012). An increase in AST also occurred in the acute toxicity of an aqueous—methanol extract of MO leaves in female Wistar Albino rats with a dose of LD50 [2,000 mg/kg body weight (BW)] (Okumu et al., 2016). Histopathological changes were also found upon examination in the form of focal hepatocyte swelling and necrosis (Kasolo et al., 2012; Okumu et al., 2016) in the area around the central and hepatic veins and hepatic vein congestion (Okumu et al., 2016). Histopathological changes were also found in the kidney and heart tissue (Kasolo et al., 2012). Meanwhile, the acute toxicity of aqueous extract of MO leaves on male Wistar Albino rats administered orally did not show any sign of toxicity, only at doses of 3,200–6,400 mg/kg BW showed a decrease in locomotion and dullness (Awodele et al., 2012). Administration of high doses of MO extract, both leaf and seed extracts, can show changes in several parameters such as blood parameters (WBC) (Kasolo et al.,

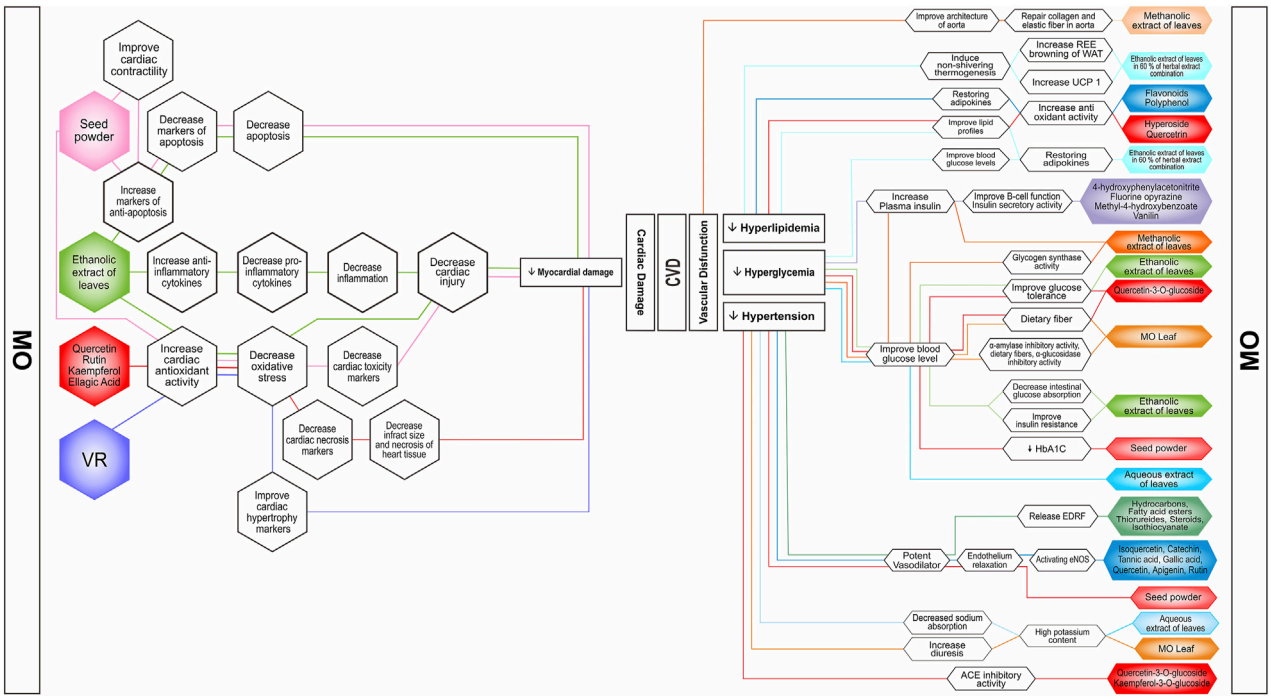

FIGURE 1 | Possible mechanism of actions of *Moringa oleifera* nutrients and bioactive compounds in combating vascular dysfunctions and myocardial damages. The bioactive compounds prevent and improve CVDs' risk factors such as hyperlipidemia, hyperglycemia, and hypertension. MO preparations are in the form of isolated metabolites, whole extracts, or pure parts. Notice that there is one promising approach to improve CVD risk by inducing non-shivering thermogenesis. ACE, angiotensin-converting enzyme; EDRF, endothelium-derived relaxing factor; eNOS, endothelial nitric oxide synthase; HbA1C, hemoglobin A1C; REE, resting energy expenditure; UCP1, uncoupling protein 1; VR, N,α-L-Rhamnopyranosyl vincosamide; WAT, white adipose tissue.

2012) and organ damage parameters such as an increase in ALT and AST (Ajibade et al., 2012; Kasolo et al., 2012; Okumu et al., 2016). On the other hand, MO leaves and seeds in low doses showed relatively safe effects (Ajibade et al., 2012; Okumu et al., 2016).

4 ROLE OF MO IN CARDIOVASCULAR DISEASES

The occurrence of CVD is inseparable from the risk factors that influence, and this section describes the role of MO in CVD and the management of classic CVD risk factors, such as hypertension, obesity, hyperglycemia, and dyslipidemia, not only *in vitro* and *in vivo* but also in clinical settings. (**Figure 1**).

4.1 The Ability of MO to Treat Obesity and Obesity-Related Cardiometabolic Abnormalities

The management of CVD risk factors such as obesity, obesity-related cardiometabolic abnormalities, and hypertension has a role in minimizing CVD incidents (Aekthammarat et al., 2019). Obesity can trigger an oxidative stress condition due to an imbalance of pro-oxidants and antioxidants in the body. In obesity, there are excessive lipogenesis and inhibition of lipolysis. Fat, especially in the visceral area, has more glucocorticoid and androgen receptors, has increased metabolic activity, is sensitive to lipolysis, and is more prone to insulin resistance. This situation can lead to dyslipidemia, insulin resistance, and inflammation that cause endothelial dysfunction (Madkhali et al., 2019).

Several studies have demonstrated the antihyperlipidemic potential of MO. This lipid lowering effect can prevent atherosclerosis incidences. In animal models, two experiments showed remarkable improvement of BW and lipid profiles in the administration of MO leaves methanolic extract in doses of 200 and 400 mg/kg BW in rats. The first study showed that administration of the extract along with high-fat diet (HFD) feeding for 49 days led to a significant increase in HDL level and decrease of BW, total cholesterol, triglycerides, LDL level, and atherogenic index (Bais et al., 2014). This study found that alkaloids, tannins, flavonoids and terpenoids, and steroids contained in MO extract were responsible for the hypolipidemic effects, due to their antioxidant activities. However, further study needs to be performed for identification of specific compounds (Bais et al., 2014). The second study that used the same kind of extract in the same doses for 3 weeks after 9 weeks administration of HFD in rats showed the improvement in BW, BMI, Lee index, and HDL. There was also an improvement of hyperlipidemic parameters

such as total cholesterol, triglyceride, LDL, and VLDL (Madkhali et al., 2019). Other important findings from this study were that administration in a dose of 400 mg/kg showed endothelium-mediated vasodilatation and improvement of aorta damage caused by HFD. MO decreased fat accumulation and repaired collagen elastic ratio, thus leading to almost normal architecture of the aorta (Madkhali et al., 2019). However, the last study did not perform phytochemical analysis to find the compounds that might be responsible for the lipid lowering activities. Both of the studies also used different extraction methods that might lead to obtaining different types and amounts of compounds (Nobossé et al., 2018). One *in vivo* study using MO ethanolic extract in a dose of 600 mg/kg BW orally for 12 weeks showed ameliorative effects in BW, atherogenic index, and insulin resistance in obese rats. This study provided molecular mechanisms to explain anti-obesity and anti-cardiometabolic abnormalities of polyphenolic and flavonoids antioxidant activities, by working directly on visceral mass and restoring mRNA expression of leptin, resistin, and adiponectin genes (Metwally et al., 2017). Cardiac ameliorative effect of MO in obese rats was investigated using administration of 200 and 400 mg of MO leaves methanolic extract orally for 12 weeks along with HFD. It was found that the extract decreased BW and improved TC, TG, HDL, and LDL profiles. In addition, the extract improved cardiac enzymes CK-MB, AST, and ALT, and decreased lipid peroxidase level by increasing SOD, CAT, and glutathione peroxidase (GPx) activities, possibly associated with antioxidant activity of phenolic compounds, mainly hyperoside and quercetrin contained in the extract (Mabrouki et al., 2020).

Research on obesity treatment has found new and promising targets. One of them is thermogenic adaptive tissue stimulation. Mitochondria in skeletal muscle and brown adipose tissue (BAT) plays a role in adaptive thermogenesis by generating heat during digestion and absorption of food to protect against environmental changes such as cold temperatures and is a thermal effect of exercise. Thereby, BAT stimulation and regulation are expected to reduce BW effectively (Tseng et al., 2010). Several natural compounds such as polyphenol and flavonoid derivatives can stimulate the proliferation and differentiation of BAT (Kang et al., 2018; Wood Dos Santos et al., 2018).

A study on MO has led to the stimulation of thermogenesis as a targeted therapy for obesity. A study using an herbal extract combination comprised of 60% MO leaves ethanolic extract in doses of 100 and 250 mg/kg BW for 28 days significantly reduced BW gain, total body fat mass, the fat cell size of inguinal and epididymal white adipose tissue (WAT), liver weight, and hepatic triglycerides and increased resting energy expenditure (REE) and fat oxidation on obese rats. The decrease of fat cell size and mass in supplemented obese rats was due to the increase energy metabolism through browning of WAT, the increase of expression of UCP1, and down-regulation expression of key adipogenic marker proteins (PPARγ, C/EBPα, CD36, aP-2α, and perilipin (Kundimi et al., 2020). However, they found that this herbal combination did not substantially affect the interscapular BAT fat mass of obese rats. This study has limitations; they did not explain whether this combined extract composition influences WAT browning or modulate BAT activation to increase energy metabolism. Another *in vivo* study demonstrated the effect of MO leaves ethanol extract on interscapular BAT. Mice were induced with HFD and given MO leaves ethanol extract in doses of 280 and 560 mg/kg BW for 7 weeks. It was found that BAT weight, BAT weight/BW ratio, BAT weight/WAT weight ratio, and BAT cell density were significantly increased in HFD-mice treated with MO compared to the HFD only mice. Also, the expression of Bone Morphogenetic Protein 7 (BMP7), a transforming growth factor–β (TGF-β) superfamily that can induce BAT adipogenesis and increase UCP1 expression, was measured. Mice given MO at dose 280 mg/kg BW significantly increase serum BMP7 levels. MO ethanol extract stimulated the development of BAT by upregulating serum BMP7 expression. This study suggested that flavonoids found in MO could modulate the BMP7 expression. However, this study did not provide phytochemical analysis, but they proposed that flavonoids were responsible for the mechanisms (Syamsunarno et al., 2021). These data were supported by an *in vitro* study that used human adipose-derived mesenchymal stem cells to investigate the effect of MO on lipids metabolism and antioxidant systems related to the adipogenesis process (Barbagallo et al., 2016). This study analyzed the expression of UCP1, Sirtuin 1 (SIRT1), peroxisome proliferator-activated receptor alpha (PPARα), and peroxisome proliferator-activated receptor-gamma coactivator 1 alpha (Pgc-1α) to evaluate the effect of MO on adipocyte thermogenic pathways. It was found that thermogenesis modulates improved metabolic rate, including glucose and lipid metabolism in humans. During adipogenic differentiation, the administration of MO significantly increased the mRNA expression of SIRT-1, PPARα, Pgc-1α, and UCP1 that indicated the activation of the heat-generating pathway, which is a lost proton pumping cycle through uncoupling proteins actions. They also measured the antioxidant activity of MO against DPPH. In particular, the percentage of DPPH inhibition resulted was about 81, 63, 42, 33, 13, and 18%, respectively, at a concentration of MO of 500–250-100–50-10–5 μg/ml. However, therapeutic efficacy of these antioxidant abilities must be confirmed by sufficient *in vivo* study due to the presence of several factors that can influence the antioxidant potential, such as physiopharmacological processes, that may lead to irrelevant results (Kasote et al., 2015). Finally, they concluded that MO has the potential to modulating lipid metabolism by upregulates the expression of SIRT-1, PPARα, Pgc-1α, and UCP1, the crucial proteins involved in thermogenesis (Barbagallo et al., 2016).

Some clinical studies were conducted to investigate the role of MO in metabolic abnormalities. Two randomized, double-blind placebo-controlled clinical studies in overweight/obese adults examined an interesting herbal extract combination comprised of 60% MO leaves ethanolic extract. The first study found that daily supplementation of this formulation in a dose of 900 mg for 8 weeks in 21 obese adults provided benefits in reducing BW and BMI, improved serum triglyceride concentration, LDL/HDL ratio, and fasting blood glucose levels. In addition, this study also found that 50 μg/ml of the extract exhibit anti-adipogenesis activity in 3T3-L1 mice adipocytes by upregulating adiponectin,

Pentraxin-3, Pref-1, and down regulating MCP-1, resistin, and PAI-1 (Sengupta et al., 2012). The following study demonstrated the benefit of this herbal formulation in 66 healthy overweight adults. It was found that daily intake in a dose of 900 mg for 16 weeks also significantly reduced BW, BMI, total body fat, waist, and hip circumferences, LDL, and increased HDL level (Dixit et al., 2018). Those results above were possibly related to the presence of three significant compounds contained in the herbal extract combination, namely, quercetin-3-O-glucoside, mahanine, and curcumin. However, how these compounds act synergistically still needs to be explained, especially when considered safe for human consumption (Sengupta et al., 2012).

Obesity, hyperglycemia, and dyslipidemia are related to each other. Although hyperglycemia does not cause CVDs directly, the treatment of hyperglycemia should be considered prevention of CVDs. Several studies have been demonstrated the potential effect of MO in lowering blood glucose in some experiments using hyperglycemic animal models. A study presented the effect of MO leaf powder in reducing blood glucose levels. Goto-Kakizaki (GK) and Wistar rats were given glucose 2 mg/kg BW orally to assess oral glucose tolerance test (OGTT). Group 1 was only given glucose, and the other group was given glucose along with MO leaf powder at a dose of 200 mg/kg BW. The treatment group showed lower fasting blood glucose levels than GK rats without MO. Blood glucose levels significantly decreased at 20, 30, 45, and 60 min for MO-treated GK rats and 10, 30, and 45 min for MO-treated Wistar rats ($p < 0.05$) compared to both controls after glucose administration. Furthermore, they analyzed the types of polyphenols in MO leaf powder by HPLC with a photodiode array detector. The result showed a high concentration of quercetin-3-glycoside, rutin, kaempferol glycosides, and other polyphenols, likely chlorogenic acid. They suggested MO has improved glucose tolerance might be stimulated by quercetin-3-glucoside, and fiber contents in MO leave powder *via* inhibition of glucose uptake and slowing gastric emptying time (Ndong et al., 2007).

Similarly, a study used MO seed powder at doses of 50 and 100 mg/kg BW mixed with feed after 4 weeks of treatment decreased by 35% and 45% fasting blood glucose and 13% and 22% HBA1c compared to the control group, respectively. In addition, interleukin-6 (IL-6) and lipid peroxidation levels increased, whereas the activity of catalase, SOD, and GSH decreased in STZ diabetic rats. Nevertheless, in STZ, diabetic rats treated with MO almost recovered these parameters to normal levels. Although it was suggested that these therapeutic effects were due to the active ingredients present in Moringa seeds, such phenolic and flavonoids contained in MO seed powder have antioxidant activity; however, this study did not perform phytochemical analysis (Al-Malki and Rabey, 2015).

Administration of MO leaves aqueous extract at a dose of 200 mg/kg BW reduced fasting blood glucose and postprandial glucose levels by 26% and 30%, respectively, in OGTT compared to the untreated group. Another group, which gave MO at a dose of 300 mg/kg BW to diabetic rats for 21 days, decreased 69% of fasting glucose and 51% of postprandial glucose levels. In addition, elevated hemoglobin and total protein levels on long-term treatment with the extract for 21 days indicated a beneficial effect in reducing the severity of diabetes. Unfortunately, they did not elucidate the hypoglycemic effect and antidiabetic mechanism of the MO leaves aqueous extract (Jaiswal et al., 2009).

In addition to using aqueous extracts and powders from MO parts, several studies have also used methanol and ethanol extracts to investigate the effectiveness of MO in controlling blood glucose. A study using oral administration of ethanol extract of MO leaves (500 mg/kg) and glibenclamide (0.5 mg/kg) as a reference drug measured fasting blood glucose and glucose tolerance. The result showed that MO ethanol extract improved hyperglycemic and glucose tolerance at 30, 90, and 120 min after glucose (2.5 g/kg) solution gavage. Furthermore, they performed plasma insulin concentration, intestinal glucose absorption, and α-amylase activity of MO extract. The result showed that intestinal glucose absorption significantly reduced and no significant induction in insulin secretion. Although α-amylase activity assay showed no significant decrease in the starch's catabolism, this promising result is important to perform with another proper method. Again, in this study, the mechanism of lowering the blood glucose effect of MO extract was not described (Azad et al., 2017). A significant decrease in blood glucose levels has been reported in treated STZ induced rats with MO leaves methanolic extract at a dose of 250 mg/kg BW for 6 weeks compared to diabetic control. However, they did not explain the mechanism of MO leaves methanolic extract in lowering blood glucose levels (Omodanisi et al., 2017).

Furthermore, another study demonstrated the effect of MO leaves methanol extract in diabetic rats. MO methanol extract at 300 and 600 mg/kg enhances glucose tolerance by 56 and 57%, and blood glucose levels were reduced by 76 and 64%, respectively, compared with the control diabetic group. Expectedly, in untreated diabetic rats, the insulin concentration was 46% lower compared with normal. In rats treated with MO at 300 and 600 mg/kg BW, plasma insulin increased by 1.6-fold ($p < 0.01$) and 1.7-fold ($p < 0.01$), respectively. Meanwhile, in untreated diabetic rats, the insulin concentration was 46% lower than normal rats, glycogen synthase activity in the liver and muscle tissues was significantly reduced, and glucose uptake was lower than normal. In rats treated with MO at doses of 300 and 600 mg/kg BW, plasma insulin increased by 1.6-fold ($p < 0.01$) and 1.7-fold ($p < 0.01$), respectively, glycogen synthase activities significantly improved in both the muscle and liver, and glucose uptake was inhibited by 49 and 59% respectively. In this study, they screened the phytochemical compounds of MO and measured the total phenolic and total flavonoids. These phytochemicals maintained beneficial effects such as reducing oxidative stress in diabetic rats, stimulating glucose transport, and inhibiting adipocyte differentiation (Olayaki et al., 2015).

Different part of MO has been evaluated as antidiabetic. The part that showed the most anti-hyperglycemic activity without causing side effects is the leaves. Natural compounds with antidiabetic activity such as phenolics, glucosinolates, isothiocyanate, syringic acid, gallic acid, and rutin are richly found in the leaves. Antidiabetic activity through insulin release activation has been reported from isolated compounds

of MO extract. A study was conducted to evaluate the potential effect of pure compounds from parts of MO extract to improve insulin secretion in the islet pancreas of male BALB/C mice. The pure compounds that were isolated and characterized are 4-hydroxyphenylacetonitrite (roots), fluorine opyrazine, methyl-4-hydroxybenzoate (roots), and vanillin (stem barks). Under basal conditions (glucose 3 mM), insulin release was similar to islet control, and these compounds have not stimulated insulin production. However, when stimulated with glucose (16.7 mM), these pure compounds showed insulin secretory activity, but the highest was fluorine opyrazine, about 230%, whereas tolbutamide, a positive drug control, obtained 282.6% of insulin secretion. This study also demonstrated the ability of kaempferol to stimulate insulin secretion as a reference compound. The data showed that kaempferol significantly induced insulin secretion (377.2%) (Hafizur et al., 2018). This study also demonstrated the antihyperglycemic of these compounds *in vivo*. Rats induced with STZ (60 mg/kg i.v.) and nicotinamide (120 mg/kg i.v.) The diabetic rats were divided into six groups: the diabetic control group and the diabetic treatment group (2–5) were given compound suspension with a 25 mg/kg BW, respectively. The diabetic group was given glibenclamide (10 mg/kg) as a reference drug. After oral administration of the drugs, blood glucose concentration was measured at 0, 1, 2, and 3 h. There was no significant reduction in blood glucose concentration measured after the 3-h oral administration of methyl-4-hydroxybenzoate and vanillin to diabetic rats. On the other hand, there was a significantly decreased blood glucose concentration in doses and time-dependent manner after administration of 4-hydroxyphenylacetonitrite and fluorine opyrazine orally. Interestingly, fluorine opyrazine showed a more obvious effect on reducing blood glucose. Blood glucose decreased significantly starting at 2 and 3 h after gavage. Glibenclamide, the standard drug, lowered blood glucose more efficiently in a time-dependent manner. Furthermore, they evaluated fluorine opyrazine to improve β-cell function and elevate plasma insulin in type 2 diabetic rats. The data showed an increased insulin secretion occurred after 30 min of glucose administration (3 g/kg), when blood glucose is higher, but not in the absence of a glucose challenge. Fluorine opyrazine stimulated insulin secretion only at higher glucose concentrations and not at lower glucose concentrations. Furthermore, an index for β-cell function, the insulinogenic index (IGI), was measured. Fluorine opyrazine-treated rats (14.8 ± 1.55 pmol insulin/mmol glucose) were 3.8-fold higher than the control rats (3.9 ± 0.69 pmol insulin/mmol glucose). The IGI proposes that fluorine opyrazine treatment ameliorated β-cell function in diabetic rats (Hafizur et al., 2018). Although they performed the effect of pure compounds of MO to induce insulin secretion *in vivo* and *in vivo* study, they did not describe the isolation methods of the compounds.

Some human studies were performed to find the potency of MO to improve glucose metabolism. A preliminary study using 10 volunteers was performed to examine the effects of MO in insulin secretion in healthy subjects. Single-dose administration of 4-g MO leaf capsule orally after overnight fast significantly increased plasma insulin (Anthanont et al., 2016). However, the following randomized placebo-controlled study in therapy-naive of 32 patients with type 2 diabetes mellitus (T2DM) conducted by the same researchers did not demonstrate the blood glucose-lowering effects of MO. Administration of 8 g per day of MO leaf capsules for 4 weeks showed that MO leaf did not affect glycemic control (HbA1C level, fasting, premeal, and post-meal plasma glucose). The limitation of the study was the use of raw material without performing phytochemical analysis that might result in the lack of active substances responsible for blood glucose-lowering agents such as quercetin, chlorogenic acid, and moringinine. In addition, the dose used in this study was reported no adverse effects on the liver and kidney function of the subjects (Taweerutchana et al., 2017). Moreover, another study found that using raw material in administrating MO to the human body might lower blood glucose levels *via* another pathway. Administration of 20 g of MO leaf powder in traditional meals to 17 diabetic subjects showed an earlier peak of postprandial glucose response with lower increments at 90, 120, and 150 min and lower mean glycemic meal response than the non-diabetic group. One of the factors that attributed to these results is the ability of high total fibers contained in MO leaf to reduce the velocity of starch ingestion in the intestine, leading to a decrease of postprandial blood glucose, despite the ability of total polyphenols to inhibit α-amylase activity (Leone et al., 2018). For further study, there is a need to isolate the exact compounds responsible for the mechanism.

4.2 The Ability of MO to Lower Blood Pressure and Improve Endothelial Dysfunctions

Several studies were conducted to support the scientific evidence of the empirical use of MO to treat hypertension. Some studies examined the ability of MO as endothelial protecting agent using L-NAME (Nω-nitro-L-arginine-methyl ester) material as hypertension-inducer. L-NAME induces high blood pressure by acting as nitric oxide synthase (NOS) inhibitor (Aekthammarat et al., 2019; Aekthammarat et al., 2020). In a study using MO leaves aqueous extract orally in 30 and 60 mg/kg/day doses for 3 weeks in L-NAME-induced hypertension in rats showed a significant decrease in blood pressure and heart rate and also reduced the impairment of mesenteric arterial relaxation induced by acetylcholine. Rats that received 0.001–3 mg bolus injection of the extract showed dose-dependent vasorelaxation in the endothelium of mesenteric arterial beds. These emphasized the ability of MO as a potent vasodilator, probably by inducing the release of endothelium-derived relaxing factors (EDRFs). The extract also decreased vascular O_2^- production and malondialdehyde (MDA) level in plasma and thoracic aorta and increased the level of SOD and CAT antioxidant enzymes, suggesting the potency of MO against oxidative stress-related hypertension in L-NAME rats (Aekthammarat et al., 2019). Further study was performed to investigate blood pressure-lowering activity of MO associated with enhanced NO production by delivering MO leaves aqueous extract in a 30 mg/kg intravenous dose after L-NAME administration in

rats. MO showed longer period of BP-lowering effect possibly by activating eNOS *via* NOS-sGC dependent signaling. This condition increased NO availability, resulting in a vasorelaxing effect in the endothelium. This study provided quantitative analysis of some phenolic compounds. Although isoquercetin, catechin, tannic acid, gallic acid, quercetin, apigenin, and rutin were found using HPLC-DAD, further studies are needed to find specific compound which responsible for MO hypotensive activity (Aekthammarat et al., 2020).

Evidently, hypotensive activity of MO *via* releasing of EDRF also occurred under normal blood pressure condition. A study demonstrated the ability of MO root petroleum ether and dichloromethane extract to lower mean arterial pressure at a dose of 30 mg/kg when given intravenously in normotensive rats. Both extracts were suggested to cause the release of nitric oxide (NO) or EDRF in smooth muscle cells in different pathways. The petroleum extract stimulated muscarinic receptor and dichloromethane extract demonstrated to promote pathways other than cholinergic. GC-MS analysis showed the presence of hydrocarbons, fatty acid esters, thiorureides, steroids, and isothiocyanate in almost all extracts. These constituents may be responsible for hypotensive potential of MO root extracts (Sana et al., 2015).

Several human studies were conducted to investigate the blood pressure-lowering effect of MO. One human study was conducted to provide scientific evidence of MO blood pressure lowering effect. Healthy participants that were given 120 g of cooked MO leaves for a week showed a decrease of 2 h postprandial blood pressure compared to the control group. This study did not perform phytochemical analysis of MO leaves; however, the possible mechanisms of the blood pressure lowering effect may be attributed to MO free radical scavenging activity of nitrile, thiocarbamate, and isothiocyanate (Chan Sun et al., 2020). A clinic-based experimental study was performed to investigate the effect of MO aqueous extract in 30 normotensive adults. Consumption of MO aqueous extract (28.5, 57, and 85.7 mg/kg) orally on three different groups significantly lowered blood pressure and intraocular pressure at 30, 60, and 90 min after administration compared to baseline values, subsequently returned to baseline values after 150 min in a dose-dependent manner compared to control group that received distilled water only. This possibly occurred due to high potassium and calcium content in MO; therefore, it prevented the excessive absorption of sodium and decreased blood pressure (George et al., 2018). A study involving 20 males with stage-1 hypertension and obesity was performed to investigate the effect of 150 ml of MO leaf juice given twice a day for 30 days. It was found that MO leaf reduced systolic and diastolic blood pressure (DBP) significantly. This study did not perform phytochemical analysis; after there, they proposed that the effects were due to the ability of flavonoids to reduce oxidative stress, subsequently induced relaxation of resistant arteries (Sailesh et al., 2018). Another study showed that daily supplementation of 30 g of MO leaf powder in 30 obese hypertensive individuals for 60 days significantly decreased BMI, systolic blood pressure (SBP), and DBP and increased urine frequency by 27.2%. This study did not perform nutrient analysis and phytochemical analysis of the preparation; however, antioxidant activities generally attributed to bioactive compounds such as flavonoids, tannins, isothiocyanate, and thiocarbamate glycosides might be responsible for the decrease of BMI and blood pressure. It was noted that MO also demonstrated diuretic activity associated with its high potassium content (Fombang et al., 2016).

Another mechanism was proposed to explain the blood pressure-lowering effect of MO. By using *in vitro* ACE inhibition assay, MO was found to have ACE inhibitory activity attributable to two compounds contained in ethyl acetate leaves extract, namely, quercetin-3-O-glucoside and kaempferol-3-O-glucoside. This ACE inhibitory activity of these compounds was even higher than Captopril that served as positive control. Administration of this extract orally in 0.01 and 0.3 g/kg/day doses in L-NAME hypertensive rats showed a significant decrease of SBP after 4 weeks of treatment. This study also revealed that crude extract of MO is safe up to 2,000 mg/kg dosage (Acuram et al., 2019).

Endothelial dysfunction also develops during aging. A study revealed that administration of MO seed powder in a 750 mg/kg/day dose for 4 weeks gave protective effects to the endothelium function of aged rats. It was suggested that MO improved endothelium relaxation by increasing Akt signaling, activating endothelial NO synthase and down-regulating arginase-1 (Randriamboavonjy et al., 2019). Phytochemical analysis was not performed in this study, but the endothelium improvement effects were most likely due to polyphenol, glucosinolate, and isothiocyanate compounds contained in MO.

4.3 Ameliorative Effects of MO in Cardiac Toxicity Condition/Myocardial Infarction

Various studies have evaluated numerous natural products that might have cardioprotective effects by using different methods in animal models, such as surgery or drug-induced cardiotoxicity methods, to mimic human myocardial infarction (MI) (Panda et al., 2013; Panda, 2015). Application of drugs or chemical products such as anticancer, antibiotic, or pesticide also caused cardiotoxicity effects. These conditions encouraged researchers to investigate the role of natural compounds in combating MI by using the drugs or chemical compounds in animal model settings. Most of the studies concluded that the antioxidant activity of MO was responsible for its cardioprotective effects.

A study using specific alkaloid from MO leaves, N,α-L-rhamnopyranosyl vincosamide (VR), for the pretreatment of ISO-induced cardiotoxicity in rat models with a dose of 40 mg/kg BW orally for 7 days showed inhibition of the ST-segment elevation, normal heart rate, and decrease of necrotic cells of cardiac muscle (Panda et al., 2013). Administration of ISO caused elevation of MI biomarkers cTnT, CK-MB, LDH, and SGPT, indicating myocardial integrity damage. Furthermore, this condition could be countered by pretreatment of VR. This study also analyzed the free radical scavenging activities of VR *in vitro* and *in vivo*. VR decreased MDA and LOOH levels by increasing SOD, CAT, GPx, and GSH enzymes activities; that was the proposed mechanisms of cardioprotective effect of VR (Panda

et al., 2013). Another study also investigated the free radical scavenging activities of VR. It was found that administration of magnetic hydrogel nanocomposite-loaded VR in doxorubicin (DOX)–induced cardiotoxicity rat models suppressed MDA by increasing GSH and SOD levels and decreasing mRNA level of cardiac hypertrophy marker ANP, BNP, and β-MHC mRNA in rat heart after 2 weeks intraperitoneal administration (Cheraghi et al., 2017). This justified the cardioprotective effect of VR mediated through its free radical scavenging activities.

Other studies using various doses of hydroalcoholic extract of MO leaves in MI animal models also showed the beneficial effects of MO in reducing myocardial damage, which was attributed to the antioxidant properties of MO. Pretreatment with butanolic fraction of MO leaves in a dose of 100 mg/kg/day for 28 days orally in ISO-induced cardiotoxicity rat models could lower MDA level and increase SOD, CAT, GPx, and total GSH. High concentration of quercetin, rutin, kaempferol, and ellagic acid contained in the extract was found responsible for these free radicals scavenging activities. These activities suppressed the increase of cardiac necrosis biomarkers LDH, CK-MB, and cTnT. This study also found the ability of the extract to reduce infarction, necrosis, and inflammation infiltrate in to the myocardium and to normalize myofibrillar structure through *in vitro* and *in vivo* analysis of cardiac tissue (Panda, 2015). A remarkable improvement of cardiac injury associated with antioxidant properties of ethanolic extract of MO leaves was also shown in benzene-induced leukemia rat models. This study aimed to assess the protective role of MO in cardiotoxic effects of DOX, an anticancer drug that is generally used to treat acute myeloid leukemia. Administration of 680 mg/day MO for 4 weeks orally in leukemia rat models significantly decreased MDA level and increased GSH and GPx levels. Interestingly, administration of MO in conjunction with DOX produced a higher ameliorative effect compared to the administration of MO alone. MO treatment significantly decreased cardiac toxicity markers ɣ-H2AX and ET-1 expressions in heart tissue, which could indicate a protective effect of MO against cardiac injury. A notably near to normal cardiac muscle appearance fibers with minute myolysis was realized from histological analysis. However, this study did not perform phytochemistry analysis to find specific MO compound, which may be responsible for the improvement of cardiac injury (Aniss et al., 2020). The seed, another interesting component of MO to explore, showed better survival rates and cardiac functions in mice with ligated left anterior descending branch of coronary artery, as a model for human MI (Li et al., 2020). Administration of MO seed powder in 600 and 900 mg/day oral doses for 28 days significantly alleviated contractile dysfunction by increasing the value of the left ventricular ejection fraction (LVEF) and left ventricular fractional shortening (LVFS). MO could also reduce infarct size and cardiac fibrosis; taken together, it might have occurred by antioxidative and antiapoptotic activities of MO compounds that were seen to decrease the apoptotic marker Bax, cytochrome-c, inducible NOS (iNOS) expression and NO level, and increase of Bcl2 marker (Li et al., 2020).

In addition to the ability to improve cardiac antioxidant status, MO has ability to ameliorate cardiac injury through its anti-inflammation and antiapoptotic potential. Administration of MO in cardiotoxicity rat models decreased inflammation markers TNF-α, NF-κB, and MCP-1 (Aniss et al., 2020). MI incident causes apoptosis and necrosis in cardiomyocyte that leads to histoarchitecture damage of cardiac tissue. MO compounds have been known to have antiapoptotic potential that may contribute to the prevention of cardiac tissue damage (Panda, 2015; Aniss et al., 2020; Khalil et al., 2020; Li et al., 2020). Administration of MO in cardiotoxicity rat models decreased apoptotic markers p53 and caspase 3 and increased antiapoptotic marker Bcl2 (Aniss et al., 2020).

The chemical structures of the prominent MO bioactive compounds described above can be seen in **Figure 2**. The studies evaluating the potency of MO for CVD are summarized in **Tables 3**, **4**.

5 DISCUSSION

The potency of MO to overcome CVD is especially through its ability as free radical scavenger, anti-inflammation, and antiapototic agent, which is associated with the richness of bioactive compounds, such as flavonoids, phenolic acids, tannins, saponin, alkaloids, glucosinolate, and glycosides with their various isolates such as quercetin, N,α-L-rhamnopyranosyl vincosamide, and isothiocyanate (**Figure 1**). MO becomes a promising resource in finding natural therapy, even for MI, which is known as the main cause of death by CVD. According to The Fourth Universal Definition of In Myocardial Infarction, the pathological analysis denotes MI as myocardial cell death due to prolonged ischemia (Thygesen et al., 2018). MO increased cardiac antioxidant status, which led to the improvement of MI biomarkers, cardiac contractility, morphology of cardiac muscle, inflammatory cytokines, and apoptotic markers (Panda et al., 2013; Panda, 2015; Khalil et al., 2020; Saka et al., 2020).

Regardless of how protocols of research using natural ingredients are performed, it is still important to find specific compounds responsible for CVD-related mechanisms. The studies that described the MO potency in CVD concluded that quercetin, N,α-L-rhamnopyranosyl vincosamide, and isothiocyanate are the promising compounds for further study.

Quercetin, one of the typical active substances in MO, is a natural flavonoid found in many fruits and vegetables. Previous studies have shown the beneficial effect of quercetin in treating atherosclerosis events *via* reducing oxidative stress, lipid metabolism modulation, and as anti-inflammatory (Deng et al., 2020). In reducing oxidative stress, quercetin can directly act as an antioxidant by inhibiting activation of NADPH oxidase and p47phox expression (Xiao et al., 2017) and increase the production and activity of antioxidants, for example, as enzyme heme oxygenase-1 (HO-1) (Luo et al., 2020), vascular endothelial NO synthase (Loke et al., 2010), and glutamate–cysteine ligase (Li et al., 2016). In addition, quercetin attenuates the pro-oxidants, such as MDA and superoxide (Loke et al., 2010). Quercetin can also mitigate

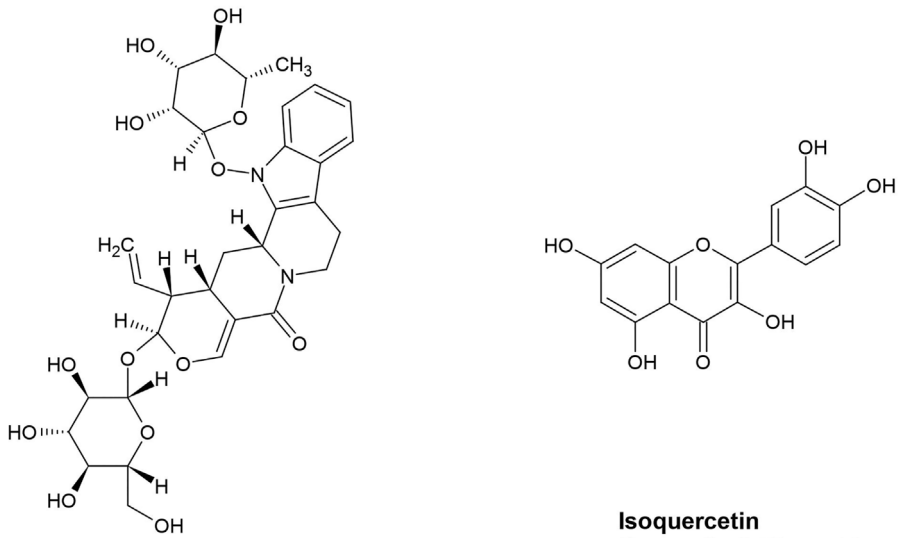

N, α–L-Rhamnopyranosyl vincosamide

Isoquercetin
Quercetin-3-Glucoside
Quercetin-3-O-Glucoside

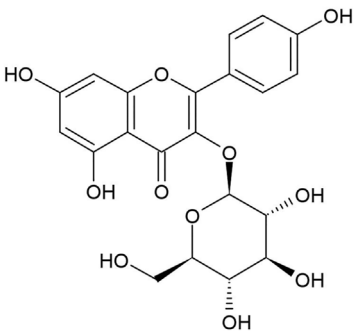

Kaempferol-3-O-glucoside

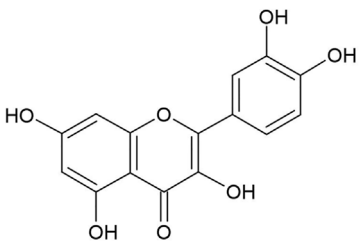

Quercetin

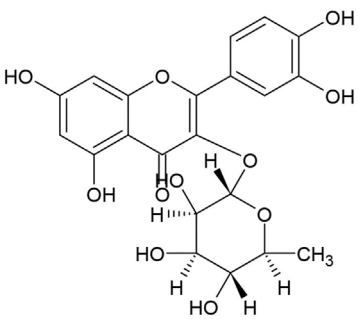

Quercetrin

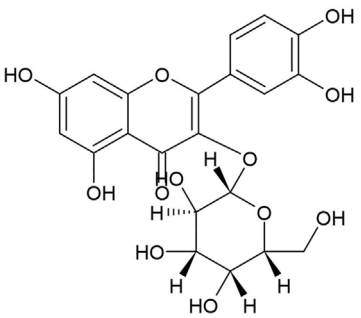

Hyperoside

FIGURE 2 | Chemical structures of prominent *Moringa oleifera* bioactive compounds that have role in combating CVDs.

atherosclerotic inflammation through modulating galectin-3 (Gal-3)-pyrin domain-containing 3 (NLRP3) (Li et al., 2021), and 5′adenosine monophosphate-activated protein kinase (AMPK)/sirtuin 1 (SIRT1)/NF-κB signaling pathway (Zhang et al., 2020) inhibits lipid droplet formation by regulating proprotein convertase subtilisin/kexin type 9 (PCSK9), ATP-binding cassette sub-family G member 1 (ABCG1), and ATP-binding cassette transporter 1

TABLE 3 | Experimental approach of *Moringa oleifera* in CVD field.

No	MO parts	Bioactive compound	Dosage	Duration	RoA	References
1	Methanolic extract of leaves	Carbohydrates, alkaloids, tannins, saponins, flavonoids, triterpenoids, and steroids	200 and 400 mg/kg/day	49 days	Oral	Bais et al. (2014)
2	Methanolic extract of leaves	Not available	200 and 400 mg/kg/day	3 weeks (after HFD feeding)	Oral	Madkhali et al. (2019)
3	Ethanolic extract of leaves	Colorimetric assay: Polyphenolic (6.98 g of gallic acid equivalent/ 100 g), flavonoids (2.85 g of rutin equivalent/100 g)	600 mg/kg	12 weeks	Oral	Metwally et al. (2017)
4	Methanolic extract of leaves	HPLC-ESI-MS analysis: hyperoside (316,822 μg/g) and quercetrin (204,685 μg/g)	200 and 400 mg/kg BW	12 weeks	Oral	Mabrouki et al. (2020)
5	Ethanolic extract of leaves of in 60% of herbal extract combination comprised of MO, Murraya koenigii, Curcuma longa (Laila Nutraceuticals Ltd.)	HPLC analysis: 0.2% Quercetin-3-O-glucoside, 0.1% Mahanine, 0.7% Curcumin	100 and 250 mg/kg/day	28 days	Oral	Kundimi et al. (2020)
6	Ethanolic extract of leaves of in 60% of herbal extract combination comprised of MO, Murraya koenigii, Curcuma longa (Laila Nutraceuticals Ltd.)	HPLC analysis: 0.2% Quercetin-3-O-glucoside, 0.1% Mahanine, 0.7% Curcumin	50 μg/ml (*in vitro*)* 900 mg/day (human study)8#	8 weeks (human study)* 16 weeks (human study)#	Oral (human study)*#	*Sengupta et al. (2012) #Dixit et al. (2018)
7	Leave powder	HPLC analysis: quercetin-3-glycoside [1,494.2 μmol/100 g dry weight (dw)], rutin (1,446.6 μmol/ 100 g dw), kaempferol glycosides (394.4 μmol/100 g dw), and chlorogenic acid (134.5 μmol/ 100 g dw)	200 mg/kg	Single dose, examined 10, 20, 30, 45, 60, 90, and 120 min after administration	Oral	Ndong et al. (2007)
8	Seed powder	Not available	50 and 100 mg/kg	4 weeks	Oral	Al-Malki and Rabey (2015)
9	Aqueous extract of leaves	Not available	200 mg/kg (for OGTT model) 300 mg/kg (for diabetic model)	21 days	Oral	Jaiswal et al. (2009)
10	Ethanolic extract of leaves	Not available	500 mg/kg	Single dose, examined after 30, 90, and 120 min after glucose gavage	Oral	Azad et al. (2017)
11	Methanolic extract of leaves	Not available	250 mg/kg	6 weeks	Oral	Omodanisi et al. (2017)
12	Methanolic extract of leaves	Qualitative methods: saponin, flavonoids, steroids, phenol, glycosides, and tannins Quantitative methods: total phenolic and total flavonoid	300 and 600 mg/kg	6 weeks	Oral	Olayaki et al. (2015)
13	Pure compounds from root and stem bark	4-hydroxyphenylacetonitrite (roots), fluorine opyrazine, methyl-4-hydroxybenzoate (roots), and vanillin (stem barks)	*In vitro*: 200 μm *In vivo*: 25 mg/kg	Right after stimulated with glucose Examine 0,1, 2, and 3 h after gavage	Islet pankreas Oral	Hafizur et al. (2018)
14	Leaves	Not available	4 g	Single dose	Oral	Anthanont et al. (2016)
15	Leaves	Prosky method: total fiber (32.8 ± 0.5 g/100 g), soluble fiber (5.7 ± 0.1 g/100 g), and insoluble fiber (27.1 ± 0.2 g/100 g) UV-Vis spectrophotometry: total polyphenols (23.91 ± 0.2 mg GAE/g), total glucosinolates (21.22 ± 3.7 mg SE/g), and total saponins (16.92 ± 0.6 mg OAE/g)	20 g	Single dose	Oral	Leone et al. (2018)

(Continued on following page)

TABLE 3 | (*Continued*) Experimental approach of *Moringa oleifera* in CVD field.

No	MO parts	Bioactive compound	Dosage	Duration	RoA	References
16	Aqueous extract of leaves	AAS model-solar 969 unicam series (acetylene flame): potassium (1,324 mg/100 g), calcium (2,003 mg/100 g)	28.5, 57, and 85.7 mg/kg	Single dose	Oral	George et al. (2018)
17	Leaf juice	Not available	150 ml	Twice daily for 30 days	Oral	Sailesh et al. (2018)
18	Leaf powder	Not available	30 g	60 days	Oral	Fombang et al. (2016)
19	Aqueous extract of leaves	HPLC-DAD-based assay: cathechin, gallic acid, isoquercetin, quercetin, tannic acid, and small amount of apigenin and rutin	MOE (30 and 60 mg/kg/day), Bolus injection of MOE (0.001–3 mg)	3 weeks	Oral, intra-arterial	Aekthammarat et al. (2019)
20	Aqueous extract of leaves	HPLC: (in mg/100 g dry extract): isoquercetin, 81.14; catechin, 76.77; tannic acid, 63.28; gallic acid, 21.23; quercetin, 20.47; apigenin, 4.03; and rutin, 0.11	Doses: 1, 3, 10, and 30 mg/kg of extract cumulative	30 min after administration of L-NAME	Intravenous	Aekthammarat et al. (2020)
21	Petroleum ether (MRP and MRP-1) and dichloromethane extracts (MRDC-IN, MRDC, and MRDC-1) of roots	GC-MS: isocyanate, isothiocyanate, thioureido, pyridine, and sesquiterpene	3 and 30 mg/kg	—	Intravenous with dose increment 60 and 120 s	Sana et al. (2015)
22	Cooked leaves	Not available	120 g of cooked *M. oleifera* leaves	A week	Oral	Chan Sun et al. (2020)
23	Crude methanol extract (ME), Ethyl acetate extracts (EA) of leaves	RP-HPLC: Quercetin-3-O-glucoside and Kaempferol-3-O-glucoside	ME (0.3 g/kg/day), ME (0.01 g/kg/), and EA (0.3 g/kg/day)	49 days: Three weeks after oral administration of L-NAME to mice, five of these animals were randomly selected and treated with ME or EA extracts (0.3 g/kg/day) during 25 days	Oral	Acuram et al. (2019)
24	Seed powder	Not available	750 mg/kg/day	4 weeks	Oral	Randriamboavonjy et al. (2019)
25	Leave extract	N,α-L-rhamnopyranosyl vincosamide (VR)	VR 40 mg/kg BW	7 days	Oral	Panda et al. (2013)
26	Leave extract	N,α-L-rhamnopyranosyl vincosamide (VR)—an indole alkaloid	200, 400, 800, 1,000, and 2,000 µg/ml	2 weeks	Intra-peritoneal	Cheraghi et al. (2017)
27	Butanolic fraction of leaves	HPLC analysis: Quercetin (980.16 µg/g), rutin (370 µg/g), kaempferol (490.5 µg/g), and ellagic acid 120.1 µg/g)	50, 100 and 150 mg/kg/day	28 days	Oral	Panda (2015)
28	Ethanolic extract of leaves	Not available	680 mg/day	4 weeks	Oral	Aniss et al. (2020)
29	Seed powder	Not available	600 mg/day or 900 mg/day	2 weeks prior to surgery and 4 weeks after surgery	Oral	Li et al. (2020)

(ABCAl) (Li et al., 2018). Furthermore, quercetin can ameliorate atherosclerotic lesions by altering the gut microbiota and depressing atherogenic lipid metabolites (Nie et al., 2019).

Alkaloid is a group of pharmacologically active compounds found in medicinal plants that mostly contain of basic nitrogen atoms (Vergara-Jimenez et al., 2017). Alkaloids successfully isolated from MO leaves are pyrrolemarumine 4″-O-α-L-rhamnopyranoside and 4′-hydroxyphenylethanamide (marumosides A and B) from pyrrole class (Sahakitpichan et al., 2011) and N,α-L-rhamnopyranosyl vincosamide from indole class (Panda et al., 2013). Alkaloids possess antioxidant, anticarcinogenic, antiviral, antifungal, and antimicrobial activities (Thawabteh et al., 2019) and also antiapoptotic and anti-inflammatory effects (Shrivastava et al., 2013). Examination using DPPH, $ABTS^{+}$, chelating and reducing power assays has showed antioxidant activity of alkaloids (Liu et al., 2014). In a study using Parkinson's rat models, alkaloid showed the ability to block the release of apoptogenic factors (cytochrome-c, caspase 3, and caspase-9), maintained the ratio of antiapoptotic factor Bcl2 with proapoptogenic factor Bax, and depleted proinflammatory cytokines TNF-α and IL-1ß, which were consistent with its antioxidant properties (Shrivastava et al., 2013). Alkaloids also showed vascular protection effects by significantly decreasing atherosclerotic lesion (Zhang et al., 2018) and caused endothelium relaxation *via* the activation of the potassium channels and reduction of calcium influx (Romero et al., 2019). Total alkaloids of MO leaves showed antihypertensive effect possibly *via* calcium channel blocker activity in isolated frog heart and tenia coli of guinea pig; however, this study did not

TABLE 4 | Functional activities of *Moringa oleifera* in CVD field.

No	Functional activities	Biological model	MO effects	References
1	Treatment of obesity and obesity-related cardiometabolic abnormalities	High-fat diet (HFD)–fed rat model	↓ Body weight (BW), total cholesterol (TC), triglycerides (TG), low density lipoprotein (LDL), and atherogenic index ↑ High density lipoprotein (HDL)	Bais et al. (2014)
		HFD-induced dyslipidemia rat model	↓ BW, Lee Index, BMI, TC, TG, LDL, and VLDL ↑ HDL endothelium-mediated vasodilatation improved architecture of aorta	Madkhali et al. (2019)
		Obese female rats	↓ BW, atherogenic index, insulin resistance, leptin, and resistin ↑ Adiponectin	Metwally et al. (2017)
		HFD-induced obesity rats	↓ BW, TC, TG, LDL, CK-MB, AST, ALT, and lipid peroxidation levels ↑ HDL, SOD, CAT, and GPx activities	Mabrouki et al. (2020)
		Obese rats	↓ BW, total body fat mass, WAT fat mass and cell size, liver weight, hepatic triglycerides, and leptin serum level ↑ Resting energy expenditure (REE), fatty oxidation Browning of WAT ↑ UCP1 ↓ PPARγ, C/EBPα, CD36, and ap-2α, perilipin	Kundimi et al. (2020)
		Overweight/obese adults; 3T3-L1 adipocyte	↓ BW, BMI, TG, and LDL/HDL ratio ↓ Fasting blood glucose ↑ Adiponectin, pref-1 protein ↓ Resistin, PAI-1	Sengupta et al. (2012)
		Overweight/obese adults	↓ BW, BMI, total body fat, waist and hip circumference, and LDL ↑ HDL	Dixit et al. (2018)
		GK and Wistar rats	↓ Fasting blood glucose Improve glucose tolerance	Ndong et al. (2007)
		STZ-induced diabetic rats	↓ Fasting blood glucose and HbA1C ↓ IL-6 and lipid peroxidase	Al-Malki and Rabey (2015)
		OGTT and diabetic rat model	↓ Fasting blood glucose and post-prandial blood glucose	Jaiswal et al. (2009)
		Type 2 diabetic rats	↓ Blood glucose Improve glucose tolerance ↓ Intestinal glucose absorption	Azad et al. (2017)
		STZ-induced diabetic rats	↓ Blood glucose	Omodanisi et al. (2017)
		Diabetic rats	↓ Blood glucose Improve glucose tolerance ↑ Plasma insulin and glycogen synthase activity	Olayaki et al. (2015)
		Diabetic mice	Insulin secretory activity of islet pancreas Improve β-cell function of the pancreas ↓ Blood glucose ↑ Plasma insulin	Hafizur et al. (2018)
		Healthy subjects	↑ Plasma insulin	Anthanont et al. (2016)
		Diabetic subjects	Earlier peak of post-prandial glucose response Lower mean glycemic meal response α-amylase inhibitory activity	Leone et al. (2018)
2	Natural vasodilator and improve endothelial dysfunctions	Nω-nitro-L-arginine-methyl ester (L-NAME)–induced high blood pressure in rats	↓BP, HR, vascular O_2^- production, and MDA level in plasma and thoracic aorta ↑SOD and CAT dose-dependent vasorelaxation in endothelium of mesenteric arterial beds	Aekthammarat et al. (2019)
		Rats that administered with L-NAME *via* catheter	↓BP possibly by activating eNOS *via* NOS-sGC dependent signaling	Aekthammarat et al. (2020)
		Normotensive rats	↓ Mean arterial blood pressure (MABP)	Sana et al. (2015)
		Healthy human	↓2 h postprandial blood pressure	Chan Sun et al. (2020)
		Normotensive adults	↓ BP and intraocular BP	George et al. (2018)
		Stage-1 hypertension subjects	↓ Systolic blood pressure (SBP) and diastolic blood pressure (DBP)	Sailesh et al. (2018)
		Obese hypertensive individual	↓ BMI, SBP, and DBP ↑ Urine frequency	Fombang et al. (2016)
		Nω-nitro-L-arginine methyl ester (L-NAME)–induced high blood pressure in rats	↓ SBP ACE inhibitory activity	Acuram et al. (2019)

(Continued on following page)

TABLE 4 | (*Continued*) Functional activities of *Moringa oleifera* in CVD field.

No	Functional activities	Biological model	MO effects	References
		Middle-age Wistar rats and young Wistar rats	Improved endothelium relaxation ↑ Akt signaling and endothelial NO synthase ↓ Arginase-1	Randriamboavonjy et al. (2019)
3	Ameliorative effects in cardiac toxicity/ cardiac infarction	Isoproterenol (ISO)–induced cardiac toxicity rat model	Inhibited ST-segment elevation and normalized HR ↓ Serum cTnT, CK-MB, LDH and SGPT, MDA, and LOOH ↑ SOD. CAT, GPx, and GSH	Panda et al. (2013)
		Doxorubicin-induced cardiac toxicity rats	↓ MDA level and mRNA level of cardiac hypertrophy markers (ANP, BNP, and β-MHC) ↑ GSH and SOD	Cheraghi et al. (2017)
		Isoproterenol (ISO)–induced cardiotoxicity rat model	↓ MDA, LDH, CK-MB, and cTnT ↑ SOD, CAT, GPx, and total GSH	Panda (2015)
		Benzene-induced leukemia rat model	↓ MDA ↑ GSH and GPx ↓ TNF-α, NF-κB, and MCP-1 ↓ p53 and caspase 3 ↑ Bcl2 ↓ cardiac ɤ-H2AX and ET-1	Aniss et al. (2020)
		Myocardial infarction (MI) mouse model by surgery	Higher survival rate ↑ LVEF and LVFS ↓ Infarct size and fibrotic scarring, apoptotic markers Bax, and cytochrome-c ↑ Bcl2 ↓ Expression of iNOS ↓ The expression of gp91phox ↓ NO level	Li et al. (2020)

confirm the specific alkaloid, which was responsible for the activity (Dangi et al., 2002). To the best of our knowledge, N,α-L-rhamnopyranosyl vincosamide is the first MO specific alkaloid that has been examined for its ability to counter cardiac damage. Further study is needed to explore any MO specific alkaloids for their CVD-related activity.

The underlying pathophysiology of CVD such as obesity, hypertension, and atherosclerosis occurred because of inflammation, with its wide array of cytokines secreted by immune cells (Tran et al., 2021). MO leaves extract could modulate humoral and cellular immunity in rats and mice (Gupta et al., 2010; Sudha et al., 2010). One of the interesting phytochemical compounds in MO leaves extract is isothiocyanates. Isothiocyanates formed by enzymatic hydrolysis of the MO glucosinolate (Mbikay, 2012; Waterman et al., 2014), and it has been shown to have strong anti-inflammatory properties. A study conducted using RAW 264.7 macrophage cell model of LPS-induced inflammation showed that MO isothiocyanates reduced iNOS and IL-1ß mRNA expression and inhibited the production of NO (Mbikay, 2012). Similarly, a reduction in gene expression of *iNOS*, *IL-1β*, and *IL-6* without affecting cell viability was reported (Jaja-Chimedza et al., 2017). An *in vitro* study reported a dose-dependent reduction in iNOS protein expression following incubation for 18 h of RAW 264.7 lipopolysaccharide-activated cells treated with different isothiocyanate concentrations from MO fruits (Cheenpracha et al., 2010). The MO anti-inflammatory activity was also examined using RAW 264.7 mouse macrophage cells, and it showed a reduction in iNOS expression, as well as a decrease in cyclooxygenase-2 (COX-2) (Park et al., 2011). These reported studies demonstrated that MO has potential in treating inflammatory-related diseases, including CVD.

6 LIMITATIONS AND RECOMMENDATION FOR FUTURE RESEARCH

All the studies mentioned above are conducted in different sample preparation, such as isolated metabolites, whole extracts, and pure MO parts, and have notable different dose range tested. There are also significant variations in the nutritional value and phytochemical content of MO. They depend on the genetic background, location, climate, and environmental factors (Valdez-Solana et al., 2015; Sultana, 2020). Furthermore, it is necessary to choose the extraction method and the solvent use because it will produce different quantity of bioactive compounds and produce different free radical abilities. For example, a study conducted on MO leaves revealed that extracts with ethanol and methanol solvents produced higher antioxidant activity than using water extract (Nobossé et al., 2018). Therefore, extraction technique must also be chosen to find suitable extract with high antioxidant activity. The identification of the plant and the use of full botanical taxonomic name are also important, especially in experimental study, to avoid inconsistency between studies.

MO is traditionally consumed in raw materials, such as fresh leaves or leaves powder, manufactured commercially by the community (Syamsunarno et al., 2021). These preparations are also applied in various human studies and become a challenge in

implementing studies that use oral administration methods due to the unpleasant odor and intolerable taste of MO leaves. The acceptability test of the MO preparation and choosing aqueous extract ("tea") or other odor and flavor masking methods are needed due to the subjects' convenience and relate to dose determination (Leone et al., 2018; Fahey et al., 2019), without omitting the benefits of the compounds. The use of MO alcoholic extracts is still in the scope of *in vitro* or *in vivo* studies, so the utilization of these extracts in human studies must undergo strict supervision due to possible undesired effects.

Nanotechnology drug delivery becomes a new promising formulation in CVD studies due to better pharmacokinetic profiles, biocompatible, low toxicity and antigenicity, and more efficiency to target mitochondria dysfunctions (Forini et al., 2020). However, this technology is still limited to preclinical studies. Surprisingly, this drug-carrier technology application was found in some MO studies. Application of magnetic hydrogel nanocomposite for delivering MO bioactive compound showed a higher pharmacokinetic profile than that of the extract alone (Cheraghi et al., 2017). An *in vitro* study that examined the cytotoxicity effect of MO against colon cancer found that incorporation of MO leaves extract with silver nanoparticles showed higher antioxidant activity compared to that of before the incorporation. This is possibly related to the ability of the preparation to increase total polyphenolic compounds (Shousha et al., 2019). Another previous study found that nano-formulations in MO seed oil have gained a higher cytotoxicity effect on various cancer cell lines through mitochondrial-mediated apoptosis with minimal harmful effects compared to that of the free seed oil (Abd-Rabou et al., 2016). Thus, it is highly expected that there will be MO preparation using nano formulations applied in human studies related to CVD management purposes.

Other limitation is not all studies performed toxicity analysis of MO extract/compound they used (Cheraghi et al., 2017; Aekthammarat et al., 2020). One review article analyzed the MO leaves' efficacy and safety. MO leaves including the extracts has high rank of safety at the doses utilized based on various *in vitro*, *in vivo*, and human studies (Stohs and Hartman, 2015). Nevertheless, preliminary studies that find the right non-toxic dosage is important, whether *in vitro* or *in vivo* as screening for study feasibility, but still, further human study is required to determine the dose safety and efficacy (Stohs and Hartman, 2015).

Apart of the ability of MO bioactive compounds to combat CVDs, MO seed oil also has potency to be investigated for further study due to its high PUFA. MO oil contains approximately 5.6–6.2% behenic acid (Nadeem and Imran, 2016). A previous study showed that daily fat supplement consisted of behenic acid from behenate oil for 1 week tended to raise total cholesterol and triacylglycerol plasma of seven mildly hypercholesterolemic men compared to other vegetable oils (Cater and Denke, 2001). This fact led to inconsideration of behenic acid for treating CVD's risk factors. Contrary, more recent findings from a cohort study involving 2,680 older adults showed that a higher level of circulating plasma phospholipid very long saturated fatty acid (VLSFA) behenic acid was associated with a 15% significant reduction in aging-related CVD events, namely, MI, heart failure, stroke, transient ischemic attack, and claudication possibly by lowering endogenous levels of shorter-chain ceramides (Bockus et al., 2021).

The traditional application of MO, such as blood pressure and glucose-lowering agents, which were mentioned earlier, has been proven through many studies. However, *in vitro* findings must be confirmed by sufficient *in vivo* and human studies, especially in clinical settings. In conclusion, there are several mechanisms of MO associated with CVD. MO has the ability to improve cardiometabolic abnormalities, hypertension condition, and endothelial dysfunctions, and, in animal model, it has a beneficial effect in cardiotoxicity condition/MI. Further studies are still needed to complete the limitations found in previous studies.

AUTHOR CONTRIBUTIONS

FA and MS made concept and design. FA dan NA made literature searching and manuscript writing. MP and MS provided helpful advice, organized the work, and revised the manuscript.

FUNDING

This work was supported by University Research Grant no: 1827/UN6.3.1/LT/2020 from the Ministry of Research and Technology of the Republic of Indonesia.

REFERENCES

Abd El-Hack, M. E., Alagawany, M., Elrys, A. S., Desoky, E. S. M., Tolba, H. M. N., Elnahal, A. S. M., et al. (2018). Effect of Forage Moringa Oleifera L. (Moringa) on Animal Health and Nutrition and its Beneficial Applications in Soil, Plants and Water Purification. *Agriculture (Switzerland)* 8 (9), 1–22. doi:10.3390/agriculture8090145

Abd-Rabou, A. A., A Zoheir, Kh. M., Kishta, M. S., Shalby, A. B., and Ezzo, M. I. (2016). Nano-micelle of Moringa Oleifera Seed Oil Triggers Mitochondrial Cancer Cell Apoptosis. *Asian Pac. J. Cancer Prev.* 17 (11), 4929–4933. doi:10.22034/APJCP.2016.17.11.4929

Acuram, L. K., and Chichioco Hernandez, C. L. (2019). Anti-hypertensive Effect of Moringa Oleifera Lam. *Cogent Biol.* 5 (1), 1596526. doi:10.1080/23312025.2019.1596526

Aekthammarat, D., Pannangpetch, P., and Tangsucharit, P. (2019). Moringa Oleifera Leaf Extract Lowers High Blood Pressure by Alleviating Vascular Dysfunction and Decreasing Oxidative Stress in L-NAME Hypertensive Rats. *Phytomedicine* 54, 9–16. doi:10.1016/j.phymed.2018.10.023

Aekthammarat, D., Tangsucharit, P., Pannangpetch, P., Sriwantana, T., and Sibmooh, N. (2020). Moringa Oleifera Leaf Extract Enhances Endothelial Nitric Oxide Production Leading to Relaxation of Resistance Artery and Lowering of Arterial Blood Pressure. *Biomed. Pharmacother.* 130 (May), 110605. doi:10.1016/j.biopha.2020.110605

Ajibade, T. O., Olayemi, F. O., and Arowolo, R. O. A. (2012). The Haematological and Biochemical Effects of Methanol Extract of the Seeds of Moringa Oleifera in Rats. *J. Med. Plants Res.* 6 (4), 615–621. doi:10.5897/jmpr11.1258

Al-Malki, A. L., and El Rabey, H. A. (2015). The Antidiabetic Effect of Low Doses ofMoringa oleiferaLam. Seeds on Streptozotocin Induced Diabetes and Diabetic

Nephropathy in Male Rats. *Biomed. Res. Int.* 2015, 1–13. doi:10.1155/2015/381040

Aniss, N. N., Rahman, Y. H. A., and Zaazaa, A. M. (2020). Cardioprotective Effect of Moringa Oleifera against Doxorubicin Cardiotoxicity in Leukemia Rat Model. *Int. J. Pharm. Phytopharmacological Res.* 10 (2), 148–161.

Anthanont, P., Lumlerdkij, N., Akarasereenont, P., Vannasaeng, S., and Sriwijitkamol, A. (2016). Moringa Oleifera Leaf Increases Insulin Secretion after Single Dose Administration: A Preliminary Study in Healthy Subjects. *J. Med. Assoc. Thai* 99 (3), 308–313.

Awodele, O., Oreagba, I. A., Odoma, S., da Silva, J. A., and Osunkalu, V. O. (2012). Toxicological Evaluation of the Aqueous Leaf Extract of Moringa Oleifera Lam. (Moringaceae). *J. Ethnopharmacol* 139 (2), 330–336. doi:10.1016/j.jep.2011.10.008

Azad, S. B., Ansari, P., Azam, S., Hossain, S. M., Shahid, M. I., Hasan, M., et al. (2017). Anti-hyperglycaemic Activity of Moringa Oleifera Is Partly Mediated by Carbohydrase Inhibition and Glucose-Fibre Binding. *Biosci. Rep.* 37 (3), 1–11. doi:10.1042/BSR20170059

Bais, S., Singh, G. S., and Sharma, R. (2014). Antiobesity and Hypolipidemic Activity of Moringa Oleifera Leaves against High Fat Diet-Induced Obesity in Rats. *Adv. Biol.* 2014, 1–9. doi:10.1155/2014/162914

Baiyeri, P., and Akinnagbe, O. M. (2013). Ethno-medicinal and Culinary Uses of Moringa Oleifera Lam. In Nigeria. *J. Med. Plants Res.* 7 (13), 799–804. doi:10.5897/JMPR12.1221

Barbagallo, I., Vanella, L., Distefano, A., Nicolosi, D., Maravigna, A., Lazzarino, G., et al. (2016). Moringa Oleifera Lam. Improves Lipid Metabolism during Adipogenic Differentiation of Human Stem Cells. *Eur. Rev. Med. Pharmacol. Sci.* 20 (24), 5223–5232.

Bockus, L. B., Biggs, M. L., Lai, H. T. M., De Olivera Otto, M. C., Fretts, A. M., McKnight, B., et al. (2021). Assessment of Plasma Phospholipid Very-Long-Chain Saturated Fatty Acid Levels and Healthy Aging. *JAMA Netw. Open* 4 (8), 1–12. doi:10.1001/jamanetworkopen.2021.20616

Borgonovo, G., De Petrocellis, L., Schiano Moriello, A., Bertoli, S., Leone, A., Battezzati, A., et al. (2020). Moringin, a Stable Isothiocyanate from Moringa Oleifera, Activates the Somatosensory and Pain Receptor TRPA1 Channel *In Vitro*. *Molecules* 25 (4), 1–12. doi:10.3390/molecules25040976

Brilhante, R. S. N., Sales, J. A., Pereira, V. S., Castelo-Branco, D. S. C. M., Cordeiro, R. A., de Souza Sampaio, C. M., et al. (2017). Research Advances on the Multiple Uses of Moringa Oleifera: A Sustainable Alternative for Socially Neglected Population. *Asian Pac. J. Trop. Med.* 10 (7), 621–630. doi:10.1016/j.apjtm.2017.07.002

Burghardt, P. R., Kemmerer, E. S., Buck, B. J., Osetek, A. J., Yan, C., Koch, L. G., et al. (2010). Dietary N-3:n-6 Fatty Acid Ratios Differentially Influence Hormonal Signature in a Rodent Model of Metabolic Syndrome Relative to Healthy Controls. *Nutr. Metab. (Lond)* 7, 53–56. doi:10.1186/1743-7075-7-53

Çakmak, H. A., and Demir, M. (2020). Microrna and Cardiovascular Diseases. *Balkan Med. J.* 37 (2), 60–71. doi:10.4274/balkanmedj.galenos.2020.2020.1.94

Cater, N. B., and Denke, M. A. (2001). Behenic Acid Is a Cholesterol-Raising Saturated Fatty Acid in Humans. *Am. J. Clin. Nutr.* 73 (1), 41–44. doi:10.1093/ajcn/73.1.41

Chan Sun, M., Ruhomally, Z. B., Boojhawon, R., and Neergheen-Bhujun, V. S. (2020). Consumption of Moringa Oleifera Lam Leaves Lowers Postprandial Blood Pressure. *J. Am. Coll. Nutr.* 39 (1), 54–62. doi:10.1080/07315724.2019.1608602

Cheenpracha, S., Park, E. J., Yoshida, W. Y., Barit, C., Wall, M., Pezzuto, J. M., et al. (2010). Potential Anti-inflammatory Phenolic Glycosides from the Medicinal Plant Moringa Oleifera Fruits. *Bioorg. Med. Chem.* 18 (17), 6598–6602. doi:10.1016/j.bmc.2010.03.057

Cheraghi, M., Namdari, M., Daraee, H., and Negahdari, B. (2017). Cardioprotective Effect of Magnetic Hydrogel Nanocomposite Loaded N,α-L-rhamnopyranosyl Vincosamide Isolated from Moringa Oleifera Leaves against Doxorubicin-Induced Cardiac Toxicity in Rats: *In Vitro* and *In Vivo* Studies. *J. Microencapsul* 34 (4), 335–341. doi:10.1080/02652048.2017.1311955

Dangi, S. Y., Jolly, C. I., and Narayanan, S. (2002). Antihypertensive Activity of the Total Alkaloids from the Leaves of Moringa Oleifera. *Pharm. Biol.* 40 (2), 144–148. doi:10.1076/phbi.40.2.144.5847

Das, A. J. (2012). Moringa oleifera(Lamm.): A Plant with Immense Importance. *J. Biologically Active Prod. Nat.* 2 (5), 307–315. doi:10.1080/22311866.2012.10719139

Deng, Q., Li, X. X., Fang, Y., Chen, X., and Xue, J. (2020). Therapeutic Potential of Quercetin as an Antiatherosclerotic Agent in Atherosclerotic Cardiovascular Disease: A Review. *Evid. Based Complement. Alternat Med.* 2020, 5926381. doi:10.1155/2020/5926381

Dixit, K., Kamath, D. V., Alluri, K. V., and Davis, B. A. (2018). Efficacy of a Novel Herbal Formulation for Weight Loss Demonstrated in a 16-week Randomized, Double-Blind, Placebo-Controlled Clinical Trial with Healthy Overweight Adults. *Diabetes Obes. Metab.* 20 (11), 2633–2641. doi:10.1111/dom.13443

El - Massry, F. H. M., Mossa, M. E., and Youssef, S. M. (2013). Moringa Oleifera Plant "Value and Utilization in Food Processing ". *Egypt. J. Agric. Res.* 91 (4), 1597–1909. doi:10.21608/ejar.2013.166383

Fahey, J. W., Wade, K. L., Stephenson, K. K., Shi, Y., Liu, H., Panjwani, A. A., et al. (2019). A Strategy to Deliver Precise Oral Doses of the Glucosinolates or Isothiocyanates from Moringa Oleifera Leaves for Use in Clinical Studies. *Nutrients* 11 (7), 1–14. doi:10.3390/nu11071547

Favero, G., Paganelli, C., Buffoli, B., Rodella, L. F., and Rezzani, R. (2014). Endothelium and its Alterations in Cardiovascular Diseases: Life Style Intervention. *Biomed. Res. Int.* 2014, 801896. doi:10.1155/2014/801896

Fombang, N. E., BlaiseBouba, B., and Ngaruoa (2016). Management of Hypertension in Normal and Obese Hypertensive Patients through Supplementation with Moringa Oleifera Lam Leaf Powder. *Indian J. Nutr.* 3 (2), 3–7. https://www.opensciencepublications.com/fulltextarticles/IJN-2395-2326-3-143.html.

Forini, F., Canale, P., Nicolini, G., and Iervasi, G. (2020). Mitochondria-targeted Drug Delivery in Cardiovascular Disease: A Long Road to Nano-Cardio Medicine. *Pharmaceutics* 12 (11), 1–24. doi:10.3390/pharmaceutics12111122

George, G. O., Ajayi, O. B., and Oyemike, A. A. (2018). Effect of Moringa Oleifera Leaf Aqueous Extract on Intraocular and Blood Pressure of Normotensive Adults in Edo State, Nigeria. *J. Niger. Optometric Assoc.* 20 (2), 75–81.

Gopalakrishnan, L., Doriya, K., and Kumar, D. S. (2016). Moringa Oleifera: A Review on Nutritive Importance and its Medicinal Application. *Food Sci. Hum. Wellness* 5 (2), 49–56. doi:10.1016/j.fshw.2016.04.001

Gupta, A., Gautam, M. K., Singh, R. K., Kumar, M. V., Rao, Ch. V., Goel, R. K., et al. (2010). Immunomodulatory Effect of Moringa Oleifera Lam. Extract on Cyclophosphamide Induced Toxicity in Mice. *Indian J. Exp. Biol.* 48 (11), 1157–1160.

Hafizur, R. M., Maryam, K., Hameed, A., zaheer, L., Bano, S., Sumbul, S., et al. (2018). Insulin Releasing Effect of Some Pure Compounds from Moringa Oleifera on Mice Islets. *Med. Chem. Res.*, 27, 1408–1418. doi:10.1007/s00044-018-2157-1

Idohou-Dossou, N., Diouf, A., Gueye, A., Guiro, A., and Wade, S. (2011). Impact of Daily Consumption of Moringa (*Moringa Oleifera*) Dry Leaf Powder on Iron Status of Senegalese Lactating Women. *Afr. J. Food Agric. Nutr. Development*, 11. doi:10.4314/ajfand.v11i4.69176

Jaiswal, D., Kumar Rai, P., Kumar, A., Mehta, S., and Watal, G. (2009). Effect of Moringa Oleifera Lam. Leaves Aqueous Extract Therapy on Hyperglycemic Rats. *J. Ethnopharmacol* 123 (3), 392–396. doi:10.1016/j.jep.2009.03.036

Jaja-Chimedza, A., Graf, B. L., Simmler, C., Kim, Y., Kuhn, P., Pauli, G. F., et al. (2017). Biochemical Characterization and Anti-inflammatory Properties of an Isothiocyanate-Enriched Moringa (Moringa Oleifera) Seed Extract. *PLoS ONE* 12 (8), e0182658–21. doi:10.1371/journal.pone.0182658

Kang, H. W., Lee, S. G., Otieno, D., and Ha, K. (2018). Flavonoids, Potential Bioactive Compounds, and Non-shivering Thermogenesis. *Nutrients* 10 (9), 1–25. doi:10.3390/nu10091168

Kasolo, J. N., Bimenya, G. S., Ojok, L., and Ogwal-Okeng, J. W. (2012). Sub-acute Toxicity Evaluation of Moringa Oleifera Leaves Aqueous and Ethanol Extracts in Swiss Albino Rats. *Int. J. Med. Plant Res.* 1 (6), 75–81.

Kasote, D. M., Katyare, S. S., Hegde, M. V., and Bae, H. (2015). Significance of Antioxidant Potential of Plants and its Relevance to Therapeutic Applications. *Int. J. Biol. Sci.* 11 (8), 982–991. doi:10.7150/ijbs.12096

Khalid Abbas, R., Elsharbasy, F. S., and Fadlelmula, A. A. (2018). Nutritional Values of Moringa Oleifera, Total Protein, Amino Acid, Vitamins, Minerals, Carbohydrates, Total Fat and Crude Fiber, under the Semi-arid Conditions of Sudan. *J. Microb. Biochem. Technology* 10 (2), 56–58. doi:10.4172/1948-5948.1000396

Khalil, S. R., Abdel-Motal, S. M., Abd-Elsalam, M., Abd El-Hameed, N. E., and Awad, A. (2020). Restoring Strategy of Ethanolic Extract of Moringa Oleifera

Leaves against Tilmicosin-Induced Cardiac Injury in Rats: Targeting Cell Apoptosis-Mediated Pathways. *Gene* 730, 144272. doi:10.1016/j.gene.2019.144272

Kundimi, S., Kavungala, K. C., Sinha, S., Tayi, V. N. R., Kundurthi, N. R., Golakoti, T., et al. (2020). Combined Extracts of Moringa Oleifera, Murraya Koeingii Leaves, and Curcuma Longa Rhizome Increases Energy Expenditure and Controls Obesity in High-Fat Diet-Fed Rats. *Lipids Health Dis.* 19 (1), 1–13. doi:10.1186/s12944-020-01376-7

Lalas, S., and Tsaknis, J. (2002). Characterization of Moringa Oleifera Seed Oil Variety "Periyakulam 1". *J. Food Compost. Anal.* 15 (1), 65–77. doi:10.1006/jfca.2001.1042

Lavie, C. J., Arena, R., Alpert, M. A., Milani, R. V., and Ventura, H. O. (2018). Management of Cardiovascular Diseases in Patients with Obesity. *Nat. Rev. Cardiol.* 15 (1), 45–56. doi:10.1038/nrcardio.2017.108

Leone, A., Bertoli, S., Di Lello, S., Bassoli, A., Ravasenghi, S., Borgonovo, G., et al. (2018). Effect of Moringa Oleifera Leaf Powder on Postprandial Blood Glucose Response: *In Vivo* Study on Saharawi People Living in Refugee Camps. *Nutrients* 10 (10), 1–14. doi:10.3390/nu10101494

Leone, A., Spada, A., Battezzati, A., Schiraldi, A., Aristil, J., and Bertoli, S. (2015). Cultivation, Genetic, Ethnopharmacology, Phytochemistry and Pharmacology of Moringa Oleifera Leaves: An Overview. *Int. J. Mol. Sci.* 16 (6), 12791–12835. doi:10.3390/ijms160612791

Leone, A., Spada, A., Battezzati, A., Schiraldi, A., Aristil, J., and Bertoli, S. (2016). Moringa Oleifera Seeds and Oil: Characteristics and Uses for Human Health. *Int. J. Mol. Sci.* 17 (12), 1–14. doi:10.3390/ijms17122141

Li, C., Zhang, W. J., Choi, J., and Frei, B. (2016). Quercetin Affects Glutathione Levels and Redox Ratio in Human Aortic Endothelial Cells Not through Oxidation but Formation and Cellular export of Quercetin-Glutathione Conjugates and Upregulation of Glutamate-Cysteine Ligase. *Redox Biol.* 9, 220–228. doi:10.1016/j.redox.2016.08.012

Li, H., Xiao, L., He, H., Zeng, H., Liu, J., Jiang, C., et al. (2021). Quercetin Attenuates Atherosclerotic Inflammation by Inhibiting Gal-3-NLRP3 Signaling Pathway. *Mol. Nutr. Food Res.* 65, e2000746. doi:10.1002/mnfr.202000746

Li, S., Cao, H., Shen, D., Jia, Q., Chen, C., and Xing, S. L. (2018). Quercetin Protects against ox-LDL-induced I-njury via R-egulation of ABCAl, LXR-α and PCSK9 in RAW264.7 M-acrophages. *Mol. Med. Rep.* 18 (1), 799–806. doi:10.3892/mmr.2018.9048

Li, W., Sun, C., Deng, W., Liu, Y., Adu-Frimpong, M., Yu, J., et al. (2019). Pharmacokinetic of Gastrodigenin Rhamnopyranoside from Moringa Seeds in Rodents. *Fitoterapia* 138 (July), 104348. doi:10.1016/j.fitote.2019.104348

Li, Y. J., Ji, Q. Q., Wang, Z., Shen, L. H., and He, B. (2020). Moringa Oleifera Seeds Mitigate Myocardial Injury and Prevent Ventricular Failure Induced by Myocardial Infarction. *Am. J. Transl Res.* 12 (8), 4511–4521.

Liu, C. M., Kao, C. L., Wu, H. M., Li, W. J., Huang, C. T., Li, H. T., et al. (2014). Antioxidant and Anticancer Aporphine Alkaloids from the Leaves of *Nelumbo nucifera* Gaertn. Cv. Rosa-Plena. *Molecules* 19 (11), 17829–17838. doi:10.3390/molecules191117829

Loke, W. M., Proudfoot, J. M., Hodgson, J. M., McKinley, A. J., Hime, N., Magat, M., et al. (2010). Specific Dietary Polyphenols Attenuate Atherosclerosis in Apolipoprotein E-Knockout Mice by Alleviating Inflammation and Endothelial Dysfunction. *Arterioscler Thromb. Vasc. Biol.* 30 (4), 749–757. doi:10.1161/ATVBAHA.109.199687

Luo, M., Tian, R., and Lu, N. (2020). Quercetin Inhibited Endothelial Dysfunction and Atherosclerosis in Apolipoprotein E-Deficient Mice: Critical Roles for NADPH Oxidase and Heme Oxygenase-1. *J. Agric. Food Chem.* 68 (39), 10875–10883. doi:10.1021/acs.jafc.0c03907

Mabrouki, L., Rjeibi, I., Taleb, J., and Zourgui, L. (2020). Cardiac Ameliorative Effect of Moringa Oleifera Leaf Extract in High-Fat Diet-Induced Obesity in Rat Model. *Biomed. Res. Int.* 2020, 6583603. doi:10.1155/2020/6583603

Madi, N., Dany, M., Abdoun, S., and Usta, J. (2016). Moringa Oleifera's Nutritious Aqueous Leaf Extract Has Anticancerous Effects by Compromising Mitochondrial Viability in an ROS-dependent Manner. *J. Am. Coll. Nutr.* 35 (7), 604–613. doi:10.1080/07315724.2015.1080128

Madkhali, H. A., Alharthy, K. M., Asiri, M. A., Ganaie, M. A., Ansari, M. N., Rehman, N. U., et al. (2019). Moringa Oleifera Lam. (Family Moringaceae) Leaf Extract Attenuates High-Fat Diet-Induced Dyslipidemia and Vascular Endothelium Dysfunction in Wistar Albino Rats. *Trop. J. Pharm. Res.* 18 (12), 2597–2604. doi:10.4314/tjpr.v18i12.20

Mayr, F. B., and Jilma, B. (2006). Current Developments in Anti-platelet Therapy. *Wien Med. Wochenschr* 156 (17–18), 472–480. doi:10.1007/s10354-006-0330-5

Mbikay, M. (2012). Therapeutic Potential of Moringa Oleifera Leaves in Chronic Hyperglycemia and Dyslipidemia : a Review. *Front. Pharmacol.* 3, 1–12. doi:10.3389/fphar.2012.00024

Metwally, F. M., Rashad, H. M., Ahmed, H. H., Mahmoud, A. A., Abdol Raouf, E. R., and Abdalla, A. M. (2017). Molecular Mechanisms of the Anti-obesity Potential Effect of Moringa Oleifera in the Experimental Model. *Asian Pac. J. Trop. Biomed.* 7 (3), 214–221. doi:10.1016/j.apjtb.2016.12.007

Nadeem, M., and Imran, M. (2016). Promising Features of Moringa Oleifera Oil: Recent Updates and Perspectives. *Lipids Health Dis.* 15 (1), 212–218. doi:10.1186/s12944-016-0379-0

Ndong, M., Uehara, M., Katsumata, S., and Suzuki, K. (2007). Effects of Oral Administration of Moringa Oleifera Lam on Glucose Tolerance in Goto-Kakizaki and Wistar Rats. *J. Clin. Biochem. Nutr.* 40 (3), 229–233. doi:10.3164/jcbn.40.229

Nie, J., Zhang, L., Zhao, G., and Du, X. (2019). Quercetin Reduces Atherosclerotic Lesions by Altering the Gut Microbiota and Reducing Atherogenic Lipid Metabolites. *J. Appl. Microbiol.* 127 (6), 1824–1834. doi:10.1111/jam.14441

Nobossé, P., Fombang, E. N., and Mbofung, C. M. F. (2018). Effects of Age and Extraction Solvent on Phytochemical Content and Antioxidant Activity of Fresh Moringa Oleifera L. Leaves. *Food Sci. Nutr.* 6 (8), 2188–2198. doi:10.1002/fsn3.783

Nouman, W., Basra, S. M. A., Siddiqui, M. T., Yasmeen, A., Gull, T., and Alcayde, M. A. C. (2014). Potential of Moringa Oleifera L. As Livestock Fodder Crop: A Review. *Turk J. Agric. For.* 38 (1), 1–14. doi:10.3906/tar-1211-66

Nouman, W., Siddiqui, M. T., Basra, S. M. A., Farooq, H., Zubair, M., and Gull, T. (2013). Biomass Production and Nutritional Quality of Moringa Oleifera as a Field Crop. *Turkish J. Agric. For.* 37 (4), 410–419. doi:10.3906/tar-1206-29

Okumu, M., Mbaria, J., Kanja, L., Gakuya, D., Kiama, S., Ochola, F., et al. (2016). Acute Toxicity of the Aqueous-Methanolic Moringa Oleifera (Lam) Leaf Extract on Female Wistar Albino Rats. *Int. J. Basic Clin. Pharmacol.* 5 (5), 1856–1861. doi:10.18203/2319-2003.ijbcp20163153

Olagbemide, P. T., and Philip, C. N. A. (2014). Proximate Analysis and Chemical Composition of Raw and Defatted Moringa Oleifera Kernel. *Adv. Life Sci. Technology* 24, 92–100.

Olayaki, L. A., Irekpita, J. E., Yakubu, M. T., and Ojo, O. O. (2015). Methanolic Extract of Moringa Oleifera Leaves Improves Glucose Tolerance, Glycogen Synthesis and Lipid Metabolism in Alloxan-Induced Diabetic Rats. *J. Basic Clin. Physiol. Pharmacol.* 26 (6), 585–593. doi:10.1515/jbcpp-2014-0129

Omodanisi, E. I., Aboua, G. Y., and Oguntibeju, O. O. (2017). Therapeutic Potentials and Pharmacological Properties of Moringa Oleifera Lam in the Treatment of Diabetes Mellitus and Related Complications. *Trop. J. Pharm. Res.* 16 (7), 1737–1746. doi:10.4314/tjpr.v16i7.35

Paikra, B. K., Dhongade, H. K. J., and Gidwani, B. (2017). Phytochemistry and Pharmacology of Moringa Oleifera Lam. *J. Pharmacopuncture* 20 (3), 194–200. doi:10.3831/KPI10.3831/KPI.2017.20.022

Panda, S. (2015). Butanolic Fraction of Moringa Oleifera Lam. (Moringaceae) Attenuates Isoprotrenol-Induced Cardiac Necrosis and Oxidative Stress in Rats: an EPR Study. *EXCLI J.* 14, 64–74. doi:10.17179/excli2014-431

Panda, S., Kar, A., Sharma, P., and Sharma, A. (2013). Cardioprotective Potential of N,α-L-rhamnopyranosyl Vincosamide, an Indole Alkaloid, Isolated from the Leaves of Moringa Oleifera in Isoproterenol Induced Cardiotoxic Rats: *In Vivo* and *In Vitro* Studies. *Bioorg. Med. Chem. Lett.* 23 (4), 959–962. doi:10.1016/j.bmcl.2012.12.060

Park, E. J., Cheenpracha, S., Chang, L. C., Kondratyuk, T. P., and Pezzuto, J. M. (2011). Inhibition of Lipopolysaccharide-Induced Cyclooxygenase-2 and Inducible Nitric Oxide Synthase Expression by 4-[(2'-O-Acetyl-α-L-Rhamnosyloxy)benzyl]isothiocyanate from Moringa Oleifera. *Nutr. Cancer* 63 (6), 971–982. doi:10.1080/01635581.2011.589960

Randriamboavonjy, J. I., Heurtebise, S., Pacaud, P., Loirand, G., and Tesse, A. (2019). Moringa Oleifera Seeds Improve Aging-Related Endothelial Dysfunction in Wistar Rats. *Oxid Med. Cell Longev* 2019, 2567198. doi:10.1155/2019/2567198

Reddy, Y. R. R., Lokanatha, O., Ratnam, K., Reddy, C. S., Raju, I. N., and Reddy, C. D. (2013). Acute and Sub Acute Toxicity of Moringa Oleifera Stem Bark Extract in Swiss Albino Mice. *Int. J. Life Sci. Biotechnol. Pharma Res.* 2 (4), 73–82.

Rockwood, J. L., Anderson, B. G., and Casamatta, D. A. (2013). Potensial Uses of Moringa Oleifera and an Examination of Antibiotic Efficacy Conferred by M. Oleifera Seed and Leaf Extracts Using Crude Extraction Techniques Available to Underserved Indigenous Populations. *Int. J. Phyotherapy Res.* 3 (2), 61–71.

Romero, F., Palacios, J., Jofré, I., Paz, C., Nwokocha, C. R., Paredes, A., et al. (2019). Aristoteline, an Indole-Alkaloid, Induces Relaxation by Activating Potassium Channels and Blocking Calcium Channels in Isolated Rat Aorta. *Molecules (Basel, Switzerland)*, 24, 2748. doi:10.3390/molecules24152748

Sahakitpichan, P., Mahidol, C., Disadee, W., Ruchirawat, S., and Kanchanapoom, T. (2011). Unusual Glycosides of Pyrrole Alkaloid and 4'-hydroxyphenylethanamide from Leaves of Moringa Oleifera. *Phytochemistry* 72 (8), 791–795. doi:10.1016/j.phytochem.2011.02.021

Sailesh, K. S., Jabir, P. K., Madhusudhan, U., Archana, R., and Mukkadan, J. K. (2018). Effect of Moringa Oliefera Leaves on Blood Pressure in Hypertensive Patients. *Indian J. Clin. Anat. Physiol.* 5 (3), 350–352. doi:10.18231/2394-2126.2018.0081

Saka, W. A., Ayoade, T. E., Akhigbe, T. M., and Akhigbe, R. E. (2020). Moringa Oleifera Seed Oil Partially Abrogates 2,3-dichlorovinyl Dimethyl Phosphate (Dichlorvos)-Induced Cardiac Injury in Rats: Evidence for the Role of Oxidative Stress. *J. Basic Clin. Physiol. Pharmacol. November* 32, 237–246. doi:10.1515/jbcpp-2019-0313

Sana, A., Saleem, R., and Faizi, S. (2015). Hypotensive Activity of Moringa Oleifera Lam (Moringaceae) Root Extracts and its Volatile Constituents. *Trop. J. Pharm. Res.* 14 (5), 823–830. doi:10.4314/tjpr.v14i5.12

Sengupta, K., Mishra, A. T., Rao, M. K., Sarma, K. V., Krishnaraju, A. V., and Trimurtulu, G. (2012). Efficacy and Tolerability of a Novel Herbal Formulation for Weight Management in Obese Subjects: A Randomized Double Blind Placebo Controlled Clinical Study. *Lipids Health Dis.* 11, 1–10. doi:10.1186/1476-511X-11-122

Shaito, A., Thuan, D. T. B., Phu, H. T., Nguyen, T. H. D., Hasan, H., Halabi, S., et al. (2020). Herbal Medicine for Cardiovascular Diseases: Efficacy, Mechanisms, and Safety. *Front. Pharmacol.* 11 (April), 422–432. doi:10.3389/fphar.2020.00422

Shousha, W. G., Aboulthana, W. M., Salama, A. H., Saleh, M. H., and Essawy, E. A. (2019). Evaluation of the Biological Activity of Moringa Oleifera Leaves Extract after Incorporating Silver Nanoparticles, *In Vitro* Study. *Bull. Natl. Res. Centre* 43. doi:10.1186/s42269-019-0221-8

Shrivastava, P., Vaibhav, K., Tabassum, R., Khan, A., Ishrat, T., Khan, M. M., et al. (2013). Anti-apoptotic and Anti-inflammatory Effect of Piperine on 6-OHDA Induced Parkinson's Rat Model. *J. Nutr. Biochem.* 24 (4), 680–687. doi:10.1016/j.jnutbio.2012.03.018

Stevens, C., Ugese, F., Otitoju, G., and Baiyeri, K. (2016). Proximate and Anti-nutritional Composition of Leaves and Seeds of *Moringa Oleifera* in Nigeria: a Comparative Study. *Agro-Sci.* 14 (2), 9. doi:10.4314/as.v14i2.2

Stohs, S. J., and Hartman, M. J. (2015). Review of the Safety and Efficacy of Moringa Oleifera. *Phytother Res.* 29 (6), 796–804. doi:10.1002/ptr.5325

Sudha, P., Asdaq, S. M. B., Dhamingi, S. S., and Chandrakala, G. K. (2010). Immunomodulatory Activity of Methanolic Leaf Extract of Moringa Oleifera in Wistar Albino Rats. *Indian J. Physiol. Pharmacol.* 54 (2), 133–140. doi:10.1515/jbcpp-2014-0104

Sultana, S. (2020). Nutritional and Functional Properties of Moringa Oleifera. *Metabol Open* 8, 100061. doi:10.1016/j.metop.2020.100061

Sun, C., Li, W., Liu, Y., Deng, W., Adu-Frimpong, M., Zhang, H., et al. (2019). *In Vitro*/*In Vivo* Hepatoprotective Properties of 1-O-(4-Hydroxymethylphenyl)-α-L-Rhamnopyranoside from Moringa Oleifera Seeds against Carbon Tetrachloride-Induced Hepatic Injury. *Food Chem. Toxicol.* 131 (May), 110531. doi:10.1016/j.fct.2019.05.039

Swati, S., Kaur Virk, A., Ali, A., Garg, P., Thakur, P., Attri, C., et al. (2018). Moringa Oleifera - a Never Die Tree: an Overview. *Asian J. Pharm. Clin. Res.* 11 (12), 57–65. doi:10.22159/ajpcr.2018.v11i12.28049

Syamsunarno, M. R. A. A., Alia, F., Anggraeni, N., Sumirat, V. A., Praptama, S., and Atik, N. (2021). Ethanol Extract from Moringa Oleifera Leaves Modulates Brown Adipose Tissue and Bone Morphogenetic Protein 7 in High-Fat Diet Mice. *Vet. World* 14 (5), 1234–1240. doi:10.14202/vetworld.2021.1234-1240

Taweerutchana, R., Lumlerdkij, N., Vannasaeng, S., Akarasereenont, P., and Sriwijitkamol, A. (2017). Effect of Moringa Oleifera Leaf Capsules on Glycemic Control in Therapy-Naïve Type 2 Diabetes Patients: A Randomized Placebo Controlled Study. *Evid. Based Complement. Alternat Med.* 2017, 6581390. doi:10.1155/2017/6581390

Thawabteh, A., Juma, S., Bader, M., Karaman, D., Scrano, L., Bufo, S. A., et al. (2019). The Biological Activity of Natural Alkaloids against Herbivores, Cancerous Cells and Pathogens. *Toxins (Basel)* 11 (656), 1–28. doi:10.3390/toxins11110656

Thygesen, K., Alpert, J. S., Jaffe, A. S., Chaitman, B. R., Bax, J. J., Morrow, D. A., et al. (2018). Fourth Universal Definition of Myocardial Infarction (2018). *Circulation* 138 (18), e618–2264. doi:10.1161/CIR.0000000000000617

Tiloke, C., Anand, K., Gengan, R. M., and Chuturgoon, A. A. (2018). Moringa Oleifera and Their Phytonanoparticles: Potential Antiproliferative Agents against Cancer. *Biomed. Pharmacother.* 108 (April), 457–466. doi:10.1016/j.biopha.2018.09.060

Tran, D. M. T., Lekhak, N., Gutierrez, K., and Moonie, S. (2021). Risk Factors Associated with Cardiovascular Disease Among Adult Nevadans. *PLoS ONE* 16 (2 February), 1–11. doi:10.1371/journal.pone.0247105

Tseng, Y. H., Cypess, A. M., and Kahn, C. R. (2010). Cellular Bioenergetics as a Target for Obesity Therapy. *Nat. Rev. Drug Discov.* 9 (6), 465–482. doi:10.1038/nrd3138

Valdez-Solana, M. A., Mejía-García, V. Y., Téllez-Valencia, A., García-Arenas, G., Salas-Pacheco, J., Alba-Romero, J. J., et al. (2015). Nutritional Content and Elemental and Phytochemical Analyses of Moringa Oleifera Grown in Mexico. *J. Chem.* 2015. doi:10.1155/2015/860381

Vergara-Jimenez, M., Almatrafi, M. M., and Fernandez, M. L. (2017). Bioactive Components in Moringa Oleifera Leaves Protect against Chronic Disease. *Antioxidants (Basel)* 6 (4), 91. doi:10.3390/antiox6040091

Waterman, C., Cheng, D. M., Rojas-silva, P., Poulev, A., Dreifus, J., Lila, M. A., et al. (2014). Stable, Water Extractable Isothiocyanates from Moringa Oleifera Leaves Attenuate Inflammation *In Vitro*. *Phytochemistry* 103 (103), 114–122. doi:10.1016/j.phytochem.2014.03.028.Stable

Wood Dos Santos, T., Cristina Pereira, Q., Teixeira, L., Gambero, A., A Villena, J., and Lima Ribeiro, M. (2018). Effects of Polyphenols on Thermogenesis and Mitochondrial Biogenesis. *Int. J. Mol. Sci.* 19, 2757. doi:10.3390/ijms19092757

World Health Organization (2021). *Cardiovascular Diseases* (Issue June). https://www.who.int/news-room/fact-sheets/detail/cardiovascular-diseases-(cvds).

Xiao, L., Liu, L., Guo, X., Zhang, S., Wang, J., Zhou, F., et al. (2017). Quercetin Attenuates High Fat Diet-Induced Atherosclerosis in Apolipoprotein E Knockout Mice: A Critical Role of NADPH Oxidase. *Food Chem. Toxicol.* 105, 22–33. doi:10.1016/j.fct.2017.03.048

Zhang, F., Feng, J., Zhang, J., Kang, X., and Qian, D. (2020). Quercetin Modulates AMPK/SIRT1/NF-κB Signaling to Inhibit Inflammatory/oxidative Stress Responses in Diabetic High Fat Diet-Induced Atherosclerosis in the Rat Carotid Artery. *Exp. Ther. Med.* 20 (6), 280–281. doi:10.3892/etm.2020.9410

Zhang, Y., Li, M., Li, X., Zhang, T., Qin, M., and Ren, L. (2018). Isoquinoline Alkaloids and Indole Alkaloids Attenuate Aortic Atherosclerosis in Apolipoprotein E Deficient Mice: A Systematic Review and Meta-Analysis. *Front. Pharmacol.* 9, 602. doi:10.3389/fphar.2018.00602

Conflict of Interest: The authors declare that the research was conducted in the absence of any commercial or financial relationships that could be construed as a potential conflict of interest.

Publisher's Note: All claims expressed in this article are solely those of the authors and do not necessarily represent those of their affiliated organizations or those of the publisher, the editors and the reviewers. Any product that may be evaluated in this article, or claim that may be made by its manufacturer, is not guaranteed or endorsed by the publisher.

Advantages of publishing in Frontiers

OPEN ACCESS
Articles are free to read for greatest visibility and readership

FAST PUBLICATION
Around 90 days from submission to decision

HIGH QUALITY PEER-REVIEW
Rigorous, collaborative, and constructive peer-review

TRANSPARENT PEER-REVIEW
Editors and reviewers acknowledged by name on published articles

Frontiers
Avenue du Tribunal-Fédéral 34
1005 Lausanne | Switzerland

Visit us: www.frontiersin.org
Contact us: frontiersin.org/about/contact

REPRODUCIBILITY OF RESEARCH
Support open data and methods to enhance research reproducibility

DIGITAL PUBLISHING
Articles designed for optimal readership across devices

FOLLOW US
@frontiersin

IMPACT METRICS
Advanced article metrics track visibility across digital media

EXTENSIVE PROMOTION
Marketing and promotion of impactful research

LOOP RESEARCH NETWORK
Our network increases your article's readership